SUCTION MEASUREMENTS AND WATER RETENTION IN UNSATURATED SOILS

Lourenço, Sérgio Duarte Nunes

SUCTION MEASUREMENTS AND WATER RETENTION IN UNSATURATED SOILS

Sérgio Duarte Nunes Lourenço

Ph.D. Thesis

September 2008

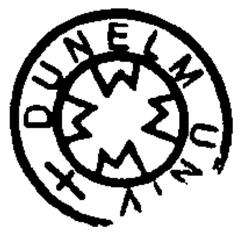

to Miguel Fernandes Lourenço

ABSTRACT

Techniques for testing unsaturated soils have been investigated where the measurement and control of parameters were done directly. Suction was measured and controlled with a new high suction tensiometer and water content through mass measurements with a balance. These techniques have been used for the determination of soil water retention curves and for the development of a suction control system using air circulation and water injection. The techniques allow the soil to be subject to the same drying and wetting conditions that occur in nature and avoid the need for elevated air pressures, as are traditionally involved in testing using the axis translation technique.

The performance of the new high suction tensiometer was evaluated, followed by its applications to soil testing. The tensiometer performance focused on the factors controlling cavitation, calibration in the negative pressure range and measurement. It was found that isotropic unloading is the most accurate technique for calibration in the negative range and that axis translation techniques can lead to errors. The research confirms high suction tensiometers are easy to use and versatile devices.

Techniques were developed to measure and control suction and water content in unconfined and confined samples. Research on the unconfined samples focused on the procedures to obtain the soil water retention curve: discrete (soil dried or wetted in stages) and continuous (soil drying continuously). While both procedures were found not to influence the curves significantly, it is demonstrated that the continuous procedure is sensitive to factors such as the exposed surface area to drying or wetting and so should be used carefully.

For confined conditions, wetting, drying, and water content measurement systems were developed. Wetting was based on the injection of water; drying was based on

air circulation through a desiccant within a closed loop system. Water content was determined from the difference between water injected and that adsorbed by the desiccant. This has been applied as part of a double cell triaxial testing system that allows continuous determination of suction, water content and volume change. A challenge of such a system was imposing an air tight environment.

The suitability of environmental scanning electron microscopy to observe unsaturated soils at the particle level was explored. The imaging of micron-sized materials at different relative humidities allowed a series of observations previously undocumented, among them: water menisci were visible, including their shape and interaction with surfaces; the contact angle between the air-water and water-solid interfaces was measurable; particle re-arrangements occurred while the Relative Humidity changed.

ACKNOWLEDGEMENTS

I would like to acknowledge my supervisors Dr. Domenico Gallipoli, Dr. David G. Toll, Dr. Charles E. Augarde. I'm particularly thankful for having involved me in the MUSE activities: the three oral presentations in the MUSE Schools, laboratory work in ENPC, and the three stays in LCPC for the centrifuge tests. Dr. Gabriela M. Medero (Heriot-Watt University) provided guidance during the second year of the PhD. The work was followed by my industrial sponsor, Mr. Fred Evans from Wykeham Farrance Division (Controls Testing).

All laboratory work in Durham was conducted with the assistance of Mr. Charles McEleavey (Bernie), Mr. Stephen Richardson (Rich) and Mr. Charantin Panesar. The idea of using silica gel as the desiccant for the suction control system comes from Bernie. Thanks are also due to Mr. Roger Little and Mr. Colin Wintrip from the mechanical workshop for the manufacturing work, Mr. Ian Hutchinson and Mr. Colin Dart from the electronics workshop for the suction control boxes, computer support by Mr. Michael Wilson, and the tensiometer photos by Ms. Julie Dodds. Changes to the TRIAX software were done by Dr. David G. Toll.

ESEM imaging was done by Ms. Helen Riggs (Chemistry Department, Durham University), Mr. David Beamer (FEI Company) and Dr. Jim Buckmann (Heriot-Watt University). The silica spheres were synthesized by Mr. Tom Smart and Dr. Aileen Congreve (Chemistry Department, Durham University). Mr. Mark Rosamond (Electronics, School of Engineering, Durham University) did the SEM images of the silica gel. Permission to use the SEM was given by Dr. Del Atkinson (Physics Department, Durham University). Mark also did the attempts to glue the 6 μm sphere to the tip of the AFM cantilever.

The centrifuge tests were conducted in the Laboratoire Centrales des Ponts et Chaussees in Nantes by Dr. Francesca Casini (Polytechnic University of Catalunia), Dr. Juan Jorge Munoz, Dr. Jean Michel Pereira from the Ecole National des Ponts et Chaussees and the author, together with the LCPC staff (Mrs. Celine Boura, Mr. Claude Favraud, Mr. Patrick Gaudicheau).

This thesis strongly benefited from discussions and work done by other colleagues in Durham: discussions on the filter paper/psychrometer and BIONICS soil data comes from Mr. João Mendes (ongoing PhD); Dr. Zulfhami Ali Rahman (PhD 2008) introduced the axis translation technique; Mr. Mark Ball (MSc. 2005), Ms. Sarah Hidayat (MSc. 2006), Mr. Phillip Wallbridge (MEng. 2007), Mr. Juan Fernandez (ERASMUS Student) and Dr. Paul Jaquin (PhD 2008) for general talks on tensiometers; Mr. Mark Donoghue (MEng. 2006) built the saturation vessel; Mr. Vincent Vercraije (MEng. 2007) for discussions on the osmotic suction; Ms. Cathy Dowding (PhD 2008) helped with the dissolved oxygen meter.

Interactions with other researchers included: tensiometer studies with Dr. A.M. Ridley (Geotechnical Observations Ltd), SWRC with tensiometers with Dr. F.A.M. Marinho (University of S. Paulo – Brazil), hygrometers with Dr. A.-M. Tang (ENPC), papers/dissertations from ENPC from Dr. Jean-Michel Pereira. Mr. João Pires (Physics Department, Durham University) helped interpreting Atchley and Prosperetti (1989) paper and all quantitative aspects of the section 'Analysis of cavitation'.

Financial support is acknowledged from the Engineering and Physical Sciences Research Council (EPSRC) of the United Kingdom for funding through a CASE research grant with Wykeham Farrance Division (Controls Testing), and the European Commission via the "Marie Curie" Research Training Network contract number MRTN-CT-2004-506861.

CONTENTS

LIST OF FIGURES

LIST OF TABLES

Chapter 1. INTRODUCTION

1.1. Suction measurements and water retention in unsaturated soils

In unsaturated conditions, soil pores are partly filled by water and air, with the water retaining at interparticle contacts and surfaces as films of water, and as bulk water enclosing particles. The relevance of partial saturation for engineering applications can be understood following the example in Figure 1.1 which links pore water pressure variations to ground deformations. The figure depicts field measurements of displacements (vertical and horizontal), rainfall and piezometric head (pore water pressures) in the slopes of a clay embankment. It shows that the slope tends to shrink when the pore water pressure reaches its minimum (during the summer) and swell when the pore water pressure increases towards zero (during the winter).

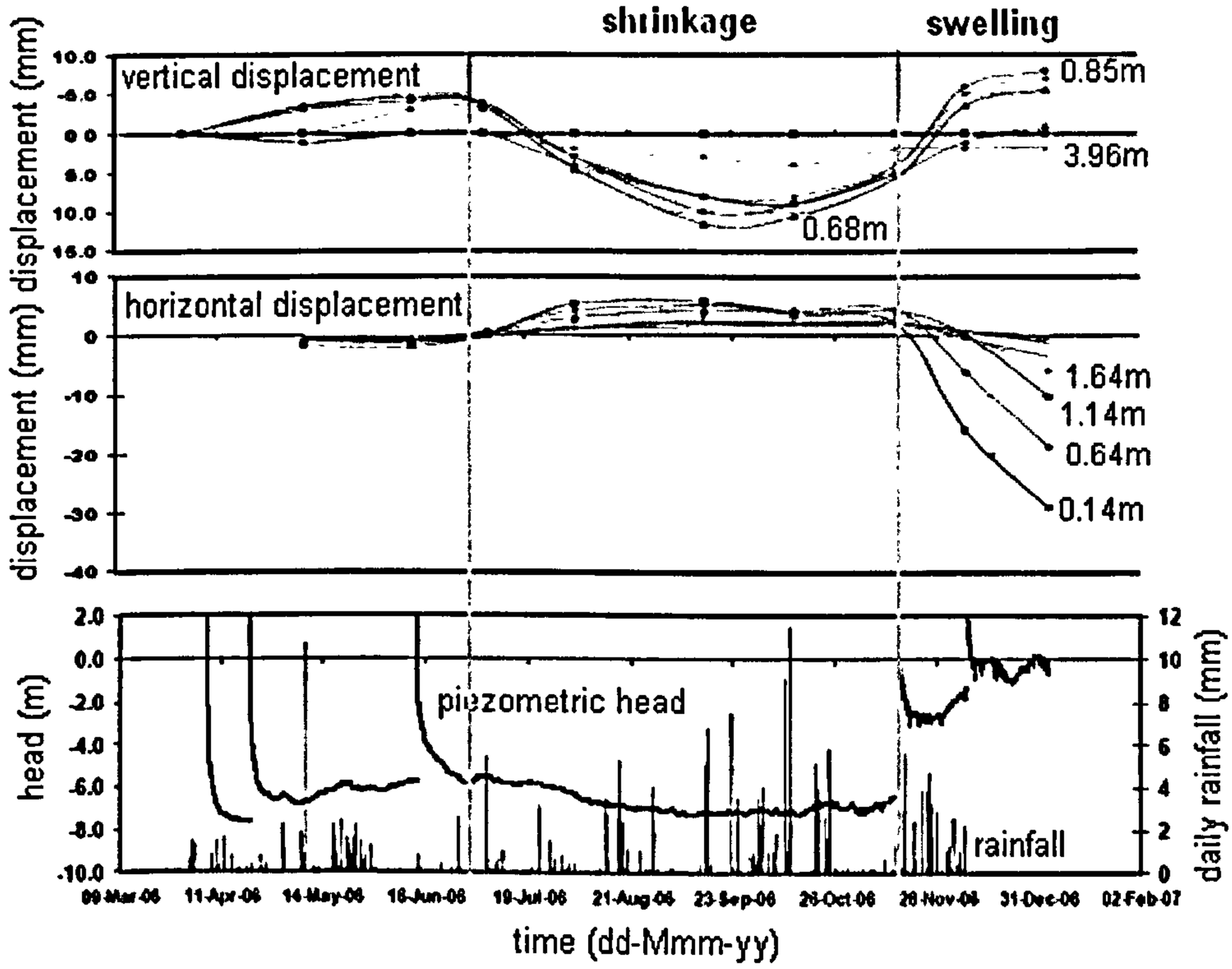

Figure 1.1: Monitoring data of a clay embankment linking negative water pressures variations to slope deformations (shrinkage and swelling) (after Ridley, 2007)

Unsaturated soils is a growing research area in different fields of science and engineering. In the ISI database, the number of papers associated to the three combinations of the following keywords: 'unsaturated – soil', 'partially – saturated – soil', 'partly – saturated – soil' increased in 1989 and has since then been increasing steadily (Figure 1.2a). Unsaturated soils cover a strongly multidisciplinary research area as proven by the fact that, from the 4676 journal papers published with the above keywords, only a small percentage appeared in geotechnical journals. Most of them were published in water sciences (9.5% in the Water Resources Research) and soil science (6.84% in the Soil Science Society of America Journal). Geotechnical engineering journals accounted for 7.74% of the 4676 papers. Environment journals also publish within the same proportion with the same keywords as geotechnical journals (Figure 1.2b).

1.1.1. Suction and water retention measurements

Known techniques to measure suction in soils include relative humidity equilibrium, which links relative humidity inside soil pores to total suction through Kelvin's equation (e.g. Alonso et al., 2005), and axis translation, which uses a raised air

pressure to measure or control suction (Hilf, 1956). Relative humidity equilibrium techniques are based on vapour transfer between soil menisci and surrounding atmosphere while axis translation techniques are based on the liquid water transfer through saturated pores or menisci. The selection of the appropriate technique depends on the suction range of interest, for low suctions (<≈1.5MPa) the axis translation is the most appropriate, while the relative humidity equilibrium covers the MPa range.

Suction and water content are either measured by directly reading their values using appropriate devices (e.g. suction is read by using tensiometers and mass is read by using a balance) or are indirectly measured by reading the value of an intermediary physical quantity, which is then related to suction or water content (e.g. the hygrometer reads relative humidity that is then converted to total suction).

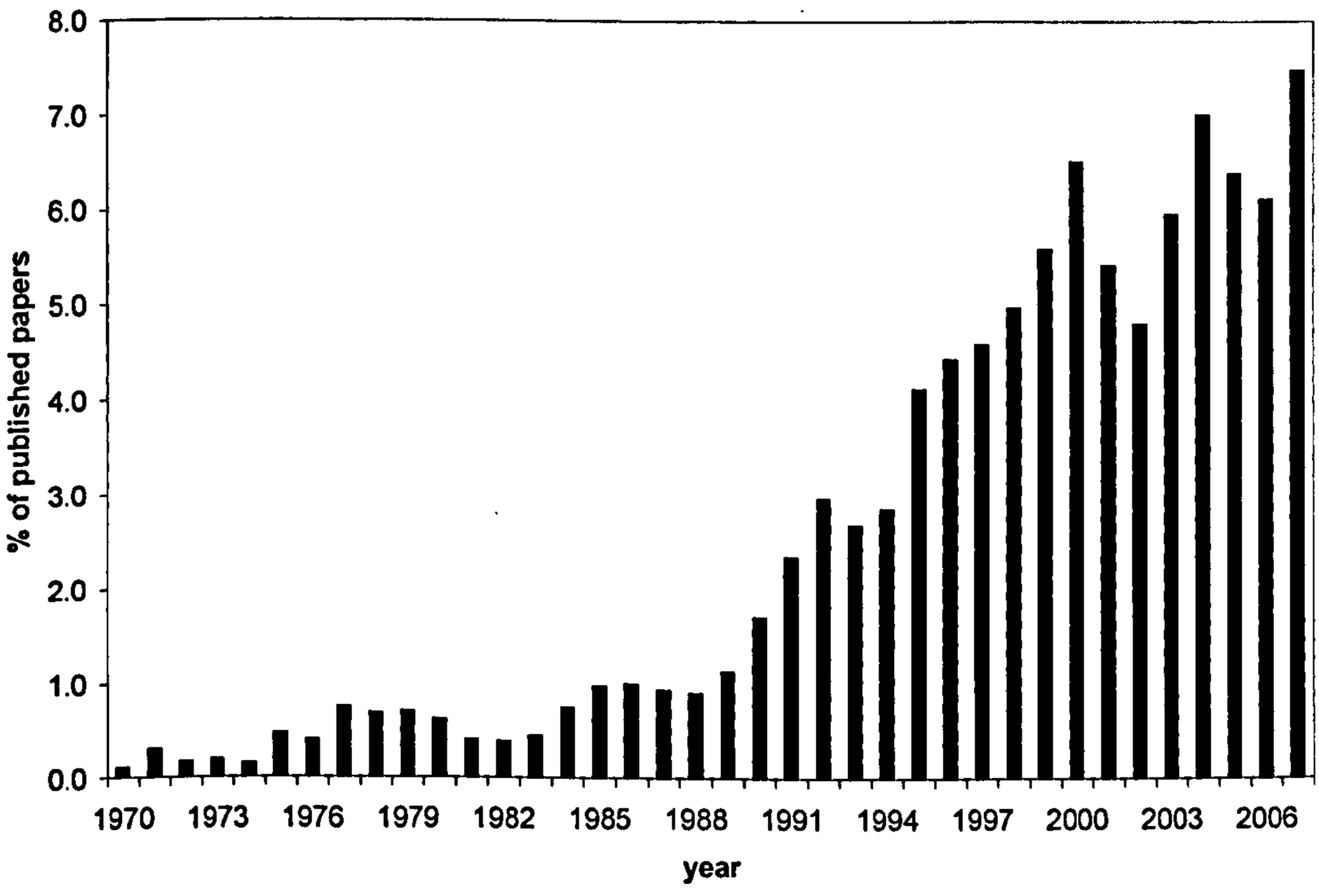

(a)

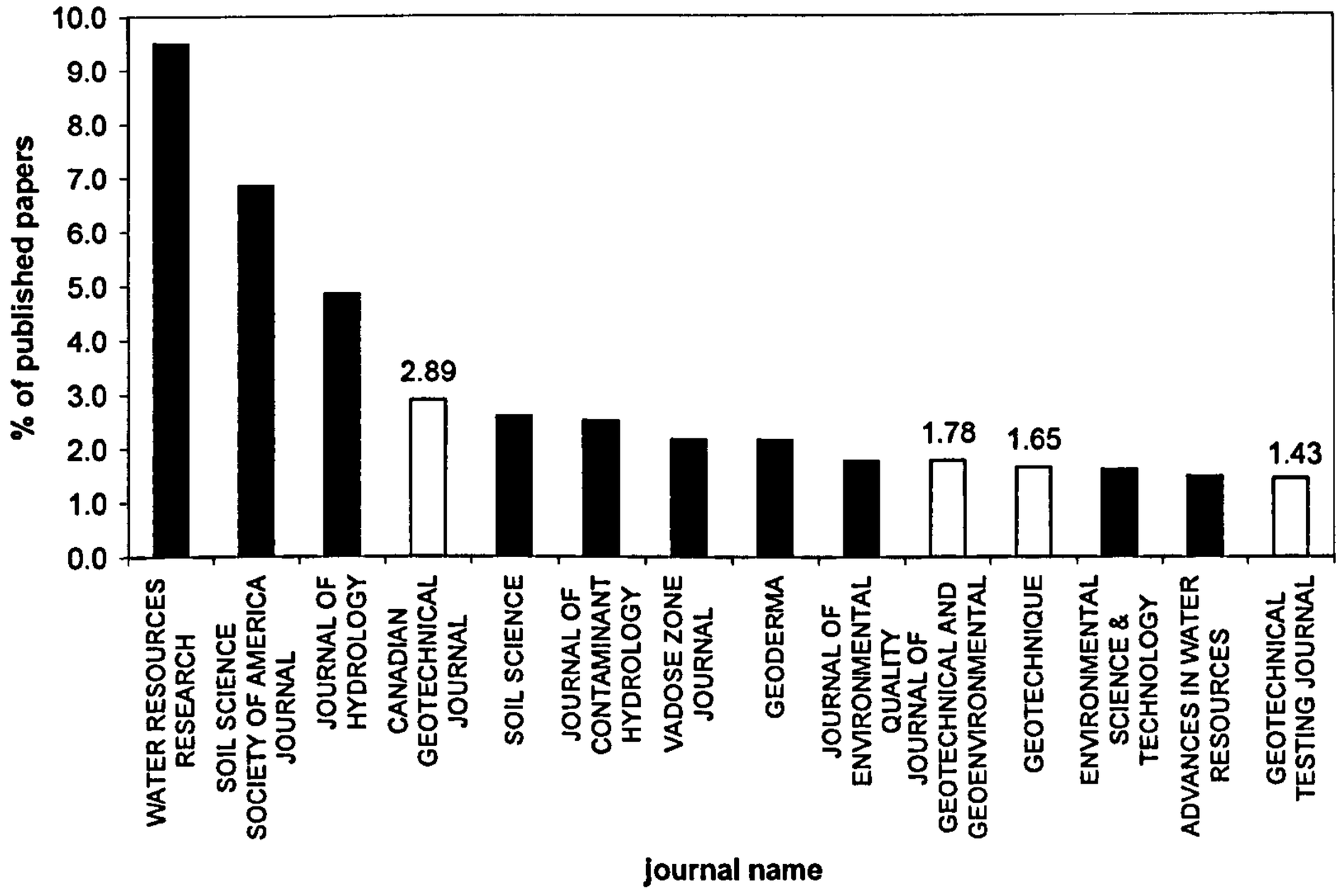

(b)

Figure 1.2: A search for the keywords 'unsaturated', 'soil', 'partially', and 'partly' in the ISI database resulted in a total of 4676 papers: (a) percentage of papers versus year of publication, (b) percentage of papers versus journal of publication - white bars correspond to the geotechnical journals (from ISI-The Thomson Corporation, 2007)

1.1.2. High suction tensiometers

Recent studies in experimental unsaturated soil mechanics have demonstrated a considerable interest in high suction tensiometers (also called high capacity tensiometers by Tarantino and Mongiovi (2001) or suction probes by Ridley and Burland (1993)) due to their fast response time, easy manoeuvrability and relatively error-free measurements. Response time of high suction tensiometers can be of the order of minutes compared to days for the filter paper and axis translation (Rahardjo and Phoon, 2006). Due to their relatively small size, high suction tensiometers can be easily transported and fitted in any device for suction measurement, e.g. centrifuge (Chiu et al., 2005), triaxial cell and oedometer (Jotisankasa, 2005), shear box (Tarantino and Tombolato, 2005) or simply to take suction measurements in soils samples wrapped in cling film (Hidayat, 2006). As they measure directly suction, errors related to indirect calibration curves, such as those used for the filter paper

and psychrometer techniques, are avoided. Tensiometers can also be used for measuring pore water pressures in saturated soils.

As tensiometers are reasonably easy to manufacture, they have received considerable interest from researchers in tropical countries where applications of unsaturated soils and suction measurements are very relevant. Mahler and Diene (2007) in Brazil developed a low cost tensiometer with acrylic body at a cost of USD 300 while Jotisankasa et al. (2007) in Thailand developed a tensiometer with a piezoresistive sensor.

1.2. Objectives and thesis structure

This dissertation is the result of a joint research project between Durham University and Wykeham Farrance Division (WF) of Controls Testing whose main objectives, as defined at the start of the research, are:

1. to develop and test a new high suction tensiometer built by WF,
2. to develop a suction control system by using the new tensiometer,

The main target was to develop a device able to measure suctions up to 1000kPa that could be commercialized. A second goal was to develop a suction control system for triaxial testing by using the tensiometer for direct measurements of suction (following the works of Cunningham (2000) and Jotisankasa (2005)).

As the research evolved with time additional research lines were followed:

3. to determine the soil water retention curve by using the new tensiometer,
4. to apply the new tensiometers to the centrifuge tests of a model foundation on an unsaturated soil layer as part of a project involving several universities within the MUSE network (this work was carried out at the Laboratoire Centrale des Ponts et Chaussees in Nantes, France),
5. to explore the effect of suction on granular materials at a microscopic scale by using environmental scanning electron microscopy. This line of investigation was initially motivated by the consideration that some of the most important physical phenomena relevant to this research (e.g., cavitation in the tensiometer) were happening at the micron-scale and these required improved understanding.

The thesis is presented in seven chapters. **Chapter 2** introduces the background to the work contained in the subsequent parts. A description of suction, water retention and volume variations of soils are introduced in Section 2.2 where hydraulic hysteresis is also reviewed in some detail. Current suction measurement and control techniques are reviewed in Section 2.3, including control and measurement techniques for water content. This focuses mainly on the testing devices used in this research or on devices with similar working principles. The chapter ends by presenting the most relevant advances in unsaturated soil testing including a description of emerging areas of research and an introduction to the high suction tensiometer in Section 2.4. **Chapter 3** concentrates on the conditioning, calibration and performance of the high suction tensiometer developed in this research. The procedures for saturation and calibration of the probe in the negative pressure range as well as the procedures for routine measurement of suction are presented in detail. Based on these results, suggestions are given regarding the most accurate technique to calibrate the tensiometer in the negative pressure range. Selected results from centrifuge tests with suction measurement using the new tensiometer are also presented in Chapter 3. **Chapter 4** and **Chapter 5** focus on the applications of the new tensiometer to laboratory testing. In particular, the procedures to obtain the soil water retention curve are presented in Chapter 4 while the development of the novel suction control system is presented in Chapter 5. **Chapter 6** presents the observations in an environmental scanning electron microscope (ESEM) of the interactions between water, gas and solid in an idealized granular material with spherical particles having diameters of the order of few microns. The observations revealed perfectly visible micron-scale water menisci at the contact between spherical grains. This Chapter also provides an initial interpretation of such microscopy observations. The dissertation ends in **Chapter 7** by summarizing the main experimental developments of this work and, based on the ESEM results, points to micromechanics as a key topic for understanding the engineering behaviour of unsaturated soils. Interpretations and discussions presented in this work are made against geotechnical and non-geotechnical literature based on papers from the various research fields listed in Figure 1.2b as well as others from physical chemistry. A list with all tests conducted for this thesis is given in the Appendix.

Chapter 2. REVIEW

2.1. INTRODUCTION

This chapter provides a brief review on suction and water retention measurements in unsaturated soils, focusing on the direct measurement of suction with high suction tensiometers and their applications to laboratory testing.

Section 2.2 introduces suction, water content, and volume variations in unsaturated soils as relevant to this thesis. At first, suction and water retention behaviour are introduced, including physical meanings and relevant laws. A distinction is made between water retention from water vapour or liquid water because both will be relevant in different parts of this research. The soil water retention curve is presented (relevant to Chapter 4) including a detailed review on the hydraulic hysteresis. Suction, water retention and volume variations are then combined to review the literature on the swelling and shrinkage of clays.

Techniques for suction measurement and control are reviewed in Section 2.3, including techniques for water content measurement. The section ends by exploring new possibilities for laboratory testing at the grain scale by Environmental Scanning Electron Microscopy.

Section 2.4 reviews high suction tensiometers. Their working principle, design and developed models are presented in 2.4.1; cavitation is introduced in 2.4.2; aspects relevant to their saturation, calibration and routine measurement are presented in sections 2.4.3, 2.4.4, 2.4.5, respectively; and end's up by reviewing applications to laboratory testing in 2.4.6.

2.2. SUCTION, WATER RETENTION, AND VOLUME VARIATIONS IN SOILS

2.2.1. Suction

2.2.1.1. Definitions

The state of water in soil is characterized by the soil water potential. According to the *Glossary of Soil Science Terms* of the *Soil Science Society of America* (SSSA) the soil water potential is defined as: "the amount of work that must be done per unit of a specified quantity of pure water in order to transport reversibly and isothermally an infinitesimal quantity of water from a specified source to a specified destination". The soil water potential is made of two components: matric potential and osmotic potential. Matric potential is the "potential energy of soil water due to the attractive forces (adhesion and cohesion) between water and the soil matrix" and the osmotic potential "the potential energy acting upon soil water due to the effect of solutes" (both SSSA definitions). From an unsaturated soil mechanics perspective, these definitions link the soil water potential to total suction, the matric potential to matric suction and the osmotic potential to osmotic suction.

Total suction is related to the water vapour pressure through Kelvin's law. If two surfaces are placed in close proximity in constant temperature and RH, water would start condensing on the surfaces until forming a liquid bridge between the two surfaces with well defined air-water menisci (Figure 2.1) (e.g. Maeda and Israelachvili, 2002, Maeda et al., 2003). The same would take place in a soil. If the pores were interconnected, water would condense in all small gaps (e.g. particle contacts) until forming a water bridge between the two surfaces. The suction corresponding to the menisci curvature can be calculated by Kelvin's equation (Fredlund and Rahardjo, 1993):

$$s = -\frac{RT}{\upsilon_{w0}\varpi_v}\ln\left(\frac{u_v}{u_{v0}}\right) \qquad (2.1)$$

Where,

s = total suction (kPa)

R = universal gas constant (8.31432 $m^3.Pa.K^{-1}.mol^{-1}$)

T = absolute temperature (273.16 + t) (K)

t = temperature (°C)

υ_{w0} = inverse of the density of water ($1/\rho_w$) (m^3/kg)

ρ_w = density of water (kg/m^3)

ω_v = molecular mass of water vapour (kg/kmol)

u_v = vapour pressure (kPa)

u_{v0} = saturation vapour pressure at a given temperature °C (kPa)

$(u_v/u_{v0})x100$ = RH (relative humidity)

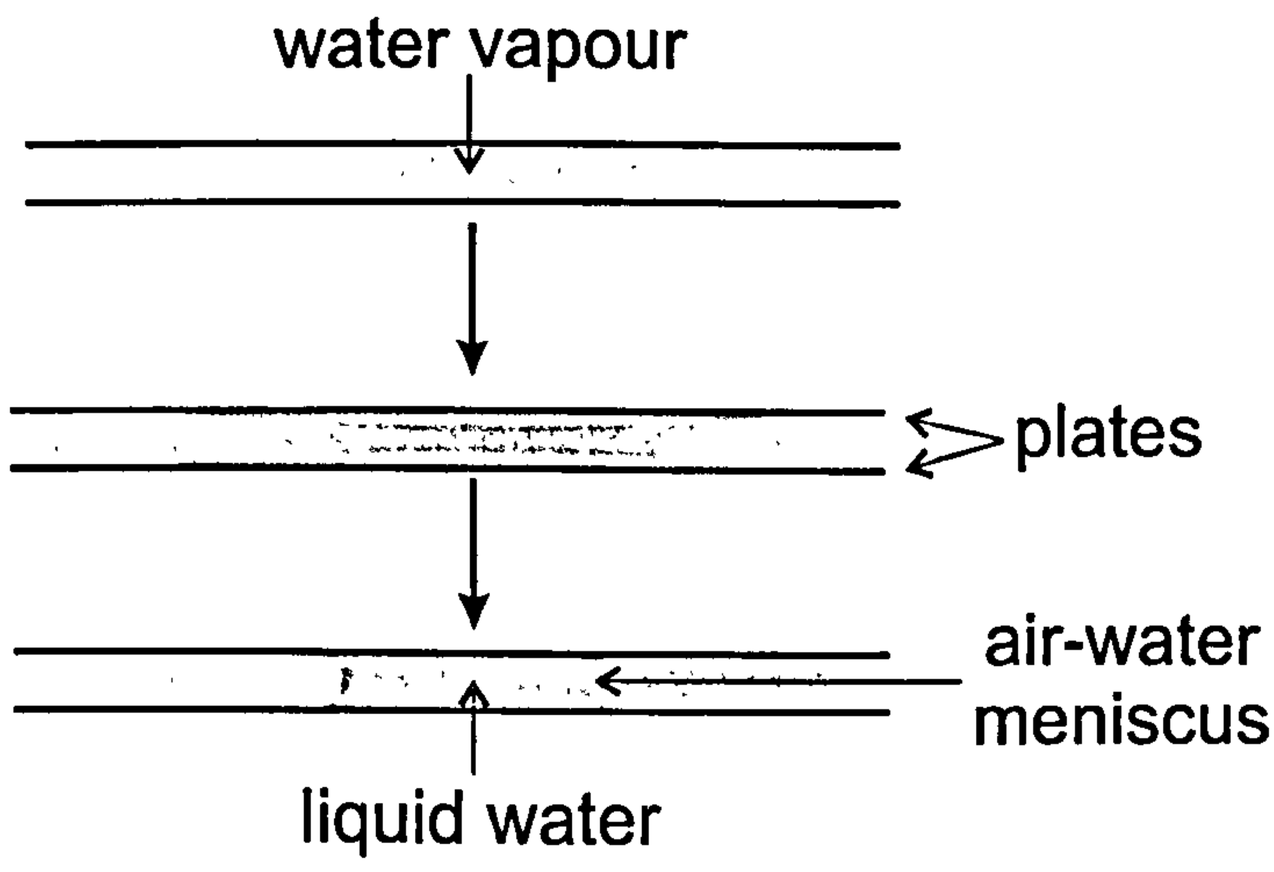

Figure 2.1: Time sequence of water condensation between 2 surfaces (after Maeda and Israelachvili, 2002, Maeda et al., 2003)

Matric suction is related to the capillary effect of water in soils through Young-Laplace equation, which relates suction to the surface tension of the air-water interface and the contact angle of the air-water interface against the solids (Figure 2.2).

$$s = \frac{2T\cos\theta}{r} \qquad (2.2)$$

Where s denotes matric suction, r denotes the radius of the menisci (the same in the direction shown in Figure 2.2 and perpendicular to it), T the air-water surface tension, and θ the contact angle of the solid-water interface. This suggests that the matric suction will be higher for soils with smaller pore diameter and higher affinity with water (low contact angles), i.e. hydrophilic clayey – silty soils.

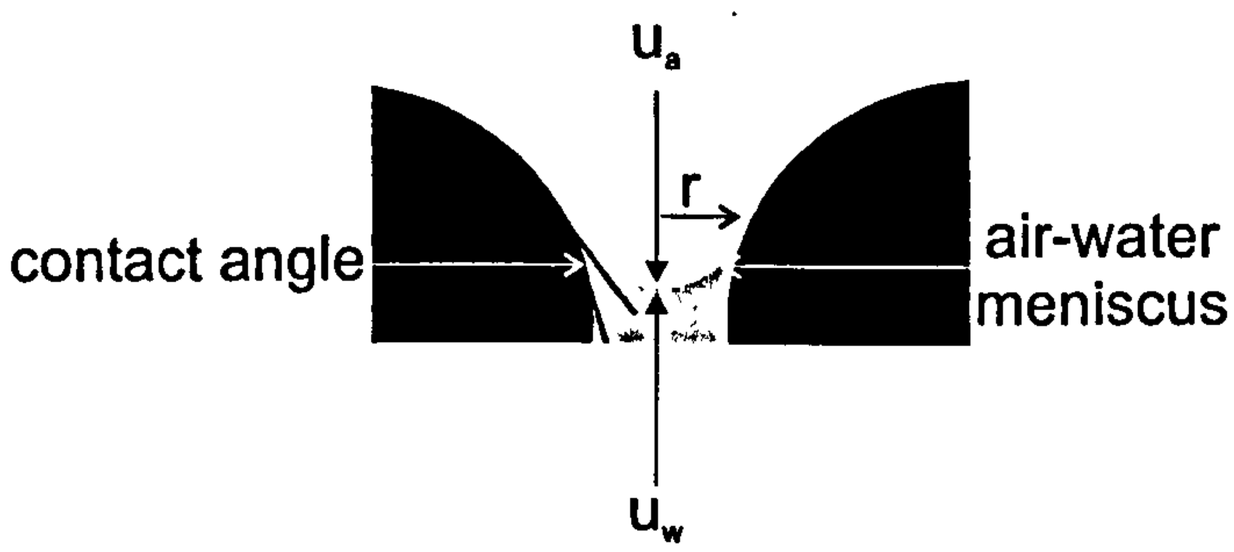

Figure 2.2: Matric suction by Young-Laplace equation

In this thesis all suction measurements are done with a high suction tensiometer and so correspond to matric suction. However, for brevity the term 'suction' will only be used.

2.2.1.2. Relevance to geotechnical engineering

Water menisci between surfaces provide an attractive force (meniscus force) that holds the soil together. This force controls the strength, stiffness and deformation behaviour of unsaturated soils. However, its effect in soils is quantified based on suction due to the difficulty in measuring the meniscus force.

The link suction – strength in soils has long been recognized. Croney and Coleman (1960), performed unconfined compression tests in undisturbed London Clay samples at increasing initial suctions and found that the unconfined compressive strength increased with the initial suction (Figure 2.3). The same trend can be observed in more recent data. Wheeler and Sivakumar (1995), for example, obtained increasing shear strengths for increasing suctions in axis translation tests in compacted kaolin (Figure 2.4).

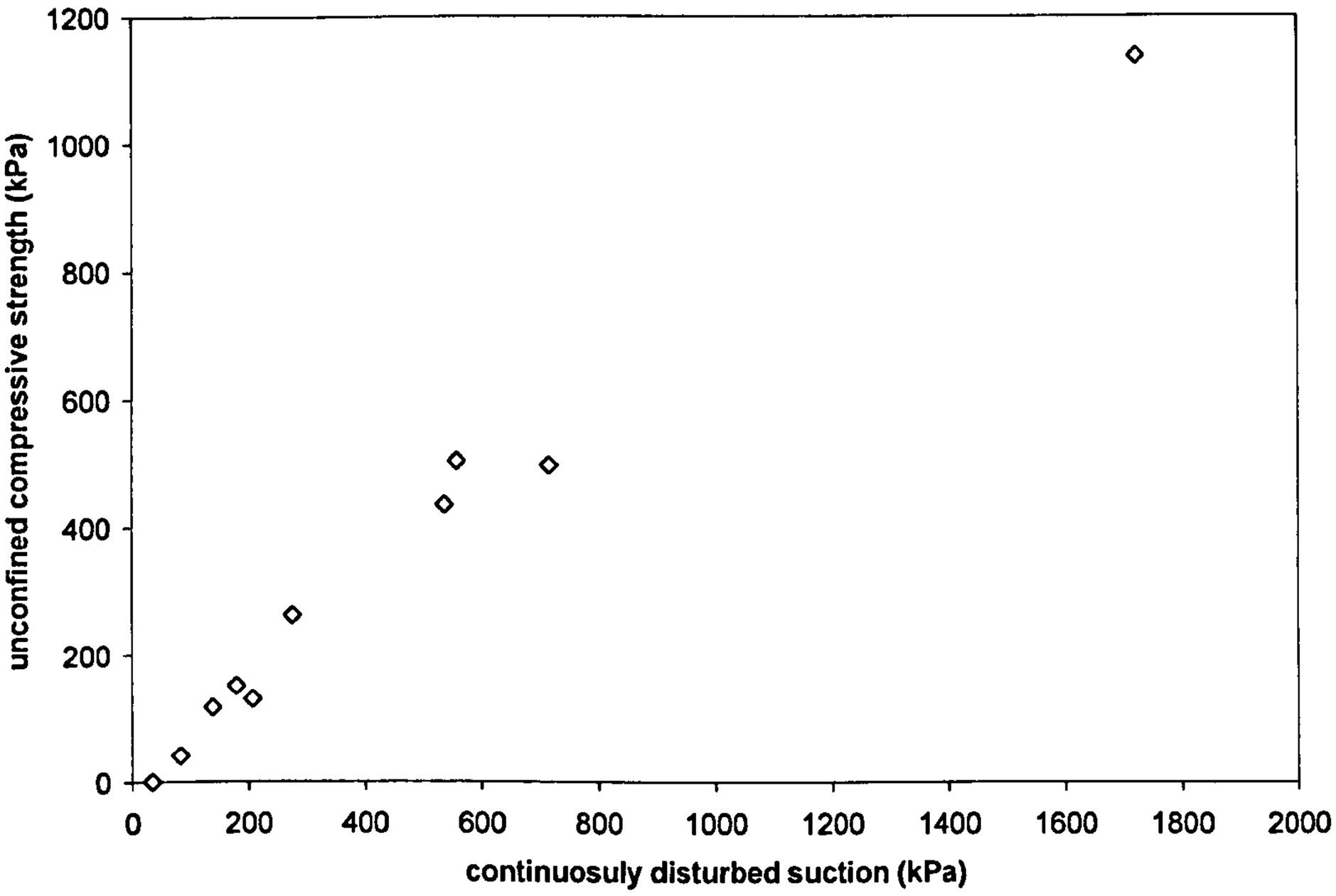

Figure 2.3: Relationship between unconfined compressive strength and suction for a heavy clay (after Croney and Coleman, 1960)

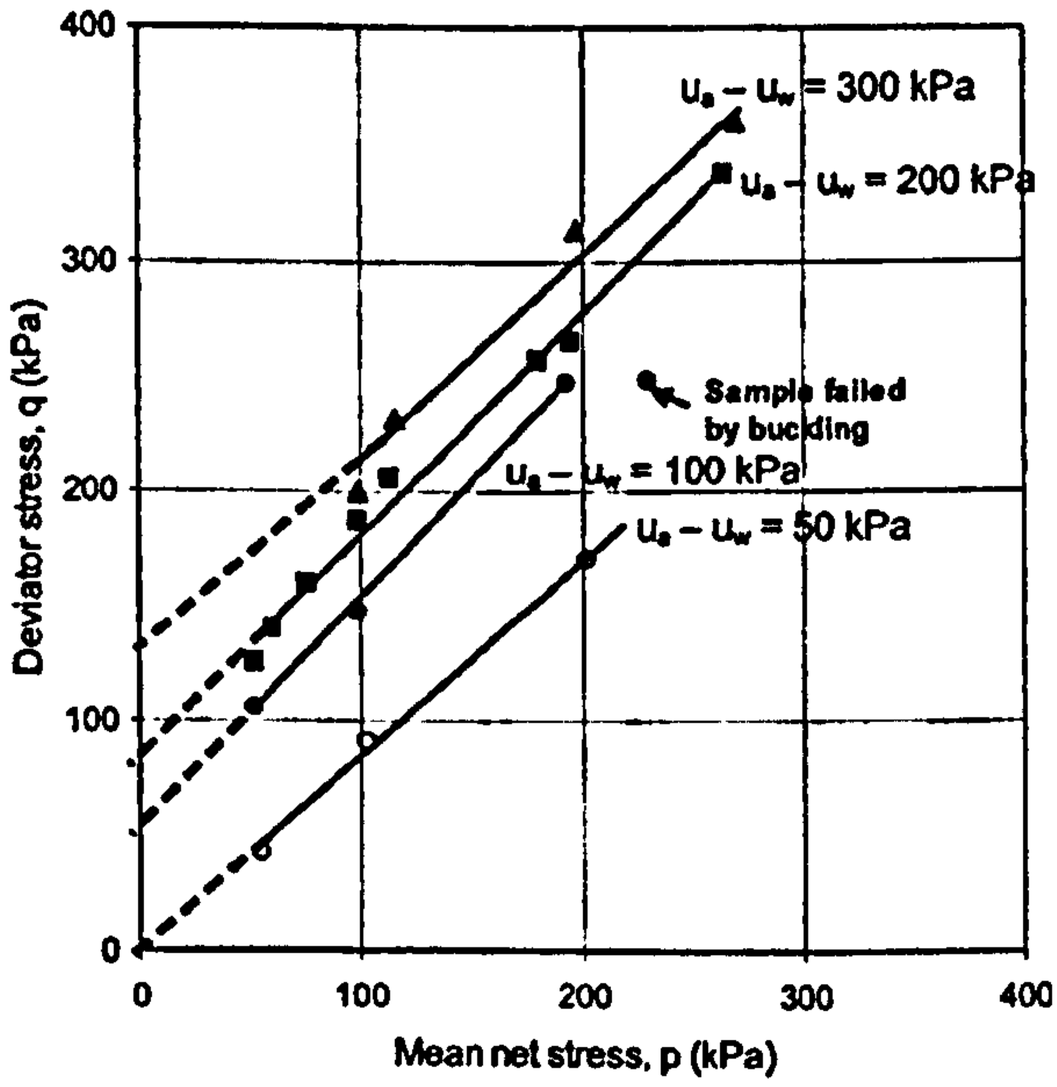

Figure 2.4: Critical shear strength results in compacted kaolin (from Wheeler and Sivakumar, 1995)

2.2.2. Water retention

2.2.2.1. From water vapour

Water retention from vapour is usually understood as an interchange of molecules between a surface and vapour, based on the Langmuir (1916) monolayer adsorption model. Langmuir regarded surfaces as adsorption sites, where each site adsorbs one molecule. If the molecule attaches, condensation occurs, if it releases, evaporation occurs. Brunauer et al. (1938) extended this model (called BET, after Brunauer-Emmett-Teller) to multilayer adsorption, where the molecules pile up in several layers (Figure 2.5a). The number of layers would be related to the ratio of partial vapour pressure / saturation vapour pressure.

Okada et al. (1998) explained the mechanism of water retention on an hydrophilic surface by the existence of OH groups which form hydrogen bonds with the water molecules in the vapour (Figure 2.5b).

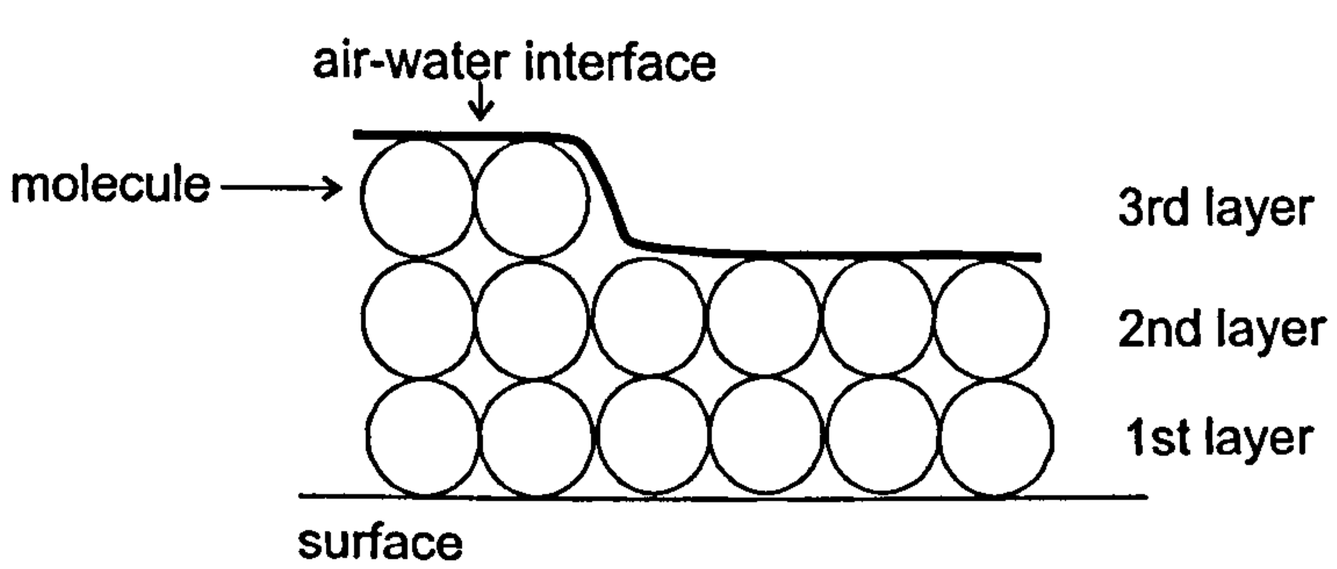

(a)

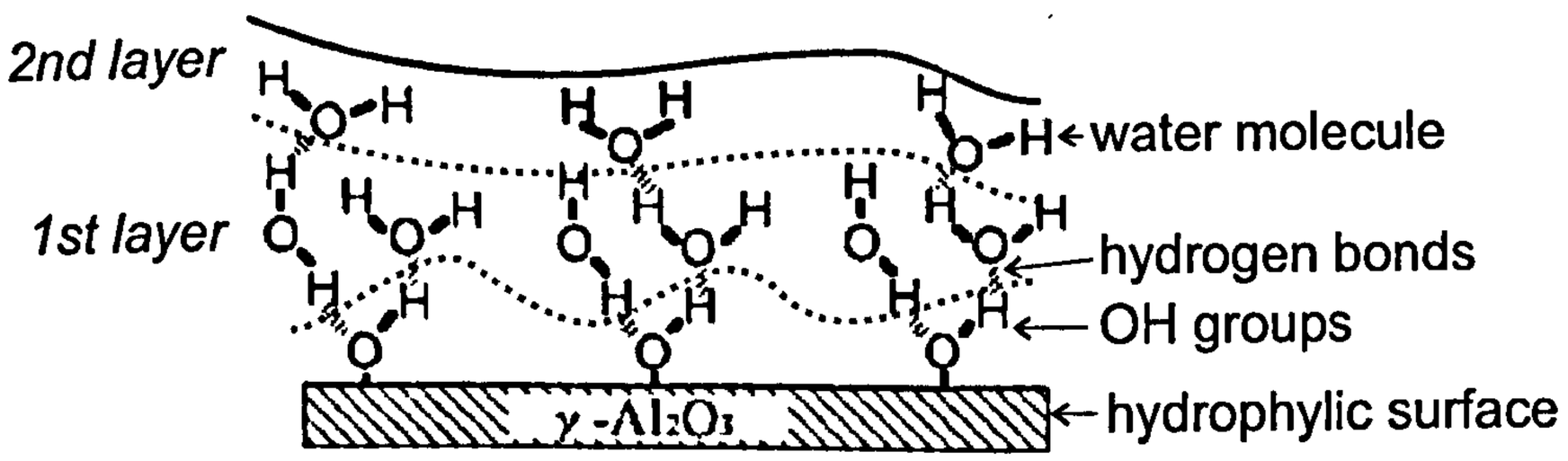

(b)

Figure 2.5: Retention of water vapour in surfaces, (a) the BET model (Gregg and Sing, 1967, Adamson and Gast, 1997, Tompsett et al., 2005), (b) adsorption in alumina (after Okada et al., 1998)

The transfer of water from vapour will occur whenever the soil and the surrounding air are not in thermodynamic equilibrium (both grain surfaces and surrounding air are at different Relative Humidity and/or temperatures). The soil will wet completely whenever the partial vapour pressure equals the saturation vapour pressure (RH of 100%), and will dry completely for very low partial vapour pressures (RH close to 0%) (e.g. NPL, 1996).

Figure 2.6 shows an example where water condenses progressively on a surface either by an increase in the partial vapour pressure to nearly 2 kPa at 20°C, or at constant vapour pressure (3kPa) by a decrease in temperature from 30°C to 25°C.

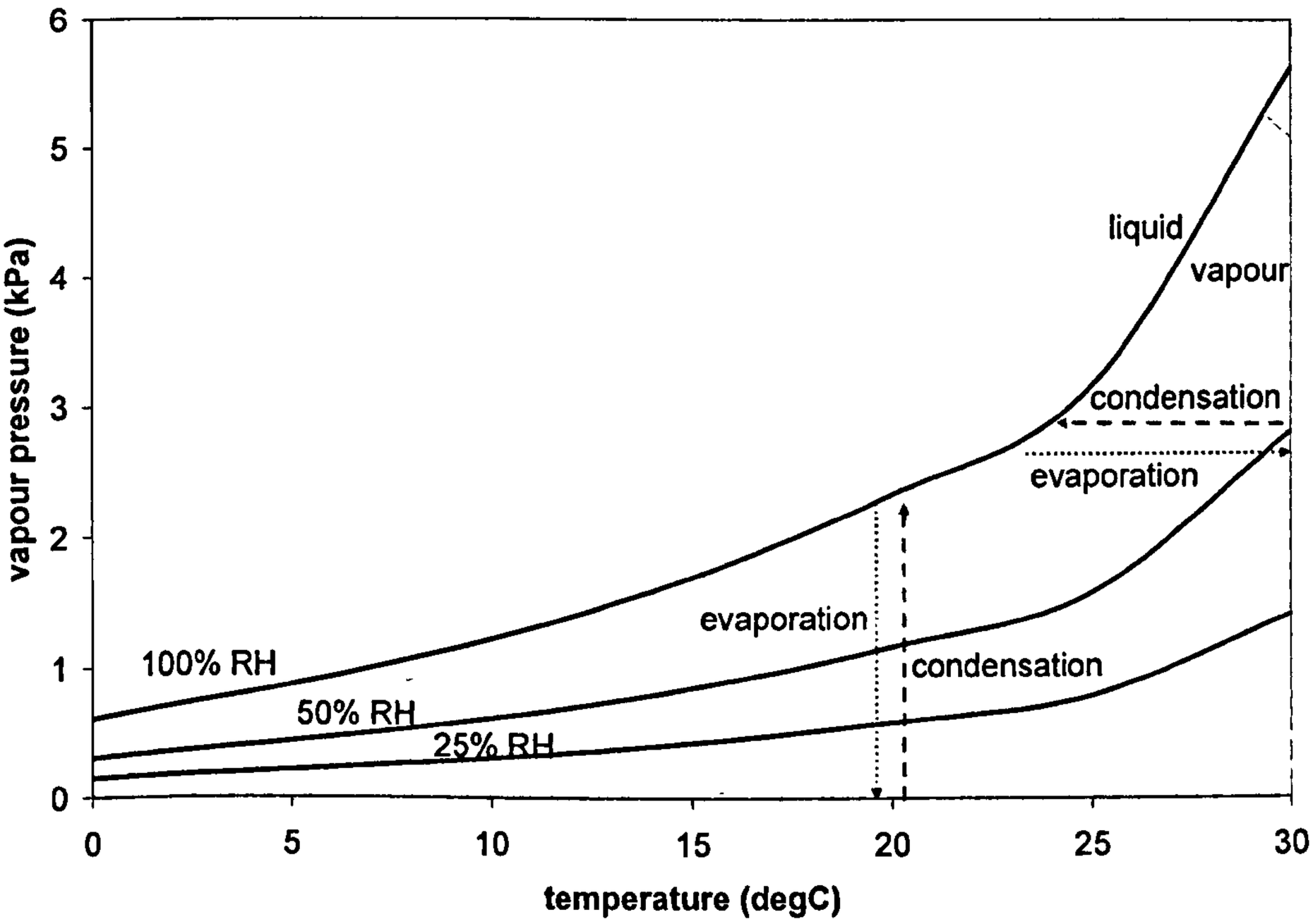

Figure 2.6: Condensation or evaporation of water due to temperature or partial vapour pressure variations

2.2.2.2. From capillary water

Water can also be retained in soils by capillary action, where the driving force is the pressure difference between air and water across the curved surface of the menisci, expressed by the Young-Laplace equation (e.g. Adamson and Gast, 1997).

Besides the capillary action, the transfer of liquid water in the ground will also depend on the existence of lateral gradients of water content, or suction, or more precisely

hydraulic heads (Fredlund and Guan, 1993). Water will flow from high to low water contents suctions or low to high suctions (Figure 2.7a). For the case of the hydraulic head (h_w) it is defined as:

$$h_w = y + \frac{u_w}{\rho_w g} \tag{2.3}$$

Where y is the gravitation head, and $(u_w/\rho_w g)$ the pressure head. The pressure head corresponds to suction and y to the elevation (either different depths or topographic variations). The hydraulic heads have to be considered because for example in the case of a slope, the soil might have the same suction (or pressure head) at the same depth but due to the different elevations there would be water flow from the higher to the lower hydraulic heads (Figure 2.7b). There could also be vertical water flow due to fluctuations in the groundwater level (there would always be a new vertical gradient of suction and water content as the groundwater level moves up and down) (Figure 2.7c).

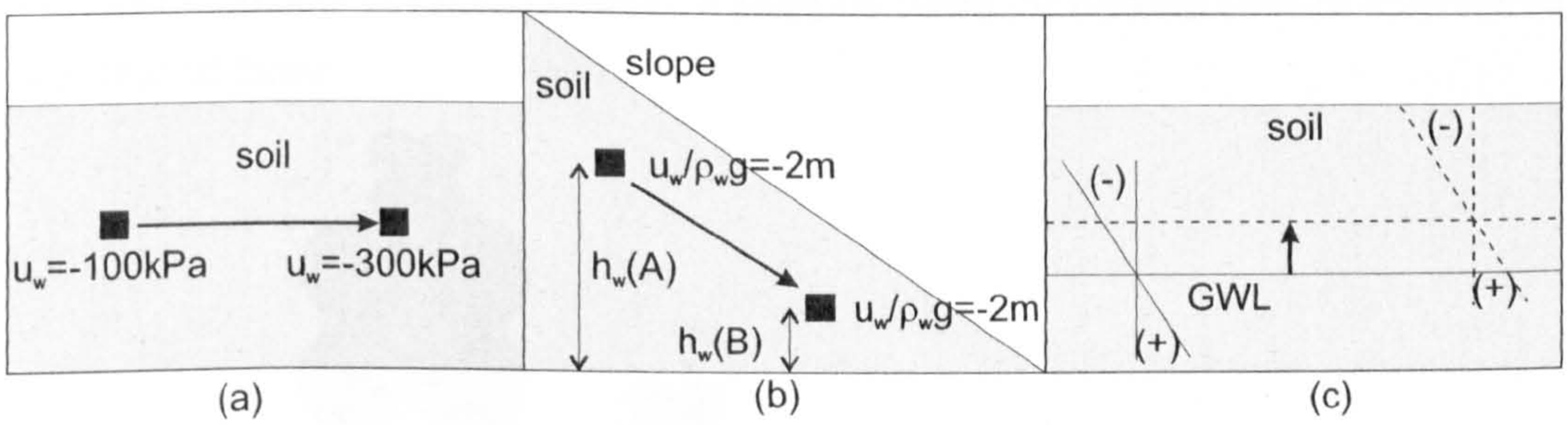

Figure 2.7: Transfer of liquid water in soil due to, (a) suction gradients, (b) hydraulic head gradients (particular case of a slope where there is an hydraulic gradient but no suction gradient), (c) fluctuations in the groundwater level (arrows show transfer direction) (after Fredlund and Guan, 1993)

2.2.3. Suction, water retention and volume variations

2.2.3.1. Soil Water Retention Curve

The soil water retention curve (SWRC) is defined as a relationship between suction and water content (Fredlund and Rahardjo, 1993). As the soil dries or wets a continuous relation between water content and suction is obtained. The SWRC is strongly dependent on the type of soil (Fredlund and Xing, 1994).

Figure 2.8 shows schematically the drying SWRC for spherical spheres. If the smaller spheres are placed on the top of the larger spheres so that only three pores exist (corresponding to u_{w1}, u_{w2}, u_{w3}) and then dried to the atmosphere from a saturated condition, the following sequence would be obtained:

1. As water evaporates the water pressure starts decreasing until reaching u_{w1}, at this moment the largest pore empties (first step in the curve).

2. If the sample keeps drying the water pressure decreases until reaching u_{w2} and the middle pore empties (second step in the graph).

3. The water pressure keeps decreasing until the smallest pore empties (at the water pressure u_{w3}).

SWRCs are smoother than in the example shown due to a wide range of pore size distribution but it is possible to obtain a stepped curve for uniform soils or soils with a well defined fabric.

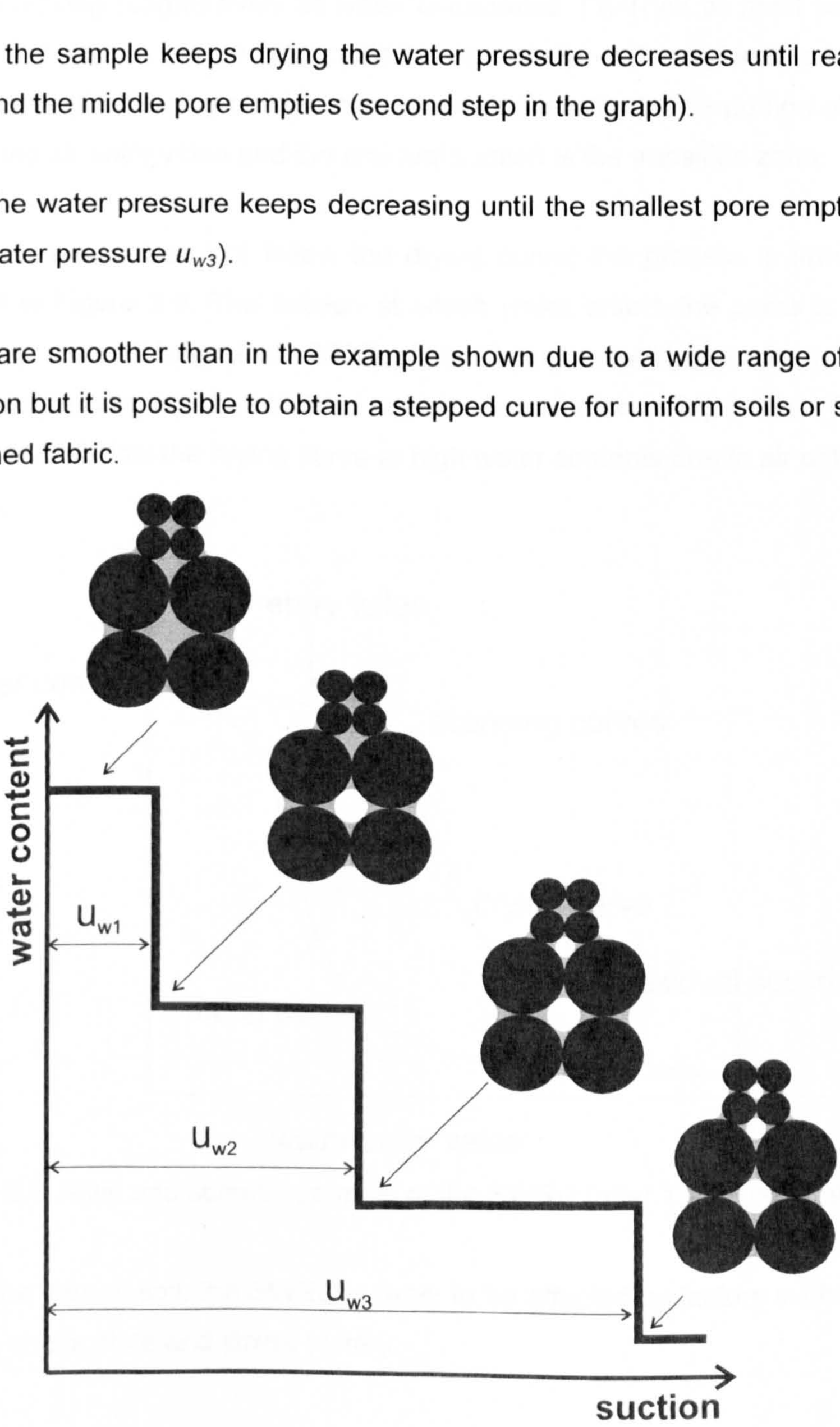

Figure 2.8: Schematics of a drying SWRC

Typical SWRCs are S-shaped with three distinct parts and can be obtained by drying or wetting (Figure 2.9) (Fredlund and Xing, 1994, Fredlund 2006). For the case of drying from a saturated condition, (1) the SWRC starts by a flat line (in the case of the degree of saturation) until curving down at the air entry value; during this stage the pores remain saturated with water under tension. (2) Once the suction value corresponding to the air entry value is reached, air enters in the larger pores (as in Figure 2.8); at this stage a continuous network of pores is formed with the volume of water decreasing progressively as water evaporates. (3) Then as most water is only concentrated at the interparticle contacts, less water will evaporate meaning that curve flattens (this turning point is named residual suction). The portion of the curve between the air entry value and the residual suction is the transition zone.

The wetting curve does not follow the drying curve; the process is irreversible as illustrated in Figure 2.9. The suction at which water enters the pores is called the water entry value (Wang et al., 2000). If the drying or wetting process is reversed during drying or wetting, the obtained curves are called scanning curves. The wetting curve might lie below the drying curve at high water contents due to air entrapment in the pores.

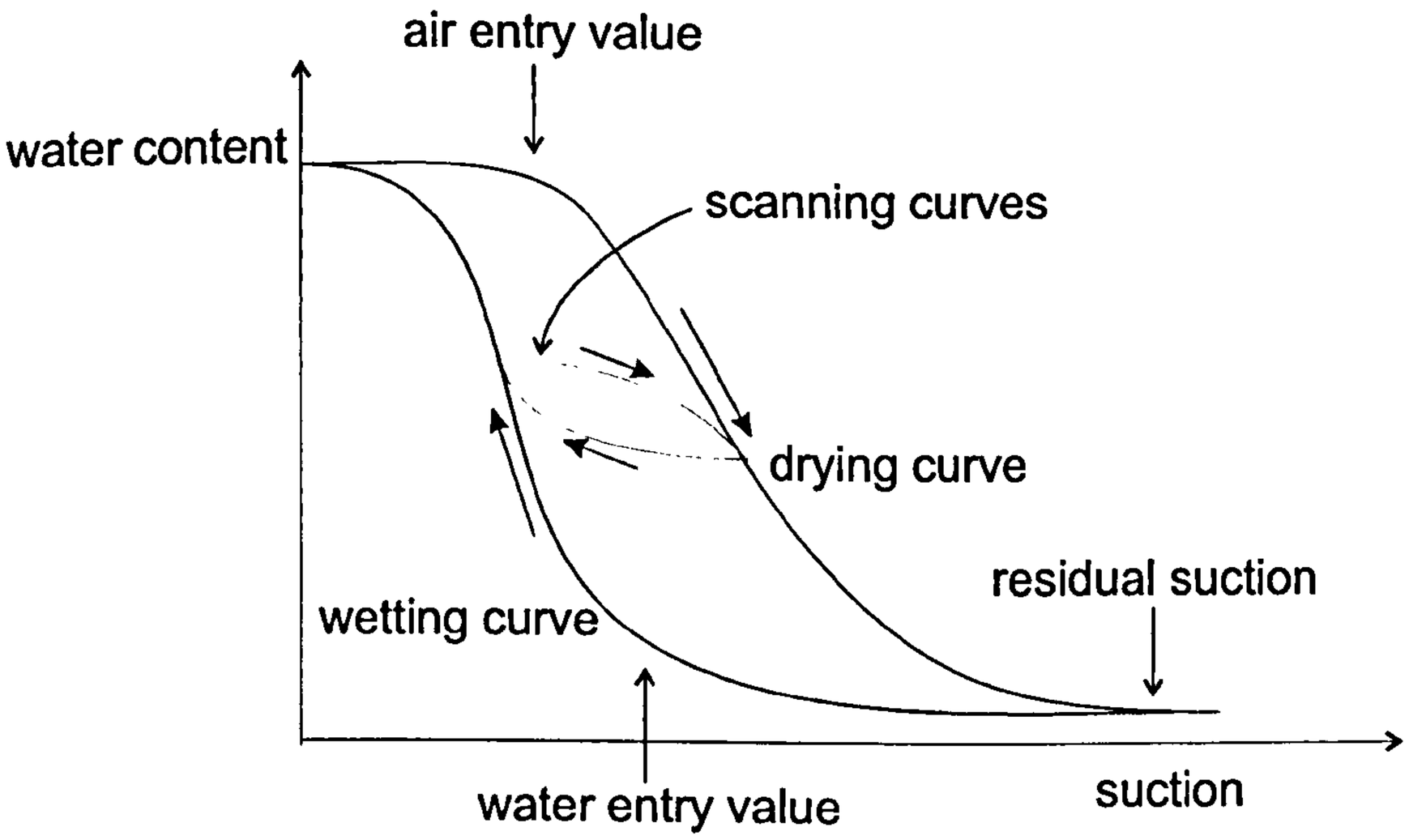

Figure 2.9: Main and scanning curves of the SWRC (after Tompsett et al., 2005)

Besides the type of soil, the SWRC is likely to be affected by factors such as the soil structure, stress state and stress history.

In a study on the effect of the structure and stress history in the SWRC, Vanapalli et al. (1999) demonstrated that the SWRC was strongly affected by the water content at compaction. Samples of a sandy clay till compacted dry of optimum showed a steeper slope comparing to samples compacted at wet of optimum. Vanapalli et al. attributed this to structure differences in the soil. Dry of optimum samples had an aggregated macrostructure while the SWRC for wet of optimum samples was governed by microstructure. This difference was visible in the low suction range (0-1500kPa), for higher suctions the SWRCs tended to overlap. Regarding the stress history (i.e. samples previously subjected to loading and unloading in the oedometer), samples compacted dry of optimum revealed a sensitivity in their water retention behaviour, while the same was not observed for samples compacted wet of optimum.

Aiming to link the water storage capacity of volcanic soils to rainfall induced landslides Ng and Pang (2000b) studied the effect of the normal stress in the SWRC. Drying-wetting paths in samples unconfined and confined at 40kPa and 80kPa revealed increasing air-entry values for increasing normal stresses, and decreasing slope inclinations for increasing normal stress (i.e. slower rates of suction increase). Recent results from Ho et al. (2007) confirm these findings.

Other factors, such as the mineralogy are likely to affect the SWRC. Williams et al. (1983) found that the presence of montmorillonite, iron oxide, vermiculite and quartz appeared to be important. In contrast, the presence of illite did not show any strong associations with a particular position or form of the SWRC.

2.2.3.2. Swelling and shrinkage of clays

Having introduced suction, water retention and the SWRC, this section adds the volume changes due to wetting and drying to review swelling and shrinkage of clays. The available literature can be grouped in the following way:

1. Swelling-shrinkage studies in expansive soils
    a. Without suction measurement
    b. With suction measurement
2. Water retention studies (with suction measurement)
3. Shear strength studies
4. Other studies

The largest numbers of papers (and oldest) are related to swelling-shrinkage studies in expansive soils Rao and Satyadas (1987), Chen and Ma (1987), Dif and Bluemel (1991), Day (1994), (Al-Homoud et al. (1995), Rao et al. (2000), Rao and Revanasiddappa (2006)). Generally the authors studied the swelling vertical strains of expansive soil samples set in an oedometer cell at increasing vertical stresses. Drying – wetting cycles varied between four Rao and Revanasiddappa (2006) and twenty Rao and Satyadas (1987) (in Figure 2.10). Most of the authors found that the axial strains stabilized after a certain number of cycles except Day (1994) who got increasing swelling and shrinkage with time. During the wetting path, Rao and Satyadas (1987) and Rao and Revanasiddappa (2006) were able to identify collapse. Some of the authors justified the various results based on microstructure changes (Al-Homoud et al. (1995), Day (1994)). Clay structure changes due to wetting - drying cycles were highlighted in a literature review by Kodikara et al. (1999).

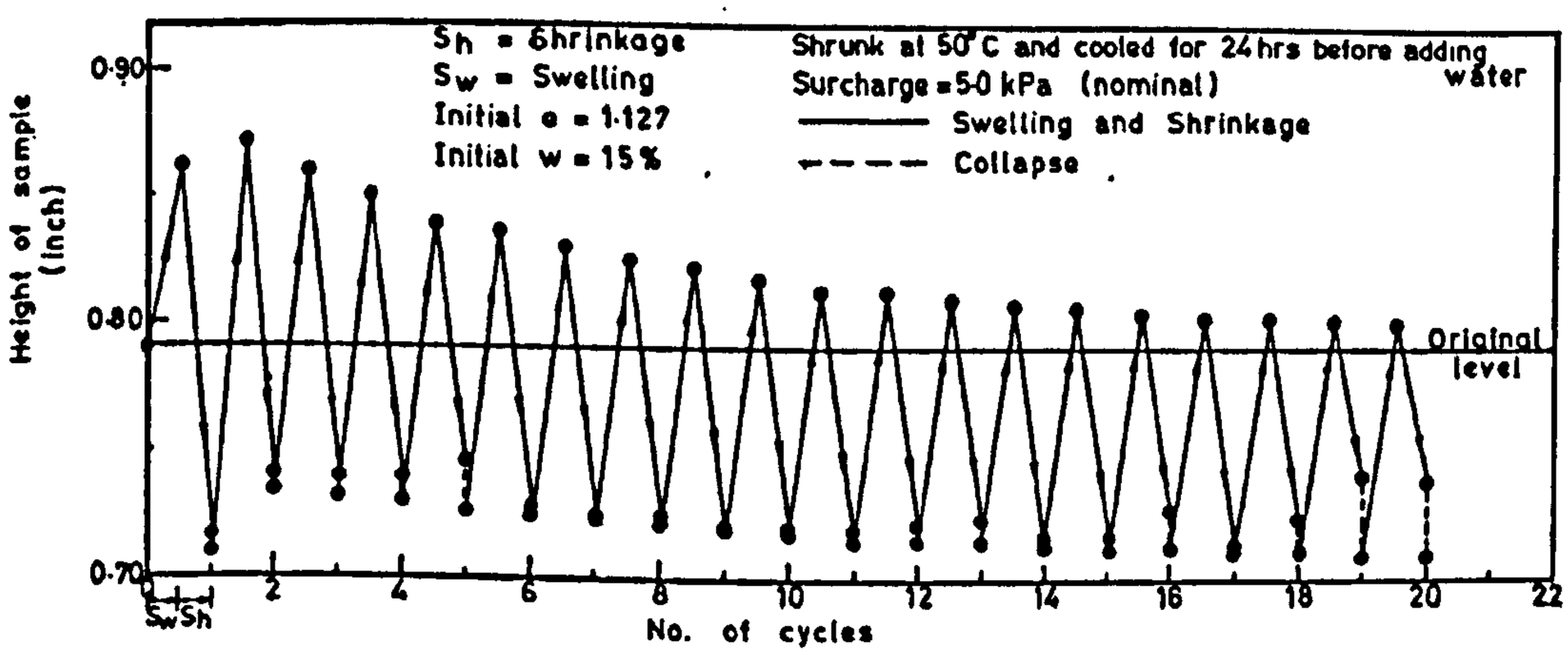

Figure 2.10: Swelling and shrinkage measurements with drying-wetting cycles in a black cotton soil; wetting done by adding water and swelling by heating the sample to 50°C (1in = 2.54cm) (from Rao and Satyadas, 1987)

Alonso et al. (2005) studied the effect of drying-wetting cycles in bentonites with suction measurement. They controlled suction through the vapour equilibrium technique in a bentonite-sand mixture at different OCRs. Up to three cycles were imposed at increasing vertical stresses. The results showed cumulative shrinkage strains as the vertical stresses increased. However there was no accumulation of swelling strains, even at elevated OCR.

The second group of tests is related to water retention studies (Ng and Pang, 2000a, Yesiller et al., 2000, Fleureau et al., 2002, Meisina, 2004). Yesiller et al. (2000) studied the cracking behaviour of low plasticity soils, with suction monitored by a psychrometer, by imposing three paths to the soil (drying – wetting – drying); the authors observed that cracking was dependent on the fines content and water content. Fleureau et al. (2002) studied the water retention behaviour of soils under different conditions: these include initial fabric (compacted versus slurry samples), relationship between the initial parameters (dry density, water content and negative pore water pressure) and the liquid limit, and aspects related to the wetting - drying paths and the compaction curve. Suction was controlled below 30kPa by using a tensiometric plate that applies a negative water pressure, at intermediate suctions (30kPa-1500kPa) with the osmotic technique, and for suctions between 2MPa and 400MPa the vapour equilibrium technique was used. A maximum of 2 cycles of suction were applied to the samples. Ng and Pang (2000a) investigated the influence of initial dry density, initial water content, number of cycles (three), soil structure and stress state with a pressure plate extractor in a decomposed volcanic soil. In a comparison between natural and recompacted samples, Ng and Pang found that the SWRC for the recompacted sample was dependent on the drying/wetting history (Figure 2.11). The authors also found the behaviour to be state-dependent. Meisina (2004) also studied the swelling-shrinking behaviour of clayey soils (associated with landslides). Meisina measured the swelling pressures and vertical strains of samples loaded in the oedometer; and determined the drying-wetting SWRCs following Fleureau et al. (2002). Only one cycle was applied to the sample. Sharma and Wheeler (2000) applied 2 drying-wetting cycles in a kaolin sample with the axis translation technique.

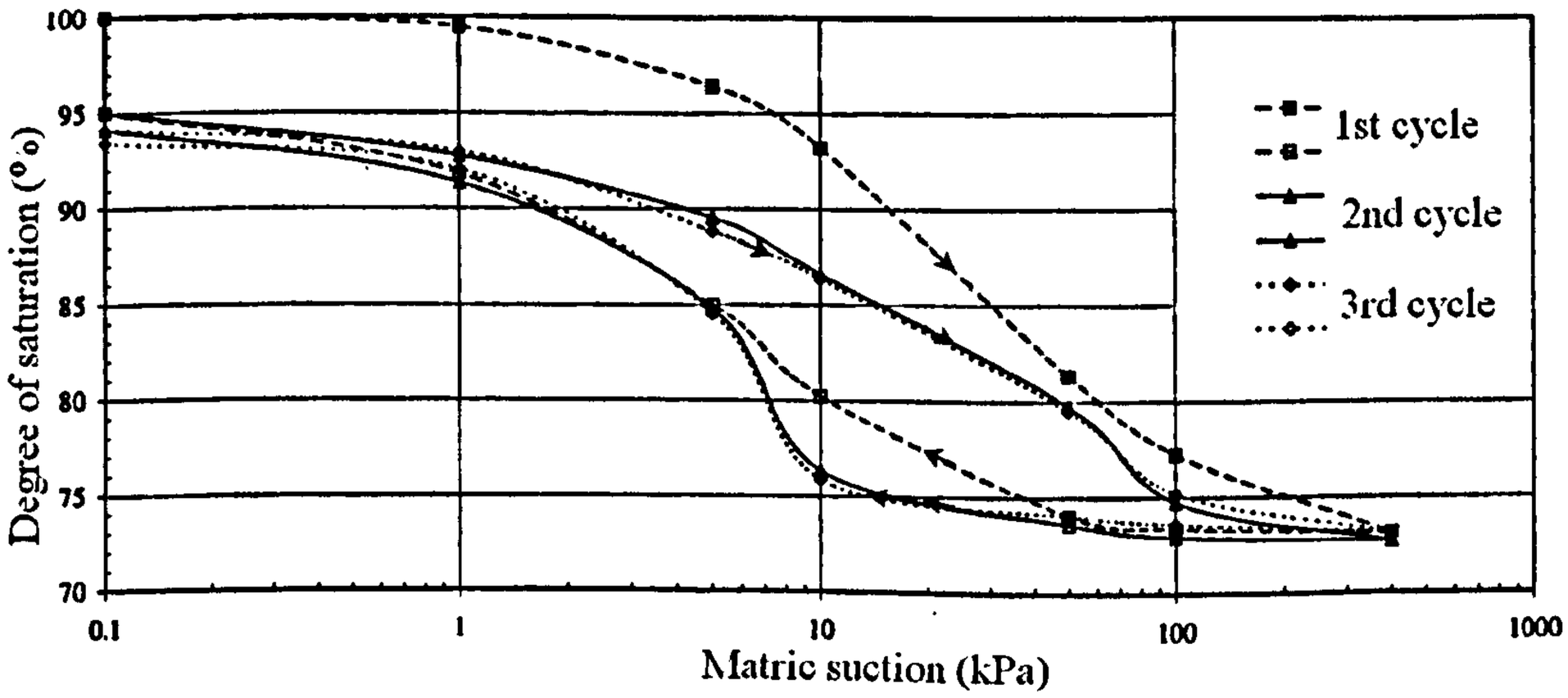

Figure 2.11: Wetting-drying cycles in a recompacted decomposed volcanic soil (after Ng and Pang, 2000a)

Allam and Sridharan (1981) studied the effect of several drying-wetting cycles on the shear strength of a residual soil. The samples were at first subjected to drying-wetting cycles (up to 60), saturated and then sheared in undrained conditions. The conclusions were: drying-wetting cycles increased the stiffness of the soil, decrease the compressibility, and increased the shear strength. More recently Tse and Ng (2008) did a similar study for unsaturated completely decomposed tuff with a shear box adapted for the axis translation technique. The direct shear tests at different parts of the SWRCs revealed a more dilative behaviour for samples tested at a higher suction level, irrespective of the path followed; and the peak strength tended to be higher for samples tested at the same suction following a drying path.

Other studies were conducted in related topics. Lehmann et al. (1998) fluctuated the water table in a sand column while measuring suction with tensiometers and the water content with Time Domain Reflectometry. The results revealed a hysteretic response of the sand with the suction and water content variations concentrated in the capillary fringe (the transition zone between the saturated and unsaturated regions). Pham et al. (2006) studied the hydromechanical behaviour of argillaceous rocks. In one drying – wetting cycle (with suction controlled by salt solutions) the authors identified hysteretic behaviour in the material evidenced by the retention curve, ultrasonic velocities and volumetric variations. The mechanical behaviour (uniaxial compression strength) was seen to depend on the suction level but was unclear whether it depended on the path followed (drying or wetting).

2.2.4. Hydraulic hysteresis

Hydraulic hysteresis is a widely studied and documented phenomenon in different fields (soil science, hydrology, and physical chemistry). Most of the understanding can easily be adapted to unsaturated soil mechanics. Table 2.1 shows the terminology used in other fields. The biggest difference is in physical chemistry where the SWRCs are termed isotherms (temperature constant and vapour pressure changing). Some terms seemed to have wrongly been used in the geotechnical literature. Ng and Pang (2006a) and Ho et al. (2006), used adsorption and desorption for wetting and drying in tests conducted with a pressure plate extractor. Adsorption/desorption refers to water retention from vapour and not from the liquid phase, which is the case of the pressure plate extractor.

2.2.4.1. Pores

Porous materials have cavities, channels or interstices with different sizes. The nature of hydraulic hysteresis is directly related to the shape and types of pores. The *International Union of Pure and Applied Chemistry* (IUPAC) classify them according to their availability to an external fluid (cited in Rouquerol et al., 1994). The different types of pores are shown in Figure 2.12. Following the IUPAC classification, there are closed pores completely isolated in a fine matrix (a), and open pores that communicate with the exterior (b), (c), (d), and (e). Some may have one end (b), or two ends (e). They can also be distinguished according to their shape, cylindrical (c), ink-bottle shaped (b), or funnel-shaped (d).

Table 2.1: Terminology for the SWRC in other fields

Soil mechanics	Physical Chemistry	Soil Science	Hydrology
soil water retention curve	adsorption-desorption isotherms	moisture characteristic curve	moisture characteristic
X-axis: suction	partial vapour pressure / saturation vapour pressure	water content	pressure head
Y-axis: water content or degree of saturation	volume adsorbed (Gregg and Sing, 1967)	matric potential (Baver et al., 1972)	moisture content (Hornberger et al., 1998)

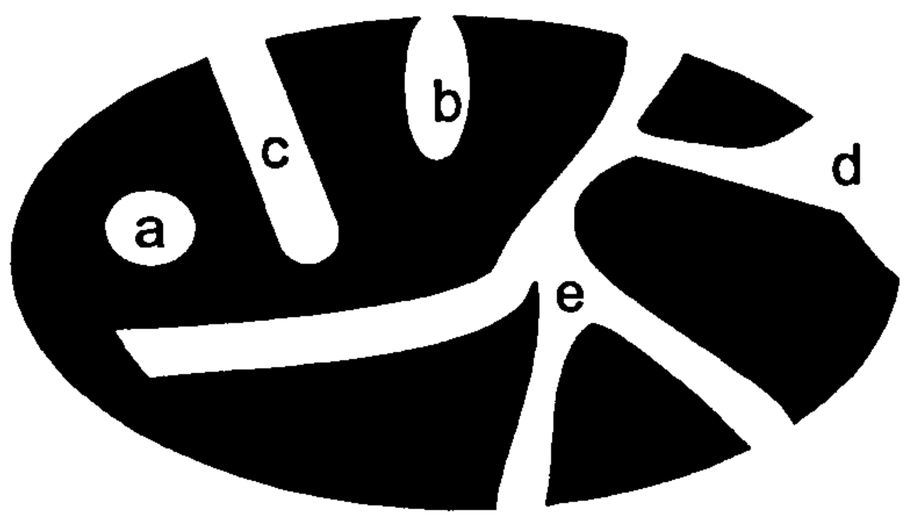

a - isolated
b - one open end ink-bottle shaped
c - one open end cylindrical shaped
d - one open end funnel shaped
e - two open ends cylindrical shaped

Figure 2.12: Types of pores (after Rouquerol et al., 1994)

2.2.4.2. Mechanisms

Soils exhibit hydraulic hysteresis, i.e. drying and wetting SWRCs do not coincide. The most common explanation for hydraulic hysteresis is pore network effects. Pore networks have enlargements and constrictions, wetting would be controlled by the pore (enlargement) dimensions, while drying would be controlled by the network of constrictions (e.g. Tompsett et al., 2005). Pores with an ink-bottle shape (narrower neck) are directly responsible for hysteresis (Figure 2.13a). The constrictions can also be obtained for groups of grains (Figure 2.13b) or clay aggregates (Figure 2.13c) arranged with an ink-bottle shape.

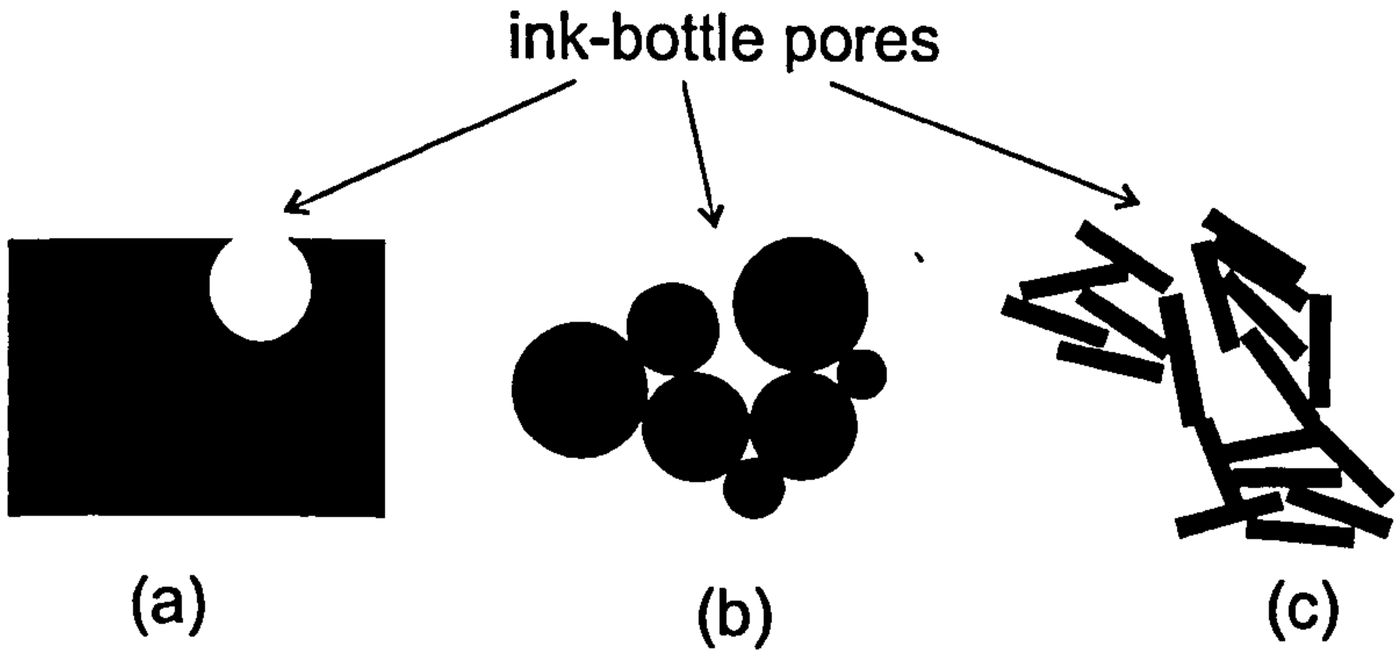

Figure 2.13: Occurrence of ink-bottle pores in, (a) surfaces, (b) granular materials, (c) aggregates

The critical part of hysteresis is the emptying of ink-bottle pores. Due to the constriction, ink-bottle pores do not empty easily. For instance, Figure 2.14 shows the emptying and filling of a group of grains with a large ink-bottle pore (left hand side figure is the initial condition, and right hand side figure the final condition). The menisci have the same curvature (hence suction) at the start and end of the test, but the volume of water retained is higher at the start.

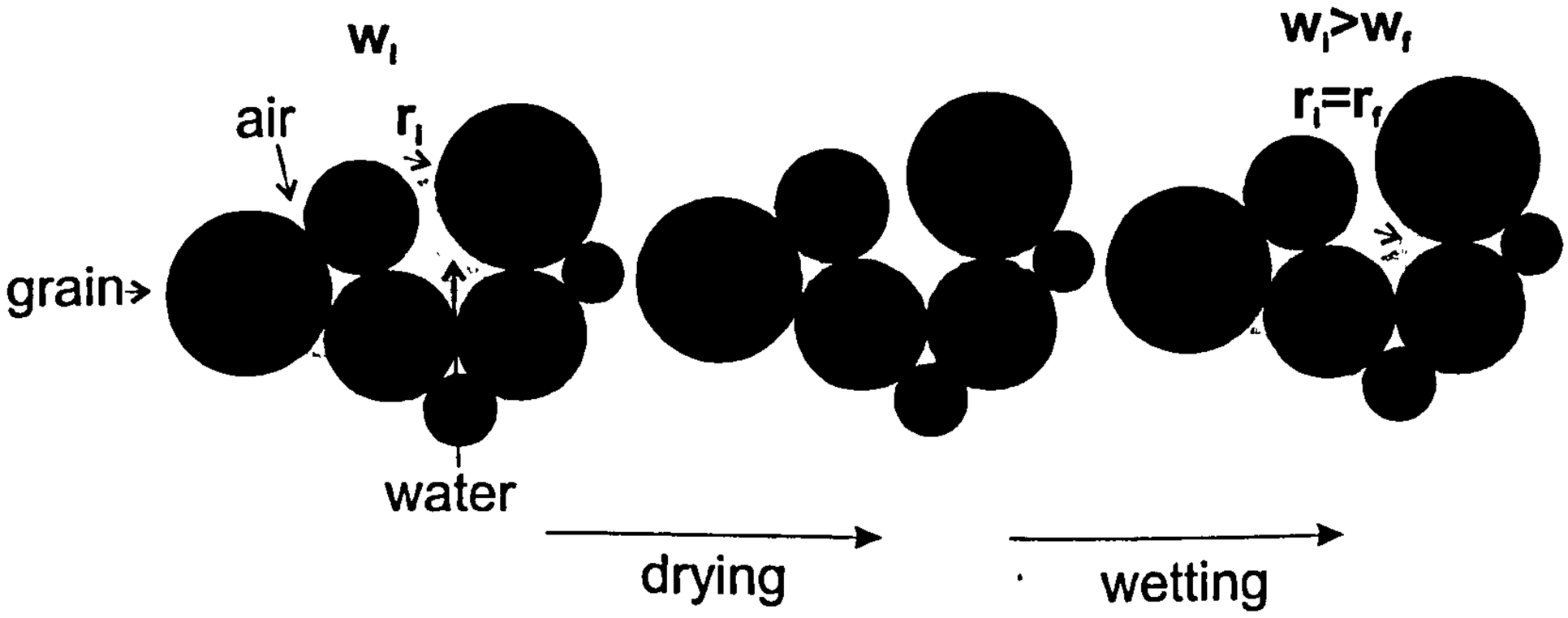

Figure 2.14: Emptying and filling of Ink-bottle pores (after Gallipoli, 2000)

Figure 2.15 illustrates the SWRC in a very simple example made of 2 pores where one is open and the second half closed (the ink-bottle pore). The sequence is based on a paper (Ravikovitch and Neimark, 2002) dedicated to emptying and filling of water from ink-bottle pores. In the example the curve starts by a completely dry state (A), with the vapour pressure increasing (RH increasing at constant temperature) until full condensation in both pores (C). From C back to D the pores dry (RH decreasing). The sequence is reversible from C to D, and irreversible afterwards. Hysteresis appears because of the smaller radius of the ink-bottle pore. If both pores were open, the SWRC would have been reversible.

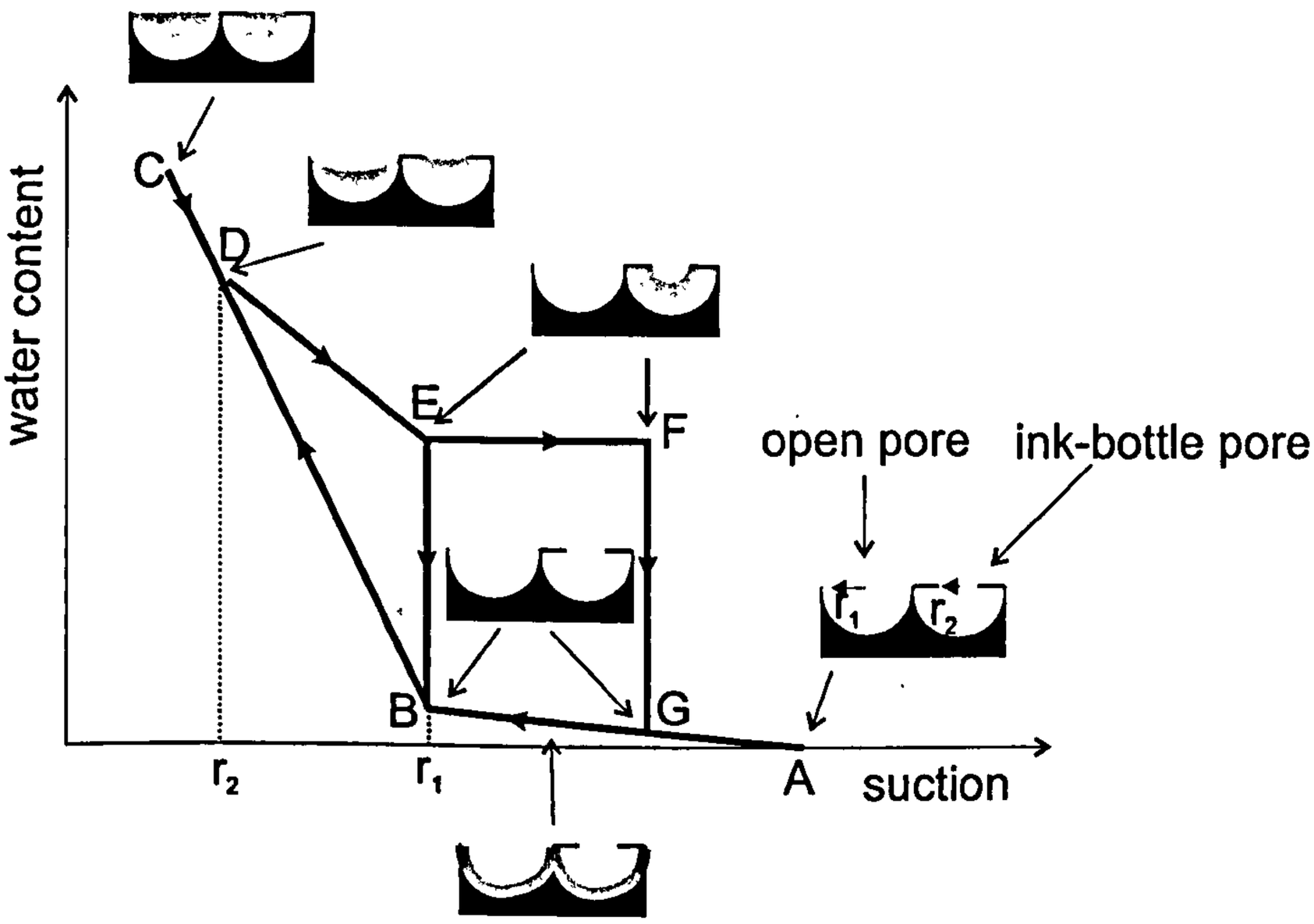

Figure 2.15: Hysteresis in an open and ink-bottle pore; start and end of the curve in A; wetting sequence A-B-C, drying sequence C-D-E-B-A or C-D-E-F-G-A

The wetting-drying sequence can be described as follows:

AB: start of wetting by increasing RH. Formation of water molecule layers

BC: as the RH reaches r_1, both pores fill completely

CD: drying starts by a decrease in RH. The process is reversible until a meniscus with a small radius is formed in both pores

DE: only the open pore empties. Water in ink-bottle pore is at increasing tension (from D to A the ink-bottle pore can empty at any suction)

EB: as suction in the water reached the r_1 radius, the ink-bottle pore empties

EF and FG: if the ink-bottle does not empty, suction will keep increasing until the water cavitates and it empties (FG)

GA: the remaining water molecules evaporate

2.2.4.3. IUPAC classification

The IUPAC defined 6 classes of isotherms for materials. Class I, II, and IV include sub-classes. All classes are illustrated in Figure 2.16.

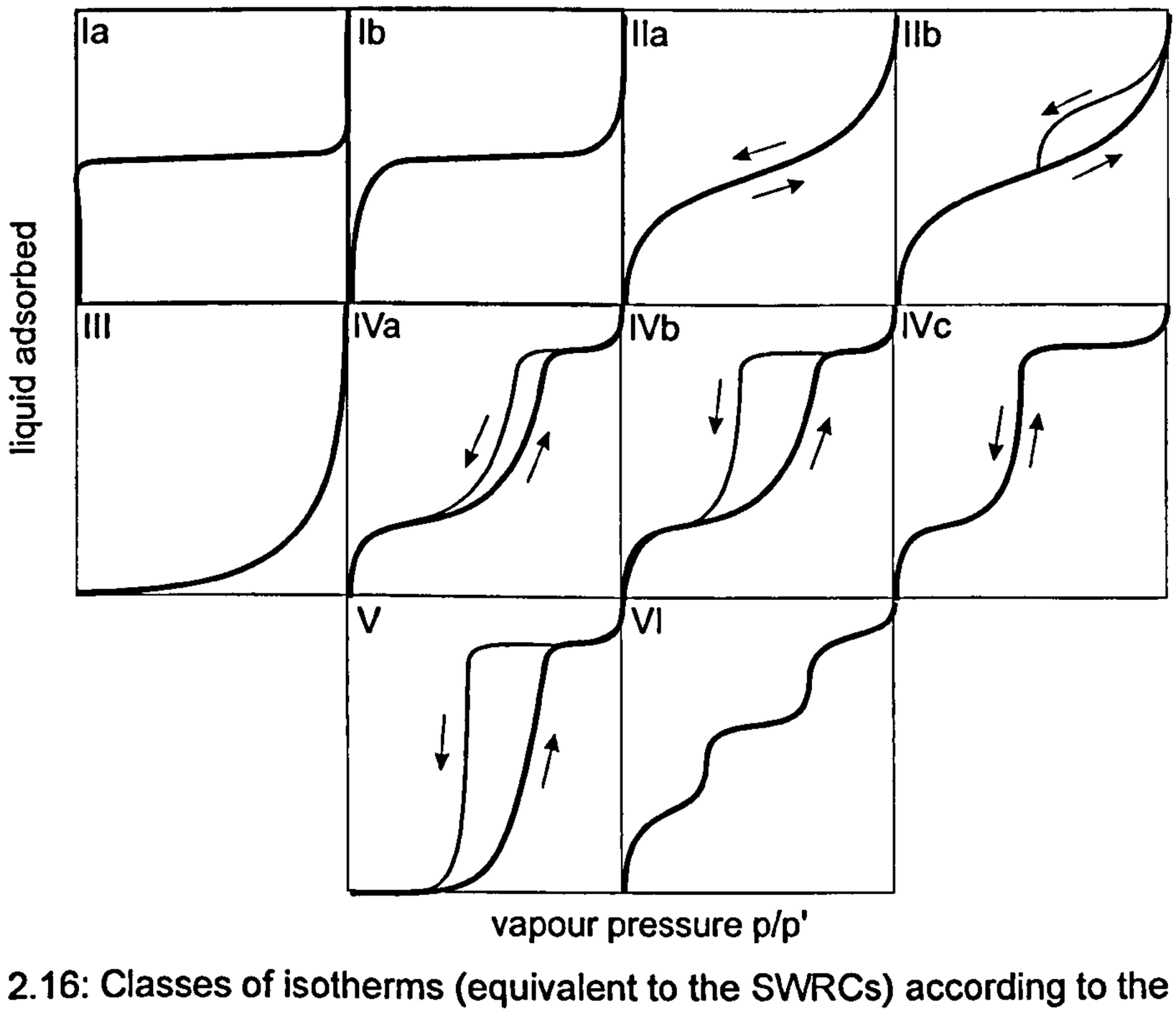

Figure 2.16: Classes of isotherms (equivalent to the SWRCs) according to the IUPAC classification , p – partial vapour pressure, p' – saturation vapour pressure; the vapour pressure increases from left to right (the reverse of SWRCs) (after Gregg and Sing, 1967, Rouquerol et al., 1999, Adamson and Gast, 1997)

The classes are defined as follows (Rouquerol et al., 1999, Gregg and Sing, 1967, Adamson and Gast, 1997):

- Class I refers to microporous or non-porous materials (diameter <2nm) and assumes that the adsorbed layer is one molecule thick (follows Langmuir, 1916) and reversible. The flat plateau corresponds to the completion of this layer. The adsorption behaviour is complex and less common.

- Class II are typical of materials that are open to the exterior (porous or non-porous). They have a concave curvature at low vapour pressures and convex curvature at high vapour pressures towards the p/p' axis. The isotherm increases sharply (from the left, it starts by a dry condition and then is wetted)

until it gets linear, the turning point is called the point B. It represents the completion of the monolayer of molecules (layer 1 only in Figure 2.5) and the beginning of the multilayer (layers 2, 3, ... in Figure 2.5). The ordinate of point B gives the amount of liquid to cover the unit mass of solid with a complete monolayer. This value can be used to calculate the surface area. If the material is rigid and all pores connected to each other, there will be a complete reversibility of adsorption-desorption isotherm (Class IIa). Non-reversible isotherms (Class IIb) are obtained with aggregates of plate-like particles which have non-rigid slit-shaped pores.

- Class III is less common and is representative of non-porous materials. It is also related to the adsorption of layers of molecules. Class V is similar to class III in the sense that it flattens at vapour pressures. The difference is that includes hysteresis due to the filling and emptying of pores.

- Class IV isotherms are similar to the Class II, but tend to level at high vapour pressures. They tend to show a marked hysteresis which is related to the filling and emptying of pores. Class IVb is dependent on pore network percolation effects.

- Class VI, or stepped isotherm, is rare and is associated to layer-by-layer adsorption.

2.2.4.4. Adsorption-desorption isotherms of gases in clays

Some of the adsorption isotherm studies have been conducted in clays. Gregg (1968) studied the adsorption behaviour of nitrogen in kaolinite in an uncompacted and compacted state. The uncompacted sample resulted in a reversible isotherm (Class IIa). The compacted sample had an hysteresis loop typical of pore filling and emptying (Class IIb). Venaruzzo et al. (2002) obtained typical Class IIb for natural bentonites from Argentina (only sieved). For vapour pressures above 0.5, the isotherms show hysteresis, but for lower values the adsorption-desorption process was reversible, indicating that only layers of molecules were evaporating or condensing (Figure 2.17).

Figure 2.18 shows examples of isotherms for water adsorption-desorption in clays. Figure 2.18a shows the water adsorption-desorption isotherm for calcined kaolinite (γ-Al_2O_3) (Okada et al., 1998). The material shows a hysteretic behaviour with two clear inflection points at 0.1 and 0.8 of vapour pressure (seems to fit into Class IVa). The first inflection point is linked to the adsorption of the first layer of water molecules to the surface and the hysteresis loop to the emptying/filling of pores. Figure 2.18b, and 2.18c, show the adsorption-desorption isotherms conducted in sodium montomorillonite (Barrer, 1989, Cases et al., 1992). Both curves have a step-like shape and marked hysteresis reaching almost the full range of the vapour pressures. Cases et al. (1992) explains it as series of layers forming in the material, below 0.16 vapour pressure just in the external surfaces, and at higher vapour pressures in the interlamellar space, as the water layers are deposited the interlamellar space increases and more water layers are deposited.

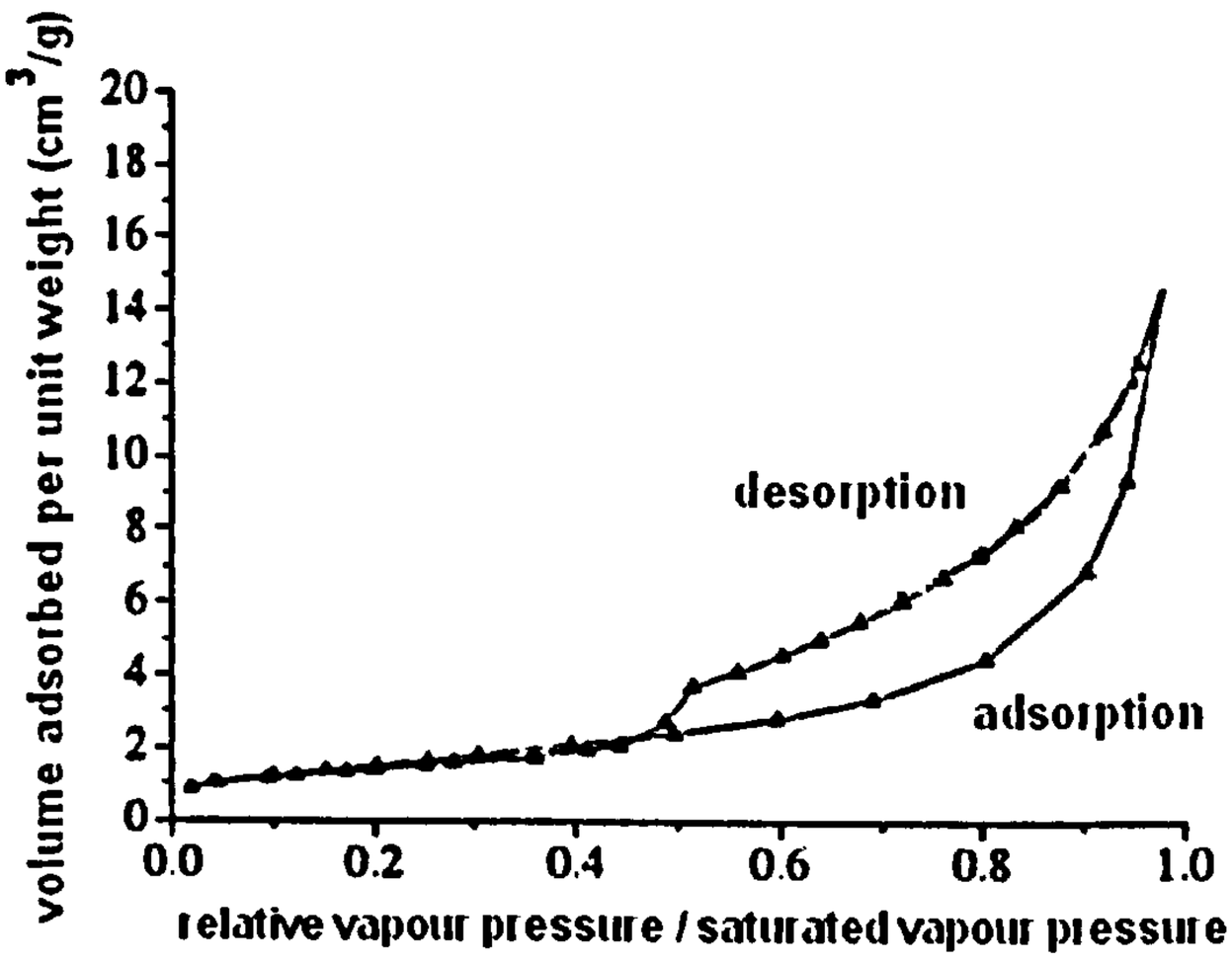

Figure 2.17: Nitrogen adsorption-desorption isotherms in bentonites from different geological formations (samples M1f, M4f) (X axis refers to the relative vapour pressure by the saturation vapour pressure of nitrogen – %/100) (after Venaruzzo et al., 2002)

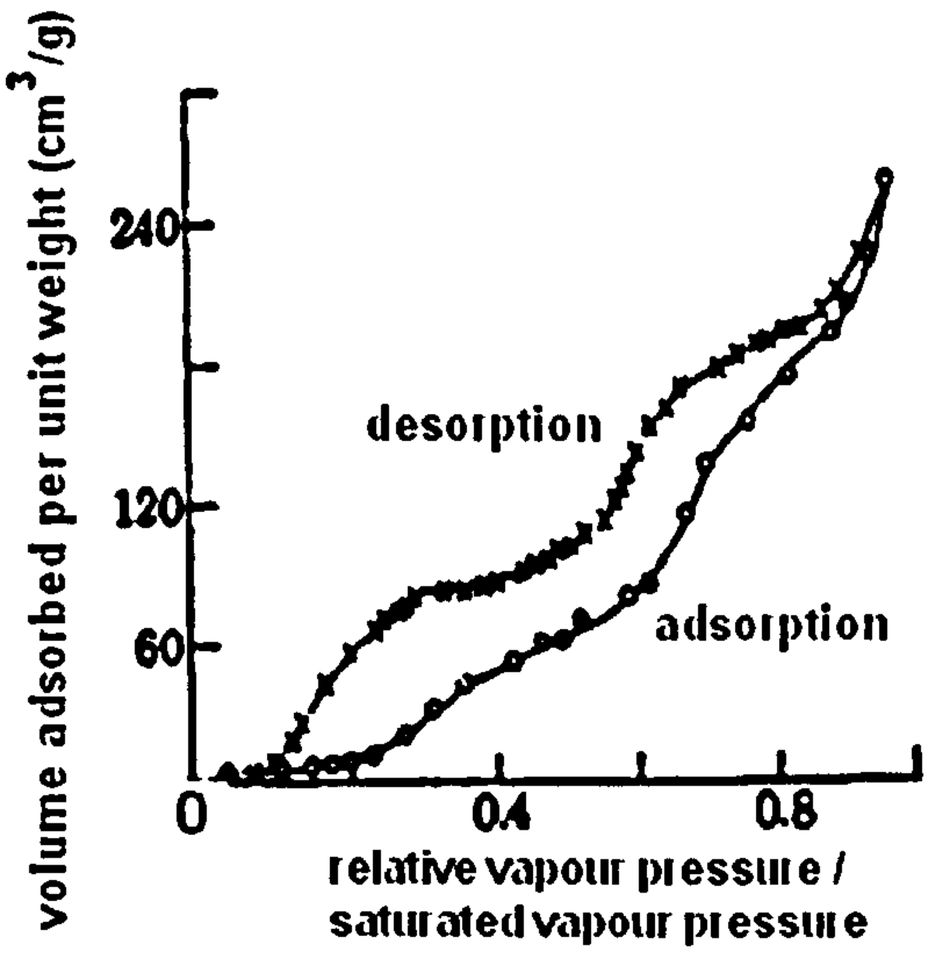

Figure 2.18: Water adsorption-desorption isotherms in a Na-rich montmorillonite (from Barrer, 1989), (c) Wyoming Na montmorillonite (after Cases et al., 1992)

2.2.4.5. Scanning curves

Figure 2.19 displays the different types of scanning curves (Tompsett et al., 2005, Ravikovitch and Neimark, 2002). As said previously they are obtained when the drying/wetting curve is reversed while the material dries or wets. The authors distinguished between ascending and descending curves, and within them, converging, crossing and returning scanning curves. Converging and crossing scanning curves are common while returning curves are rare. All types are related to the pore network openings/constrictions. An example of descending scanning curves is shown in Figure 2.20.

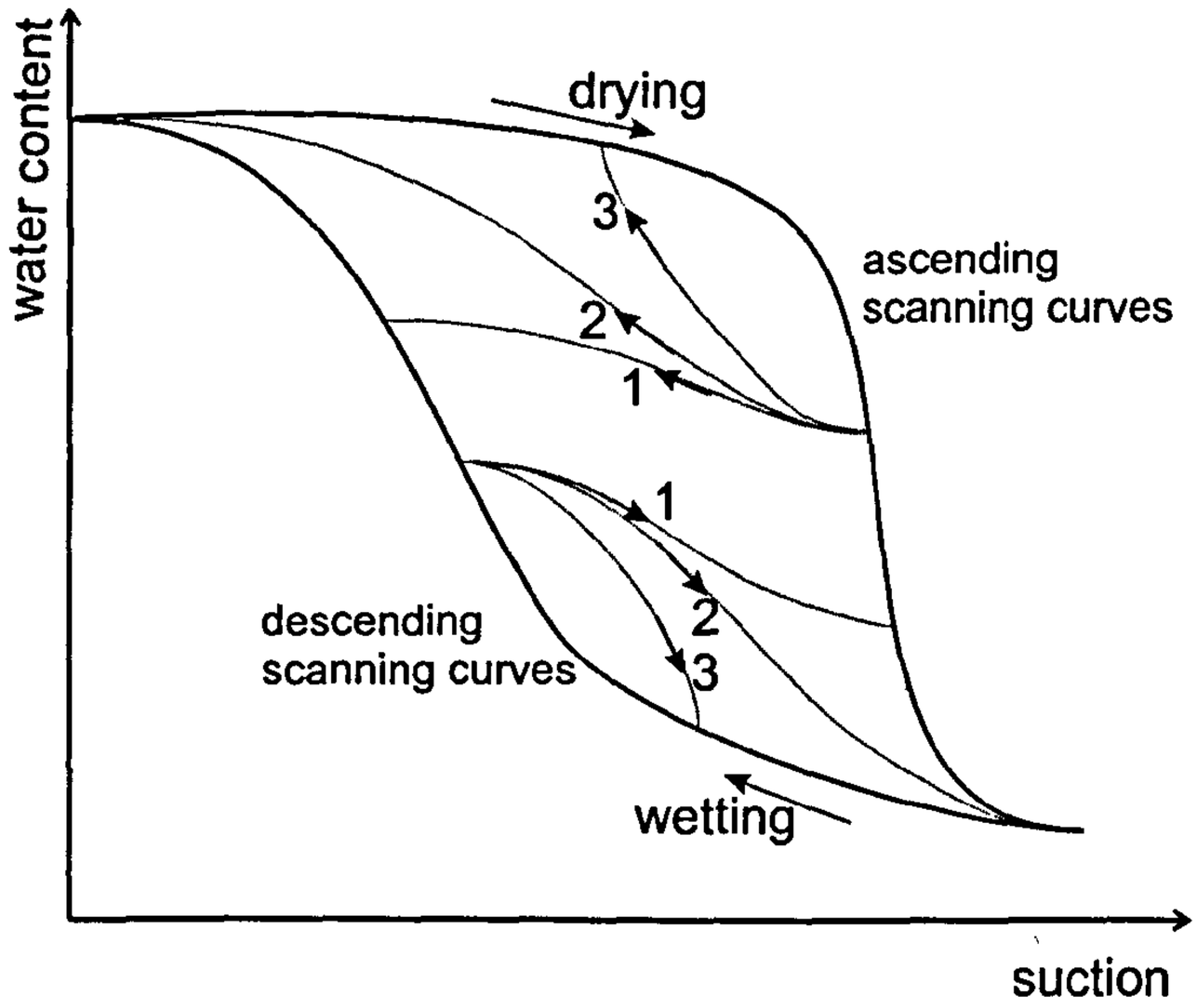

Figure 2.19: Scanning curves from the main drying and wetting curves; 1 – crossing, 2 – converging, 3 – returning (after Tompsett et al., 2005, Ravikovitch and Neimark, 2002)

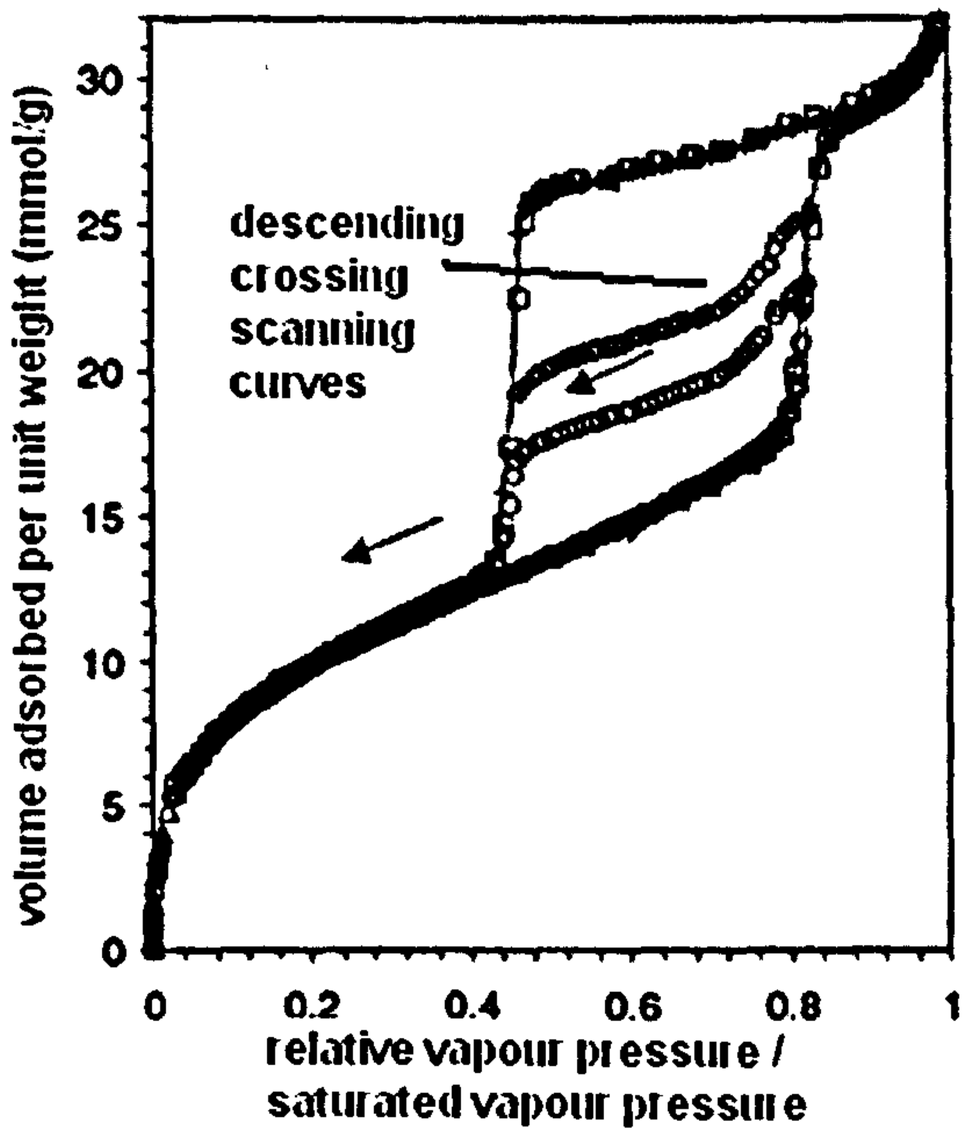

Figure 2.20: Class IV isotherms with descending crossing scanning curves (after Ravikovitch and Neimark, 2002)

2.2.4.6. Meaning of the SWRC

The IUPAC classification and the review on hysteresis shown above have several implications to the SWRCs. Some of these implications will be discussed next.

Classification of SWRCs

It could be of interest to geotechnical engineering to standardize SWRCs. This would allow a better communication between researchers/engineers and immediate recognition of the type of soil and other characteristics. The biggest advantage of the IUPAC classification is that it offers the opportunity to set a terminology in common with other fields. However, this might not be straightforward because, (1) it might be difficult to obtain complete SWRCs with the current suction measurement techniques and, (2) soils have a wide pore size distribution with different materials, therefore the most probable is to obtain mixed type of curves.

A second point is that the IUPAC classification was obtained for changes in vapour pressure, where the soil wets or dries from the water phase. It is not clear if the same classification can be adapted to SWRCs obtained by liquid water transfer (the case of the axis translation).

Wetting curve

To obtain a main wetting curve the IUPAC classification shows that a soil has to be dried completely. However, as the complete drying curve is rarely obtained (in none of the literature shown above the soil was dried completely), the main wetting curve is never obtained. They are instead ascending scanning curves. This suggests that if the main wetting curve is to be obtained, then suction measurements should be conducted to suctions as high as possible.

Ho et al. (2007) showed SWRCs where the drying and wetting lines coincide at higher suctions (upper curve in Figure 2.21). In this case the obtained wetting curve is correct.

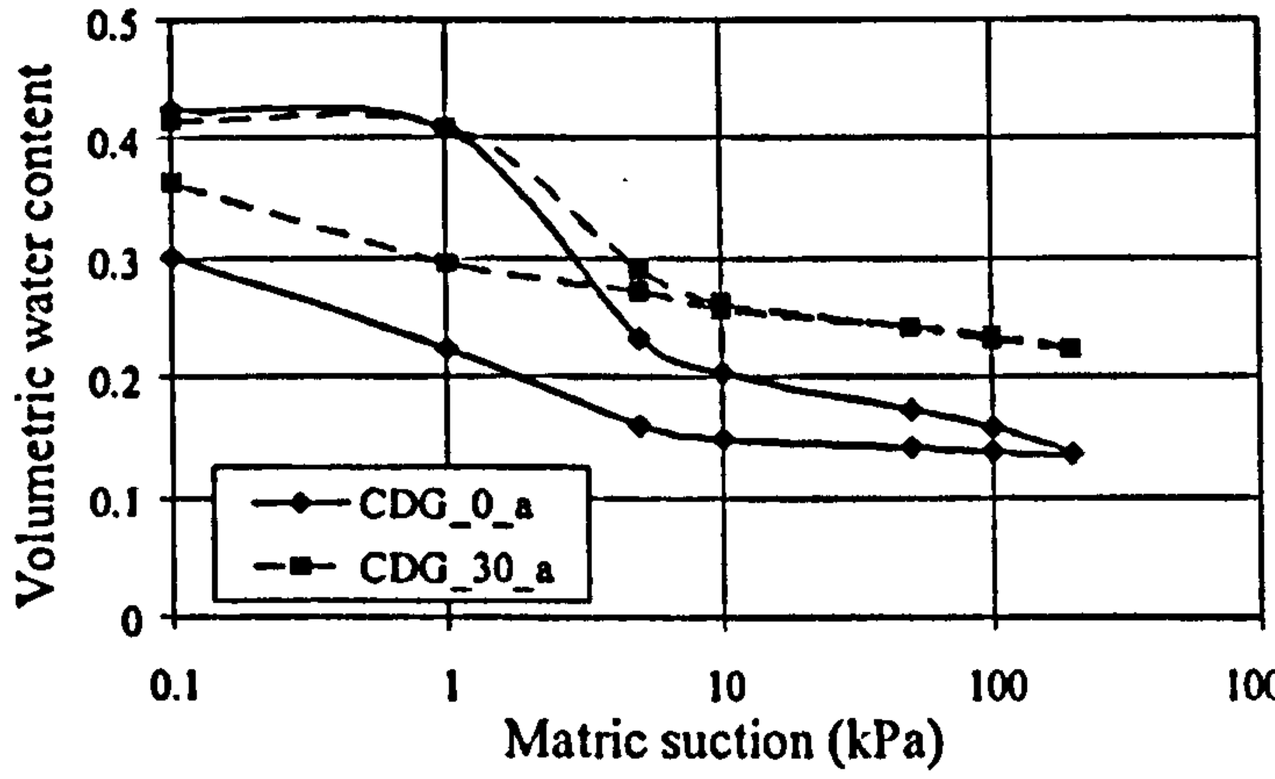

Figure 2.21: SWRCs in decomposed granite at different stress levels (0kPa for the bottom curve and 30kPa for the upper curve); the upper SWRC closes at lower suctions suggesting that the wetting curve is the main wetting and not a scanning curve (from Ho et al., 2007)

The importance of obtaining a complete wetting curve is particularly evident in Blight's (2007) work. In drying-wetting tests in Nylsvley clay, the author shows that after the first drying there is a complete absence of hysteresis, claiming that the wetting-drying process become reversible (Figure 2.22). The most likely explanation for this behaviour is that the ink-bottle pores remained filled with water during the subsequent cycles and so there was no hysteresis. The minimum water content at the highest suction is high ~36%. It is almost certain that if the soil had been further dried, hysteresis would appear.

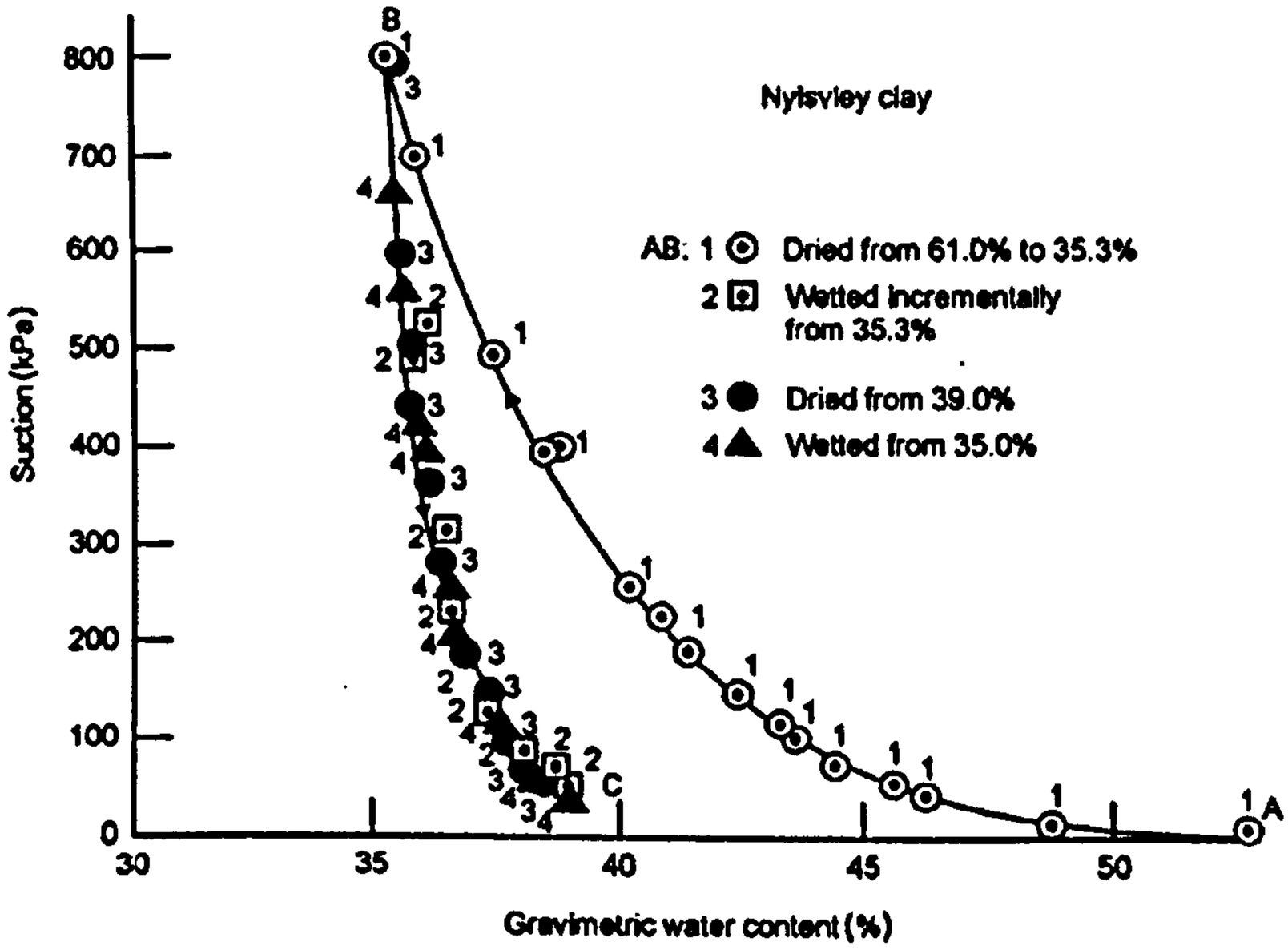

Figure 2.22: Wetting-drying cycles in Nylsvley clay (numbers denote the cycles) (from Blight, 2007)

2.3 SUCTION AND WATER CONTENT MEASUREMENT AND CONTROL

2.3.1 Introduction

Suction and water content control require a measurement device, a control device and a control system (usually a feedback system). The values read from the measurement devices are compared to the desired values and the feedback system adjusts the control device until the desired values are achieved. The measurement device or technique is used to read the values (e.g. Relative Humidity, water pressure, air pressure). The control device is a means of controlling suction or water content by, for example, varying the air or water pressure in an axis translation system to adjust suction or circulating air with different RHs to adjust water content. The feedback system can be manual (the person doing the tests) or automatic (controlling software).

2.3.2 Suction measurement and control

An overview of techniques for suction measurement and control is provided in the following. Only techniques used for this research (e.g. axis translation) or related to topics developed in the following chapters are presented. Three suction measurement techniques are introduced: the filter paper, and RH equilibrium techniques (psychrometer, hygrometer), while for the suction control the axis translation and osmotic technique (Figure 2.23). Extensive reviews that provide detailed discussions of the techniques for suction measurement and control can be found in: Ridley and Wray (1996), Lee and Wray (1995), Fredlund and Rahardjo (1993), Rahardjo and Leong (2006), Bulut and Leong (2008) and Delage et al. (2008).

The selection of the appropriate technique for testing is dependent on the suction to be measured (total, matric or osmotic) and suction range of interest. From the techniques mentioned above, the filter paper (with no contact with the soil) and relative humidity equilibrium techniques are employed for high suctions (>1500kPa) while the axis translation and osmotic technique are used for low suctions (<1500kPa).

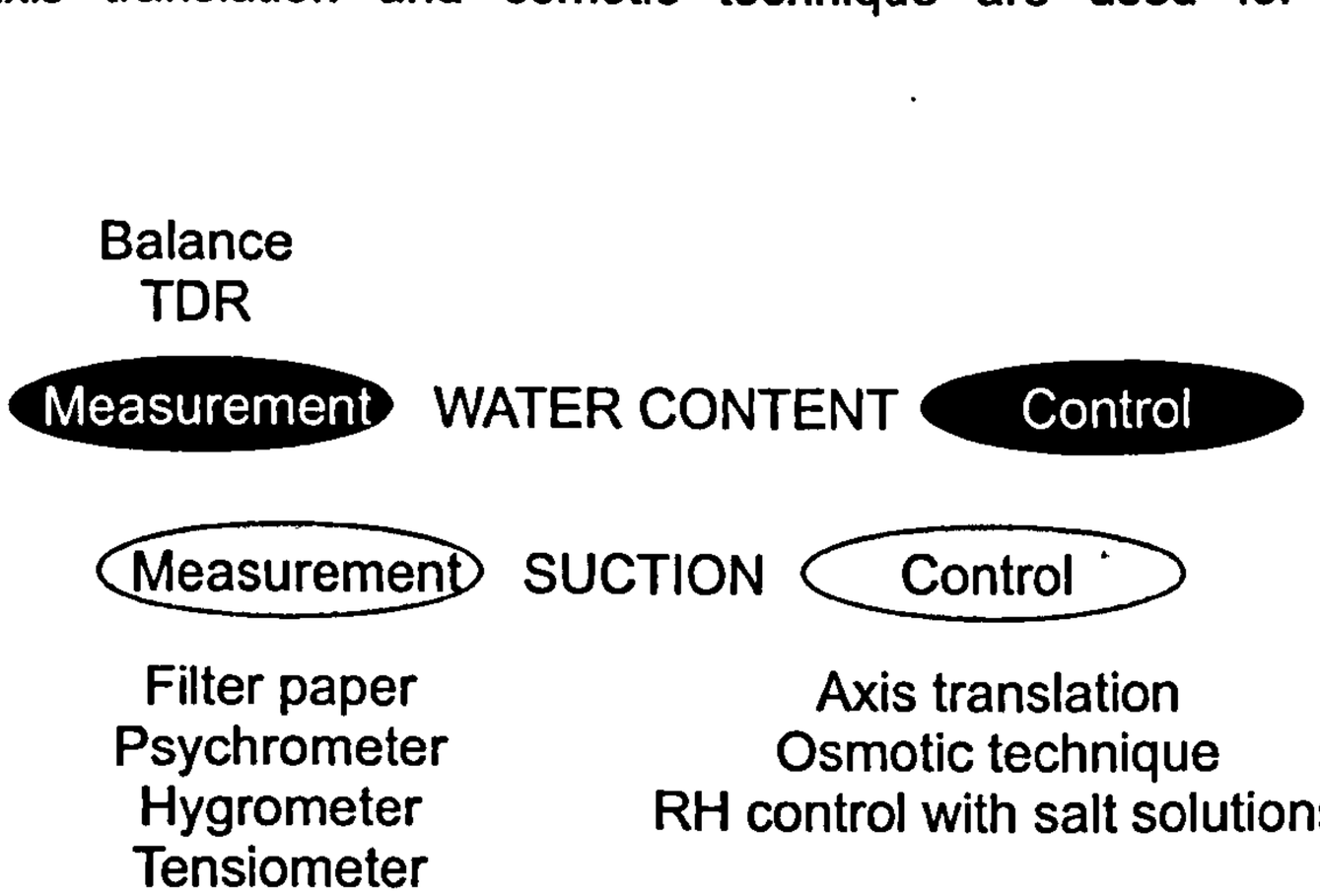

Figure 2.23: Techniques to measure and control suction and water content

2.3.2.1 Suction measurement

For the filter paper method, a soil sample is placed in a container at constant RH together with a filter paper. When equilibrium is reached, the water content of the filter paper is determined. With this value suction is determined via a calibration curve of the filter paper. The total suction is determined if the filter paper is separated from the soil, and the matric suction if in contact. For the matric suction, suction gets in

equilibrium through liquid water movement between the filter paper and soil (e.g. Bulut and Leong, 2008).

The psychrometer can be distinguished between thermocouple and transistor type. The transistor type consists in two thermometers in two bulbs, one dry and the other wet. When a sample is placed in a closed chamber with the two bulbs, water evaporates for the wet bulb until reaching an equilibrium condition between the dry bulb, wet bulb, sample and internal walls of the chamber. As water evaporates from the wet bulb, the temperature of the wet bulb decreases (which also leads to a decrease in saturation temperature). The RH is then determined from the difference of temperature of the two bulbs. For instance, if no evaporation from the wet bulb occurs it means that the ambient air was already saturated and so the RH is 100% (e.g. NPL, 1996). The second type (thermocouple psychrometer) has a similar working principle as the transistor. A cooling current is used to cool the thermocouple below the dew point of the air surrounding the sample causing water to condense on the thermocouple. Water evaporation and condensation is equilibrated with the sample and a voltage is created. This voltage is then converted to total suction. Psychrometers have also been used in triaxial tests by Blatz and Graham (2000).

Hygrometers can also be used to measure the RH (e.g. Tang and Cui, 2005, Leong et al., 2003). The most accurate are the optical dew-point type, which measure the temperature at which condensation occurs by cooling a small mirror. The onset of condensation is determined optically, by detecting changes on how the mirror reflects. Another type (use in this research) measures the RH by a capacitive sensor. Changes in humidity are measured as a change in the sensor's electrical capacitance.

2.3.2.2 Suction control

For the axis translation technique, suction is imposed by controlling the air and water pressure. The water pressure is kept at a given value by placing a soil sample in contact with a saturated porous stone with a given air entry value, and the air pressure is increased until the desired difference between the air and water pressure. As in the RH equilibrium techniques, the sample is in equilibrium when the sample's mass is constant with time. At this time no more water transfer occurs between the soil and porous stone. The technique was developed to avoid cavitation in the pipes connected to the transducers and to apply suctions higher than 100kPa (Hilf, 1956).

This technique is in part equivalent to the backpressure for saturated soils which raises the pore water pressure in the soil to avoid cavitation in the pipes when testing dilative samples (Figure 2.24). It can be used to impose suction in triaxial cells or oedometers, or be used in a purpose made device for suction measurement: the pressure plate. The pressure plate consists of a chamber with a porous stone, with a free upper face and water reservoir in the bottom face enclosed in a flexible membrane. There are numerous works conducted with the axis translation, some examples are: Buckingham (1907), Toll (1988), Wheeler and Sivakumar (1995), Tinjun et al. (1997), Ali Rahman (2008). Further details will be given in Chapter 3.

The osmotic technique works with a similar principle as the axis translation. The technique consists in enclosing a sample in a semi-permeable membrane with the external face of the membrane in a Polyethylene Glycol (PEG) solution. The membrane is only permeable to water. Due to a difference in concentration of PEG molecules across the membrane, water flows from the lower concentrations in the sample to the high concentrations of the PEG solution, generating a negative water pressure in the sample (e.g. Cui and Delage, 1996). The suction applied can be regulated by the concentration of the PEG solution (higher concentrations lead to higher suctions).

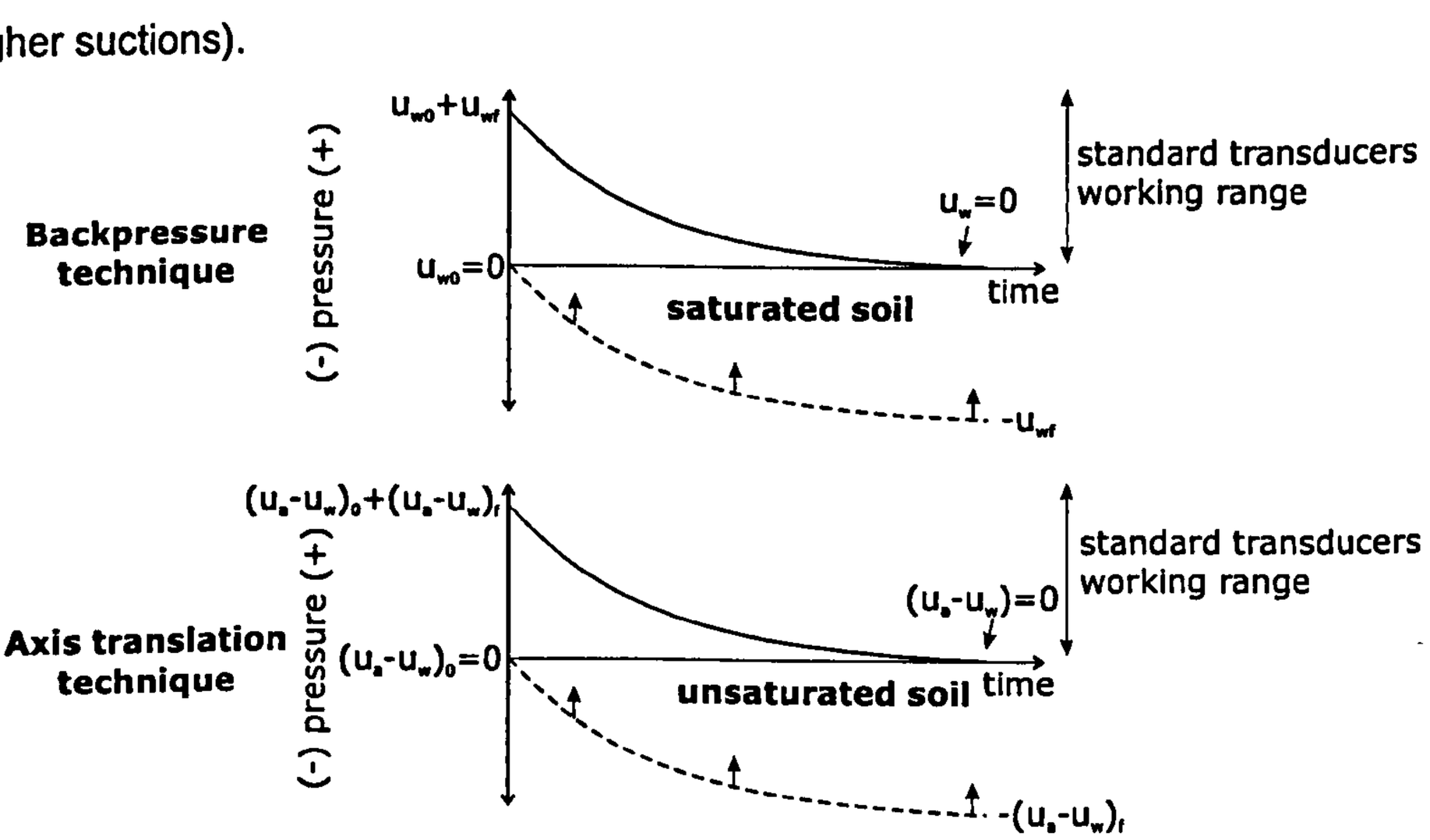

Figure 2.24: Comparison between the axis translation and backpressure technique

2.3.3 Water content measurement and control

The water content determination is commonly done by the oven drying technique (BS1377) where the mass of a soil sample is taken in a wet and dry state with a balance to obtain the mass of water in the soil. If the dry mass of the soil is initially

known, the water content of a drying/wetting sample can be measured continuously with a balance (explored in Chapter 5).

Water content measurements can also be determined indirectly by Time Domain Reflectometry (TDR). TDR determines the dielectric constant of an object by measuring the propagation time of electromagnetic waves sent from a pulse generator of a cable tester immersed in a medium. The dielectric constant of water is much higher that the soil (80 for water and 2.5 for dry sand), therefore it can be used to determine the water content of soil by using a calibration curve empirically determined by Topp et al. (1980). TDR probes consist of three pointed rods and a head. Probes by Campbell Scientific (2008) have a length between 30cm to 7.5cm. Noborio (2001), Jones et al. (2002) and Tarantino et al. (2008) provide a detailed review of the TDR technique.

Water content control requires a system to wet or dry soil and a feedback system that quantifies the water content in a soil sample. To the author's knowledge there is no such system. A system that can be run under water content control conditions is presented in Chapter 5.

2.3.4 Recent advances

2.3.4.1 Technical developments

Recent developments in unsaturated soil testing have been centred on improvements to the devices that measure suction, and to the techniques used to test under very specific conditions (e.g. with large samples, with temperature control). Examples of improvements will be presented in the following.

Leong et al. (2004) presented a modified version of the pressure plate. The pressure plate device has several limitations: (1) the air pressure increases the concentration of air in the water below the stone leading to the formation of air bubbles which can interrupt the natural outflow of water; (2) wetting is limited to the initial volume of water below the stone and (3) cracking can occur if the stone deflects too much (Figure 2.25). Leong et al. proposed that bubble formation can be avoided by flushing the water below the stone through two tubes connected to two pots, water flows by adjusting to different heights the pots. Wetting tests can be conducted by filing the pots to different levels. The flexible rubber membrane below the stone enclosing the

reservoir was removed and a grooved reservoir made. Cracking was avoided by gluing the ceramic stone to a softer acrylic sheet (makes the transition to the stainless steel and takes part of the deformations).

A common problem in unsaturated soil testing is the difficulty in avoiding air and water leakages. Wang and Benson (2004) developed a leak-free pressure plate extractor by using square instead of circular o-rings. The o-rings sealed the ceramic plate against the top lid and lower chamber. Another common problem is in making volume measurements of samples prepared from slurries. Usually the slurry cracks in the middle while it shrinks. Peron et al. (2007) proposed a solution which consisted of adding Teflon tape (a hydrophobic material) to the inner surface of the mould and further smearing it with a hydrophobic gel. With this arrangement the soil detached from the inner wall without cracking (Figure 2.26).

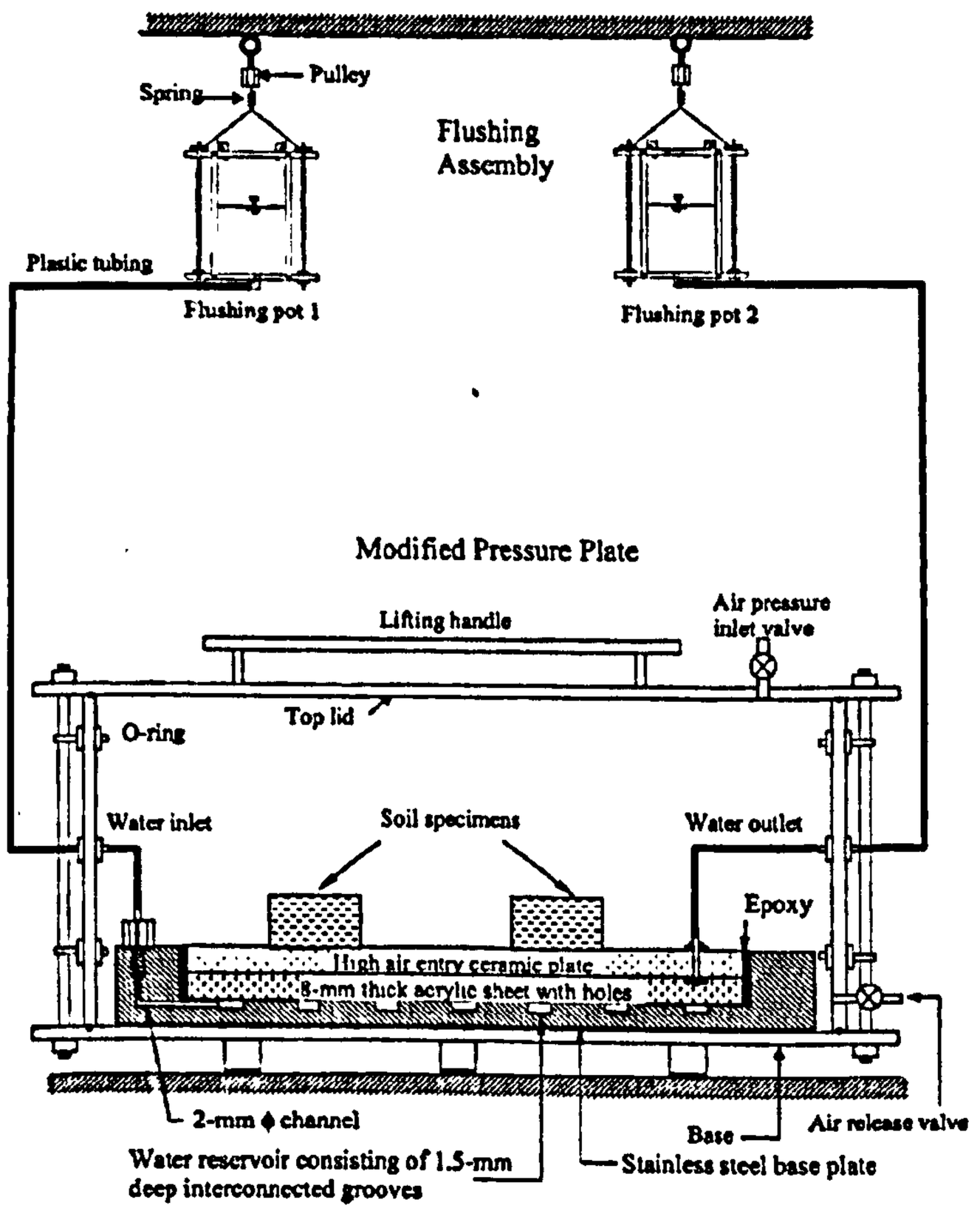

Figure 2.25: Modified pressure plate apparatus (from Leong et al., 2004)

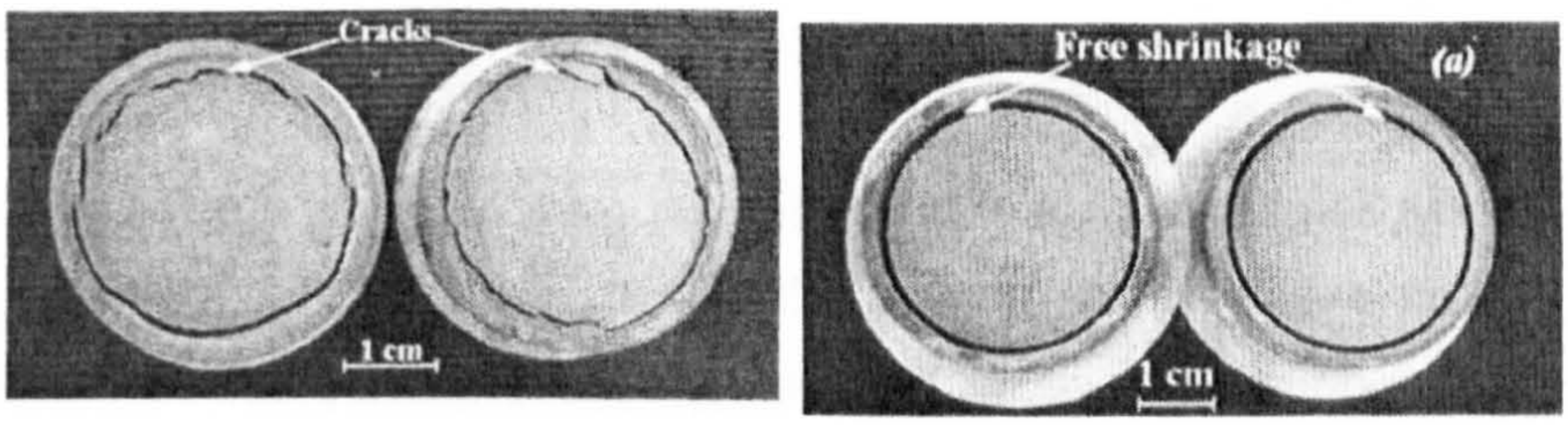

Figure 2.26: Avoiding cracking of a drying slurry in a mould by adding Teflon tape to the inner wall (right image), no Teflon in the left image (from Peron et al., 2007)

Regarding advances in suction control techniques, Arifin and Schanz (2007) studied the effect of temperature on the swelling pressure of bentonites in a constant volume cell by controlling temperature through a flexible wire heater attached to the outer wall of the cell. This device was able to control temperature up to 80°C (Figure 2.27). A very similar study was conducted by Sanchez et al. (2008) which required adapting an oedometer for high temperature testing.

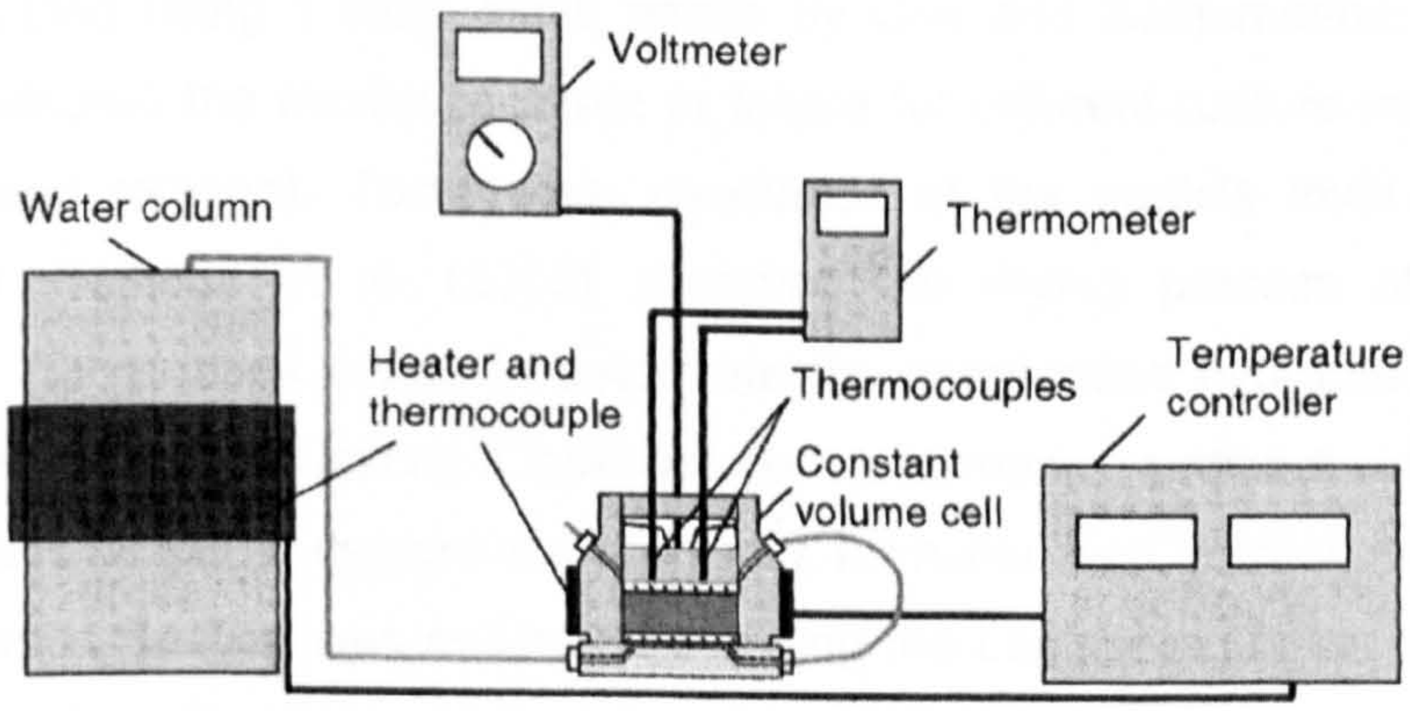

Figure 2.27: Temperature controlled test with the RH equilibrium technique in a constant volume cell (from Arifin and Schanz, 2007)

Time Domain Reflectrometry (presented in Section 2.3.3) is probably one of the most important recent advances relevant to water content measurement. It is the only technique available to measure water content (apart from the balance) and can be used for field or lab measurements. It is also sensitive to water chemistry (Jones et al., 2002). Besides geotechnical engineering, it is being actively studied in soil science and hydrology. In experimental unsaturated soil mechanics it was used recently to measure the water content component of the SWRC (Ekblad and Isacsson, 2007). However its use in confined samples that are sheared or compressed might not be straightforward as the device is brittle and has relatively large size (given in Section 2.3.3).

2.3.4.2 Particle-level testing

There is a need to start developing techniques to test at very small scales (micron-level) because direct evidence of most of the phenomena discussed in 2.2 is limited or non-existent. For instance, unsaturated soil behaviour strongly relies on the meniscus force between soil particles. However its direct measurement has never been carried out. Even direct evidence of water menisci at small scales (microns) is very limited. The reason for this is that testing at such small scales requires technology which geotechnical engineers are either unfamiliar or which is not immediately available. The solution has been to develop custom made devices (Cho and Santamarina, 2001) or to limit to observations with familiar devices (e.g. optic microscope, scanning electron microscope).

The smallest particle-level studies with direct measurements in unsaturated soils were conducted using 1.6mm glass beads by Cho and Santamarina (2001). The authors measured the meniscus strain at failure for different rupture modes (shear, extension and rotation). Tests were conducted at the particle level with optical microscopy. Reinson et al. (2005) observed the drying process of a material comprising 12mm glass beads to determine the unsaturated hydraulic conductivity and the water retention curve. Observations were made by digital videography in grouped glass beads to capture the meniscus formation and to track the movement of a dye tracer. Suction was estimated by using the Laplace equation based on the observations for a cubic packing arrangement. Computed Tomography (CT) was used by Wong and Wibowo (2000) to estimate the 3D spatial distribution of porosity, air and water saturation during water flow in a silty sand soil column. Wildenschild et al. (2002) showed that the air-water interfaces in sands could be observed by CT while Cnudde et al. (2006) reviewed the potential of CT in geo-disciplines.

The conventional SEM uses high vacuum to obtain good resolution images. As a result, imaging of wet samples is not possible and special sample preparation procedures are needed. In unsaturated soils, the SEM has traditionally been used for fabric studies, mostly to observe the orientation and packing of particles, and voids (e.g. Gasparre et al., 2007).

2.3.4.3 Environmental Scanning Electron Microscopy

The Environmental SEM permits observation of hydrated samples in their original state (e.g. Donald, 2003, Redwood et al., 2005). This increased versatility allows the application of the ESEM to various new research fields including, for example, the study of colloids (e.g. Donald et al., 2000). The studies conducted so far with the ESEM in rock and soil mechanics have focused on: wettability of reservoir rocks in petroleum engineering (e.g. Combes et al., 1998, Buckman et al., 2000, Skauge et al., 2006); hydraulic behaviour of mine marls (Sorgi and De Gennaro, 2006, 2007) and hydration of geopolymer concrete (Zhang et al., 2005). In unsaturated soils, the ESEM was used in the static 'mode' to observe the fabric of bentonites by Musso et al. (2003) and Baker et al. (1995). Montes-H. (2005) and Montes-H. et al. (2005) seem to have been the first to use the ESEM for dynamic studies in unsaturated soils. They imposed wetting-drying cycles on bentonite MX80 aggregates while monitoring the structural changes and volume variations. The swelling-shrinkage was measured by a coupled digital image analysis program. Due to the aggregated nature of the material, the scale of observation was relatively large (20μm) and the study was conducted more at a larger scale rather than at a microscale. Regarding the fabric changes, it was possible to observe cracking and swelling of the aggregates and to quantify the swelling-shrinking potential by measuring volume changes (Figure 2.28).

Working principle

The conventional SEM works by emitting an electron beam towards a conductive sample in high vacuum conditions. Secondary electrons are released from the sample, collected by a detector and amplified to produce an image. The conductive coating of the sample (usually made of gold) improves the image quality and the vacuum ensures the effective operation of the electron gun.

In the presence of water vapour inside the microscope chamber, the emitted secondary electrons collide with the water molecules generating positive ions that are directed towards the sample. This causes overcharging of the sample surface and the consequent loss of image quality. In the ESEM a high vacuum condition is ensured only in a limited zone surrounding the electron gun while the relative humidity around the sample stays relatively high. This working mode ensures imaging of hydrated samples in their natural state. Further details about the physical

principles governing the operation of the ESEM can be found in Donald (2003) and Stokes (2003).

Within the ESEM it is possible to induce changes of relative humidity, i.e. leading to water condensation in the sample or evaporation from the sample by controlling the values of water vapour pressure and temperature. The temperature is controlled by means of a Peltier cooling stage, which can impose temperatures up to 20°C (however temperatures are usually kept at low values between 2°C and 6°C during tests) while the value of vapour pressure can be increased up to 2.339 kPa. The control of relative humidity (RH) inside the microscope chamber is based on the phase diagram of water. Figure 2.6 shows the boundary of this diagram separating the region in which vapour pressure at equilibrium is saturated (RH=100%) from the region where vapour pressure at equilibrium is not saturated (RH<100%).

ESEM imaging has normally been done in static 'mode', under constant relative humidity and constant temperature, i.e. under a constant total suction, to observe a specimen in that particular state. However, it is also possible to use the ESEM in a dynamic 'mode' to observe a sample's response to changes of relative humidity. and/or temperature (i.e. to a change of total suction). Dynamic observations can be carried out in situ without removing the sample from the microscope chamber.

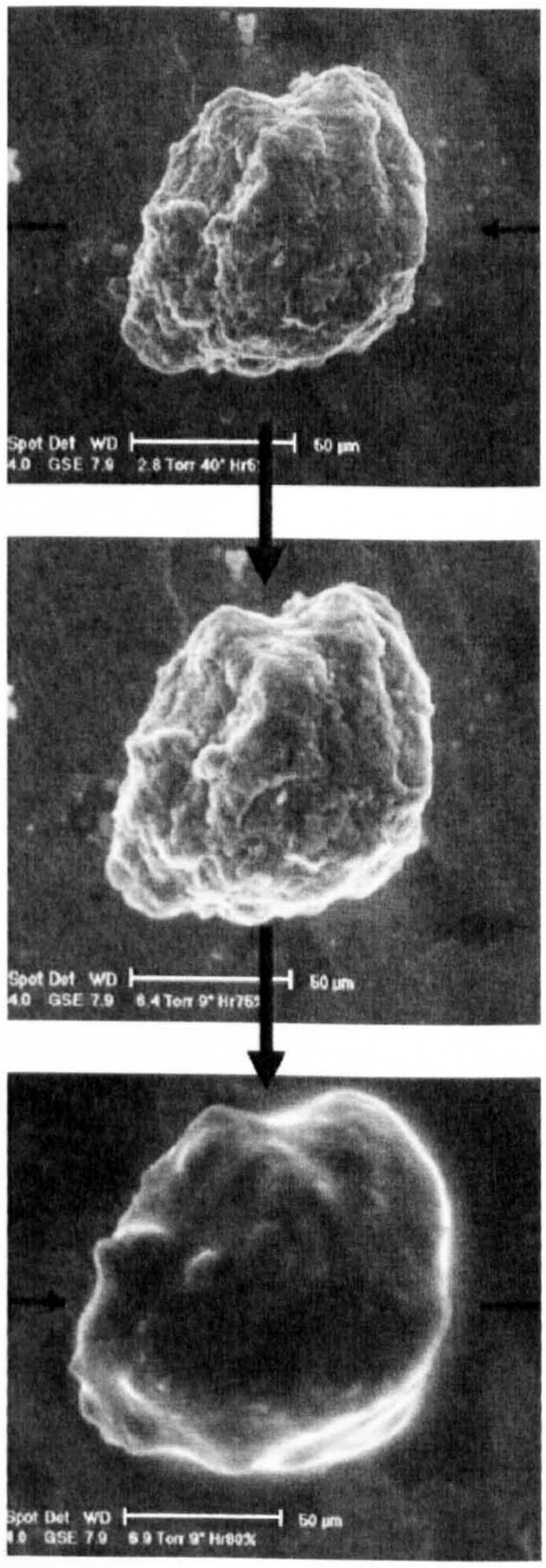

Figure 2.28: ESEM microphotograph of a bentonite aggregate (wetting from top to bottom image) (from Montes-H. et al., 2005)

Mechanical testing

Stokes and Donald (2000) developed a technique in which quantitative stress-strain relationships can be obtained whilst allowing simultaneous imaging of hydrated samples, by ESEM. The authors carried out a study on bread crumbs including a series of compression tests at different humidities in a custom built straining stage able to work in compression/extension fitted below with a Peltier stage. Figure 2.29a shows the stress-strain curves for the material under compression at different RHs (20%, 30%, and 100%). The curves appear to follow expectations in that the sample

tested at the lowest humidity reaches the highest peak strength (≈0.19MPa). Figure 2.29b shows the material deforming and rupturing as it is sheared, however, water menisci are not visible in any of the images presented. This seems to be the only published study on mechanical testing in an ESEM.

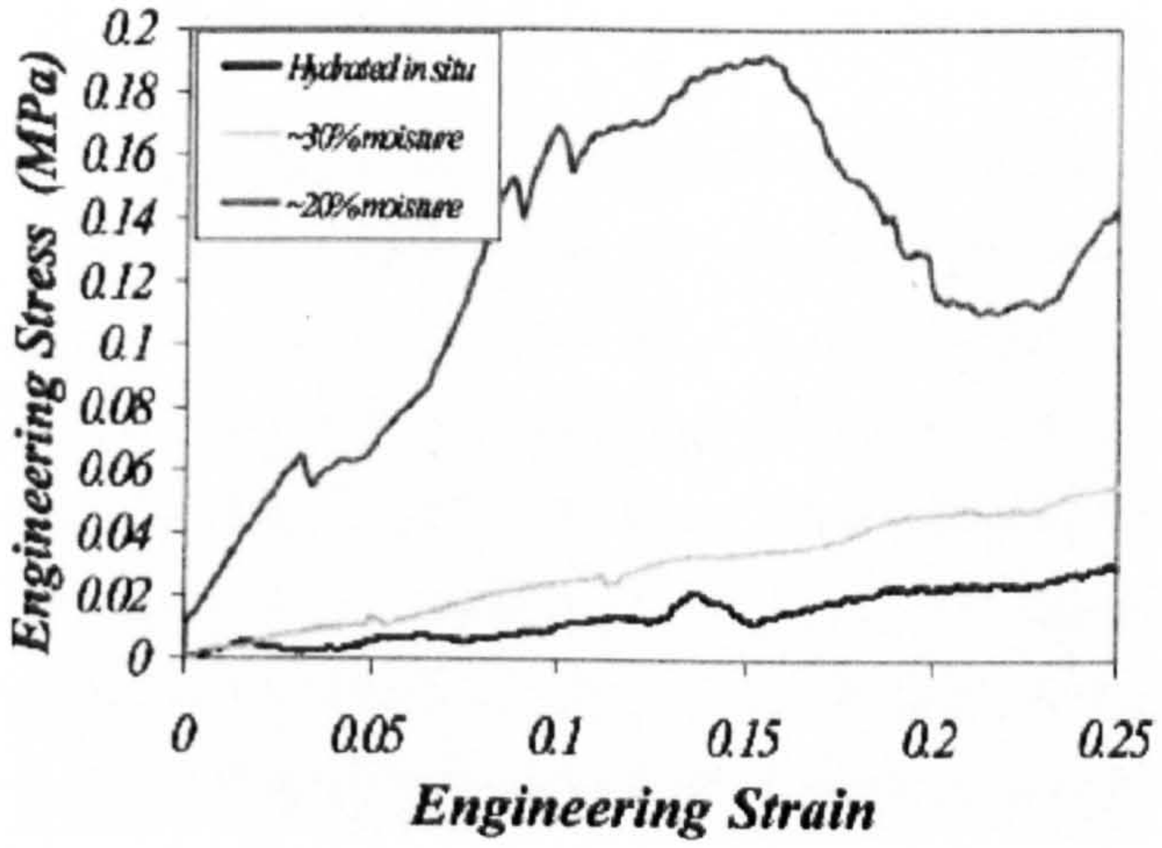

(a)

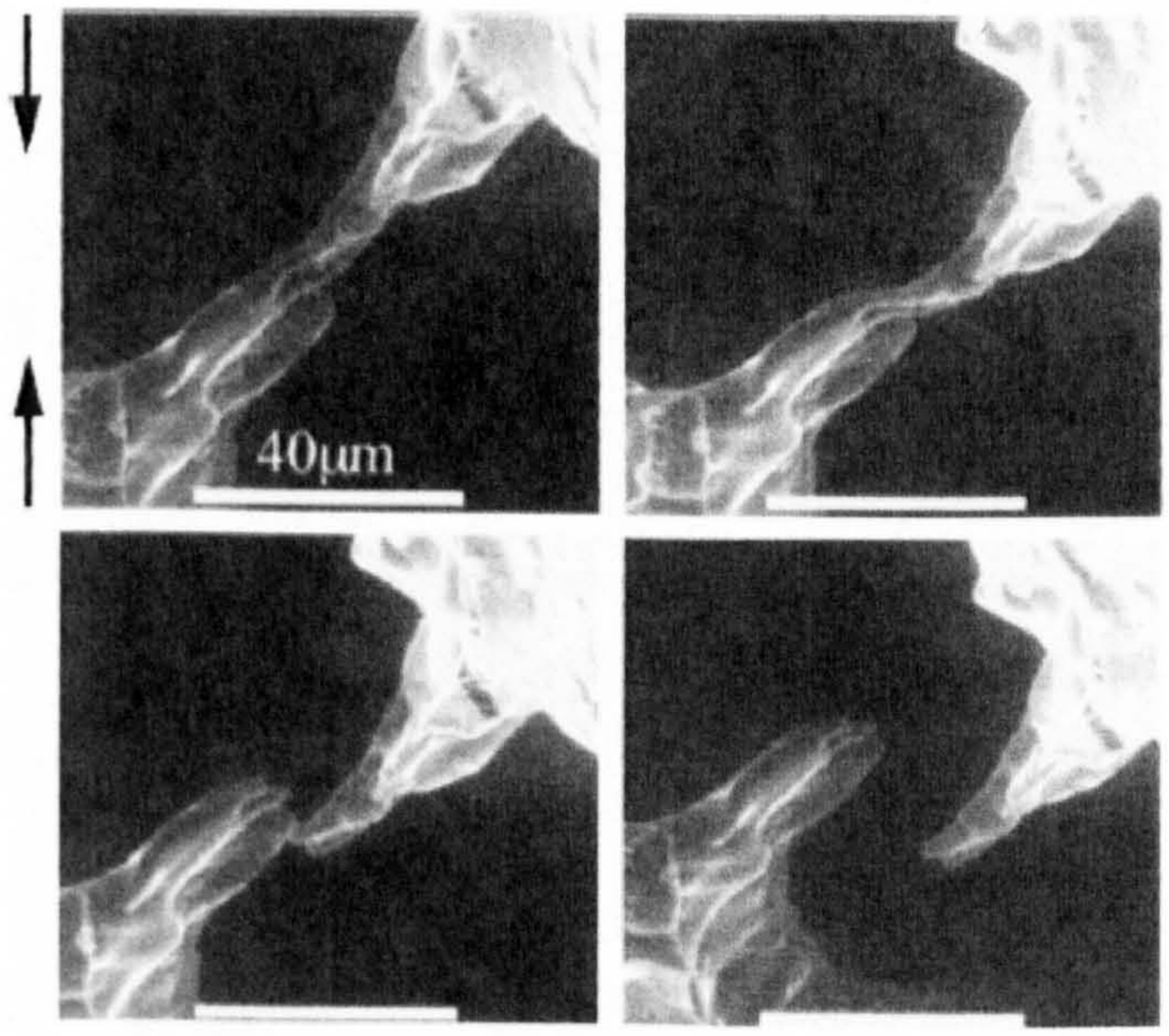

(b)

Figure 2.29: Mechanical testing in the ESEM, (a) stress-strain plot of the bred crumb at different RH, (b) microphotographs of the bread crumb under compression (RH 30%) (from Stokes and Donald, 2000)

2.4. HIGH SUCTION TENSIOMETERS

2.4.1. Characteristics and working principle

2.4.1.1. Working principle

High suction tensiometers are small probes fitted with a porous stone and pressure transducer able to measure negative water pressure smaller than -100kPa relative to atmospheric pressure. The porous stone acts as an interface soil-transducer and controls the maximum suction to be measured. If the stone is well saturated, the maximum suction is only limited by the air entry value of the stone. If not, cavitation occurs in the porous stone or reservoir. Between the porous stone and the transducer there is an open space to allow the deflection of the diaphragm when water is in tension. The transducer measures directly the pressure value.

High suction tensiometers measure directly the water tensile strength in the water menisci present in the soil by allowing the pressure within a miniature water-filled reservoir inside the probe to attain equilibrium with the soil pore water pressure through a high air entry value porous stone. During equilibration as water is sucked from the porous stone to the soil, a small volume of water flows from the reservoir through the porous disk to the soil producing a deformation of the diaphragm in the direction of the soil. This deformation is read by the strain gauge as a value of pressure. Once this transfer ends, the water in the tensiometer will have the same value of negative pressure (Figure 2.30) as the water in the soil. The volume of water transferred from the tensiometer is small enough so that it can be considered negligible, and therefore the water content of the sample is not affected.

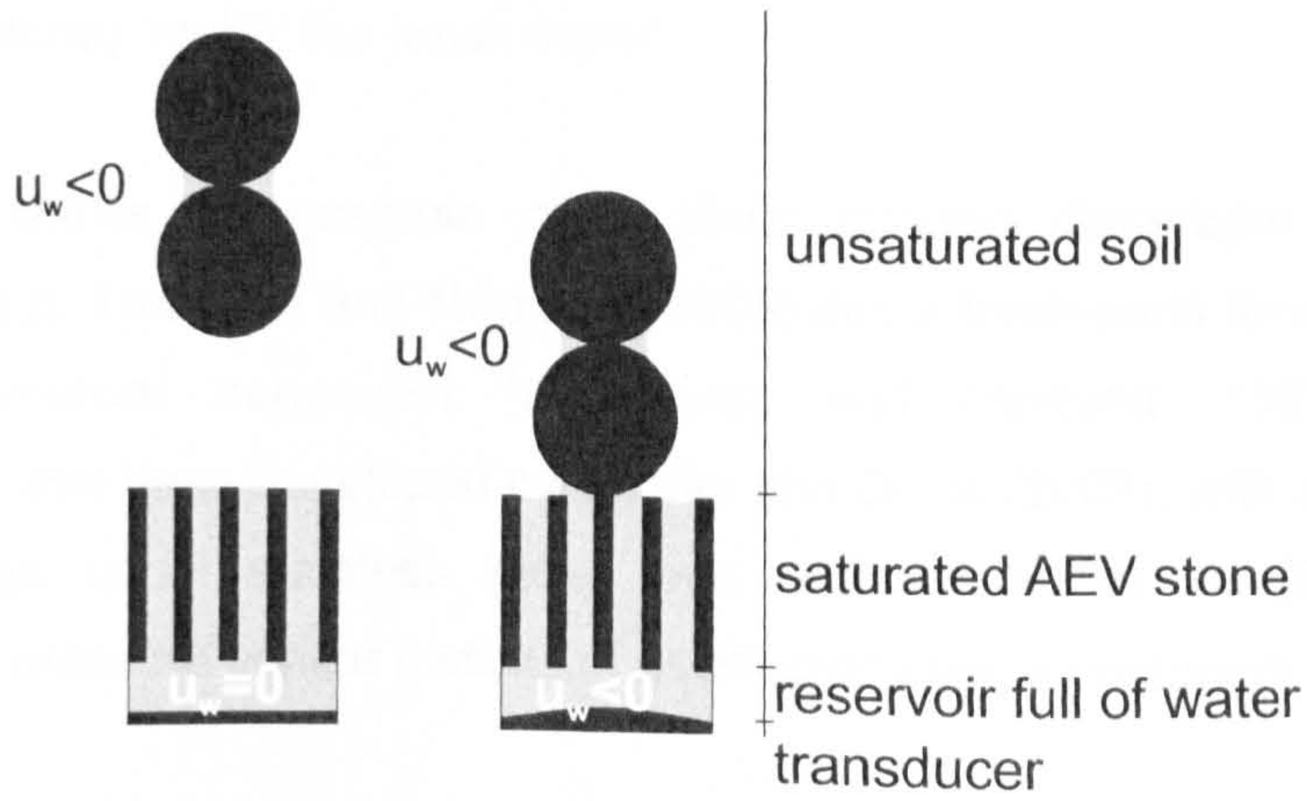

Figure 2.30: Scheme of tensiometer operation

2.4.1.2. Developed tensiometers

Eleven different designs of high suction tensiometers have been developed so far by Ridley and Burland (1993), Guan and Fredlund (1997), Sjoblom (2000), Tarantino and Mongiovi (2003), Mantho (2005), Meilani et al. (2002), Ridley et al. (2003), Take and Bolton (2004), Mahler and Diene (2007), Jotisankasa et al. (2007) and Rojas et al. (2008). F.A.M. Marinho also developed a tensiometer at the University of São Paulo, Brazil although no data has been published so far. The initial design of the high suction tensiometer by Ridley and Burland (1993) was subsequently improved by Ridley et al. (2003). The main characteristics of all these tensiometers are summarized in Table 2.2.

High suction tensiometers can be classified based on the air entry value of the stones or construction. Nearly half of the tensiometers in Table 2.2 operate at the high suction range (up to 1500kPa) while the remaining ones operate at low suctions (up to 500kPa). The high suction tensiometers by Tarantino and Mongiovi (2003), Ridley et al. (2003) and Mantho (2005) are strain gauged tensiometers, where a strain gauge was attached to the back of a flexible diaphragm. In the case of Tarantino and Mongiovi (2003) and Mantho (2005) the tensiometer body is made of a single piece and the diaphragm is machined as part of the body. Most of the high suction tensiometers listed in Table 2.2 are built from commercial transducers, which have been slightly machined to improve their response at high suctions. For example, Ridley and Burland (1993) used the model Entran EPX-500, Meilani et al. (2002) the model Druck PCDR-81 and Take and Bolton (2004) Entran EPB-C1. Some designs use commercial transducers enclosed in a stainless steel housing and fitted with a detachable porous stone, hence three separate parts (transducer, housing and stone) 'make' the tensiometer.

Figure 2.31 shows an example of a strain gauged diaphragm single-bodied tensiometer (e.g. Tarantino and Mongiovi, 2003) and a three-parts tensiometer made from a commercial transducer (e.g. Guan and Fredlund, 1997). Low cost tensiometers have been developed by Mahler and Diene (2007), with an acrylic body instead of the usual stainless steel, and Jotisankasa et al. (2007), with a piezoresistive pressure sensor instead of usual capacitive transducers.

Table 2.2: Characteristics of the tensiometers developed so far

	Porous stone AEV (bar)	Pressure transducer suction (kPa)	Water reservoir volume (mm^3)	Design	Notes
Ridley and Burland (1993)	15	3500	-	modified commercial transducer	-
Guan and Fredlund (1997)	15	15000	~20	modified commercial transducer	-
Sjoblom (2000)	-	1380	-	modified commercial transducer	stone made of sintered silica gels
Tarantino and Mongiovi (2003)	15	-	<4.5	strain gauged diaphragm, single body	-
Mantho (2005)	15	-	height 0.1mm	strain gauged diaphragm single body	-
Meilani et al. (2002)	5	1500	-	modified commercial transducer	1mm thick porous stone
Ridley et al. (2003)	15	8000	~3	strain gauged diaphragm	-
Take and Bolton (2004)	3	700	-	modified commercial transducer	-
Poirier et al. (2005)	5	1380	-	modified commercial transducer	-
Mahler and Diene (2007)	5 & 15	-	5-112	modified commercial transducer	tensiometer body in acrylic
Jotisankasa et al. (2007)	5	-	60	modified commercial transducer	piezoresistive pressure sensor

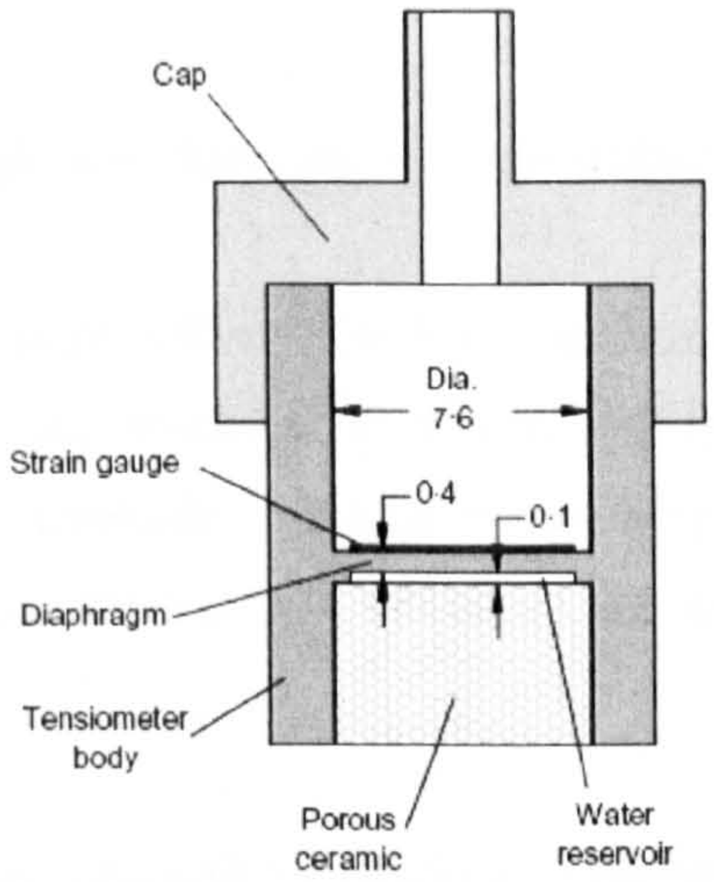

Tarantino and Mongiovi (2003)

(a)

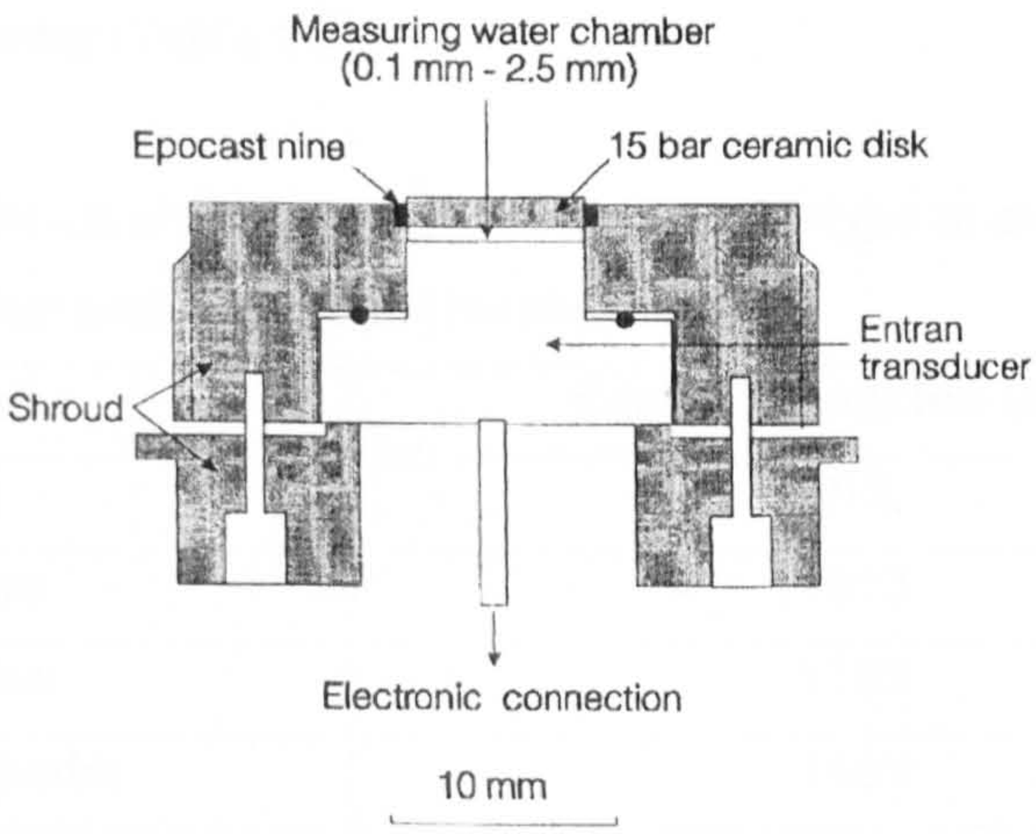

Guan and Fredlund (1997)

(b)

Figure 2.31: Different examples of tensiometer design, (a) Tarantino and Mongiovi (2003) type (units are in 'mm'); (b) Guan and Fredlund (1997) type (0.1mm-2.5mm corresponds to the height of the water reservoir)

2.4.2. Cavitation

2.4.2.1. Origin and formation of air bubbles in water

The general term of 'cavitation' will be used in this thesis to indicate the process of formation and growth of air bubbles in the water reservoir of a high suction tensiometer. In particular, cavitation can be induced by distinct physical processes such as water rupture (cavitation), air diffusion, air entry or when immersing a material in water.

Water rupture is induced by subjecting a liquid to a negative pressure in excess of its tensile strength at constant temperature (Brennen, 1995). The tensile strength of pure water has been estimated at 405MPa (Tabor, 1969) and it also depends on the amount of dissolved air in water (Table 2.3).

Table 2.3: Dependence of the breaking tension on the type of water
(after Sedgwick and Trevena, 1976)

Type of water	Breaking tension (kPa)
Tap-water	912
Deionised water	1013
Boiled tap-water	1165
Boiled deionised water	1469

Diffusion is the process by which a pre-existing bubble in water will change in volume depending on the difference of gas pressure inside the bubble and the surrounding water. The stability of a free bubble will be discussed in Section 3.3.

The process of air entry through the porous stone will depend on the air and liquid pressures, radius of the pores, and advancing and receding contact angles of the air-water interfaces.

The dynamics controlling the formation and growth of bubbles during water rupture, diffusion or air entry is variable – in particular, diffusion is a slow process while water rupture and air entry are fast processes.

Air might also get trapped on the surface of the tensiometer reservoir during a wetting process, as shown in Figure 2.32 where air is trapped in a surface crevice. The amount of air trapped depends on the geometry of the crevice and advancing contact angle of the liquid (Jones et al., 1998). Hydrophobic surfaces can trap air easily due to the high contact angle (Ishida et al., 2000).

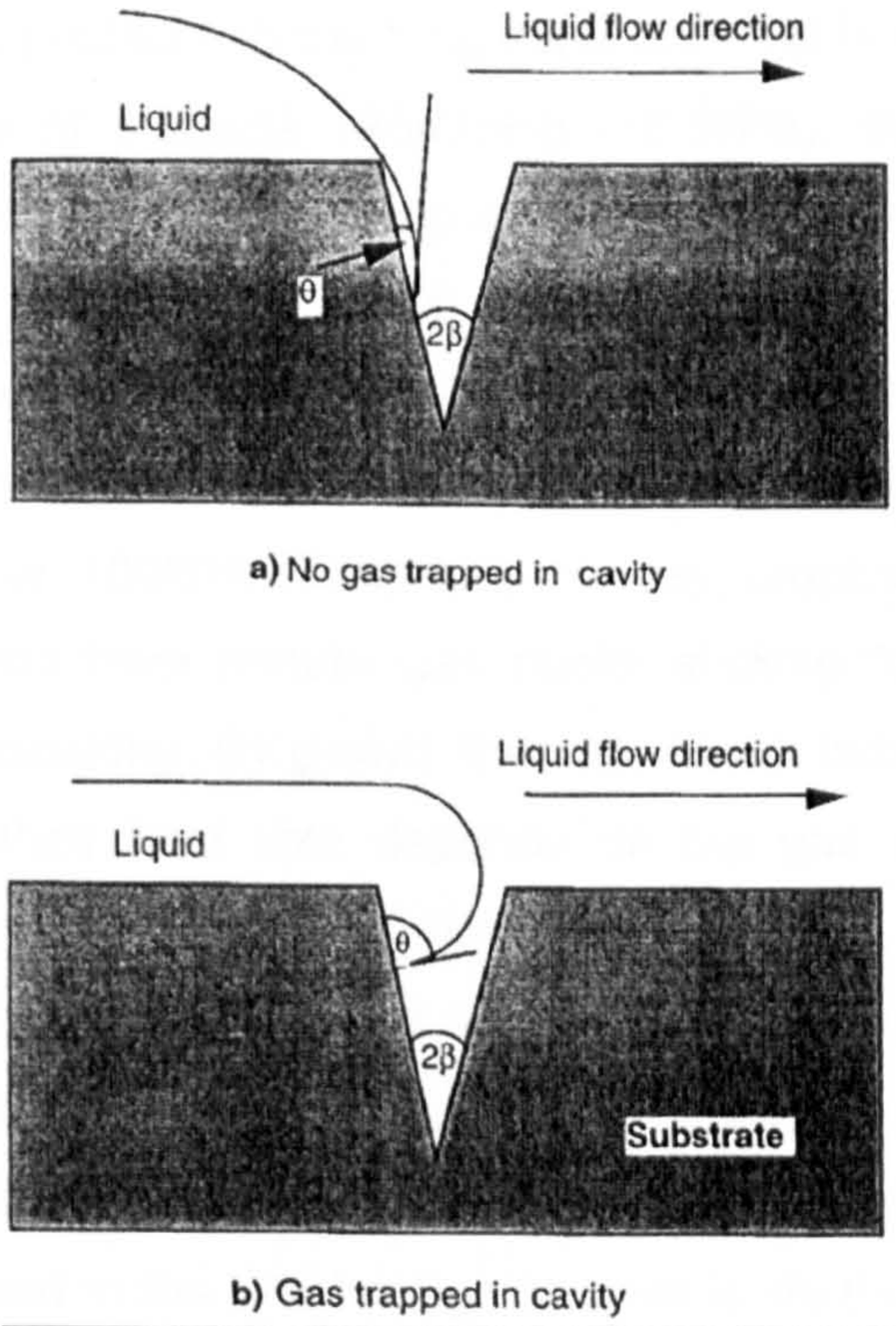

Figure 2.32: Air entrapment in a crevice depending on the advancing contact angle of the liquid, a) with a low contact angle less air gets trapped, b) with a high contact angle more air gets trapped (from Jones et al., 1999)

Key works on cavitation (water rupture), as relevant to high suction tensiometers, will be reviewed in the following. The classic paper by Harvey et al. (1944) that states that cavitation starts from small bubbles stick to surfaces will be reviewed first, followed by Ishida et al. (2000) that provide evidence of nano-sized bubbles in surfaces that could constitute potential cavitation nuclei. A recent paper by Bremond et al. (2005) that shows bubbles being released from surfaces as the water is subjected to pulses of tension is also reviewed. Cavitation in soils will also be introduced (particularly important for Chapter 3). The papers reviewed will provide background to discuss the current standing of cavitation in high suction tensiometers at the end of the section.

2.4.2.2. Harvey et al. (1944) study on bubble formation in animals

In 1944, Harvey and colleagues reported that bubbles form abundantly in both arteries and veins of animals after compression-decompression cycles. However, the blood pressures changes observed in animals were not high enough to explain this bubble formation. For instance, at the sea level the blood comes into equilibrium with 1atm (~101kPa) of gas pressure in the lung capillaries but is quickly subjected to an arterial blood pressure of perhaps 125mmHg (16.6kPa), therefore the maximum pressure difference (gas pressure-blood pressure) or *suction* it will be subjected is 101-16.6=84.4kPa. On the top of Mt. Everest the pressure difference is approximately 55.8kPa. If we consider bubble formation by decompression, the pressure variation is extremely small 84.4-55.8=28.6kPa and, in any case, well below 405MPa and still below 100kPa. Therefore Harvey proposed that most bubbles formed in animals come from minute gas nuclei sticking to the surface of cells, instead of pure liquid fracturing. By growth they appear as bubbles in blood, lymph or intercellular fluid and their final size depends on the gas available. More recent studies confirm Harvey's theory. Decompression sickness, as it is known, is a common problem for divers, aviators and astronauts (e.g. Yount and Strauss, 1976). Gas bubbles release from the organs and arteries walls to the blood during the ascending stage of divers or descent of astronauts. The bubbles obstruct blood circulation and if localized in the heart, lungs or brain is life threatening (e.g. Souders et al., 1999).

2.4.2.3. Evidence of nano-sized bubbles on surfaces

Evidence of undissolved micron-scale bubbles that could represent potential cavitation nuclei have been given by Ishida et al. (2000) for the case of hydrophobic surfaces. The authors immersed a hydrophobized silicon wafer in water to observe the surface in-situ by tapping-mode Atomic Force Microscopy (AFM). Figure 2.33 show the in-situ height (top image) and the cross sections (bottom graphs) along the lines shown on the top image. The circular structures that appear randomly on the surface are air bubbles with a height and diameter between 650nm and 40nm. There seems to be no direct evidence in the literature at such small scales for air entrapment in crevices.

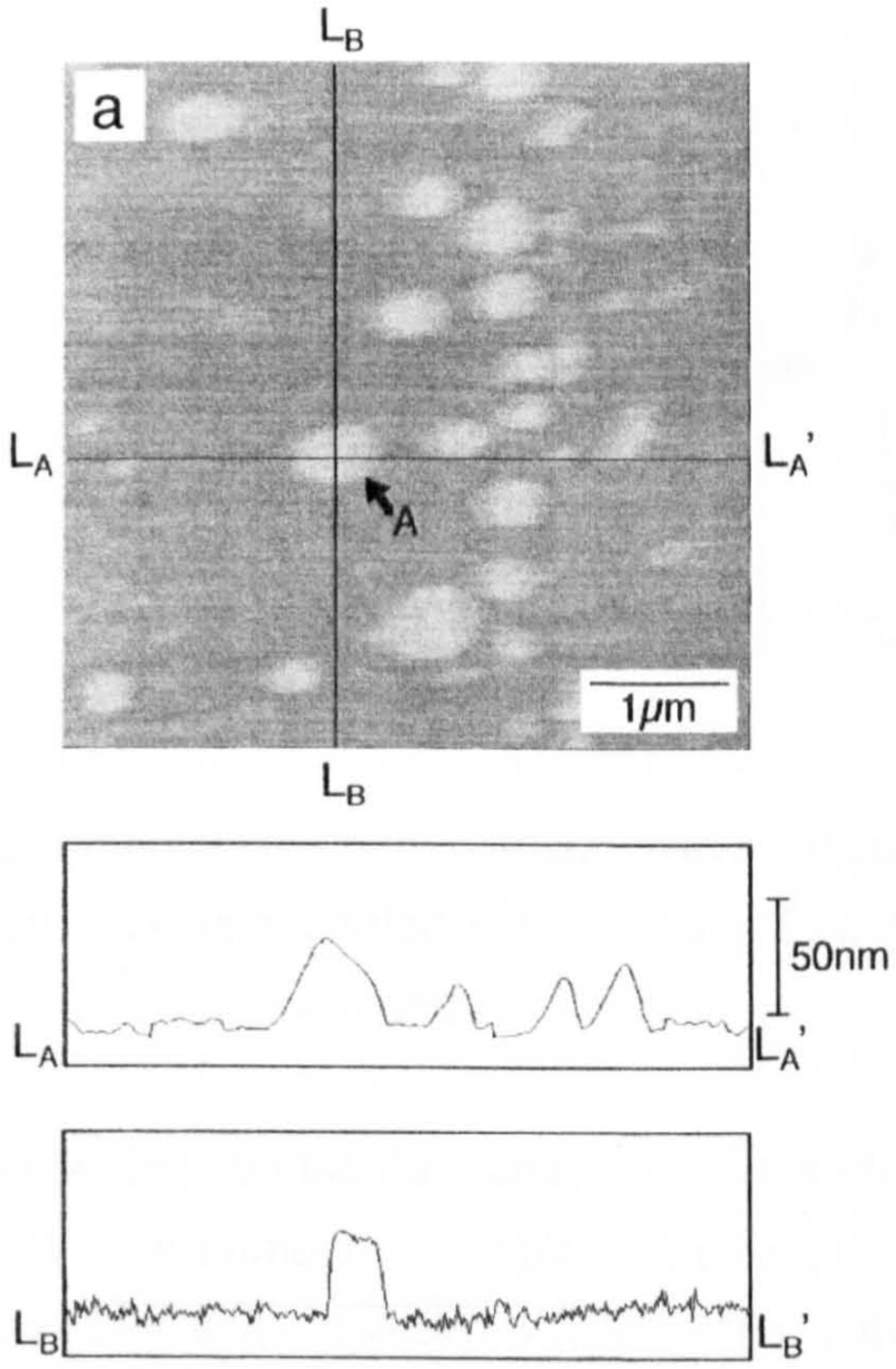

Figure 2.33: Evidence of nano bubbles attached to an hydrophobic surface in water; top image shows the AFM height image and the bottom graphs the cross-sectional views (from Ishida et al., 2000)

2.4.2.4. Bremond et al. (2005) study on cavitation on surfaces

More recently, Bremond et al. (2005) did an interesting work on cavitation on surfaces with findings that are extremely relevant to high suction tensiometers. The authors did an investigation on the presence of gas on hydrophobic surfaces immersed in water by cavitating the water under negative liquid pressures (ranging between -2 and -11MPa) by acoustic emission. A lithotripter is used as a pressure wave generator through the water (Figure 2.34a) generating a positive pressure front followed by a negative pressure pulse (Figure 2.34b). The bubbles were attached to two substrates, one flat and another with micro-asperities. The bubbles formed after immersing the substrates into water and had initial radii ranging between 13 and 37nm.

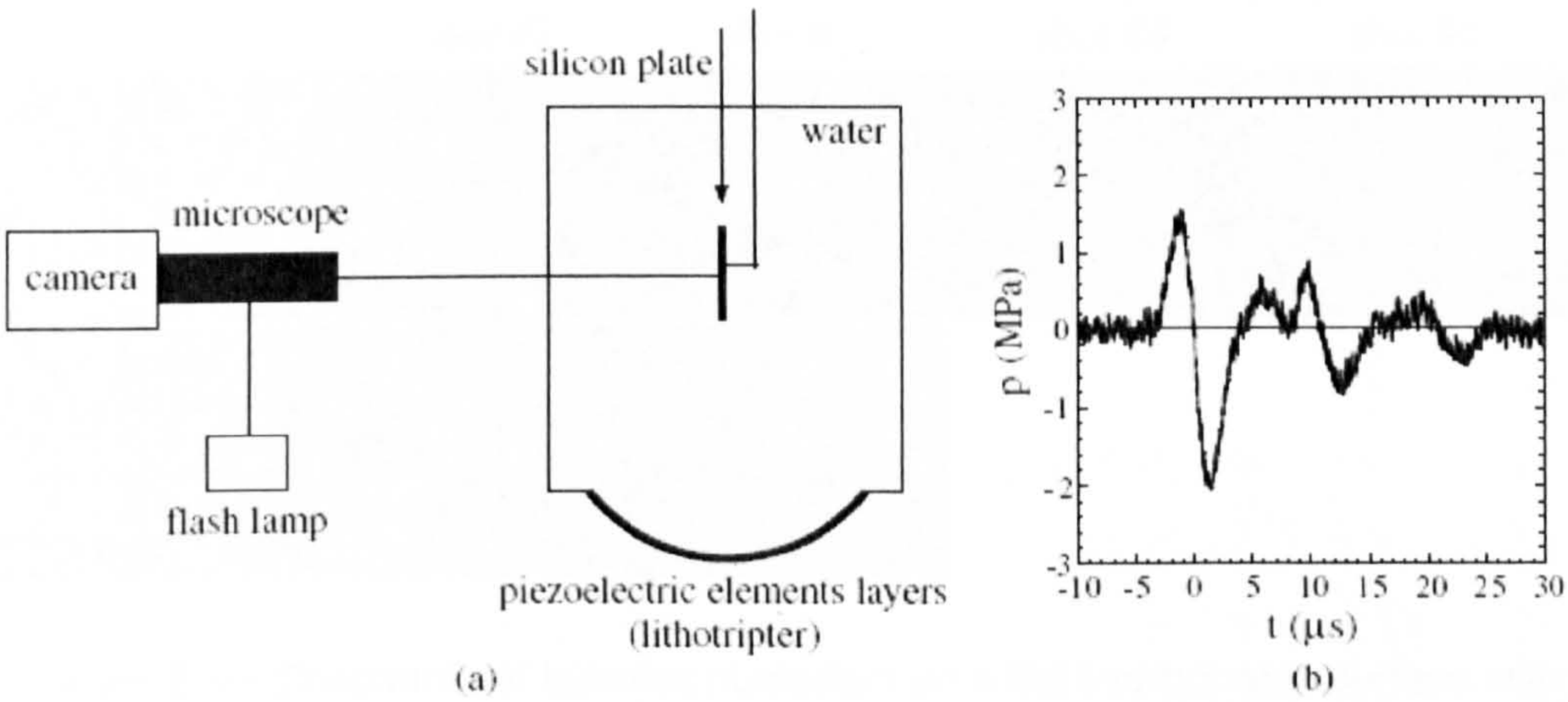

Figure 2.34: Experimental set-up, a) pressure wave generator and optical visualization, (b) pressure signal recorded with an optical fibre (from Bremond et al., 2005)

Figure 2.35 shows the bubbles on the flat surface after one -4MPa shot followed by another one of -11MPa. The number of bubbles remained more or less the same between the shots (pressure wave applied). However the authors state that, under repeated shots, the density of bubbles (number of bubbles per unit area) would decrease, which suggests that bubbles were being released from the surface. This is easily seen in Figure 2.36.

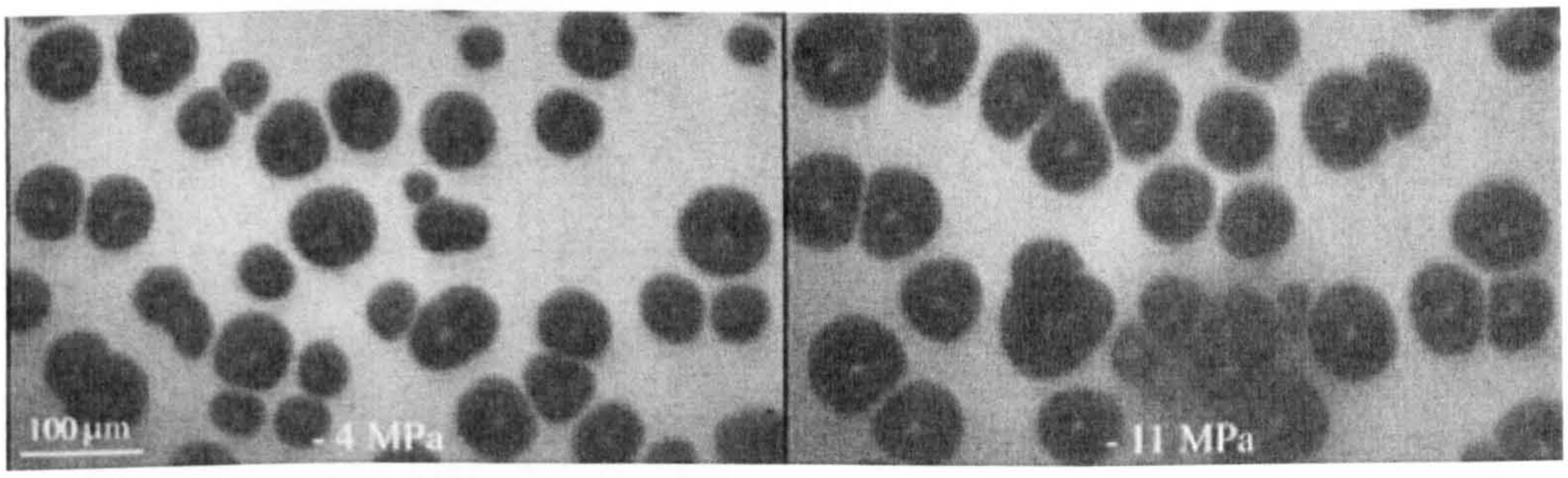

Figure 2.35: Snapshots of bubbles nucleated on a flat and smooth hydrophobic surface after the passage of pressure pulses with minimum pressures of −4 and −11MPa (from Bremond et al., 2005)

For the case of Figure 2.36 the immersed substrate had microcavities with a diameter of 2µm (Figure 2.36a), and 4µm in Figure 2.36b. As shown the number of bubbles decreased with number of shots, but the decrease was much faster for the larger cavities (4µm).

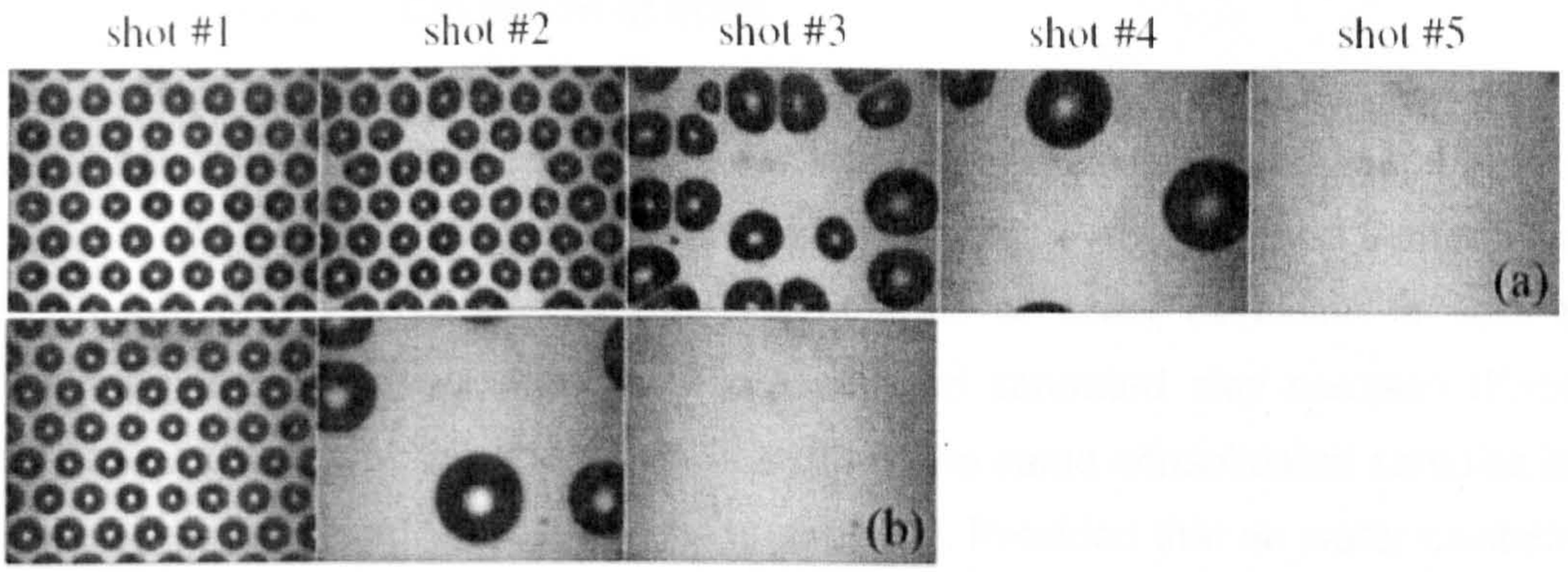

Figure 2.36: Snapshots of bubbles nucleated on a flat hydrophobic surface with cavities having diameter of 2μm (a) and 4μm (b) after successive low pressure pulses with minimum pressure of −2MPa (from Bremond et al., 2005)

Figure 2.37 shows the complete sequence of bubbles cavitating. Two microphotographs of a single bubble and a pair of bubbles are displayed in Figure 2.37a and Figure 2.37b. The evolution of the radius with time of an isolated bubble is plotted in Figure 2.37c. The bubbles were subjected to the pressure wave of Figure 2.34b.

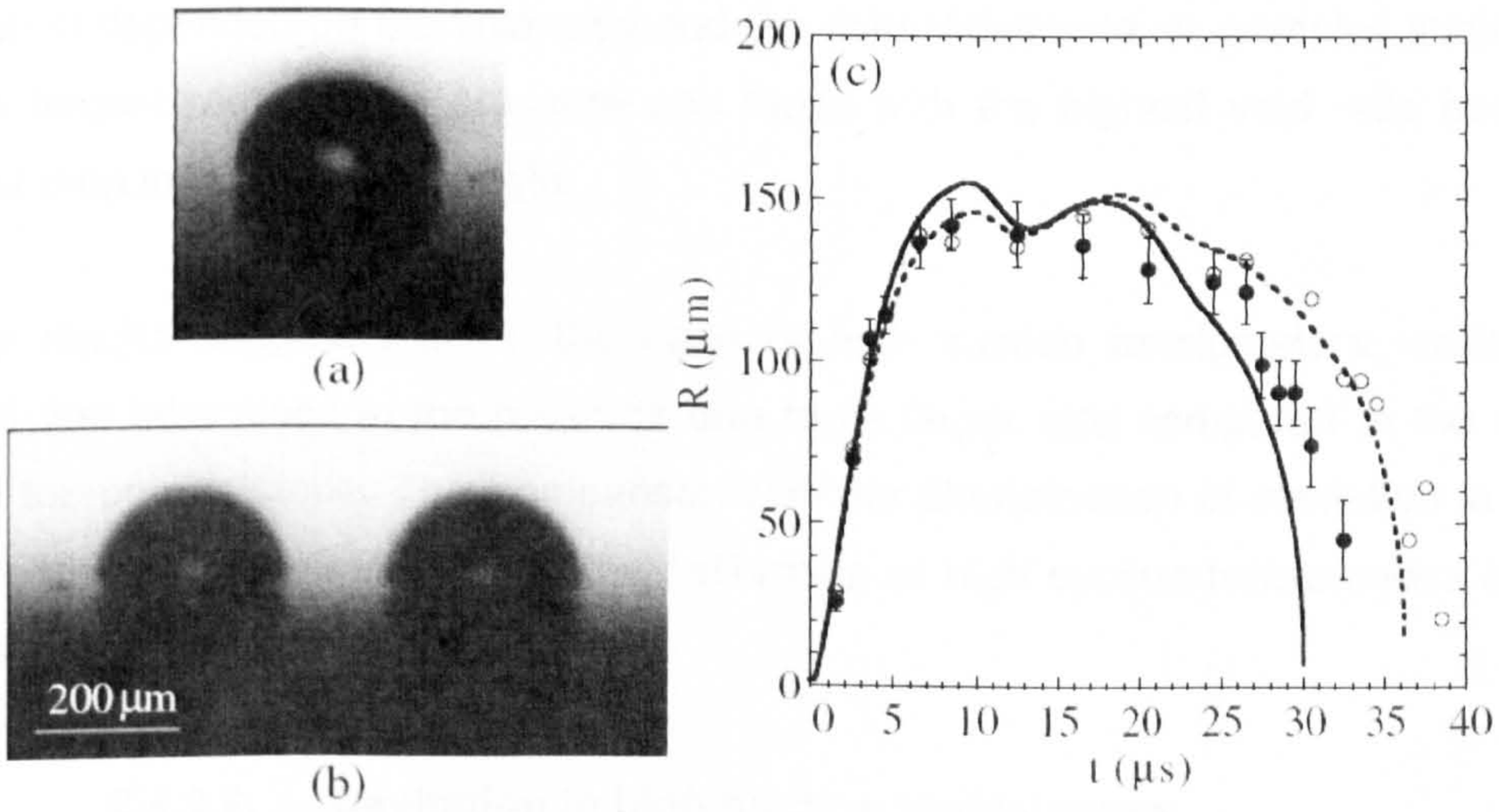

Figure 2.37: (a) Side view of a single expanding bubble on a solid surface, (b) two bubbles initially 400μm apart and (c) evolution of the bubble radius versus time for a single cavity (•) and two cavities 400μm apart (◦); the length scales in (a) and (b) are the same and the snapshots correspond to t = 8.5μs (from Bremond et al., 2005)

2.4.2.5. Cavitation in soils

The study of the formation and growth of air bubbles within soil pores might also be helpful to the understanding of cavitation in high suction tensiometers. Bishop et al. (1975) and Mair (1979) studied the phenomenon of water cavitation in soils by comparing the undrained strength of consolidated saturated clay samples (Kaolin and London Clay) with the undrained strength of the same consolidated samples but subjected to undrained unloading prior to shearing. Provided that no water cavitation takes place, the negative water pressure created during undrained unloading should be equal and opposite to the applied consolidation stress and therefore there would be no change in effective stress. Bishop et al. (1975) found, however, that for consolidation stresses ranging between 1MPa and 8MPa, the undrained strength of the unloaded samples was 65% lower than the undrained strength of samples sheared without prior unloading. For samples consolidated at low confining stresses, i.e. between 200kPa and 900kPa, the undrained strength of the unloaded samples was 40% lower than the undrained strength of samples sheared without prior unloading (Mair, 1979). The loss in strength suggested that water cavitation had indeed occurred inside the soil pores during unloading, thus reducing the induced suction and reducing the effective stress. Both authors noted that the effect of cavitation depended on the void ratio and the consolidation level; samples subjected to the largest reduction in pressure and those with the highest void ratio had the largest drop in undrained strength.

These results suggest that, in the case of high suction tensiometers, cavitation should first take place in the reservoir due to its larger size compared to the voids inside the porous stone. This comparison with the phenomenon of cavitation in soils will also be of interest later when the calibration of high suction tensiometers in the negative range will be discussed.

2.4.2.6. Cavitation in high suction tensiometers

The studies on the phenomenon of cavitation in blood (e.g. Van Lieuw and Burkard, 1993) can also be adapted to explain cavitation in high suction tensiometers. Based on Harvey's model, Ridley (1993), Take (2003) and Guan (1996) linked the phenomenon of cavitation in high suction tensiometers to the expansion of trapped gas inside the probe. Figure 2.38 shows a cavitation model presented by Take (2003), where an air bubble, initially shrunk inside a crevice of the solid surface,

grows back as water is subjected to increasing levels of tension. If water had not been pressurized (Figure 2.38a) an air bubble would be released as tension increases in the water and cavitation would occur while, if pressurization had taken place (Figure 2.38b), the air would remain trapped into the crevice and cavitation would not occur.

Current understanding of cavitation in high suction tensiometers can be summarized as follows:

- If cavitation inside the tensiometer occurs at a suction similar to the air entry value of the porous stone, it is reasonable to assume that air has broken into the tensiometer from the atmosphere through the porous stone (e.g. Ridley et al., 2003).

- The porous stone inhibits the passage of air into the water reservoir and maintains separation between the water inside the tensiometer and the air outside. Therefore the maximum suction that can be measured by a high suction tensiometer cannot exceed significantly the air entry value of the porous stone (for instance, Meilani et al. (2002) measured a maximum of 495kPa by using tensiometers fitted with a 5bar air entry value porous stone).
- On the other hand, when cavitation occurs at suctions lower than the air entry value of the porous stone, it is reasonable to assume that a bubble has formed in the water reservoir. This is due to the release of trapped gas from small crevices (having dimensions of the order of microns) as suggested by Ridley (1993), Ridley et al. (2003) and Take (2003) (see Figure 2.38).

- Air diffusion can also play an important role in the formation of bubbles inside tensiometers. Ridley et al. (2003) state that air will diffuse in from the air saturated water in the soil to the de-aired water in the tensiometer contributing to the volume increase of any pre-existing bubble.

- Cavitation should start in the water reservoir due to its larger volume (see Bishop et al., 1975, Toll and Hight (unpublished), Mair, 1979) compared to the size of voids inside the porous stone.

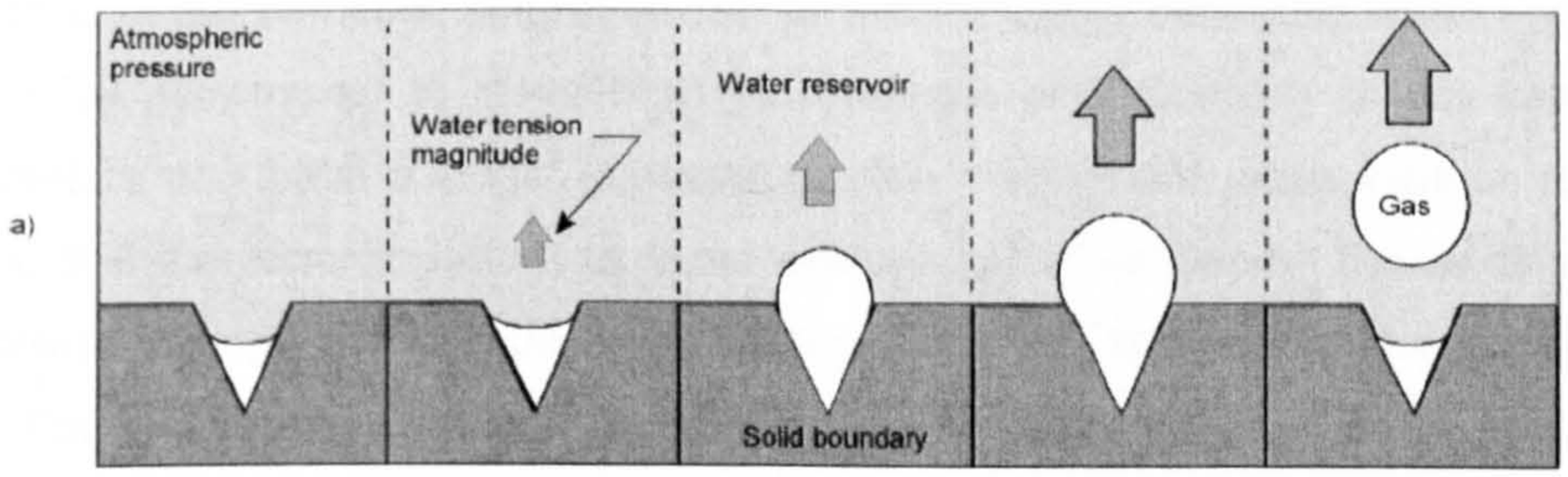

Figure 2.38: A model for cavitation in tensiometers by Take (2003); bubble growth in a crevice as water tensile stress increases: (a) no pressurization of water (cavitation occurs) (b) pressurization of water (cavitation does not occur)

2.4.3. Saturation

2.4.3.1. Procedures to saturate tensiometers

From the above discussion it follows that the reliability and measurement range of high suction tensiometers depends critically on the absence of any trapped air inside the device. The saturation of the water reservoir and the porous stone is usually performed in a similar way as for the saturation of soil samples, i.e. by applying high values of positive water pressures to force any residual air volume present in the porous stone and reservoir to dissolve in water. For the saturation of soil samples, Black and Lee (1973) divided the pressurization process in two stages: the first stage corresponds to a reduction of the size of gas bubbles due to compression under increasing water pressure while the second stage corresponds to the dissolution of the gas from the bubbles into the water. The first stage is dominant at low degrees of saturation when the gas phase is continuous while the second stage corresponds to the case where high degrees of saturation (i.e. isolated bubbles) exist. Both these stages can occur in the saturation to high suction tensiometers, with the second stage being particularly important to achieve full saturation of the tensiometer and to eliminate microbubbles acting as potential cavitation nuclei.

In the case of soil samples, saturation can be performed by infiltrating water from one end and by allowing air to leave from the opposite end. Contrary to soil samples, tensiometers only have a single exposed surface from where pressurization can be applied. It is therefore important to avoid entrapment of air behind the wetting front that moves through the porous stone during the initial flooding of the probe with water. For this reason, the first immersion of the tensiometer in water is usually performed under vacuum. The application of vacuum ensures that only a minimum amount of air is present inside the porous stone and water reservoir at the moment of immersion.

Following initial immersion in water, the tensiometers are subjected to positive values of pressure to eliminate residual air trapped inside the probe. Maximum pressures applied during this stage have attained values as high as 12 MPa (Guan and Fredlund, 1997). Some authors apply cycles of pressures over a given period of time (Guan and Fredlund, 1997, Take, 2003, Mantho, 2005) whereas other authors prefer to use a constant value of pressure (Ridley, 1993).

Other specific procedures were employed by various authors to extend the measurement range of the high suction tensiometers. For example, Mantho (2005) subjected the tensiometer to a number of initial cavitations to improve the probe performance. On the other hand, Take (2003) dried the tensiometer after each cavitation and always flooded it under vacuum before pressurization. In particular, Take (2003) explained the inability of the tensiometers to achieve full saturation after initial flooding with the presence of water menisci trapping air bubbles within the porous stone. To solve this, the saturation chamber and tensiometer were subjected to several hours of drying in an oven at a temperature of 60°C. Sjoblom (1996) changed the initial porous stone from Soil Moisture Corp. to a uniformly graded granular material fabricated in Japan and the result was a jump of the maximum measurable suction from 1500kPa to 2000kPa.

Other factors are also likely to increase suction at cavitation. For example, Richards and Trevena (1976) found that the water tension at cavitation peaked at a temperature of approximately 4°C, the temperature at which water is at its densest condition (Figure 2.39).

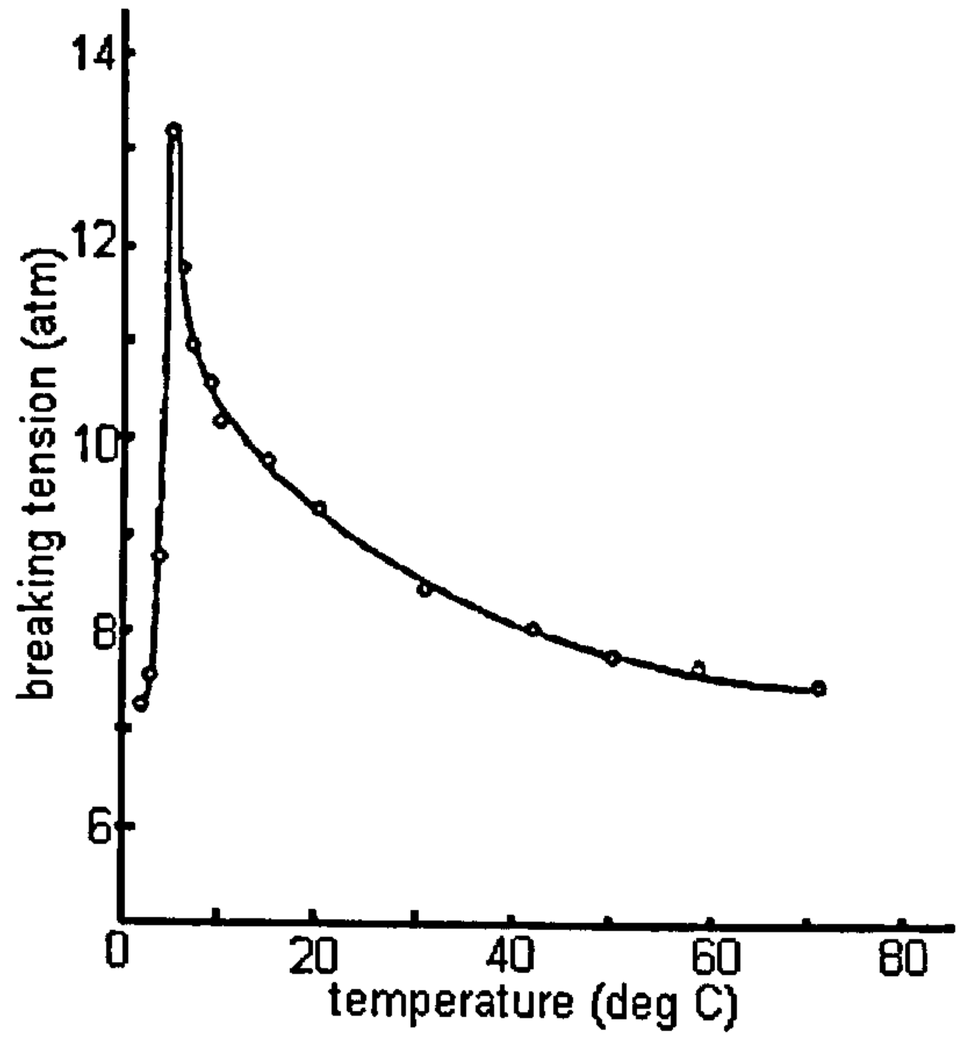

Figure 2.39: Temperature influence in cavitation; the suction at cavitation (breaking tension on the vertical axis of the above figure) is highest at a temperature of 4°C (1atm = 101.3kPa) (after Sedgewick and Trevena, 1976)

2.4.3.2. Suction range

In general, all studies published in the literature emphasize the importance of pressurization to delay cavitation. However, other factors known to have an effect are summarized in Table 2.4.

Table 2.4: Developed tensiometers and saturation procedure

	Suction at cavitation (kPa)	Saturation procedure	Factors to achieve high suction
Ridley and Burland (1993)	1250	Constant pressurization at 6MPa for 24h	Small reservoir size
Guan and Fredlund (1997)	1600	Cyclic pressurization with 6 cycles (12MPa for 1h and -85kPa for 1h)	Pressurization in cycles
Sjoblom (2000)	2000	Flooding under vacuum and constant pressurization from 12h up to 1 week	Nature of the porous stone
Tarantino and Mangiovi (2001)*	2584	Flooding under vacuum and constant pressurization at 4MPa for 24h	Cavitation history
Mantho, (2005)	1573	Flooding under vacuum and constant pressurization at 4MPa for 24h followed by pressurization-cavitation cycles	Pressurization-cavitation cycles
Meilani et al. (2002)	495	Constant pressurization at 800kPa for 4 days	-
Ridley et al., (2003)	-	Constant pressurization at 4MPa up to 6MPa	-
Take and Bolton (2003)	530	Initial drying of tensiometer, flooding under vacuum, cyclic pressurization with multiple cycles (1MPa for 1h)	Small dimensions of the stone and reservoir
Poirier et al. (2005)	<100	-	-
Mahler and Diene (2007)	800 (5 bar porous stone) and 1465 (15 bar porous stone)	Flooding under vacuum, cyclic pressurization	Smoothness of the acrylic housing
Jotisankasa et al. (2007)	350	Flooding under vacuum, constant pressurization at 1500kPa	-

*by using Ridley et al. (2003) tensiometer

Ridley et al. (2003) and Take and Bolton (2003) highlighted the importance of performing the first immersion of the probe in water under vacuum and, in particular, Take and Bolton (2003) stressed the importance of fully drying the tensiometer before the first contact with water. Guan and Fredlund (1997) highlighted the importance of applying cyclic pressurization while Tarantino and Mongiovi (2001) found that the subsequent cavitations increased the maximum measurable suction. On the other hand, Sjoblom (1996) emphasized the importance of the shape of the porous stone and the distribution of voids inside it.

2.4.4. Calibration

The performance of tensiometers strongly depends on their saturation (as this controls the maximum measurable suction) but also in their accurate calibration. Recent studies have focused on the former, particularly aspects of the pre-conditioning procedure employed for saturation, such as the magnitude and duration of the positive pressurization stage and the effect of initial flooding of the tensiometer under vacuum (e.g. Take and Bolton, 2004, Tarantino and Mongiovi, 2001). Calibration has however received less attention, with only one dedicated study by Tarantino and Mongiovi (2003) to the author's knowledge.

Calibration is the relation between a known imposed value (input) and the read value (output). For a tensiometer the input is water pressure and the output is a DC voltage. A calibration factor, *m* is derived (assuming a linear relationship between input and output using a least-squares regression technique) where *m* is the ratio of water pressure in kPa to voltage in μV. Calibration error is the difference between an imposed value of suction and the value obtained from the calibration equation using the measured output. As tensiometers work in the negative pressure range, calibration should ideally be done by imposing negative pressure values. However, due to the difficulty in generating negative water pressures within the environment of conventional soil mechanics laboratories, tensiometers are generally calibrated in the positive range and a linear extrapolation of the calibration equation is assumed to the negative range (Sjoblom, 2000, Take and Bolton, 2004, Meilani et al., 2002).

Table 2.5 contains a summary of tensiometer calibration methods which will be examined in turn below. The only direct method to calibrate in the negative pressure range (suitable for high suction tensiometers) employs pressurization from the back of the tensiometer. This technique has the advantage of replicating the exact

conditions in which the tensiometer will be used. Pressurization from the back of the tensiometer induces a deflection of the transducer diaphragm in the direction of the soil, i.e. in the same direction as a negative pressure in the reservoir. In Tarantino and Mongiovi (2003) a similar tensiometer was used but with a strain gauged diaphragm replacing the transducer, behind which was a sealed chamber that could be pressurized. The extrapolation error was found to be 1-1.5% which, the authors state, justifies extrapolation in this case.

Table 2.5: Methods of tensiometer calibration

Range	Technique	Direct or Indirect?	Imposed	Medium in which measurement is taken
positive	transducer	direct	water pressure	water
negative	vacuum	direct	water pressure (>-100kPa)	water
	isotropic unloading	indirect	water pressure in cell	saturated soil
	axis translation	indirect	air pressure	saturated/ unsaturated soil
	back pressurization	direct	air pressure	air

The technique proposed by Tarantino and Mongiovi (2003) is probably the most suitable for calibration since it replicates the effect of a negative pressure in the diaphragm. However the technique requires adapting the tensiometer for air pressure application from the back, which implies that each tensiometer has to be designed and built so that it can easily be switched between calibration, saturation and use. This makes the technique somewhat impractical and complex. In the case of the tensiometer used for this research, it was not possible to pressurize through the electrical wires because a cement sealant completely isolates the back of the transducer. This is a necessary feature for a tensiometer that may be used in a submersible environment, such as a triaxial cell.

Indirect methods to assess the validity of extrapolation have greater applicability than the direct method described above and have been more widely used in the past. These include the axis translation method and the isotropic unloading method. Both techniques impose a known suction to an instrumented soil sample. The suction read by a tensiometer attached to the sample using the extrapolated calibration equation is then compared to the applied suction and accuracy of extrapolation is then measured. In addition it is possible to apply small negative pressures (down to -100 kPa) using a vacuum pump attached to a triaxial cell but this has limited application for high suction tensiometers.

The axis translation technique imposes a known value of suction on an unsaturated soil sample by elevating the pore air pressure while keeping pore water pressure at atmospheric value. The air pressure is subsequently reduced in steps preventing water inflow to the sample while a tensiometer in contact with the soil sample measures the corresponding decreases of pore water pressure (in the negative range). Assuming that equilibrium is attained at the imposed value of suction, the tensiometer should read a negative value of pore water pressure identical to the corresponding reduction in pore air pressure. Guan and Fredlund (1997) used this technique to investigate the accuracy of extrapolation on clay and silt samples in the pressure plate. The calibration error was between 0.5% and 8.5%. However these values should be taken as indicative because the tensiometer used by the authors had a resolution of approximately ±20kPa and the difference between the measured and imposed values was within 2kPa to 26kPa. In Guan and Fredlund (1997) study the observed tendency was for suction to stabilize at smaller values than those imposed, after each drop of the air pressure. This was interpreted as water transfer from the porous stone to the sample.

The isotropic unloading technique uses a tensiometer to read the negative pore water pressure imposed by undrained unloading of a soil sample initially consolidated to a given effective stress under a backpressure equal to or greater than zero. According to the effective stress principle, any change in mean total stresses in undrained conditions should generate an equal pore water pressure change. Ridley and Burland (1993) tested kaolin samples consolidated to different values of effective stresses (up to ~1500kPa) with a constant backpressure of 200kPa. The samples were then unloaded with the drainage line closed while the generated soil suction was measured by the tensiometer. Subsequently the samples were re-loaded still under undrained conditions to the same initial total stress and the backpressure was

again measured to calculate the corresponding effective stress (which was in general different from the value initially imposed). The error was calculated as the difference between the suction measured by the tensiometer and the imposed effective stress. Ridley and Burland (1993) found that the error was smaller if the effective stress measured after reloading was used in the calculation, as the suction read by the tensiometer was noticeably smaller than the effective stress initially imposed (i.e. before unloading of the sample). The lower effective stress measured after reloading was attributed to the occurrence of swelling associated with air coming out of solution during unloading.

2.4.5. Measurement

From the three parts of tensiometer studies (saturation, calibration and measurement), measurement has received less attention. Aspects related to the installation of the tensiometer or contact soil-stone are equally important to obtain suction values representative of the sample conditions. For example, a measurement of suction at constant water content should give a flat line where suction increases and flattens (top curve in Figure 2.40). Any deviation from this implies that the measurement is not correct. In the case of a slowly descending line it might be thought that the water evaporates because the box where the measurement is done is not air tight enough, however it was found in this research that if there are open spaces in the box water evaporates and condenses in the walls. Therefore the simple requirement of a well closed box is not enough to explain a slowly descending curve and to get an accurate measurement (this is illustrated schematically in Figure 2.40).

In the literature, topics related to the measurement appear spread in papers related to the saturation or calibration of tensiometers. The topics studied include the contact between the soil and the porous stone, set up and equipment for suction measurement, osmotic efficiency of the stone, and types of curves of suction measurement and their meaning.

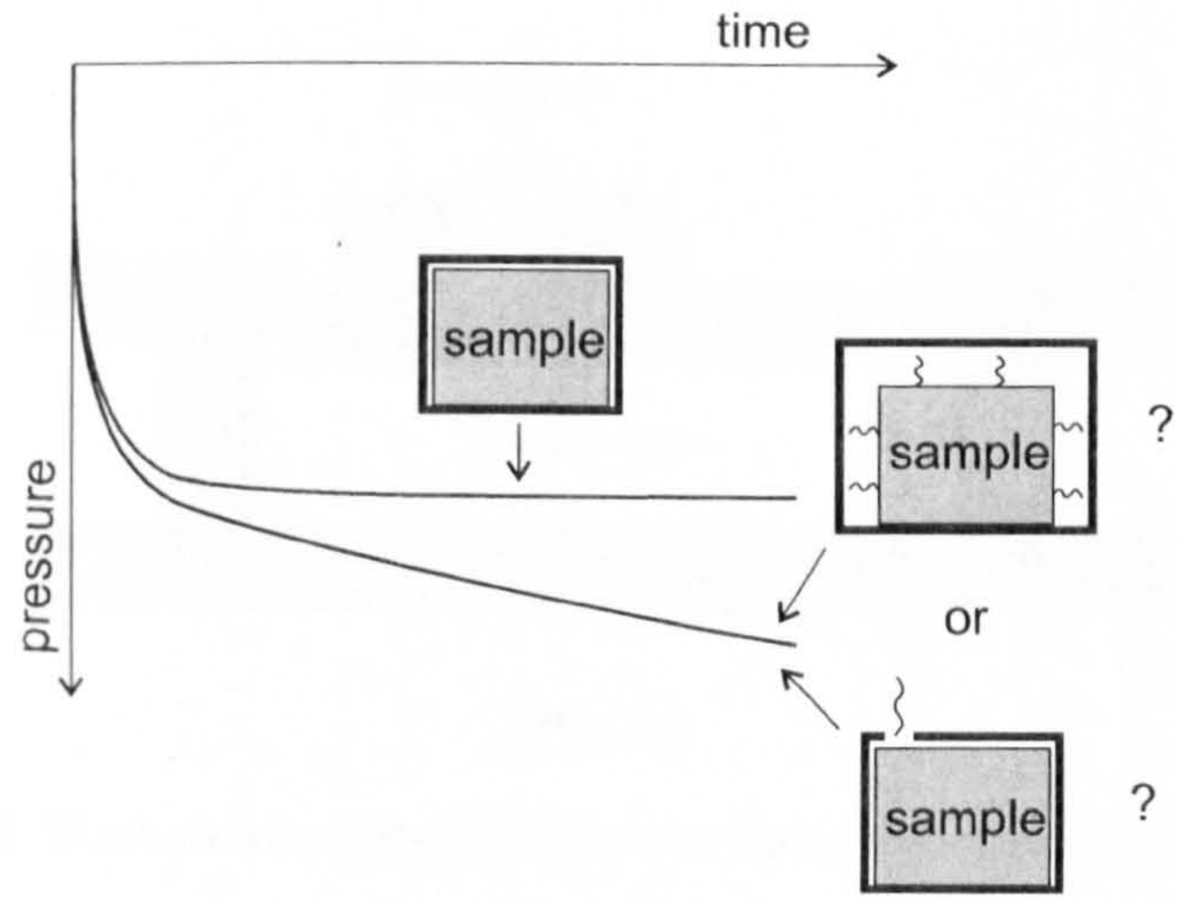

Figure 2.40: Schematic illustration of the factors affecting the correct measurement of suction

To improve the contact porous stone – soil, the usual adopted solution is to add a clay paste between the porous stone and sample. The paste acts as a second deformable interface (the porous stone is also an interface but is rigid), that links the stone to the soil. This solution was commonly adopted by various authors (e.g. Oliveira and Marinho (2008), Ridley and Burland (2003), Cunningham (2000) irrespective of the soil tested. Mantho (2005) considered the paste essential because some of his measurements were conducted in chalk. Interestingly, Mantho (2005) also states that that another reason to use the paste is that it slows down the suction increase and so prevents premature cavitation.

Suction measurements at constant water content have been carried out in air tight boxes with holes to insert the tensiometers (Figure 2.41). In Tarantino and Mongiovi (2003) set-up, the tensiometer is positioned above, while for Ridley et al. (2003) the tensiometer is below the sample. Other authors add a weight on the top of the sample to force the contact (Mantho, 2005).

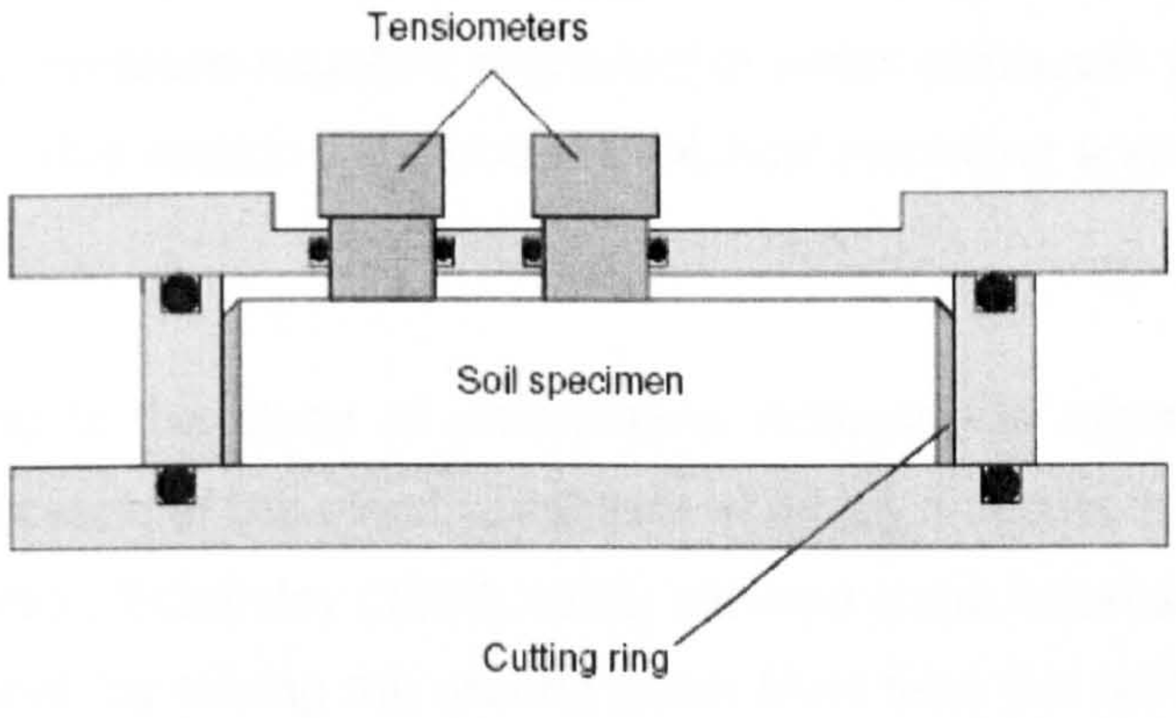

Figure 2.41: Suction measurement box by Tarantino and Mongiovi (2003)

Ridley et al. (2003) showed that the shape of the suction curve depends on external factors. For example, in Figure 2.42 it is shown that if the tensiometer's stone has no film of water, the readings overshoot the soil's suction.

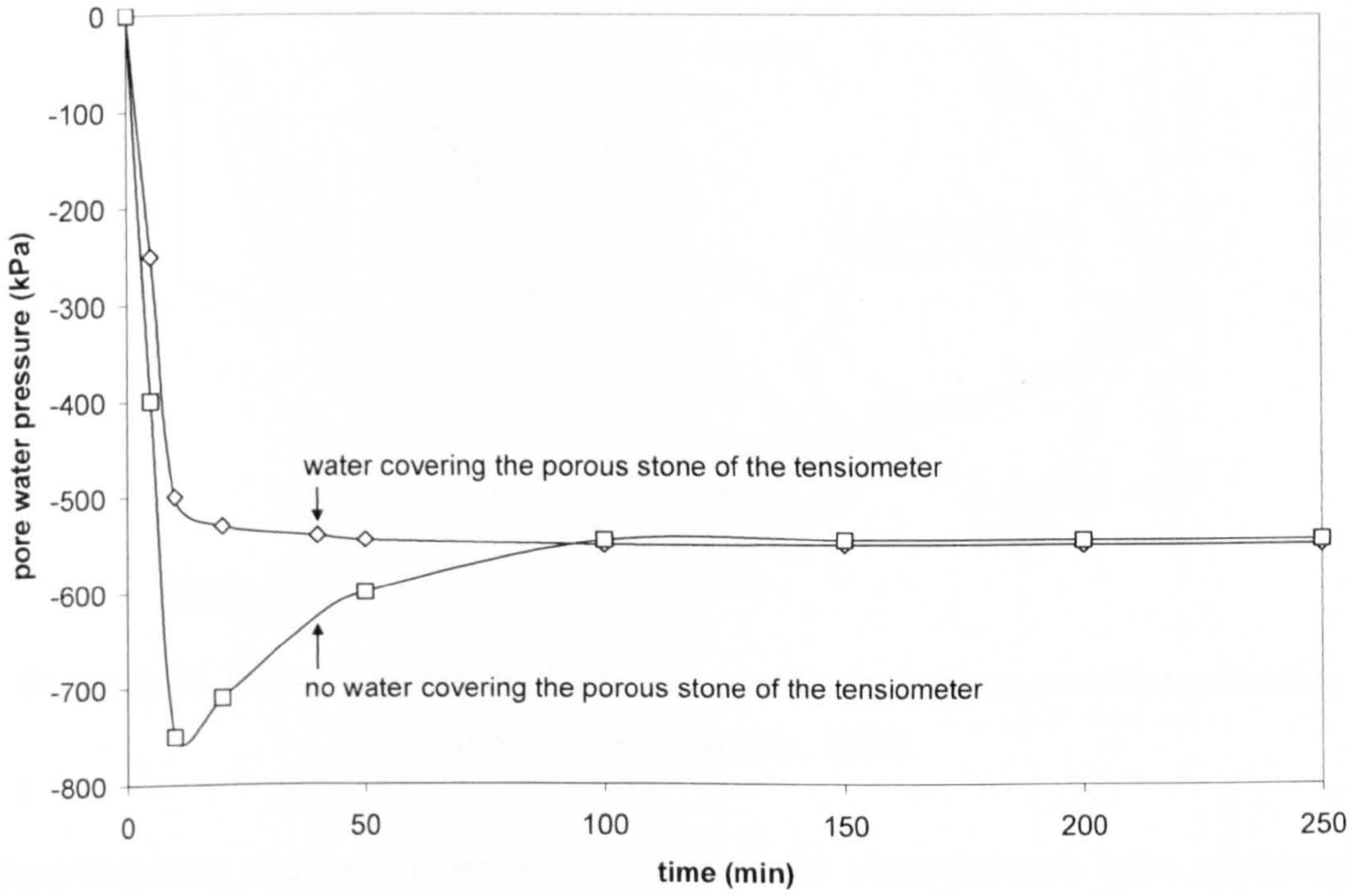

Figure 2.42: Influence of moisture in the stone on the suction measurement (after Ridley et al., 2003)

Guan (1996) checked the osmotic efficiency of the Saskatchewan tensiometer by placing it saturated in sucrose solutions. The attempts gave a null reading. Therefore the probe had no osmotic efficiency.

High suction tensiometers have been employed in centrifuge tests due to their small size and ability to measure negative and positive water pressures (Take, 2003 and Chiu et al., 2005). This section will introduce physical modelling and review Take and Chiu et al. studies.

Physical modelling is the study of phenomena occurring in nature or man-made structures by replication of the exact conditions at which it occurs in laboratory scale models. For instance, Eckersley (1986, 1990) induced slope failures in small models made of coking coal, by raising the ground water level from the bottom, to study the failure pattern and the pore water pressures developing just before failure (Figure 2.43). Lourenço et al. (2006a) did similar tests in two layer physical models.

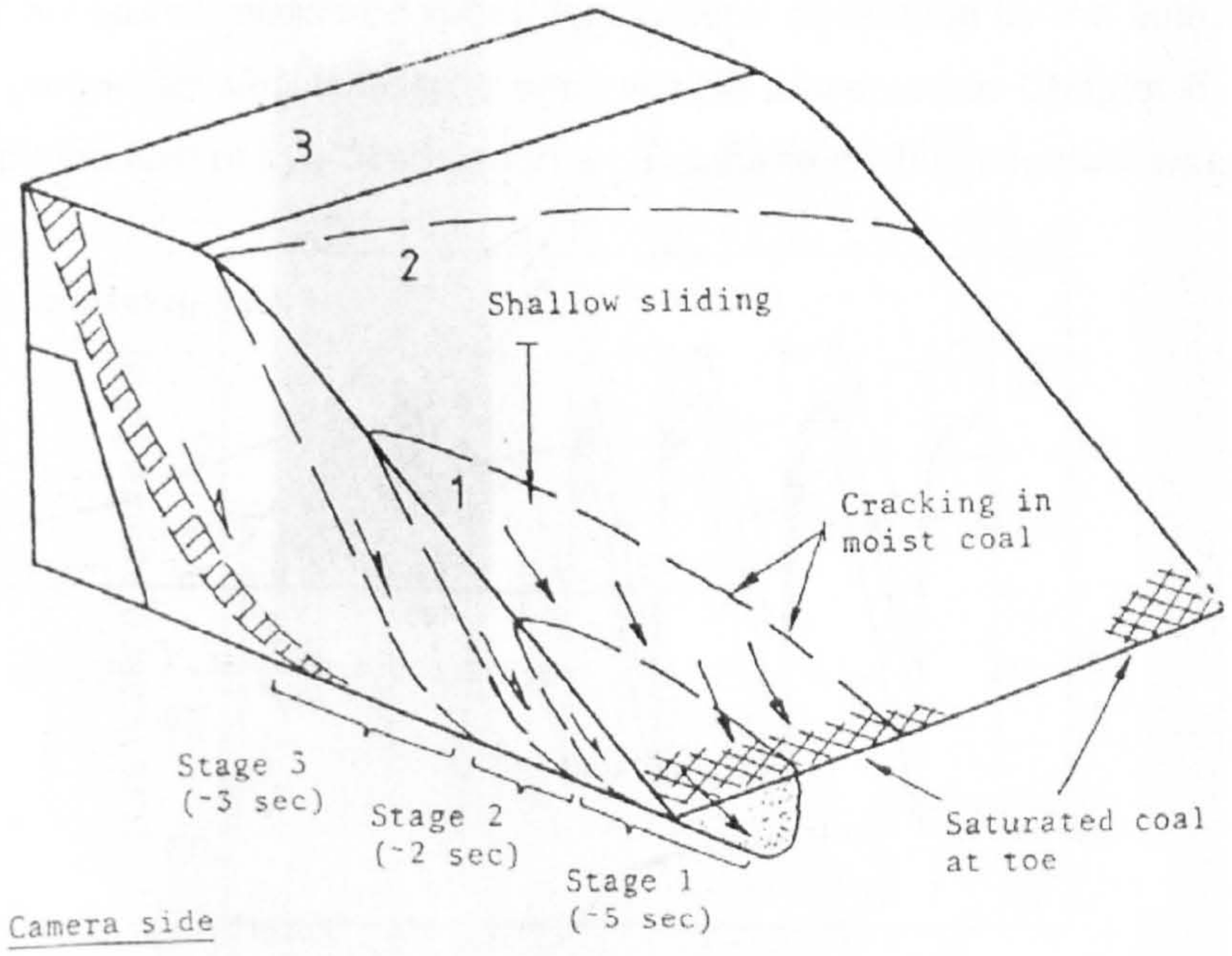

Figure 2.43: Physical modelling the failure sequence of coking coal in small scale models (from Eckerley, 1986)

Materials have a stress dependent behaviour. For instance, soils have increasing peak shear strengths for increasing confining pressures. This mean's that the same material will be more 'stable' at higher than lower confining pressures. The volumetric response also differs, at low confining pressures it tends to be dilative switching to contractive at higher pressures (e.g. Ali Rahman, 2008). These details are not immediately reproducible in the above models were tests were conducted at a gravity of 1g. However, if the small laboratory model is subjected to a centrifugal acceleration (by spinning it) it will become heavier resembling the real stress conditions. This can be understood following an example given in UCD (2005). If a

1m deep model container is filled with soil, placed at the end of a centrifuge and subject to a centrifugal acceleration of 50g, the stresses are increased by a factor of 50. So, the vertical stress at the base of the model container is equivalent to the vertical stress at a depth of 1m x 50 = 50m in the earth, the 1m deep model represents 50m of prototype soil.

There are at least two centrifuge studies in unsaturated soils with the water pressure measured by tensiometers (Take, 2003 and Chiu et al., 2005). Take (2003) study, investigated the behaviour of model clay embankments to a sequence of wetting/drying cycles in an atmospheric chamber. The measured pore water pressures are displayed in Figure 2.44. Tests were conducted at controlled RH with pore water pressures measured with a tensiometer developed by the author. Chiu et al. (2005) performed similar tests to what will be presented in Chapter 5. The goal was to study the flow of hydrocarbons in an unsaturated silt at constant water table.

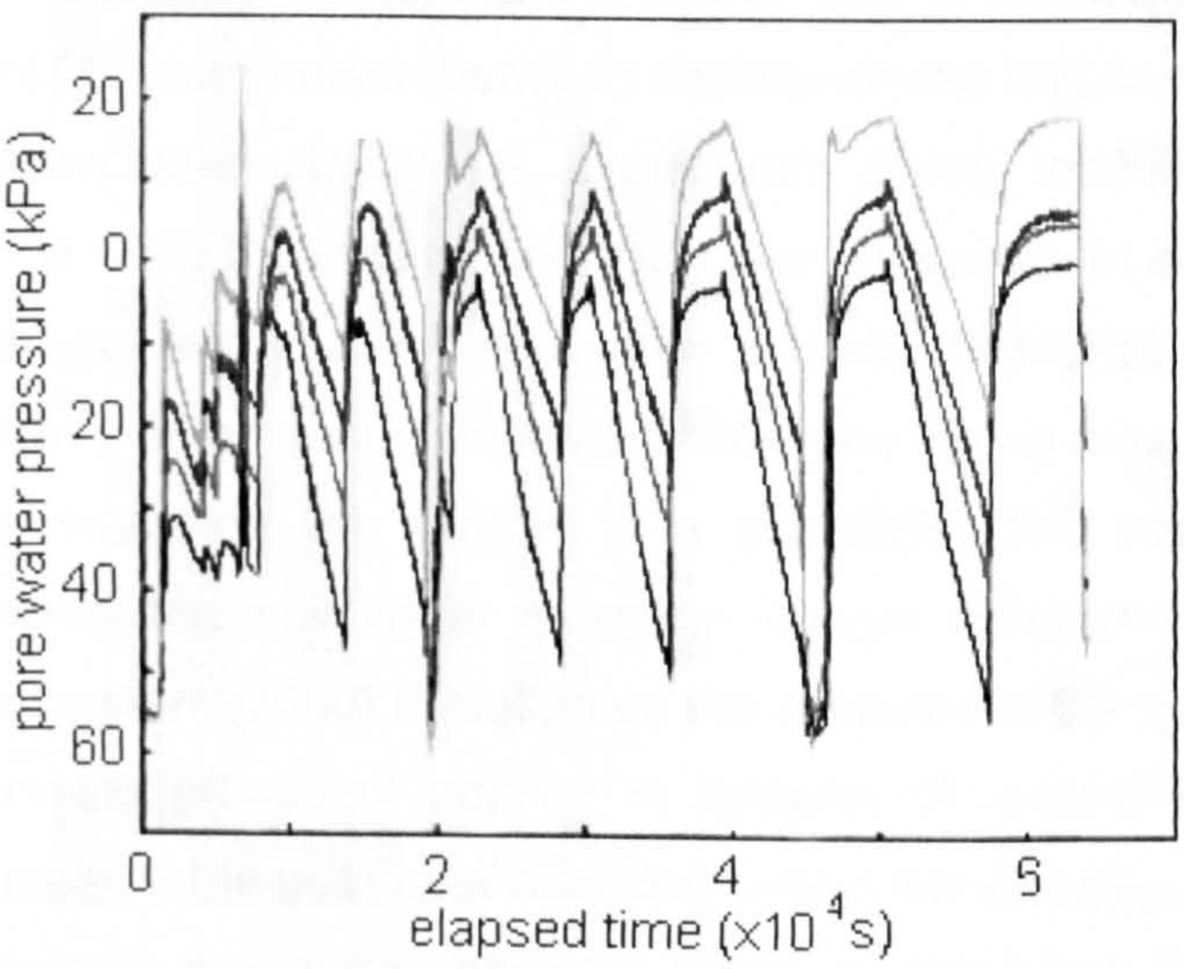

Figure 2.44: Wetting/drying cycles imposed to model clay embankments in centrifuge tests (each line represents the pore water pressure measured at different locations) (after Take, 2003)

2.4.6. Applications

Some applications of high suction tensiometers to laboratory testing will be reviewed in this section. Previous work on the soil water retention curve and suction control systems that use high suction tensiometers will be introduced next.

2.4.6.1. Soil Water Retention Curve

Recently, high suction tensiometers have emerged as an alternative instrument for the determination of the soil water retention curve, since they directly measure the water tensile stress and are faster than other suction measurement techniques.

Cunningham (2000), Toker et al. (2004), Boso et al. (2003), and Teixeira and Marinho (2006) determined the soil water retention curve by using an electronic balance to record the water content and a tensiometer to measure suction. Boso et al. (2003) presented a comparison between discrete drying and continuous drying for a sample of reconstituted clayey silt. Continuous drying mean's that the soil is continuously drying while the suction and mass are measured. In discrete drying, the soil is dried in stages with suction and water content measured after each drying stage in an air tight environment. The evaporation rate during continuous drying was slowed down by wrapping the sample in a geotextile. The results revealed no differences between the soil water retention curves determined using the two procedures. Cunningham (2000) investigated the influence of the evaporation rate for the continuous drying procedure applied to samples of reconstituted silty clay. In particular, he compared the soil water retention curves obtained by drying the sample continuously either to the atmosphere or inside a controlled humidity chamber. Similar results were obtained from the two procedures suggesting that the evaporation rate had little or no influence on the resulting soil water retention curve. Cunningham's study was the first for the determination of the SWRC with tensiometers. Figure 2.45a shows the set-up for continuous drying to the atmosphere and Figure 2.45b a comparison between the tensiometer data and the filter paper. These two studies also confirmed that tensiometers could be used to determine the SWRC in a significantly shorter period of time in comparison to other conventional testing techniques. Toker et al. (2004) did an in depth study on the continuous drying procedure in granular materials. Teixeira and Marinho (2006) used the discrete procedure to determine the SWRC and compared this to other techniques (pressure plate and suction plate).

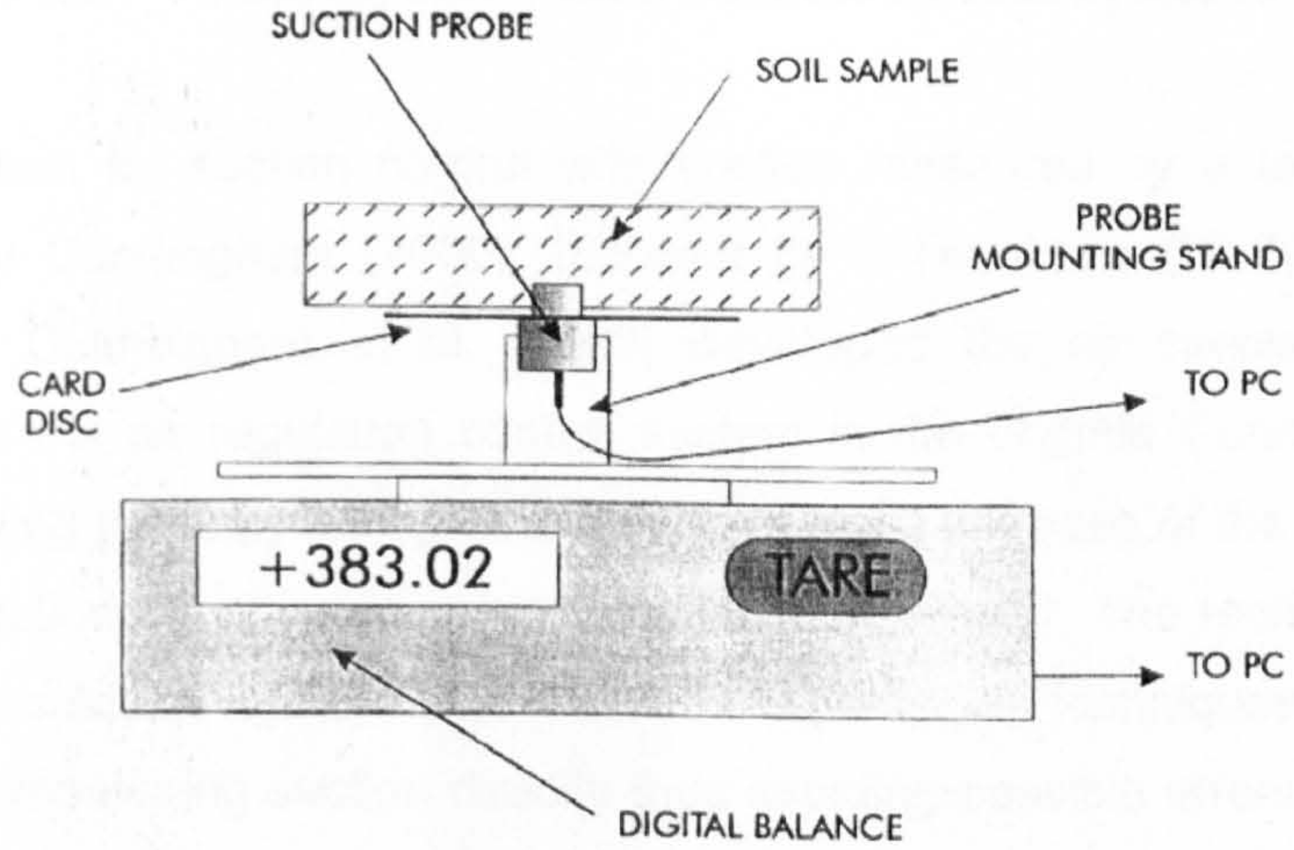

(a)

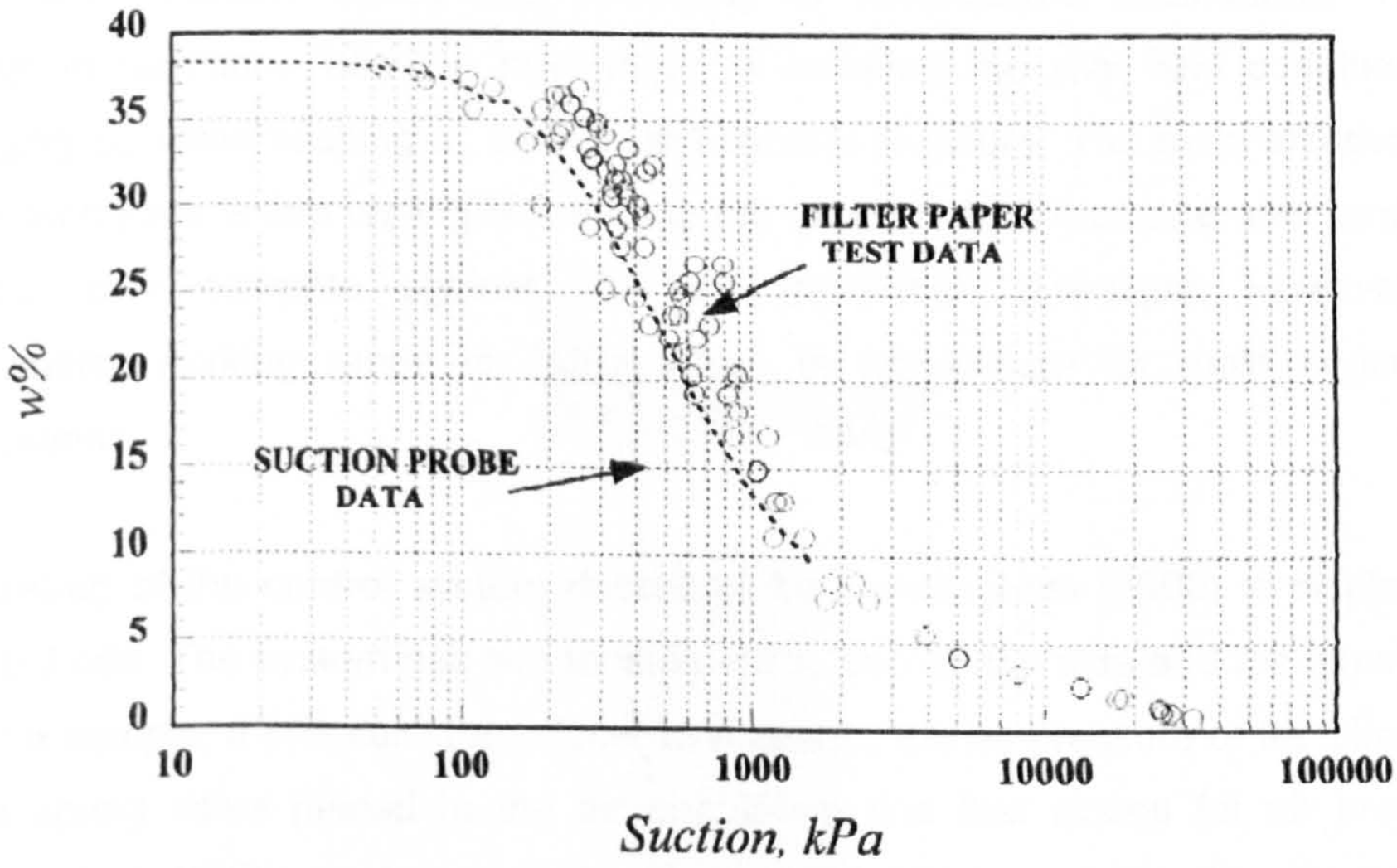

(b)

Figure 2.45: First study conducted on the determination of the SWRC with tensiometers, (a) set-up for continuous drying, (b) comparison between the continuous drying and filter paper data (from Cunningham, 2000)

2.4.6.2. Tensiometer based suction control systems

The first system for suction control with suction measured by a tensiometer was introduced by Cunningham (2000), followed by Jotisankasa (2005). Cunningham (2000) and Cunningham et al. (2003) developed the air circulation technique (described as the air regulation control system in the original Cunningham (2000) article) for drying paths by letting air circulate through the base of the sample and by measuring suction directly with a high suction tensiometer. The technique is based on an air circulation system like the RH equilibrium techniques, but has the advantage of measuring suction directly thus avoiding possible errors due to indirect nature of measurements of the hygrometer (Tang and Cui, 2005) or psychrometer (Blatz and Graham, 2000) and sensitivity to temperature fluctuations. The air circulation technique has the advantage of imitating the real field conditions, by changing u_w while keeping u_a at the atmospheric pressure. The main disadvantage of the technique is that testing is limited to the tensiometer's measurement range and so can only compete against the axis translation technique. However, the tensiometer working range is 2MPa which is appropriate for most engineering applications.

The set-up of the control system described by Cunningham (2000) is displayed in Figure 2.46a. The system has two tensiometers, one on the side and the other at the top of a sample, a pressure transducer to measure the air pressure of the circulating air, a spring valve placed in the air circulation line that closes for air pressures smaller than 15kPa, and a control software (TRIAX) to regulate the air pressure source. The control system worked by circulating air at the base of the sample and setting a target value of suction. When the target was reached, TRIAX would reduce the air pressure to below 15kPa to stop drying. As soon as suction had reduced to 5kPa less than the target value, the system responded by switching the air supply back on. The system was just for monotonic drying. Wetting paths could not be followed. A further limitation was that water content measurements were not incorporated.

Figure 2.46b plots suction measured by the top and middle tensiometers against time for a sample initially saturated that was dried until 850kPa, loaded isotropically to a confining stress of 400kPa, and then sheared at constant suction. Both the isotropic stress and deviatoric stress were applied at constant suction in such a way that suction did not exceeded ±15kPa of the target value.

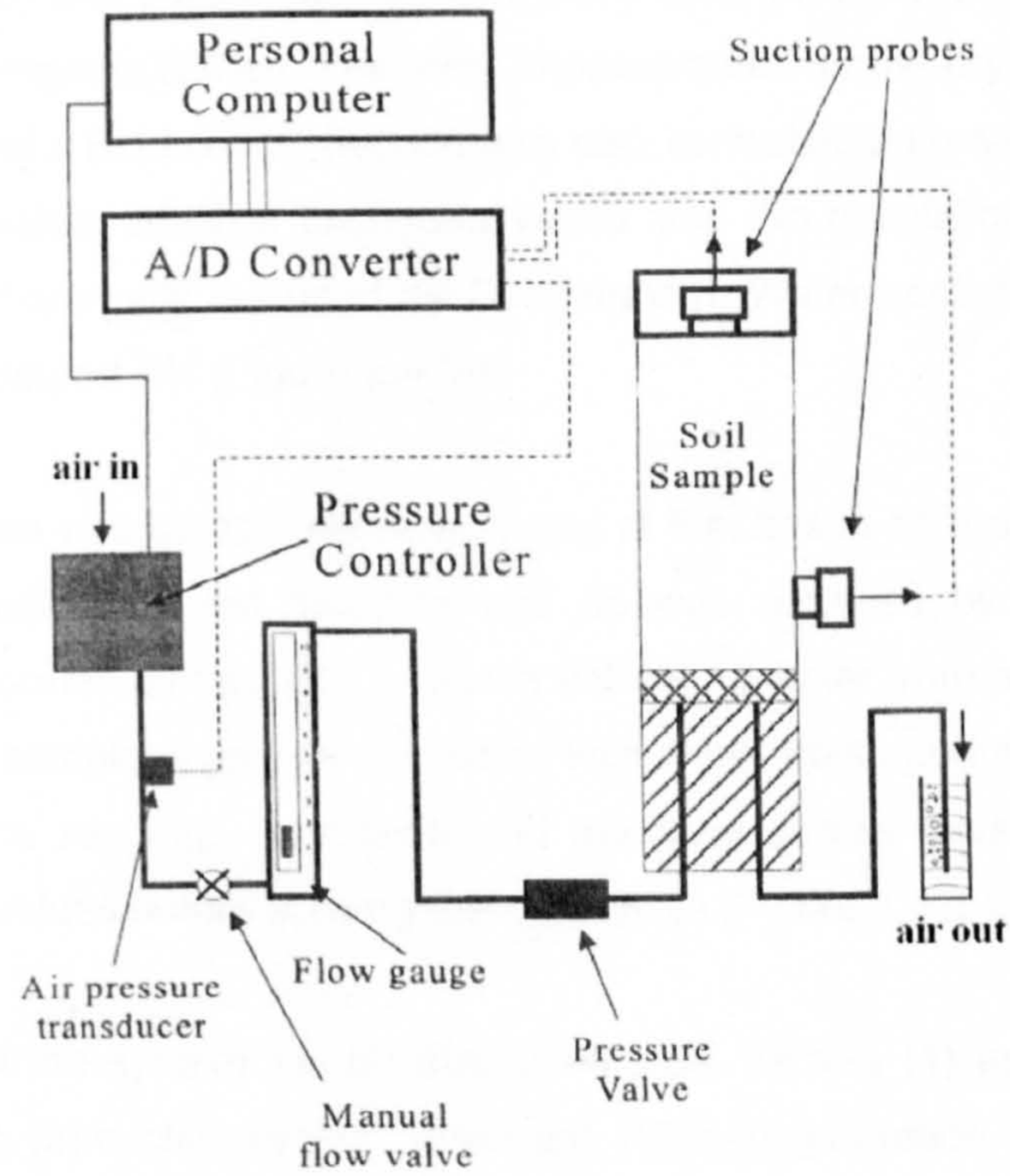

(a)

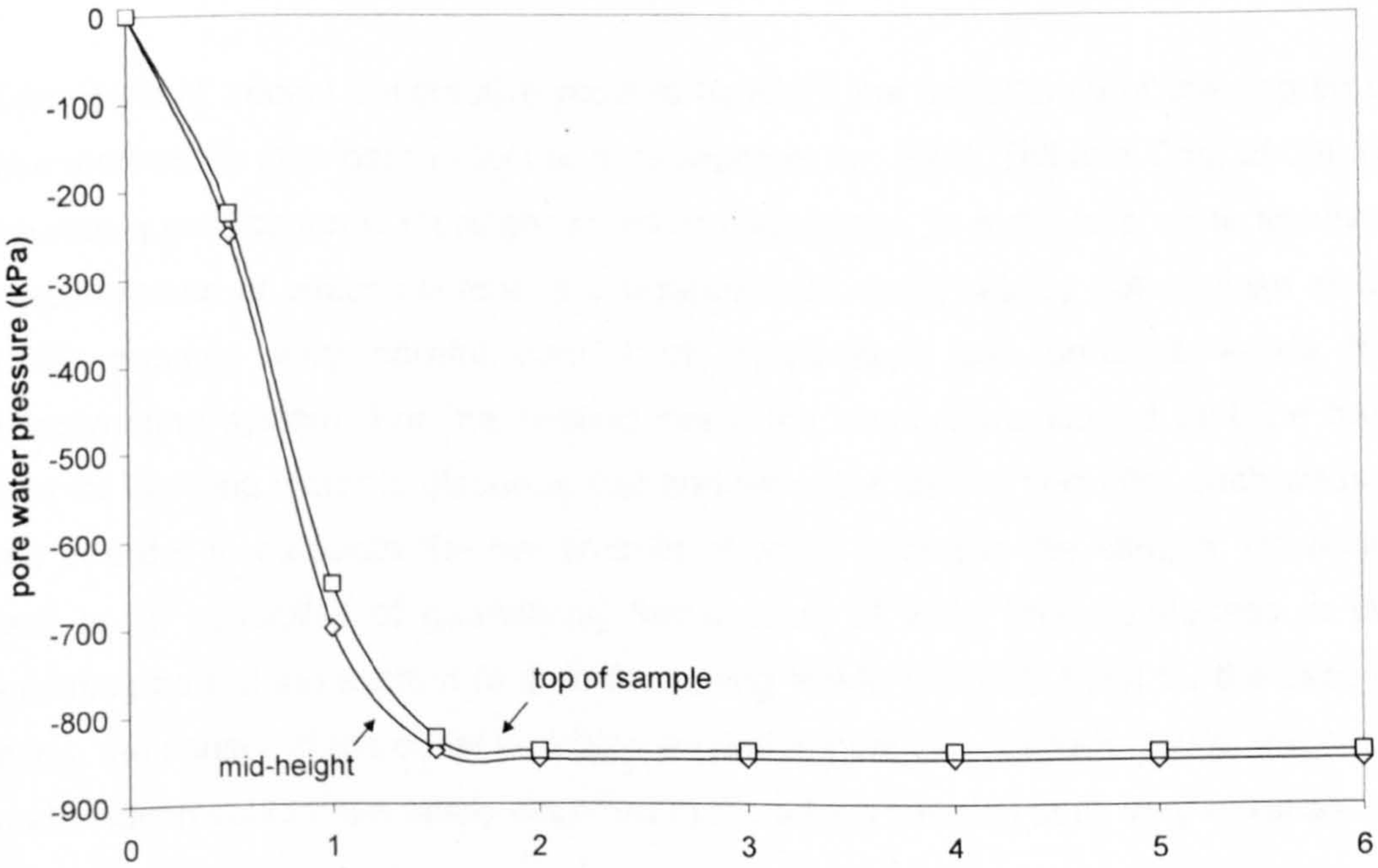

(b)

Figure 2.46: The air circulation system by Cunningham (2000), (a) set-up for drying, (b) results (after Cunningham et al., 2003)

Jotisankasa (2005) and Jotisankasa et al. (2007) describe a further development of the work by Cunningham (2000). The main improvements for the drying system were the incorporation of a RH sensor. Suction was also controlled automatically by setting a suction target value, which if exceeded would stop the circulation. Air circulation was through the base only, as used by Cunningham. Water content was estimated based on the measured RH (Figure 2.47a).

The wetting system was completely new. It was at first based on moist air circulation but proved ineffective to wet samples and so was replaced by water injection. Wetting was performed by injecting a known volume of water from a pipe connected to the top of the sample. Injection was done with a peristaltic pump in stages. After each injection, the readings of suction and the local strains were monitored until achieving stable values before starting the next stage (Figure 2.47b).

Some features of the system will be discussed next, namely (1) aspects related to the water content, (2) suction cycles (reversals), (3) testing duration and, (4) pressure gradients across the sample. The analysis presented below summarizes a discussion by Lourenço et al. (2007b).

Water content: recent constitutive models highlight the importance of the degree of saturation within their parameters (e.g. Gallipoli et al., 2003, Toll and Ong, 2003). Its accurate quantification is therefore of prime importance. In order to provide accurate measurements of water content, the arrangement described by Jotisankasa et al. (2007) requires very careful control of temperature and pressure inside the drying/wetting system. For the wetting case, the authors mentioned that the tube used for injecting water is disconnected and weighted before and after each wetting step in order to calculate the net amount of water added to the sample. However, there is no possibility of quantifying the amount of water that condenses in the remaining part of the system (e.g. in the tubing inside the cell). Even for the case of drying, the sensor at the outlet indicates a relative humidity of nearly 100%; therefore condensation could have easily occurred in the tubing carrying such very moist air.

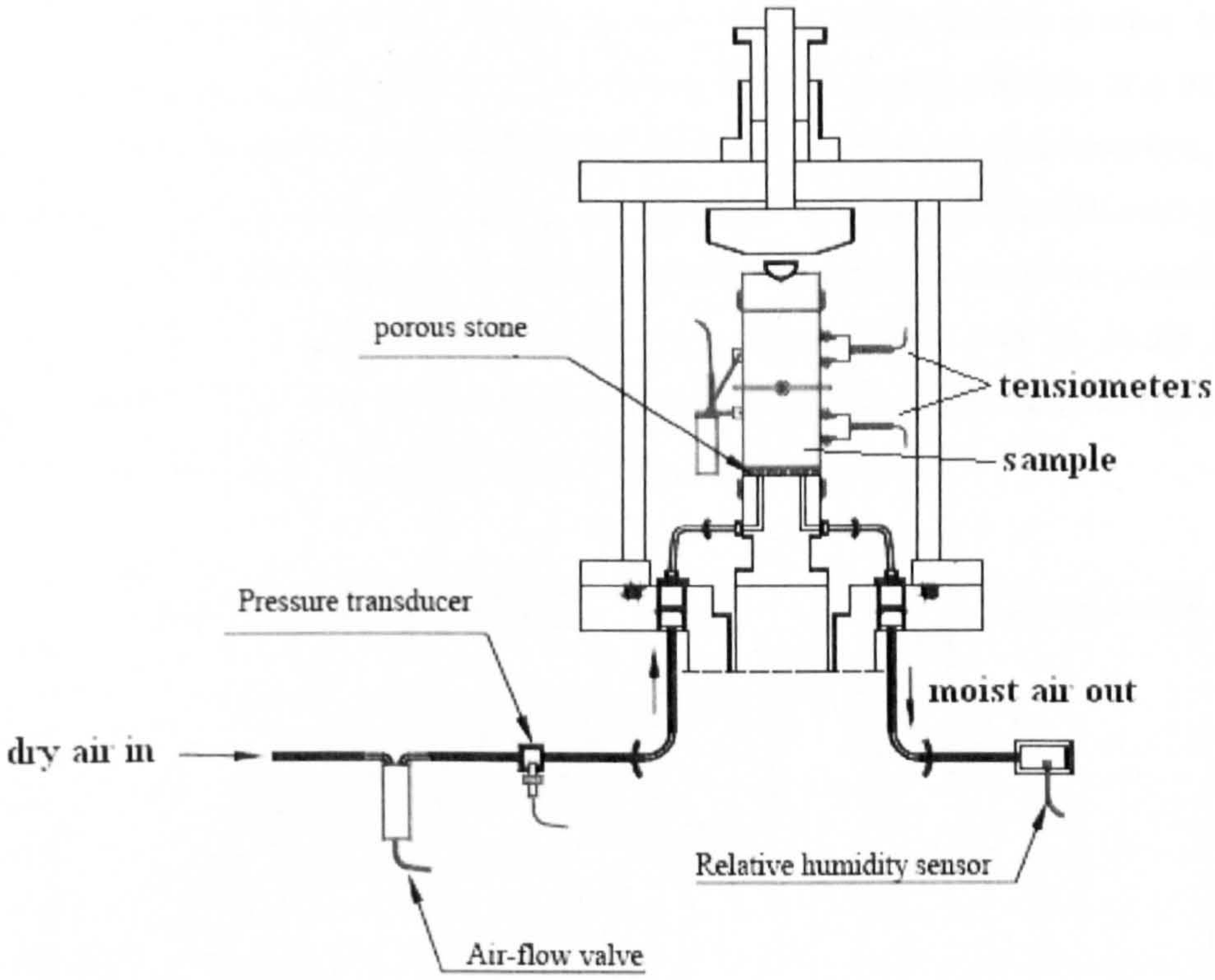

(a)

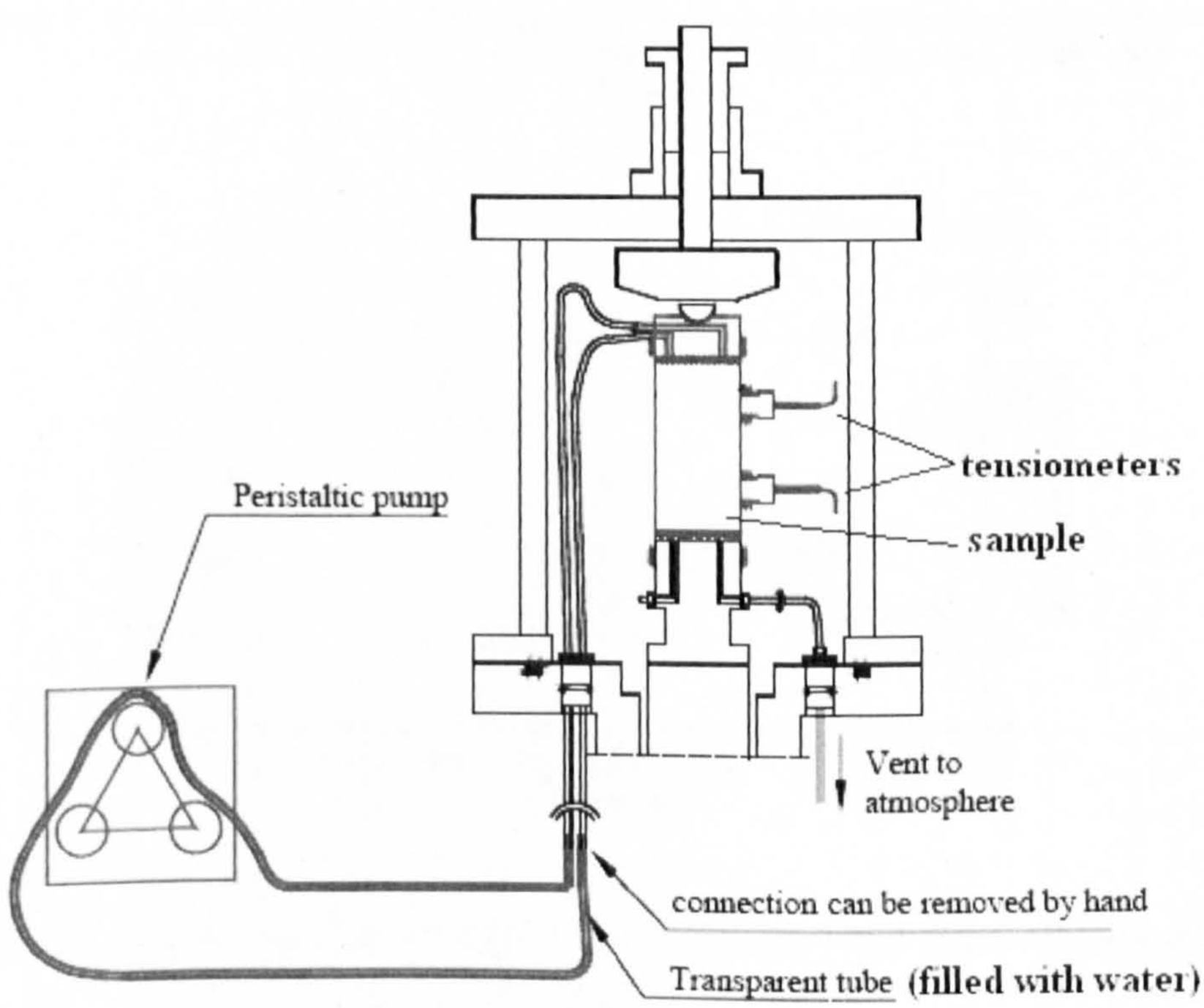

(b)

Figure 2.47: The air circulation system by Jotisankasa (2005), (a) drying system, (b) wetting system

Suction cycles (reversals): the wetting test in Figure 2.48a shows wetting being controlled in a series of coarse 'steps' (each involving a manual addition of a certain volume of water) followed by an equalisation process in which suction reverses. The suction changes are rather large, involving a reduction of about 80kPa followed by an increase of about 50kPa. Suction reversals should instead be as small as possible in order to preserve the monotonic nature of the stress path and to avoid local irreversible changes of volumetric and hydraulic properties of the soil during cyclic variations (Wheeler et al., 2003) (will be discussed in Chapter 3).

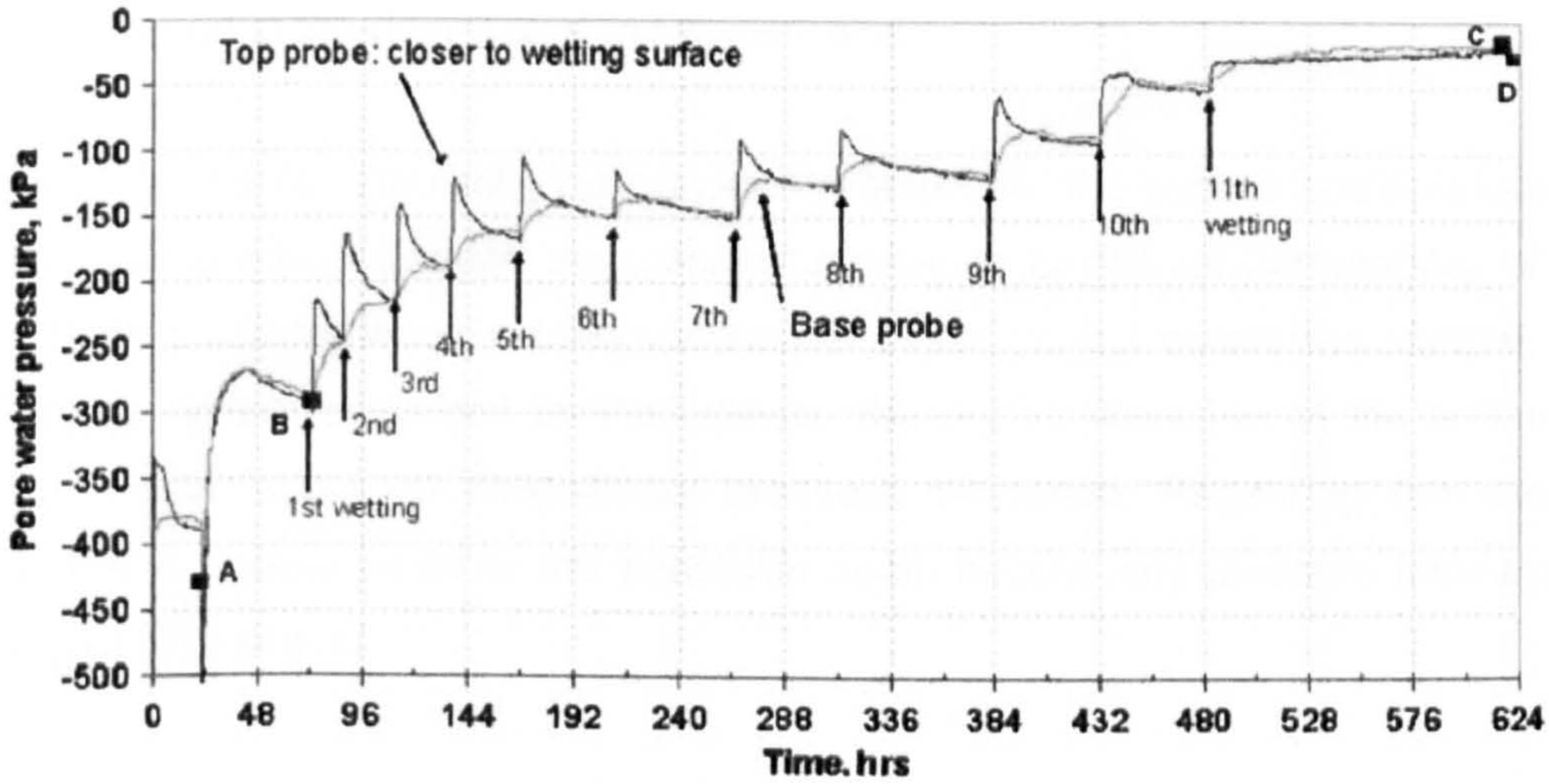

(a)

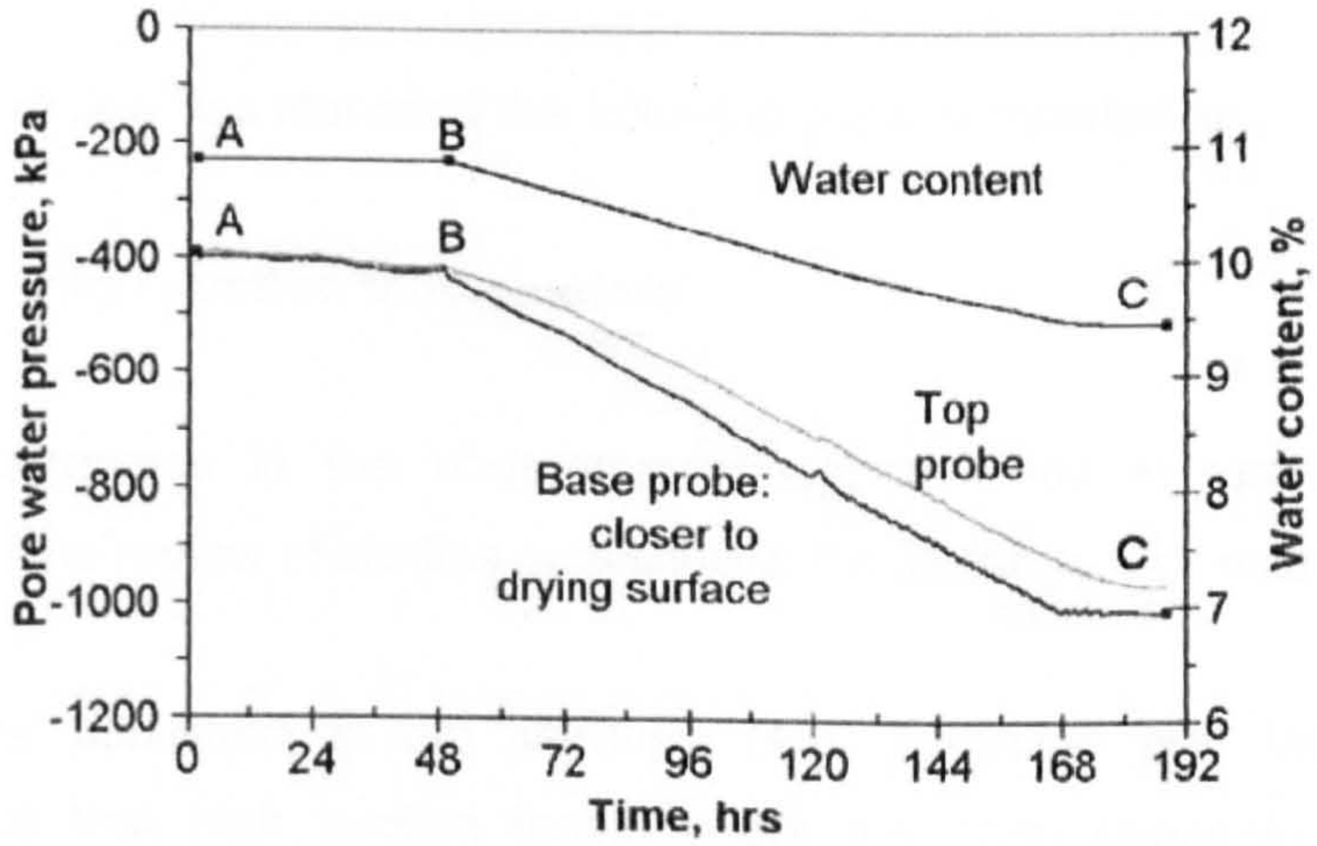

(b)

Figure 2.48: Time series of a drying test, (a) TC27, (b) TC23 (from Jotisankasa et al., 2007)

In the drying system section, Jotisankasa et al. say that "in order to dry the sample in a suction-controlled manner, an air-flow valve was introduced for switching the flow on and off, depending on the suction reading from the suction probe that was closest to the drying surface". The drying test in Figure 2.48b does not show any suction reversals (unless the suction reversals are so small that they cannot be detected by visual inspection).

Testing duration: it is interesting to note that the test duration for the drying test from point B to C (Figure 2.48b) was three times faster than the wetting test (for a greater suction change in the drying test) in Figure 2.48a.

Pressure gradients: circulating air only at the bottom of the sample could induce an air pressure gradient through the sample (depending on the air permeability of the soil). Such gradients would unbalance the net stress (σ_3-u_a) across the sample. For the drying system described by the authors, the dry air flowed in at the bottom at 10kPa, which is not an insignificant pressure difference. Regarding the wetting system, it is unclear whether the peristaltic pump caused any pressure increase at the top of the sample.

2.5. GAPS IN KNOWLEDGE

The literature review has identified the following gaps in knowledge:

2.5.1. High suction tensiometers

Some inconsistencies in the understanding of cavitation in tensiometers have emerged from the review of studies published in the literature. For example:

a) Results published in the literature (e.g. Tarantino and Mongiovi, 2001) indicate that high suction tensiometers are often capabale of measuring suctions well above the air entry value of the porous stone.

b) Progressive air diffusion from the atmosphere into the tensiometer would facilitate cavitation as described by Ridley et al. (2003). On the other hand, this is not compatible with work by Tarantino and Mongiovi (2001) where it is shown that the prolonged use of tensiometers for suction measurement on

soil samples seem to improve their performance. A similar response was found for the Imperial College tensiometers by Jotisankasa (2007).

c) No one has attempted to predict quantitatively cavitation in tensiometers for suctions higher than 100kPa. The conceptual model by Take (2003) and Ridley et al. (2003) do not include some essential aspects. For instance, Take's model does not include the flooding stage, and both authors do not take into consideration the contact angles.

d) There is not general agreement between different studies on the most important factors of the saturation process for the achievement of high values of suction at cavitation. Authors that applied higher pressurization values measured suctions at cavitation that were lower than those measured by authors who applied lower pressurization values. For instance, Guan and Fredlund (1996) applied a pressurization stage of 12MPa for 24h and measured a cavitation suction of 1600kPa while Tarantino and Mongiovi (2001) applied a pressurization stage of 4MPa during 24h and measured a cavitation suction of 2500kPa. Therefore a simple direct relationship linking pressurization magnitude to maximum suction at cavitation is not valid and additional factors controlling cavitation must be accounted for.

It is still unclear whether the calibration in the negative range by extrapolation from the positive is correct. The errors obtained in the above studies are variable and in some cases large (0.5-8.5% for Guan and Fredlund, 1997). The errors also seem to depend on the technique and procedure. Both Ridley and Burland (1993) and Tarantino and Mongiovi (2003) got lower errors, but in the case of Ridley and Burland (1993) it depended on the value of cell pressure and backpressure picked up (before unloading or after reloading). Therefore, more work is needed on the calibration of high suction tensiometers in the negative range.

The main question regarding suction measurement with tensiometers is: how do we know that the suction measured is 'correct'? or, how do we know that the equilibrium conditions were reached so that we could take the correct value of suction? While some work has already been done, most of the understanding is incipient. Other gaps include:

(1) According to Kelvin's law it could be possible to measure total suction with the tensiometer because if the RH is sufficiently high, water menisci would condense between the porous stone grains until reaching equilibrium with the imposed RH.

(2) There are no studies quantifying the response time of tensiometers, or on the implications of the response time for a sample that is continuously drying or wetting.

(3) With only two studies conducted, there is still much to explore in unsaturated soil testing with the centrifuge. One topic that comes from the two studies presented above is the time for suction to reach equilibrium. Chiu et al. (2005) shows the curves flattening, but not Take (2003) data, where suction increases linearly during drying and is suddenly reversed due to wetting. This topic will be further discussed in Chapter 3.

Chapter 3 will attempt to clarify some of these inconsistencies and questions.

2.5.2. Applications of high suction tensiometers

The main disadvantages of current suction measurement systems is that, with the exception of the tensiometer, no other provides direct measurements of suction. For water content there seem to be no systems for controlling this variable.

The literature review on the SWRC with tensiometers revealed some contradictory results. For instance, Cunningham (2000) says that the evaporation rate had little or no influence on the SWRC, while Boso et al. (2003) concluded that continuous drying agrees with discrete drying curves only if the evaporation rate is decreased. It is clear that further research is needed and this lead to the study in Chapter 4 on the procedures for the determination of the SWRC with the tensiometers.

The following limitations were found in the tensiometer based suction control systems reported by Cunningham and Jotisankasa: suction reversals for the wetting surface are too large (>50kPa); the wetting system and drying systems do not consider condensation in the pipes during drying or retained droplets in the pipes for wetting; the water content measurement is calculated indirectly based on assumptions (constant RH/air flow rate) of the air flowing out. These two works do add greatly to

the development of unsaturated soil testing. With the development of commercially available tensiometers having capacities exceeding 1500kPa such test procedures are likely to become common-place, once the limitations of the control systems discussed have been overcome. A more sophisticated automated system for suction control with water content measurement, building on the work of Cunningham (2000) and Jotisankasa (2005), is described in Chapter 5.

2.5.3. Particle level testing

There is a need to start developing techniques for "testing" at small scales because unsaturated soil behaviour is controlled at the particle level. The techniques to be employed will depend on: (1) the accuracy required: whether measurements (quantitative) or estimations (qualitative) are obtained; (2) the parameter to be measured: stress, strain, suction, water content; (3) particle size scale: mm (sand) to μm (clay); (4) number of particles to be tested: single particle to particle contact or group of particles. A technique with particular interest to unsaturated soil mechanics is the Environmental Scanning Electron Microscope (ESEM). It allows hydrated samples to be observed in their original state, unlike the conventional Scanning Electron Microscope (SEM) where samples dry during observation. Mechanical testing also appears to be possible. The ESEM has also the capability of conducting dynamic experiments where the total suction in the sample can be varied by changing the relative humidity and temperature inside the microscope chamber. Chapter 6 explores the potential of Environmental Scanning Electron Microscopy for particle level studies in unsaturated soils.

2.6. CHAPTER SUMMARY

2.6.1. Suction, water retention and volume variations in soils

This section has reviewed basic concepts of unsaturated soil mechanics relevant to this dissertation. All work conducted (experimental developments or soil studies) surrounded three aspects of behaviour: suction, water retention and volume variations. Suction and water retention were reviewed separately (in sections 2.2.1 and 2.2.2) and then combined to include the volumetric component in section 2.2.3. Suction was defined in terms of capillarity and through Kelvin's law; its significance to soil mechanics was expressed in terms of meniscus forces. For the water retention,

both retention from vapour or capillary water were presented. Section 2.2.3 includes a review of the shrinkage and swelling of soils and the SWRC was introduced. Non-geotechnical literature was also reviewed. Unsaturated porous media is a topic of interest also to soil science, physical hydrology and physical chemistry. There are a huge number of papers in these fields, particularly in physical chemistry, with knowledge than can be adapted to geotechnical engineering. One of the topics, hydraulic hysteresis, has been extensively studied so it has been presented in more detail in section 2.2.4.

2.6.2. High suction tensiometers

All existing tensiometers were presented, including their structure and working principle. The current understanding of cavitation was reviewed focusing on cavitation from surfaces which is likely to be the true origin of bubbles in tensiometers. Key works on cavitation from surfaces were reviewed in detail (Harvey et al., 1944) and other more recent works that show micron-sized bubbles (Ishida et al., 2000) and cavitation from similar size bubbles (Bremond et al., 2005). Then cavitation in tensiometers was reviewed with the current cavitation mechanisms detailed. The procedures to saturate tensiometers were presented.

The literature on tensiometers calibration was reviewed. Because tensiometers measure water pressure well below -100kPa, special techniques are needed to create such values. Most common procedure is to calibrate in the positive range and extrapolate this relation to the negative. However, some authors worked directly in the negative range by using different techniques. Guan and Fredlund (1997) used the axis translation technique, Ridley and Burland (1993) isotropic unloading, and Tarantino and Mongiovi (2003) pressurization from the back. Even if the errors obtained were considerably small, they seemed to depend on the technique used and the procedures followed for each technique.

In order to obtain correct values of suction, the measurement is as relevant as cavitation and calibration. The literature review revealed that it is not enough to place the tensiometer in contact with the soil. If the stone has too much water, suction will overshoot the sample's suction. Someone inexperienced with tensiometers could stop the test at the turning part of the curve and assume 750kPa as the correct value of suction, instead of 570 kPa as the actual value. Therefore, there are a series of factors (some of them identified in the gaps of knowledge) that are able to mask the

correct measurement of suction (e.g. response time). Physical modelling is an attractive experimental approach to study complex geotechnical phenomena (e.g., soil-structure interactions, tunnelling) under stress conditions equivalent to the field. Tensiometers can be used for such studies due to their small size and ability to measure pore water pressure directly. Two studies that used tensiometers were reviewed (Take, 2003 and Chiu et al., 2005). Take (2003) imposed a sequence of dry and wet conditions through the RH to study the long-term stability of clay slopes while Chiu et al. (2005) measured suction at different depths at a constant water level.

2.6.3. Tensiometer applications and recent developments in unsaturated soil testing

Previous work conducted for the determination of the Soil Water Retention Curve (SWRC) with tensiometers and tensiometer based suction control systems were reviewed. Four studies on the SWRC, one of them not published (Cunningham, 2000), were presented. All works were introductory and focused in particular aspects (e.g. testing procedure only, relative humidity effects).

Cunningham (2000) and Jotisankasa (2005) have presented a new suction control system for unsaturated soils based on air circulation with independent drying and wetting systems and direct measurement of suction. This new technique has several advantages: (1) as stated by Jotisankasa et al. (2007) "the principal advantage of these systems is that high suction can be controlled without raising the ambient air pressures as is required with the axis-translation technique"; (2) it measures suction directly by means of a high suction tensiometer able to reach 1500kPa while, for example, techniques based on the relative humidity equilibrium of the system calculate suction indirectly via a thermodynamic relation with the water vapour pressure; (3) the suction range (up to 1500kPa depending on the tensiometer) provided by this new technique is of most interest for geotechnical engineering problems. This new technique can therefore constitute a reliable alternative to the commonly used axis-translation technique. While the technique described by Jotisankasa et al. (2007) is a major advance in unsaturated soil testing, there are some limitations in what they propose. Recent developments in experimental unsaturated soil mechanics have been centred on improvements to standard devices to measure suction, or on improving the techniques that control suction. Some of these 'improvements' were presented in this Chapter.

Chapter 3. A HIGH SUCTION TENSIOMETER

3.1. INTRODUCTION

Chapter 2 reviewed the tensiometers developed so far, their working principles and the prerequisites to measure suction. The phenomenon and importance of cavitation was discussed and the saturation and calibration procedures followed by other authors presented. Within this context, this chapter presents a new tensiometer in Section 3.2, examines the factors controlling cavitation in Section 3.3 and the calibration procedures in Section 3.4. Suction measurements with tensiometers have specific problems related to the fact that water pressure is measured directly and that they have a small contact area with the soil. Topics related to set-up, installation and factors affecting suction measurement will be addressed in Section 3.5. Findings are summarized in Section 3.6. As a result of these studies, the design of the tensiometer was modified and further alterations were proposed to Wykeham Farrance to improve its performance.

3.2. A NEW TENSIOMETER

3.2.1. Design

The new high suction tensiometer, in Figure 3.1a, is composed of (1) a porous stone (or filter) by Soil Moisture Corporation with an air entry value (AEV) of 15bar, (2) a reservoir of small dimensions ($5mm^3$) and, (3) a ceramic sensor to measure pressure. The length of the stainless steel casing is 23mm and is 14mm wide. The total mass (including the cable but not the electrical plug) is approximately 72g.

Chapter 3. A HIGH SUCTION TENSIOMETER

3.1. INTRODUCTION

Chapter 2 reviewed the tensiometers developed so far, their working principles and the prerequisites to measure suction. The phenomenon and importance of cavitation was discussed and the saturation and calibration procedures followed by other authors presented. Within this context, this chapter presents a new tensiometer in Section 3.2, examines the factors controlling cavitation in Section 3.3 and the calibration procedures in Section 3.4. Suction measurements with tensiometers have specific problems related to the fact that water pressure is measured directly and that they have a small contact area with the soil. Topics related to set-up, installation and factors affecting suction measurement will be addressed in Section 3.5. Findings are summarized in Section 3.6. As a result of these studies, the design of the tensiometer was modified and further alterations were proposed to Wykeham Farrance to improve its performance.

3.2. A NEW TENSIOMETER

3.2.1. Design

The new high suction tensiometer, in Figure 3.1a, is composed of (1) a porous stone (or filter) by Soil Moisture Corporation with an air entry value (AEV) of 15bar, (2) a reservoir of small dimensions ($5mm^3$) and, (3) a ceramic sensor to measure pressure. The length of the stainless steel casing is 23mm and is 14mm wide. The total mass (including the cable but not the electrical plug) is approximately 72g.

The tensiometer was assembled by gluing the 3 parts into a stainless steel casing to form a single piece. None of the parts can be removed after assemblage. The transducer is separated from the porous stone by a metallic spacer. The tensiometer inner parts are shown in Figure 3.1.

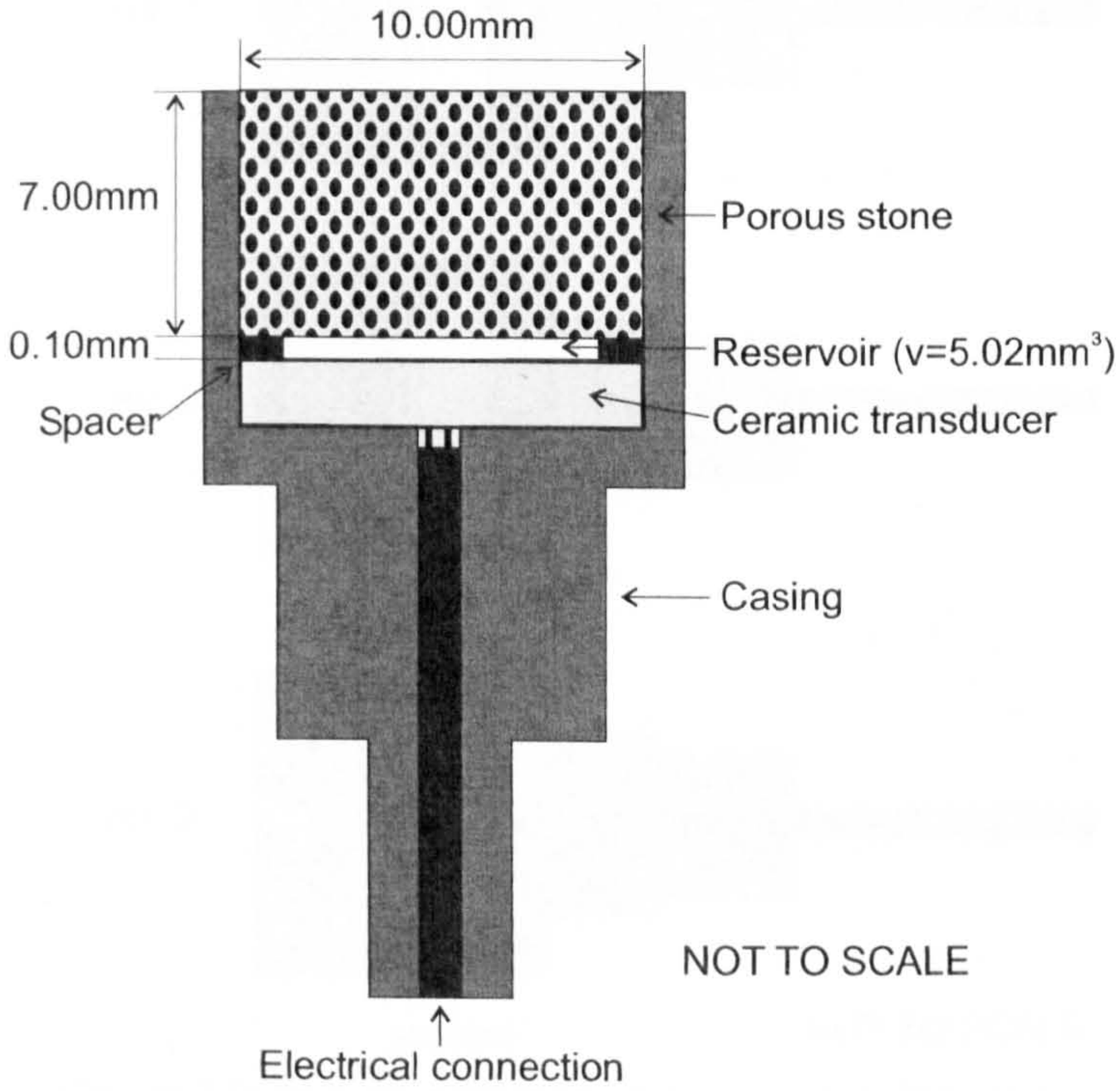

Figure 3.1: The new tensiometer

3.2.2. Design evolution

During the course of this research changes were made to the tensiometer design. Most of them concerned the sealing of the tensiometer. The sealing was done with glue to ensure that all parts (casing, stone, transducer and spacer) fitted together and to prevent water leakages to the electrical components. The first version (version 1 in Figure 3.2) had no internal sealing, so as soon as it was pressurized with the water, the readings became non-sense. Version 2 had sealing but it was soon observed that some of the tensiometers leaked through the cable giving wrong readings. This happened because the glue used for sealing was only filling some gaps (Figure 3.3). This explained the water flowing out of the cable during pressurization. All version 2 tensiometers stopped functioning within 1 year except one that continued working properly for two years (tensiometer II2). Usually the failure occurred during pressurization. The sealing was improved with holes drilled on the casing of the version 3 tensiometers to force glue out during installation of the transducer and

stone. This was done by filling the casing with glue and pushing the transducer, spacer and stone inside while the glue was flowing out from the holes.

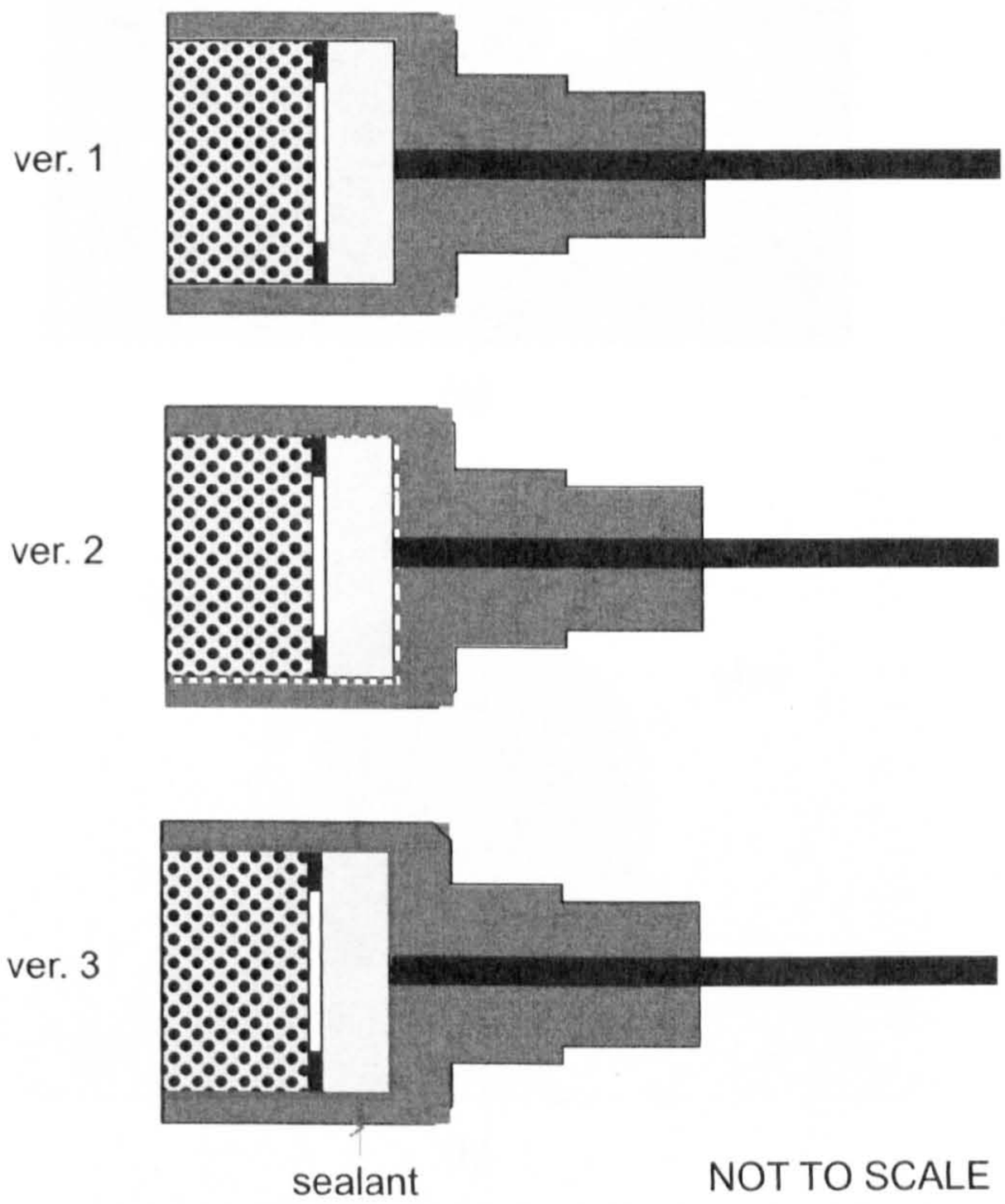

Figure 3.2: Design evolution of the new tensiometers

The leakage seemed to have been fixed in the version 3 tensiometers, however most of them had a new problem, they were unable to measure suctions higher than 300kPa. After saturation, they would stop at low suctions and then cavitate during a drying test (Figure 3.4a). All of them were however properly working within the positive range. One of these faulty tensiometers was dismantled and it was observed that part of the stone was glued to the transducer. This was believed to be the reason for the limited increase of suction not increasing during a drying test (Figure 3.4b).

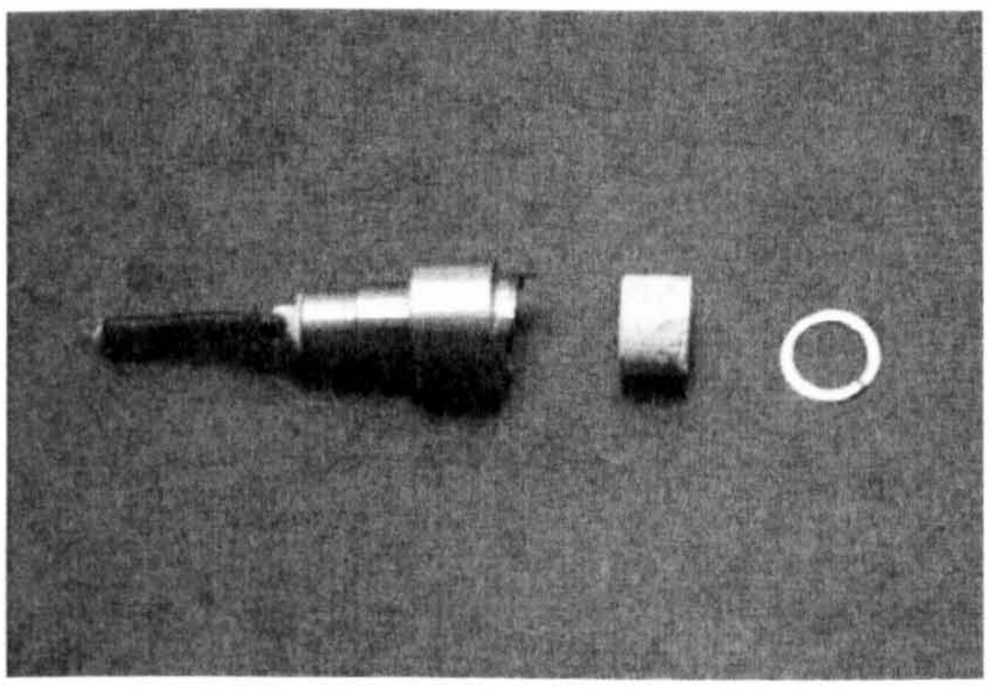

(a)

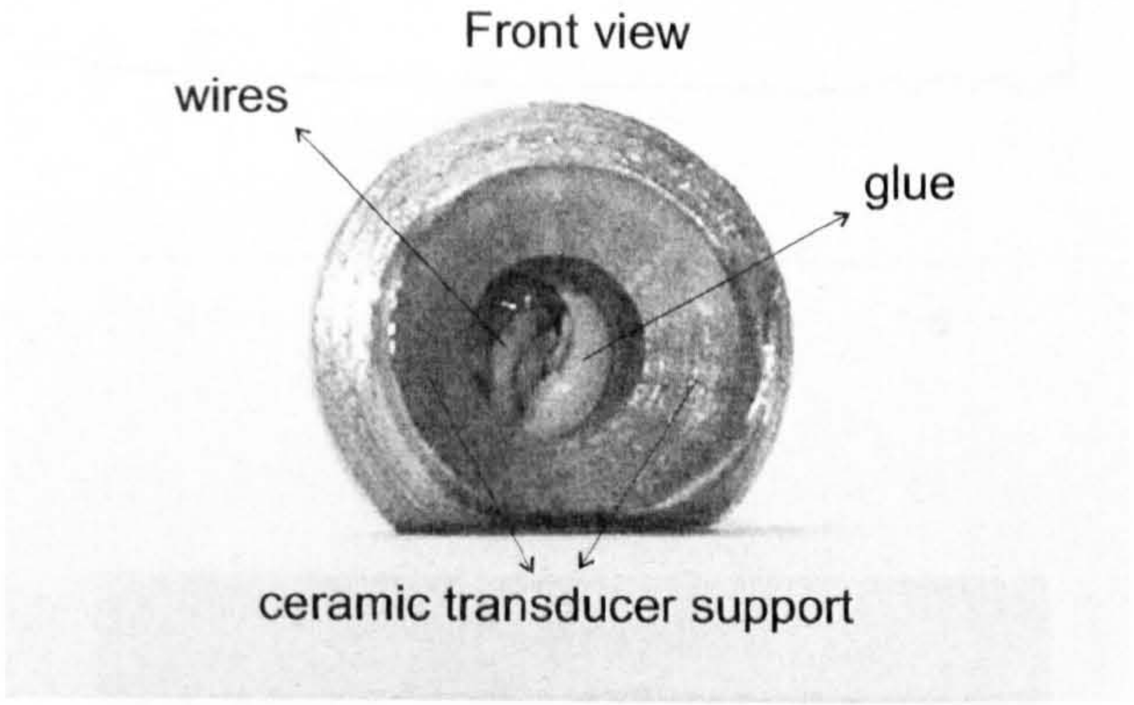

(b)

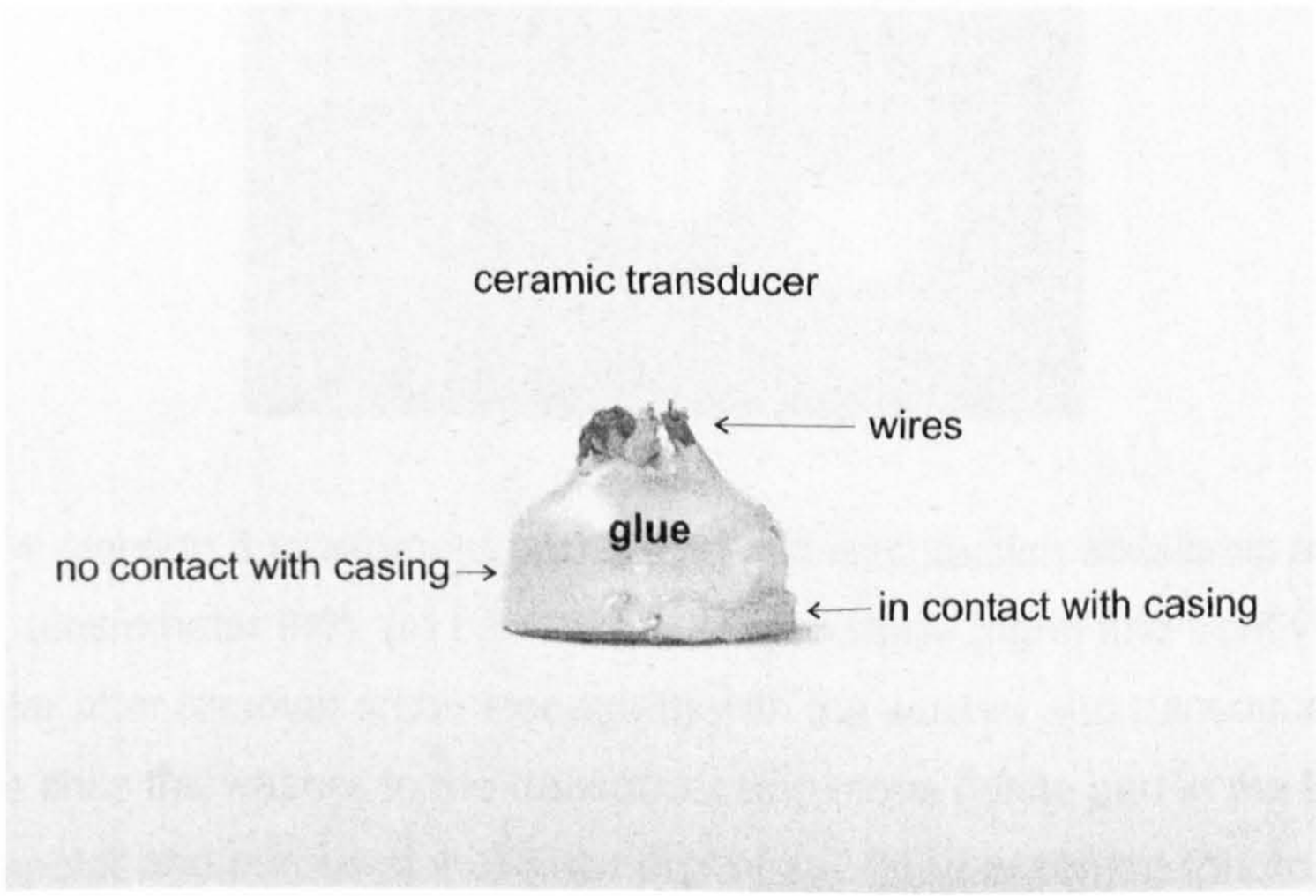

(c)

Figure 3.3: Poor sealing of the version 2 tensiometers, (a) the 3 parts of the tensiometer: washer, porous stone and part of the tensiometer body (transducer is inside), (b) front view of the tensiometer without the internal parts, (c) side view of the ceramic transducer, glue was locally in contact with the stainless steel (diameter of the stone and transducer is 10mm) (photos J. Dodds)

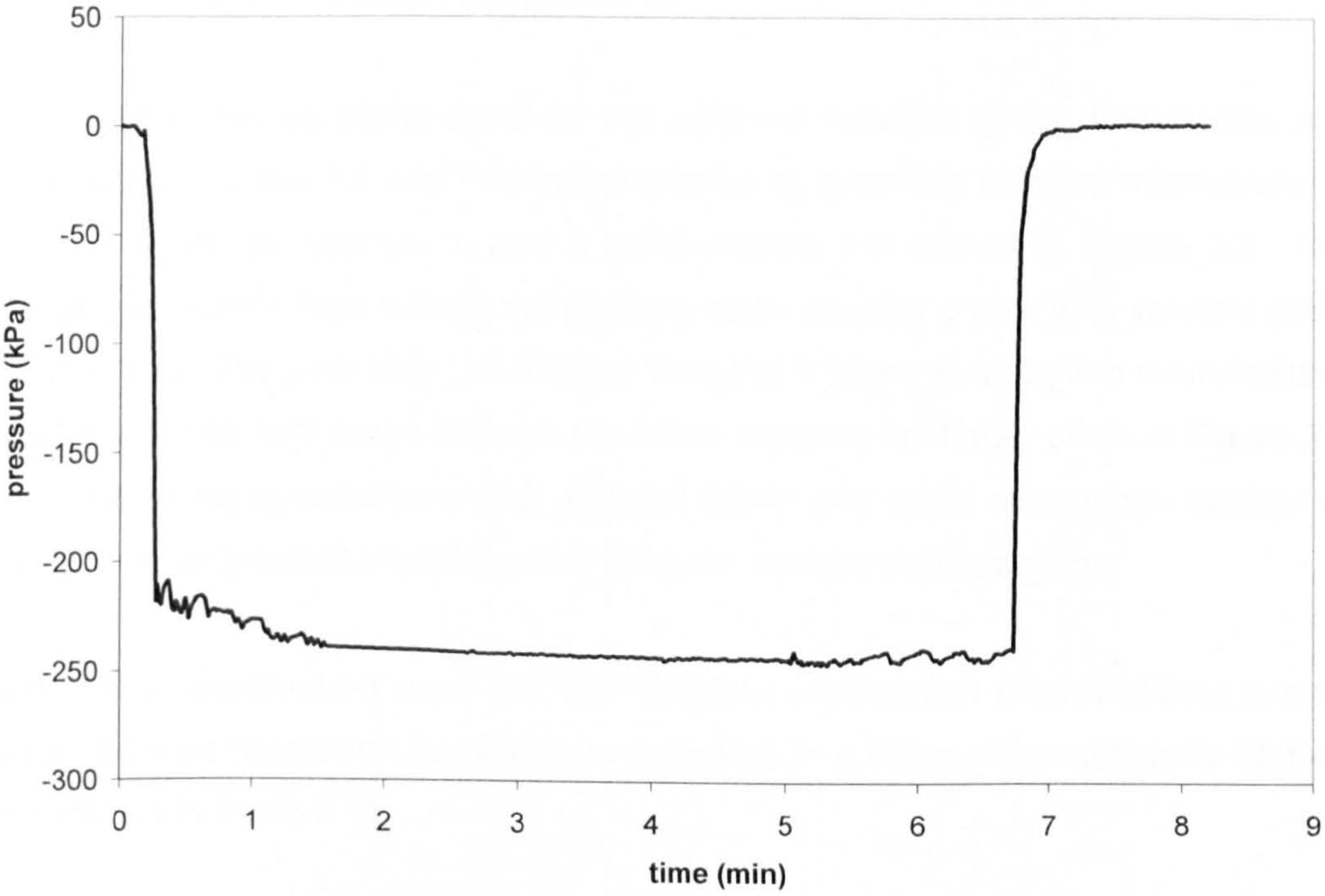

(a)

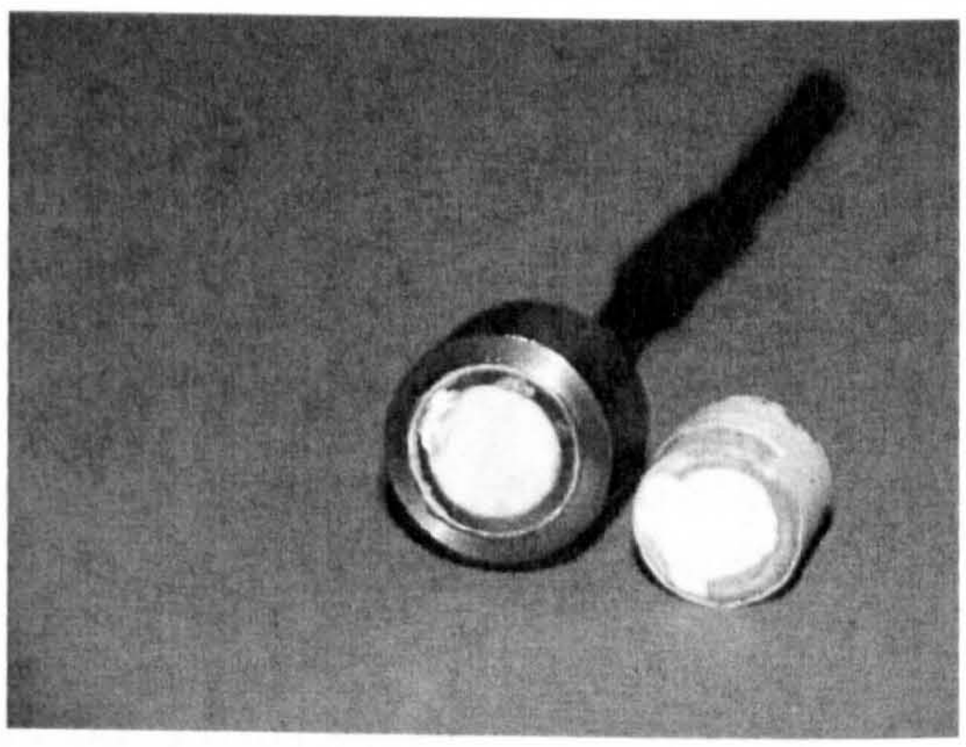

(b)

Figure 3.4: Version 3 tensiometer, (a) drying test with suction stabilizing at 250kPa (test Td1, tensiometer III6), (b) back of the porous stone (right) and front view of the tensiometer after removal of the stone (left) with the washer and transducer (white), some glue links the washer to the transducer and stone (white part in the left side of the tensiometer and porous stone) (diameter of the stone is 10mm) (photo J. Dodds)

3.2.2.1. Design components

Details of the porous stone used for the different versions of the tensiometer are summarized in Table 3.1 and microphotographs by scanning electron microscope of a porous stone for version 1 and 2 tensiometers are shown in Figure 3.5. The micrographs, made from a fresh cut surface, show angular grains with variable grain and pore size. The pore size looks larger than the 0.16μm given by the manufacturer and closer to the 1μm range instead. However, some of the larger pores in Figure 3.5 might not be representative of the material fabric and could correspond instead to small pieces of material breaking away from the surface during cutting.

Most of the tensiometers used the Soil Moisture Corporation porous stones except version 3 tensiometers that have a stone supplied by a different manufacturer (details are included in Table 3.1).

Table 3.1: Properties of the porous stones

	Air entry value (bar)	Composition	Approximate porosity (%)	Maximum pore size (μm)
Version 1 and 2	15 (Soil Moisture)	Kaolin, Talc, Alumina, Ball clay, Feldspathic mineralsa	32b	0.16b
Version 3	15	Alumina (60%), Silica (37%), trace elementsc	40-50c	0.2c

[a] from Sjoblom (2000)

[b] Porous Ceramics Catalogue (Soil Moisture Corporation)

[c] Personal communication from Fred Evans

(a)

(b)

Figure 3.5: SEM micrographs of a 15 bar Soil Moisture ceramic stone at two different magnifications, x5000 times in (a) and x10000 times in (b)

All versions of the tensiometer used a ceramic pressure sensor with a capacity of 10bar whose technical specifications are given in Table 3.2.

Table 3.2: Electrical characteristics of the ceramic pressure sensor

Range	Overpressure	Excitation	Signal output	Non-linearity	Temperature coefficient
0-1000 kPa	x2	1V through 20V	6mV/V	<0.5% FSD	0.05%/°C

Automated data acquisition was accomplished by connecting the tensiometers to a data logger for conversion of the signal from analogue to digital. The digital signal was then read by a PC equipped with the TRIAX logging software (Toll, 1999).

3.2.2.2. Identification of the tensiometers

Each tensiometer was identified by a code consisting of the symbol I, II, or III followed by a number. The roman numbers refer to the sequential batch received from Wykeham Farrance, i.e. three different batches of tensiometers were provided by Wykeham Farrance. The batch sequential numbers are not directly linked to the versions numbers above. All II tensiometers correspond to version 2 while III tensiometers correspond to both version 2 and version 3 (the same for version I tensiometers). The second number (1,2,3,...) is to differentiate tensiometers within the same batch. Table 3.3 lists the tensiometers used for the different studies described in this dissertation.

Table 3.3: Tensiometers used throughout the studies described in this thesis

Tensiometer ID	Saturation (Chapter 3)	Calibration (Chapter 3)	Centrifuge (Chapter 3)	SWRC (Chapter 4)	Control System (Chapter 5)
II1	■	■	■	■	■
II2	■	■	■	■	■
II3	■	■			
II4	■				
III1				■	
III2		■			
III3	■	■	■	■	■
III4	■	■	■	■	
III5	■			■	
III6		■			

3.2.3. Testing rationale

This tensiometers used in this research had been all recently manufactured and had never been previously used. Hence, before they could measure suction, they had to be calibrated and saturated. A calibration in the positive range was done first with pressurized air, to make sure that there was linear relation between applied pressure and voltage. After calibration the saturation process started.

The goal of the saturation process is to saturate all voids in the porous stone and the entire space in the reservoir with water. The achievement of full saturation was subsequently assessed by triggering cavitation in the tensiometer by means of a drying test. The maximum suction measured indicates how well the tensiometer is saturated and if the suction values read by the tensiometers are within the desired range. A second calibration in the negative range was also conducted (according to the procedures in Section 3.4) for each tensiometer to confirm the calibration in the positive. After this, the tensiometers were ready for the relevant application and were left in a cup with distilled water until further use. The initial conditioning of all tensiometers used in this dissertation followed the above sequence.

3.3. SATURATION

3.3.1. Introduction

The literature review has identified research gaps which will be addressed in this section, among them a frequently discussed topic is the capability of tensiometers to measure suction above the AEV of the stone. It challenges the belief that the maximum suction is limited by the AEV of the stone. Or, a better understanding is needed on which factors extend the measurement range of tensiometers. There is little agreement between the different studies.

In order to clarify some of these questions and others raised in Chapter 2, the testing program included: the effect of the saturation procedure, time (continuous use of the tensiometer and measurement of suction for prolonged periods of time), and temperature on the suction at cavitation. The tensiometer behaviour at and after cavitation was also studied. The results were re-interpreted by comparison with

existing literature focusing on aspects related to the cavitation process, location of cavitation, saturation, and measurement range.

3.3.2. Saturation procedure

3.3.2.1. Assessment of oxygen content in water

One of the key factors to ensure full saturation of the tensiometers is the low air content of the water used. De-airing of the water is usually assessed indirectly, by applying vacuum above the water surface until no more bubbles are released. When this condition is reached, the water is considered de-aired.

In order to give a more precise measurement, a dissolved oxygen (DO) meter was used in this work to quantify the percentage of oxygen in the water. The DO meter is frequently used in water quality analysis to measure the percentage of oxygen dissolved in water in comparison to the amount of oxygen in the air (100%). However it only gives a measurement of oxygen, and does not include other common gases such as nitrogen. Therefore it will not give a complete measure of de-airiness in water but will only refer to the part of the air that includes oxygen. Other measurements on the water used for saturation of the tensiometers were also conducted such as measurement of electrical conductivity (related to the amount of dissolved ions) and pH.

A comparison was made between 3 different types of water: tap water, distilled water, and de-aired (with the vacuum pump) distilled water. Within the de-aired distilled water, the water properties were checked just after de-airing and 2 days after de-airing (the water was closed in a container during this time, not exposed to the atmosphere). All tests were conducted in 3 different samples and then averaged.

All measurements, shown in Table 3.4, indicate that the dissolved oxygen decreased continuously from the tap water to the distilled water and to the de-aired distilled water. It decreased by 15% from the tap water to the distilled, and by a further 8% from the distilled water to the de-aired distilled water. Even if there is no way of assessing whether the measured values are good enough, it looks as 53.9% is too high and probably an indication the vacuum system does not de-air properly. As a comparison, bacteria-rich water in a closed environment (closed bottle) reaches DO values much lower than this (~10%). The EC shows that the distilled water is in a

nearly pure state. The pH is slightly acidic and could be related to the low salts percentage of water. For this research, the water with the lowest percentage of dissolved oxygen was always used (distilled just de-aired water).

Table 3.4: Properties of the water used to saturate the tensiometers

Water condition	Dissolved oxygen [%]	Electrical conductivity [µS/m]*	pH
De-aired distilled (48h after de-airing)	53.9	34.7	5.7
De-aired distilled (just after de-airing)	53.6	30.7	5.9
Distilled	61.1	36.2	5.8
Tap water	76.6	226.5	7.6

*µS/m = micron Siemens per metre

3.3.2.2. Saturation procedure

Saturation was conducted at first in a Perspex cell during the first eleven months of experimentation and afterwards in a purpose-made saturation vessel. Maximum pressure applied by the Perspex cell was limited to 800-1000kPa due to water leakage at higher pressure. The use of the Perspex cell was abandoned when a new saturation vessel was built of brass (Donoghue, 2006), which could reach pressures up to several MPa. However, due to the sealing problems of the tensiometers reported in Section 3.2.2, the maximum pressure applied was within 1500-2000kPa and in most cases was ~1500kPa. The outlines of both saturation arrangements are similar and included a vacuum pump, a pressure controller, an adequate tensiometer fitting and de-aired water lines. Figure 3.6a shows the outline of the Perspex vessel while Figure 3.6c shows a picture of the brass saturation vessel.

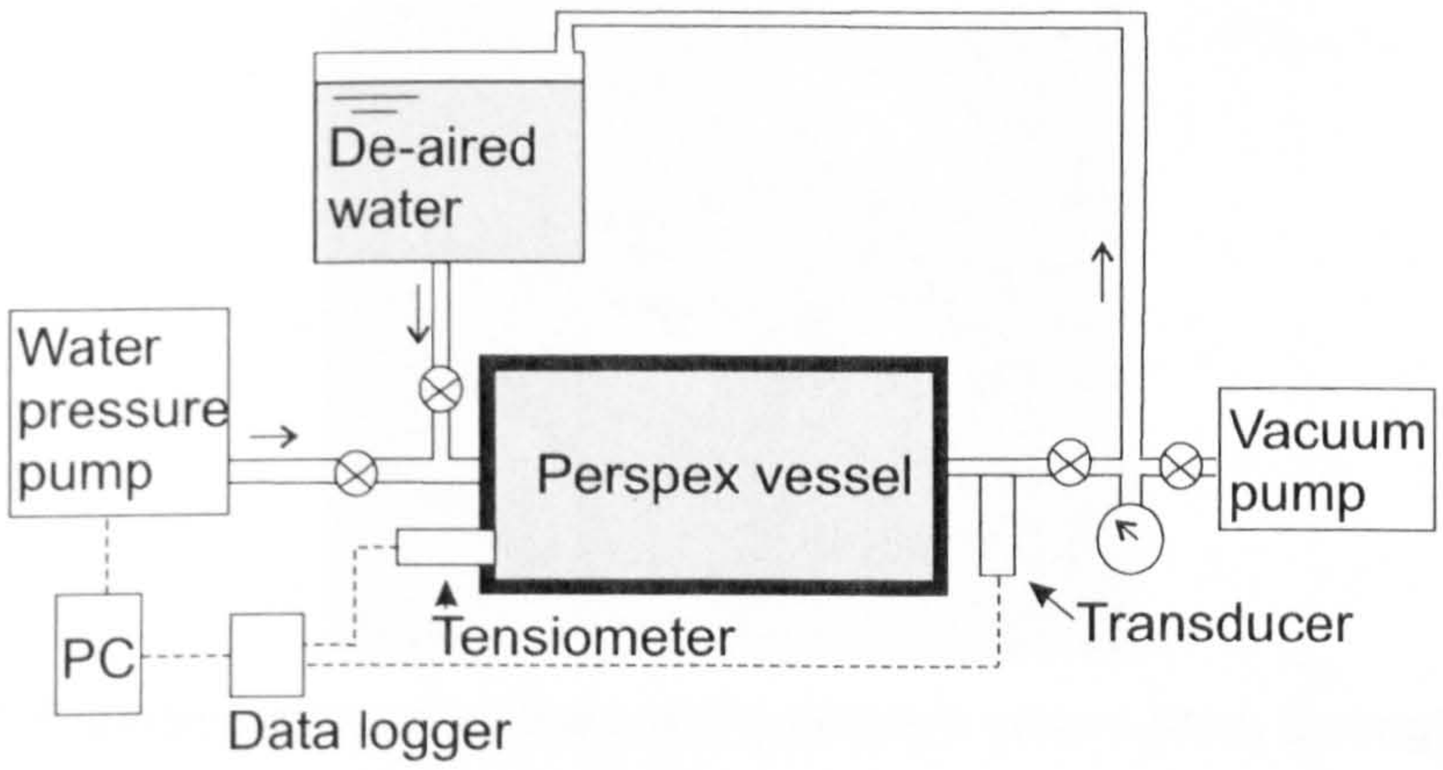

(a)

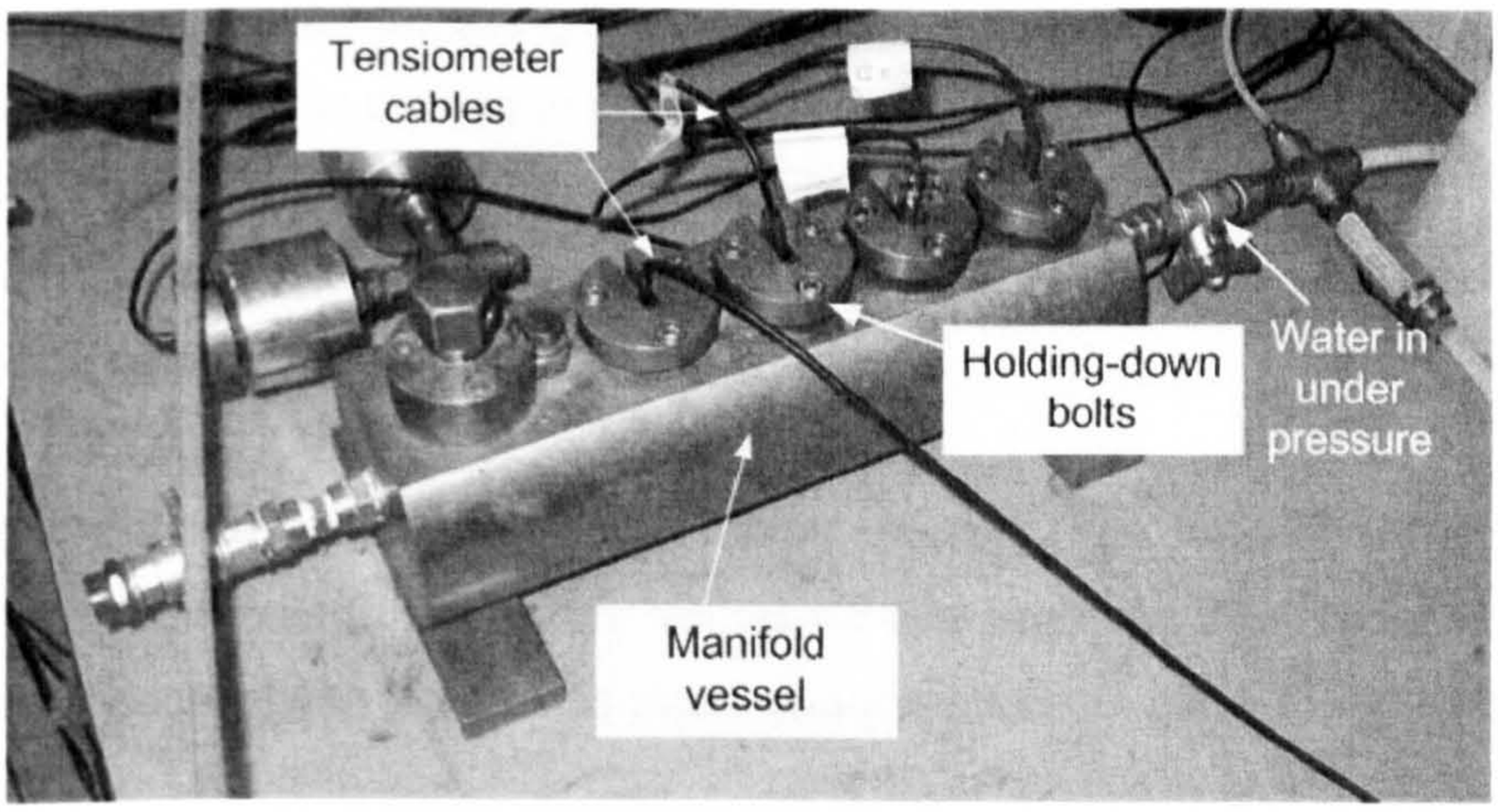

(b)

Figure 3.6: Pressurization set-up, (a) pressurization in Perspex vessel (dashed lines represent electric connections and open lines represent hydraulic lines), (b) manifold (photo C.E. Augarde)

Fixing of the tensiometer in the brass vessel was done by placing first the o-ring and metallic ring in the appropriate slot and then pushing the tensiometer through them followed by the holder and bolts. The purpose of the metallic ring with an inclined inner side was to squeeze the o-ring against the side of the tensiometer body to prevent any leakage at higher pressures (Figure 3.7). Clamping of the holder with bolts was done gently, just with enough force to avoid any leaks. As will be discussed in Section 3.4, the tensiometer body is deformable under the action of surrounding pressures and therefore excessive tightening could induce deflection of the pressure transducer and affect calibration.

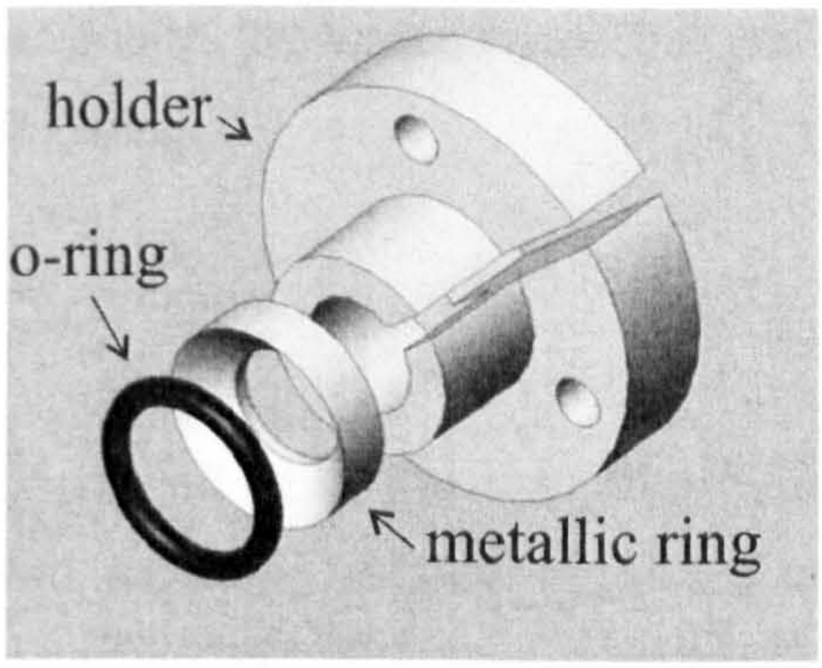

Figure 3.7: Clamping system for the small saturation vessel (from Donoghue, 2006)

The procedure followed for the initial saturation of the new tensiometer, based on Ridley et al. (2003), was divided in three stages:

1. Vacuum stage: the tensiometer was placed in the saturation vessel and vacuum applied for a minimum of 10 minutes.

2. Flooding under vacuum stage: while under vacuum, the de-aired water line was opened and left running through the vessel for few seconds. This ensured that the water was in contact with the porous stone under a pressure close to -100kPa.

3. Pressurization stage: 1500kPa was applied via a piston controller for approximately 24h or for sufficient time (dependent on the extent of desaturation of the tensiometer) in the brass vessel.

After saturation, cavitation was triggered by leaving the tensiometer to dry in the atmosphere after wiping the porous stone with clean paper tissue or placing a small quantity of soil on it. Guan and Fredlund (1997) call such experiments “drying tests” or “evaporation tests”. The presence of soil has the advantage of controlling the speed of suction increase, while the direct drying to the atmosphere is faster.

Special care was taken when inserting a cavitated tensiometer back in the vessel for subsequent pressurization. With the holder removed, the vessel would be filled again with de-aired distilled water until the top. The tensiometer would then be inserted in a tilted position to ensure that no air bubbles were trapped at the face.

Attention was given to the cleanliness of the porous stone and tensiometer body. After use, the porous stone and body of each tensiometer was carefully cleaned to

avoid any clogging. Occasionally, the water inside the vessel was also replaced as impurities tended to accumulate.

3.3.3. Results

In the following results on the effect of the saturation procedure on the suction at cavitation will be presented, including aspects regarding to cavitation (behaviour of the tensiometer just after and before cavitation). The procedures and results for the temperature effect will be presented, and some evidence that suction at cavitation increases with the continuous use of the tensiometer.

3.3.3.1. Cavitation behaviour

A typical sequence of saturation and cavitation triggering is shown in Figure 3.8. With reference to this particular test, the tensiometer was saturated at 1000kPa for a period of 6.6h and then subjected to a drying test. In this case the maximum suction measured was 700kPa and the tensiometer was afterwards plunged in free water.

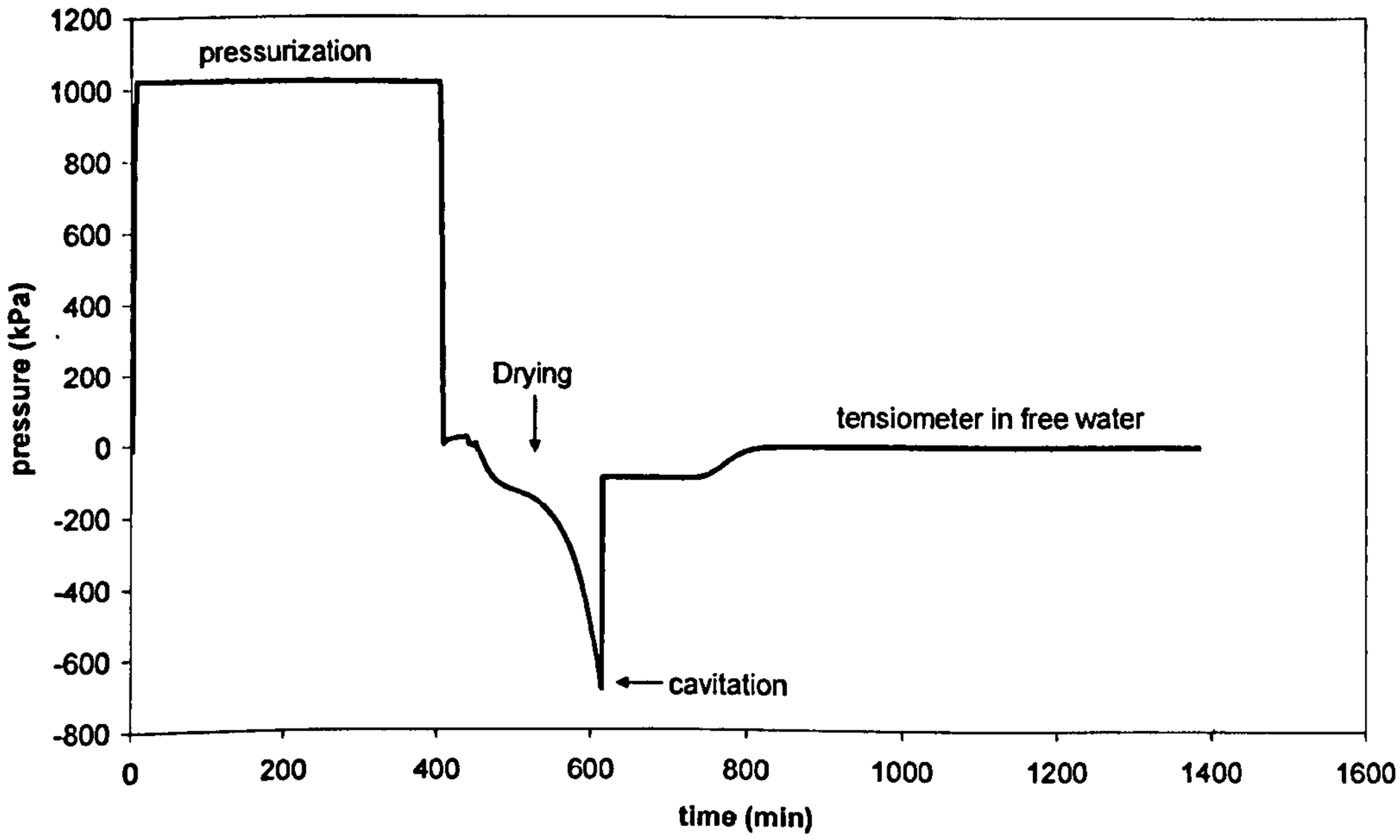

Figure 3.8: Sequence of pressurization and cavitation triggering in a tensiometer (test T24, tensiometer II5)

During drying, as water evaporates out of the stone, suction increases until the readings jump back to 100kPa. This is referred as cavitation and corresponds to the formation of a gas bubble inside the porous stone or reservoir. Cavitation occurs fast, a recording rate of 0.5 reading per second is not enough to capture the cavitation process. Data from Bremond et al. (2005) indicates cavitation happens at the micron-second scale. Other studies with different types of tensiometers show the same jump to 100kPa (e.g. Ridley and Wray, 1996). In this research no click was heard during cavitation unlike other authors (e.g. Guan and Fredlund, 1997).

Opposite to soils which undergo a strain rate increase when approaching failure in stress controlled conditions, there are no precursory phenomena leading to cavitation. From the suction versus time curves it is not possible to predict the moment cavitation will occur. Figure 3.9a shows a typical variation of the suction change rate with time during drying and it can be observed that the suction change rate was approximately constant when cavitation occurred. The only exception to this behaviour was observed during one drying test where unusually high values of suction were recorded as shown in Figure 3.9b. The suction versus time curve shows two step changes during the minutes immediately preceding cavitation, which could be perhaps be interpreted as 'aborted' cavitations.

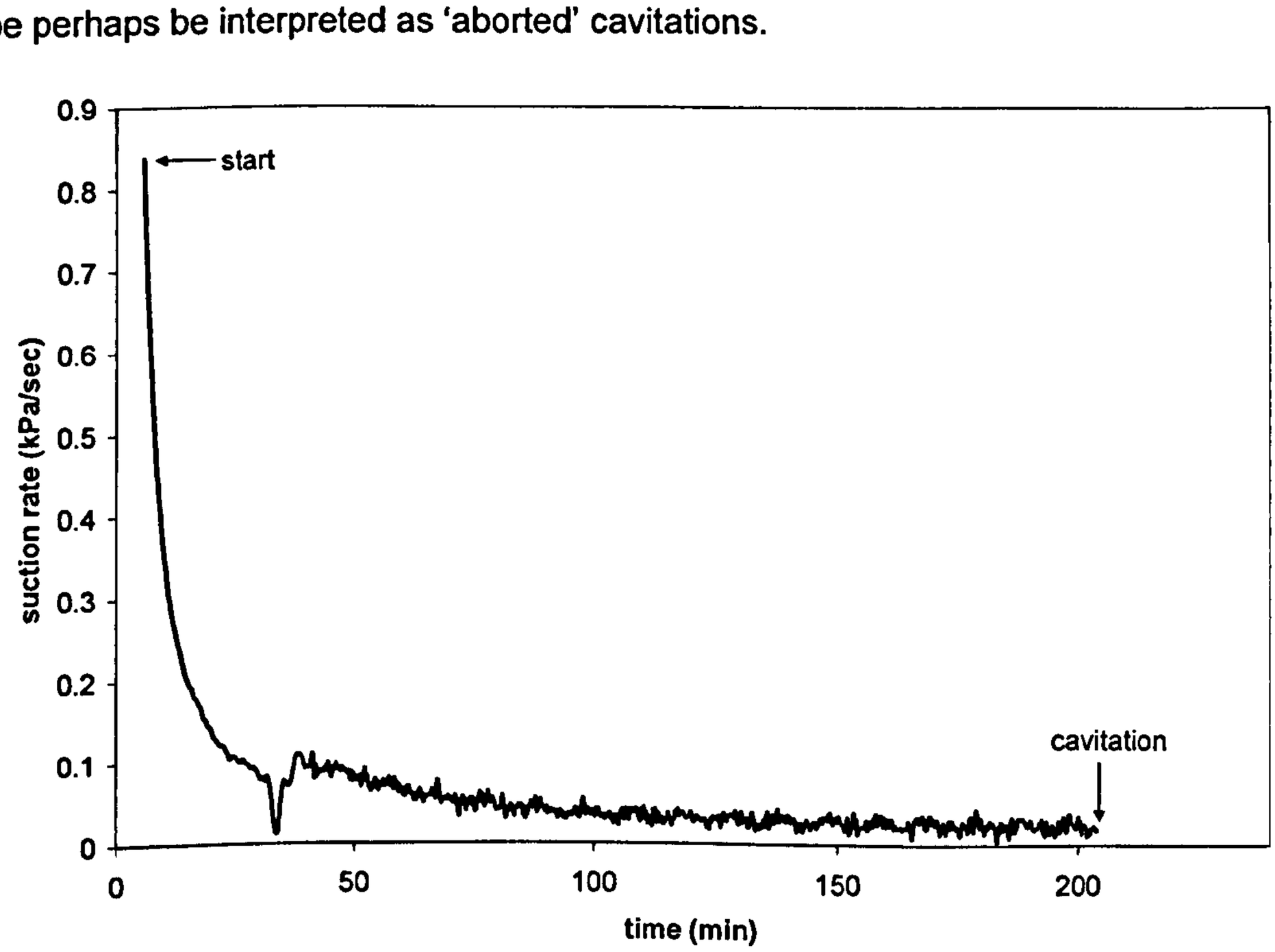

(a)

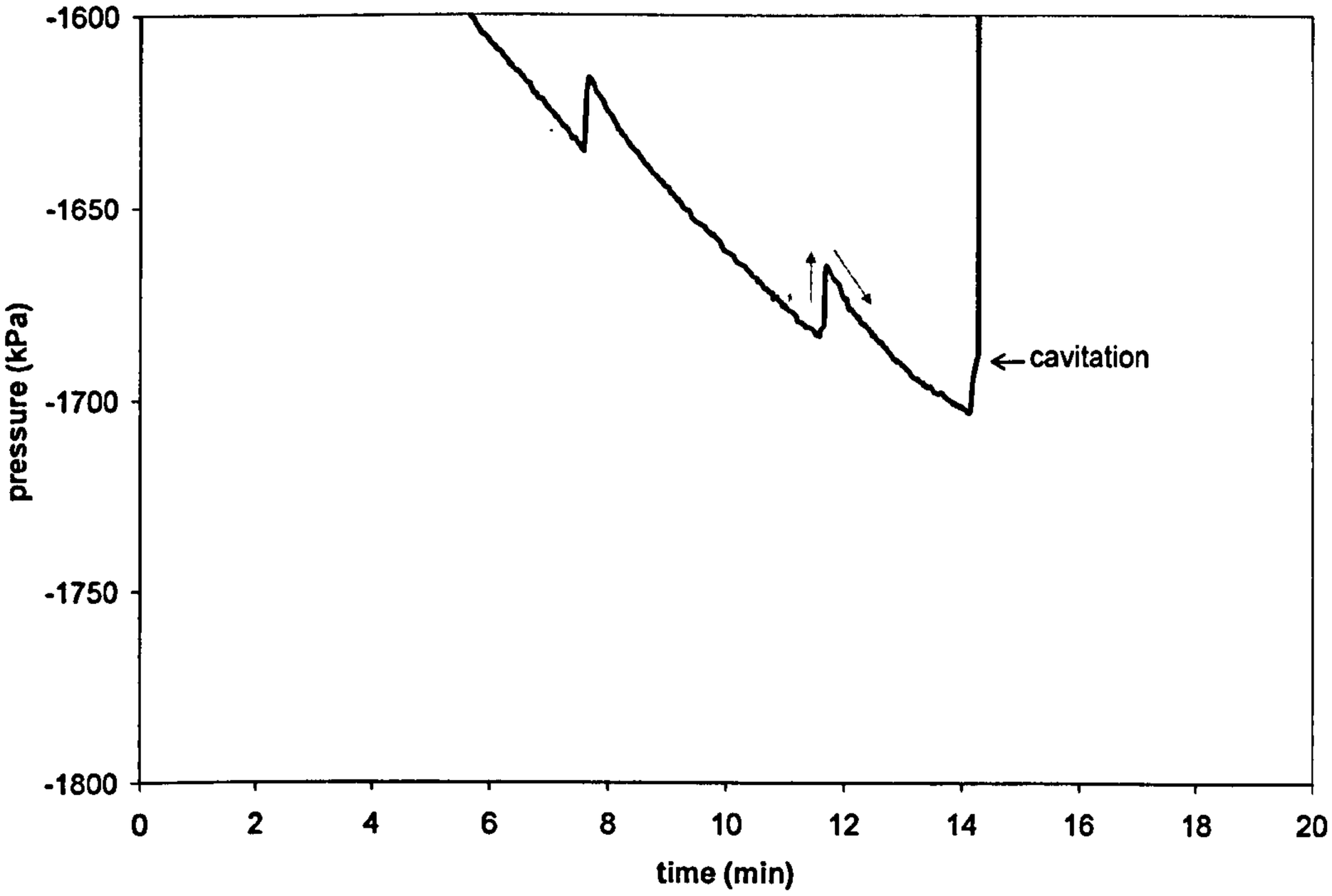

(b)

Figure 3.9: Pre-cavitation behaviour of the tensiometer; (a) typical suction change rate versus time during drying (test T24, tensiometer II3 with kaolin paste), (b) tensiometer behaviour at high suctions showing a 'stepped cavitation' (test Tt9, tensiometer III4)

The highest suction measured during this research was 2087.1kPa by tensiometer III4 (Figure 3.10) followed by 2045.5kPa by tensiometer II2 (Figure 3.12). These are the second highest suction measurements by tensiometers reported in the literature after the value of 2584kPa measured by Tarantino and Mongiovi (2001).

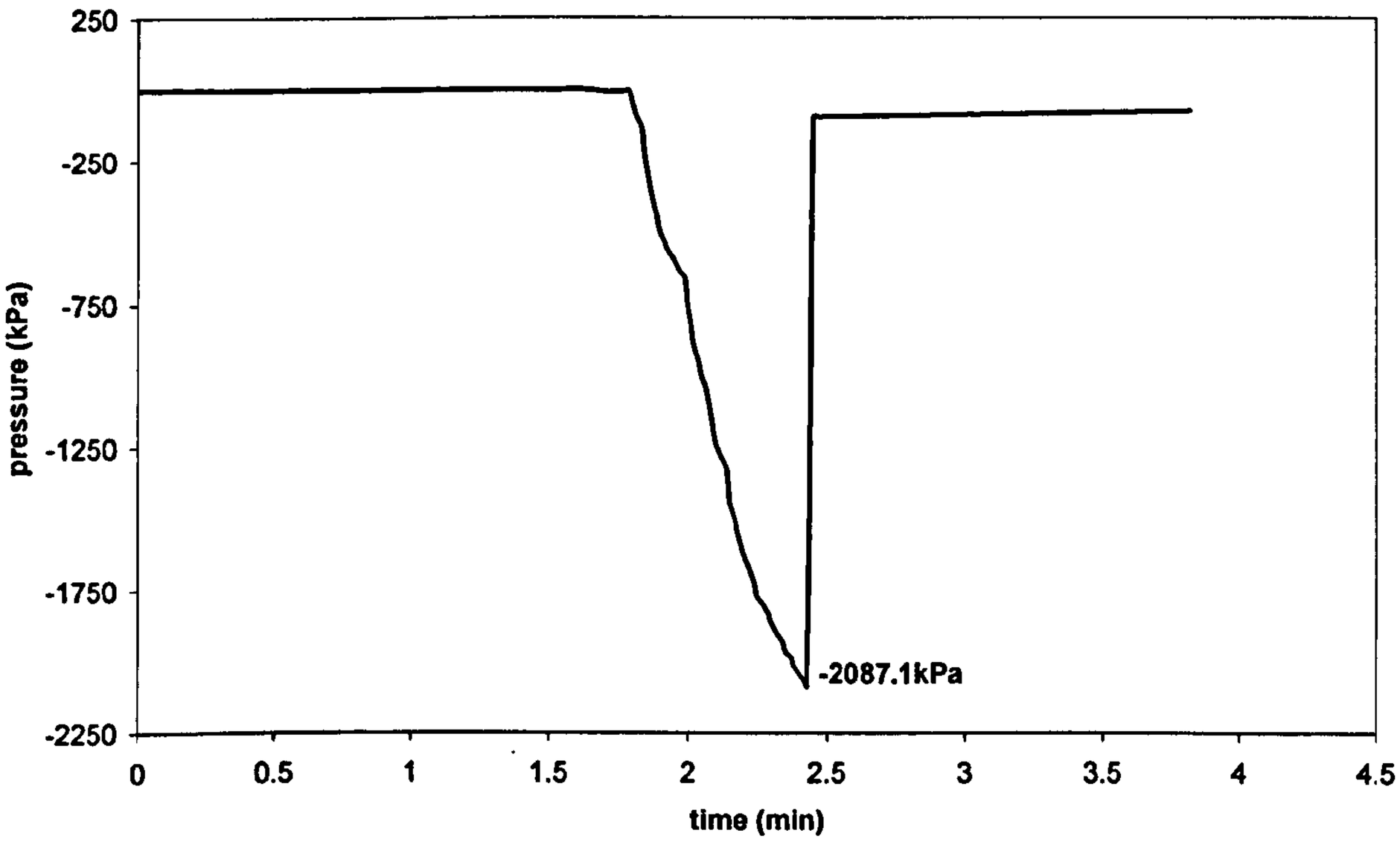

Figure 3.10: Highest suction measured in this research with a tensiometer (test T31, tensiometer III4)

If the tensiometer is plunged in free water immediately after cavitation it reads approximately 0kPa the same value is read if the tensiometer is left drying to the atmosphere for enough time. After cavitation the tensiometer is incapable of measuring suction values in excess of 100kPa (Figure 3.11) suggesting that there is a discontinuity (air bubble) in the water between the transducer and the soil. It is therefore necessary to subject the tensiometer to a pressurization stage with the application of high values of positive pressures through the porous stone to recover its ability to measure suction values in excess of 100kPa.

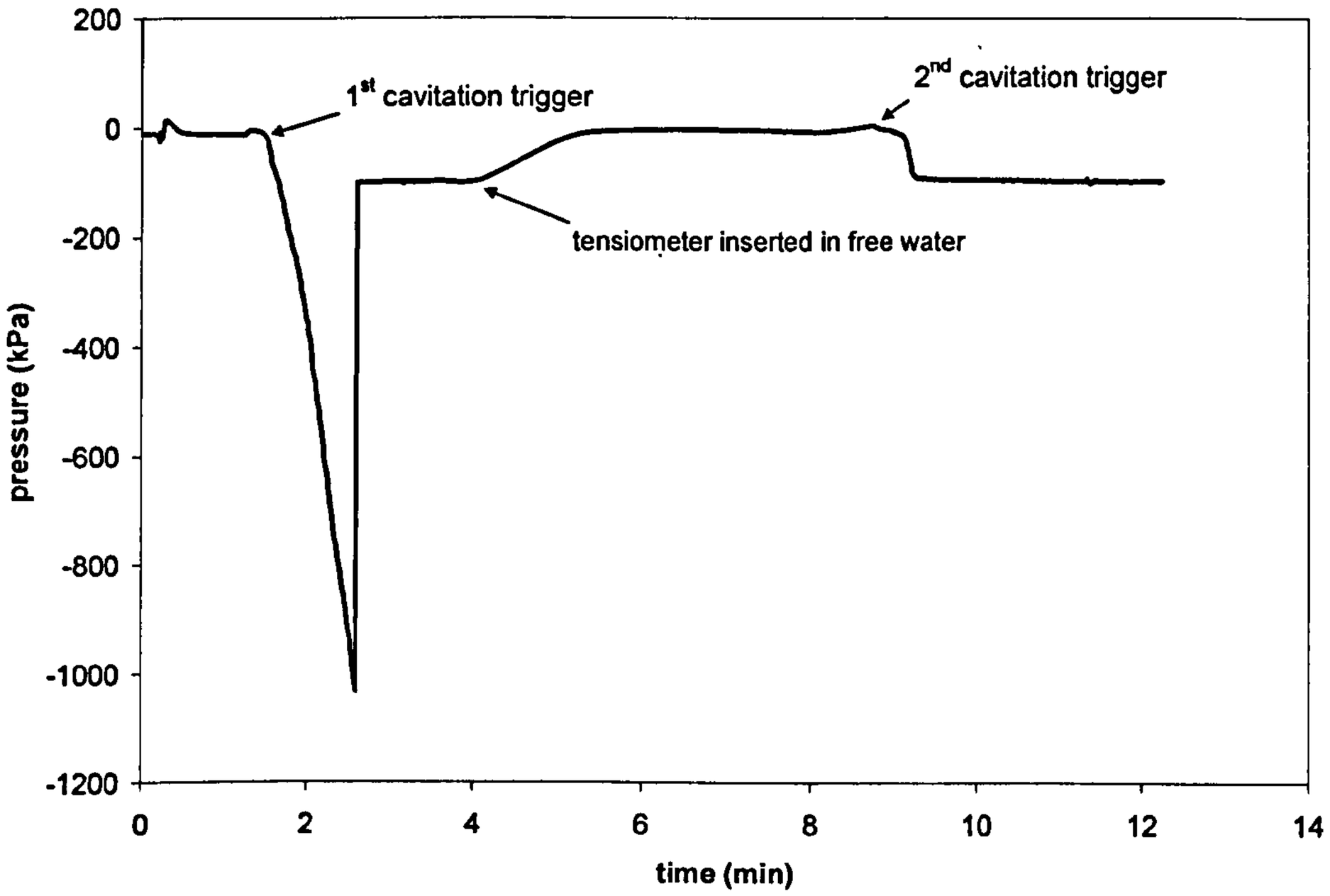

Figure 3.11: Two consecutive drying tests in a tensiometer; after the first cavitation, the tensiometer is unable to measure suction in excess of 100kPa (test T28, tensiometer II4)

3.3.3.2. Effect of saturation procedure

During the early stages of this research a small testing program was devised to try to increase the maximum suction. The most obvious factor to change would be the maximum pressure applied during the pressurization stage but, as this was limited to 800-1000kPa, the following factors were chosen: (1) pressurization duration, (2) method for triggering cavitation and, (3) time taken to cavitation. A series of 9 tests were conducted in the old Perspex cell at the maximum allowed pressure (800-1000kPa).

Results of the saturation program are shown in Table 3.5. The table shows the maximum pressure applied and duration to saturate the tensiometers, the procedure (placing kaolin on the stone or leaving it to dry to the atmosphere) and time taken for cavitation to occur. Maximum suctions are in the range 800-1000kPa which correlate well with applied pressures (800-1000kPa). Table 3.5 also shows the highest suction was measured by tensiometers that had been used for a prolonged period of time since last pressurization stage. Influence of other factors namely the duration and

material used to trigger cavitation, and duration of the pressurization seemed to be irrelevant.

Table 3.5: Saturation testing program

Tensiometer nr	Test nr	Pressurization		Cavitation		Suction at cavitation (kPa)
		Pressure (kPa)	Duration (h)	Material	Time (min)	
II1	T11	800	72	Kaolin	45	981.9
	T12	800	24	Kaolin	60	917.3
	T13	800	5	Kaolin	60	990.3
	T34	1000	-	Air drying	2	1043.0
II2	T15	800	60	Kaolin	120	858.6
	T16	800	24	Kaolin	60	792.1
	T25*	-	-	Kaolin	158	1230.9
II3	T18	800	48	Kaolin	30	903.7
	T27*	-	-	Kaolin	150	818.2
	T29*	930	5	Air drying	12	1047.7
II4	T20	-	-	-	-	870
	T28	800-1000	4-14	Air drying	1	1032.1
	T30*	-	-	Air drying	3	994.9

*used for 1 month after pressurization

Donoghue (2006) studied the influence of pressure cycles on the maximum measured values of suction. The results showed suction at cavitation increasing with the number of cycles (maximum pressure applied was 2MPa for a period of 2h), and that the optimum number of cycles was around 15. When more than 15 cycles were carried out, the maximum suction showed no improvement.

3.3.3.3. • Effect of temperature

As discussed in Chapter 2, low temperatures are likely to increase the suction measurement range of tensiometers. To investigate this, a testing program was carried out at controlled temperatures (between 4°C and 20°C). The temperature control was ensured by half-filling a polystyrene box with liquid nitrogen. Ice was used at first but it melted and so could not keep low temperatures constant for enough time. Liquid nitrogen was a good alternative as it did not vaporize

immediately and was able to provide a much cooler environment. Temperature was measured by attaching a thermocouple directly to the tensiometers body.

After pressurization, the cable of the tensiometer was inserted through an orifice in the cover of the polystyrene box and the tensiometer was left hanging at a small distance (~1cm) from the liquid nitrogen (Figure 3.12). In order to slow down drying and to give enough time for the tensiometer temperature to equalize with the surrounding environment, the tensiometer was placed in the box with the stone completely wet, i.e. without previous wiping of excess water.

This testing programme consisted in series of 13 drying tests, conducted on tensiometers II2, III3, and III4 (Table 3.6).

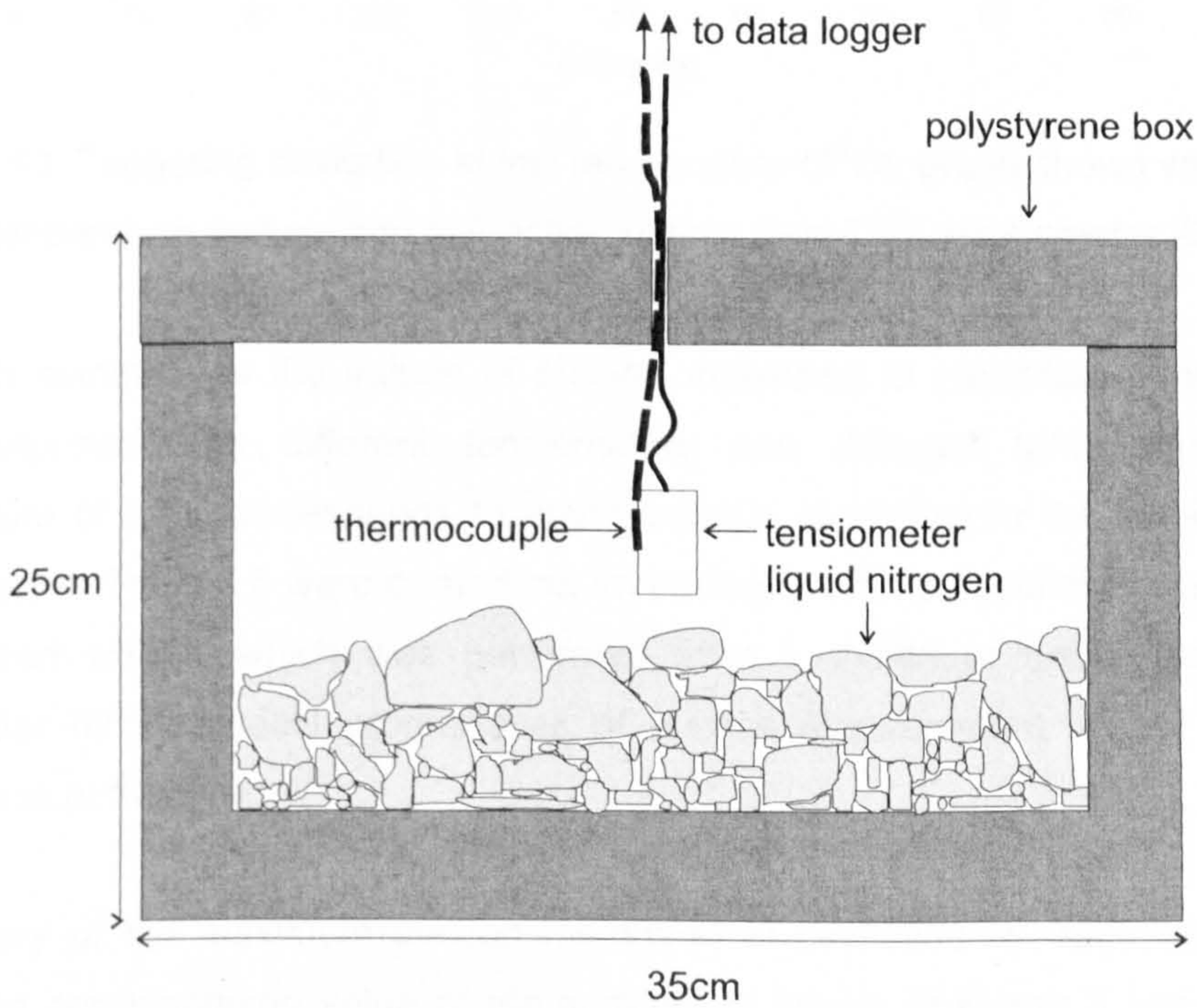

Figure 3.12: Testing set-up for the low temperature tests

An example of a cavitation occurring at a temperature of ~5°C is shown in Figure 3.13, which also corresponds to the highest suction value measured by tensiometer II2 (2045.5kPa). It can be seen that the temperature remained constant for a total of about 1h, i.e. 30min before suction started increasing and 30min while suction increased. However such stable values of temperature were difficult to achieve in all tests and earlier tests, where ice was used instead of liquid nitrogen, because of temperature fluctuations (mainly linked to the opening of the box to refill it with more ice).

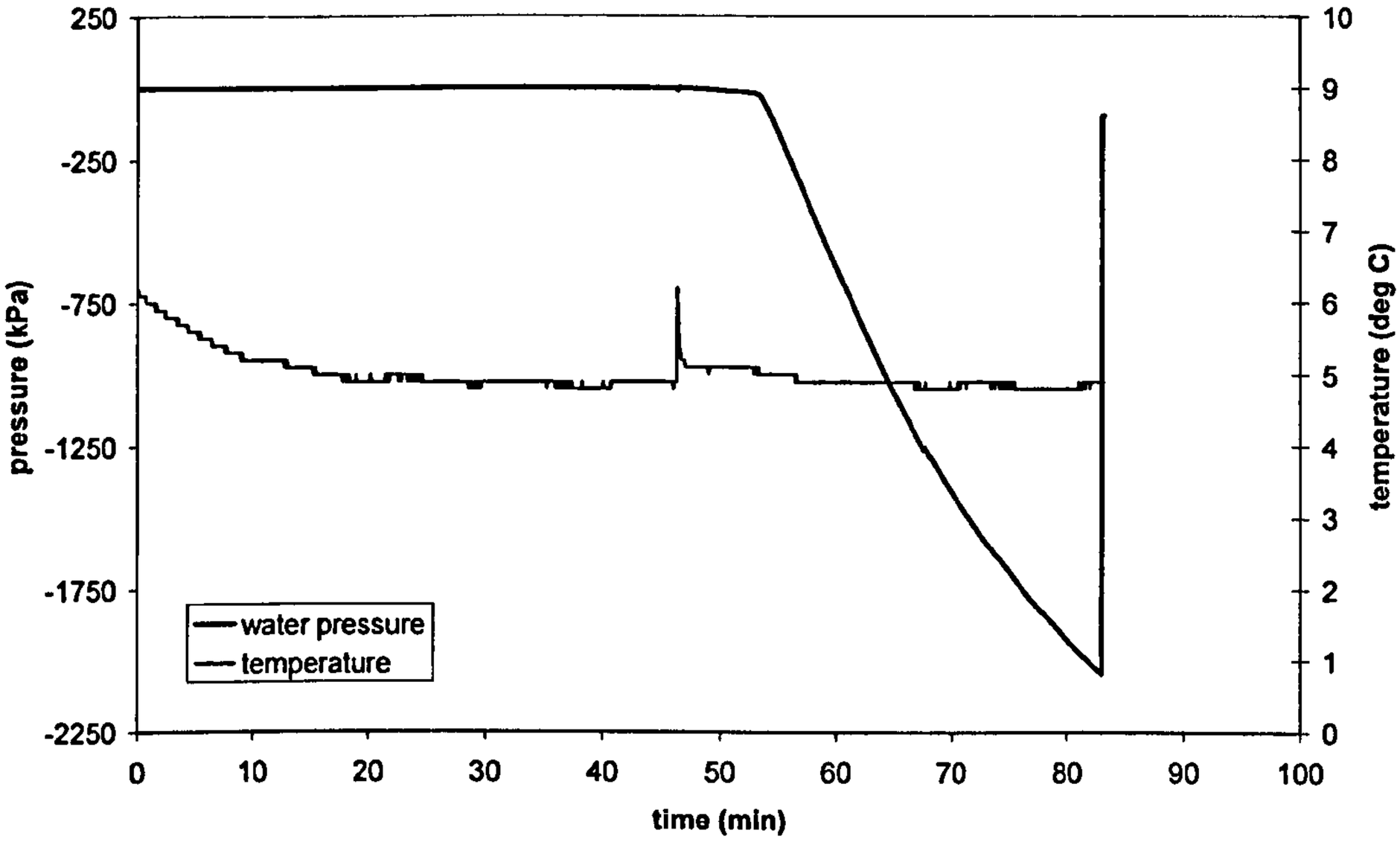

Figure 3.13: Triggering cavitation at low temperature (5°C); graph shows variation of temperature and suction in function of time (test Tt10, tensiometer II2)

Table 3.6 summarizes the values of suction measured at cavitation during drying tests performed with different tensiometers and different temperatures. The temperature of 22°C corresponds to environmental conditions in the laboratory. All drying tests in Table 3.6 were carried out immediately after pressurization except the test marked with *, which was performed after 1 month of continuous use of tensiometer II2 in parallel programmes of suction measurement on soil samples taking place at the time.

A summary of the maximum suction measured at cavitation by each tensiometer versus the corresponding value of temperature is shown in Figure 3.14a. As tests were done in sequence, the suction at cavitation was also plotted against the sequential cavitation number for each tensiometer (Figure 3.14b). Figure 3.14a shows that the maximum measured value of suction increases with decreasing temperature with the exception of tensiometer III3, which recorded a drop of the suction corresponding to the lowest temperature. Figure 3.14b shows that suction increased with the number of successive cavitations except in the last test for all 3 tensiometers (for tensiometer III3 the maximum suction decreased in the last two tests).

Table 3.6: Maximum suctions measured at different temperatures (sequence of tests displayed is the same as during the testing period)

Tensiometer ID	Suction at cavitation [kPa]	Temperature [deg C]
III3	1147.5	22
III4	1262.9	22
III4	1478.1	22
II2*	1536.8	22
III4	1489.5	22
II2	1903.6	~11
III4	1700.0	10
III3	1772.4	10
III4	1703.0	~4
II2	2045.5	~5
III3	1332.4	~10
III3	1266.8	~5
II2	1908.8	~8
III4	1608.6	~14

*after 1 month of continuous measurement of suction

In order to conclude from these results that temperature has an effect on the maximum suction at cavitation, the calibration of the tensiometer must remain unaffected by the temperature. A calibration in the positive range at low temperature was conducted by applying increasing air pressures. Due to the difficulty of inserting the saturation vessel inside the polystyrene box together with the several cables and air pipe, the calibration was conducted outdoors where the temperature was at 4°C. Two calibrations were conducted during a period of 2h in order to give enough time for the temperature to come to equilibrium with the tensiometers. The calibration factors obtained at 4°C were 0.0112 and 0.0110. The calibration factor at room temperature (21°C) obtained previously was 0.0112. This shows almost no influence of the temperature. However these results should be taken as indicative, because even if the tensiometer parts were at 4°C, the compressed air in contact with the ceramic transducer was not, so there could have been a temperature gradient between the tensiometer external surface and the transducer.

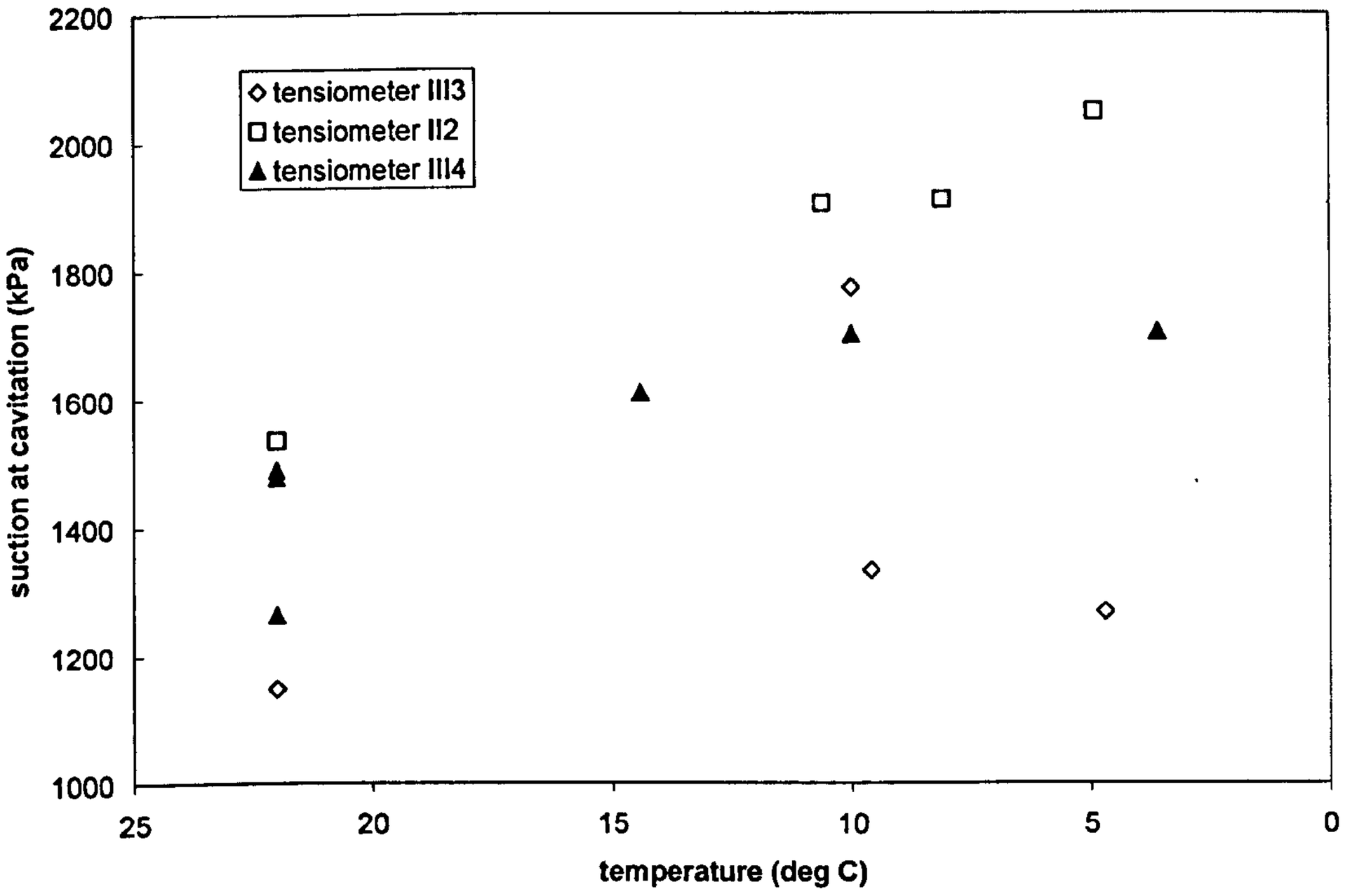

(a)

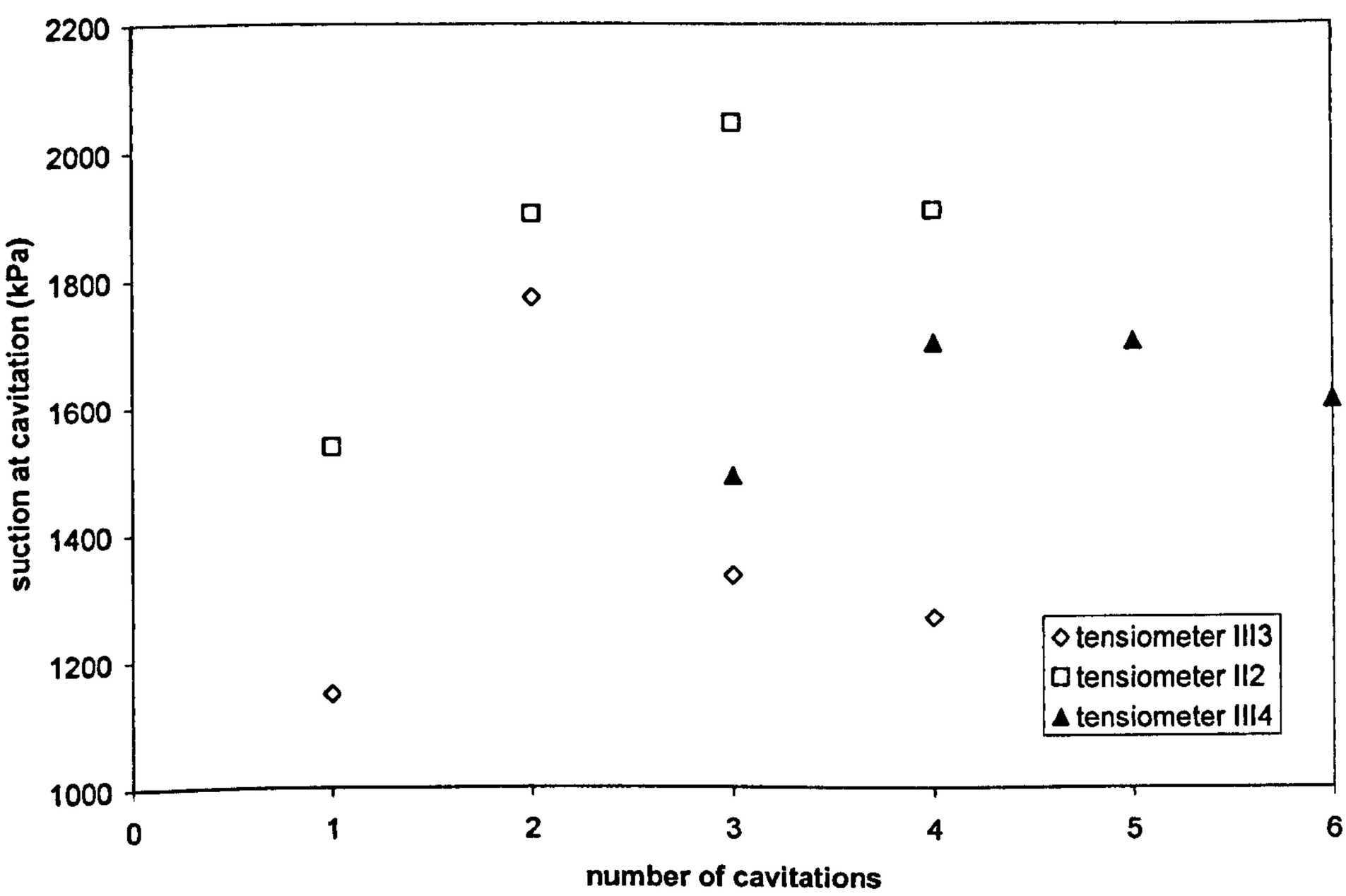

(b)

Figure 3.14: Low temperature effect in suction at cavitation, (a) suction at cavitation versus temperature, (b) suction at cavitation versus number of cavitations (tests Tt1 to Tt14, tensiometers II2, III3, III4)

3.3.3.4. Effect of time

It was found that the suction range of the tensiometer increases with duration of use. Ball (2006) after using the same tensiometer for approximately 1 month, triggered cavitation reading a maximum value of 1231kPa (the first highest suction measured with tensiometer II2 shown as test T25 in Table 3.5). Similarly, Hidayat (2006) used the same tensiometer for 1 month in bentonite-sand mixtures measuring small suction (<600kPa) without cavitation occurring. Afterwards, without pressurizing, the tensiometer was cavitated and the maximum suction measured was 1537kPa (corresponds to the first value for II2 in Table 3.6).

The highest suction readings were consistently obtained by the same tensiometrers. Tensiometer II2 (from the oldest batch) tended to read the highest values of suction, e.g. it was the first tensiometer to measure ~1200kPa (Ball, 2006) and subsequently attained readings of 1627kPa (Donoghue, 2006) and 2045kPa. The same for tensiometer III4, which initially measured a value of suction of 1703kPa and subsequently attained a maximum reading of 2087kPa. Mendes (2007a), who is currently using the same batch of tensiometers, has also reported that III4 is the best-performing tensiometer. Such consistency of performance was also identified by Jotisankasa (2007c) for the Imperial College tensiometers.

Donoghue (2006) found that another dominant factor in increasing the range of suction measurements was the number of cavitations. Tests conducted with tensiometers II2 and II3 show an increase of suction at cavitation with time. However tensiometer II2 shows an upper suction limit of 1600kPa and, after having attained such measurement, it returns to read lower values. A similar finding is already reported in the literature by Tarantino and Mongiovi (2001).

It was also found that the time to re-saturate previously used tensiometers from a dry condition was much greater than for new tensiometers. New tensiometers that had never been used before achieved suctions >1000kPa, after 1-2 weeks of pressurization. For previously used tensiometers, this period was extended to 1-2 months to reach similar levels suction. This was evident in the tensiometers III9 and III10 that were saturated from completely dry.

3.3.3.5. Tensiometer behaviour after extensive drying

An interesting finding was that dry tensiometers recorded increasing pressures when plunged in free water. In Figure 3.15, a tensiometer was cavitated and then left drying to the atmosphere for a period of 12h. When in contact with free water it recorded increasing positive pressures up to 250kPa. This response was observed whenever the tensiometer dried for longer periods of time, either in contact with a soil sample or just drying to the atmosphere.

This phenomenon is believed to be related to the porous nature of the stone. By capillarity, the stone absorbed water and the resulting wetting front moved inside trapping and squeezing the air. The increasing pressure is therefore generated by the air being compressed.

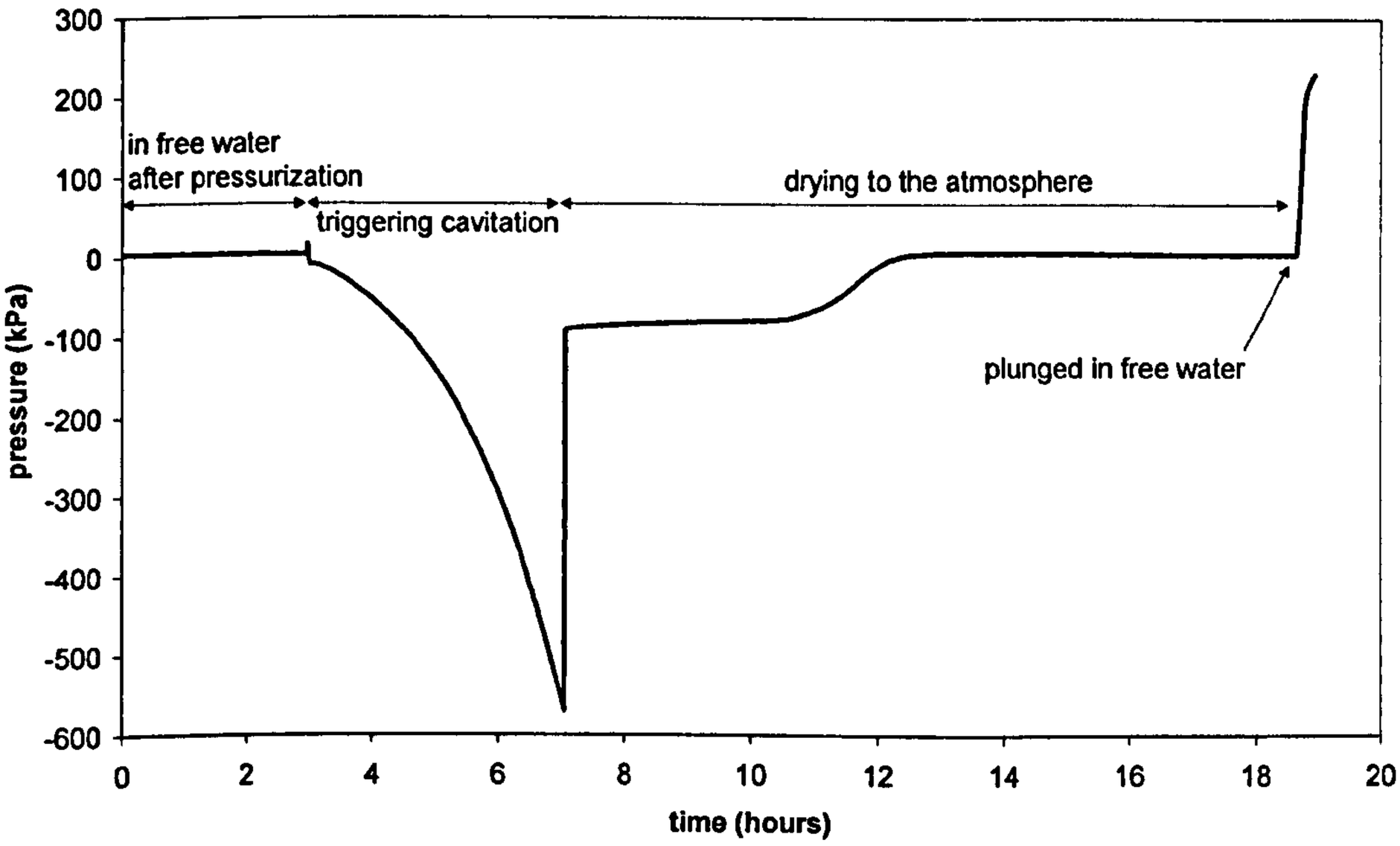

Figure 3.15: Tensiometer response when in contact with free water after cavitation and extensive drying (test T35, tensiometer II1)

Such response was investigated by leaving the tensiometers submerged in free water until readings stabilized (Figure 3.16a) or by removing the tensiometer from water during the pressure increase (Figure 3.16b). Figure 3.16a show that the pressure peaked at 700kPa and then decreased smoothly and slowly with time until stabilizing 2 months later at approximately -40kPa. The decrease is interpreted as air diffusing into the water leaving most of the reservoir filled with water. In Figure 3.16b, the tensiometer was removed from water at 250kPa and wiped clean. Pressure still

increased up to 320kPa and then stabilized at zero 1h later. The decrease in this case is interpreted as a decompression of the air as water evaporates from the stone.

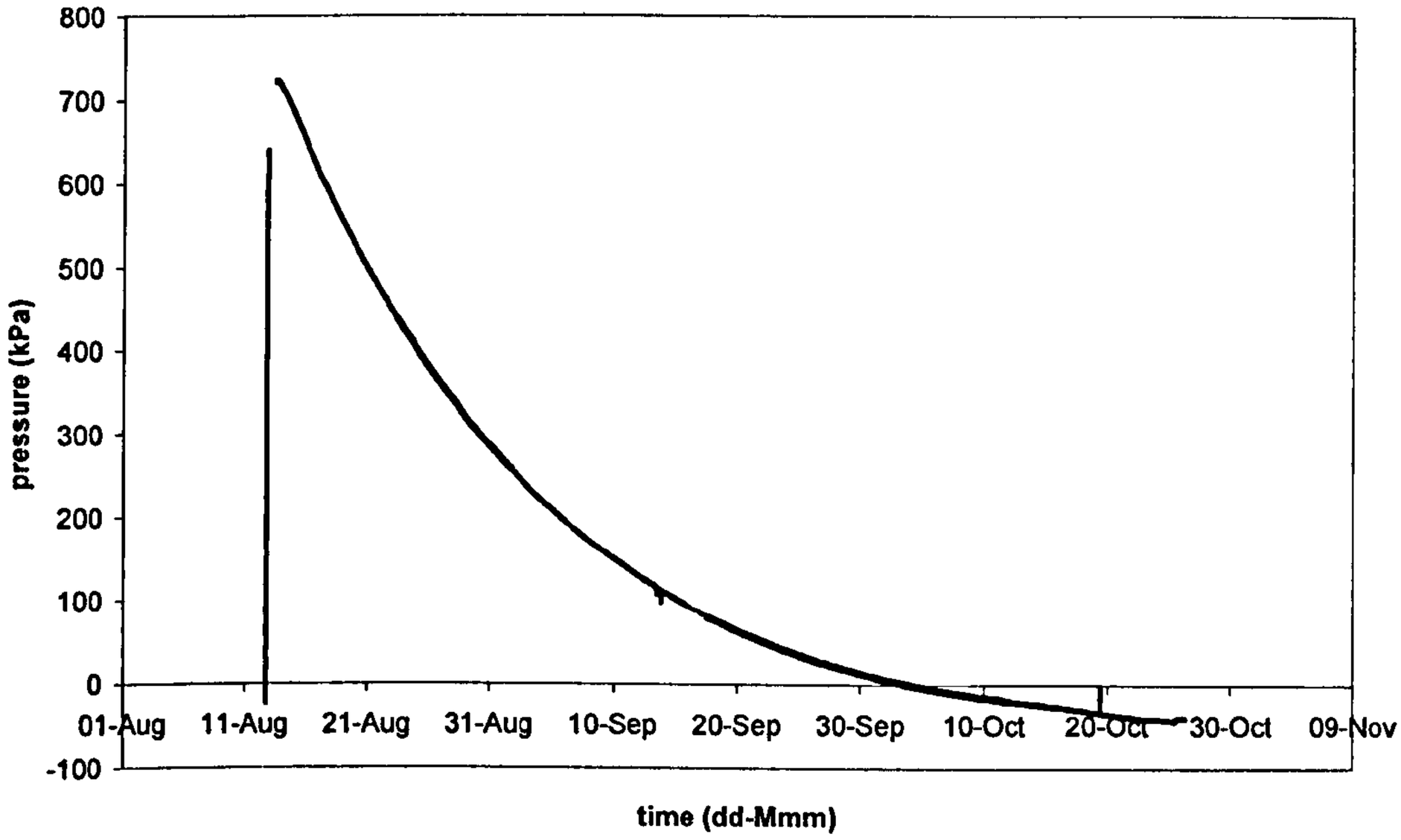

(a)

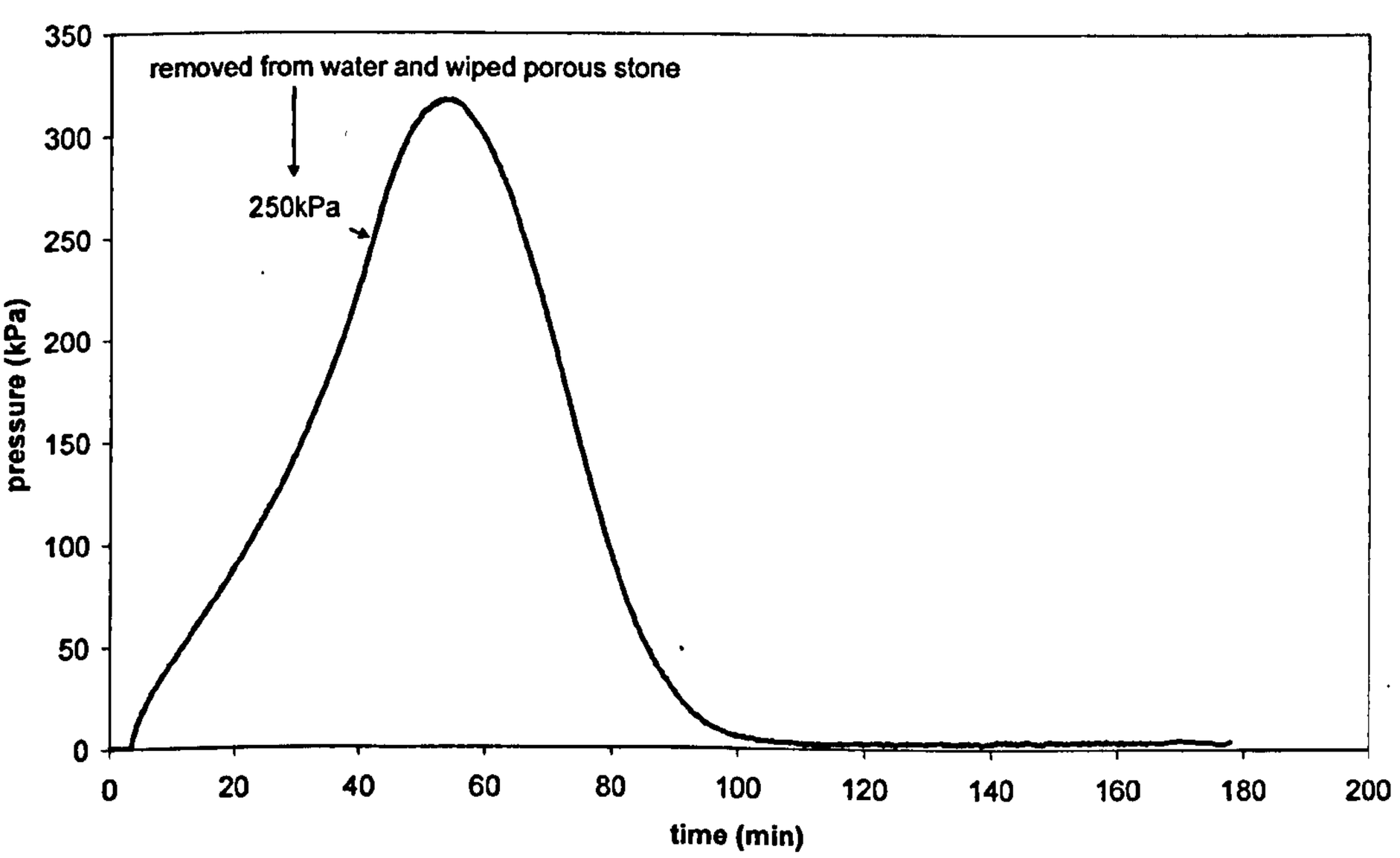

(b)

Figure 3.16: Response of a tensiometer plunged dry in free water, (a) tensiometer was left in water until readings stabilized by air dissolution in water (test Tpc1, tensiometer III5), (b) tensiometer was removed from water at 250kPa (test Tpc2, tensiometer III5)

Further tests were carried out by performing mass measurements during the pressure increase. If the pressure increase was due to capillarity, then the water content of the stone should increase. The mass measurements were done with a Sartorius balance with a precision of ±0.0001g. However, it is expected that the precision considered is of ±0.001g (1 order less) because the cable might have been contaminated by dust as it was used. The tensiometer was initially dried in silica gel and then plunged in free water.

Figure 3.17a clearly shows the mass increasing with pressure until approximately 830kPa and then just increasing a little. Most of the mass increase (0.18g) was until pressure reached approximately 700kPa. From 700kPa to 830kPa the increase was in the order of 0.01g (Figure 3.17b).

The excess air pressure phenomenon can also be observed when applying cycles of water pressure to an initially dry stone (Donoghue, 2006). In Figure 3.18 as the applied pressure increases and decreases back to zero (the transducer readings), a residual positive air pressure due to capillarity remains between the ceramic transducer and the wetting front. So when the applied pressure returns to zero, the tensiometer readings stop at a value which corresponds to the pressure of the trapped air. The subsequent cycles of water pressure progressively replace the air by water until most of the reservoir is saturated. The shape of the tensiometer curve is similar as in Figure 3.16a.

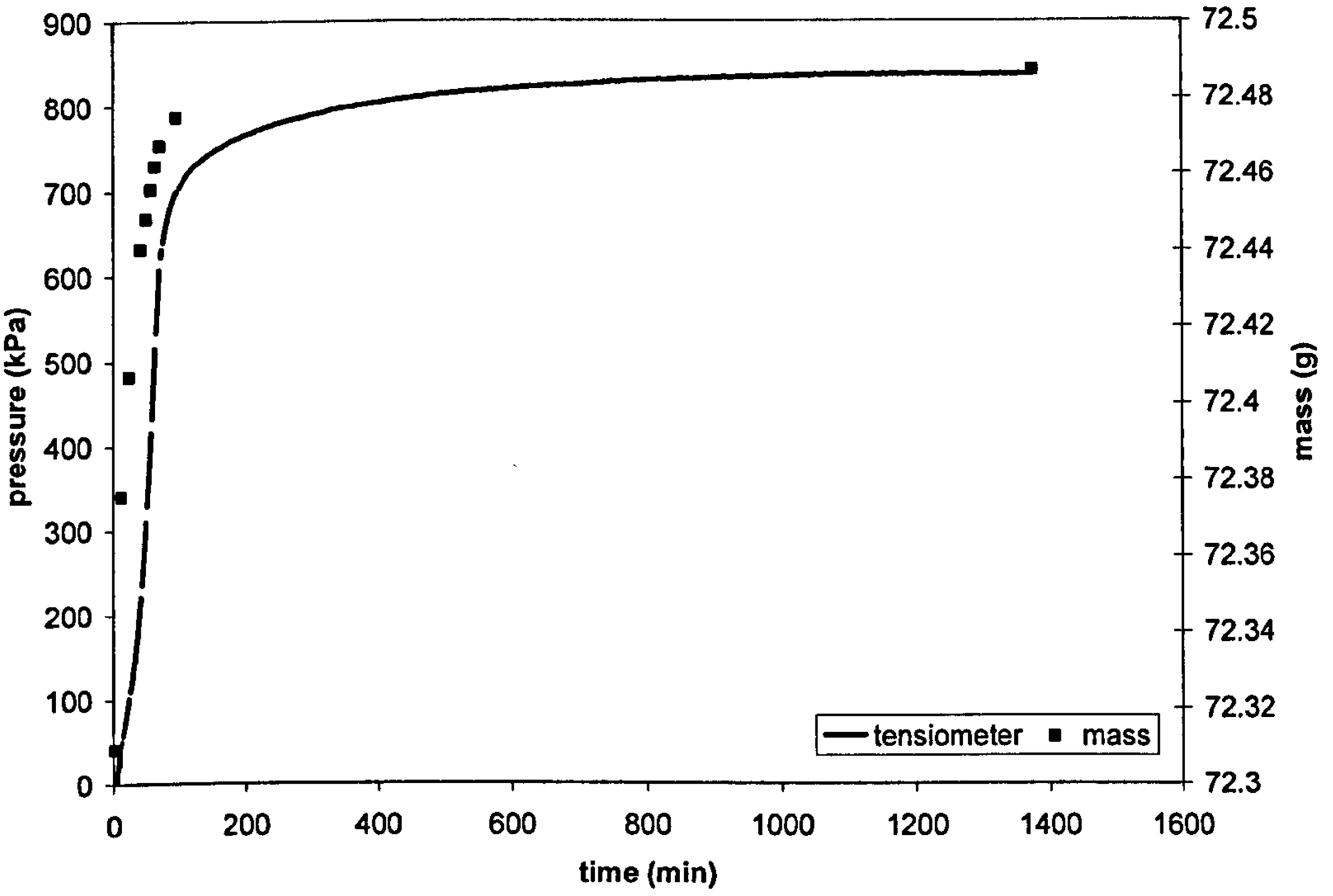

(a)

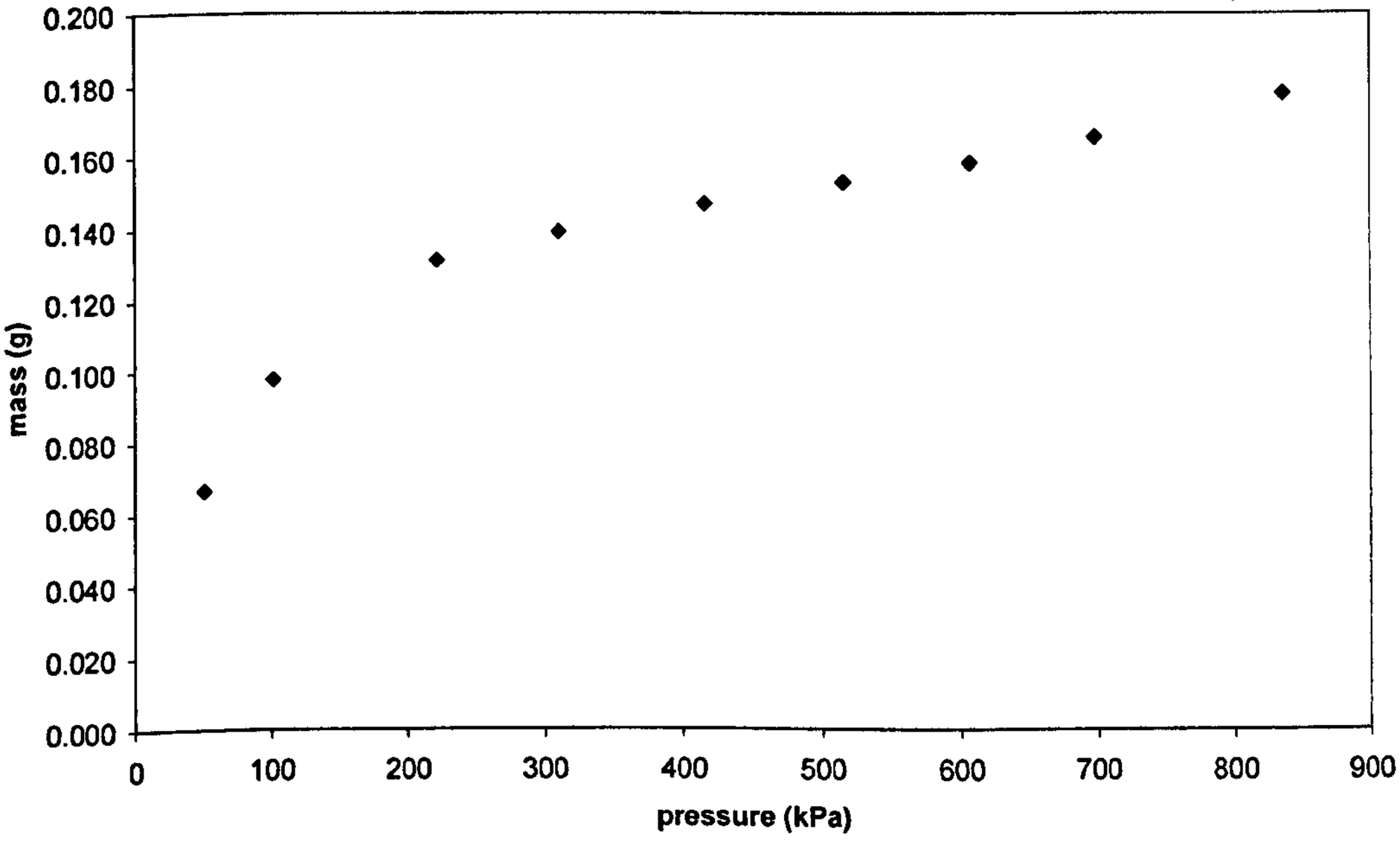

(b)

Figure 3.17: Mass measurements of the tensiometer during the pressure increase (test Tpc3, tensiometer III5), (a) time series, (b) mass versus pressure

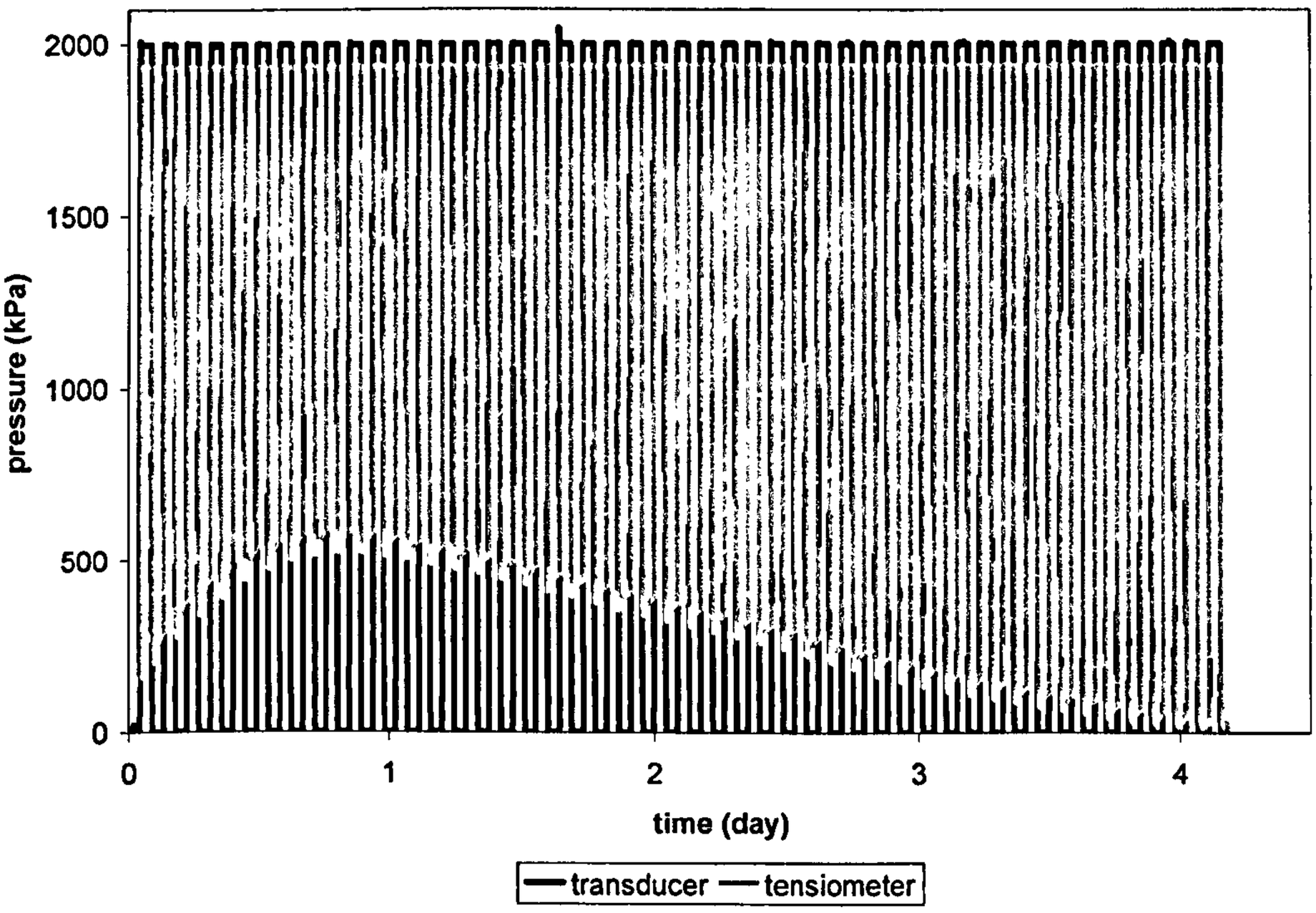

Figure 3.18: Water pressure cycles applied to a dry tensiometer (applied water pressure measured by a transducer and monitored by the tensiometer) (after Donoghue, 2006)

3.3.4. Discussion

3.3.4.1. Evaluation of the saturation degree

Besides the usual way of evaluating the degree of saturation of tensiometers by triggering cavitation, an alternative way is to look at the speed of response of the tensiometer either in the positive or negative range. For example, the delayed response in Figure 3.19 to a pressure increase implies poor saturation. The same in the negative range, fast increases after cleaning the stone is a sign of high saturation, and consequently high suction.

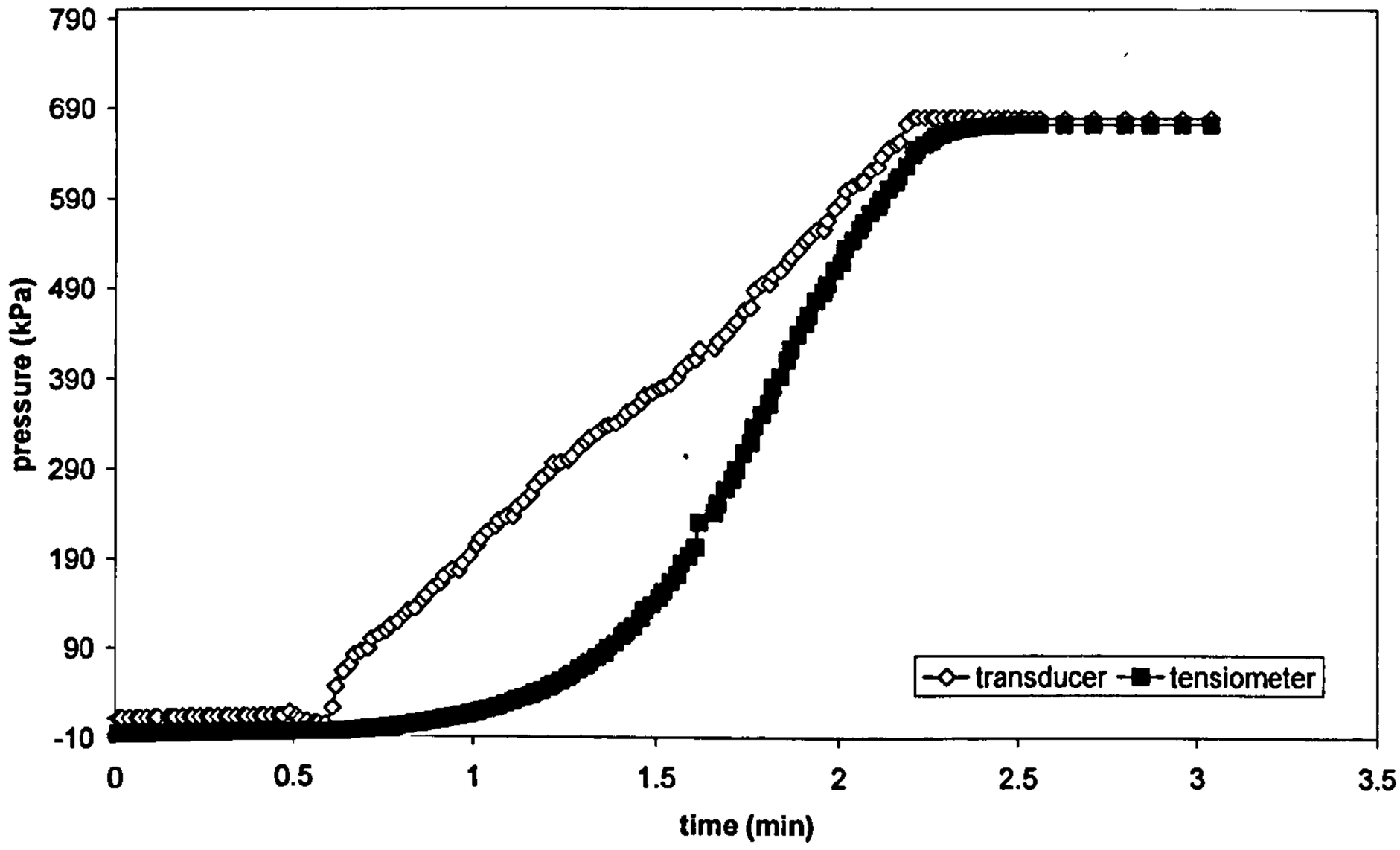

Figure 3.19: Evaluation of the saturation degree of tensiometers by the speed of response (test T36, tensiometer II2)

3.3.4.2. Excess air pressure

Figure 3.17 can be further analyzed by plotting the degree of saturation versus pressure. The degree of saturation was estimated based on data from the Porous Ceramics Catalogue (S.M.C.). The degree of saturation curves were calculated for two densities due to the density variation of the 15 bar AEV stones (1.73-2.48g/cm^3 according to the SMC catalogue). The specific gravity was estimated in 2.6.

Both curves for two different tests (the one from Figure 3.17 and a second called 'test 2') in Figure 3.20 show that most of the stone is saturated when the air pressure reached its maximum, particularly when the highest density is considered.

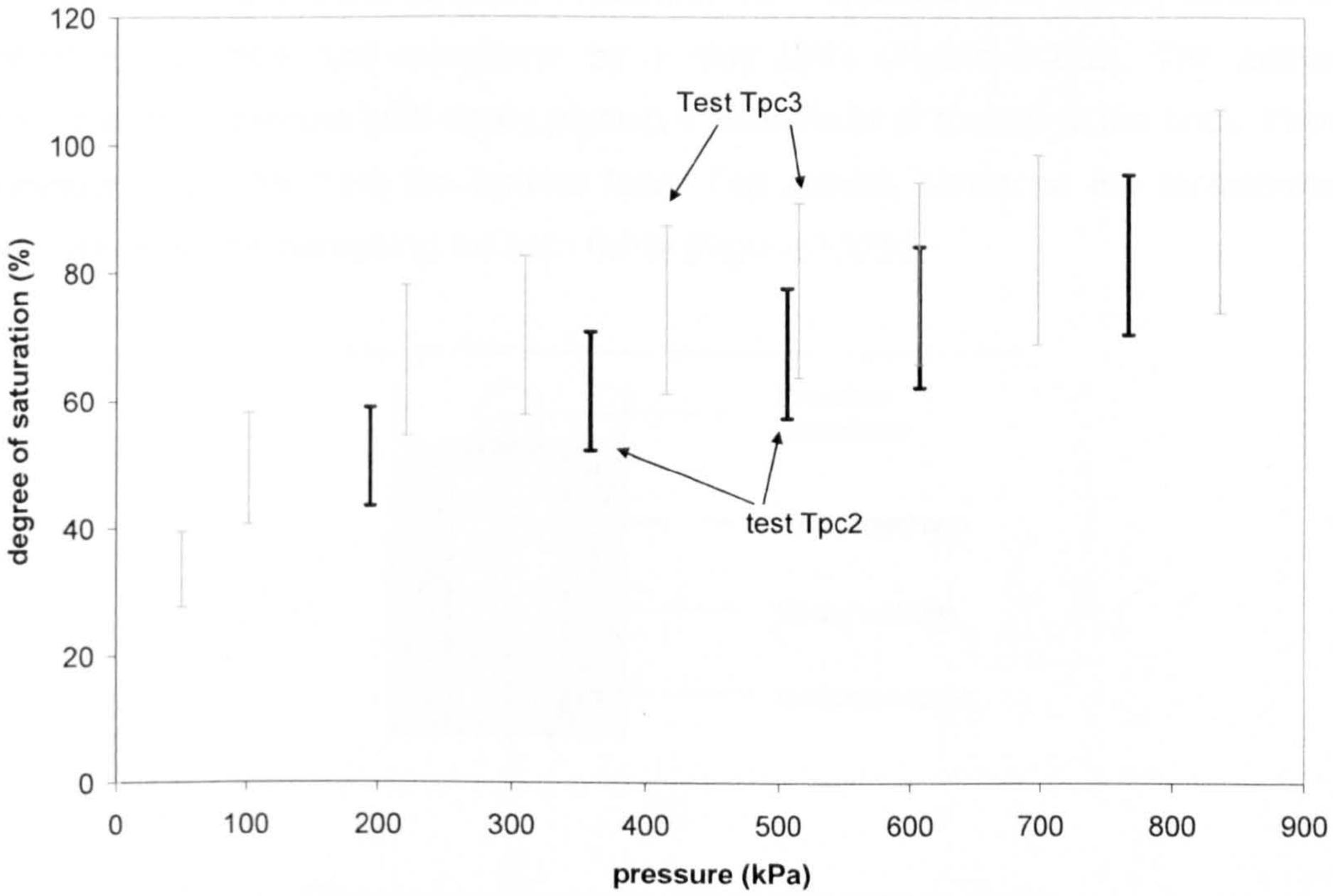

Figure 3.20: Degree of saturation versus excess air pressure for tests Tpc2, Tpc3 (n=32%, e=0.471, G_s=2.6, m_1=0.95g, m_2=1.36g; n is porosity, e void ratio, G_s the specific gravity, m_1 and m_2 are the mass of the stone for the 2 densities)

The mechanism previously explained for the excess air pressure generation is schematically shown in Figure 3.21. The inward movement of water by capillarity traps and compresses air ahead of the wetting front leading to the strain gauge deforming to the positive side as if under positive water pressures until an equilibrium condition is reached. Then, the pressure readings start decreasing to zero as air diffuses into water and the reservoir is filled.

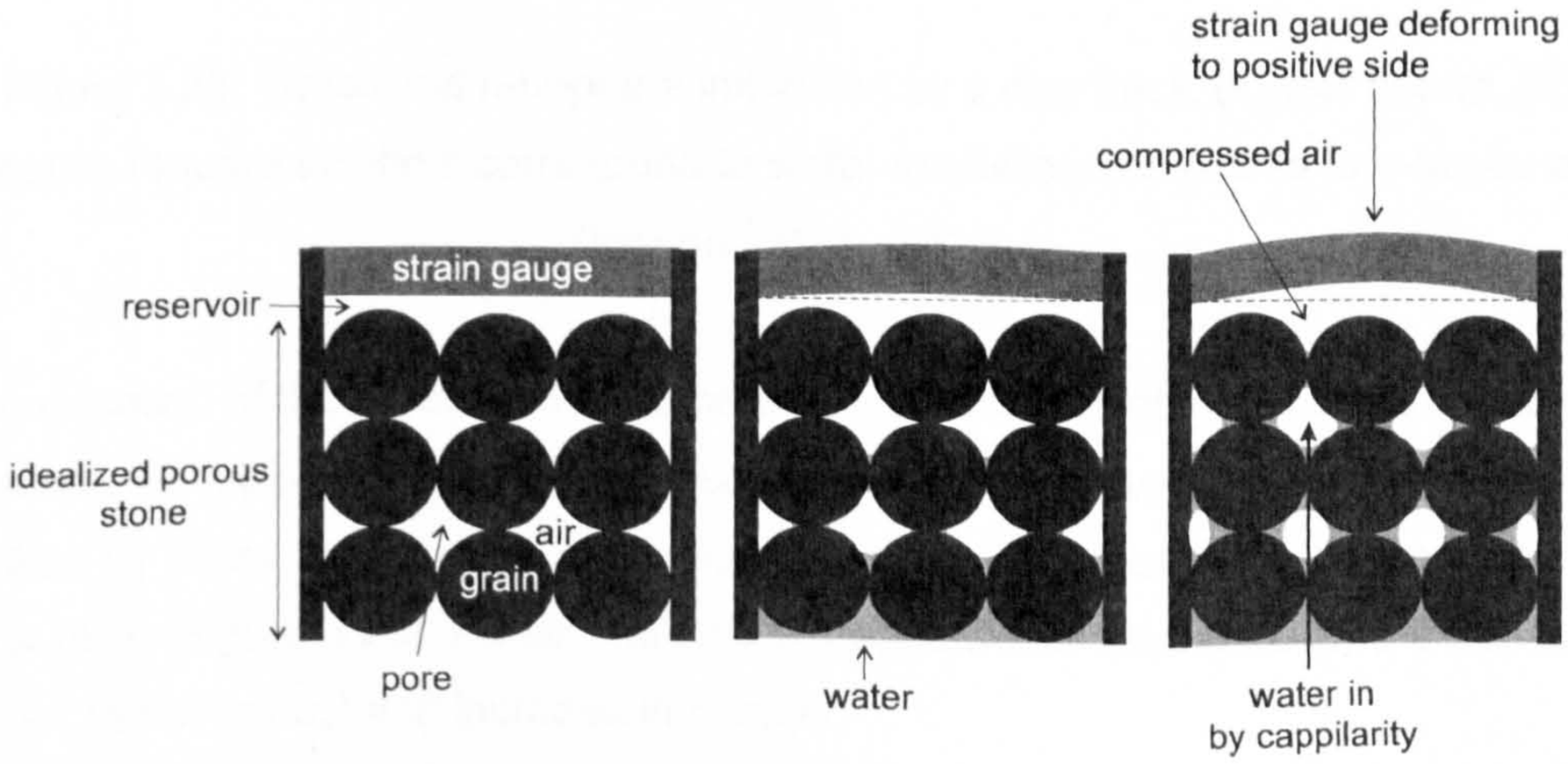

Figure 3.21: Schematic diagram for the excess air pressure mechanism

Similar results have been reported in the literature. Ioannou et al. (2003) studied the imbibition of water and *n*-heptane by a clay brick (Figure 3.22a). The authors measured the pressure built-up by placing a transducer at the top of the brick. Water imbibition was only from the bottom face. The results, similar to the tensiometer, show air pressure increasing for both fluids (Figure 3.22b).

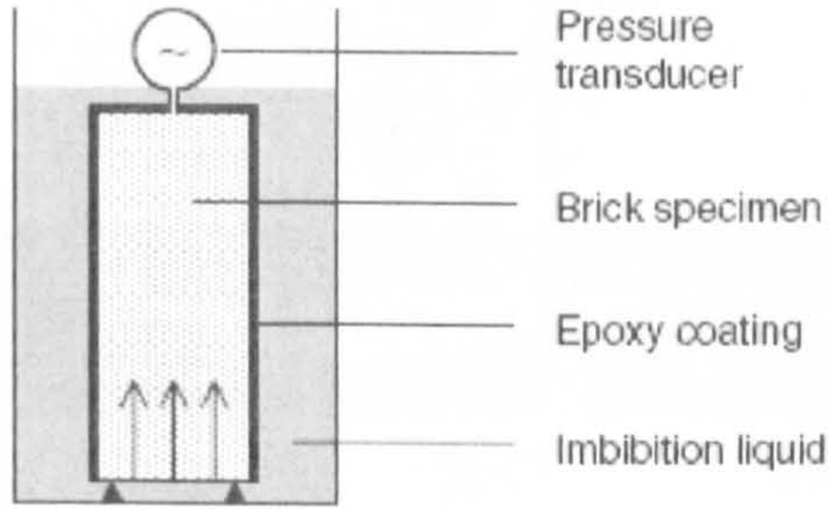

(a)

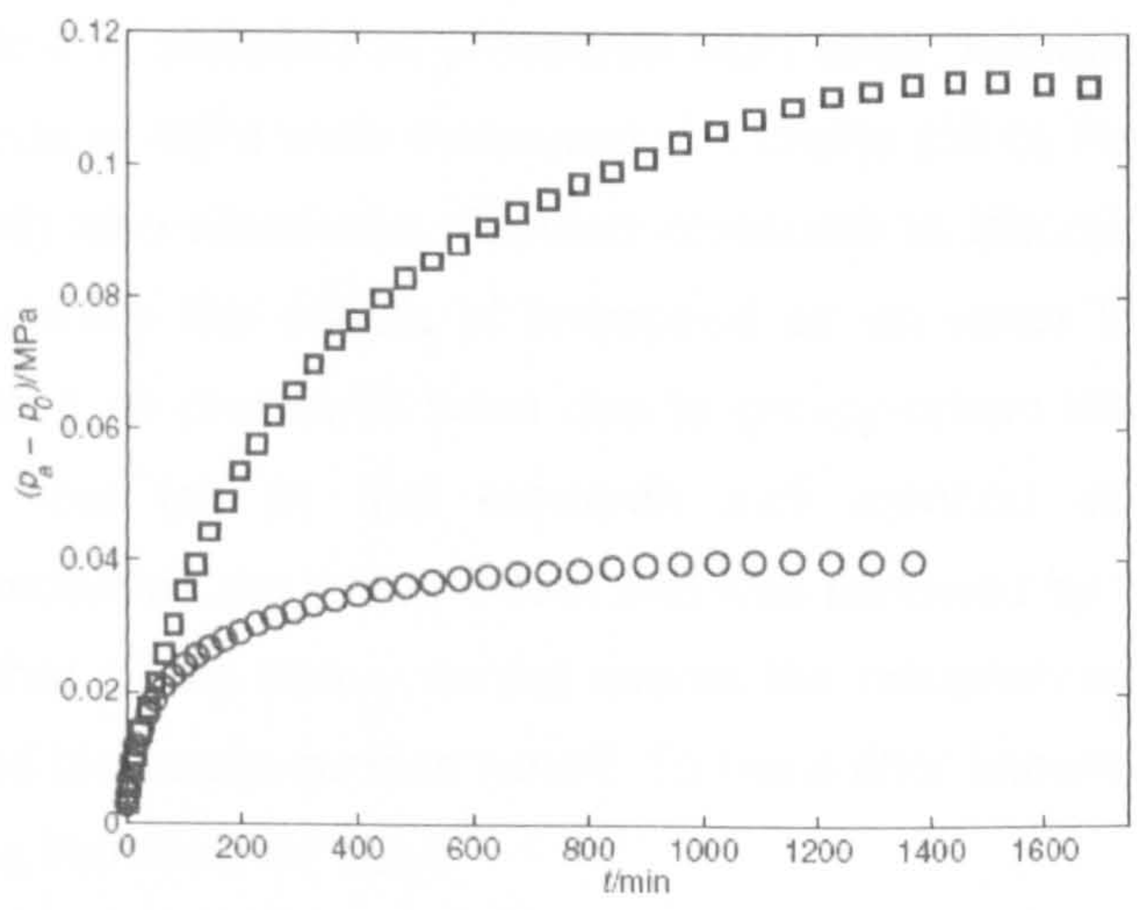

(b)

Figure 3.22: Water and *n*-heptane imbibition by a clay brick, (a) test set-up, (b) results (square symbols correspond to water imbibition and circles to *n*-heptane) (Ioannou et al., 2003)

An implication of these results is that pore air in the field might not be at atmospheric pressure. Pockets of elevated air pressure can develop during wetting if air flow is blocked by water saturated barriers, e.g. a wetting front meeting a concave-shaped water table (Figure 3.23). An air pressure increase would contribute for a decrease in the net stress (σ_3-u_a) and increase in suction.

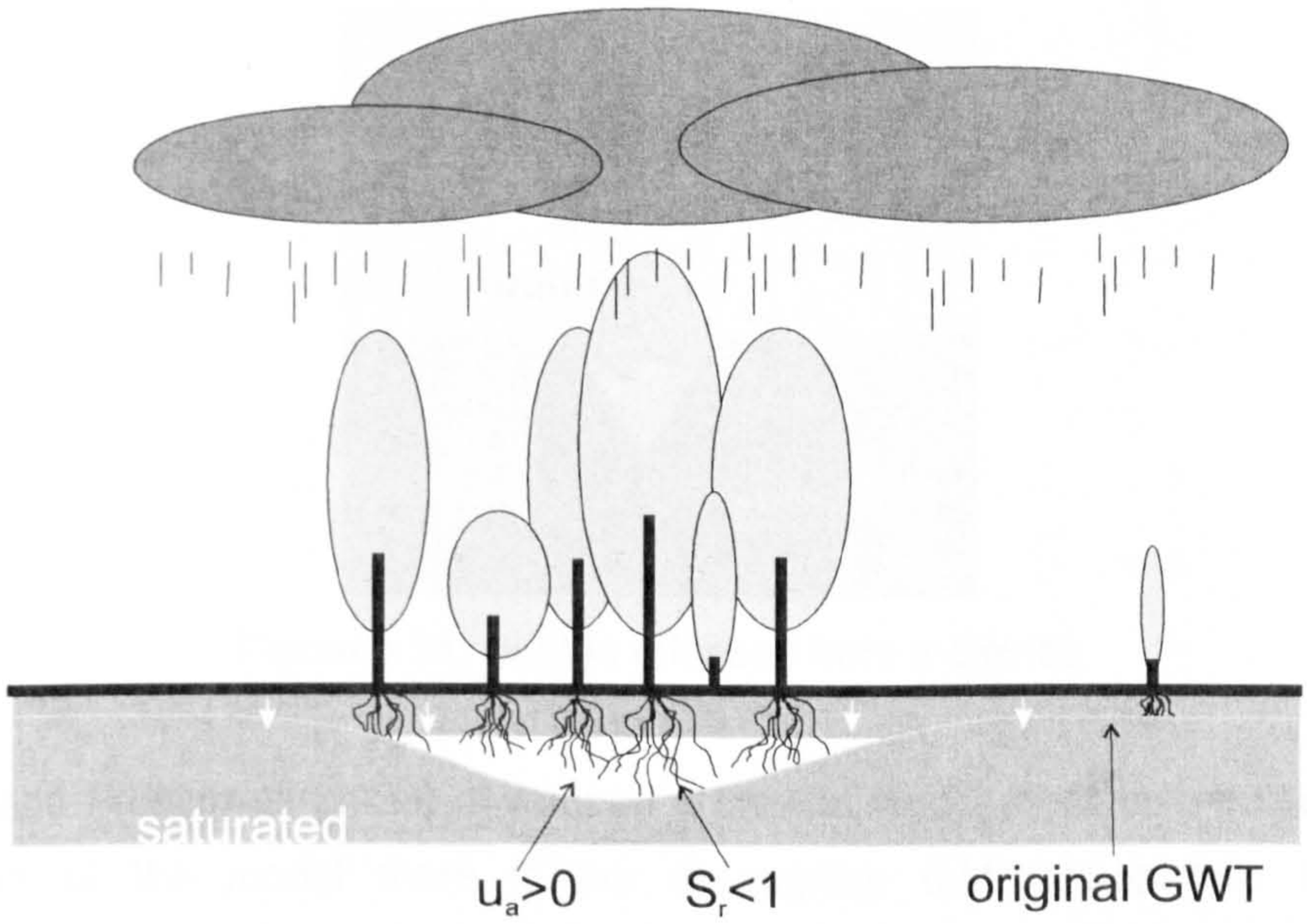

Figure 3.23: Possible example of elevated air pressures in the field

Field measurements of elevated air pressures have been documented. Maximum air pressures variations of 4kPa were measured in a prairie soil by Renault et al. (1998). Wang et al. (1998) also measured elevated pressures in laboratory experiments in loamy sand to quantify the effects of entrapped air on water infiltration. For both studies the elevated air pressures were due to gravity-driven infiltration rather than capillarity-driven flow (as in this research and Ioannou et al., 2003). This phenomenon is known as the 'Lisse' effect and was reviewed by Weeks (2002). The consequence is that during heavy rainfall events the compressed air decreases the infiltration rate and increases surface runoff. To the author knowledge this effect was not reported in the literature for clays.

3.3.4.3. Analysis of cavitation

Cavitation in tensiometers has been mainly associated to the formation of bubbles from gas trapped in crevices at the interface between water and tensiometer as shown in Figure 3.24 (e.g. Ridley et al., 2003). The gas trapped in crevices slowly grows until it is released in the form of a bubble when a critical condition is reached. What is commonly referred to as 'cavitation' in tensiometers correspond to the sudden release of a bubble from a crevice. Explanations of bubble growth and release from crevices during cavitation in tensiometers tend to be general and neglect key factors as discussed in Section 2.4.

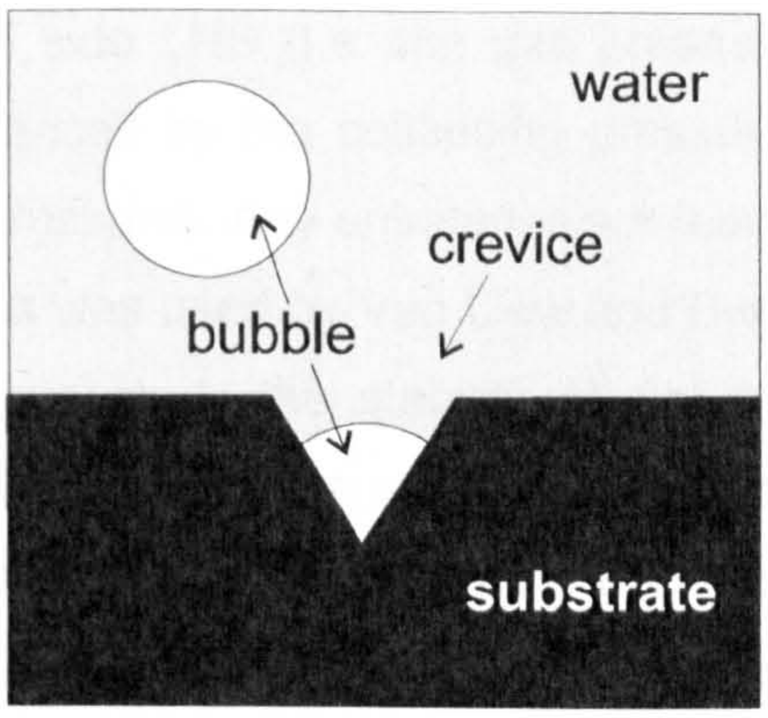

Figure 3.24: Bubble released from a crevice

Atchley and Prosperetti (1989) developed a crevice model for bubble nucleation. At the basis of the model there is the assumption that hydrophobic impurities congregate at the bottom of crevices preventing the water from making contact with solid surfaces. Following on Harvey et al. (1944), the model describes bubble growth and release from microscopic crevices due to a decrease of liquid pressure. In particular, it predicts the liquid pressure at which cavitation occurs depending on the geometry of the crevice, contact angles of the air-water interfaces, gas saturation and other physical variables. Examples presented in Atchley and Prosperetti (1989) show that the liquid pressure at cavitation ranges from -4 to -10bar for crevices with dimensions at μm scale and initial volumes of trapped gas of few μm^3. Cavitation is triggered by a decrease in liquid pressure (instead of an increase of gas pressure inside the bubble).

The model as presented by Atchley and Prosperetti (1989) provides a quantitative insight into bubble growth and release and suits very well the physical process occurring during cavitation in tensiometers. The subsequent part of this section will therefore interpret the model of Atchley and Prosperetti (1989) with the objective of linking it to the phenomenon of cavitation in tensiometers.

The equilibrium equation of a spherical free bubble in water is:

$$p_A + p_V = p_L + \frac{2\sigma}{R} \tag{3.1}$$

where p_A is the partial absolute pressure of air inside the bubble, p_V is the partial absolute pressure of vapour inside the bubble, p_L is the liquid absolute pressure outside the bubble, σ is the surface tension of water, and R is the radius of the spherical bubble. Equation (3.1) indicates that, at equilibrium, the expanding

pressures in the left-hand side LHS (i.e. the gas pressure sum of air and vapour partial pressures) are balanced by the collapsing pressures on the right-hand side RHS (liquid and Laplace pressure). Any unbalance will lead to a bubble size increase or decrease. This approach was used by Van Liew and Burkard (1995) and Van Liew and Raychaudhuri (1997) to study the stability of gas bubbles in the blood. The collapsing forces were controlled by the surface tension of the gas-blood interface and the expanding forces (called by the authors mechanical stabilizers) tended to resist the tendency for decrease in surface area. The same rationale applies to free air bubbles in the reservoir or porous stone of the tensiometer. Any bubbles will easily tend to expand for decreasing liquid pressures, depending on partial absolute pressure of air and vapour inside the bubbles. Therefore, as tensiometers measure suctions up to 2MPa, cavitation cannot start from undissolved air bubbles. The most likely alternative is bubble release from microscopic crevices in the reservoir, porous stone or floating impurities.

The treatment of the crevice model by Harvey et al. (1944) identifies cavitation with the value of the liquid pressure at which the contact angle θ between the air-water interface and the crevice surface reaches the receding value θ_R. Any subsequent decrease of liquid pressure would produce corresponding changes of the radius of curvature and gas pressure resulting in a continuous growth of the bubble. This is illustrated in Figure 3.25 for different receding contact angles. In Figure 3.25a, if the pressure of the liquid is gradually decreased, the bubble grows in size from the initial position corresponding to the advancing value of contact angle θ_A, until a minimum of the contact angle given by the receding value θ_R. The bubble, however, might detach before such minimum value of the contact angle is achieved if the gas pressure becomes greater than the surface tension effect and liquid pressure. If θ_R is larger, as in Figure 3.25b, the contact angle will reduce only slightly from its initial value (different in this case from the advancing contact angle) until $\theta=\theta_R$. At this point the contact angle has reached its minimum and the bubble moves outward on the side of the cavity with $\theta=\theta_R$ until the expanding forces of the enlarging bubble pull it away from the cavity. In Figure 3.25c the bubble has initially a convex curvature towards the gas and, at this initial position, the contact angle is equal to the receding value θ_R, so any liquid pressure decrease leads to a movement up in the crevice with the curvature unchanged.

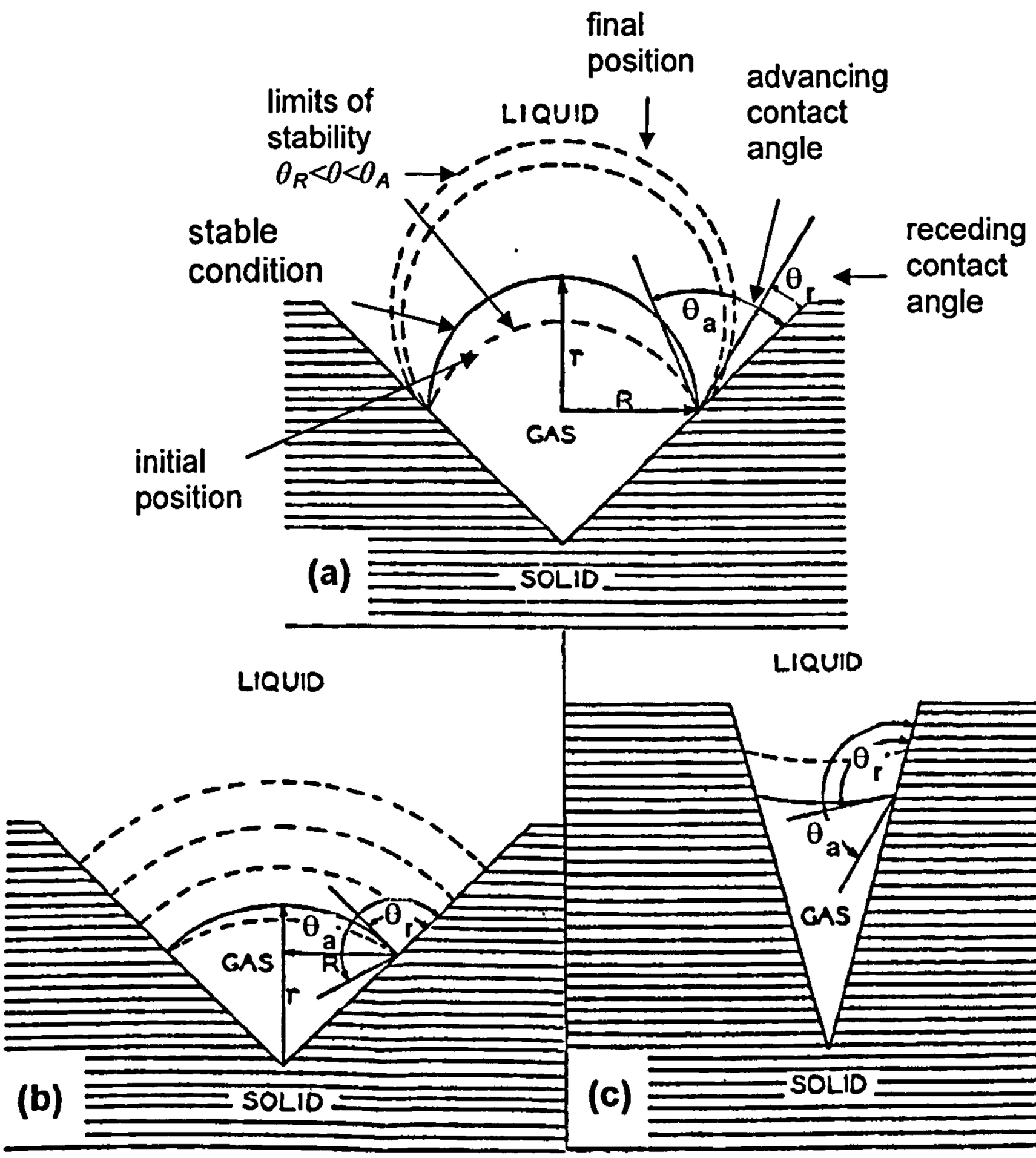

Figure 3.25: An air bubble in a conical cavity with (a) small receding contact angle, (b) large receding contact angle and (c) initial contact angle equal to the receding contact angle (after Harvey et al., 1944)

Atchley and Prosperetti (1989) re-examined the crevice model as presented by Harvey et al. (1944) and concluded that the model overlooks the fact that the upward motion of the interface causes both the Laplace pressure and the gas pressure to decrease. Harvey's model is only valid if the gas pressure decreases faster than the Laplace pressure but, if the pressure differential across the interface decreases faster, than the gas pressure instability could occur even if the condition $\theta=\theta_R$ is not met. Atchley and Prosperetti (1989) took this in consideration and developed a model where the gas pressure changes proportionally to the volume, i.e. if the pressure of the liquid decreases and the bubble volume increases, the pressure of the gas will decrease. Note that the model does not account for diffusion across the air-water interface. Atchley and Prosperetti (1989) use the equilibrium equation (3.1) and calculate the liquid pressure under the following limit conditions:

(1) p_L^A, when $\theta=\theta_R$, with the bubble inside the crevice (Figure 3.26a)

(2) p_L^B, when $r=R$, with the bubble inside the crevice (Figure 3.26b)

(3) p_L^C, when $\theta=\theta_R$, with the bubble outside the crevice (Figure 3.26c)

(4) p_L^D, when $r=R$, with the bubble outside the crevice (Figure 3.26d)

The condition $r=R$ corresponds to the formation of a hemisphere.

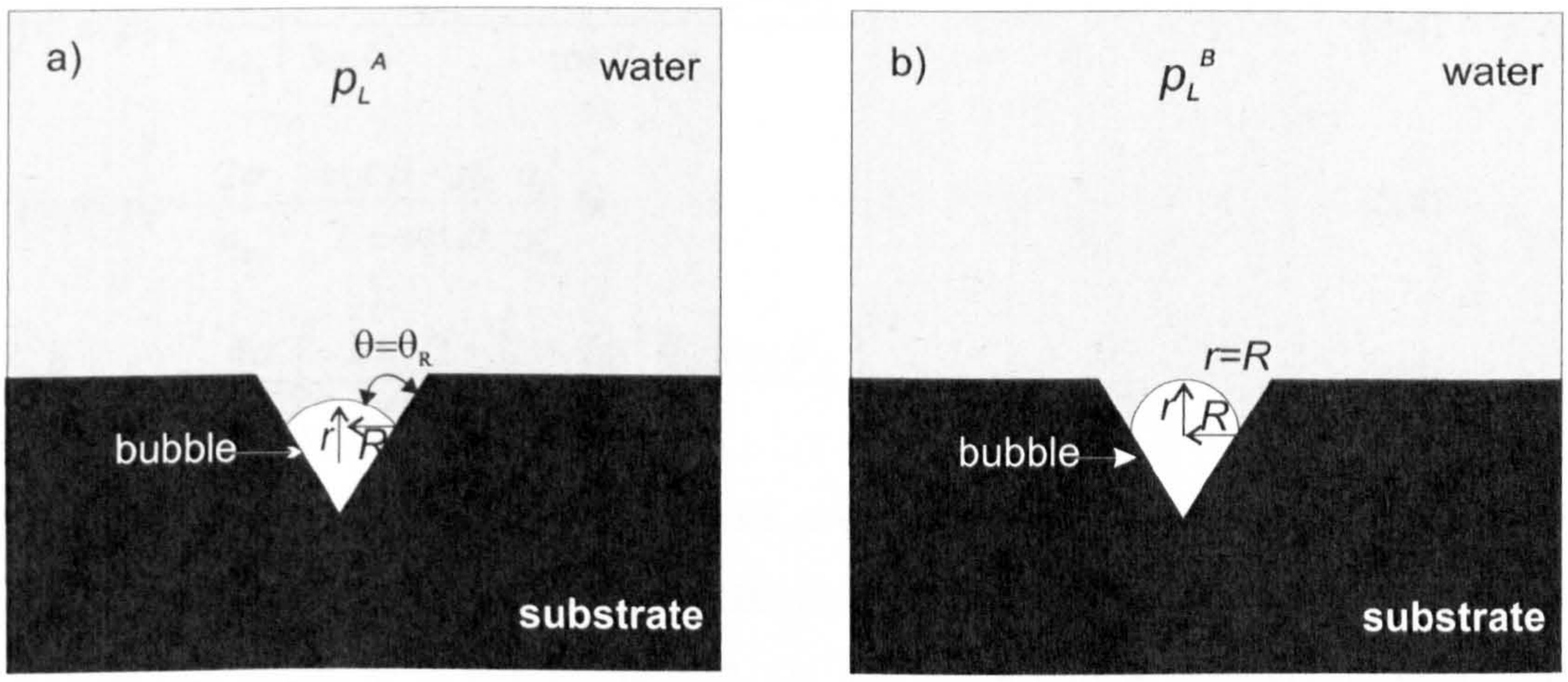

Figure 3.26: Schematic drawing for the different limit conditions; (a) p_L^A calculated when the moving contact angle θ equals the receding contact angle θ_R with the bubble inside the crevice; (b) p_L^B calculated when bubble forms a hemisphere ($r=R$) inside the crevice; (c) p_L^C calculated when $\theta=\theta_R$ with the bubble outside the crevice; (d) p_L^D calculated when bubble forms a hemisphere ($r=R$) outside the crevice

Special values of liquid pressure are identified for the 4 previous conditions. For cavitation to occur, the liquid pressure must fall below one of the liquid pressures corresponding to one of the above conditions defined through the following equations:

$$p_L^A = p_V + \frac{\cot\beta - \eta_0}{\cot\beta \pm \eta_R} G \mp \frac{2\sigma}{a_0} \left|\cos(\theta_R - \beta)\right| \tag{3.2}$$

$$p_L^B = p_V - \frac{4\sigma}{3a_0}\left(\frac{2\sigma}{3a_0 G}\frac{(\cot\beta + \eta_R)\left|\cos(\theta_R - \beta)\right|^3}{\cot\beta - \eta_0}\right)^{1/2} \tag{3.3}$$

$$p_L^C \approx p_V - \frac{2\sigma}{a_m} + \frac{\cot\beta - \eta_0}{2 + \cot\beta}\frac{a_0^3}{a_m^3} G \tag{3.4}$$

$$p_L^D \approx p_V - \frac{4\sigma}{3a_0}\left(\frac{2\sigma}{3a_0 G}\frac{2 + \left(2 + \sin^2\theta_R\right)\cos\theta_R}{\cot\beta - \eta_0}\right)^{1/2} \tag{3.5}$$

where p_L^A, p_L^B, p_L^C, p_L^D are the liquid pressures corresponding respectively to conditions a), b), c) and d) in Figure 3.26; p_V is the partial vapour pressure; β is the crevice half-angle; G is the air tension, i.e. the initial partial pressure of air in the bubble (it is different from p_G that is the total gas pressure inside the bubble, i.e. the sum of air partial pressure and vapour partial pressure); σ is the air-water surface tension; a_0 is the initial radius of the generic ring of contact; θ_R is the final radius of the ring of contact (the receding contact angle); a_m is the radius of the crevice mouth; η_0 and η_R are functions of θ and β. Figure 3.27 shows schematically the meaning of these notations.

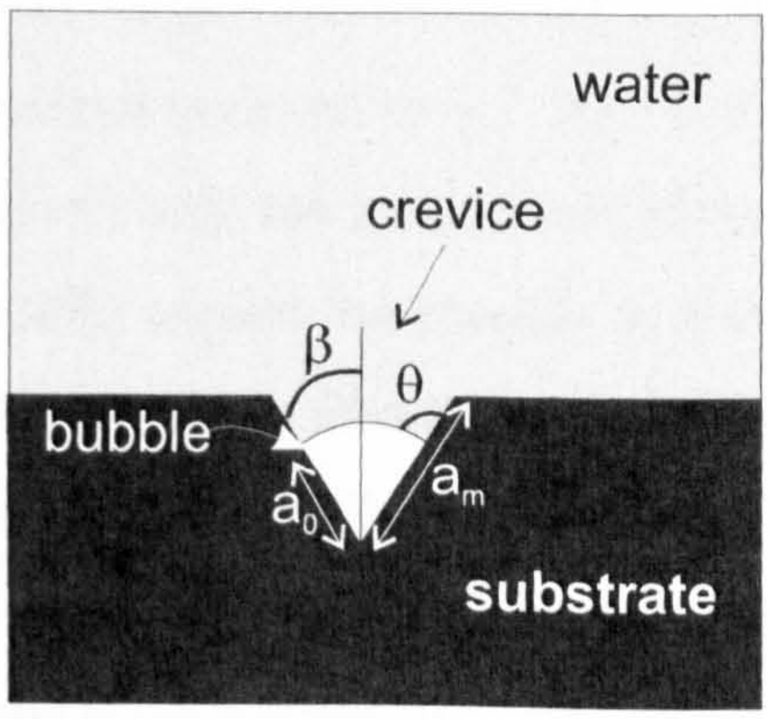

Figure 3.27: Geometry of a bubble in a crevice

All the above equations were derived from eq. (3.1). The derivation process of these equations as presented in Atchley and Prosperetti (1989) is long and consists of a sequence of 72 equations, therefore no details will be presented here. The equations

define the liquid pressures at which unstable growth inside or outside the crevice starts, which will occur when the receding contact angle is reached ($\theta=\theta_R$) or mechanical stability is lost ($r=R$). For cavitation to occur, the liquid pressure must fall below one of these thresholds. Therefore the thresholds have to be calculated for each of the 4 conditions and, depending on the geometry and location of the initial interface (inside or outside the crevice), the lowest value among the 4 values of p_L given by equations (3.2.), (3.3), (3.4) and (3.5) is chosen as the cavitation pressure. If the initial position of the air-water interface is outside the crevice, then it is not necessary to calculate p_L^A and p_L^B as these two values define threshold pressures inside the crevice and the cavitation pressure would be defined by the lowest of p_L^C and p_L^D.

An example of these thresholds is represented in Figure 3.28. The curve in Figure 3.28 was obtained for the following conditions: air-water interface is initially horizontal at the mouth of the crevice (Figure 3.29a) with a_m=0.35mm, θ_R=94°, β=15°, σ=0.072N/m, p_{L0}=0.975bar (the initial liquid pressure), p_v=0.025bar, G=0.975 bar, η_o=0.0131 and η_R=0.145. The interpretation of Figure 3.28 can be as follows: as the liquid pressure is decreased from 0.975bar, the interface bows outward until reaching the receding contact angle (Figure 3.29b). This value of pressure p_L^A is given by equation (3.2) and corresponds to a value of (p_v- p_L^A) equal to -0.15bar. According to Harvey's model, cavitation would occur at this point. However, if we keep decreasing the liquid pressure, a smaller value corresponding to p_L^B is attained (p_v- p_L^B=0.27bar) indicating that instability had not occurred for p_L^A. If p_L is still decreased, the interface goes from forming an angle θ_R with the crevice wall to forming an angle θ_R with the horizontal plane (Figure 3.29c) around the crevice. At this position p_v- p_L^C is 3.5bar. Afterwards the bubble will increase in size by keeping the same contact angle with the horizontal plane (Figure 3.29d). In these circumstances, the conditions to determine p_L^D will never be met, therefore p_L^D is irrelevant and the liquid pressure at cavitation should correspond to p_L^C in Figure 3.29c.

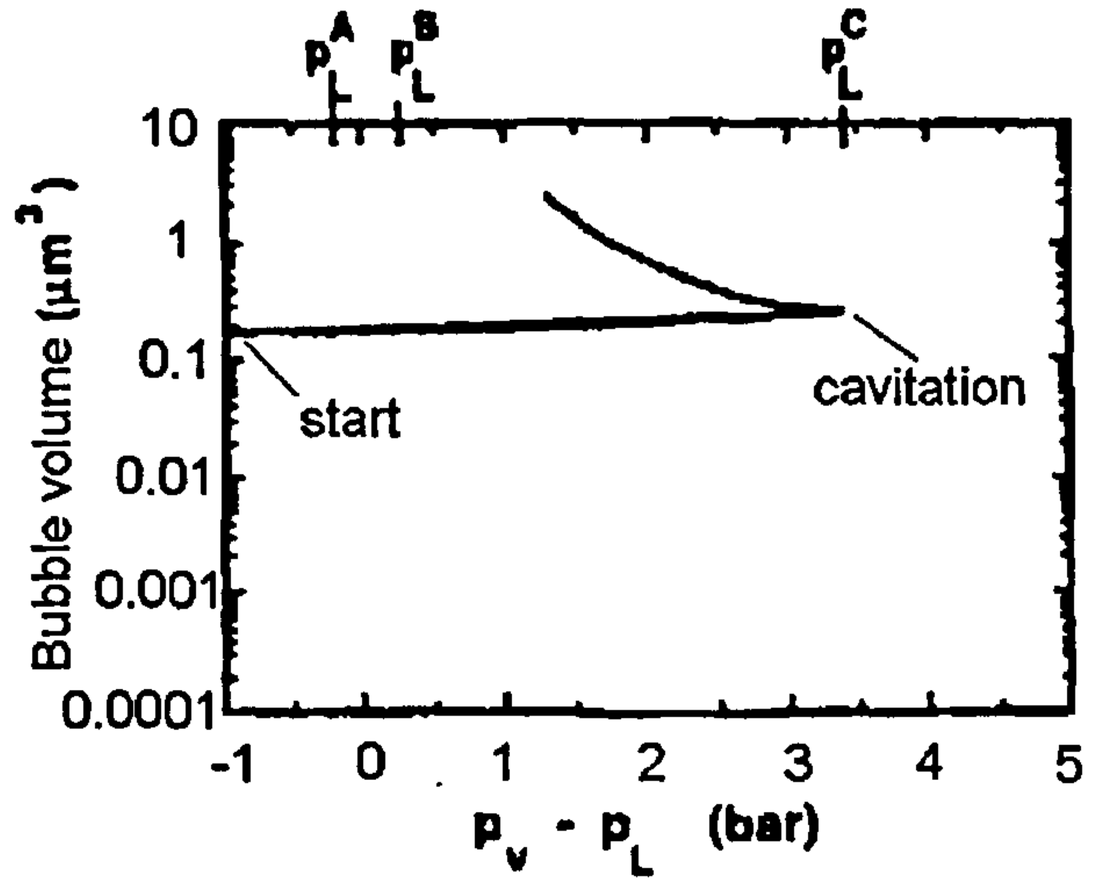

Figure 3.28: Atchley and Prosperetti (1989) predict cavitation in similar conditions to the tensiometer (the values noted in the figure are in the form $p_v - p_L^X$, rather than p_L^X)

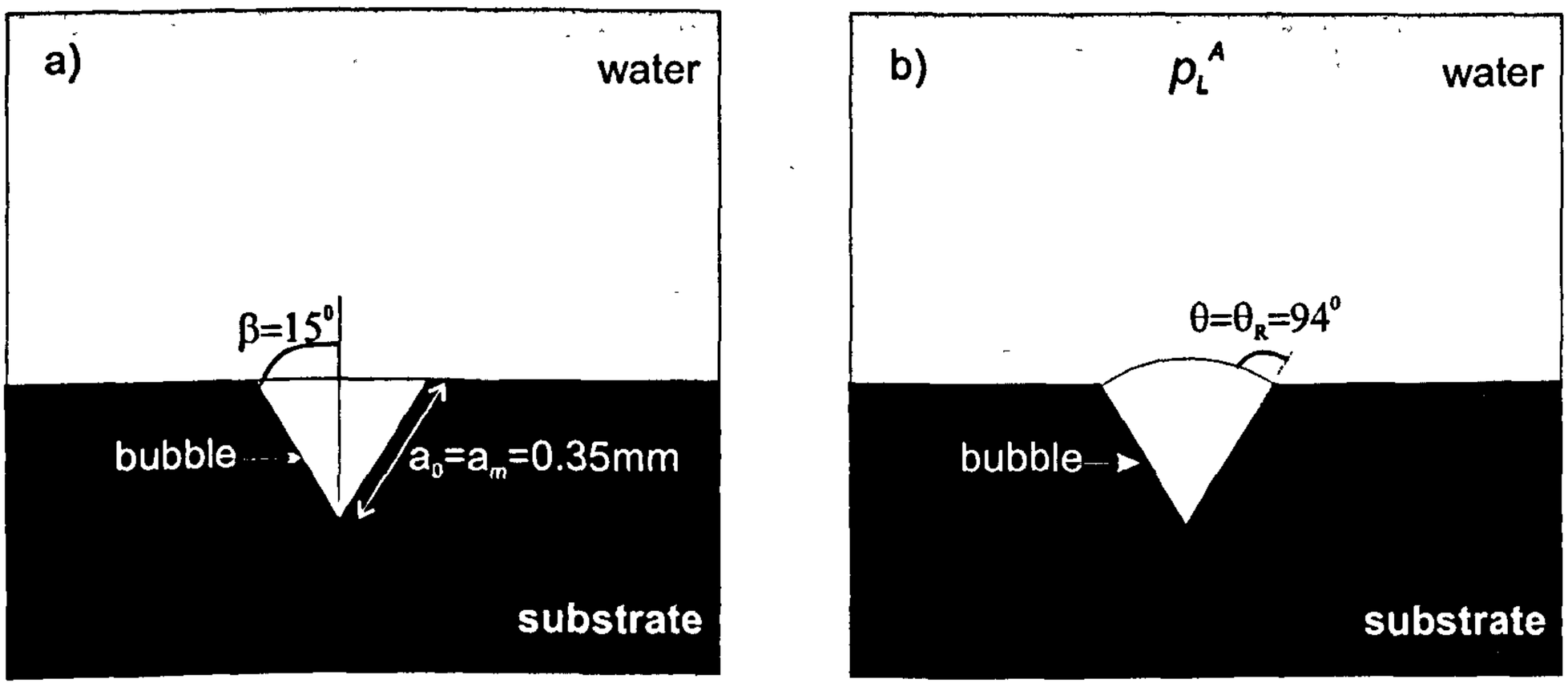

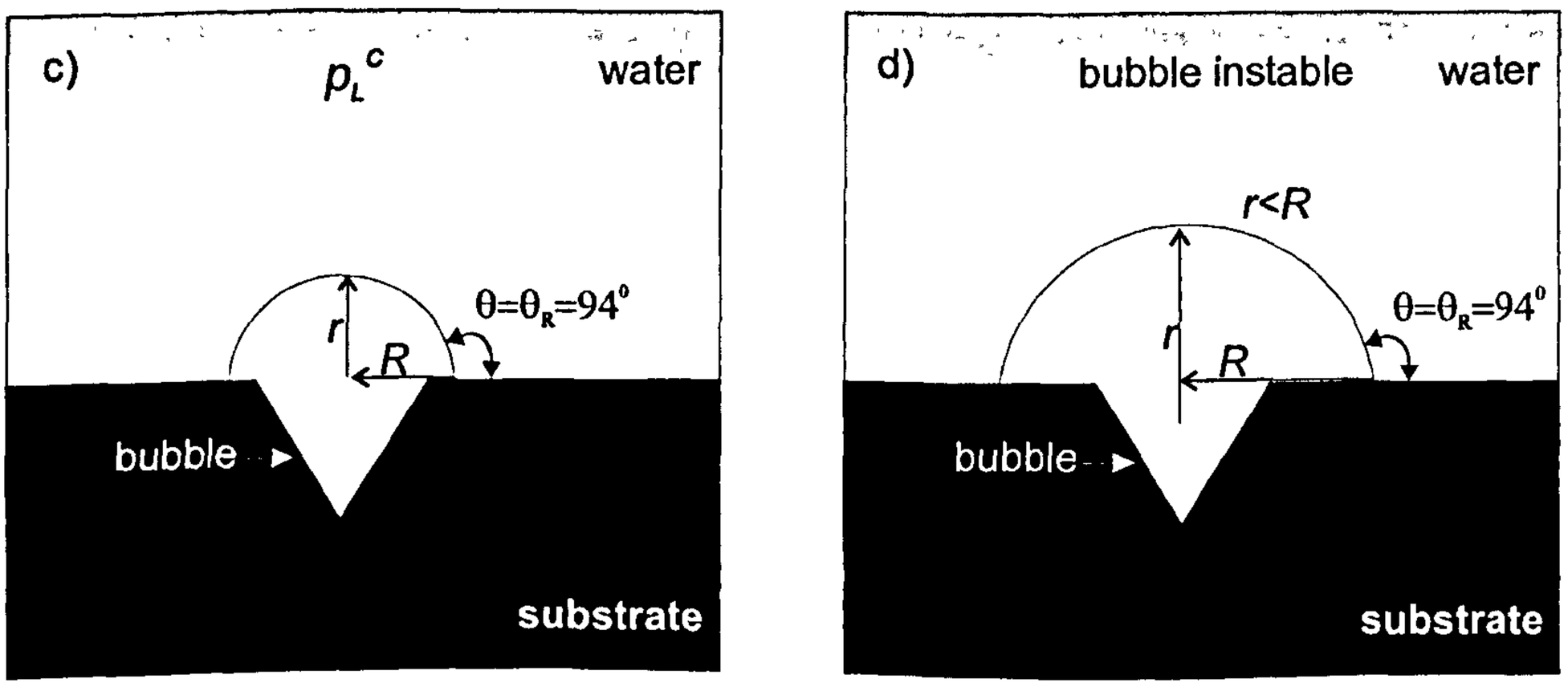

Figure 3.29: Bubble evolution for the test in Figure 3.28

The above considerations on the liquid pressure to trigger cavitation are complex, nonetheless they show that cavitation from a crevice can be predicted and depends on the values of the contact angles and the geometrical parameters of the crevice. The crevice model seems to fit well in tensiometers, the example in Figure 3.28 shows that cavitation occurs within the range of liquid pressures similar to tensiometers (~-4bar) for crevice dimensions probably equivalent to crevices located in the reservoir or porous stone of the tensiometers. However, it has to be said that the model was developed for acoustic cavitation (or fast cavitations) and so neglects gas-diffusion effects. In the case of the tensiometer, this model will only be relevant if suction changes fast.

3.3.4.4. Factors controlling cavitation

The above sections have presented the factors that influence cavitation, and have demonstrated how cavitation could occur in a tensiometer according to a theoretical model. This section will start by discussing the likely location where cavitation occurs in tensiometers. It will then review the key factors for measuring high suctions. Most of the existing literature has provided little investigation on the increase of the maximum suction measured by tensiometers with time of use. Factors controlling measurement of high suction values to be considered here include: maximum pressure applied during saturation, nature of the porous stone, temperature, and long term measurement of suction and cavitation history.

Location of cavitation

Knowing the location where cavitation starts in tensiometers would help improving the current design of these probes to extend their measurement range. There has been significant debate on such topic and studies on cavitation seem to point to different conclusions. Based on a literature review, different hypotheses about where cavitation starts are presented next.

- Cavitation starts anywhere in the stone or reservoir

(1) The study by Ishida et al. (2000), reviewed in Chapter 2, demonstrates that nano-sized bubbles attach to hydrophobic surfaces. Therefore bubbles of such size could adhere in all internal parts of the tensiometer, depending on the shape of the surface and the affinity of those surfaces to water.

(2) The study by Bremond et al. (2005), also reviewed in Chapter 2, has also demonstrated that bubbles release from surfaces, either flat or with microaspereties.

From both these studies, one can conclude that cavitation could start from any internal surface of the tensiometer.

- Cavitation starts in the porous stone

(1) Following the crevice model and looking at the images of the porous stone in Figure 3.5, it seems intuitive to assume that cavitation occurs within the porous stone. The highly angular and heterogeneous features of the stone provide excellent traps for air bubbles (many angular crevices have the dimensions and shape of the example of Figure 3.29).

(2) Tarantino and Mongiovi (2001) also proposed a mechanism with cavitation starting in the porous stone but did not explain the reason why cavitation should start there.

- Cavitation starts in the reservoir

(1) Bishop et al. (1975), Mair (1979) and Toll and Hight (unpublished) state that cavitation depends on the pores size, with smaller pores capable of maintaining higher suctions. According to this, cavitation should start in the reservoir due to the larger dimension compared to the pores of the ceramic stone (as if the reservoir was a crevice itself). A bubble of the size of the reservoir would have a volume in the order of mm^3 instead of μm^3. A bubble of this size will not withstand high suctions, expanding as soon as suction reached 100kPa. This simple link between cavitation location and dimensions of the pores is not however sufficient to conclude that cavitation starts in the reservoir.

(2) Guan (1996) gave relevant evidence that cavitation should start in the reservoir. The author placed a cellulose membrane in the reservoir and then triggered cavitations. The maximum suction immediately increased to 900kPa (Figure 3.30). Previous tests without the membrane reached suctions in the

order of 600kPa. According to the author, the tensiometer behaved much better as soon as the membrane was placed in the reservoir and this clearly demonstrates that the dimension of the reservoir plays a very important role in delaying cavitation.

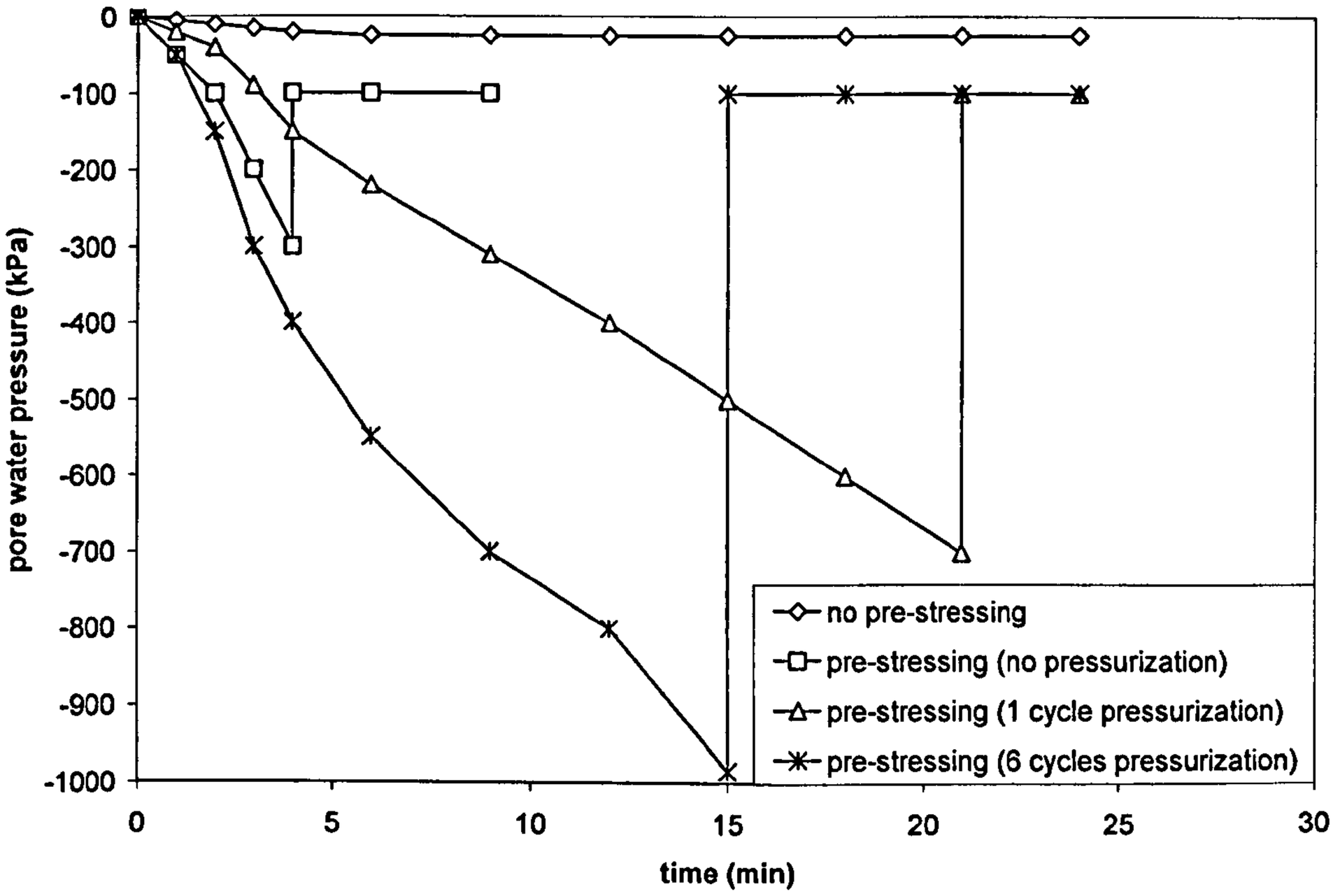

Figure 3.30: Improved response of the Saskatchewan tensiometer by placing a cellulose membrane in the reservoir; pre-stressing indicates that a pressure is applied to the membrane during placement in the reservoir (after Guan, 1996)

- Conclusion: cavitation starts anywhere with enough space for bubbles to grow

The only difference between cavitation starting in the reservoir or stone is that the pores in the stone are in a confined environment, i.e. any bubble growth would be constrained physically by the presence of the grains of the porous stone, while in the reservoir the bubble would be able to expand freely or coalesce with others forming a larger bubble. Guan (1996) clearly showed that decreasing the volume of the reservoir increased the cavitation threshold and this suggests that the onset of cavitation might depend on the availability of space for a bubble to grow.

Works published in physics journals (e.g. Atcheley and Prosperetti, 1989 or Bremond et al., 2005) are based on experiments performed on relatively large volumes of

water, where bubbles are free to release from surfaces or crevices but, to the author knowledge, there is no investigation on cavitation occurring in confined spaces.

Even if a bubble managed to release within the porous stone of a tensiometer, it would be immediately trapped by the surrounding grains while the relatively large volume of the reservoir allows bubbles to expand and coalesce. Although small bubbles can form anywhere either in the porous stone or reservoir, they can only coalesce to create an air discontinuity inside the reservoir due its larger volume. This seems to indicate that the critical aspect to achieve measurement of high suctions is the size of the reservoir and having a reservoir as small as possible is probably even more important than smoothness of internal surfaces or material affinity to water.

Factors controlling measurement of high suction

In the following the factors enabling the measurement of high suctions by tensiometers are presented. The discussion is mainly based on the author's experience and combines the results presented throughout Chapter 3 with related works published in the literature.

- Saturation procedure

Results from Table 3.5 show that no application of high positive pressures is required to saturate the tensiometers and pressures as low as 800-1000kPa were enough to reach suctions around 1000kPa. The pressures applied during conditioning of tensiometers, as reported in the literature, range between 4MPa (Tarantino and Mongiovi, 2001, Ridley et al., 2003) and 16MPa (Guan and Fredlund, 1998). It however appears from this work that such high pressures would only speed up the saturation time but they will not significantly affect the measurement range.

A practical aspect that emerged from this work is the large time required to re-saturate a tensiometer by pressurization after the stone has fully dried (Section 3.3.2). It is, therefore, crucial to ensure that the tensiometer does not dry in any circumstance to avoid delay of testing programmes. Within this context, flooding under vacuum did not look very important in terms of extending the measurement range to high values of suction. Dried tensiometers were re-saturated by flooding under vacuum and the benefits were not clear in terms of saturation time or increase of measurement range.

- Time effect on cavitation

There are two different effects of time on the occurrence of cavitation in tensiometers: (1) one relates to the rate of suction increase during measurement and the other (2) to the time of use of tensiometers. Regarding (1), results presented by Tarantino and Mongiovi (2001), where the maximum measured suction increases with the number of cavitations, were obtained for slow increases of suction. Tests took between 1h-14h (while in this research tests took seconds to few minutes). The slow increase of suction could have contributed to the measurement of high suction values at cavitation. Figure 3.31 shows the time to cavitation based on Tables 1, 2 and 3 from Tarantino and Mongiovi (2001) which provide details about the sequence of measurements, suction at cavitation and measurement durations. Only cavitation at high suctions (>2000kPa) are shown while for lower cavitation suctions (~1200kPa), the data is not clear. In Figure 3.31a the value of suction at cavitation tends to increase with the test duration except Series 2 data.

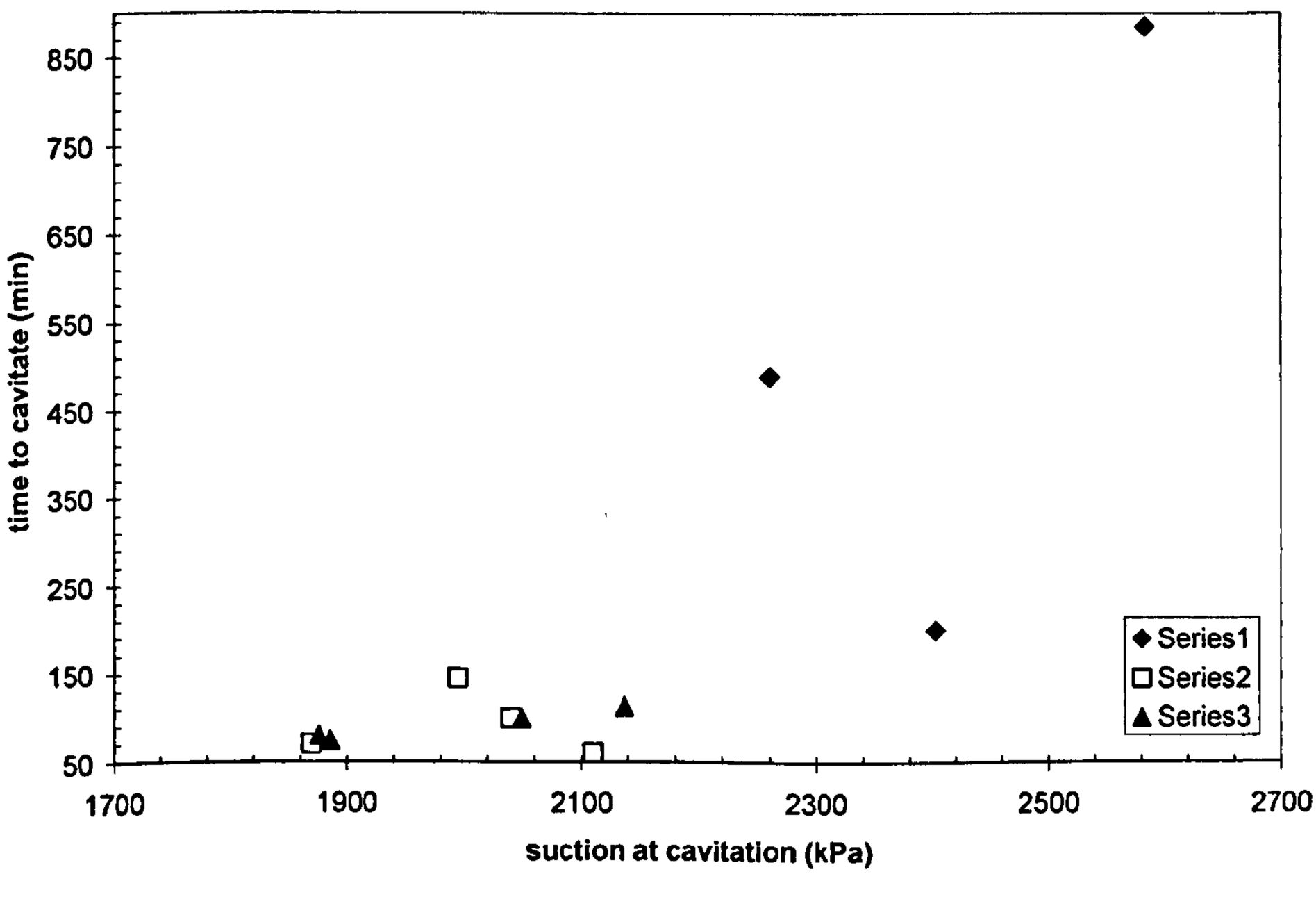

Figure 3.31: Suction at cavitation versus time to cavitation; series 1, 2, 3 correspond to suction measurements and are taken from Tables 1, 2, 3 respectively, from Tarantino and Mongiovi (2001)

A similar effect of time on the suction measured at cavitation has also been reported elsewhere. Trevena (1982) analyzed cavitation results that partly support the previous results. In Berthelot tube experiments, where cavitation is triggered by cooling enclosed water, the author found that cooling in intervals with waiting periods of several minutes lead to higher cavitation thresholds than continuous cooling. However opposite results were obtained when cavitatation was achieved by dynamic stressing, which consisted in applying a shot with a bullet against a piston filled with water. The impact of the bullet generates a compression pulse, which travels upward and is then reflected at the upper free surface of the liquid as a descending pulse of tension. Trevena (1982) states that in the Berthelot tube cavitation starts from bubbles in the walls of the device while by dynamic stressing cavitation starts in the liquid itself. How a slow increase of suction can extend the cavitation threshold is still unclear. Trevena (1982) do not provide a reason and Tarantino and Mongiovi (2001) did not mention such effect. One possibility is that that the achievement of high suction values at cavitation is controlled by air diffusion, given the strong dependency of air diffusion on time, but how diffusion could delay cavitation is still unclear.

Secondly, the time of use of tensiometers also has an effect on the measurement of high suctions at cavitation. Results presented in Section 3.3.2 showed that the suction range measured by tensiometers increased with time of use. In general, experience from the present research showed that older tensiometers performed better than the relatively young ones.

The cavitation threshold could increase with time due to pore clogging of the porous stone. If finer materials deposit physically or precipitate inside the porous stone, the corresponding air entry value of suction would tend to increase. Wenzel and Wieshammer (1995) state that clogging of pores may occur through precipitation of compounds from supersaturated soil solution, or by biofilm growth and trace metal adsorption. Clogging by filtration does not happen in tensiometers because water does not flow continuously through the stone. Direct evidence of clogging of the stone was found earlier in this research when testing a calcium rich soil (see Section 3.5) and by the larger time required to saturate tensiometers used continuously (as presented in Section 3.3.2). In the latter case, the longer time required for saturation (1-2 months instead 1-2 weeks) suggests that pore size is smaller, or at least that are 'obstructions' are impeding water flow. Clogging could have also occurred physically when wiping the stone, forcing finer particles to penetrate inside the pores. Comparing to other devices that use porous stones, tensiometers are likely to remain

indefinitely clogged because there is no way of flushing the impurities out of the porous stone. The long-term contact of a porous stone with soil could have lead to pore filling by precipitation or physical action, which could have increased the air entry pressure of the stone and consequently the cavitation threshold (where the term cavitation is also used to identify breakage of air through the stone).

- Cavitation history

The theory put forward by Atcheley and Prosperetti (1989) could partially explain the results obtained by Tarantino and Mongiovi (2001) that the suction at cavitation increases with the number of cavitations. According to this theory the bubbles to be first released should be those with a larger volume. As cavitation occurs and the tensiometer is re-pressurized, any bubble previously released from the crevice dissolves into water and the next bubble to pull away from a crevice will have a smaller volume and so would cavitate at a smaller liquid pressure. This could explain why a succession of cavitations might progressively increase the value of suction measured at cavitation.

Similar effects of cavitation history have already been reported in the literature. In dynamic stressing experiments, the application of successive shots (Sedgwick and Trevena, 1976) water at 3 min intervals produced a increase of the breaking tension with time until a stable value was achieved (Figure 3.32). Sedgwick and Trevena (1976) concluded that air nuclei present are 'cleaned up' by successive shots until when most of these nuclei are removed and the breaking tension stabilized around an upper limit of about 1100kPa (11.0atm). This is also in agreement with Bremond et al. (2005), who showed that the number of bubbles after cavitation decreased with the number of shots (reviewed in Chapter 2).

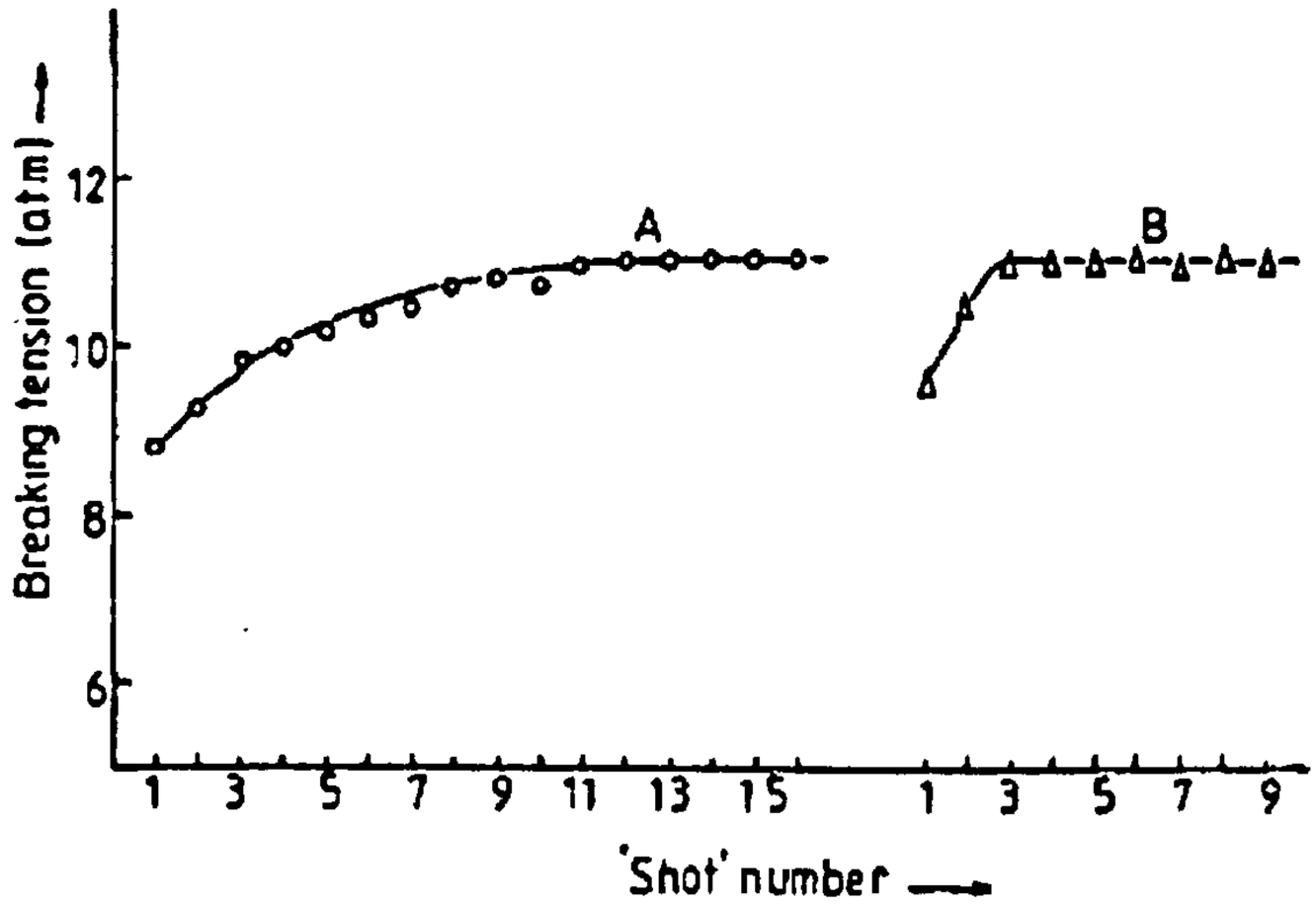

Figure 3.32: Influence of cavitation history on the breaking tension of water (by subjecting a tap water sample to successive stressing shots in curve A and after a waiting period of 24h in curve B) (1atm = 101.3kPa) (from Sedgwick and Trevena, 1976)

The long term integrity of the stone might also be affected by internal erosion due to the consecutive cavitations resulting, eventually, in a decrease of cavitation thresholds with time. Such erosive process might lead to material loss and formation of large cavities (Tomlinson and Mathews, 1995, Litzow et al., 2006). Tomlinson and Mathews (1995) studied the erosion of ceramics with an ultrasonic vibratory facility. The material made of 97.5% Al_2O_3 was submerged in water and submitted to continuous cavitation for several hours. Figure 3.33a shows the material lost approximately 175mg in 30h. Figure 3.33b shows the stone polished before the test while Figure 3.33c shows the same stone eroded after 1h of continuous cavitations. In reality, the number of cavitations to reach the conditions of Figure 3.33c would be relatively large and, therefore, cavity erosion could not affect the life-span of tensiometers.

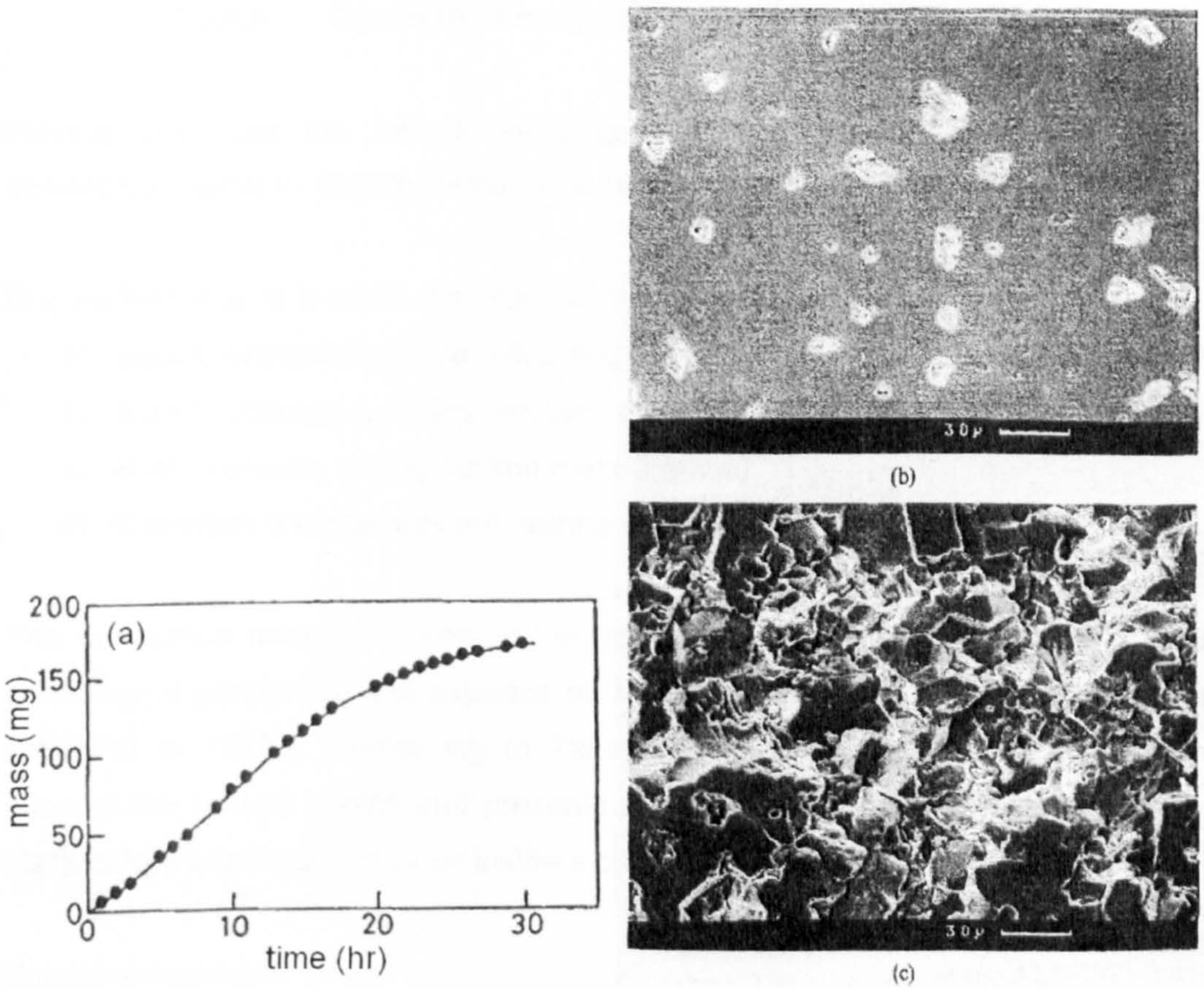

Figure 3.33: Cavitation erosion in a ceramic material (Al_2O_3), (a) mass loss *w* as a function of time *t*, (b) SEM micrograph of the ceramic before the test and, (c) after erosion for 1h (from Tomlinson and Matthews, 1994)

- Other factors

The nature of the porous stone might also play a role in the measurement of high suction values at cavitation. The change of the suction measurement range when using tensiometers fitted with different porous stones, as observed by Sjoblom (2000), can be interpreted as an effect of the different geometry or surface properties of the material forming the stone. In particular, Sjoblom (2000) states that a high interconnectivity of pores inside the stone improves the saturation process.

The study about the influence of low temperatures on cavitation performed in this research (Section 3.3.2) suggests that using tensiometers at temperatures near 4°C (i.e. the temperature at which the water is at its densest state) could increase the cavitation threshold. Testing at such low temperatures might however introduce additional experimental shortcomings such as an effect of temperature on calibration and a change of properties for soils with a temperature dependent behaviour.

3.3.4.5. Conceptual model for bubble formation

Having described the factors affecting bubbles formation in tensiometers, a conceptual model for bubble formation in high capacity tensiometers is proposed.

Bubble formation in tensiometers can be divided into four stages:

a) Bubble entrapment, during flooding
b) Bubble shrinkage, during pressurization
c) Bubble growth, during suction measurement
d) Cavitation (bubble release), during suction measurement

This conceptual model is based on the work of Jones et al. (1999), where a similar sequence is presented, and expands on the ideas put forward by Take (2003) and Ridley et al. (2003). Comparing to Take (2003) model (Figure 2.9), it takes into account the contact angles and presents a complete sequence of bubble formation starting by the entrapment of air inside a crevice until its release as a bubble.

Bubble entrapment

As water flood the tensiometer under vacuum, residual air gets trapped inside crevices assuming a geometry that depends on the advancing contact angle and crevice dimensions (Figure 3.34).

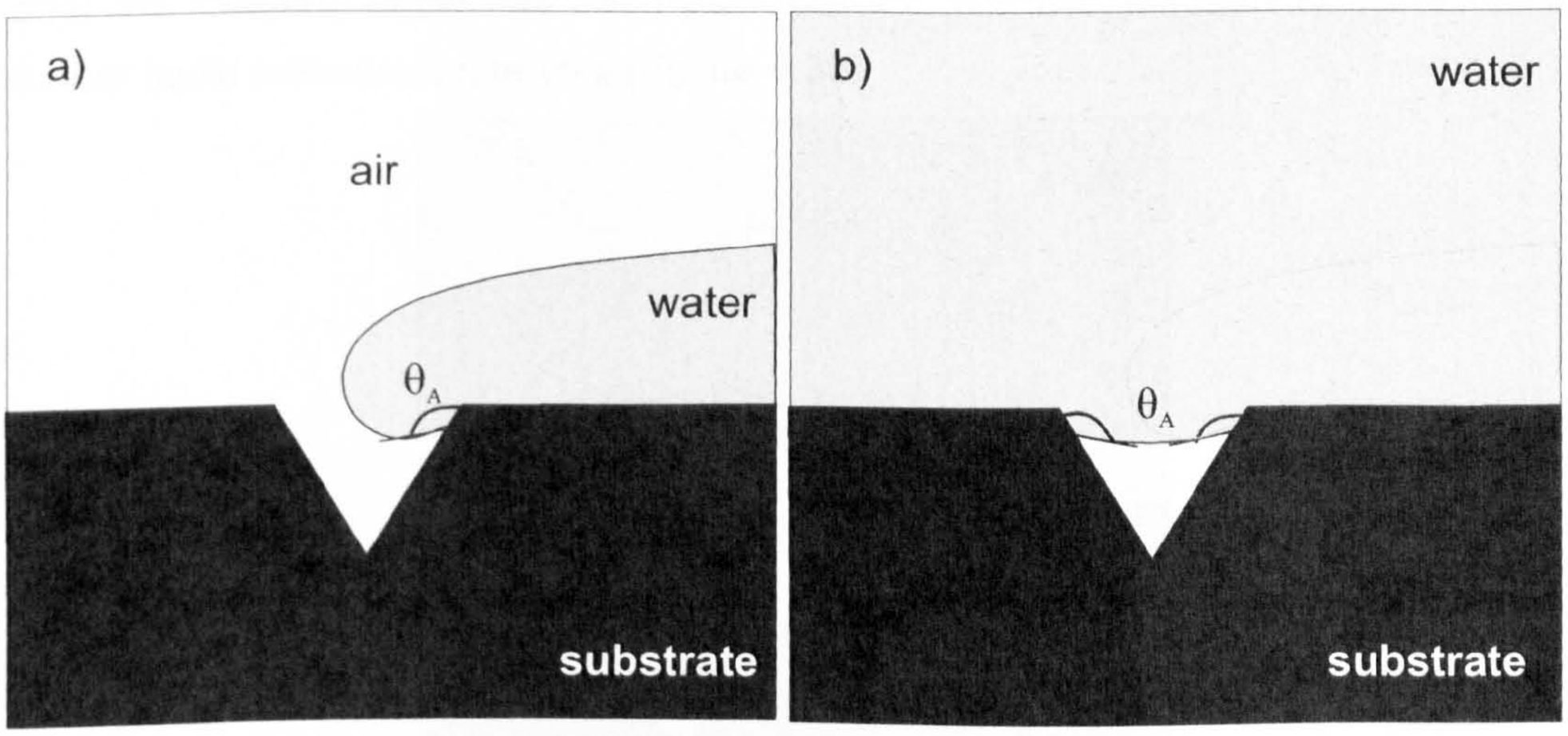

Figure 3.34: Bubble entrapment in a crevice (bubble volume will depend on the contact angles and geometry of the crevice)

Bubble shrinkage

As the tensiometer is pressurized, trapped bubbles decrease in volume by air diffusion to the surrounding water (Figure 3.35). The changing curvature of the interface would be limited by the advancing contact angle.

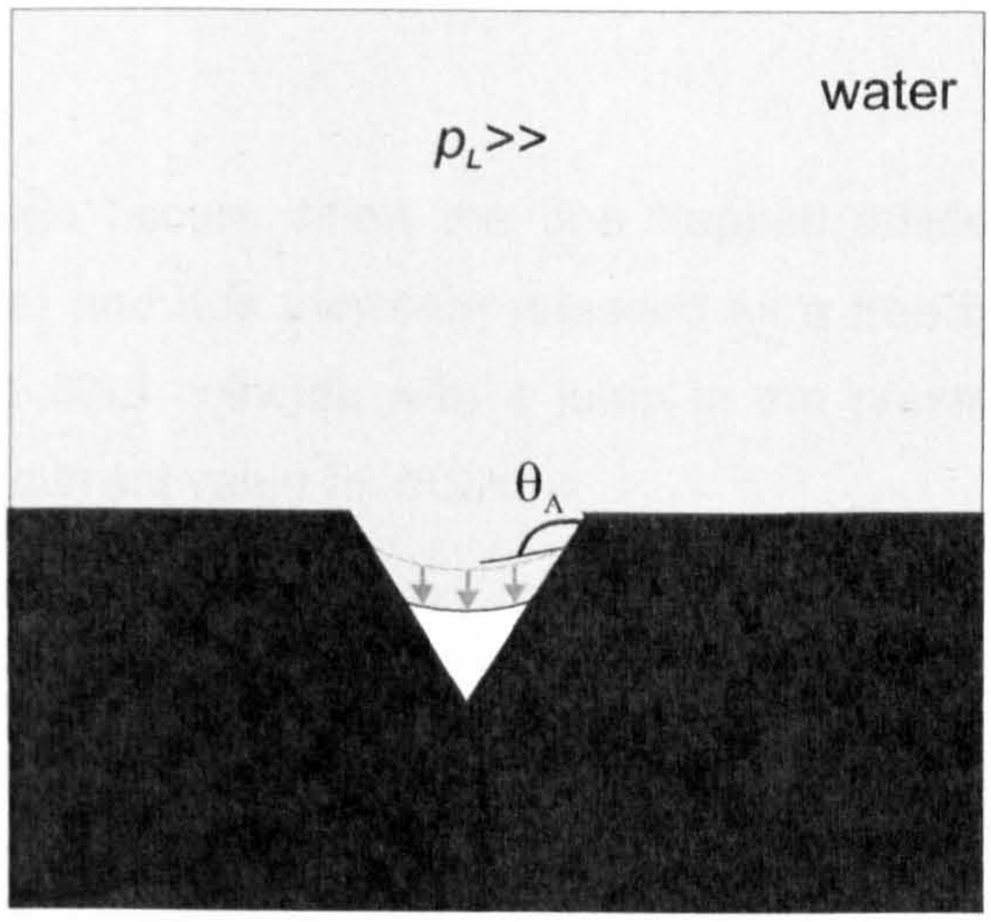

Figure 3.35: Bubble shrinkage during pressurization

Bubble growth

As the pressure is reduced, the attachment of the interface with the crevice wall will not change in position but the contact angle will progressively change from advancing to receding, i.e. the interface will pivot around the attachment point. Only after the receding angle has been achieved the interface will start to move under further liquid pressure decreases (Figure 3.36).

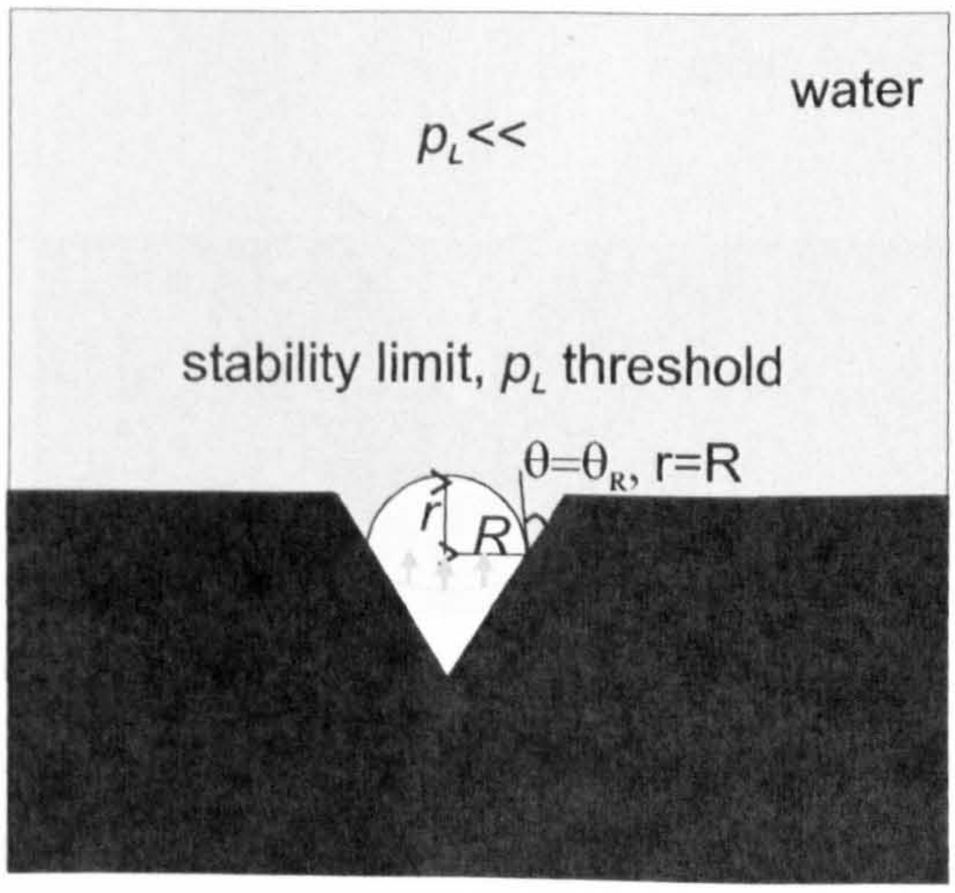

Figure 3.36: Bubble growth under decreasing liquid pressure

Bubble release (cavitation)

There are at least two scenarios to explain cavitation, one is the progressive expansion of a single free bubble released from a crevice and the other is the coalescence of one or more bubbles forming a discontinuity inside the water reservoir.

Free bubble expansion occurs when the gas trapped inside a crevice becomes instable (Figure 3.37a) and it is therefore released as a free bubble (Figure 3.37b). This instant (Figure 3.37c) coincide with a jump in the pressure measured by the tensiometer from the current value to -100kPa.

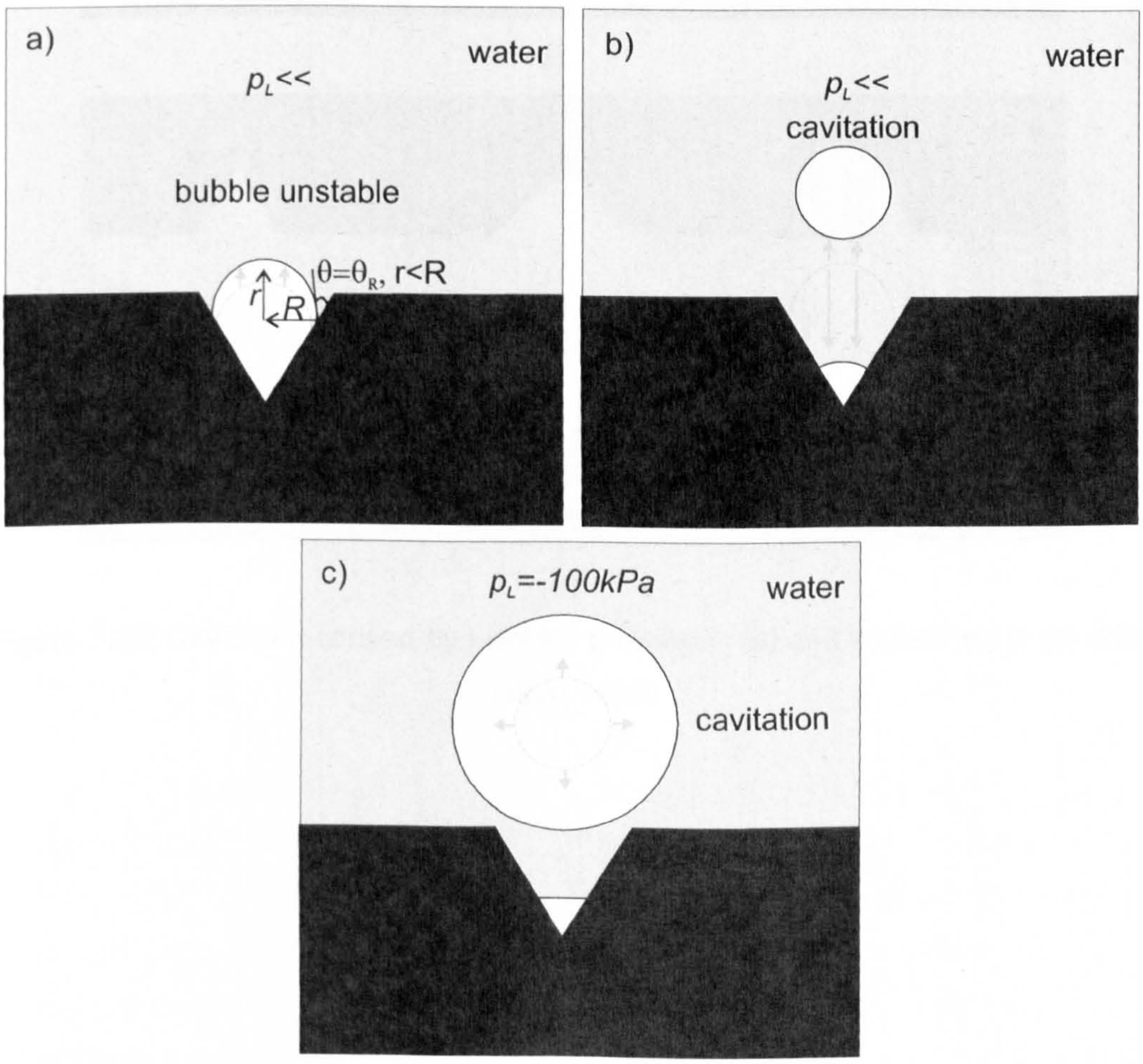

Figure 3.37: The cavitation process for a free bubble released from a crevice, (a) bubble reaches an unstable condition, (b) bubble is released from the crevice to form a free bubble, (c) bubble expands due to large pressure difference across the air-water interface

The second possibility is that small bubbles grow and coalesce inside the water reservoir. This will create a larger bubble breaking through the water forming a discontinuity between the transducer and soil (Figure 3.38).

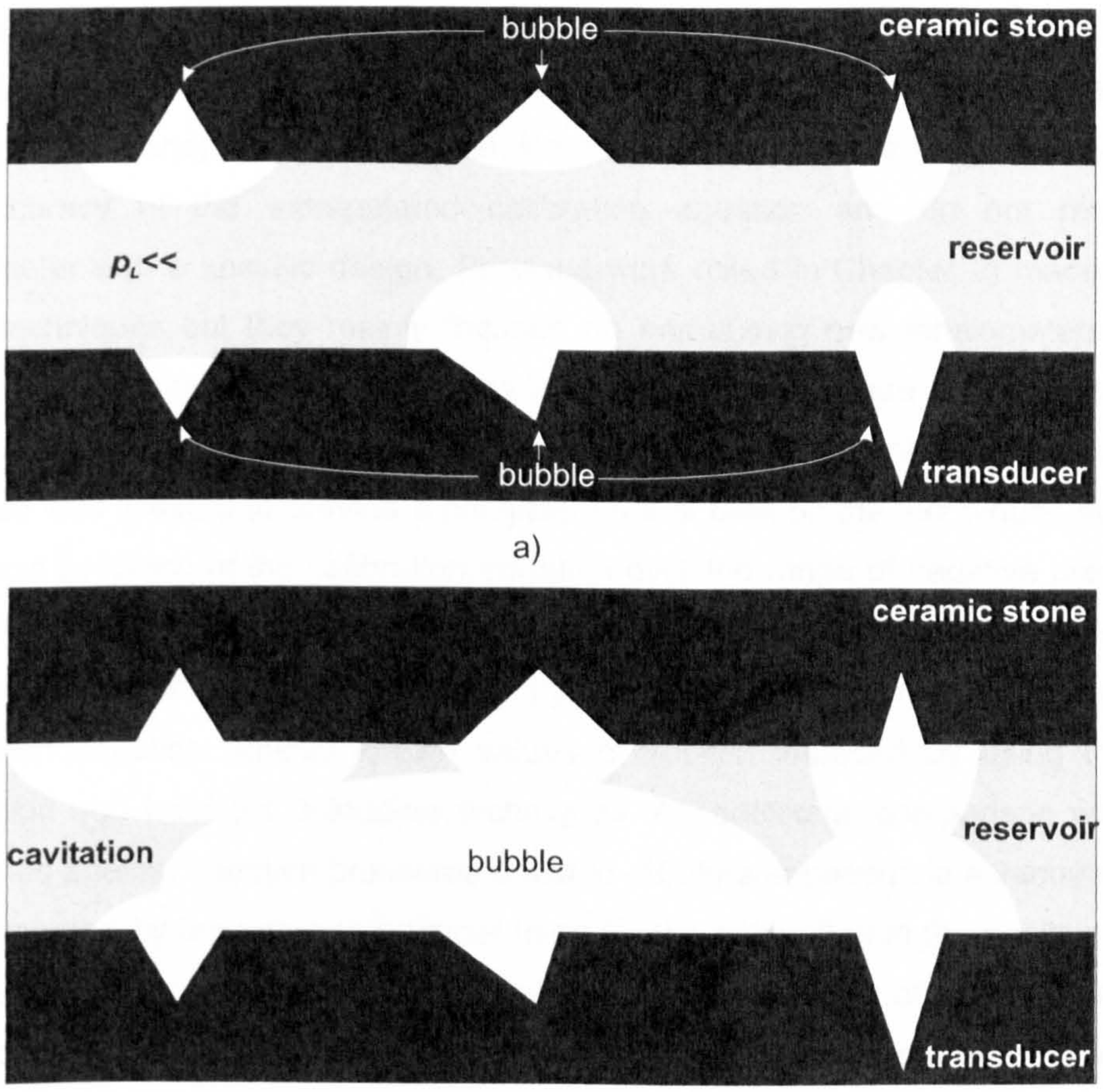

Figure 3.38: Cavitation caused by bubbles growing in (a) and coalescing in (b) (after Guan 1996)

3.4. CALIBRATION

3.4.1. Introduction

The indirect methods outlined in Chapter 2 (axis translation and isotropic unloading) use equipment easily available in laboratories (e.g. a triaxial cell with a high air entry value porous stone) for calibrating tensiometers in the negative range or assessing the accuracy of the extrapolated calibration equation and do not require a tensiometer with a specific design. Previous work (cited in Chapter 2) made use of these techniques but they mainly focused on introducing new tensiometers to the geotechnical community and it remains unclear which technique provides the most accurate way of calibrating tensiometers. In the light of these limitations, the present research was initiated to provide a consistent set of data on the techniques available to assess accuracy of the calibration equation over the range of negative pressures. The testing program consisted of calibrating a tensiometer in the positive range and then comparing the suction measured by the tensiometer using the extrapolated calibration equation against known values of suction imposed by using the axis translation and isotropic unloading techniques. An additional comparison was also performed against negative pressures down to -100kPa imposed via a vacuum pump and measured by the same transducer used for the calibration in the positive range. Calibration equations were obtained for single or several cycles of imposed pressure (to study any hysteretical effect of the calibration equation). Related aspects are also discussed, namely the influence of external forces, error calculation, hysteresis of the calibration equation and alternative techniques to assess the calibration of the tensiometer in the negative range.

A series of tests were carried out in which target negative pressures (suctions) were applied to a tensiometer (directly or by means of a soil sample) and compared to the values derived from a calibration curve extrapolated from the positive pressure range. This section discusses features of the tests themselves as well as the effect of cyclical variation of pressure on tensiometer performance. Following this, a comparison is made with calibrations in the positive range to assess the accuracy of extrapolation. Throughout the following, the error e in using extrapolation is the ratio

$$e = \frac{\left|(u_w)_e - (u_w)_a\right|}{\left|(u_w)_a\right|} \times 100\% \qquad (3.6)$$

where $(u_w)_a$ is the applied target negative pressure and $(u_w)_e$ is the estimated pressure measured by the tensiometer using the extrapolation of the positive calibration curve to the negative pressure range. The results presented below are summarized in Lourenço et al. (2006c, 2008a, 2008b).

3.4.2. Equipment and material

The tensiometer used was the same as described early in this chapter. Calibration in the positive range was conducted in a purpose built saturation manifold (Donoghue, 2006), shown in Figure 3.6, and in a triaxial cell. In the saturation manifold the tensiometer is fastened from the back and sealed on the sides by an o-ring and a metallic ring (the metallic ring was designed to improve the sealing at high pressures). The calibration in the positive range was performed against a standard transducer (maximum capacity of 2000kPa) previously calibrated against a dead load machine. This same transducer was used as the reference measure for the air pressure imposed in the axis translation technique, the cell pressure or backpressure imposed in the isotropic unloading technique and for the negative pressure imposed by the vacuum pump. The axis translation tests and isotropic unloading tests were conducted in a triaxial cell fitted with a pedestal containing a porous stone with an air entry value of 500kPa. This allowed easier control of the water conditions below the porous stone, compared to the pressure plate used by Guan and Fredlund (1997). TRIAX software was used for data acquisition (Toll, 1999).

Reconstituted Speswhite kaolin samples were used for the tests using the isotropic unloading and axis translation techniques. Speswhite kaolin was chosen due to its availability, homogeneity (ensuring reproducibility) and the ability to cover the suction range of the tensiometer with a relatively high cavitation limit. It is also non-expansive and reasonably permeable (for a clay), avoids effects related to temperature fluctuations and enables relatively fast equalization of pore water pressure. Kaolin was initially mixed with distilled water at a water content of 200% to form a slurry and placed in a Rowe cell for one dimensional consolidation at 250kPa. Samples were then cored using 38mm samplers, and coated with liquid wax paraffin in several layers to prevent moisture losses. All samples had a water content of approximately 42%, initial void ratio of 1.13 and degree of saturation of 98.7%.

3.4.3. Calibration in the positive range

3.4.3.1. Procedure

In order to study the validity of extrapolation, it was first necessary to obtain a calibration in the positive range for the tensiometer used. This calibration was performed in three ways. Calibrations were carried out in the saturation manifold, with different holding down forces applied to the tensiometer in the seating. Two further calibrations were then carried out with the tensiometer inside a triaxial cell. First, a calibration was carried out in what we term 'isotropic' conditions, by submerging the probe in water and increasing the cell pressure in steps. This calibration method corresponds to a condition where the pressure applied to the inner transducer through the ceramic stone is the same as the pressure applied externally to the probe's body. Secondly, a calibration was carried out in what we term "anisotropic" conditions, by consolidating a soil sample at a given cell pressure and applying increasing backpressures until reaching an effective stress of approximately zero. At the same time, the tensiometer was maintained directly in contact with the soil through a grommet on the sample's side, sealed by o-rings and painted with several layers of liquid latex rubber. The procedure for placing the tensiometer in contact with the sample is similar to that described by Hight (1982) for sealing a piezometer probe on a sample's side during saturated triaxial tests and has been used frequently since (e.g. Wong et al., 2001, Jotisankasa, 2005). This calibration method corresponds to a condition where the pressure applied to the transducer through the ceramic stone was equal to the backpressure inside the sample and different from the cell pressure applied externally to the tensiometer's body.

3.4.3.2. Results and discussion

The calibration factors, *m* obtained for the four cases described above are shown in Figure 3.39 together with the plots of voltage against applied pressure. There is a clear difference between these calibration methods. The effect of loose or tight fitting in the saturation manifold is significant while tests conducted with the tensiometer in 'isotropic' or 'anisotropic' conditions inside the triaxial cell show closer calibration factors. The two calibration factors that differed most (i.e. for the tensiometer fixed tightly in the saturation manifold and in 'isotropic' conditions respectively) show a difference of 9.8% indicating that, in order to obtain accurate measurement of

suctions, the tensiometer should ideally be calibrated using a method that resembles conditions of use. Further possible evidence for this can be found in the study by Jotisankasa (2005). Given our findings here, the calibration factor used later to check extrapolation to the negative pressure range was that obtained under 'isotropic' conditions.

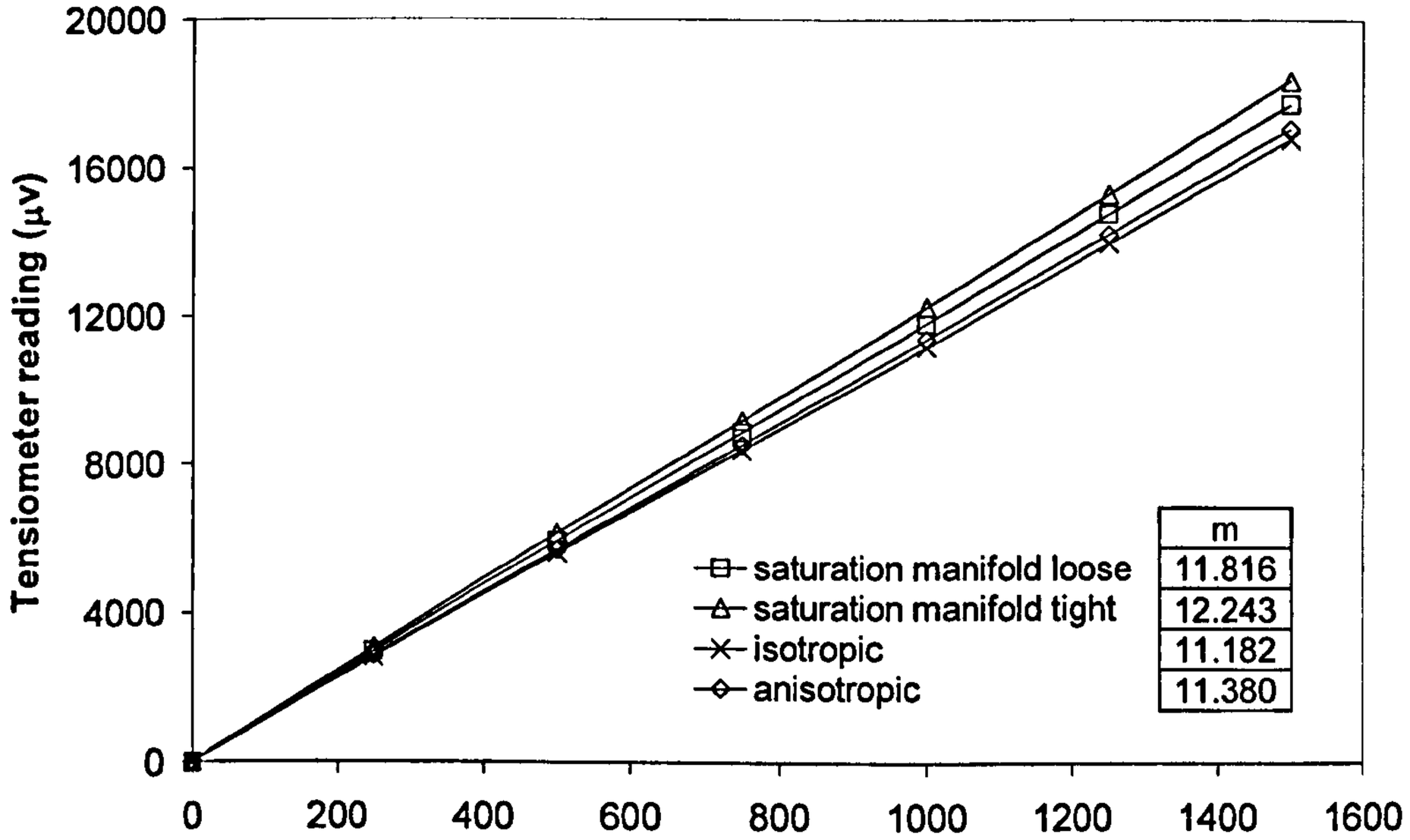

Figure 3.39: Calibration in the positive range (tests Tc1 to Tc4, tensiometer III3)

Hysteretic effects due to imposed positive pressure changes were also studied. The procedure followed consisted of submerging the tensiometer in water in a triaxial cell and applying five cycles of cell pressure between zero and 600kPa. The changes of cell pressure were applied in steps followed by waiting periods to ensure that the tensiometer readings achieved equilibrium. Data for these pressure cycles are shown in Figure 3.40, where the series of loops corresponding to consecutive changes of cell pressure could be attributed to the low permeability of the stone causing a delay in the tensiometer response. As the diaphragm deflects a small amount of water flows inwards or outwards depending on whether pressure increases or decreases respectively. After each change of pressure, a period of time of 1 to 2 minutes is necessary for this flow process to complete and for tensiometer readings to stabilize. By considering only the final equilibrium points for each change of cell pressure, the same calibration factor as given in Figure 3.39 for 'isotropic' conditions is obtained.

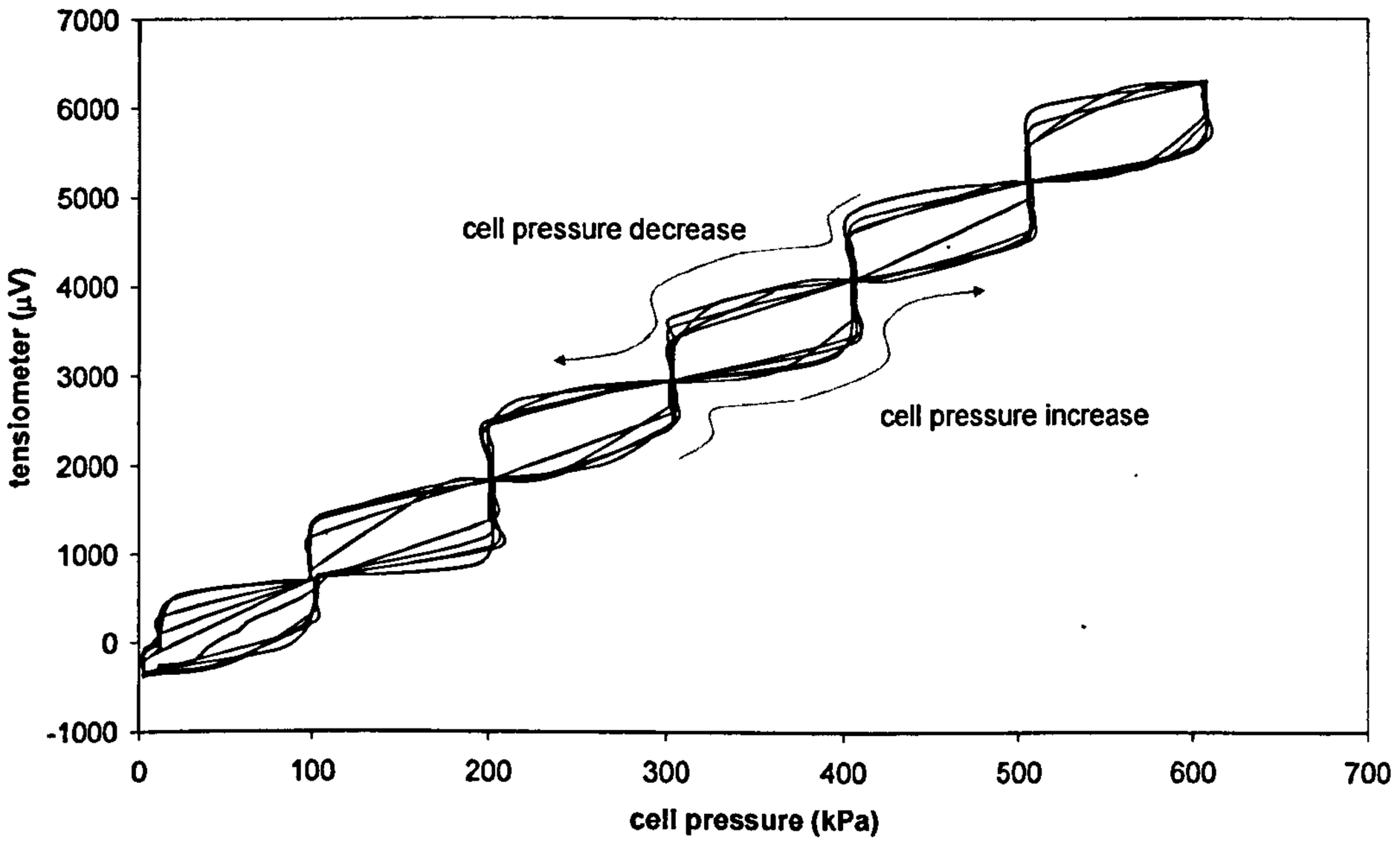

Figure 3.40: Response of the tensiometer submerged in the triaxial cell to increasing and decreasing cycles of cell pressure (test Tc3, tensiometer III3)

The importance of using an appropriate calibration procedure in the positive range is particularly evident in the study by Jotisankasa (2005). That author compares the readings by two tensiometers set on the side of a dummy sample inside a the triaxial cell. The sample was free to drain under a zero value of backpressure while the cell pressure was increased to 800kPa. One tensiometer recorded a decrease of pressure of 35kPa as the cell pressure was increased, while the other remained at zero (Figure 3.41). This discrepancy of response was justified by Jotisankasa (2005) based on manufacturing differences between tensiometers and water infiltration from the back of the tensiometer. Both tensiometers were calibrated over the positive range inside a manifold, i.e. in a completely different pressure environment with respect to their use inside a triaxial cell. The present research has shown that calibration inside a manifold can be very inaccurate and the negative pressure of -35kPa, measured by the tensiometer under a cell pressure of 800kPa in Figure 3.41, is well within the range of calibration errors found in this research. The measurement of such negative value of pressure could therefore be attributable to the difference in the pressure regime acting on the body of the tensiometer during use inside the triaxial cell and calibration inside the manifold.

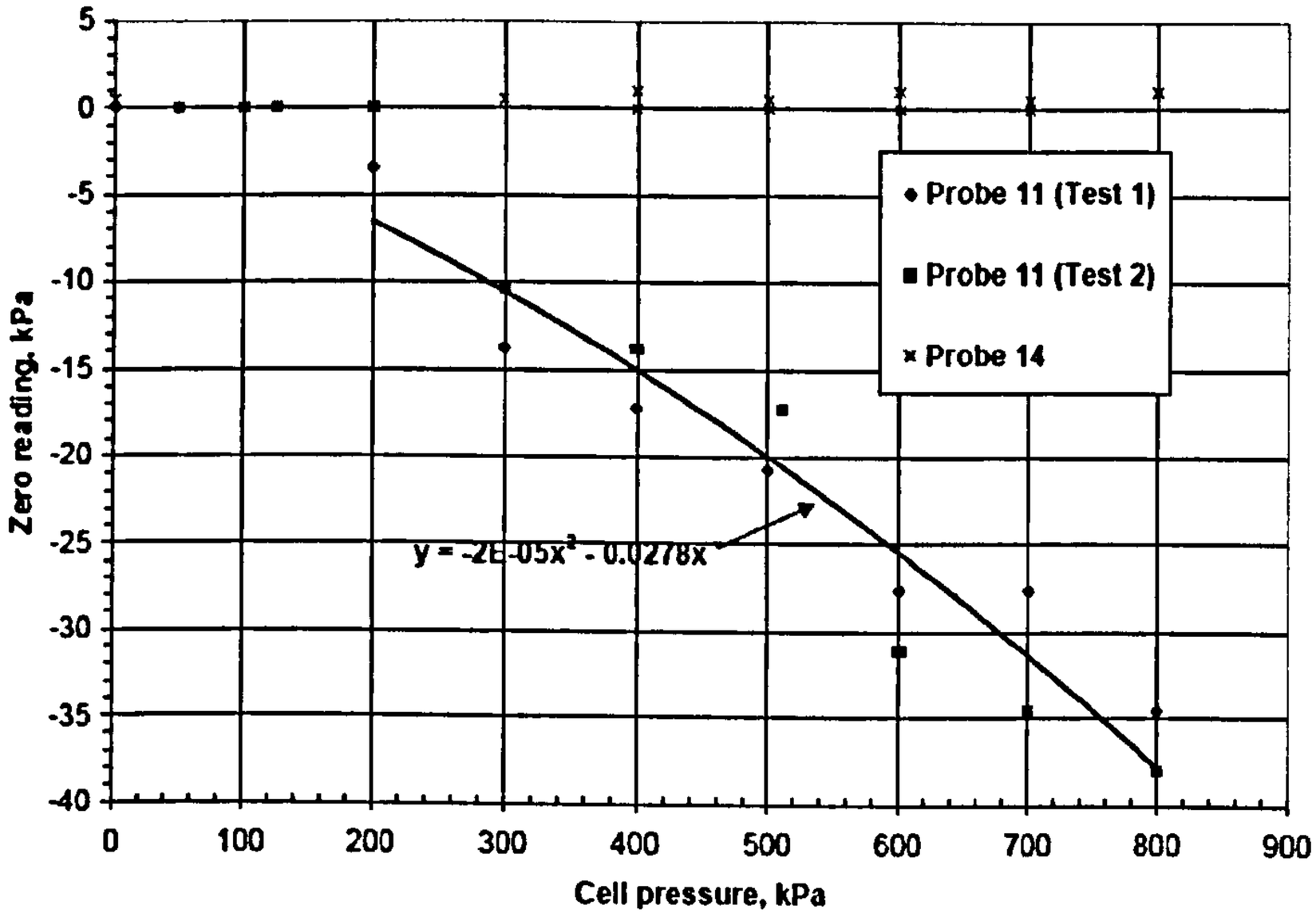

Figure 3.41: Response of Imperial College tensiometers to an increase in cell pressure (in the figure probe is equivalent to tensiometer) (from Jotisankasa, 2005)

Having obtained a calibration in the positive pressure range, three methods (one direct method and two indirect methods) were investigated to check the extrapolation of such calibration to the negative pressure range.

3.4.4. Application of vacuum

3.4.4.1. Procedure

The first extrapolation check used a direct method of applying negative pressures down to –100kPa by means of a vacuum pump. Despite its limitations for high suction tensiometers, it was thought useful to include such a method in this study as a comparison with other indirect techniques. The tensiometer was submerged in a cup in free water placed inside a triaxial cell. Vacuum was applied inside the cell in three different cycles and maintained constant for short periods of time at different stages during each cycle (see Figure 3.42). Tensiometer readings (using the calibration factor extrapolated from the 'isotropic' method in the positive range) were compared against the imposed negative pressure (measured by the same transducer used during calibration in the positive range).

3.4.4.2. Results and discussion

The results in Figure 3.42 show that the pressure transducer controlling the vacuum returns to zero after each cycle whereas the tensiometer shows a slight shift in measurements throughout the three cycles. With the cell pressure at zero, the tensiometer reading after the second cycle was approximately 2kPa and after the third was 3kPa. This suggests that calibration could be drifting as pressures are ranged between zero and -100kPa but there is no evidence of a change of the calibration factor, *m*.

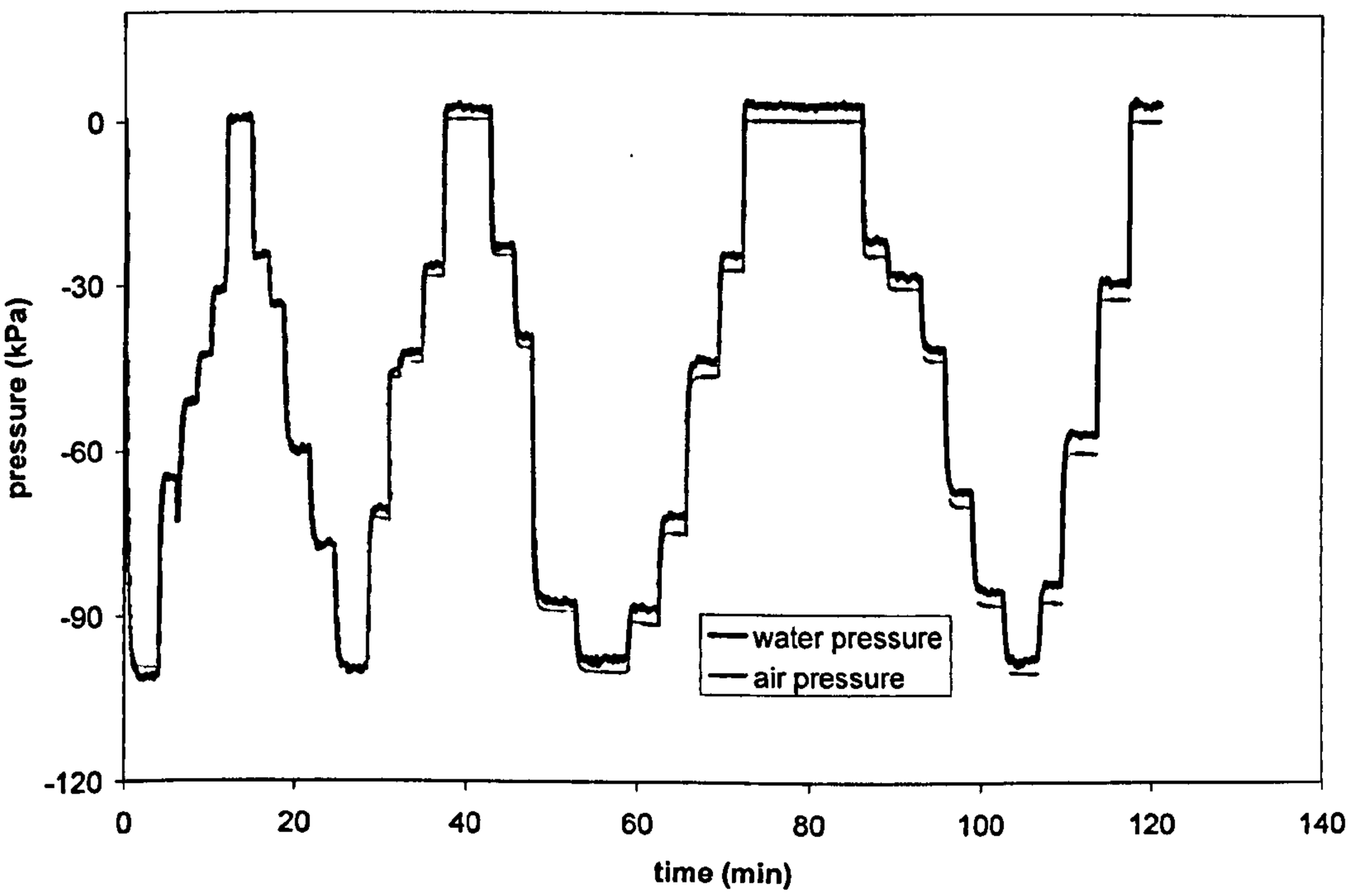

Figure 3.42: Cycles of pressure applied using the vacuum method (test Tc5, tensiometer III4)

Suction-induced hysteresis

Suction-induced hysteresis of this nature has also been seen in studies involving the continuous use of a tensiometer for soil testing where values read by the tensiometer, when plunged in free water before and after a test, were seen to change up to 14kPa (although values were usually below 5kPa) as shown in Table 3.7. This might be explained by a small calibration drift when the tensiometer is working in the negative range, which however would only be significant at very low suctions given that the calibration factor, *m* remains unchanged. There is also the possibility that this

phenomenon only appears when using tensiometers at low suctions, but this seems unlikely as it has been seen in tensiometers used continuously for a period of one year regardless of the suctions measured. While the nature of this drift is unclear, it seems to be restricted to the negative pressure range. When pressure was cycled in the positive range between zero and 600kPa, as previously described, the tensiometer reading always returned to zero at the end of each cycle. Tarantino and Mongiovi (2003) also found a change in the calibration when tensiometers were used in the negative range. For those authors quick cycles of negative pressure were seen to improve the measurement accuracy.

Table 3.7: Drift of the calibration zero for tensiometers III3 and III1 after prolonged period of testing

	tensiometer III3	**tensiometer III1**
reading in free water (kPa)	-2.5	-14
	-2.7	-1
	-6.9	-1
	-1.5	-1
	0.9	-1.4
	-1	
	-1.4	

3.4.5. Undrained unloading

3.4.5.1. Procedures

The procedure followed for the isotropic unloading test in this research had one difference from that described by Ridley and Burland (1993). A zero pore water pressure, instead of 200kPa of backpressure, was imposed on the sample before unloading. Therefore the suction read by the tensiometer was compared to the initial total stress applied to the sample (which in this case is equal to the effective stresses). In this initial test, a sample was enclosed in a latex membrane and mounted in the triaxial cell with the drainage line open to the atmosphere to ensure a zero pore water pressure. The tensiometer was set directly in contact with the sample through a grommet as in the 'anisotropic' positive pressure calibration described above. The arrangement for the isotropic unloading tests is shown in

Figure 3.43. Cell pressure was then quickly increased producing a build up of excess pore water pressures read by the tensiometer. After dissipation of the excess pore water pressure and with the tensiometer reading zero, the backpressure drainage line was shut and the cell pressure was decreased while the tensiometer measurements were recorded (using the extrapolated positive calibration).

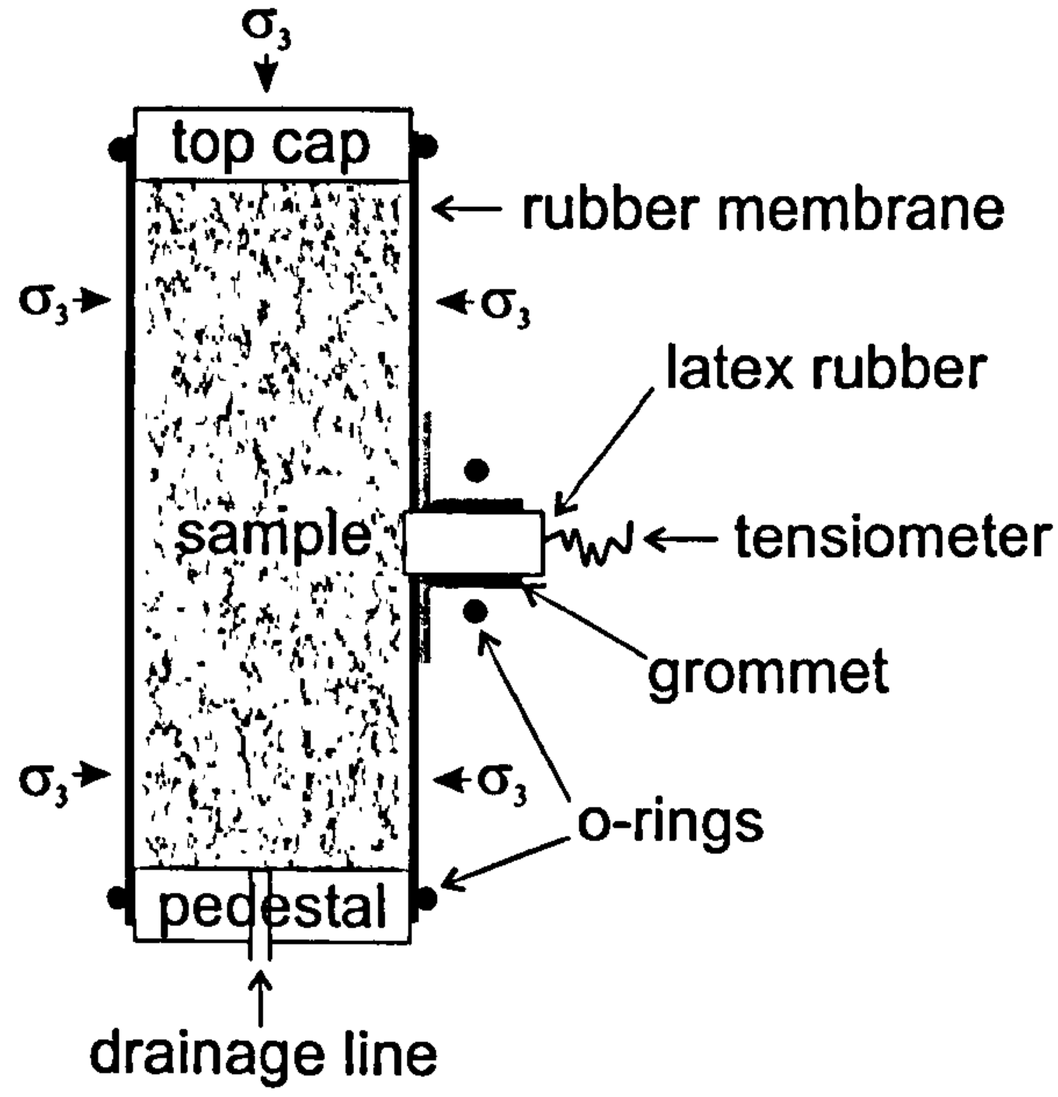

Figure 3.43: Arrangement for the isotropic unloading tests

3.4.5.2. Results and discussion

Results from an initial test are shown in Figure 3.44. Due to the high degree of saturation (98.7%), it was considered unnecessary to saturate the sample under a back pressure. The sample was initially consolidated to 454kPa of effective stress and, with the tensiometer reading zero, the drainage line was closed before decreasing the cell pressure first to 253kPa and then to zero. For the first drop, the cell pressure decreased by 201kPa while the suction measured by the tensiometer was equal to 190kPa. The ratio between the target and measured values of suction is therefore 0.944 and the extrapolation error is about 5.6%. For the second drop in cell pressure the error is similar, i.e. about 5.4%. Both errors are quite large but comparable to those obtained by Guan and Fredlund (1997) by using the axis translation technique.

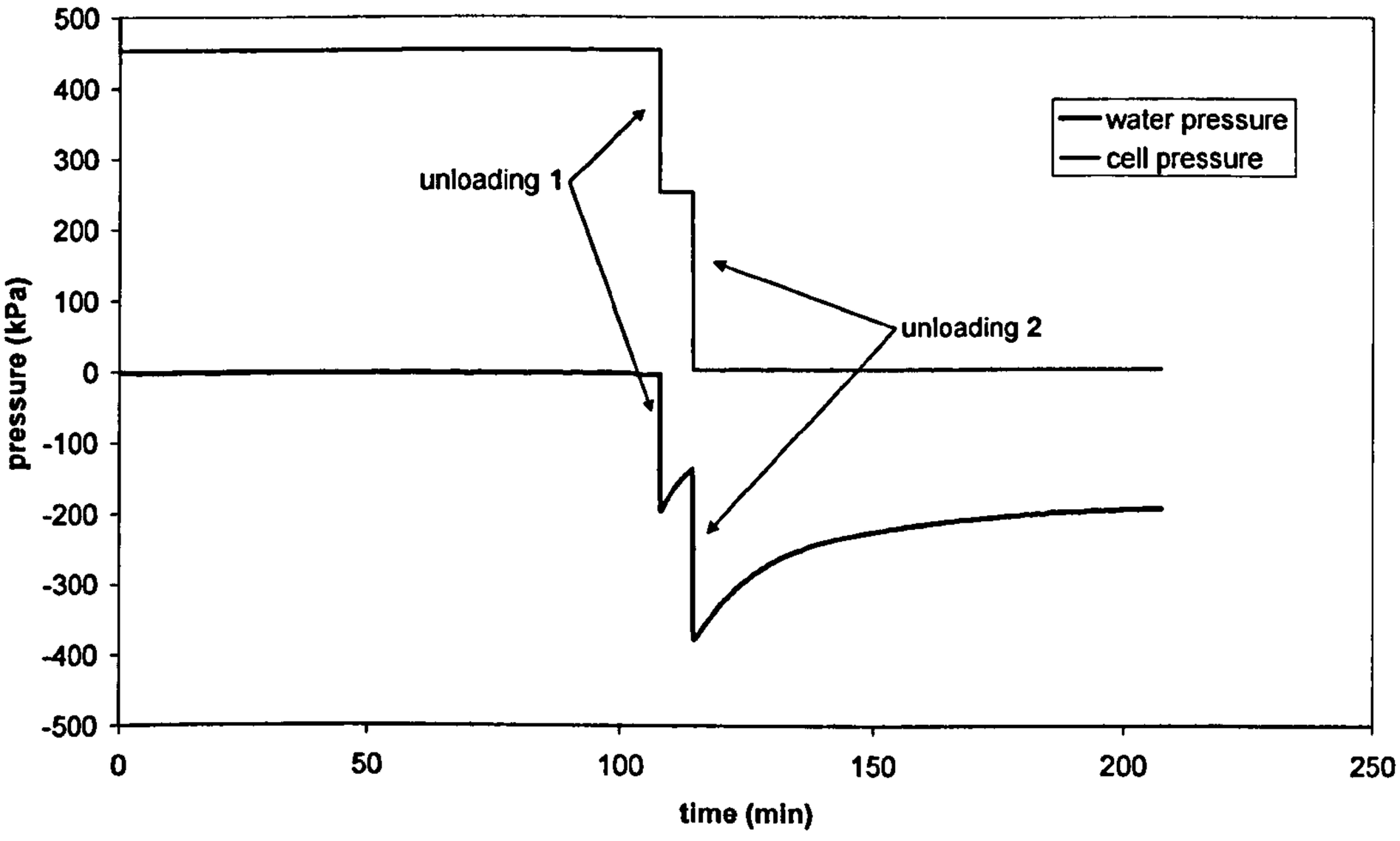

Figure 3.44: Initial isotropic unloading test (test T13, tensiometer III4, kaolin)

The results also revealed an unexpected increase of the pore water pressure after unloading and this was attributed to water adsorption from the sample. After ending the test, it was found that the latex rubber had detached from the sample's membrane which could have lead to water infiltrating from the cell to the sample through the grommet. Water imbibition could have also occurred from the porous stone or from the reservoir below the porous stone in the pedestal of the triaxial cell. Also, as water pressure decreases below the -100kPa threshold, cavitation could have occurred in the drainage tubing. There is also the possibility that cavitation could have occurred within the pores of the kaolin resulting in a decrease of suction due to the formation of small air bubbles.

To overcome some of these problems, a second test was carried out, in which the sealing of the sample was improved by eliminating the tube connecting the top cap to the triaxial base. A system was also introduced for blowing dry air through the drainage system below the porous stone in the pedestal of the triaxial cell before unloading. This follows the example of Bishop et al. (1975) who modified a triaxial cell base so that water could be removed when required. To avoid the water leaks through the grommet the entire sample was painted with the liquid latex (including the grommet) in several layers, and was then sealed with extra o-rings at the top cap, pedestal and around the grommet (Figure 3.45a). The improved sealing removed the

suction decrease after unloading but resulted in a similar extrapolation error of approximately 5.0% (Figure 3.45b).

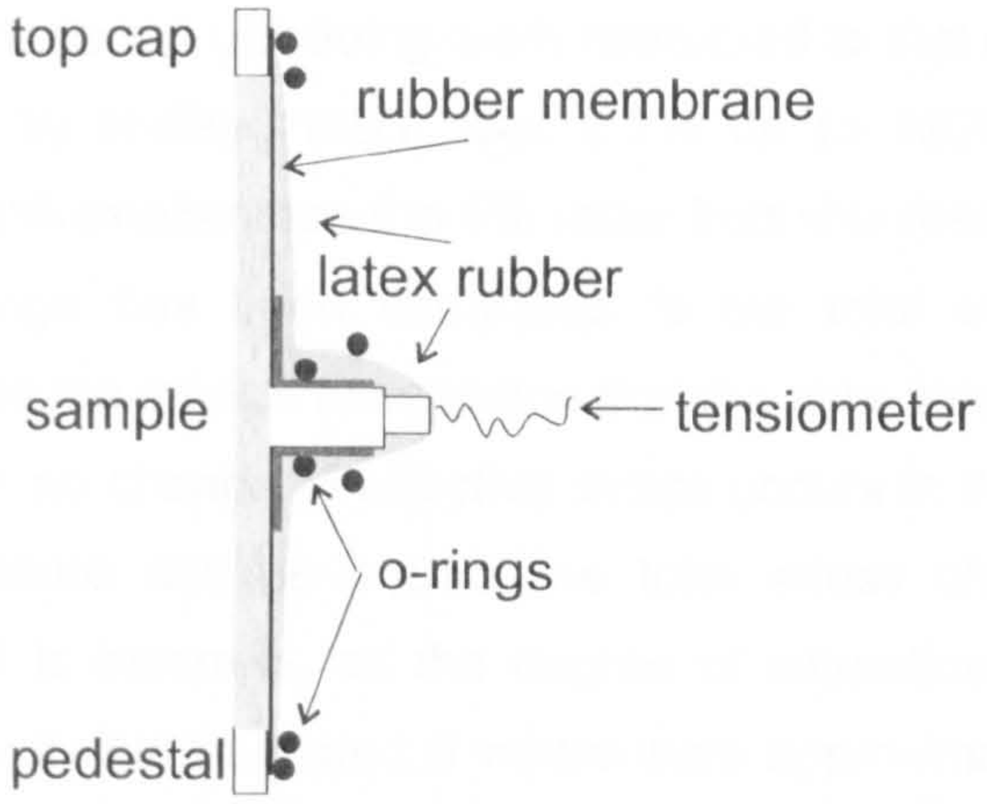

(a)

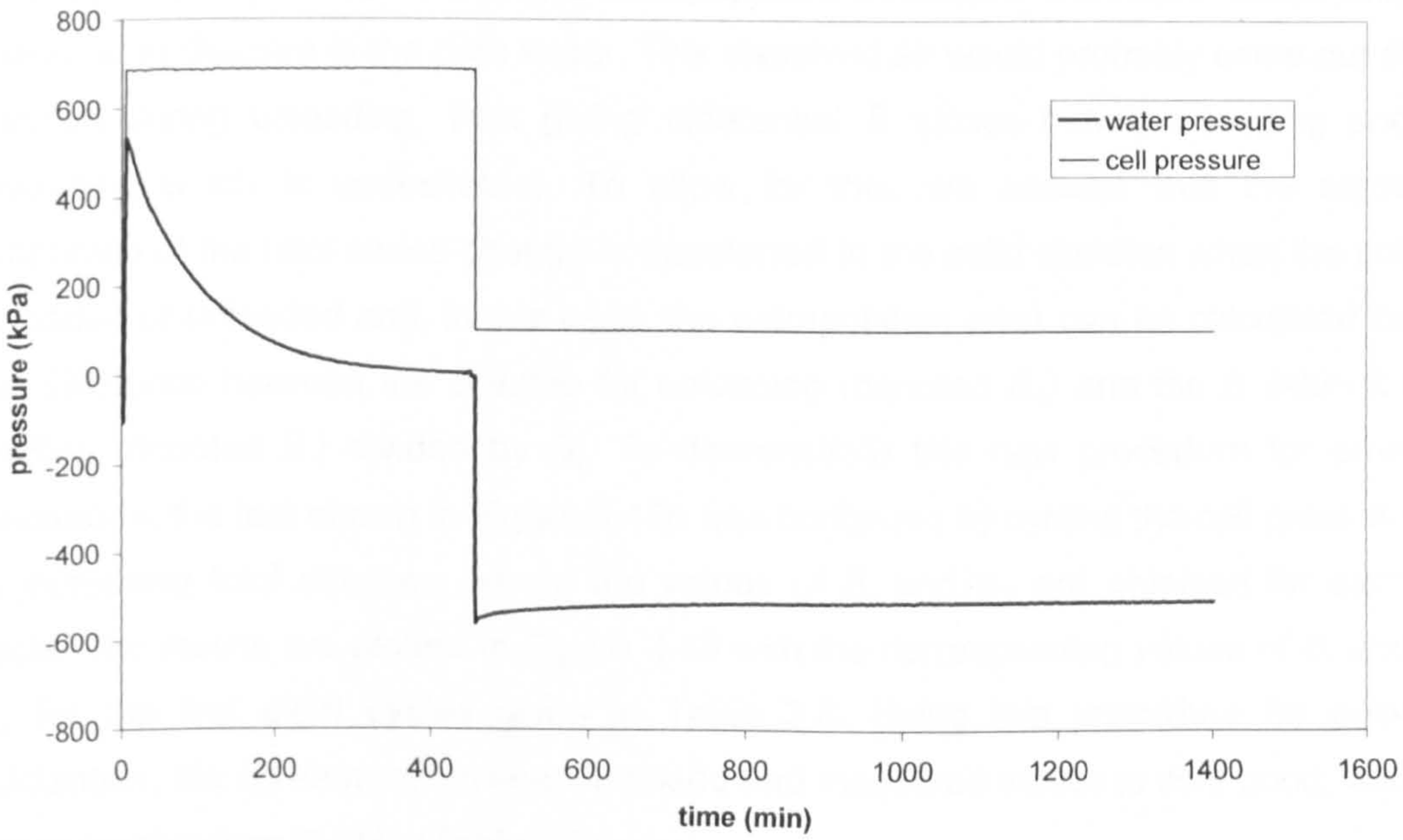

(b)

Figure 3.45: Isotropic unloading test with improved sealing, a) schematic drawing of sealing, b) tensiometer response (test Tc15, tensiometer III4, kaolin)

New error calculation

In Ridley (1993) specimens were reloaded after the unloading stage and the changes in pore water pressure during unloading were compared to that during reloading. The difference observed by Ridley (1993) was 2.2% up to 1200kPa and increasing afterwards, but was still smaller than the 5% value from this research. So far the pore water pressure change has been compared to the total stress change during unloading. This makes the implicit assumption that the pore pressure parameter, B is equal to unity so that no change of effective stress occurs in the solid skeleton and the pore water pressure change equals the total stress change. However, the assumption of $B = 1$ is incorrect, as the degree of saturation was not 100% (but 98.7% as stated above) and measured B values were approximately 0.96. (Note that, while the samples were not fully saturated, the B values were above the limit of 0.95 as prescribed by BS1377. Using a backpressure saturation technique would only cause air to dissolve in the pore water. This dissolved air would probably come out of solution during unloading, thus giving differential B values between loading and unloading which is undesirable). To allow for this, we assume that the same proportion of the total stress change is transferred to the solid skeleton when the soil is loaded or unloaded and, in this case, the extrapolation error can be calculated as the difference between the B value for unloading (denoted B_u) and the B value for loading (denoted B_l) divided by B_l. To demonstrate this new procedure for error calculation, the test shown in Figure 3.45b was continued by cycling the cell pressure at increasing total stresses, where the values of B_l and B_u are obtained for each cycle. The results are plotted in Figure 3.46 with the corresponding values of B_l and B_u for the first eight cycles given in Table 3.8. Using this procedure for error calculation, the agreement between imposed and measured values is very good, with errors smaller than 0.81% (Table 3.8).

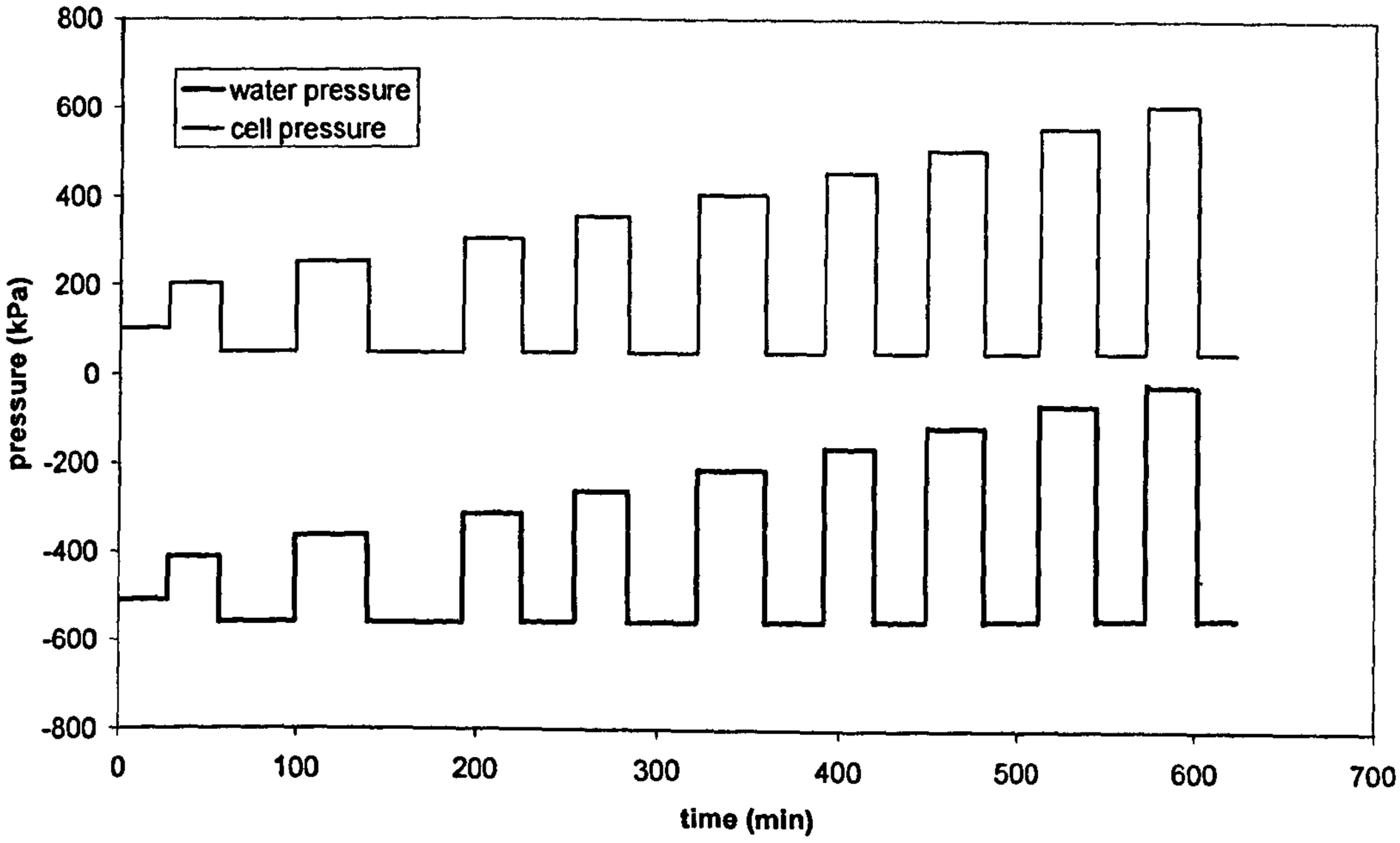
water pressure
cell pressure
pressure (kPa)
800
600
400
200
0
-200
-400
-600
-800
0
100
200
300
400
500
600
700
time (min)

(a)

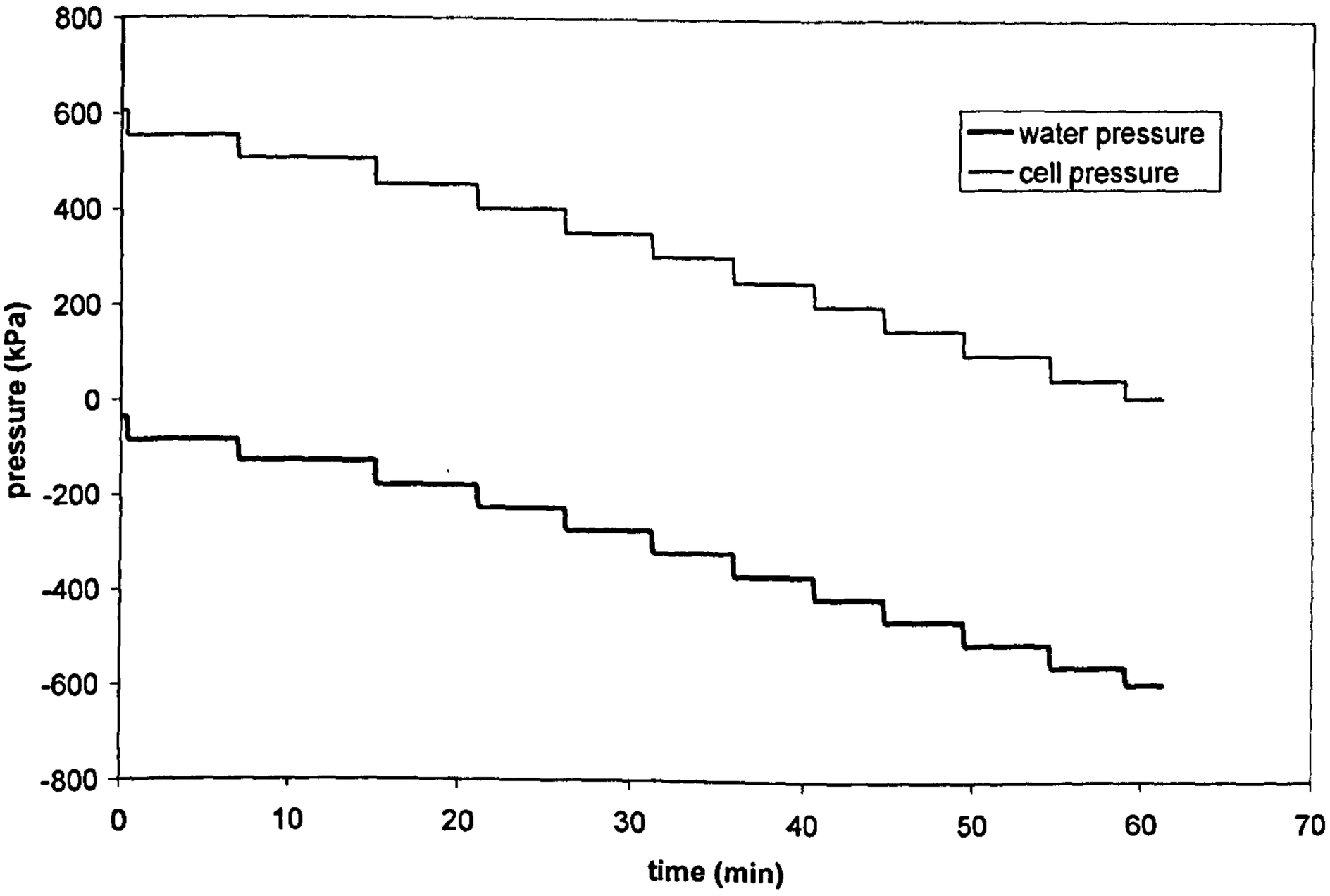
water pressure
cell pressure
pressure (kPa)
800
600
400
200
0
-200
-400
-600
-800
0
10
20
30
40
50
60
70
time (min)

(b)

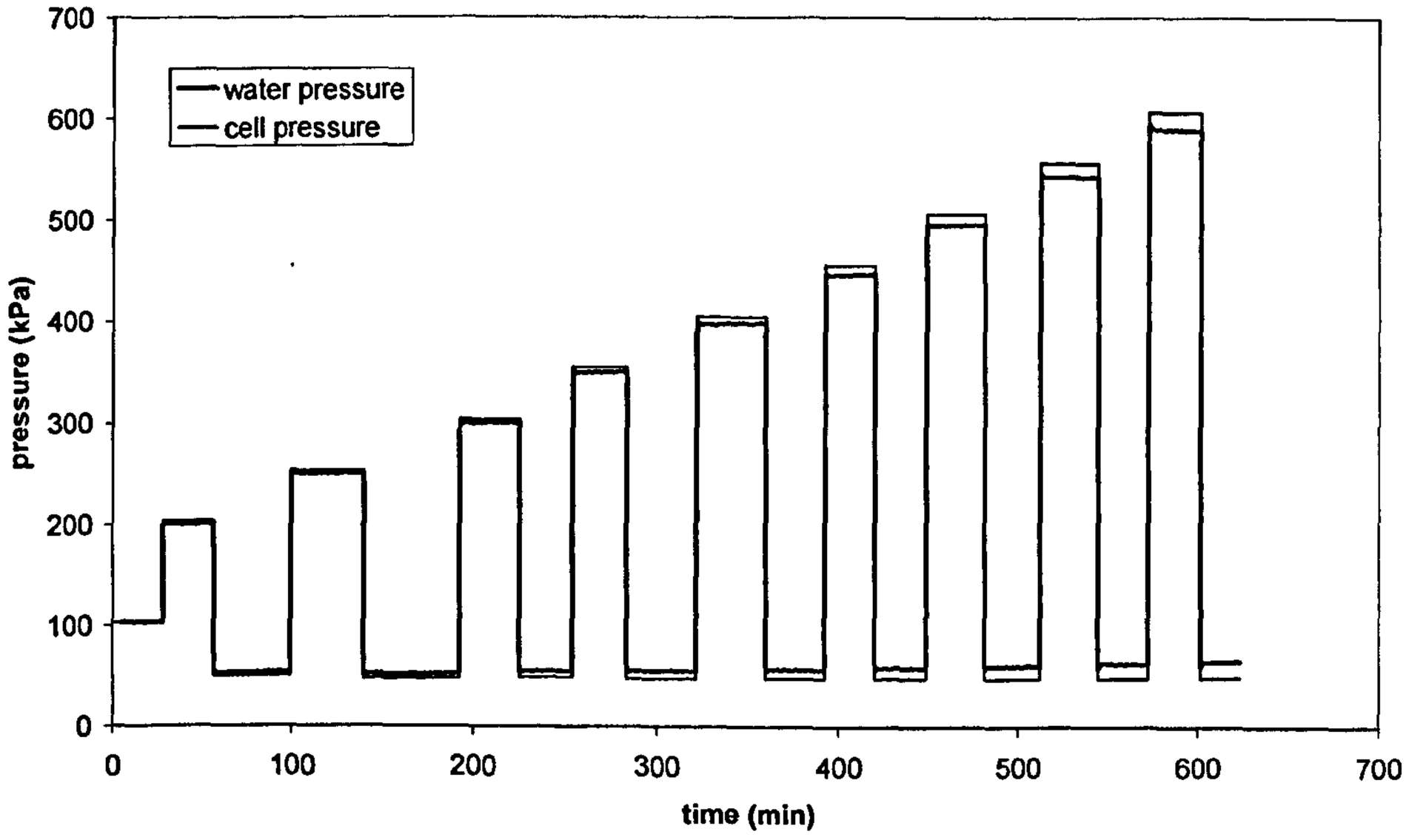

(c)

Figure 3.46: Undrained unloading test (test Tc15, tensiometer III4, kaolin); (a) cycles of loading and unloading; (b) continuation of a) with the cell pressure decreasing in steps; (c) with 2 curves of (a) superimposed

Table 3.8: Cycles of loading and unloading in the isotropic unloading test

Imposed change in cell pressure Δp (kPa)	Difference in water pressure read by tensiometer during loading Δu_l (kPa)	Difference in water pressure read by tensiometer during unloading Δu_u (kPa)	Water pressure parameter during loading $B_l = \frac{\Delta u_l}{\Delta p}$	Water pressure parameter during unloading $B_u = \frac{\Delta u_u}{\Delta p}$	Extrapolation error $e = \frac{\lvert B_u - B_l \rvert}{B_l}\%$
±101	97.9	-97.7	0.969	0.967	0.20
±203	197.3	-197	0.972	0.970	0.15
±256	246.3	-248.3	0.962	0.970	0.81
±306	295.2	-295.1	0.965	0.964	0.03
±357	342.7	-343.5	0.960	0.962	0.23
±407	390.3	-389.7	0.959	0.957	0.15
±457	435.1	-436.9	0.952	0.956	0.41
±509	485.2	-482.3	0.953	0.948	0.60

3.4.6. Axis translation

3.4.6.1. Testing program

The second indirect method used in this work to check extrapolation of the calibration curve to the negative pressure range was based on the axis translation technique. A sample was placed on a previously saturated high air entry value porous stone (with air entry value of 500kPa). The tensiometer was set in contact with the top of the sample. No membrane was used to contain the sample and the pore air pressure was applied all around the specimen (Figure 3.47).

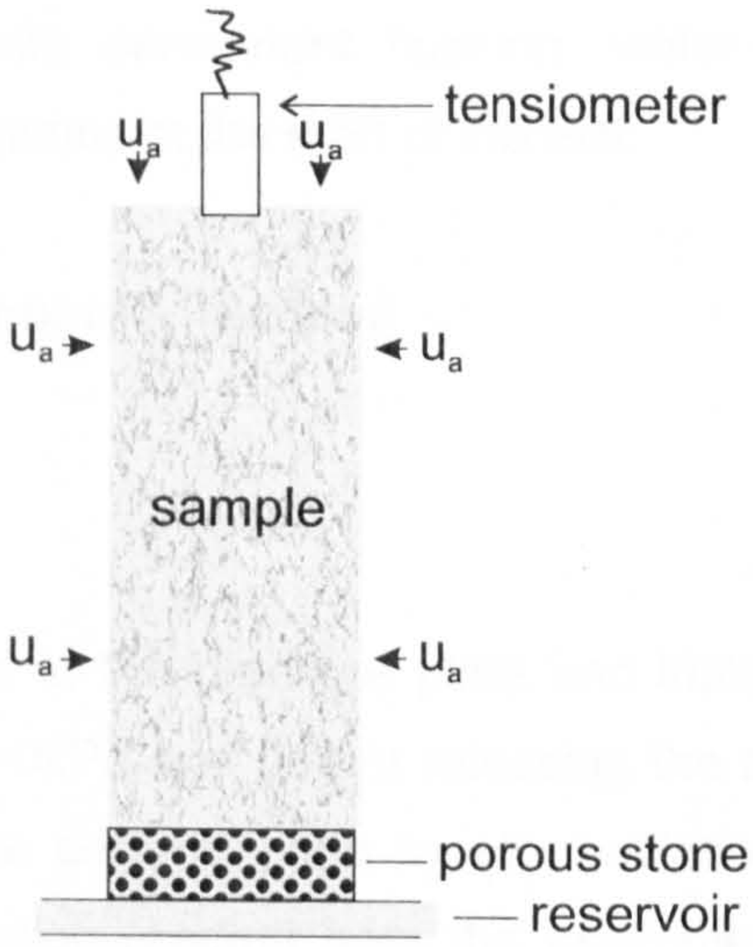

Figure 3.47: Set-up for the axis translation tests

Suction was imposed to the sample inside a pressure plate or triaxial cell by quickly raising the air pressure to the required value while pore water backpressure was maintained at atmospheric value. As soon as the air pressure was raised, the tensiometer (placed on the top of the sample) recorded a positive excess pore water pressure, which subsequently started to dissipate. Once the pore water pressure read by the tensiometer dropped back to zero, it was assumed that equilibrium was achieved throughout the sample. The air pressure was then reduced to the atmospheric value and the corresponding negative pore water pressure generated inside the sample was measured by the tensiometer. Increasing values of suction were applied and measured on the sample in a sequence up to a maximum value of 500kPa corresponding to the air entry value of the ceramic plates in both the triaxial cell and the pressure plate.

It was observed that the suction value measured by the tensiometer was sensitive to the water conditions below the porous stone. The following three distinct testing programs were therefore carried out to account for such effect:

- Axis translation with temporary flushing: water below the porous stone flushed out during the air pressure release but flushed back in during the subsequent air pressure increase.

- Axis translation with temporary flushing and sample mass measurements: same as above but with measurement of change in water content during the equalization stage.

- Axis translation with permanent flushing: water below the porous stone flushed out permanently at the start of the test.

3.4.6.2. Temporary flushing

Procedures

The tests were performed in the pressure plate and triaxial cell. In the triaxial cell, after suction equalized at 0kPa and before releasing the air pressure to zero, water was flushed out below the ceramic plate by air circulation. Once the cell pressure was reduced and the suction reading from the tensiometer was taken, water was restored below the ceramic for the application of the next suction stage. In the pressure plate, due to the specific characteristics of this piece of equipment, water at atmospheric pressure was present in the compartment below the ceramic plate throughout the entire test. Tests were conducted at first in a pressure plate but a triaxial cell was subsequently used because it allowed better control of the water conditions below the porous stone.

Results and discussion

Similar behaviour to that observed in the isotropic unloading tests was also observed during the axis translation tests. On releasing the air pressure, there was an immediate decrease of pore water pressure but thereafter the pore water pressure increased back with time.

Figure 3.48a shows the results for the test performed in the pressure plate. Inspection of Figure 3.48a indicates that, after the air pressure was increased to 187.6kPa, the pore water pressure measured by the tensiometer instantaneously increased by about the same amount and then progressively dissipated back to zero. After equilibrium was achieved, air pressure was reduced to zero and this induced a reduction of the pore water pressure from zero to -149.2kPa, i.e. a reduction about 20% smaller than the corresponding reduction in air pressure. Subsequently, the air pressure was increased again to a higher level of 396.5kPa and, after dissipation of the excess pore water pressure, was reduced again to zero. Also in this case, the corresponding reduction of pore water pressure from zero to -278.5kPa was about 30 % smaller than the corresponding reduction of air pressure.

For the case of Figure 3.48b, the air pressure was increased in 4 stages to 99.6kPa, 200kPa, 299.4kPa, and 400kPa. The corresponding water pressures measured by the tensiometer, on releasing air pressure to zero, were 95.7kPa, 191.4kPa, 284.9kPa, and 381.6kPa. Comparing to Figure 3.48a, the differences between the imposed and measured values of suction were smaller.

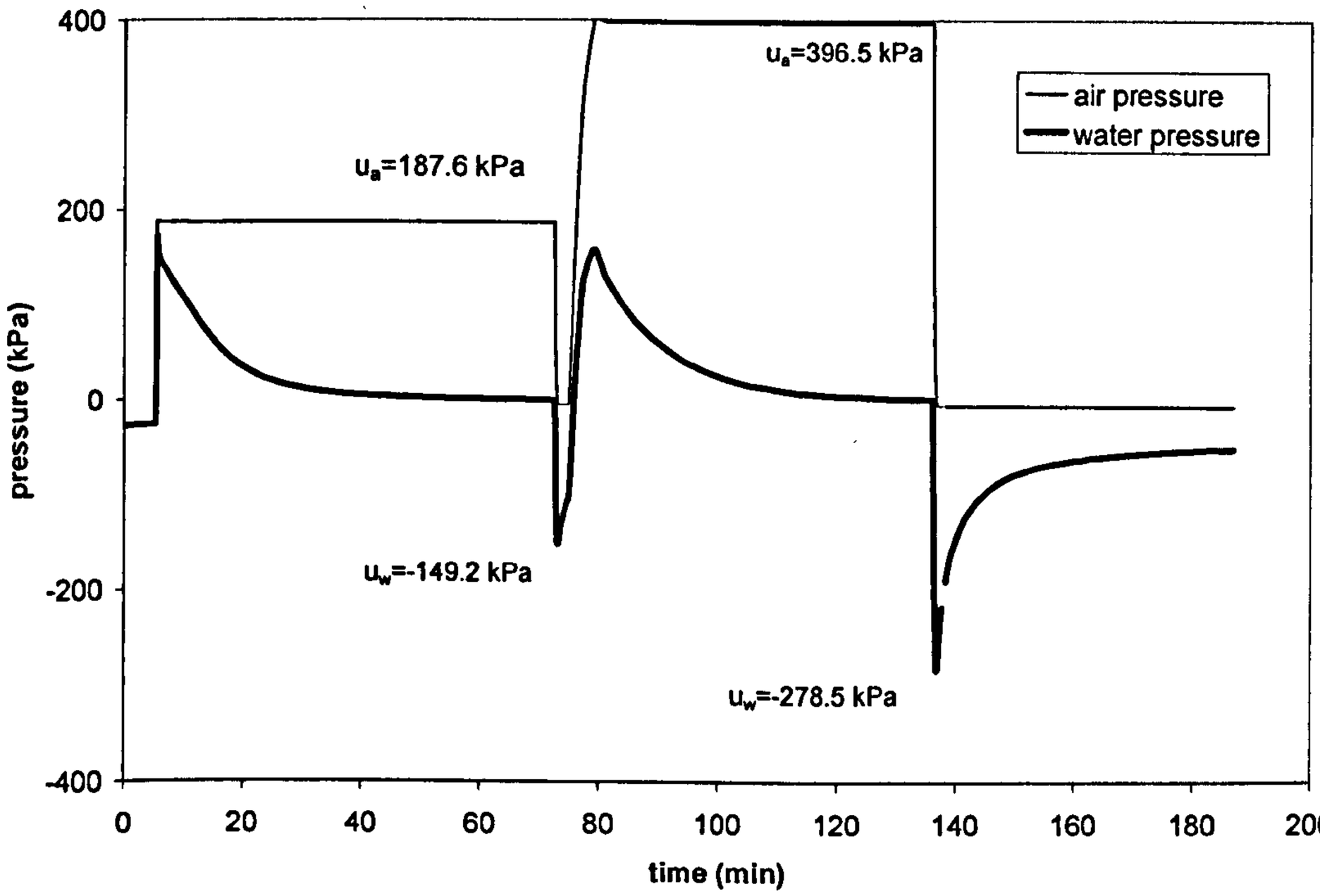

(a)

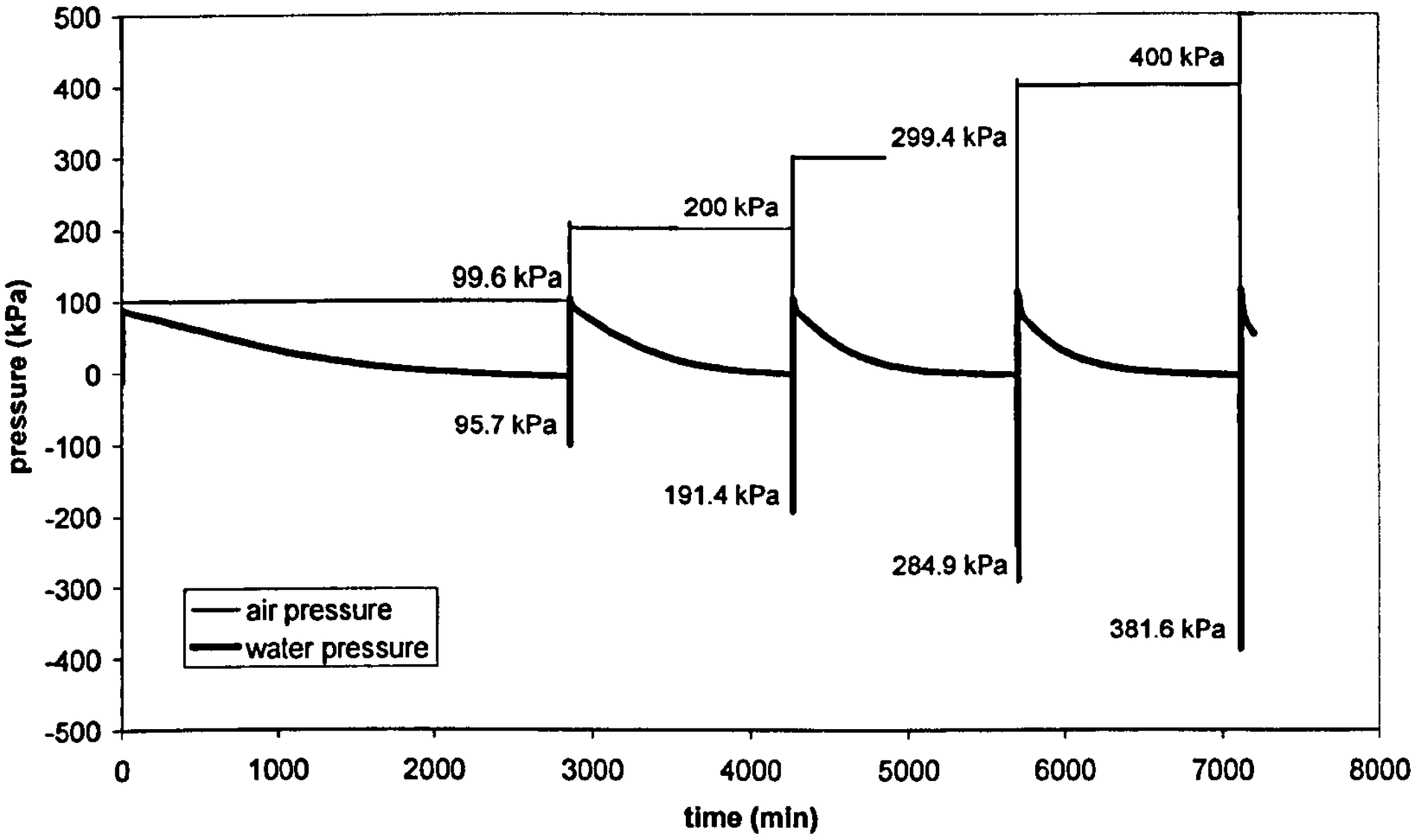

(b)

Figure 3.48: Axis translation tests with temporary flushing, conducted in the (a) pressure plate (test Tc16, tensiometer II1, kaolin) and (b) triaxial cell (test Tc23, tensiometer II1, kaolin)

Table 3.9 shows the error range for each test performed in this work, where the error is defined similarly to eq. 3.6 as the difference between the measured and imposed suction divided by the imposed suction. Such error was seen to vary throughout a test, i.e. it could vary by a significant margin between each air pressure release. For instance, in test T14 shown in Figure 3.48a, the error corresponding to the first air pressure release is around -20.4% while, for the second air pressure release, the error increases to -30.5%. Previous work by Guan and Fredlund (1997) showed similar results, with the suction measured by the tensiometer smaller than the suction imposed by the axis translation technique by a margin ranging between -0.5% to -8.5%.

Table 3.9: Errors in measured suction for tests performed with temporary flushing

Test nr	Device	Error, *e* (%)
T14	Pressure plate	-20.4 to -30.5
T17	Pressure plate	-12.5 to -18.2
T31	Triaxial cell	-10.5 to -11.0
T35	Triaxial cell	-4.6 to -10.5
T36	Triaxial cell	-12.5 to -16.25
T38	Triaxial cell	-14.2 to -17.2
T39	Triaxial cell	-4.3 to -6.0
T40	Triaxial cell	-4.3 to -4.6

Figure 3.49a shows an expanded view of the final part of the test shown in Figure 3.49a. It can be seen that, after the instantaneous initial drop in pore water pressure, the pore water pressure slowly rises over a period of about 20 minutes until it stabilises at a value of approximately -73kPa. A similar result is shown in Figure 3.49b, which presents part of a test carried out in the triaxial cell where the pore water pressure recorded by the tensiometer, after an initial instantaneous drop, rises under constant air pressure and stabilises at a value of -335kPa.This was a common feature of behaviour observed in all tests where the air pressure was maintained at zero for some time, after reducing it from the imposed value of suction. This result might be a consequence of the availability of free water inside the ceramic plate or below it. This water is sucked into the sample under the action of the negative pore water pressures generated by the air pressure drop, thus increasing water content and reducing soil suction.

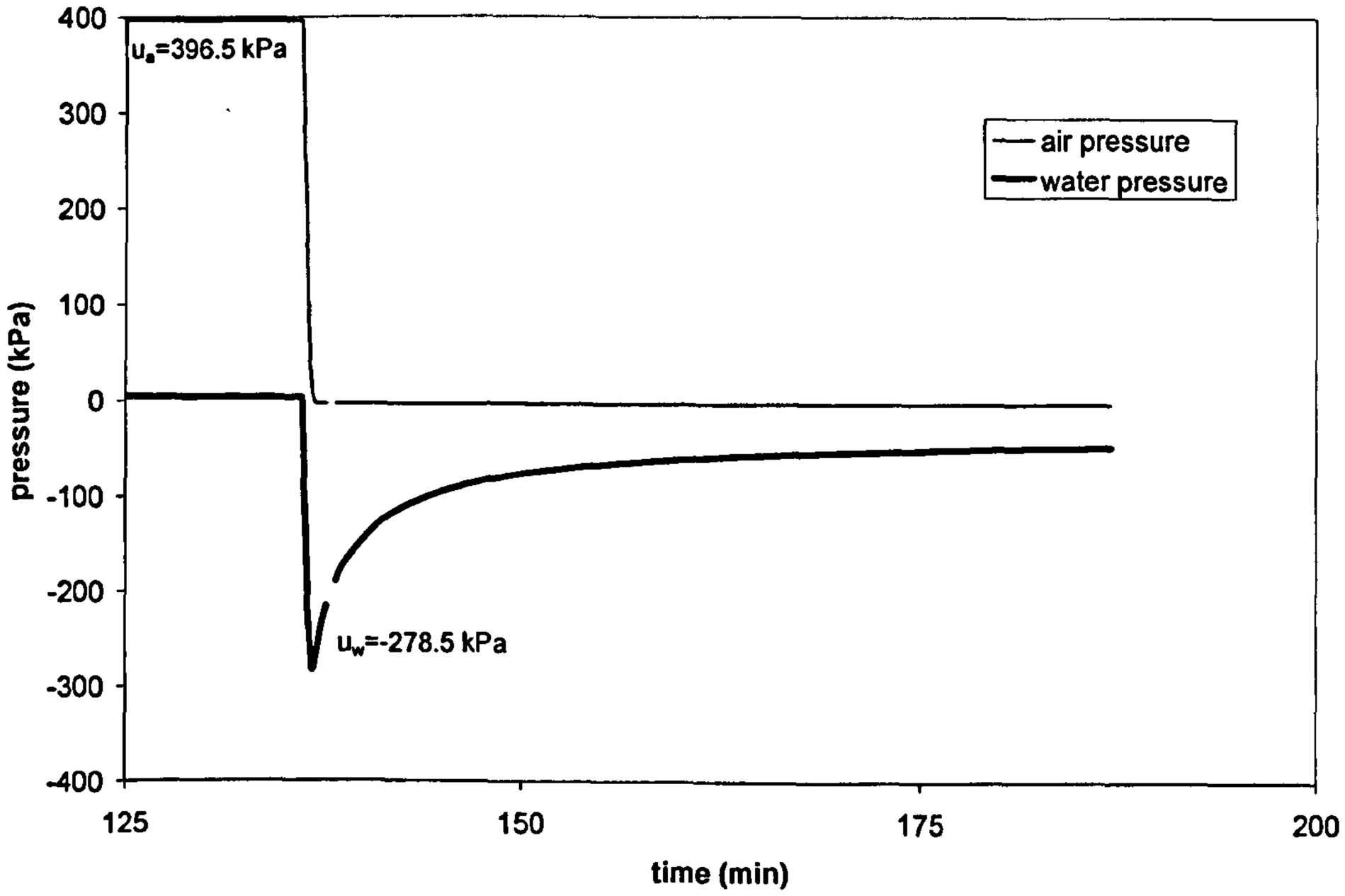

(a)

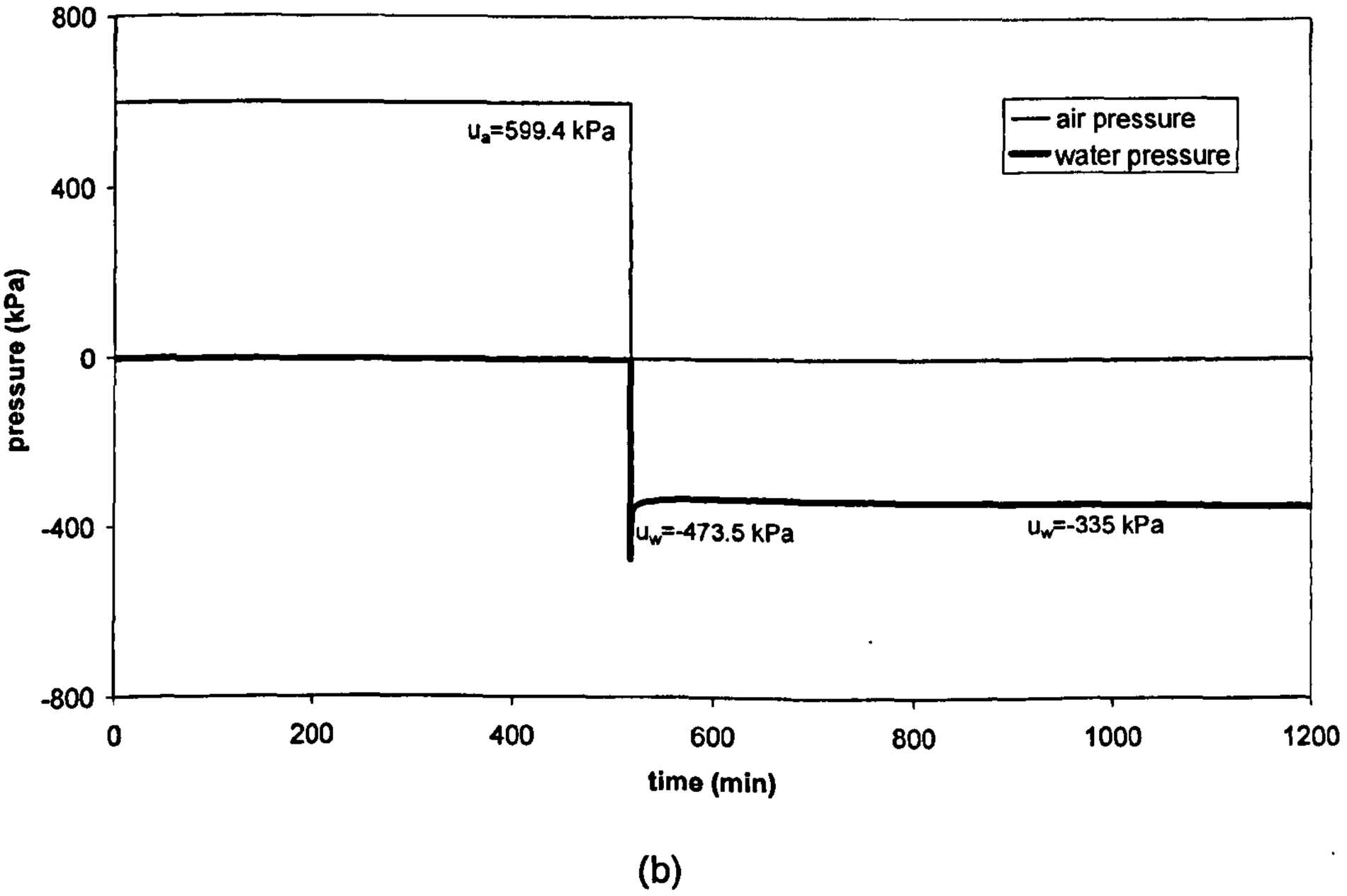

(b)

Figure 3.49: Sample response after releasing air pressure a) in the pressure plate (test Tc16, tensiometer II1, kaolin) b) in the triaxial cell (test Tc19, tensiometer II3, kaolin)

There are two possible explanations for the fact that the instantaneous pore water pressure decrease recorded by the tensiometer is generally smaller than the imposed drop of air pressure:

(1) One possibility is that, despite the air pressure drop being applied almost instantaneously, some water is still sucked back into the sample, which limits the magnitude of the measured pore water pressure reduction. This explanation seems consistent with the observation that pore water pressure reductions tends to be proportionally smaller for tests carried out in the pressure plate, where water is permanently present below the ceramic plate, than for tests carried out in the triaxial cell, where water below the ceramic plate is flushed out before each air pressure drop.

(2) The other is that the water content in the soil sample had not yet come to equilibrium, despite the pore water pressure having done so. Equilibrium was assumed to be achieved at each imposed value of suction when the tensiometer read a value of zero pore water pressure. After this condition was attained, the air pressure was decreased and the corresponding negative pore water pressure drop was measured by the tensiometer. However, although the pore water pressure is equal to zero throughout the specimen, it is possible that water content is still reducing inside the sample due to a slow rearrangement of water menisci at the interface between gas and liquid phases inside the pores. Such a hypothesis seems to be supported by the observation that pressure plate tests published in the literature (where the achievement of equilibrium is based on the measurement of the sample mass during equalisation) usually require significantly longer time than the tests reported in this work (where the achievement of equilibrium is based on the dissipation of the excess pore water pressures measured by the tensiometer). For example, the tests shown in Figure 3.48a and Figure 3.48b, both of which involved imposing more than one suction value to the sample, took overall 4 hours and 5 days respectively. Tinjun et al. (1997) and Vanapalli et al. (1997) reported equalisation times for clay samples of 5-8 days and 6-7 days respectively for each imposed value of suction in the pressure plate. In both these cases equilibrium conditions were assumed when the outward flow of water from the sample stopped.

If the above hypothesis were true, the dissipation of pore water pressure to zero would not be enough to conclude that a given suction 'is imposed' on the sample, as assumed by Guan and Fredlund (1997). Hence, the difference between the measured and imposed suction is simply due to lack of equilibrium in terms of water content. The tensiometer would be expected to measure suctions closer to the imposed ones if longer periods of time are waited during equalisation. In order to confirm such hypothesis, an additional testing program was undertaken as described below.

3.4.6.3. Temporary flushing with mass measurement

Procedure

In this case the experimental procedure was exactly the same as in the testing programme undertaken in the triaxial cell described above, except that, following air pressure release, the sample was removed from the cell and weighted. This procedure was repeated several times until mass measurements had stabilized under a given cell air pressure. Two air pressure levels were applied (300kPa, 400kPa) while mass measurements were taken by a balance with a precision of 0.00001g.

Results and discussion

Figure 3.50a shows the variation of suction with time for both imposed cell air pressures of 300kPa and 400kPa. Figure 3.50b displays the variation of mass with time while Figures 3.50c and 3.50d show the variation of the measurement error with time and mass respectively. Inspection of Figure 3.50b indicates that, for both applied levels of air pressure, the mass tended to decrease but it did not achieve equilibrium over a relatively prolonged period of time. Such decrease of water content was only clearly matched by a corresponding decrease of the error in the case of an air pressure of 300kPa. For an air pressure of 400kPa, although the error trend was less clear, a very small error of 0.44% was recorded at the end of the test. In both case the maximum errors are quite similar to those observed during the previous testing programme summarized in Table 3.9.

Although Figures 3.50c and 3.50d are not conclusive regarding the effect of equalization time, they clearly show that water content still tends to decrease despite the reading from the tensiometer indicates that equilibrium of pressures has been achieved throughout the sample. It is also worth noting that the lowest measurement errors (i.e. -0.99 %, +0.45 %) were measured in this test in comparison to both the previous testing programme and the one described in the next section.

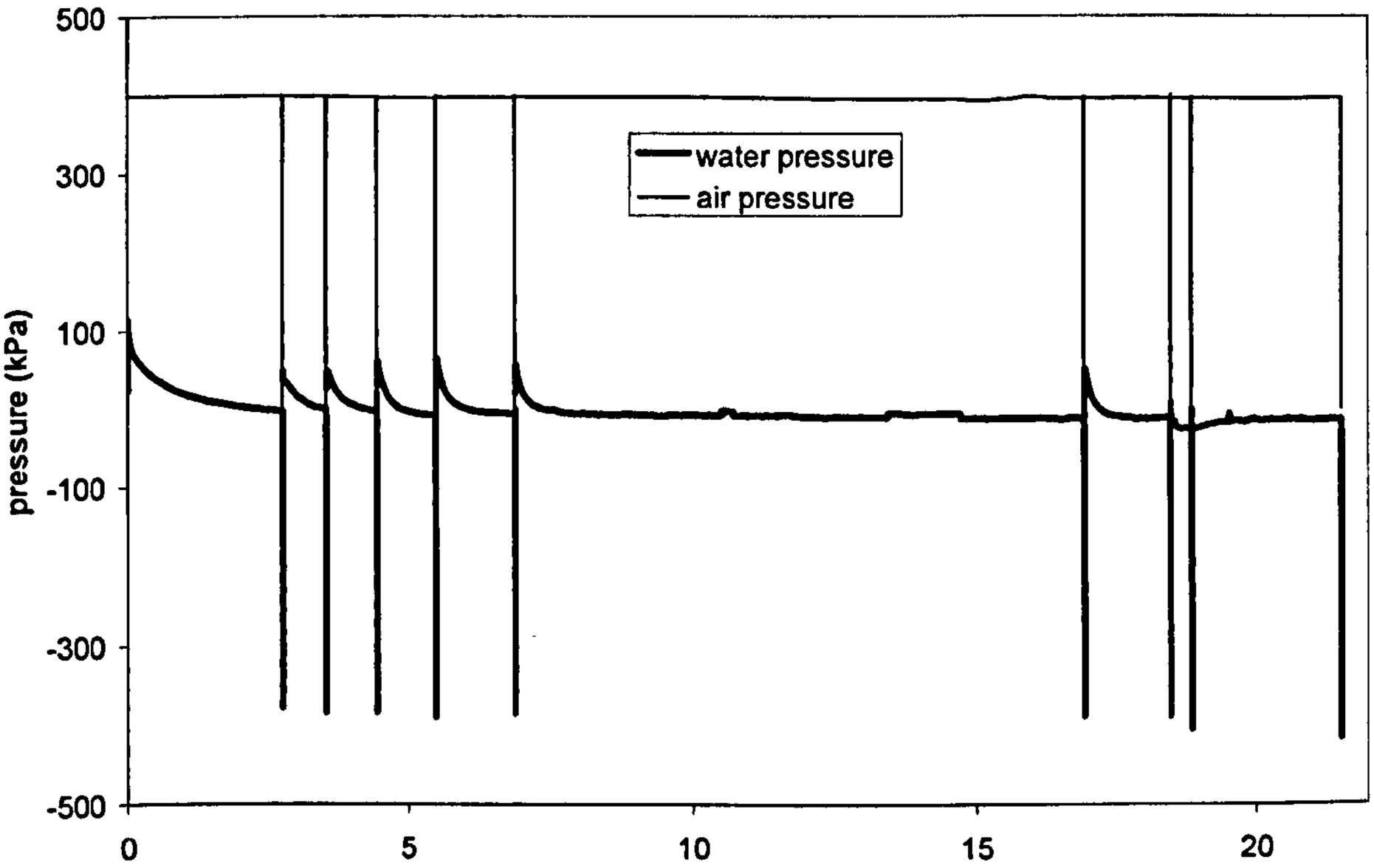

(a)

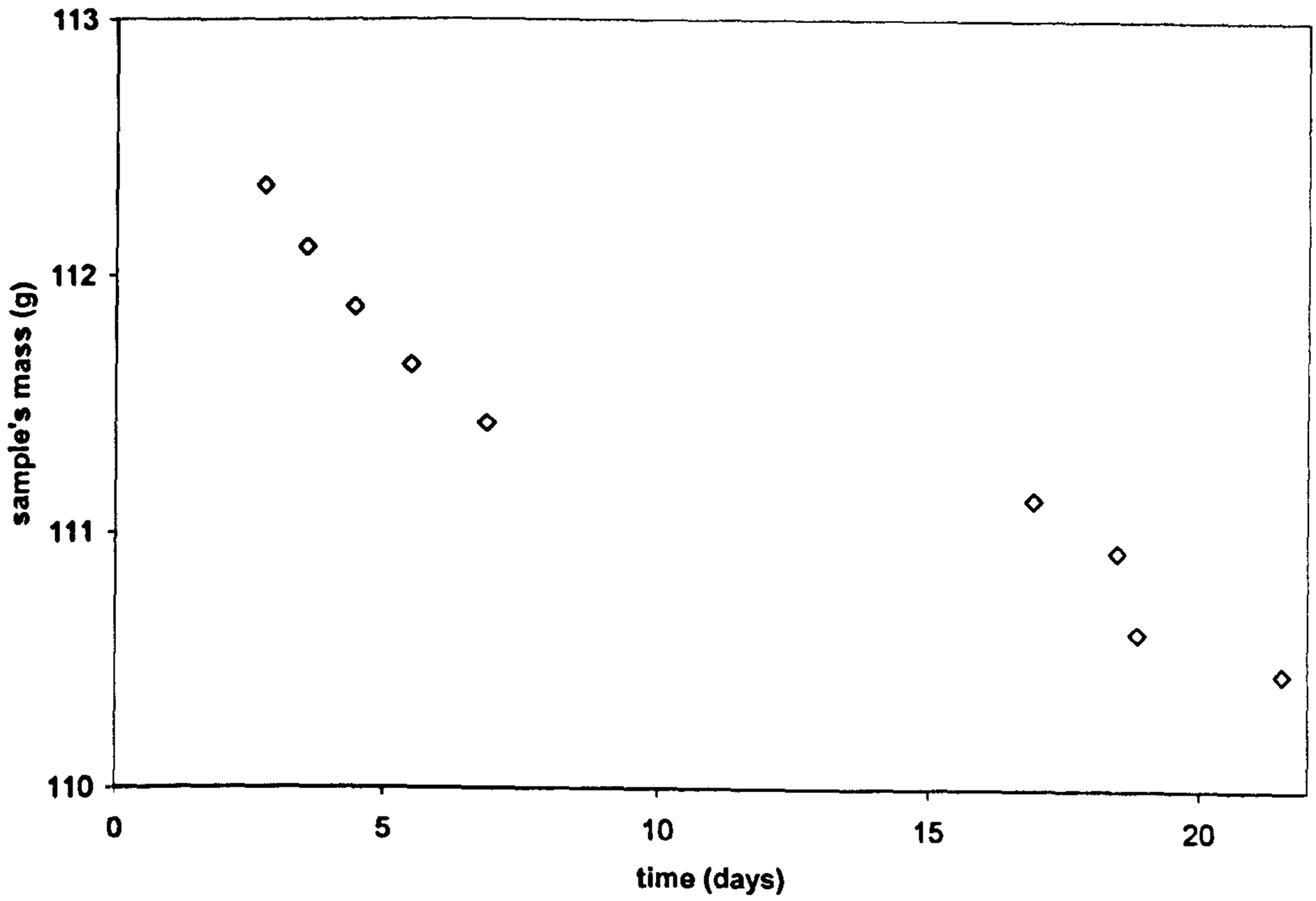
113
112
111
110
sample's mass (g)
0
5
10
15
20
time (days)

(b)

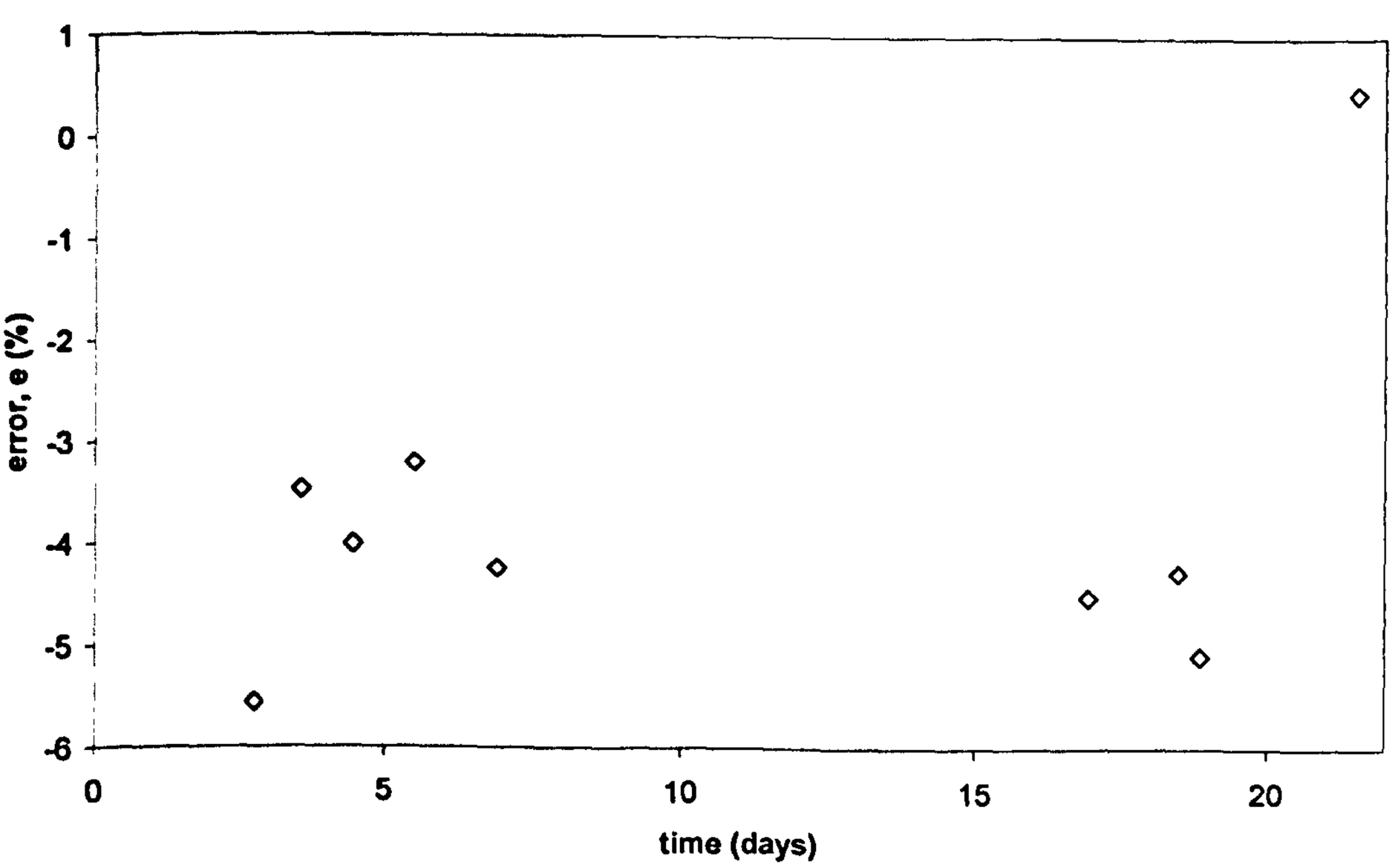
1
0
-1
-2
-3
-4
-5
-6
error, e (%)
0
5
10
15
20
time (days)

(c)

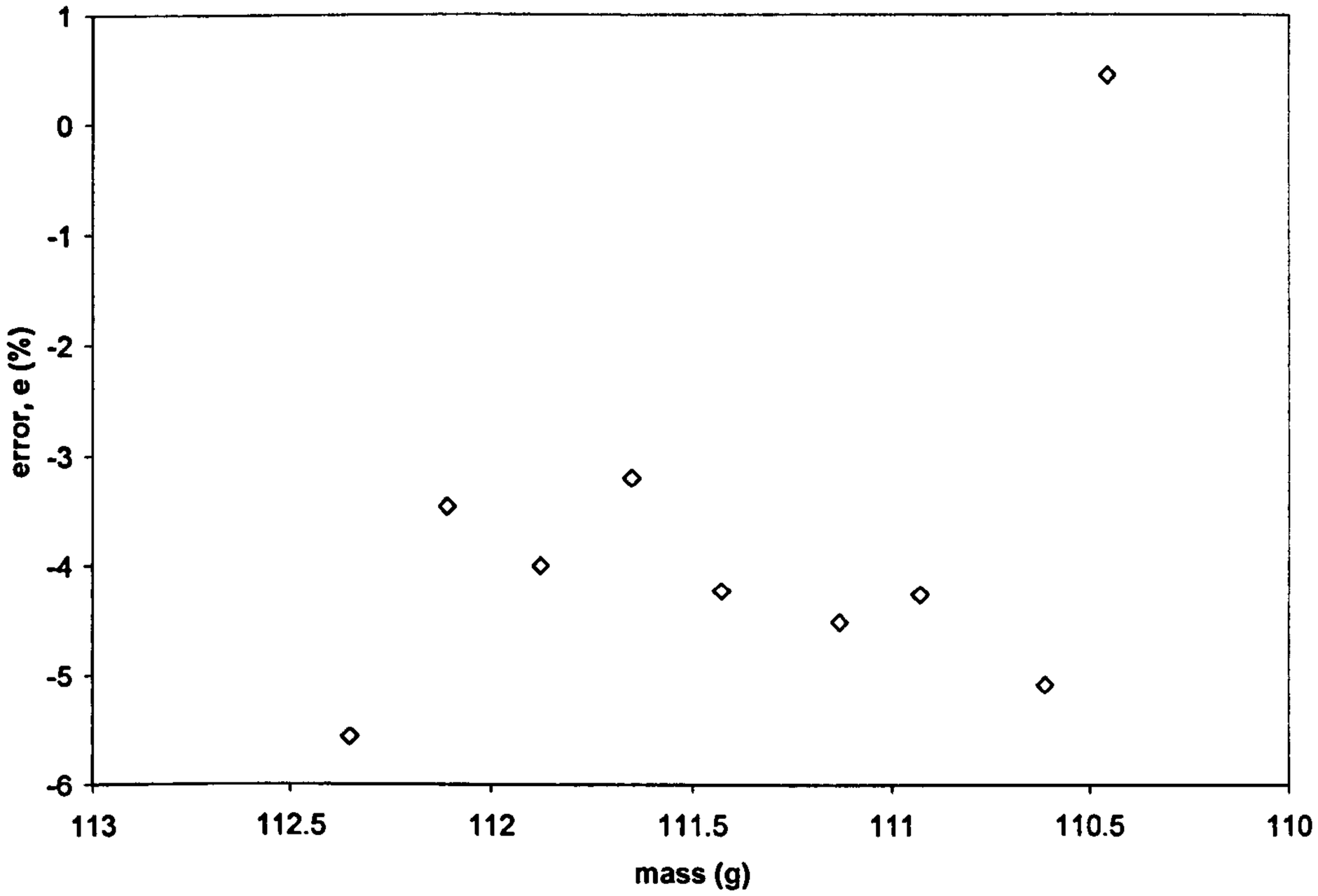

(d)

Figure 3.50: Axis translation tests with temporary flushing and sample mass measurements (test Tc24, tensiometer III4, kaolin); a) test time series, b) sample mass versus time, c) error versus time, d) error versus sample mass

3.4.6.4. Permanent flushing

In order to further study the effect of water conditions below the porous stone on the suction measured by the tensiometer, a third testing program was devised whereby water was permanently flushed out below the porous stone at the beginning of the test.

Procedures

Having removed all water from below the porous stone by flushing air through the backpressure line the pore air pressure was changed in steps (e.g. reducing from 600kPa to zero then increasing in similar steps back to 600kPa). The air pressure was, in this case, changed in steps to ensure that any remaining water below the porous stone would be absorbed gradually by the sample instead of in a single instance. A series of three cycles were imposed to the sample with the pore water pressure, measured by the tensiometer, compared to the applied pore air pressure,

read by the same pressure transducer used for the calibration of the tensiometer in the positive range.

Results and discussion

Plots of applied pore air pressure and measured pore water pressure are given in Figure 3.51a and show the following:

(1) After each decrease of pore air pressure, the pore water pressure instantaneously decreased. However, it subsequently increased back while pore air pressure was held constant and stabilized at a higher value than that imposed. This can be clearly seen in the first two unloading steps in cycle 1 where, although the tensiometer reading dropped immediately on reducing pressure, it then started to move back towards zero. The same effect can be seen in Figure 3.51b which shows cycle 3 on an expanded time scale. The likely reason for this is again that water is being drawn out of the porous stone. This effect disappeared as pore air pressure decreased, suggesting that all free water had been removed by this stage.

(2) During the ascending part of the curves the pore water pressure increased instantaneously after an increase of pore air pressure, showing a tendency to reduce slowly with time while air pressure was kept constant after each stage. This effect can be explained by water evaporating from the sample in an attempt to establish equilibrium with the relative humidity inside the cell. As a note, the degree of saturation at the end of the test was 92.3% (initial degree of saturation in section 3.4.2 was 98.7%). Table 3.10 shows the results in terms of the change of pore water pressure instantaneously measured after each step change of pore air pressure in cycle 3. The error is rather large, with the measured change of pore water pressure tending to be generally greater than the imposed change of air pressure by an amount that could be as big as 8%. Error is also seen to increase at higher suctions. Only at the end of the first cycle, a change of water pressure significantly smaller that the increase of air pressure was observed. This can be explained by the fact that, in this case, the pore air pressure was slowly increased to 600kPa and the pore water pressure started dissipating as it became positive. Since the water channels below the porous stone had been blown dry, water under positive pressure would be able to flow out of the specimen and into space below the porous stone.

Table 3.10: Difference between imposed and measured values of suction for cycle 3 of the axis translation test with permanent flushing

Decrease (D) or increase (I)	Measured difference in water pressure (kPa)	Imposed difference in air pressure (kPa)	Error, *e* (%)
D	103.1	102.2	+0.88
D	104.5	101.3	+3.16
D	105.0	102.5	+2.44
D	109.0	102.4	+6.45
D	89.9	85.5	+5.15
I	94.2	87.3	+7.90
I	104.4	99.9	+4.50
I	104.6	97.5	+7.28
I	104.2	101.1	+3.07
I	105.0	101.3	+3.65

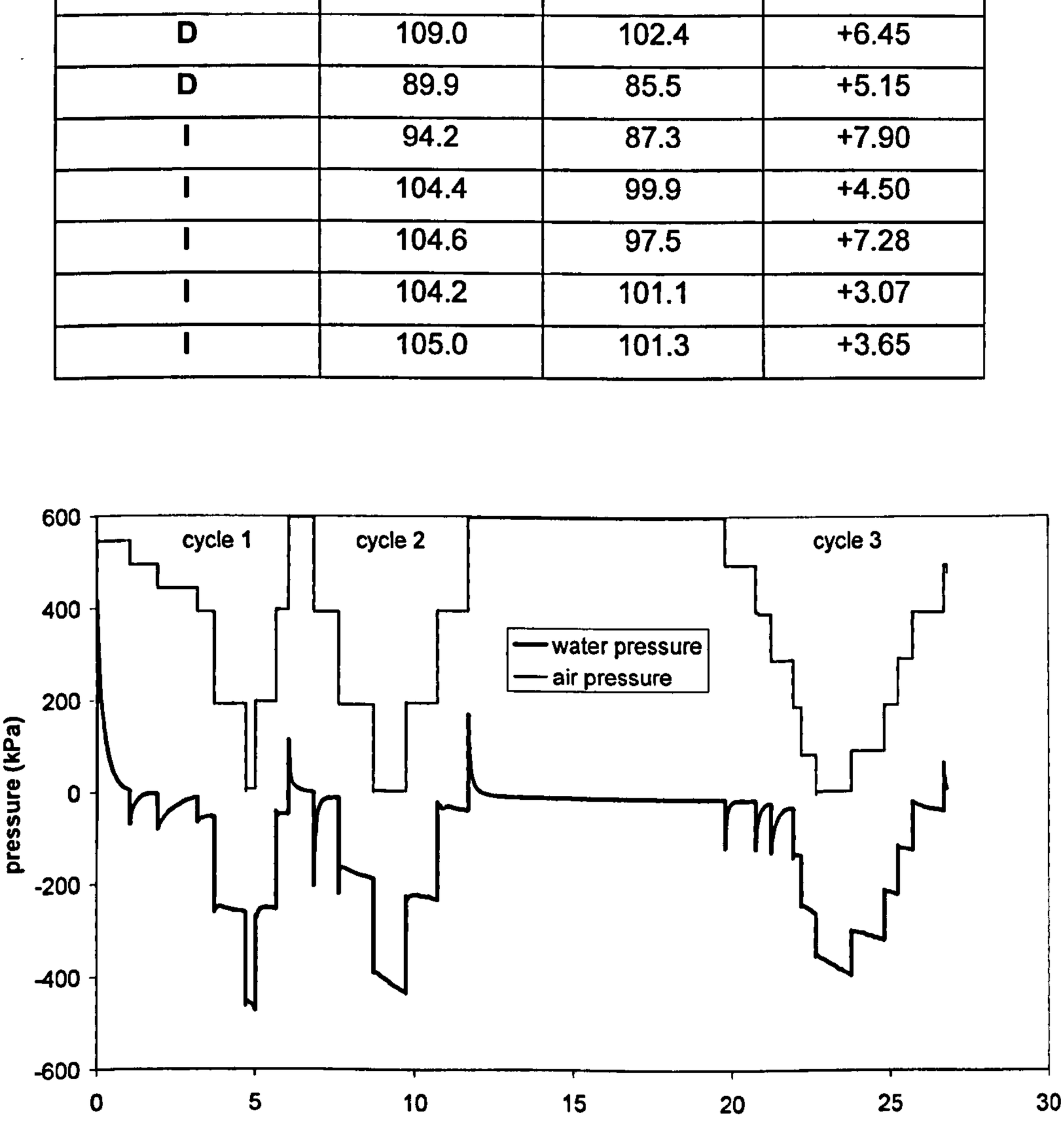

(a)

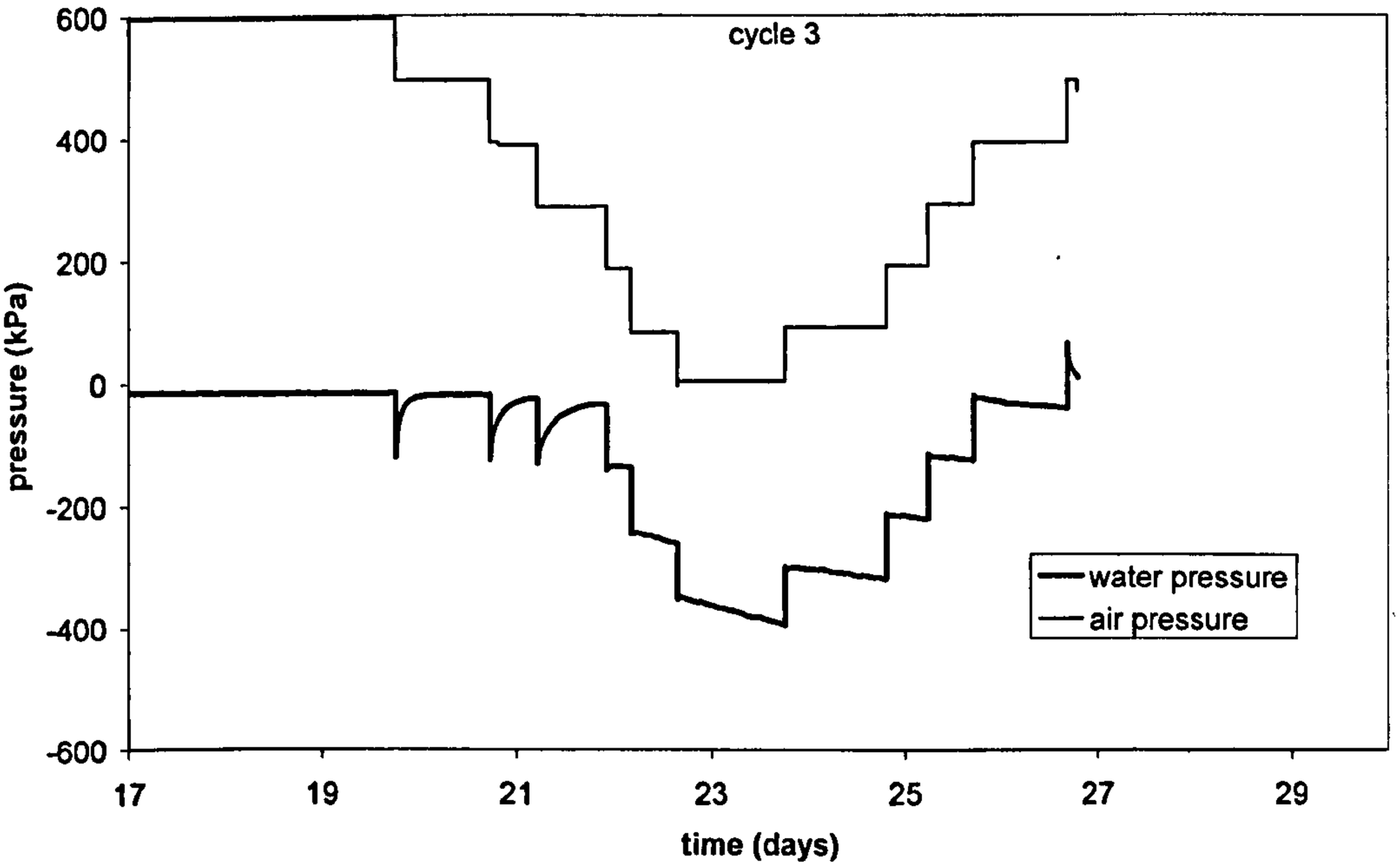

(b)

Figure 3.51: Axis translation test with permanent flushing (test Tc25, tensiometer III4, kaolin), a) all cycles, b) cycle 3 only

In contrast to the above, the previous two testing programs showed changes of pore water pressures whose magnitude was always smaller than the corresponding changes of air pressure. In those tests, however, the water channels beneath the porous stone of the pressure plate were filled with free water, rather than being blown dry. Guan and Fredlund (1997) reported similar results to this study for some tests where the pore water pressure increase measured by the tensiometer was higher than the air pressure increase by about 5%. Those authors give no reason for such behaviour.

When air pressure in the cell is decreasing, there would be a tendency for the pressure difference between the air pressure on the top surface and the water pressure inside the stone to decrease. However, this tendency will progressively reduce as availability of free water vanishes and negative pore water pressures are generated inside the stone. At the same time, at the base of the stone, the pressure difference between the atmospheric air pressure and the water pressure inside the stone is increasing. This could lead to water rearrangement within the porous stone, potentially increasing suction even more than the imposed value. However, while this

might explain the descending part of the curves it does not explain the ascending parts.

There is also the possibility that the sample dried during the release of air pressure, however this is unlikely to have any effect because pore air pressure is changed rapidly (in a few seconds) so there would be no time for water to evaporate from the sample. Nevertheless, it could be that the suction change produced in the sample by a reduction in cell air pressure is affected by previous drying during equalisation periods between pressure drops.

3.4.6.5. Summary

Axis translation was used in this research as an indirect technique to validate the extrapolation of tensiometer calibration from the positive to the negative range. In particular, three separate testing programs have been conducted: a first testing programme where water is flushed out below the porous stone when suction measurements are taken but it flushed back in during the intermediate equalization stages, a second testing programme similar to the previous one but including additional measurements of sample mass during intermediate equalization stages and a third testing programme where water is permanently flushed out from below the porous stone since the start of the test. The two main conclusions that can be drawn from this study are:

(1) The suction generated inside the porous stone, following each air pressure release, depends on the presence of water below the porous stone and is likely to affect also the suction measured by the tensiometer. If there is water below the porous stone, suction changes measured by the tensiometer tend to be lower than the imposed air pressure change. However, if there is no water, suction changes tend to be greater than the imposed air pressure change (i.e. up to 8% greater than the imposed air pressure change).

(2) As shown in the second testing program, a measurement of zero pressure by the tensiometer during equalization stages is not necessarily an indication of hydraulic equilibrium throughout the sample. Test results clearly indicate that longer equalization periods, with periodic measurement of the sample mass, are needed to ensure that equilibrium is achieved in the soil specimen.

3.4.7. Discussion

3.4.7.1. Technique selection

The previous sections have discussed aspects of individual direct and indirect methods of evaluating tensiometer calibration over the negative pressure range. It was assumed that extrapolation from the positive range is acceptable in order to observe features of the tests in isolation and to express results in terms of pressures. In the following we will compare these methods of obtaining a calibration factor working in terms of the raw output from the tensiometer, the DC voltage.

The results in previous sections indicates that, from a practical point of view, the isotropic unloading method of checking extrapolation for tensiometer calibration is most suitable and, while slightly more complicated to carry out, provides less disadvantages than the axis translation method.

Figure 3.52 shows plots of imposed known negative pressures against tensiometer transducer output voltages for the three methods described above. Also shown is the calibration line extrapolated from the positive range for the 'isotropic' calibration procedure. All results shown here use the same tensiometer (including the extrapolated calibration curve) but are different to the results discussed in previous sections (which used a different tensiometer). Table 3.11 shows the calibration factors for the three methods previously described and compares them with the assumption of extrapolation from the positive range using an error measure similar to eq. (3.6) in terms of *m*. The vacuum method provides a calibration that is the closest to the extrapolated curve followed by the isotropic unloading method.

Table 3.11: Comparison of calibration factors for different methods

Method	Calibration factor *m*	Error if extrapolation used (%)
Vacuum	11.071	-0.59
Isotropic unloading	10.921	-0.78
Axis translation (for permanent flushing)	11.438	+3.78
(Extrapolation from positive range)	(11.006)	

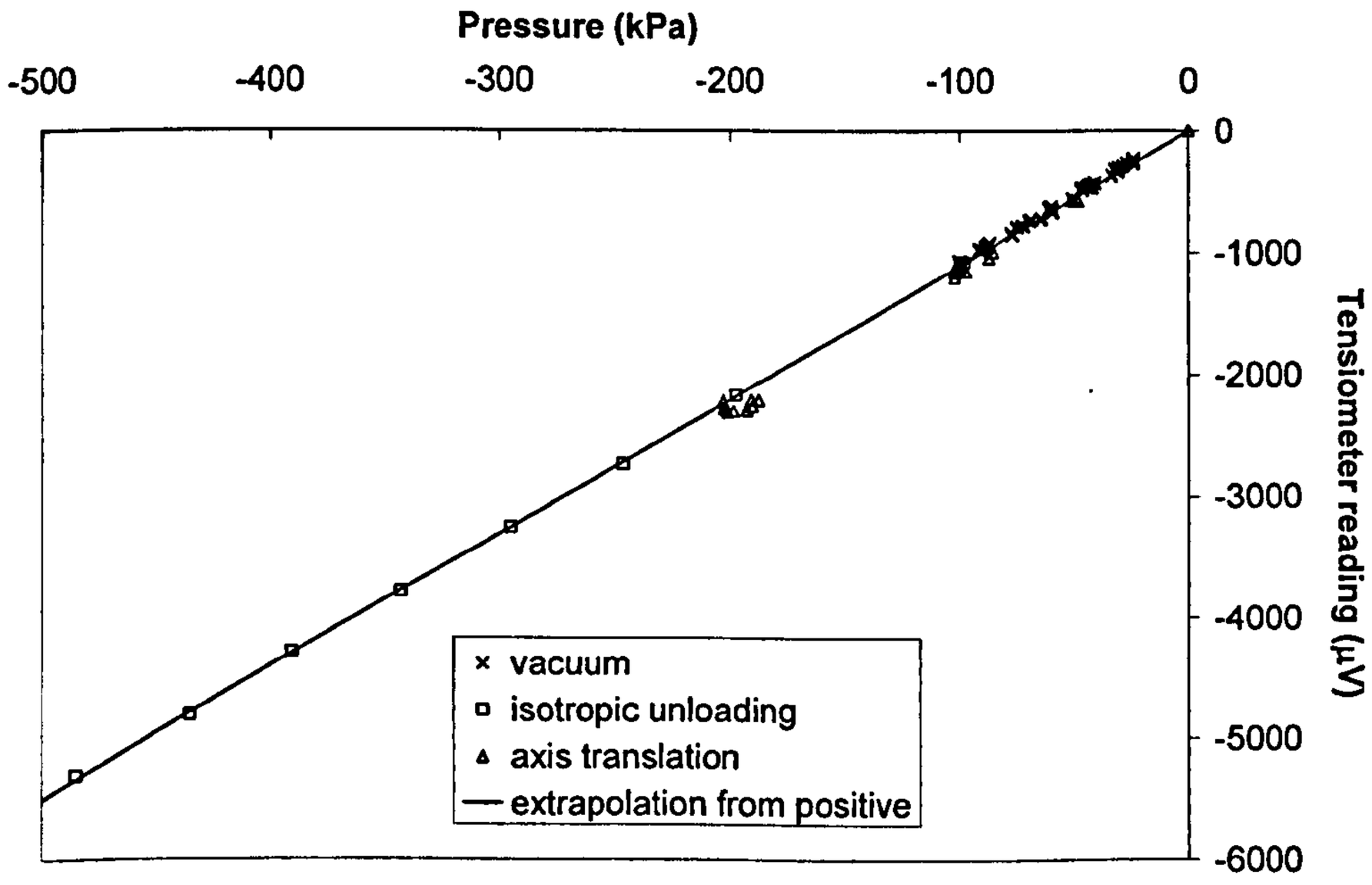

Figure 3.52: Comparison of calibrations in the negative range with extrapolation from the positive range

The high sensitivity of the axis translation method to the presence of water inside and below the porous stone indicates that it probably should not be used to check the extrapolation of the calibration curve to the negative range. It also suggests that special procedures have to be followed when using the pressure plate. The most immediate is that samples should be removed as soon as the air pressure is released. Depending on the mass of sample and shape of the soil water retention curve the error obtained could be considerable, as shown by the tests conducted in the pressure plate.

Isotropic unloading and the vacuum method give smaller errors and seem to be less dependent on external factors. It also suggests that calibration in the positive range with extrapolation to the negative could be accurate enough, but only if the tensiometer is calibrated in the same conditions as it will be used.

Application of these results to other tensiometers might not be straightforward because of design differences among tensiometers. Differences in dimensions, materials, sealants and construction would certainly affect the calibration differently in the positive range, as forces would be transmitted differently through the body (and should also influence the tensiometer response in the negative range). For instance, tensiometers developed by Tarantino and Mongiovi (2003) and Ridley et al. (2003) have the diaphragm embodied in the casing as a single piece, while the tensiometers developed by Guan and Fredlund (1997) and in this research have separate transducers that are glued or fixed to the casing. In general, it is suggested that at least one calibration in the negative range should be done in order to assess the validity of the extrapolation of the calibration curve from the positive range.

3.4.7.2. Alternative calibration techniques

An alternative technique (not used in this research) to calibrate the tensiometer in the negative range might consist in placing a material with a smooth surface in contact with the porous stone of a saturated tensiometer as shown in Figure 3.53. After sealing around the contact between the tensiometer and the smooth surface, a tensile force is applied to pull the tensiometer away from the smooth surface. If the contact between such surface and the tensiometer is very smooth and the tensiometer is fully saturated and well sealed, then any tension applied will result in a negative water pressure inside the tensiometer, which can then be related to the magnitude of the external pull.

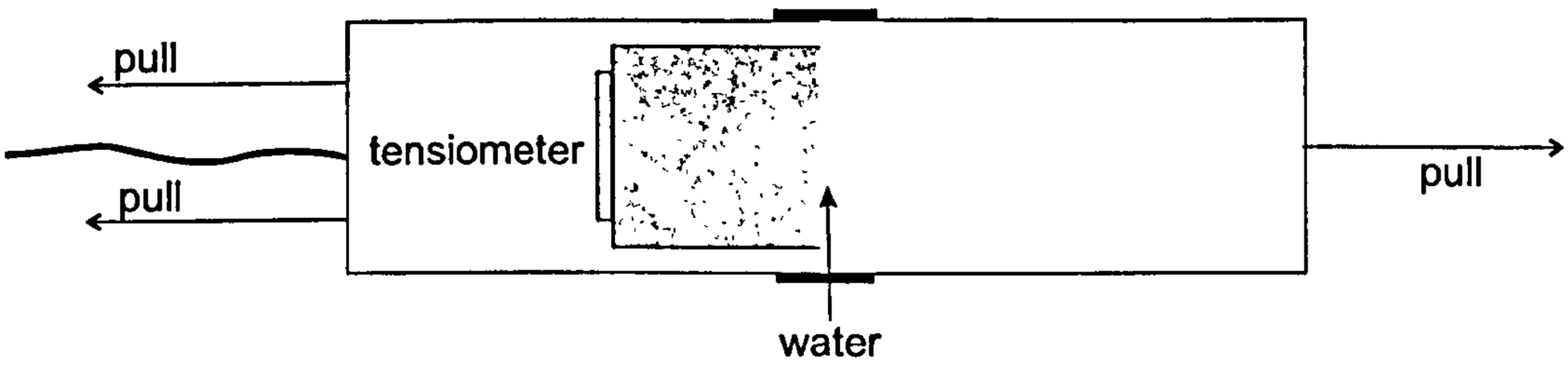

Figure 3.53: An alternative direct technique for tensiometer calibration

3.4.7.3. Quick assessment of the reliability of calibration

A good indication of the accuracy of the calibration is given by the pressure the tensiometer reads immediately after cavitation, which should be approximately -100kPa, as shown by many studies on high suction tensiometers. If it does not give this reading, then there has been a shift in the calibration, or the calibration is not correct. Cavitation following measurement of high suction is shown, for one of the tensiometers used in this study, in Figure 3.54 and indication of correct calibration can be seen in the very small deviation from -100kPa following cavitation.

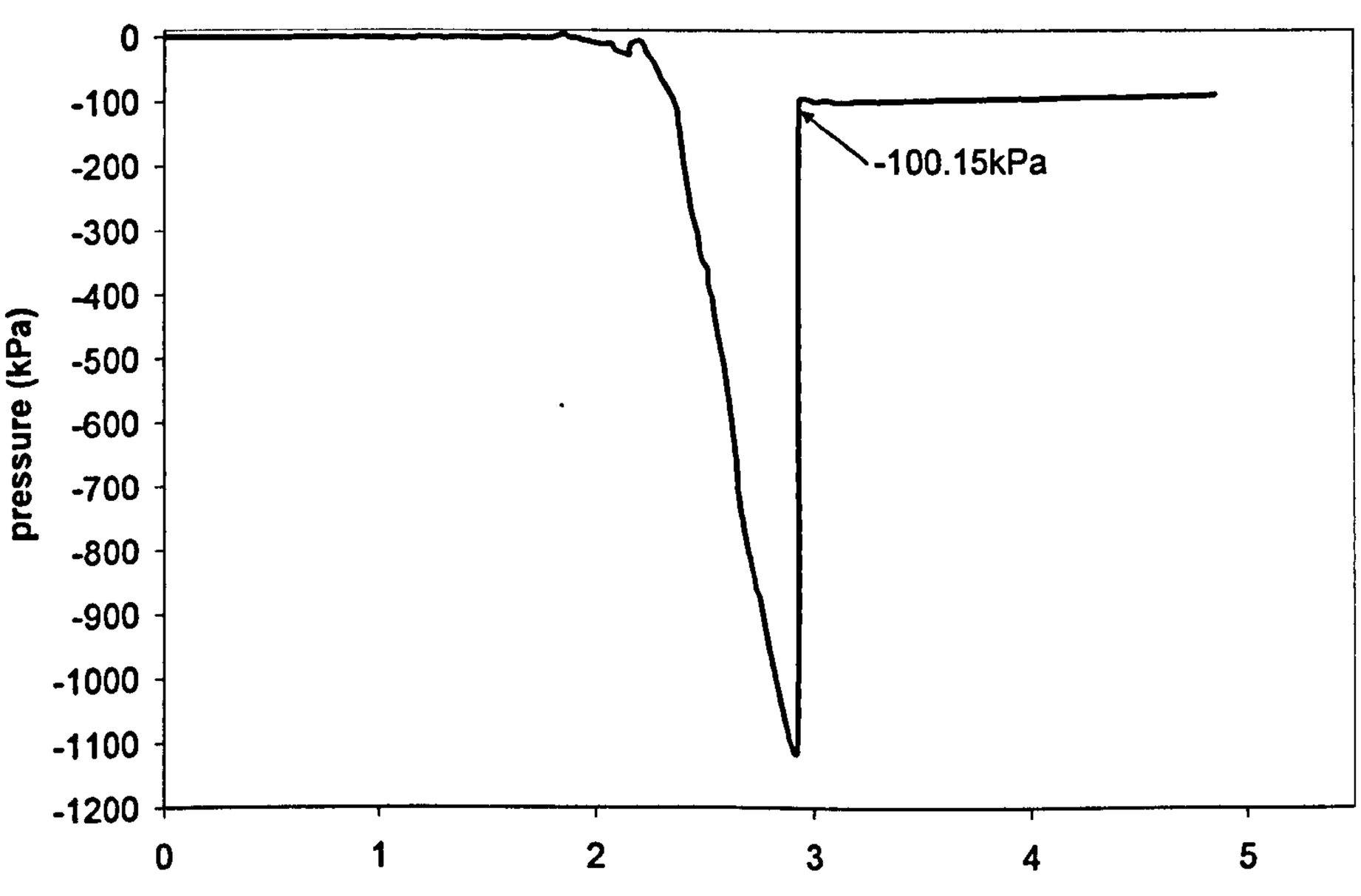

Figure 3.54: Tensiometer reading after cavitation (test Tc25, tensiometer III5)

Similarly an useful procedure for assessing any change of the calibration factor or a shift in the calibration zero (perhaps due to device hysteresis) at pressures lower than -100kPa consists in performing repeated suction measurements on the same

soil sample to check whether the same reading is obtained. For example, figure 3.55 shows a good agreement in the suction measured several times on a sandy clay sample by one of the tensiometers used in this research.

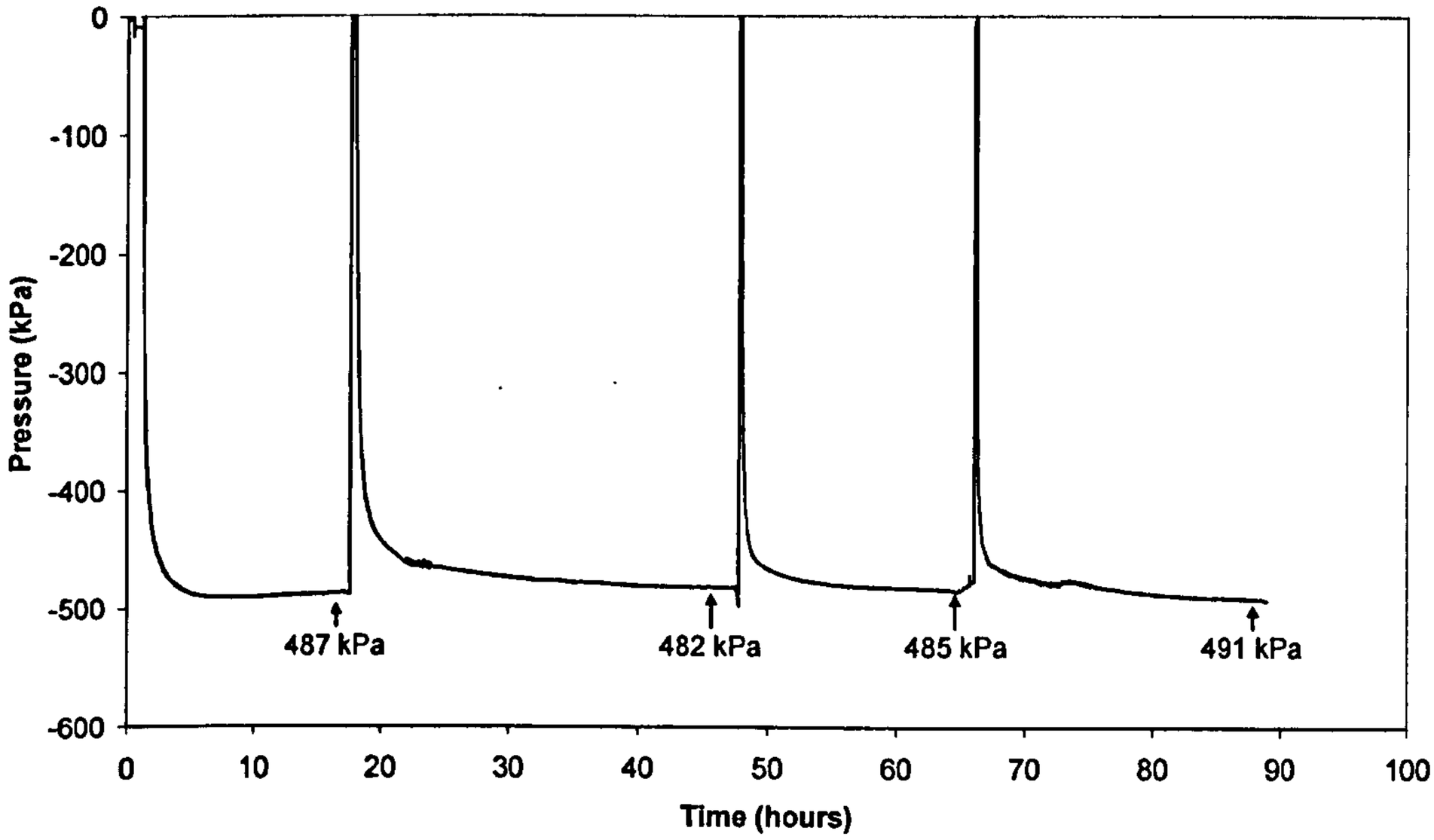

Figure 3.55: Repeated readings to assess calibration reliability (test Tc27, tensiometer II1, BIONICS)

3.5. MEASUREMENT

3.5.1. Introduction

This section will start by defining the factors affecting suction measurement and will then move to address some of the gaps of knowledge raised in Chapter 2. In particular it aims to answer the question first asked in Chapter 2: 'how do we know that the suction measured is correct?'

3.5.1.1. Factors affecting suction measurement

The factors affecting suction measurement by tensiometers include:

(1) Rate of suction change in the soil. The rate of suction change in the soil must be slower than the response time of the tensiometer. The rate of suction change in the soil might also depend on the sample's water content and tends to be faster for drier samples. The rate of soil suction change during laboratory tests can be controlled by imposing slower rates of water content change.

(2) Contact porous stone-soil. It is very important that a good contact is achieved between the porous stone and the sample to ensure continuity of water pressure between the soil and the measuring device. This contact can be improved by adding a fine soil paste to the surface of the porous stone before.

(3) Electro-mechanical aspects of the tensiometer. The tensiometer readings might be affected by the temperature, external pressures on the tensiometer body, calibration, infiltrations from the back of the tensiometer and fluctuations of the input voltage.

3.5.1.2. Types of measurement

Suction measurements taken by tensiometers can be grouped in two categories: discrete measurements or continuous measurements. Discrete measurements are performed at constant water content on a sample placed inside a sealed cell. In this research discrete measurements were performed using the sealed cell shown in

Figure 3.56. On the other hand, continuous measurements are performed on soil samples while suction and water content are progressively changing with time (e.g. triaxial testing, field measurements, oedometer testing).

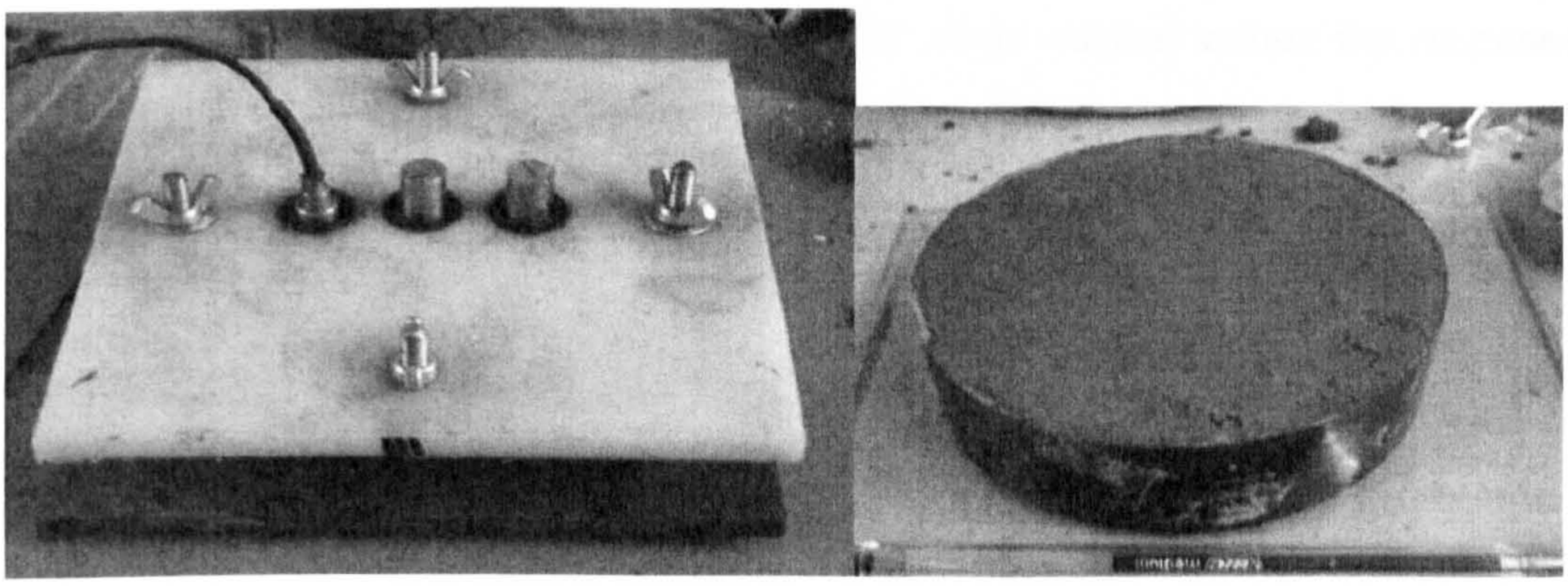

Figure 3.56: Equipment for the discrete measurement of suction: cell made of 2 plates with a ring in the middle and tensiometer inserted through the top plate (left); the ring is shown with a sample inside in right hand side image

3.5.2. Time dependency

Tensiometers take a certain amount of time to measure suction, which will depend on the rate of water transfer between the tensiometer and the soil. The rate of water transfer to the soil is influenced by the hydraulic conductivity of the soil and porous stone, and the volume of water transferred (e.g. Klute and Gardner, 1962, Hayashi et al., 1997, Towner, 1980).

For high suction tensiometers, the response time is particularly relevant for cases where the suction and water content of the soil change with time. If the rate of change is faster than the response time of the tensiometer, the values measured will be incorrect. The response time might also be affected by electro-mechanical aspects of the tensiometer (thickness of the diaphragm and temperature) and, as discussed in Section 3.3, by the degree of saturation of the porous stone.

The response times of the tensiometers vary between 8-350min as suggested by Figure 3.57 where measurements taken on a number of different soil samples at different suctions are shown. If the four dark points are neglected (these correspond to measurements taken early in this research in different locations of the same sample), the response times vary between 8-160min.

It was expected that the response times would increase with suction, because at higher suctions the volume of water to be transferred from the tensiometer to the soil would be greater, although this is not evident from the 24 suction measurements shown in Figure 3.57. It can be noticed however that for suctions higher than 500kPa the minimum response time is 50min, while for lower suction values the response time is much smaller (minimum of 8min).

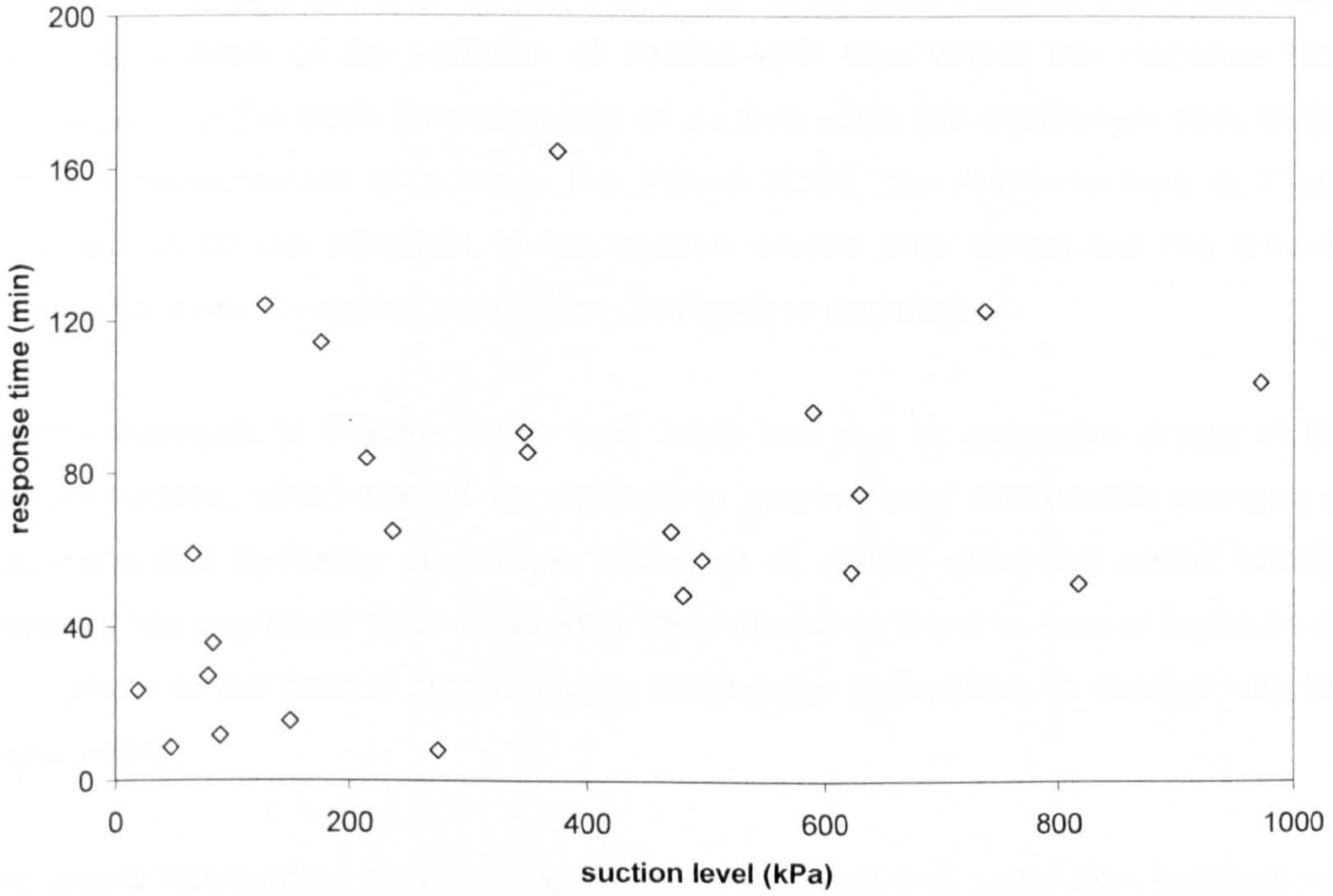

Figure 3.57: Response time at different suctions

Oliveira and Marinho (2008) studied the factors affecting the equilibrium time in a gneissic residual soil with a high suction tensiometer. The authors found that the time to equilibrium was affected by the structure of the soil. Samples were compacted for water contents dry of optimum, at the optimum water content, and wet of optimum. Oliveira and Marinho also found that the time to equilibrium increased with the suction level.

If suction has equalized throughout the soil sample, the time for the tensiometer to read such equilibrium value of suction is the same as the response time. In this case the suction read by the tensiometer progressively reduces with time until the curve flattens at a constant suction value (Figure 3.58a). There are however cases when the variation of suction with time does not follow the trend of Figure 3.58a and, in

these cases, the definition of the response time differ from that of the equilibrium time.

Figures 3.58b, 3.58c, and 3.58d show different measurements of suction taken in this research where the time to reach equilibrium is greater than the response time. All measurements were taken on samples previously dried from a higher water content and sealed inside a cell such as that shown in Figure 3.56. Figures 3.58b and 3.58c display a reversal of the variation of suction with time where the response time corresponds to the peak measurement of suction while the equilibrium time to the constant measurement of suction. For Figure 3.58d, the response time is 75min (corresponds to the inflection in the suction versus time curve) but the time to equilibrium is never reached as suction continues to decrease.

Suction reversals in Figures 3.58b and 3.58c are due to excessive drying of the sample surface, which should be avoided to prevent local irreversible changes of volumetric and hydraulic properties. Ridley et al. (2003) observed similar suction reversals but explained them differently; they attributed them to excess moisture on the surface of the porous stone prior to placing the soil sample in contact with the tensiometer.

The slowly descending curve of Figure 3.58d indicates that water was continuously evaporating from the sample, which was initially explained by a faulty sealing of the cell. However it was later found that there was no clear leak in the sealing and water was instead evaporating from the sample and condensing on the inner walls of the cell. This also suggests that, in order to reach equilibrium, the gap around the sample should be as small as possible.

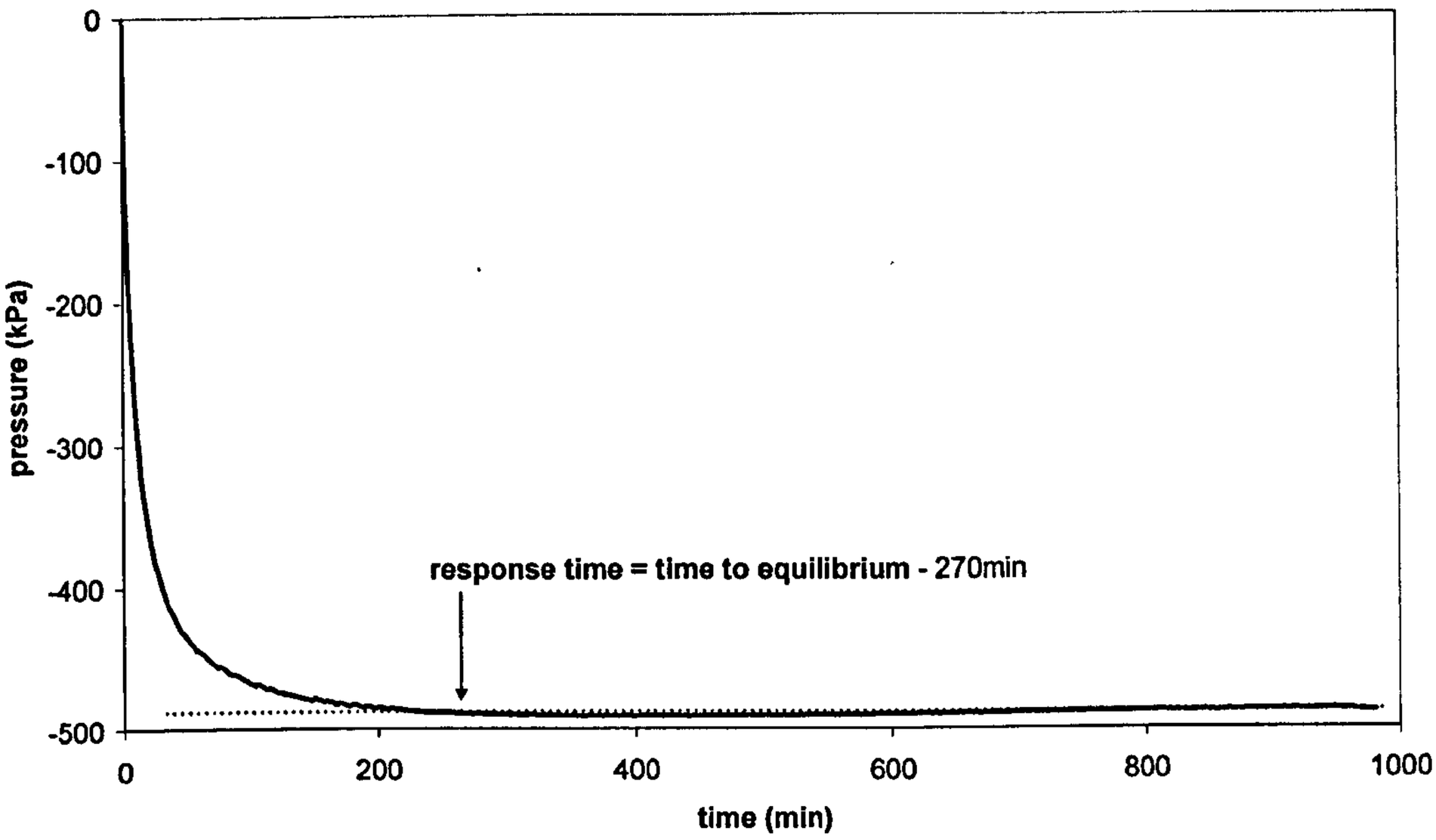
0
-100
-200
-300
-400
-500
pressure (kPa)
response time = time to equilibrium - 270min
0
200
400
600
800
1000
time (min)

(a)

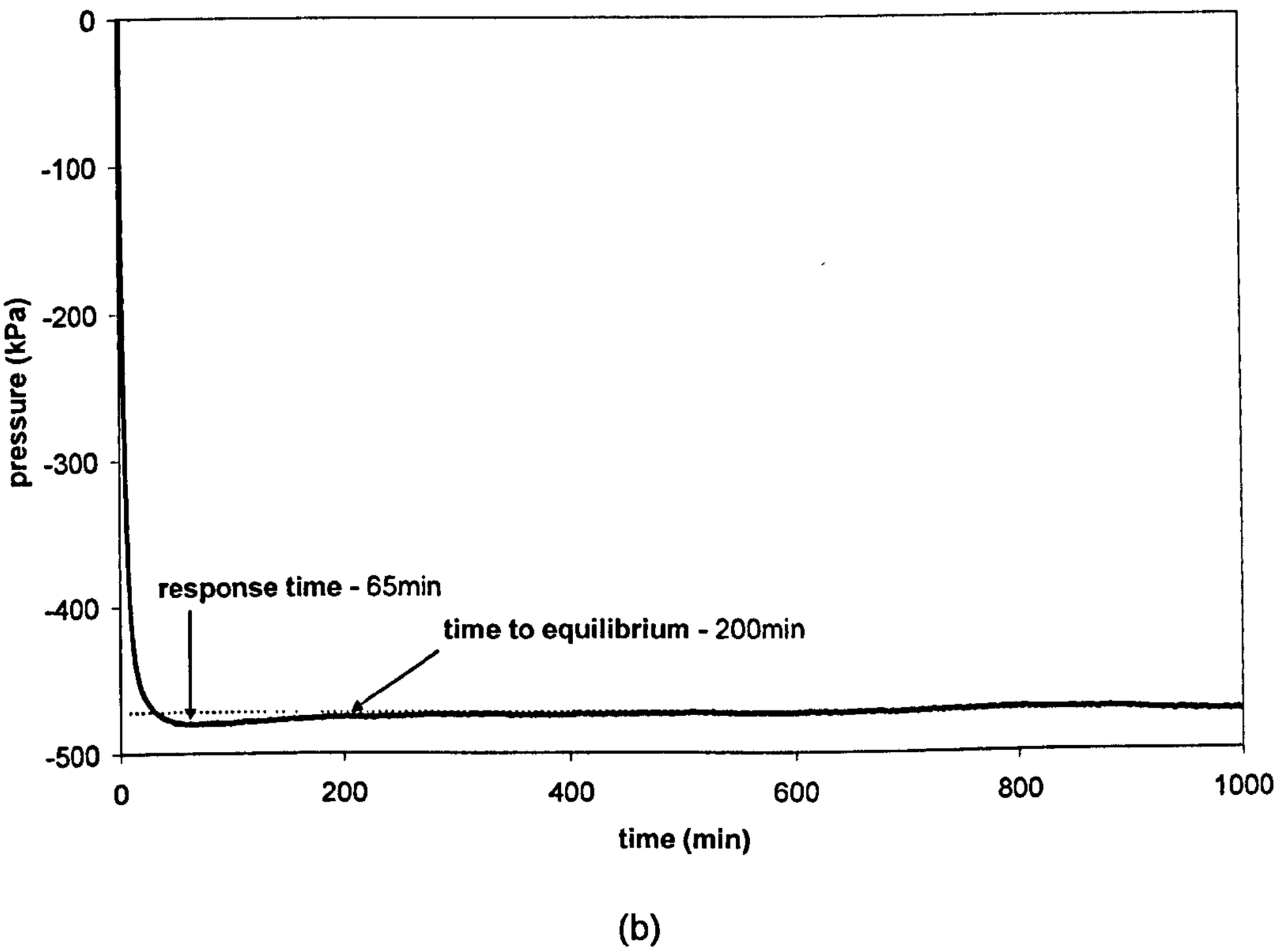
0
-100
-200
-300
-400
-500
pressure (kPa)
response time - 65min
time to equilibrium - 200min
0
200
400
600
800
1000
time (min)

(b)

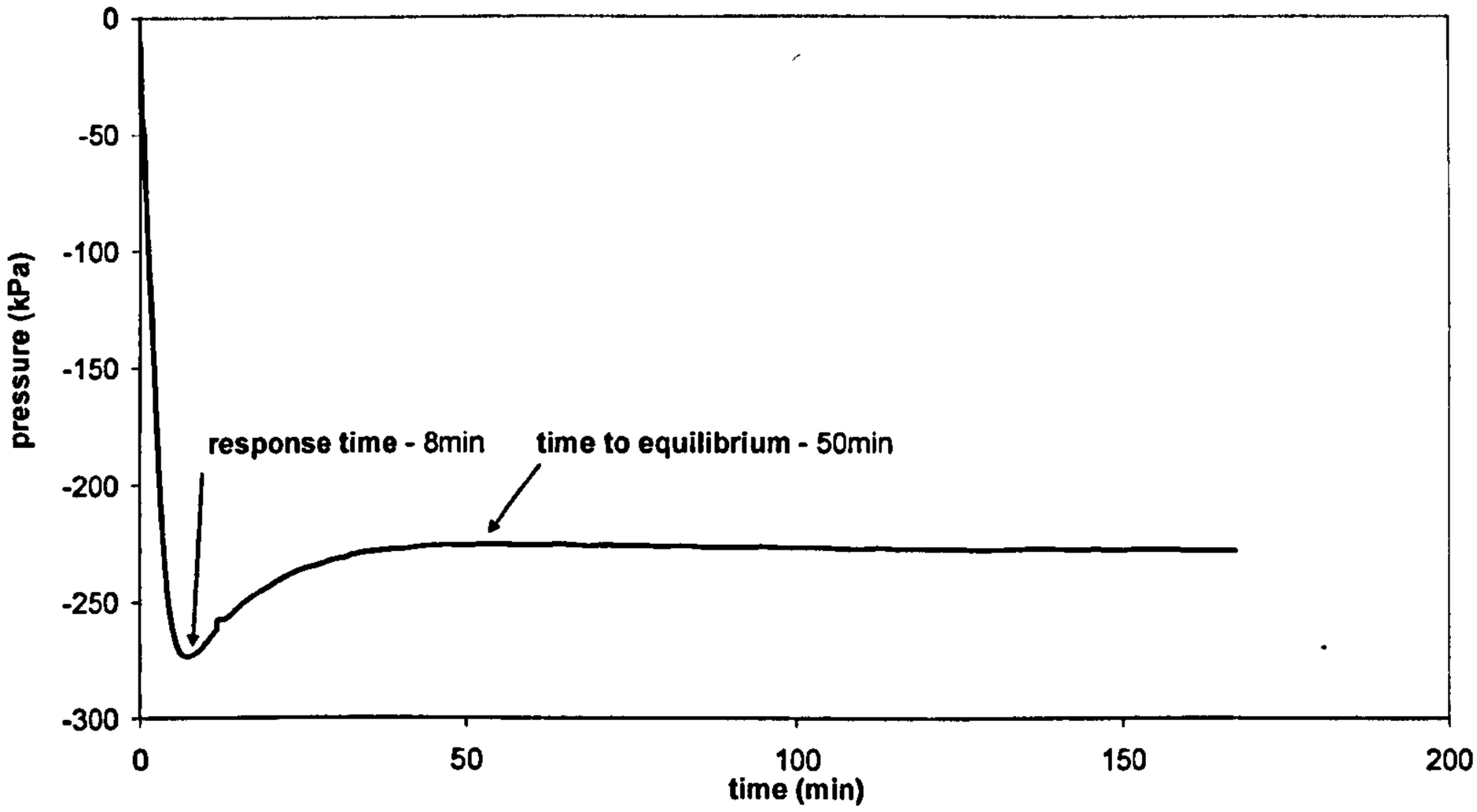

(c)

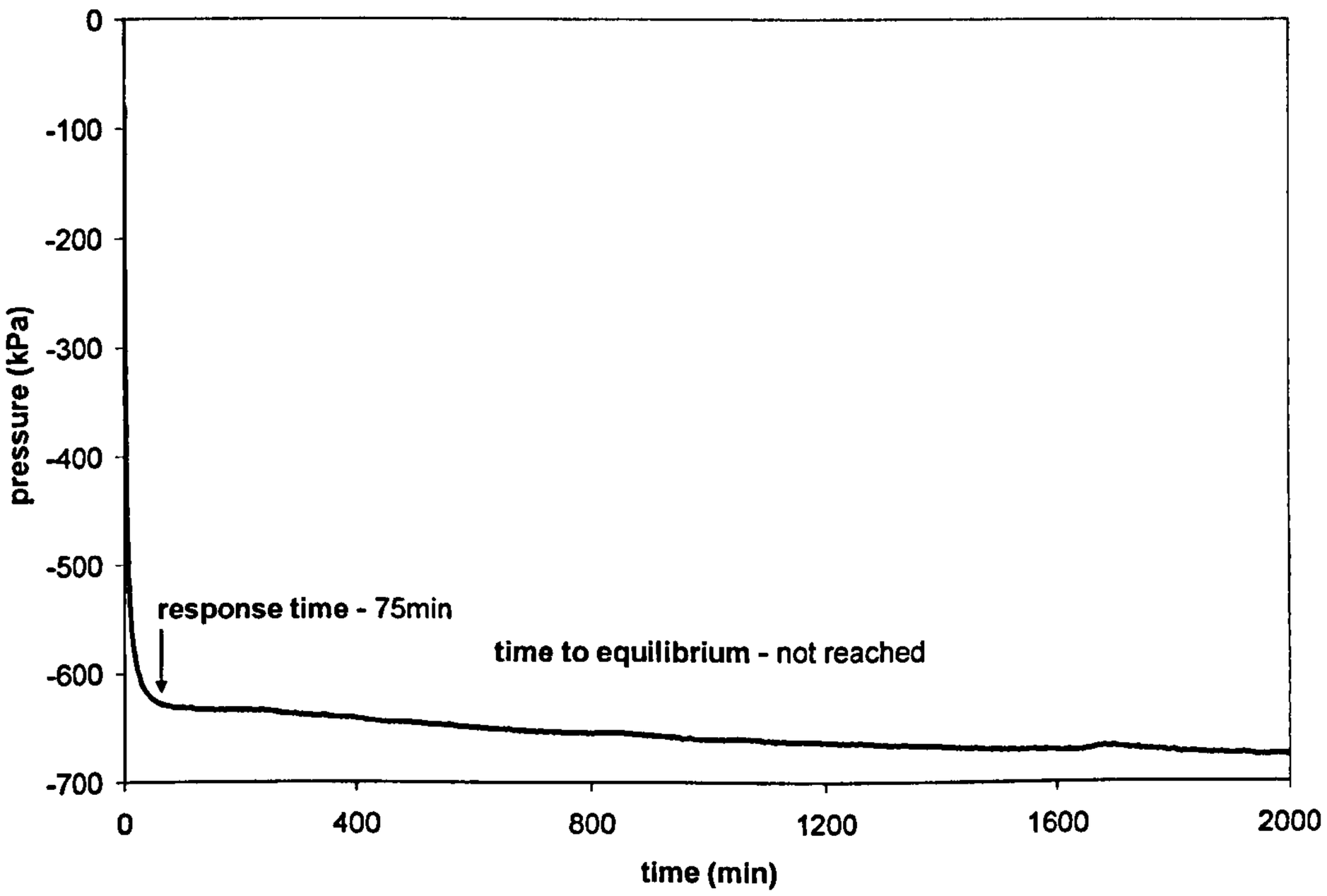

(d)

Figure 3.58: Response and equilibrium times for four different suction measurements: (a) sample having achieved suction equalization prior to measurement (test Tc27, tensiometer II1, BIONICS), (b) (test Df1, tensiometer III4, BIONICS) and (c) samples with incomplete suction equalization prior to measurement (testDi2, tensiometer II1, BIONICS) and (d) sample surrounded by large air gap during measurement (test Df5, tensiometer III3, BIONICS)

3.5.3. Measurement

3.5.3.1. Contact soil-porous stone

The accuracy of suction measurement depends on the quality of the contact between the porous stone and the soil. If the contact is good and there is continuity of water between the soil and the porous stone, the pore water pressure in the soil is measured. The quality of such contact depends on four main soil characteristics: (1) grain size distribution, (2) fabric (e.g. presence of large pores), (3) stiffness and (4) brittleness. For instance, a good contact is usually achieved when measuring suction in any soft soil (as the soil can be easily moulded to the porous stone). The opposite case is given by a natural collapsible soil (e.g. loess) where a good contact is more difficult to achieve due to the roughness of the surface and the brittleness of the material, which tends to crumble if a slight pressure is applied by the tensiometer.

All tests for this dissertation were conducted either on a sandy clay or on kaolin and the tensiometers were always placed in direct contact with the sample, i.e. no clay paste was applied on the porous stone prior to the measurement. At high water contents the contact was good because the samples were very soft. As the water content decreased the samples became stiffer and, in this case, a thin film of water was placed on the porous stone to help continuity of the water between the soil and the tensiometer. The disadvantage of placing a clay paste or a thin water film on the porous stone is that, in the case of small samples, this might induce errors in the measurement of water content. Contrary to what is claimed by other researchers (e.g. Oliveira and Marinho, 2008), the use of a clay paste is not essential to obtain a good contact. If the material is soft and fine, a good contact is easily attained.

In this work the contact between the porous stone and the sample was ensured by pressing the tensiometer against the soil and forcing it to penetrate by 2-3mm. Good contact was assumed when the force applied to the tensiometer produced an increase of pore pressures in the positive range. At lower water contents, in addition to exerting a small pressure against the soil and having the stone covered with water, light rotating movements were applied to soothe the interface. If an excessive pressure is applied, however, the volume of the sample could change inducing errors in the determination of the degree of saturation.

As shown in the previous section, measurements are sensitive to external pressures acting on the tensiometer body and, therefore, tensiometers should be calibrated while the probe's body is subjected to similar external forces as those existing during use. For tests where the tensiometer is submerged in water (e.g. during triaxial tests where the tensiometer is placed on the lateral surface of the sample), good sealing is required to prevent infiltration through the electrical connections at the back of the tensiometer. Jotisankasa (2005) reported water infiltrations through the back of his tensiometers. In this work, for the undrained unloading tests conducted in Section 3.4, a heat shrink sleeve was used to cover from the stainless casing to the electrical cable. In addition, the tensiometer was placed in contact with the sample through a grommet, sealed by o-rings and painted with several layers of liquid latex rubber. The procedure is similar to that described by Hight (1982) for sealing a piezometer probe on a sample's side for triaxial tests in saturated soils, and has been used frequently since (e.g. Wong et al., 2001, Jotisankasa, 2005).

3.5.3.2. Measurement of total and osmotic suction

Figure 3.59a shows a suction measurement where an imperfect contact between the tensiometer's porous stone and the soil was achieved. The sample was initially saturated and the maximum suction to be measured should have been around 10kPa, but instead suction increased to more than 300kPa and fluctuated within 100kPa. This was an unusual response when compared to any of the measurements previously shown in Figure 3.58. The observed variation of suction with time was compared to the temperature continuously measured in the lab and it was found that the temperature peaks matched well with the suction peaks (Figure 3.59b). It can also be seen that a variation of 0.1°C seems to correspond to a change of suction of about 100kPa. Could this mean that the tensiometer was measuring total suction instead of matric suction?

In order to answer this question, the total suction change was calculated for a temperature change from 21.65°C to 21.73°C (this is the same as the maximum fluctuation shown in Figure 3.59b) for an initial relative humidity of 99.8%, which corresponds to a total suction of 200kPa according to Kelvin's law. By definition, the relative humidity is the ratio of the vapour pressure to the saturation vapour pressure at a given temperature. As the saturation vapour pressure at 21.65°C is 2589.33Pa, a relative humidity of 99.8% implies that the water vapour pressure at such temperature is 2584.154Pa. As the temperature increases to 21.73°C, the saturation

vapour pressure increases to 2602.03Pa and, assuming that the water vapour pressure remains the same, the relative humidity decreases to 99.3% which corresponds to a total suction of 1000kPa according to Kelvin's law.

From this very simple calculation, it can be concluded that the total suction change for a temperature change from 21.65°C to 21.73°C and an initial relative humidity of 99.8% is 800kPa, which is well above the fluctuation of about 100kPa shown in Figure 3.59b). This can possibly be explained by the fact that the porous stone was only partly exposed to the atmosphere and a limited contact with the soil sample was still retained.

In order to explore further whether the tensiometer was capable of reading total suction as well as matric suction, an additional experiment was carried out where the tensiometer was enclosed in an air tight cell containing de-ionized water with the porous stone exposed to the atmosphere inside the cell. The tensiometer was first saturated and, after applying a thin film of water to the porous stone, it was suspended upside down inside the cell at 2cm from the water surface.

Figure 3.60 shows that after nearly 24h the tensiometer cavitated. It was also visible that the film of water covering the stone was gradually evaporating, while water was condensing in the container's walls, which would suggest the system tensiometer-water-container was not in isothermal conditions. This experiment was therefore not conclusive and could not confirm whether the tensiometer is able to measure total suction.

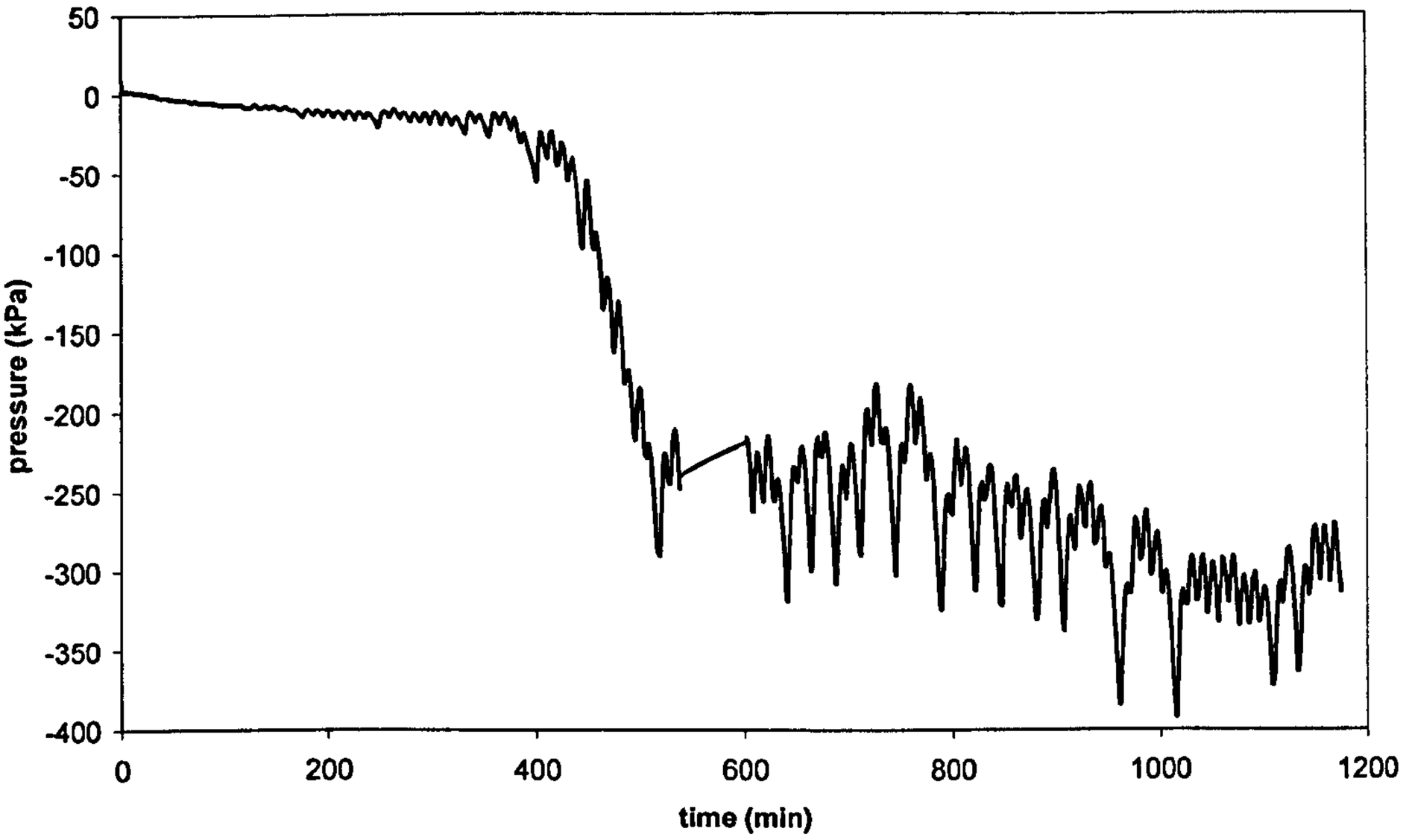

(a)

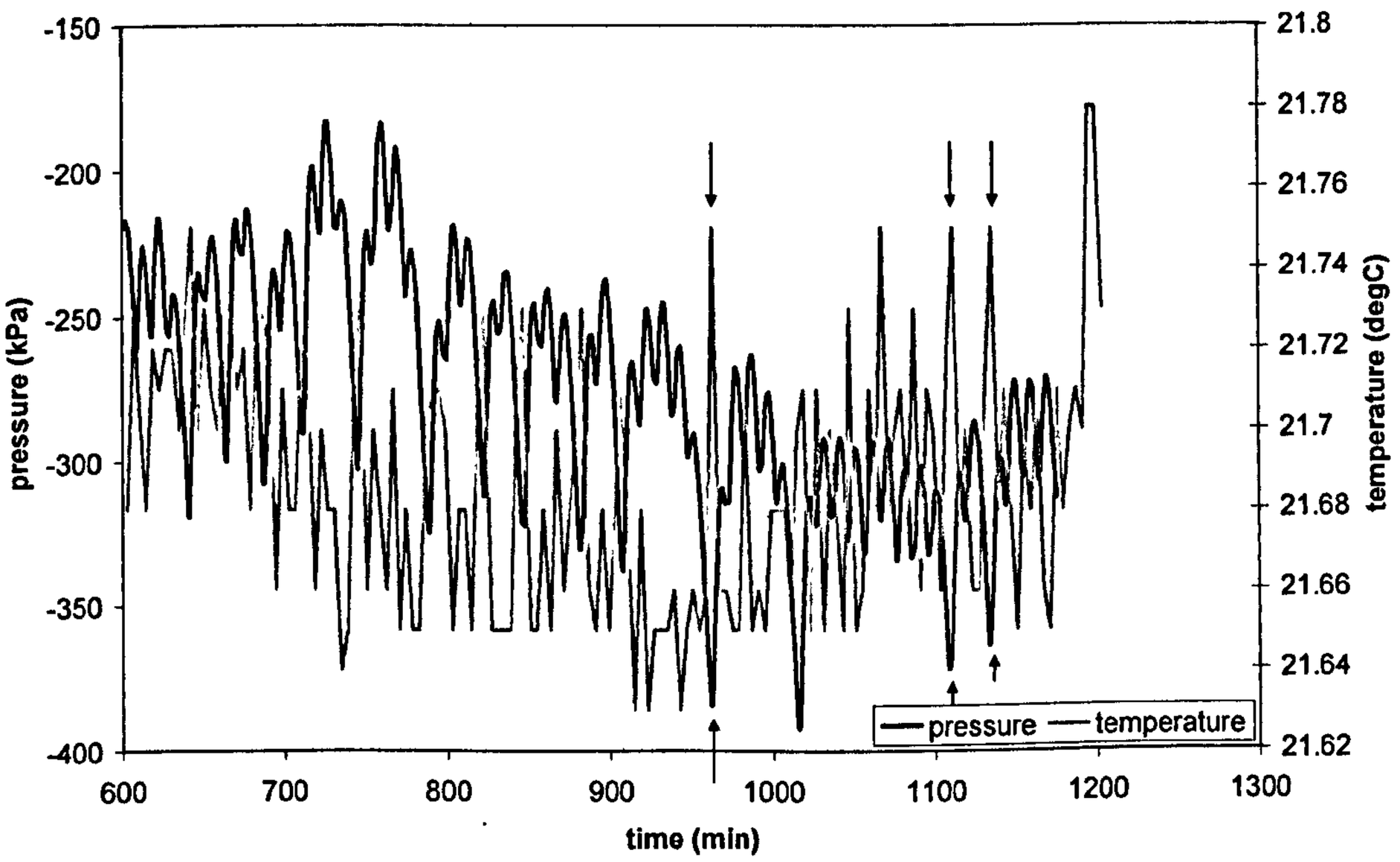

(b)

Figure 3.59: Example of suction measurement with poor contact between the soil and the porous stone: (a) variation of pressure with time and (b) correlation between variations of pressure and temperature (arrows point to corresponding peaks of temperature and pressure) (test Tm1, tensiometer III3, BIONICS)

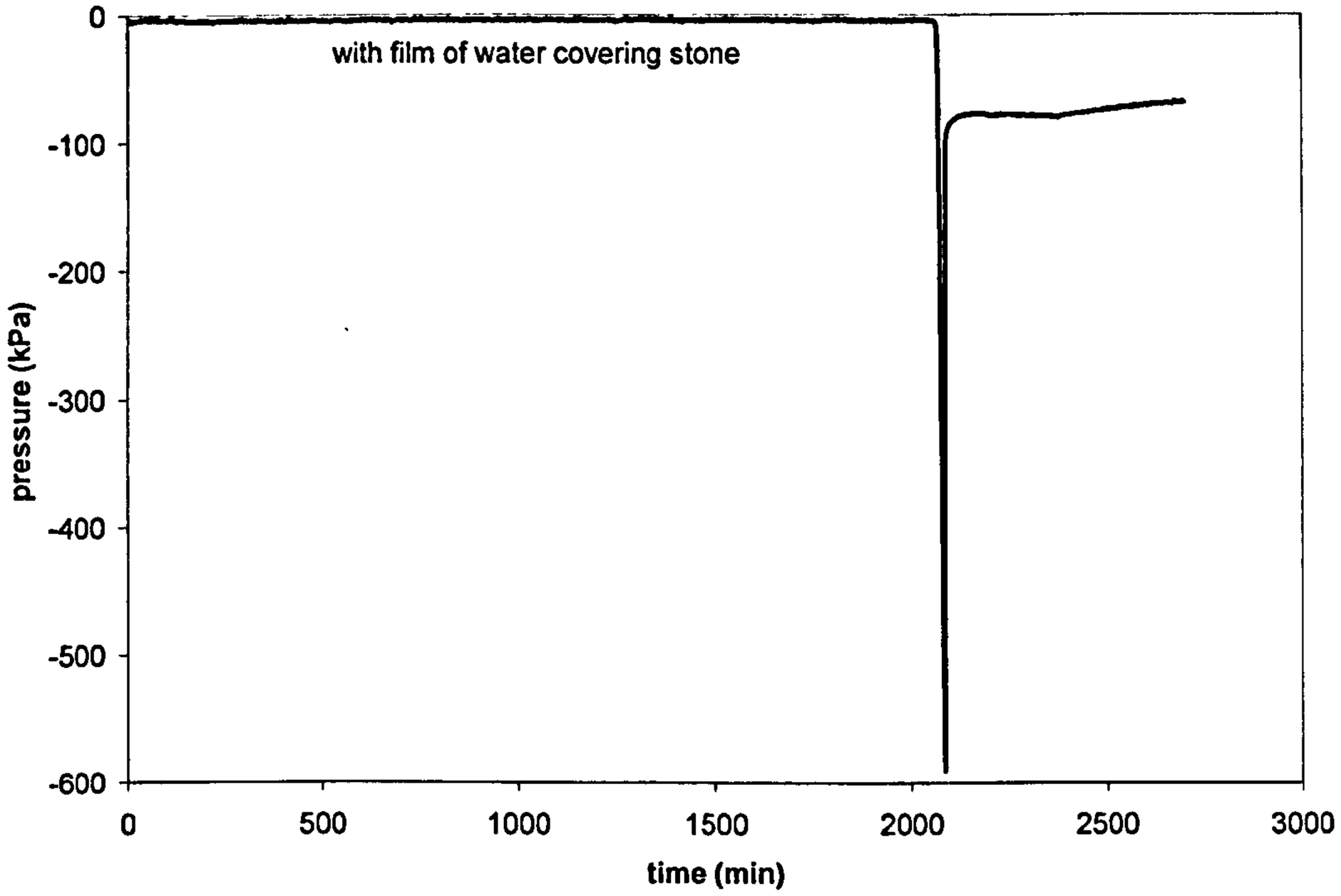

Figure 3.60: Measurement by a tensiometer exposed to a vapour saturated atmosphere (test Tm3, tensiometer III5)

Additional experiments were carried out by Vercraeije (2007) to investigate whether the same tensiometers used in this research were able to measure the osmotic component of suction. The procedure consisted in compacting samples at water contents of 15% with NaCl concentrations of 0.5M, 0.7M, 1.0M or 1.5M and imposing a suction value of 300kPa to the samples by using the pressure plate. The tensiometer was then used to measure suction on the same samples and the readings by the tensiometer were compared to the suction imposed by the pressure plate.

Figure 3.61 shows the tensiometer measurements from Vercraeije (2007), who states that, out of the twelve measurements, there were only three cases where the tensiometer recorded a suction near 300kPa while, in four cases, the suction was less than half this value.

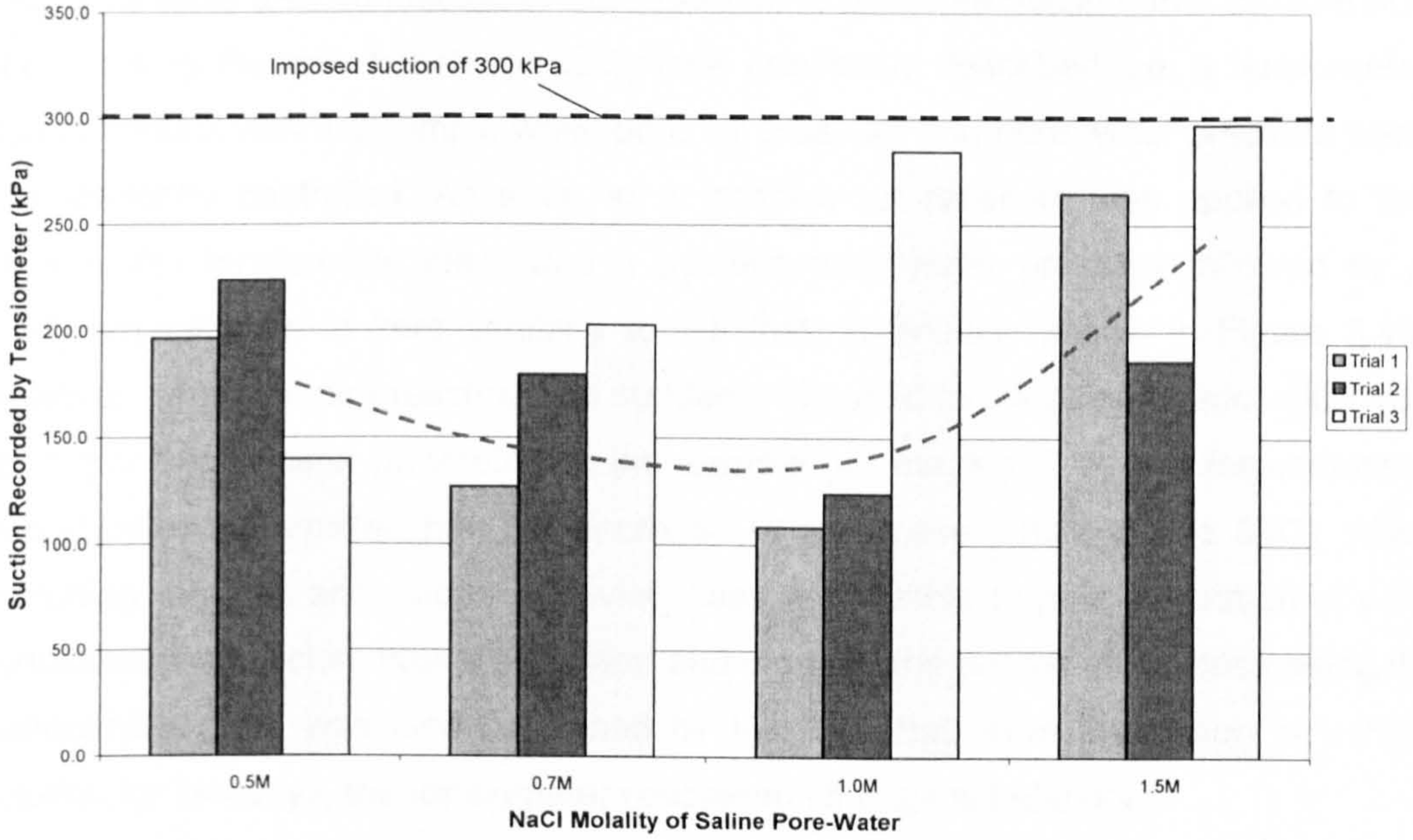

Figure 3.61: Tensiometer measurements on samples compacted with water solutions of different NaCl molalities and subjected to an initial suction of 300kPa by the pressure plate (trial 1, 2, 3 refers to test no. 1, 2 3) (from Vercraeije, 2007)

Vercraeije (2007) also performed a second series of experiments with distilled water and, in this case, he noticed that suction values read by the tensiometers were generally higher than those imposed by the pressure plate. This indicates that the presence of saline pore water could have an effect on the suction measured by the tensiometer but, if the tensiometer were capable of measuring an osmotic component of suction, the suction measurements during the first series of experiments should have been higher than those during the second series of experiments. On the basis of such results, Vercraeije (2007) deduced that tensiometers are not able to measure osmotic suction. However, there is one important shortcoming in the experimental procedure employed by Vercraeije (2007) that should be considered before drawing any conclusion. During measurements by the tensiometers, a semi-permeable membrane should have been placed between the porous stone and the soil containing saline pore water so that only pure water would pass through from the sample to the tensiometer making sure that the osmotic component of suction could be measured. In the absence of results using such procedure, it would be inappropriate to make a conclusive statement whether the tensiometers used in this research are indeed capable of measuring osmotic suction.

Few tests were also conducted in this research to measure suction on a calcium rich soil by using the axis translation technique previously described, i.e. a tensiometer was in contact with the sample while pore air pressure and pore water pressure were independently controlled. As soon as a positive air pressure was applied to the sample, the tensiometer measured a positive pore water pressure followed by a gentle equalization to zero similarly to the tests previously shown in Figure 3.48. However, when the air pressure was suddenly released to the atmospheric value, the corresponding suction generated in the sample (as measured by the tensiometer), was significantly smaller than the decrease of air pressure (see Figure 3.62). After excluding that this anomalous behaviour was attributable to poor saturation, it was concluded that calcium had precipitated and clogged the porous stone decreasing its permeability. This was also confirmed by the fact that, after immersion in a HCl solution for few days, the tensiometer recovered its original behaviour.

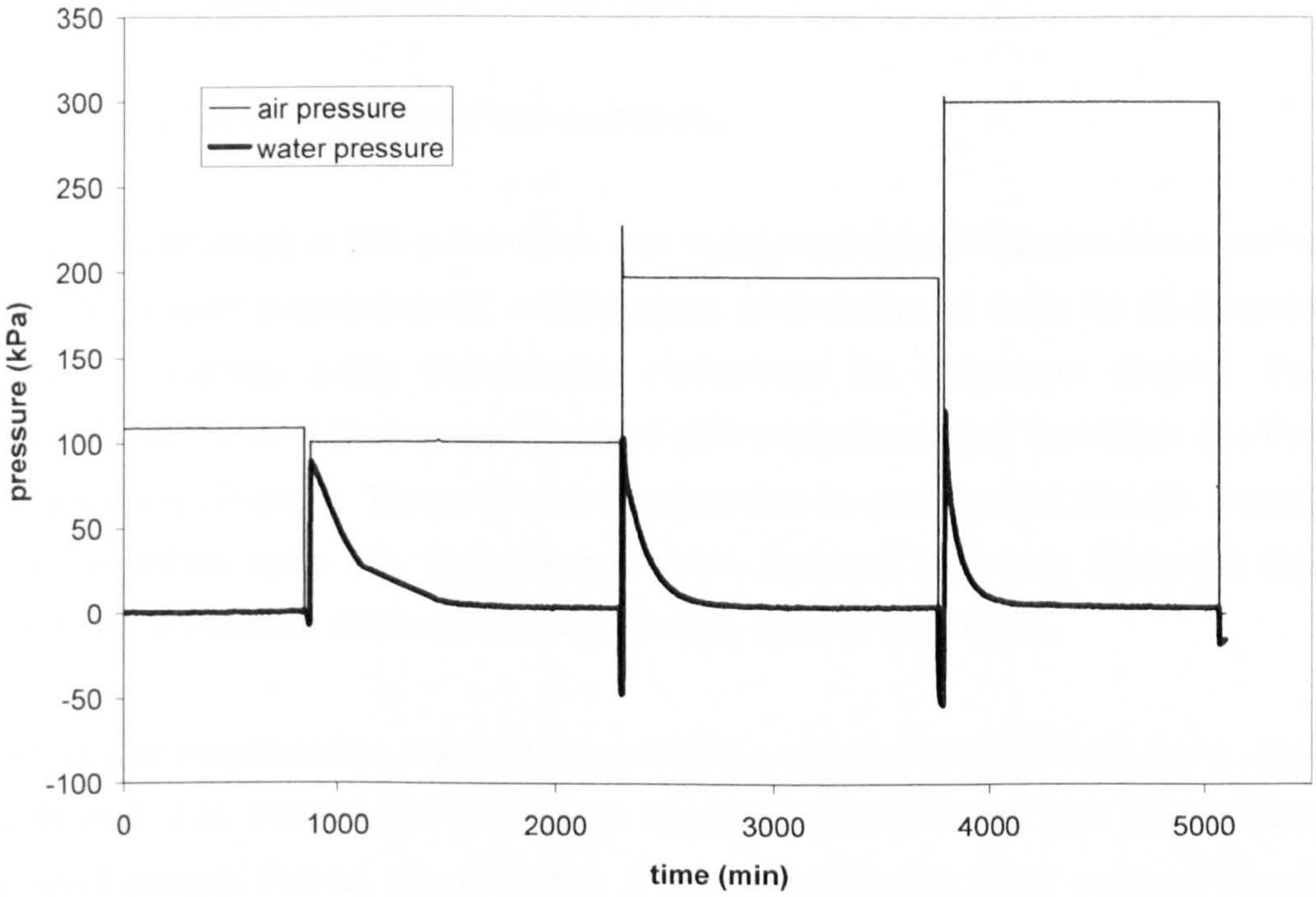

(a)

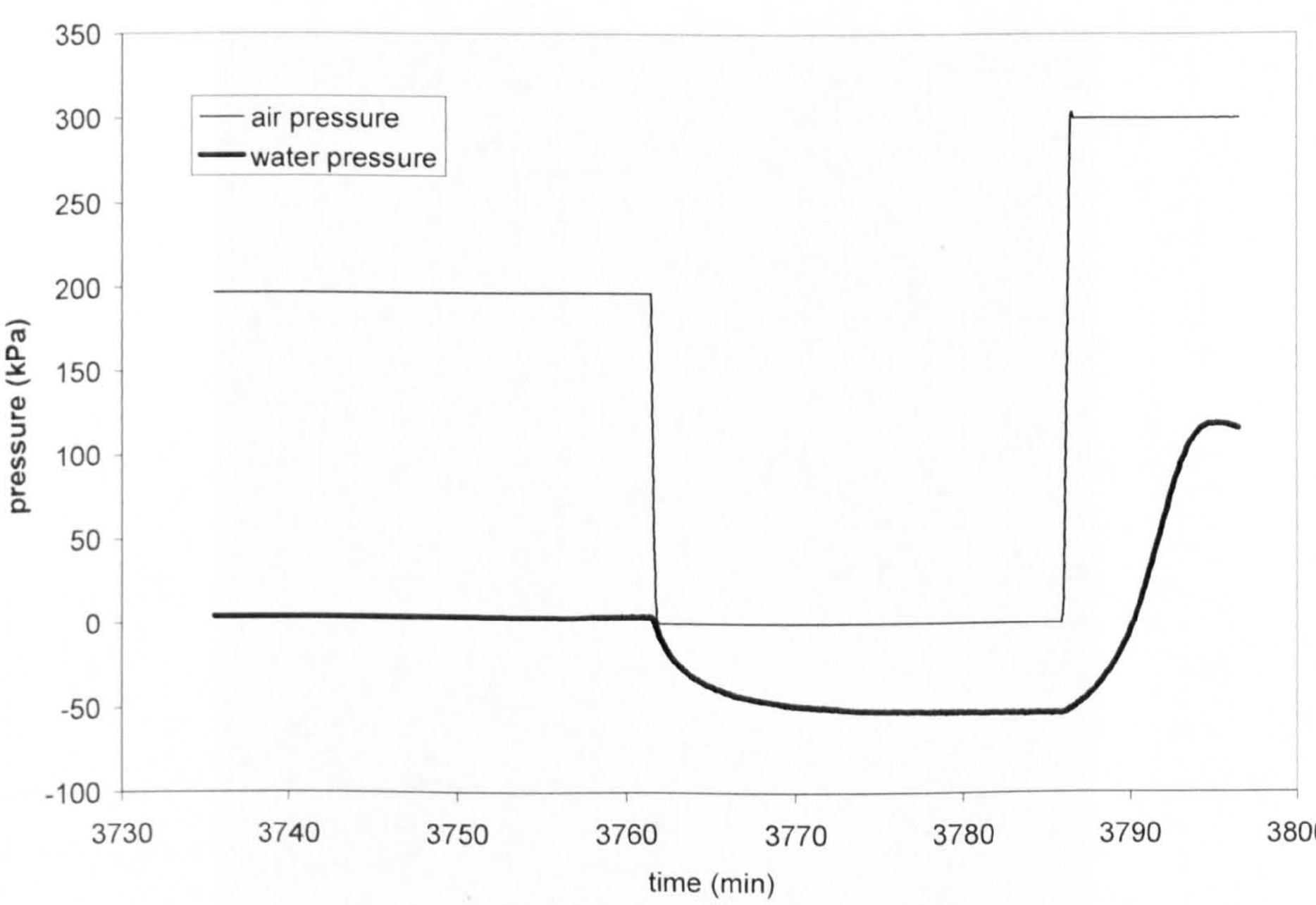

(b)

Figure 3.62: Tensiometer measurements on a calcium rich soil, (a) entire test, (b) detail of single suction measurement (test Tm4, tensiometer II3, lime)

3.5.4. Measurement in a centrifuge

3.5.4.1. Scope of the research

The work described in this subsection was conducted jointly between three partners of an EU funded project (MUSE – Mechanics of Unsaturated Soils for Engineering): Durham University (UK), Universidad Politecnica de Catalunya (Spain), Ecole National des Ponts et Chaussees (France) with the Laboratoires Centrales des Ponts et Chaussees (France). The goal of the project was to model physically the response of a foundation on a silt. Tensiometers from Durham University (DU) and Ecole National des Ponts et Chaussees (ENPC) were used in the project.

Testing was conducted in the centrifuge facility in Nantes (Figure 3.63) by F. Casini, J.J. Munoz, J.M. Pereira and the author, together with the LCPC staff (Celine Boura, Claude Favraud, Patrick Gaudicheau). It was conducted in three periods: June'06, August'06 and November'06.

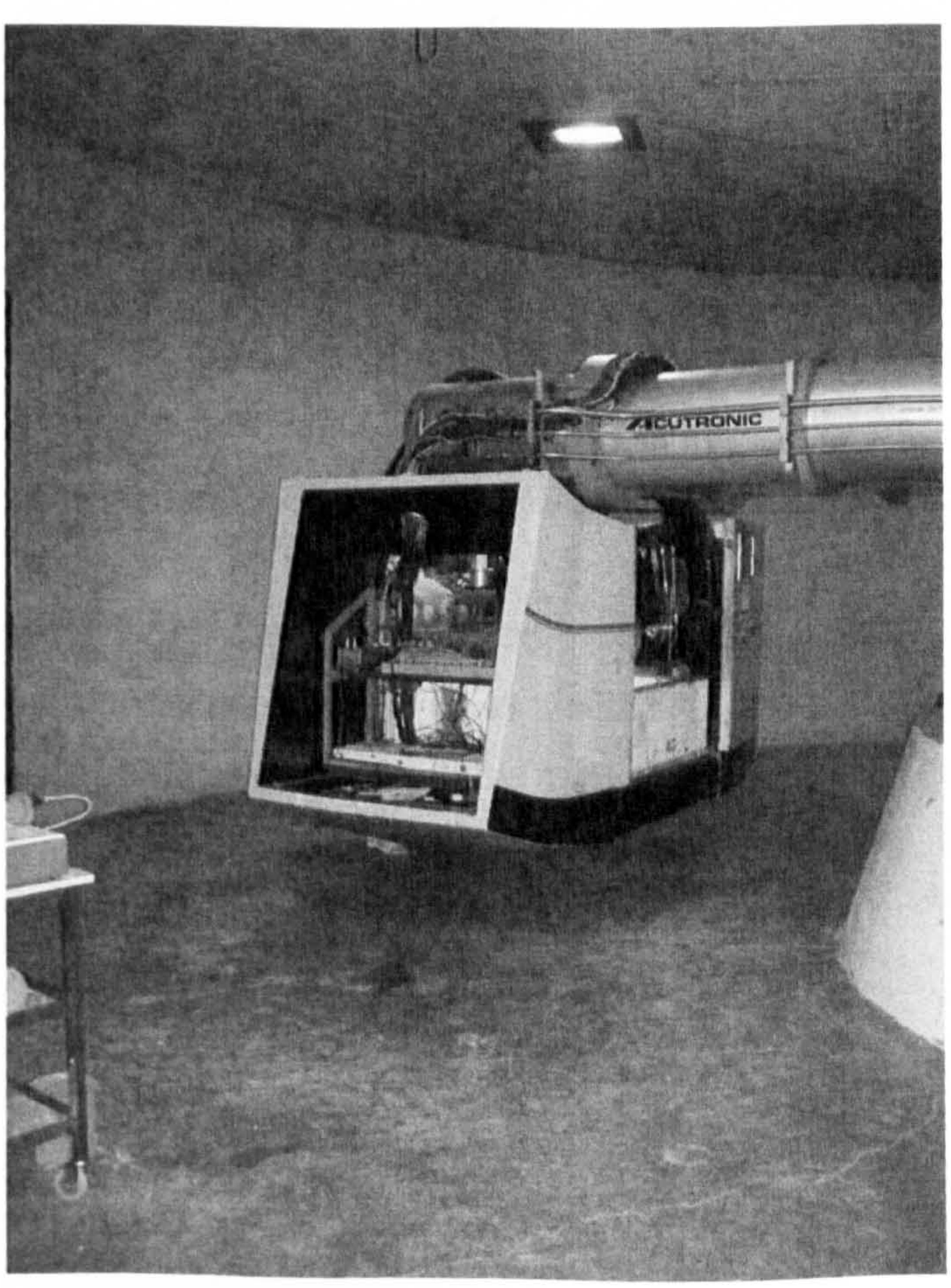

Figure 3.63: The centrifuge of LCPC (photo J.J. Munoz)

It is not the intention to present all obtained results here. An internal report has been written by Casini et al. (2007). This subsection will only present selected results. It will follow the research line of this dissertation focusing on the tensiometer performance (at 50g) and unsaturated soil behaviour (suction, water retention, volume variations).

3.5.4.2. Testing program

The model simulates a circular foundation with a diameter of 1.5m (30mm in the model) in a soil with a depth of 15m (300mm depth in the model). The testing program consisted in 3 tests (Figure 3.64):

1. Loading in saturated conditions (water level at the top of the sample)
2. Loading in unsaturated conditions with wetting (loading followed by wetting)
3. Loading in unsaturated conditions (water level at the bottom of the sample)

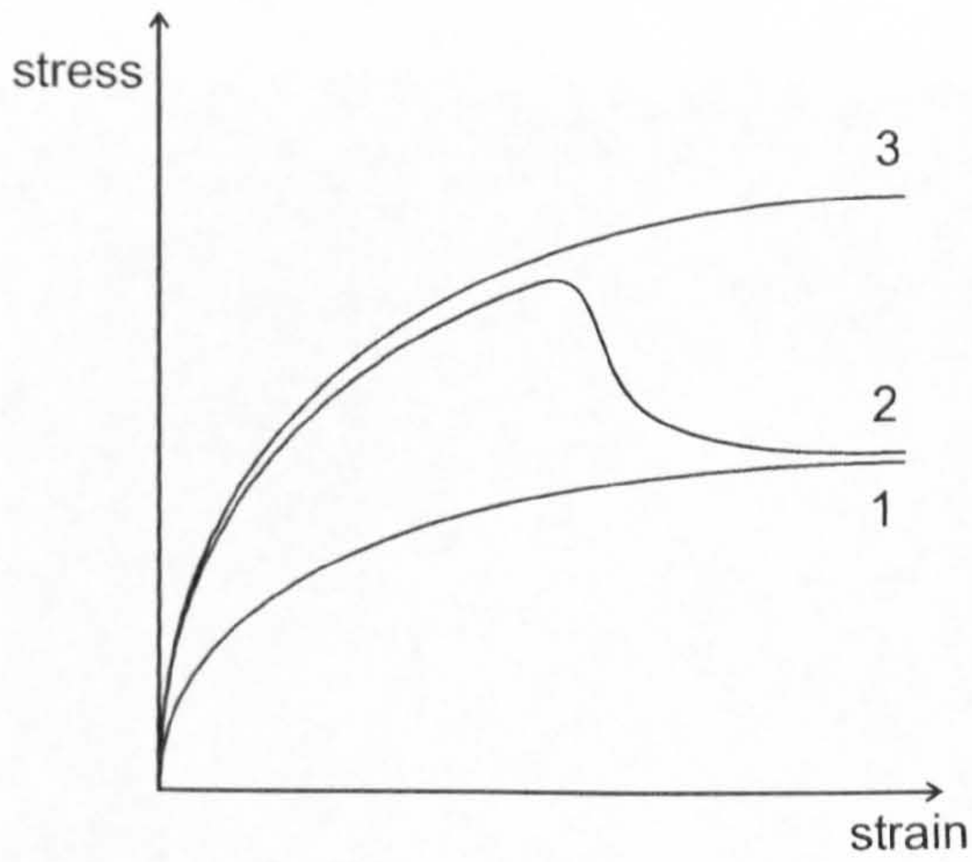

Figure 3.64: Planned loading tests in the centrifuge (after Vaunat, 2006)

The material used was Jossigny silt, prepared at w=13%, statically compacted to obtain γ_d=14.5kN/m^3. The initial suction was estimated at 200kPa according to the SWRC obtained by Mercury Intrusion Porosimetry. The silty soil rested on a sand layer of 3cm separated by a geotextile. The dimensions and location of the tensiometers are shown in Figure 3.65a.

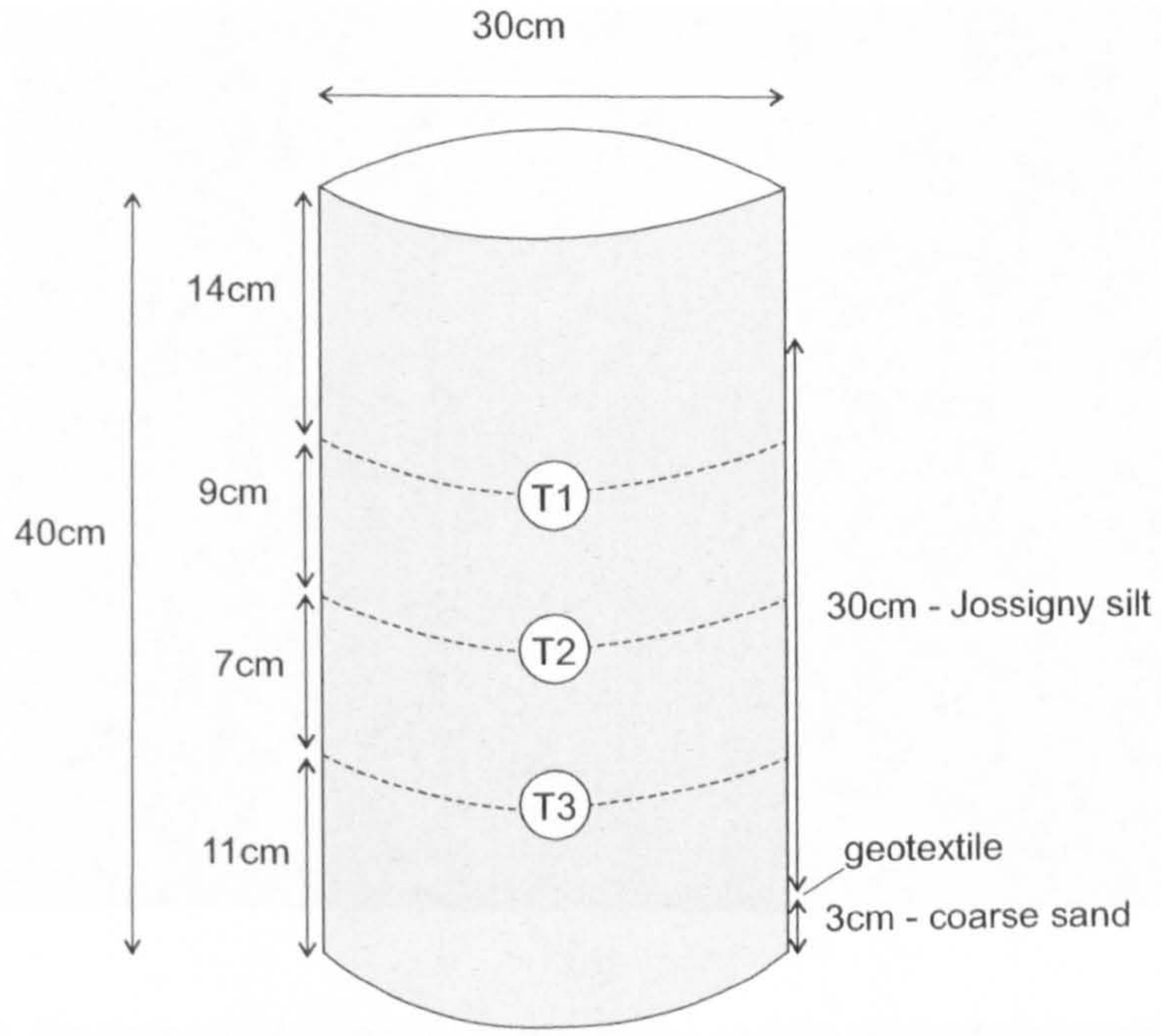
30cm
14cm
9cm
40cm
T1
30cm - Jossigny silt
7cm
T2
T3
11cm
geotextile
3cm - coarse sand

(a)

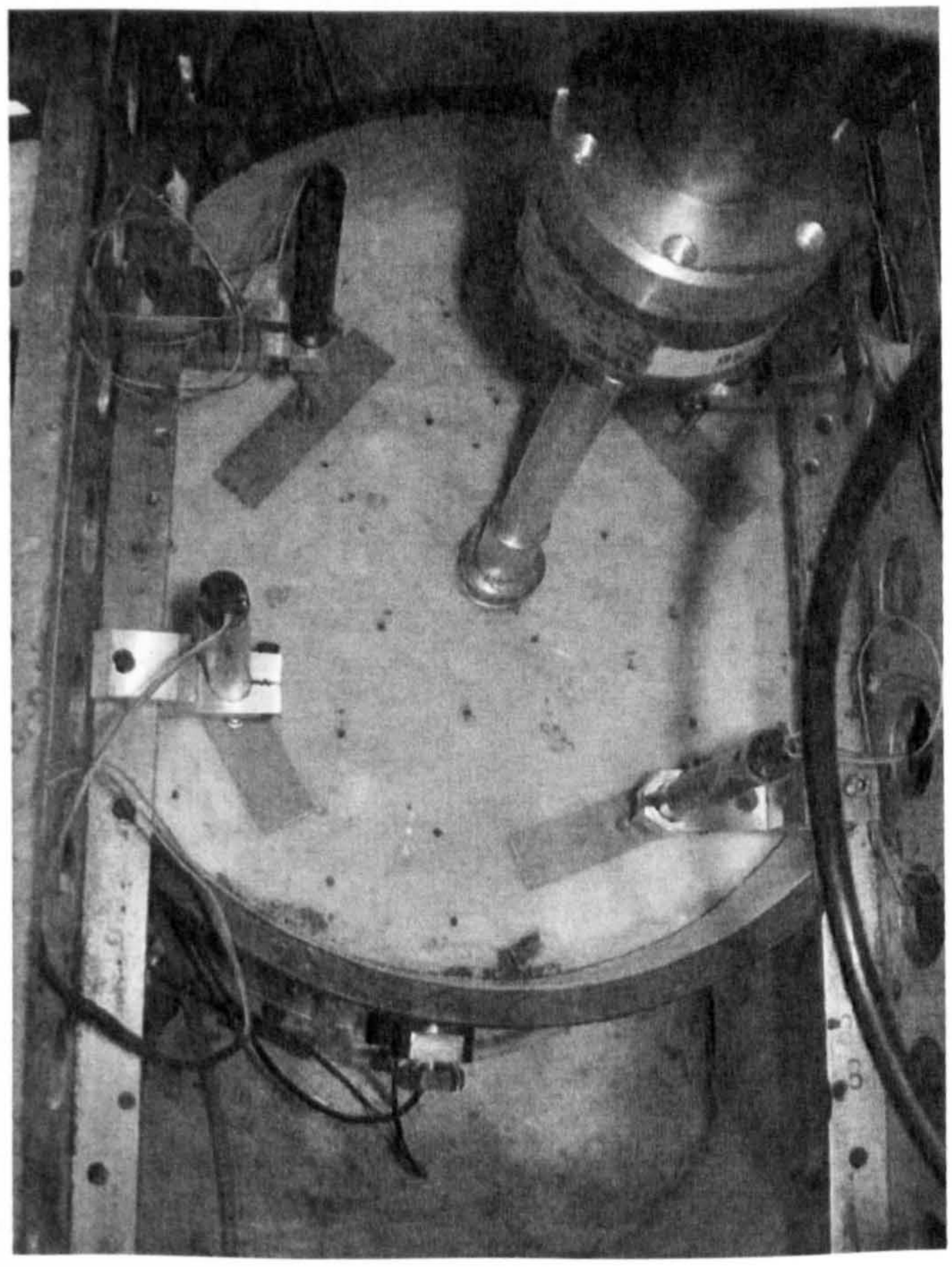

(b)

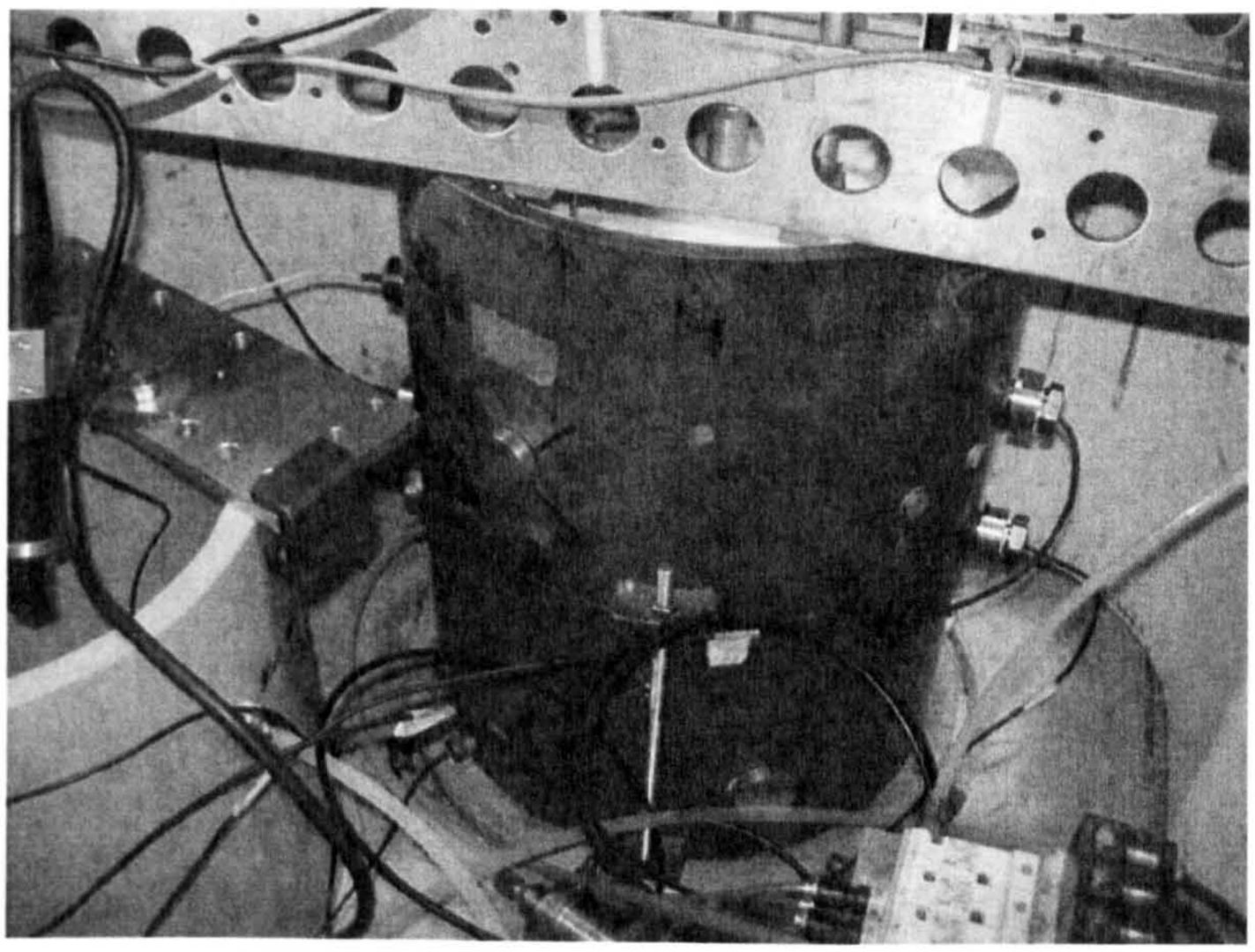

(c)

Figure 3.65: Equipment, (a) mould dimensions and tensiometers location, (b) view from above with the four displacement transducers and the piston (white colour is due to paraffin wax to avoid evaporation) (photo J.J. Munoz), (c) side view of the mould with the DU tensiometers on the right hand side (photo J.J. Munoz)

The tests were conducted in a centrifuge with a maximum acceleration of 200g, radius of 5.5m and package of 2 tonnes. The equipment used included: high suction tensiometers from DU (2 initially and then 3) and ENPC (3), LVDTs (4) to measure displacement of the soil surface and for the pile, one load cell and one displacement transducer. Pore water pressure transducers were also included, one to measure water level in the sand layer and the other to measure the water level in the mould during the saturation stage. The two groups of tensiometers were placed on the sides of the mould at different heights facing each other. They were calibrated first in the centrifuge equipment. Figure 3.65b and 3.65c shows photos of the mould with all the equipment.

After the sample preparation, the mould was set in the centrifuge's basket. The test started by increasing the gravitational force 50 times. While in flight the water level was regulated to be in contact with the bottom of the silt in order to provide the suction gradient corresponding to the real 15m height (for the unsaturated condition). An equilibration time was allowed until suction stabilized. Then depending on the test, the water level was raised in the mould for saturation and the piston moved

down to load the soil, or the soil was simply loaded in an unsaturated condition (with the water level at the bottom of the silt).

3.5.4.3. Results

Tensiometer performance at 50g

The response of the tensiometers was unsteady with some noise (observed in a static and spinning condition). This was different to all other measurements made in the laboratory in Durham.

The response time was fast with the tensiometers recording any external events (increase in *g*, water level changes) immediately and simultaneously. For instance, water level fluctuations produced clear and fast changes of suction when setting the water level in contact with the silt or during saturation. No significant changes of suction occurred during loading for any of the tests (Figure 3.66b).

When the acceleration was increased from 1 to 50g, suction increased to a maximum and then stabilized at a lower value (Figure 3.66b). One possible explanation could be that once *g* starts increasing the soil is pushed against the tensiometer's porous stone leading to a decrease in suction (the same effect as pushing manually the tensiometer against the soil).

Unsaturated silt behaviour at 50g

Two selected tests (Tcen1, Tcen3) are shown in Figure 3.66a and 3.66b. For test Tcen3, the three tensiometers were placed on the side of the mould and left to equalize. The top and middle tensiometer read similar values (approximately 120kPa) while the bottom one read a smaller value (approximately 100kPa). The mould was then put in flight at slowly increasing acceleration. A new suction profile developed in the soil, with the bottom tensiometer reading a similar value as at 1g, but the middle and top increasing. The increase in the water level (in three steps) produced well marked settlements of the soil that could be associated with changes in readings of the tensiometers. When the flight stage was stopped, the bottom tensiometer decreased to near zero values indicating the presence of bulk water in the pores.

The response of the silt was in general clearer for test Tcen3 (only two tensiometers used). The tensiometers were placed in the mould and suction left to equalize (all the peaks before the flight stage were due to further adjustments of the tensiometers against the soil). Immediately after increasing the acceleration to 50g, the water level was adjusted to the bottom of the silt to create the unsaturated condition. During this time both suctions equalized well (better than Tcen3). The water level was then increased until the surface of the soil to create a saturated condition. The tensiometers responded immediately with a decrease in suction and increase of positive pore water pressures. The displacement transducers recorded a sharp downward movement of the soil surface (interpreted as a collapse phenomenon). The surface was then loaded in displacement controlled conditions by 5mm. The maximum vertical stress measured was 6.5kPa, a very small value showing that the soil was in a very soft condition. The tensiometers and displacement transducers did not detect the loading, eventually because they were at some distance from the loaded area.

Figure 3.67 shows the suction profiles at equilibrium measured by the tensiometer with the water level at the bottom of the silt (depth of 0.3m). Equilibrium here means just before saturation (in Figure 3.66b) or when stopping the centrifuge (in Figure 3.66a). The calculated hydrostatic profile is shown by black symbols and the measured suction profiles (7) by open symbols in Figure 3.67. All profiles except two showed the same tendency, measuring higher suctions at the top, intermediate suctions in the middle and lower suctions at the bottom. This provides proof that a profile close to the hydrostatic suction profile at 50g had developed in the silt. However, most profiles are displaced to the higher suctions side, suggesting that the water at the base of the mould was not in contact with the silt. The higher the initial suction, the more to the right hand side of the graph the suction profile would be.

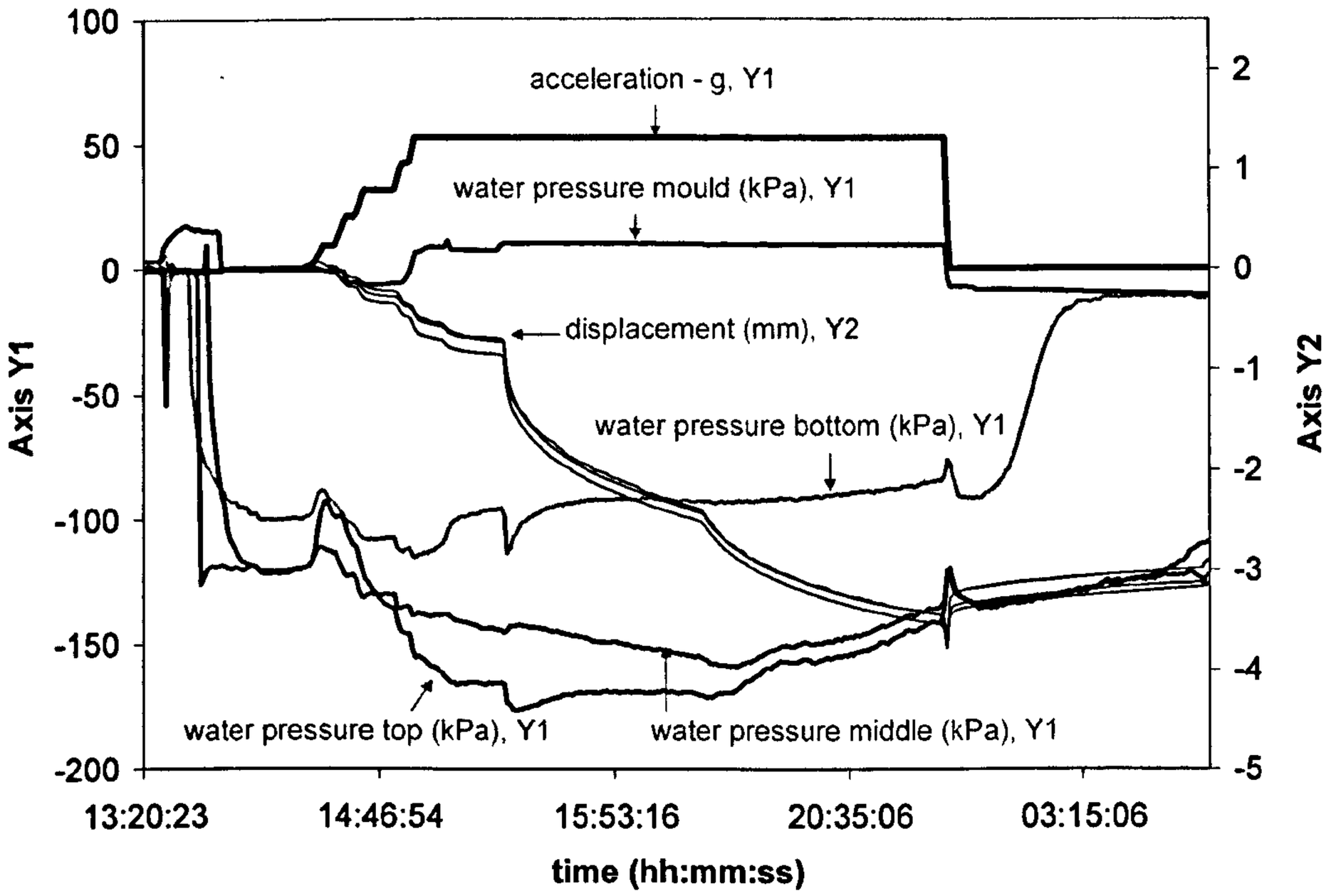

(a)

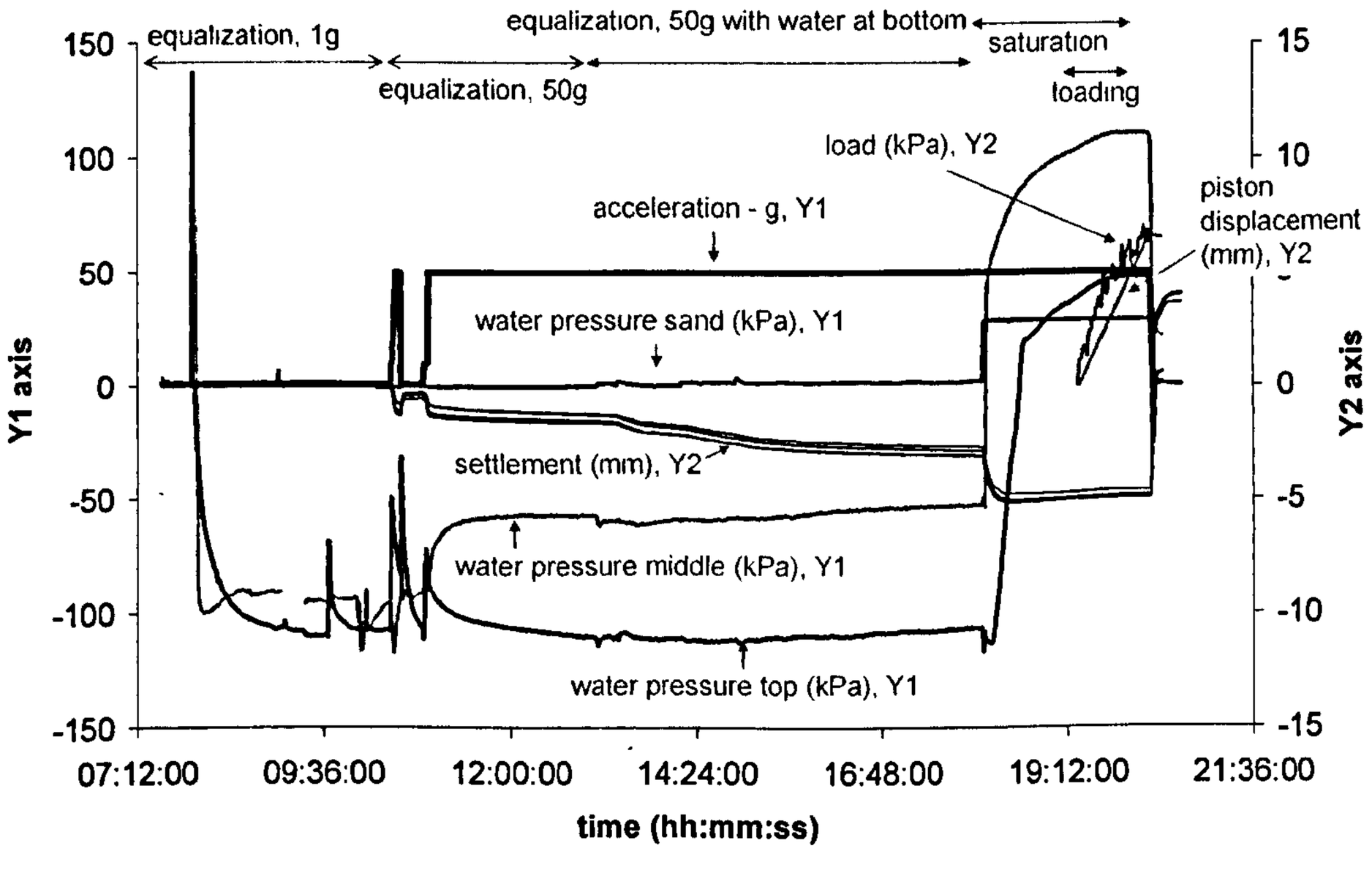

(b)

Figure 3.66: Centrifuge tests in a silty soil at 50g, (a) unsaturated condition (test Tcen3, tensiometers III3, III4, III6, Jossigny silt), (b) started in an unsaturated condition followed by saturation and loading (test Tcen1, tensiometers II1, II2, Jossigny silt)

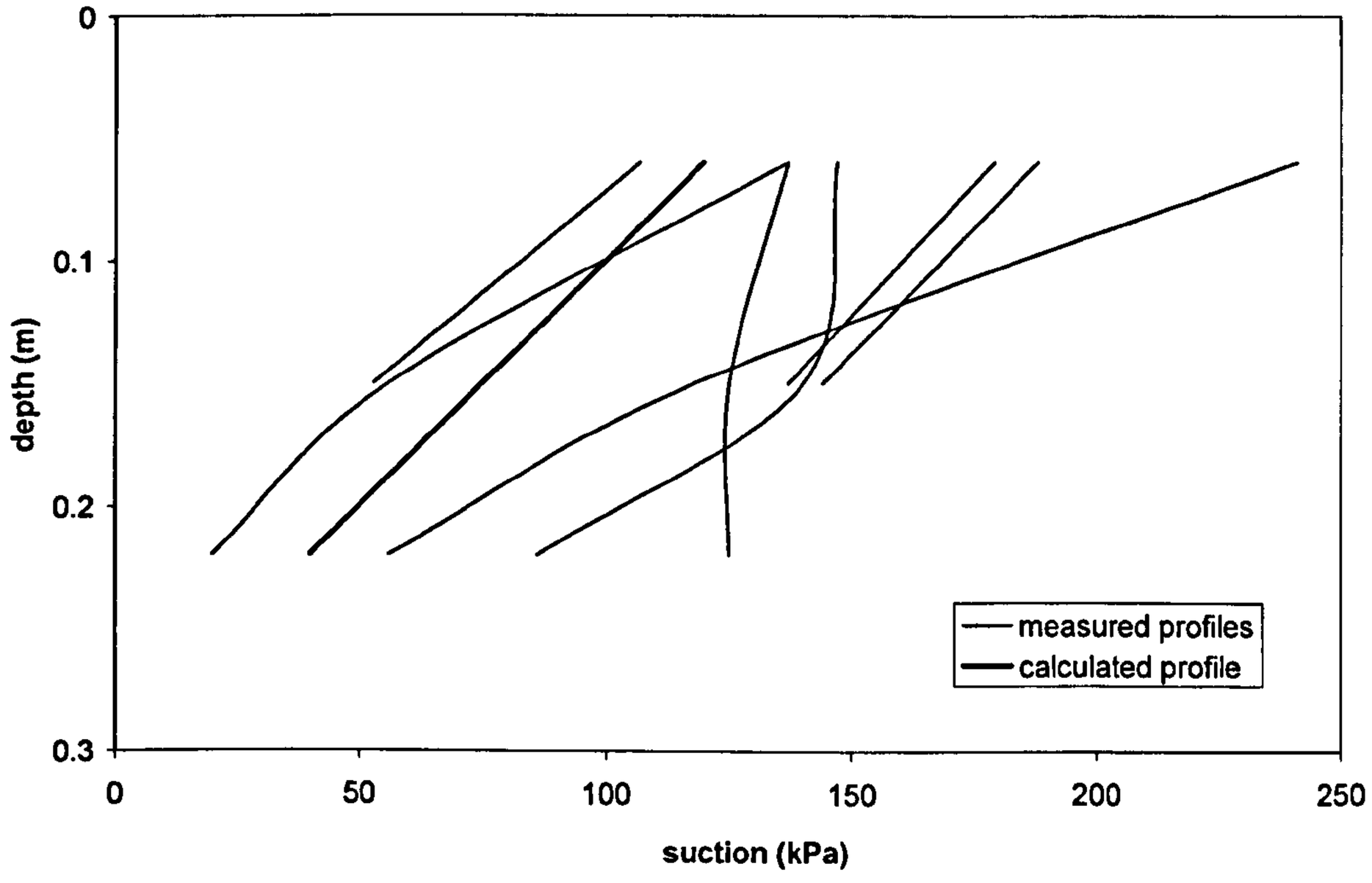

Figure 3.67: Suction profiles at equilibrium at 50g, with the water level at the bottom of the silt – 0.3m (open symbols correspond to measured values and black signs to the calculated hydrostatic profile)

One of the main issues of the centrifuge tests was the time required for suction equilibrium. This was identified in the early tests by Chiu et al. (2005) but seems not to have been considered by Take (2003). From this research, not much time was required for suction to stabilize (from Figure 3.66b it took 4h), Chiu et al. (2005) states 7h, but from Take data there was no waiting time (Figure 2.44a), pore water pressure tends to stabilize quickly during the wetting periods but not during the dry periods.

3.6. CHAPTER SUMMARY

A new tensiometer was presented. Its design, parts and design evolution.

3.6.1. Saturation

The main findings from this part of the research are:

- The concentration of oxygen in the water used for the saturation of the tensiometers was measured by using a dissolved oxygen meter, instead of relying on the absence of bubbles during de-aeration.

- The positive pressure applied during saturation of the tensiometer does not need to be very high. Pressures in the order of 1500kPa are sufficient to achieve good saturation and the advantages of using more complex procedures, e.g. flooding under vacuum and cycles of pressure, were not immediately obvious.

- Early results suggest that decrease of temperature could increase the measurement range of suctions.

- If a dry tensiometer was plunged in water, it would record increasing positive pressures. This was found to be due to the porous nature of stone that sucked water by capillarity trapping air behind.

- Continuous use of tensiometers increased the suction measurement range.

Published studies on cavitation have proven essential to understand behaviour of tensiometers. The work by Atchley and Prosperetti (1989) predict suction values at cavitation similar to those obtained in tensiometers (under conditions that could resemble those in tensiometers). Bremond et al. (2005) provided an insight into the progressive formation of bubbles under a sequence of cavitations.

In the discussion it was proposed that the key element controlling cavitation is the availability of space for a bubble to grow. Bubbles can grow from anywhere, either

the porous stone or reservoir, but the reservoir is the only place where they can coalesce with other bubbles until forming an air discontinuity throughout the water.

Data from this research, as well as other studies, clearly suggest that there is an effect of time on the response by tensiometers. In this study it was observed that the suction measurement range tends to increase with time of use. A longer saturation period was also required for tensiometers that had been used during prolonged experimental programmes, suggesting that the porosity of the stone had decreased with time leading to an increase of the air entry value of suction.

The suction measurement range tends to increase following consecutive cavitations. This can be explained again by the crevice model of Atchley and Prosperetti (1989) and the work of Bremond et al. (2005). The largest bubbles are first released from crevices with relatively small values of suction at cavitation. However, as consecutive cavitations occur, bubbles become progressively smaller and higher cavitation suctions are achieved until a steady state is attained after a large number of cavitations.

Experiments by other authors showed that extensive erosion of the porous stone could happen due repeated cavitations. This is however unlikely to occur with the same severity in tensiometers because of the relatively limited number of cavitations to which a tensiometer is subjected during its entire life (whereas the mentioned experiments refer to continuous cavitations).

Finally, a conceptual model was proposed that shows two possible alternative mechanisms for the formation and evolution of bubbles leading to cavitation.

3.6.2. Calibration

Techniques to validate the extrapolation of the calibration of high suction tensiometers from the positive to the negative pressure range have been studied. The tensiometers have been calibrated in the positive range against a standard transducer. The results show that calibration in the positive range is sensitive to the way the tensiometer is fixed inside the saturation manifold, since the biggest source of error is due to the external forces holding the device in place. The immediate implication is that the calibration should be conducted under the same external force regime as will be applied to the body of the tensiometer when it is used.

The calibration extrapolated from the positive pressure range has then been used to read known values of suction imposed on soil samples by using two different techniques, i.e. the axis translation technique and isotropic unloading. Readings from the tensiometer have also been compared against known value of negative pressures (down to -100kPa), which have been directly imposed to the tensiometer by using a vacuum pump. Extrapolation appeared to be satisfactory when the isotropic unloading technique and the method using the vacuum pump were used. For isotropic unloading, allowance has to be made for a *B* value that may not equal unity. If this is allowed for, calibration errors were less than 0.77%. The axis translation technique seems to be the least suited for validating the extrapolation of the calibration equation to the negative pressure range as the suction generated in the sample is strongly dependent on the water conditions underneath the porous stone of the device used to impose such suction.

Long term monitoring of the use of tensiometers shows that changes of the calibration do occur (with time or with use). This is seen as a non-zero value at the end of a test when the tensiometer is submerged in free water. These shifts of the calibration zero tend to occur when the tensiometer is used to measure pressures in the negative range but not in the positive range. This shift of the calibration zero is generally low (about 5kPa) and should only pose a problem if the tensiometer is used to measure low suctions.

Differences between tensiometer types could lead to different results to those observed for the particular tensiometer used in this study, so it is suggested at least one check on the validity of the extrapolated calibration equation should always be done. Isotropic unloading and the direct application of negative pressures down to -100kPa seem to be the best options for checking whether an extrapolation from the positive range is sufficiently accurate for the intended use.

3.6.3. Measurement

The response time of a tensiometer is crucial for tests where suction changes continuously with time. For measurements to be correct, the response time has to be shorter than the rate of suction change. For the particular tensiometer used in this work, the response time ranged between 8min and 160min and did not depend on the suction level. The suction measurements conducted in this research also showed

that the response time does not necessarily coincide with the time for the sample to reach equilibrium. If suction has not fully equalized throughout the sample (e.g. the surface where the measurement is taken is drier), the measured suction tends to reach a peak before dropping back to the equilibrium value.

During suction measurements at constant water content, despite care was taken in sealing the sample inside a cell, suction still tended to continuously increase with time if a large air gap existed around the sample. Because the system sample – tensiometer – cell was not in isothermal conditions, water would evaporate from the sample and condensate on the cooler internal cell surfaces. This sort of response (see Figure 3.58d as an example) was observed several times during the suction measurements performed in this research.

Ensuring a good contact between porous stone and soil is very important to obtain an accurate measurement of suction. If the contact is imperfect, the tensiometer might cavitate or the suction measurement might be affected by the relative humidity of the surrounding air (see Figure 3.59). Many authors have suggested adding a clay paste to the porous stone before taking suction measurements. In this research, a good contact between the porous stone and the soil was ensured just by pressing the tensiometer against the sample. This worked fine if the soil was soft but, for stiffer samples, a thin film of water had also to be placed on the porous stone so that it could easily stick to the soil. Finally few examples of suction measurements taken by tensiometers on a chemically active soil were presented.

The second part presented centrifuge tests conducted in LCPC – Nantes (France) as a joint research project between 3 universities to study the behaviour of a foundation during loading in unsaturated and saturated conditions on a silty soil. The tensiometers performed well, with suction profiles not far from those expected. Suction readings were sensitive to changes in the water level and acceleration.

Chapter 4. SOIL WATER RETENTION CURVE

4.1. INTRODUCTION

In this chapter Soil Water Retention Curves (SWRC) are determined using high suction tensiometers of the type described in Chapter 3. Procedures using continuous drying and discrete drying/wetting are described and compared. Discrete drying/wetting involves halting the drying or wetting process at different stages to ensure equalization within the sample.

Previous studies of the determination of SWRC using tensiometers by other authors presented in Chapter 2 do not provide sufficient details of the procedures followed to allow consistent results to be achieved. Also none of the studies have included wetting paths and volume change measurements. Therefore, the present research was initiated to provide a set of testing procedures for the determination of the SWRC using tensiometers, following either a drying or wetting path, and to validate it against a known technique. Testing with the continuous procedure focused on drying only (due to the difficulty in imposing a RH of 100% to achieve wetting). Parts of the results shown in this chapter are summarized in Lourenço et al. (2007a). Testing was divided into 5 parts:

(a) Continuous drying

(b) Discrete drying

(c) Discrete wetting

(d) Volume measurements were included for both procedures to determine the void ratio and degree of saturation

(e) Validation against the pressure plate for the drying path

This Chapter aims to address two questions:

1. Which procedure (discrete or continuous) provides the true (or more correct) SWRC?

2. How do we know that the obtained SWRC is correct?

4.2. FACTORS AFFECTING THE SWRC DETERMINED WITH TENSIOMETERS

A series of factors are likely to influence the shape of the SWRC determined with high suction tensiometers (Figure 4.1). The first is the procedure itself (continuous or discrete). Within the procedures, the discrete procedure is expected to yield the most accurate results as suction is measured while the sample achieves equalization, while continuous drying is likely to introduce inaccuracies due to the lack of equalization through the sample. The lack of equalization is influenced by:

(1) Drying/wetting rate (controlled by Relative Humidity, RH)
(2) Surface area exposed to drying/wetting

Further factors that may affect the SWRC determination are:
(3) Suction measurement location
(4) Experimental setup (e.g. cable effects)

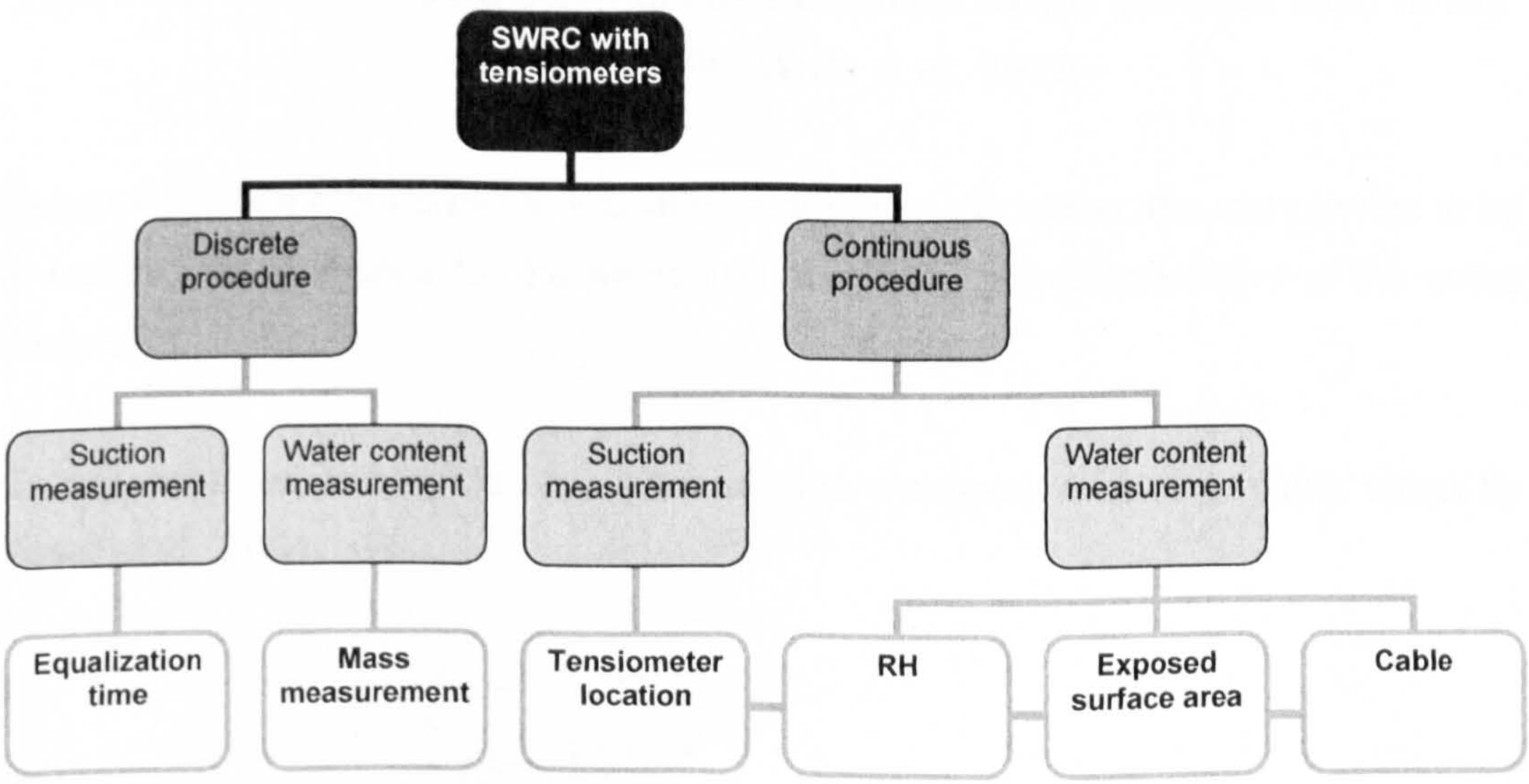

Figure 4.1: Factors affecting the determination of the SWRC with tensiometers

The drying/wetting rate and the exposed surface area to wetting/drying are related to the equilibrium conditions in the sample (constant water content/suction). For instance, there will be no equilibrium if the drying/wetting rate is too fast or if the surface area is too small. White et al. (1972) showed that the ratio of exposed surface to volume of laboratory samples produces a change in the relationship between the degree of saturation and suction (Figure 4.2). The surface areas in the figure (0%, 33%, 67%, and 100%) represent the ratio between the exposed surface area to the sample volume.

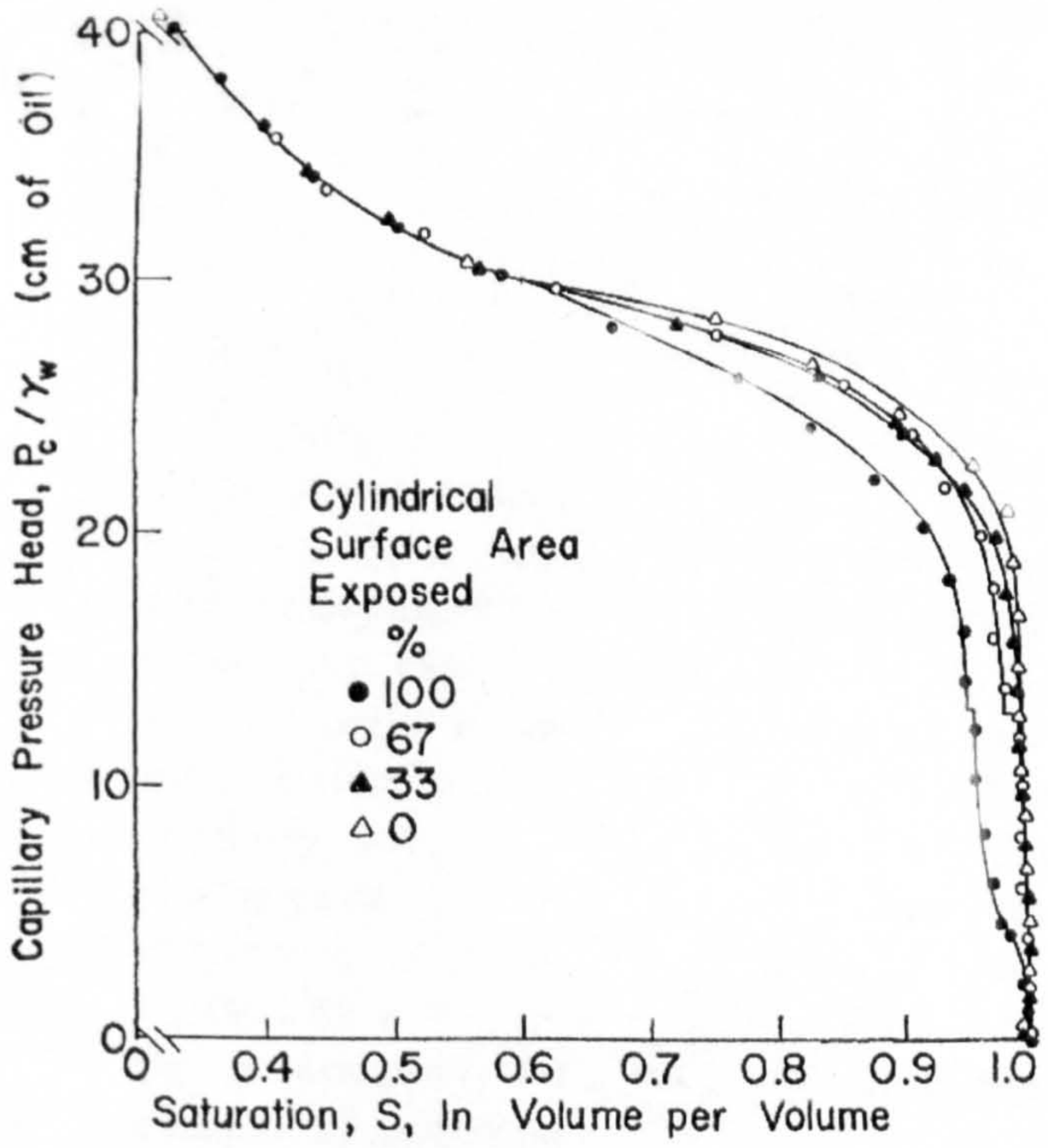

Figure 4.2: Effect of the exposed surface area on the SWRC (pressure head versus saturation) (after White et al., 1972)

Because tensiometers provide a local measurement of suction, the sample has to be in equilibrium conditions for the measured suction to be representative of the entire sample.

Experimental aspects could also influence the measurements (e.g. cable effect by Toker et al., 2004).

4.3. MATERIAL AND EQUIPMENT

4.3.1. Material characterization

A sandy clay of intermediate plasticity with PL = 19.7%, LL = 43.3% and grain size distribution shown in Figure 4.3 (Mendes, 2008a) has been used in this study. The soil was taken from the BIONICS embankment (Glendinning et al., 2006). All samples were compacted according to the standard Proctor test (BS light compaction, BS 1377-4, 1990) at an initial water content of 25% (optimum water content is 18%).

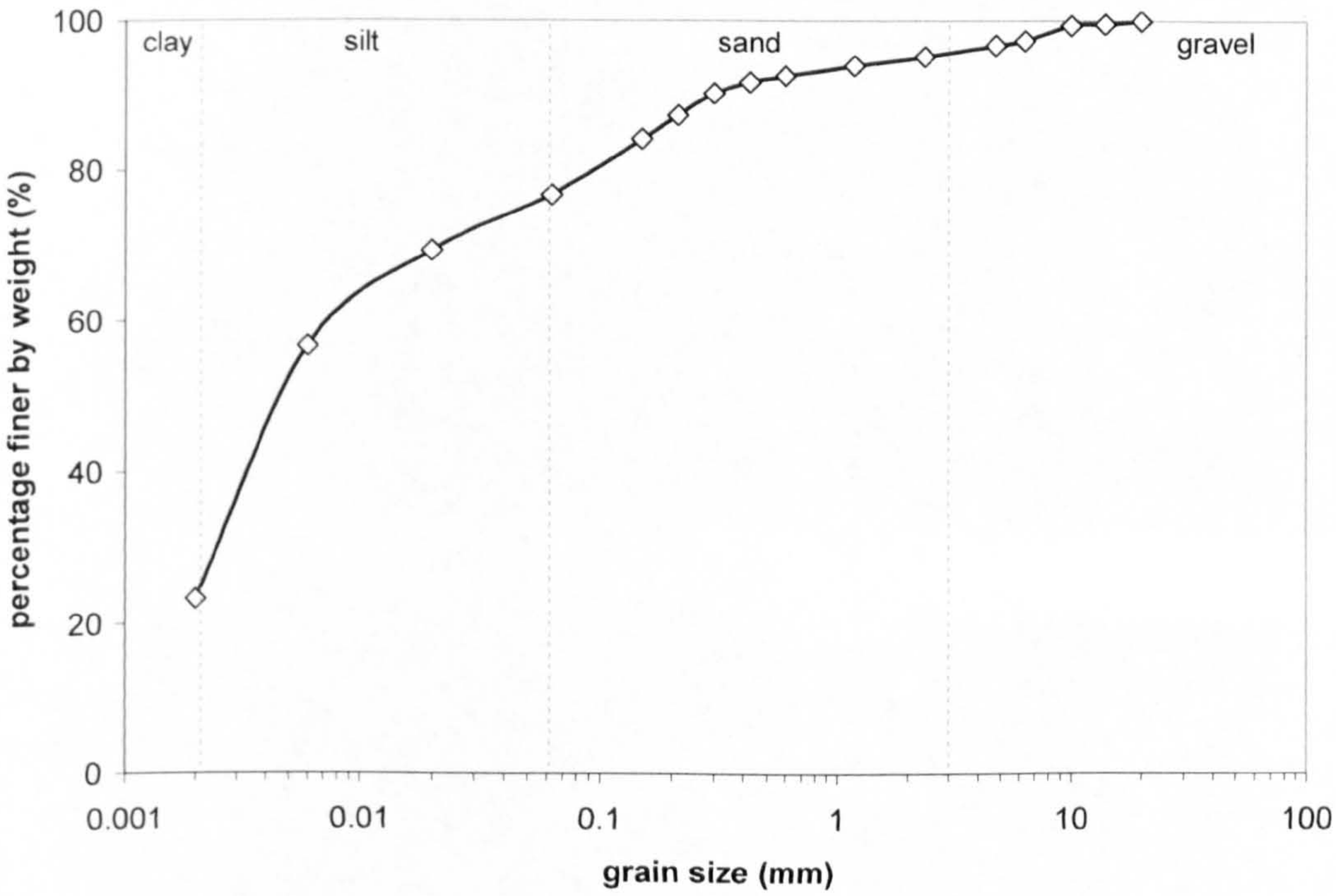

Figure 4.3: Grain size distribution of BIONICS soil (from Mendes, 2008a)

Scanning Electron Microscope images of the BIONICS soil at different scales are shown in Figure 4.4. The samples show different macro and micro features. At a larger scale, Figure 4.4a shows several pathways where air could circulate freely. It can also be seen that the right part of the image seems to have a lower porosity (or higher amount of fines) than the left side. In Figure 4.4b clay platelets can easily be recognized (with a length smaller than 10μm) but they do not seem to be arranged in a particular way. Figure 4.4c also shows many small rounded particles (different from the clay particles) and larger grain with a planar surface (mineral?). Some of the

rounded grains are as small as 5μm and fit into the grain size range of fine silt (2-6μm according to BS5930, 1999).

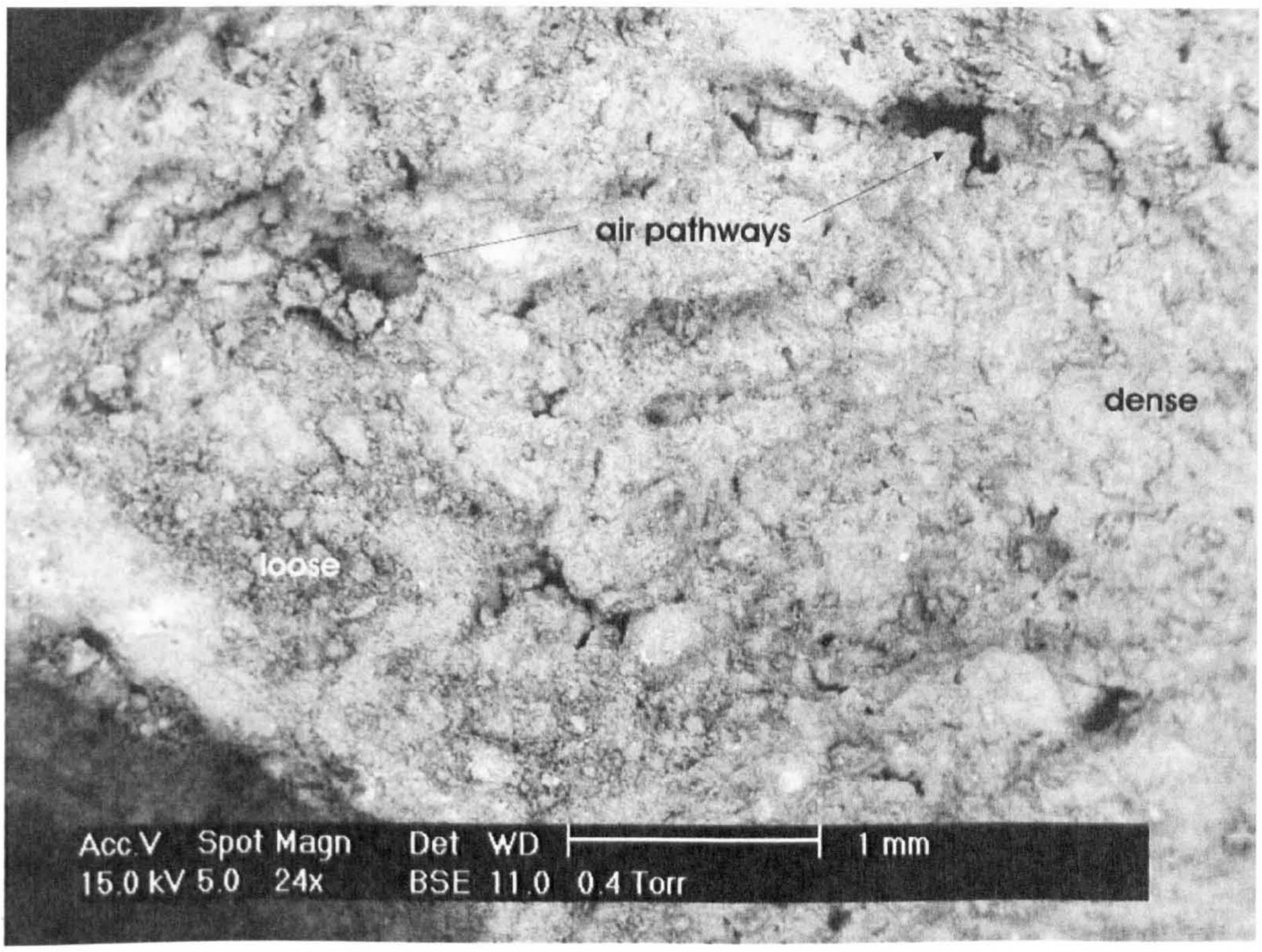

(a)

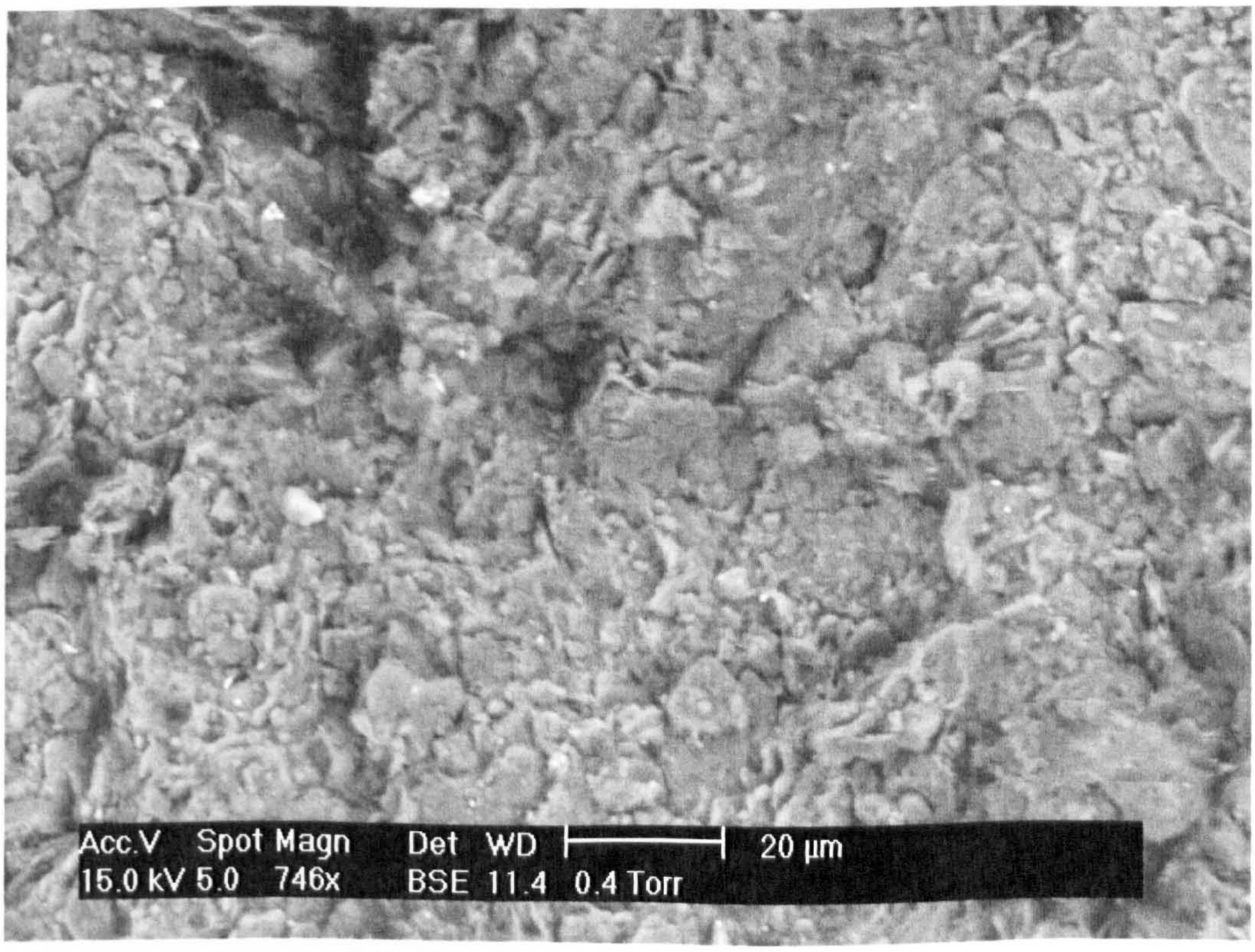

(b)

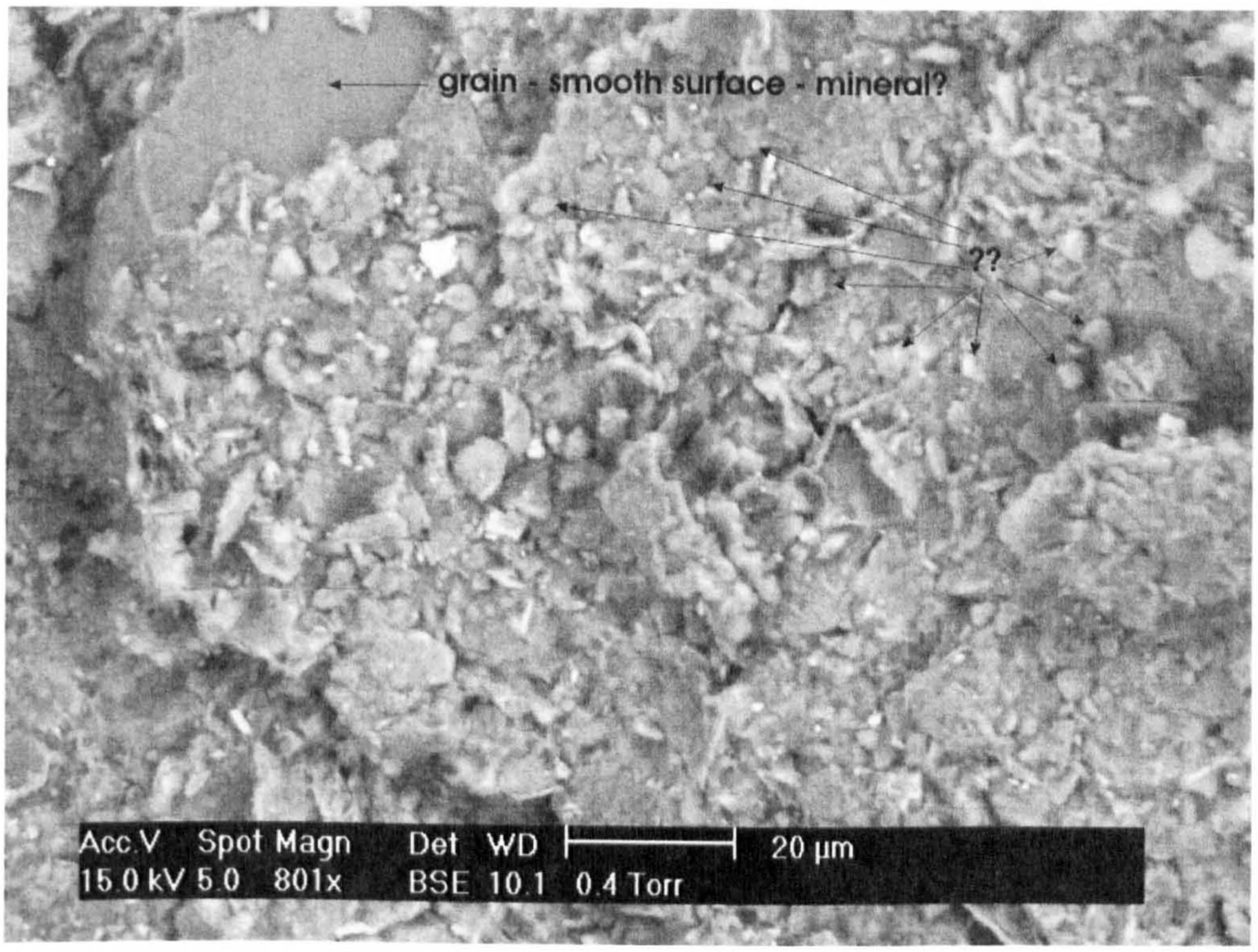

(c)

Figure 4.4: (a), (b), and (c) SEM photographs of BIONICS soil fabric and composition (photos by Helen Riggs)

BIONICS soil exhibited a tendency for volume decrease upon drying. Figure 4.5 shows a sample in a wet state (w=25%) and with a reduced size after drying to the atmosphere. The shrinkage limit was determined for three samples (S1 to S3) prepared at an initial water content of 25%. Accurate volume change measurements were done with a mercury porometer (details given in following section). The shrinkage limit of the soil is approximately 14% (Figure 4.6).

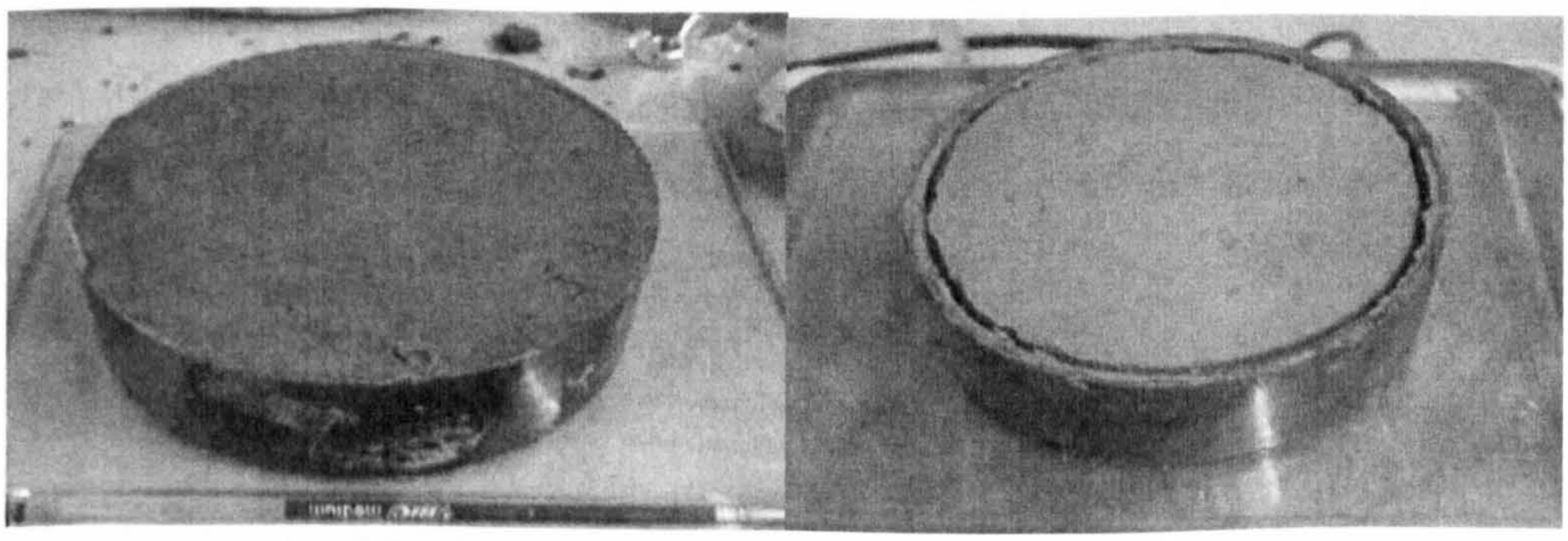

Figure 4.5: Photographs showing shrinkage of BIONICS soil, initial state in the left hand side, after drying in the right hand side

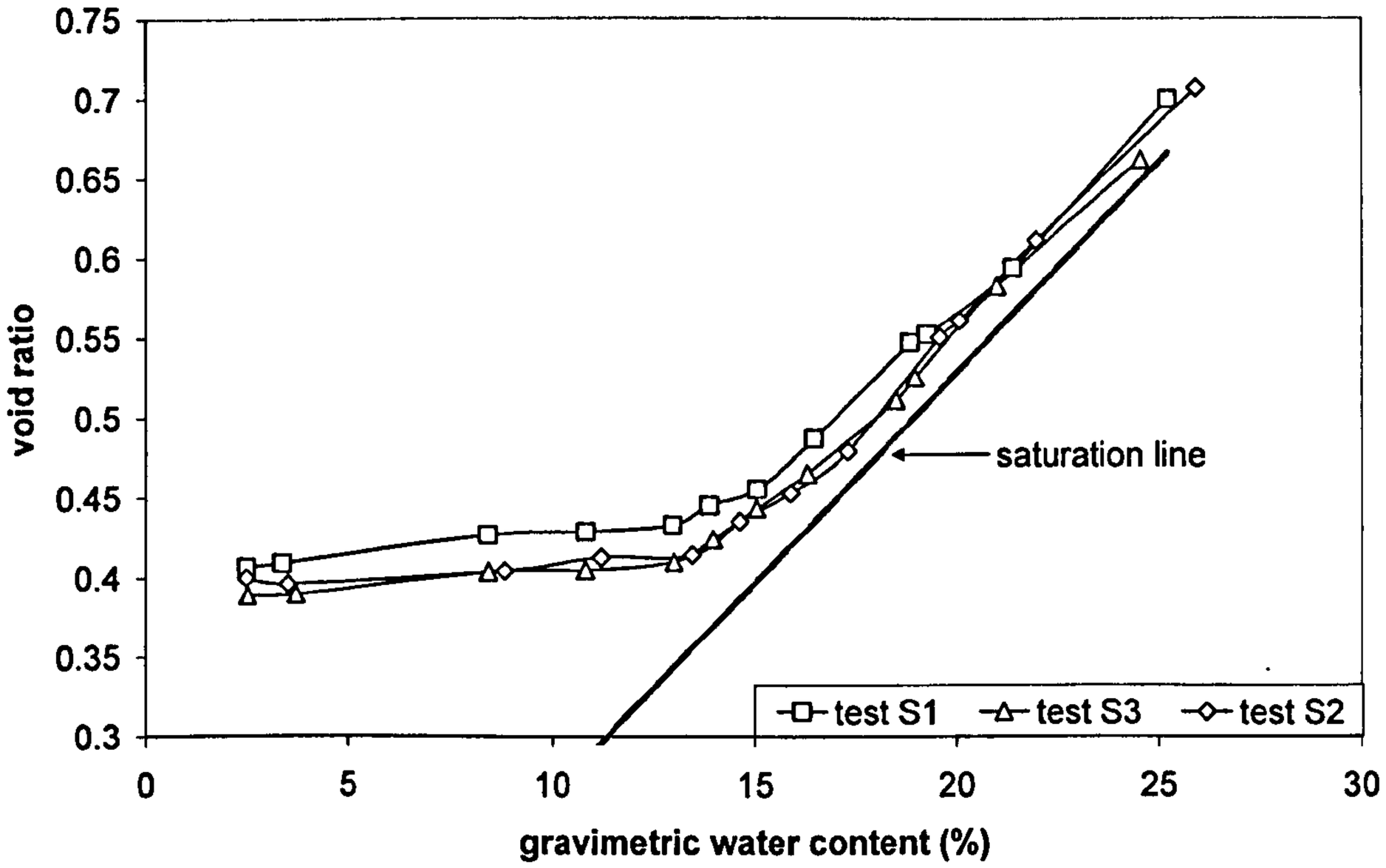

Figure 4.6: Shrinkage behaviour of BIONICS soil (void ratio versus gravimetric water content) (tests S1 to S3, BIONICS)

4.3.2. Equipment

Suction was measured with the high suction tensiometers presented in Chapter 3. For the discrete drying and wetting, the suction measurements were done in the suction measurement box shown in Figure 3.56 (in Chapter 3). A humidifier was used as the wetting source for the discrete wetting (Mendes et al., 2007b). The humidifier consists of a large container with two baskets with water placed inside. A mist environment was then created by placing small foggers submerged in the water with the sample resting on a grid inside the container. Wetting was by the water vapour. All measurements were conducted in a temperature controlled room with the RH and temperature continuously monitored (relevant to the continuous drying tests). The ambient temperature and RH was measured continuously by a Hygroclip-IC-1 probe. The RH measurement accuracy is variable. According to the calibration data supplied by the manufacturer, the probe can read RH 9.9±0.6 at 9.9%, RH 35±0.4 at 35%, and RH 95.1±1 at 95.1%, for RH values imposed by saline solutions. The sample's mass was measured by a digital balance (Oertling balance with accuracy ±0.1g) logged with a data acquisition system via a RS 232 interface.

Two different volume measurement techniques were used due to the different set up of the procedures. The volume change measurements for the discrete procedure were conducted using a Rusca Universal Porometer (accuracy 0.01cm^3/div). For the continuous procedure, displacement transducers (accuracy ±0.001mm) were mounted (detailed in the procedures section).

The pressure plate test was conducted in a pressure plate device manufactured by Soil Moisture Corp, California, fitted with a 500kPa air entry value (AEV) stone.

4.4. PROCEDURES AND RESULTS

The study started with an initial set-up following the works of Cunningham (2000), Toker et al. (2004), Boso et al. (2003), and Teixeira and Marinho (2006) and was then improved as problems were solved until a final set-up was achieved.

4.4.1. Continuous drying

This section presents the initial tests for the continuous drying procedure focusing on the factors affecting the shape of the SWRC (tensiometer's cable, exposed surface area to drying, RH, suction measurement location) and ends by proposing a final set-up that minimizes the effect of these factors.

4.4.1.1. Initial set-up

Influence of the tensiometer's cable

For the continuous drying procedure, a compacted sample with dimensions 30mmx100mm and volume of 235cm^3 was placed on the balance together with the sampling ring as shown in Figure 4.7. Two purpose-made rings were used, a plastic and a steel one. The internal diameter was 100mm to give a tight fit to the sample. The tensiometer was gently pushed into the top surface of the sample to a depth of approximately 3mm. This ensured a good contact with the soil and lateral support so that the tensiometer would not fall to the side. The entire length of the tensiometer cable was also supported (by resting it on still surfaces) to minimize any influence of its stiffness on the mass measurements. Pore water was left to evaporate through the exposed top surface of the sample while the decrease of water content was

observed through the change in mass (recorded by the balance) and increase of suction measured by the tensiometer were continuously recorded. The initial sample conditions and a summary of the key results are shown in Table 4.1. Fourteen tests were conducted, Ci1 to Ci14 (*C* for continuous drying and *i* for initial set-up). Ci1 to Ci10 were statically compacted and Ci11 to Ci14 dynamically compacted (the reason for this will be given later in this chapter).

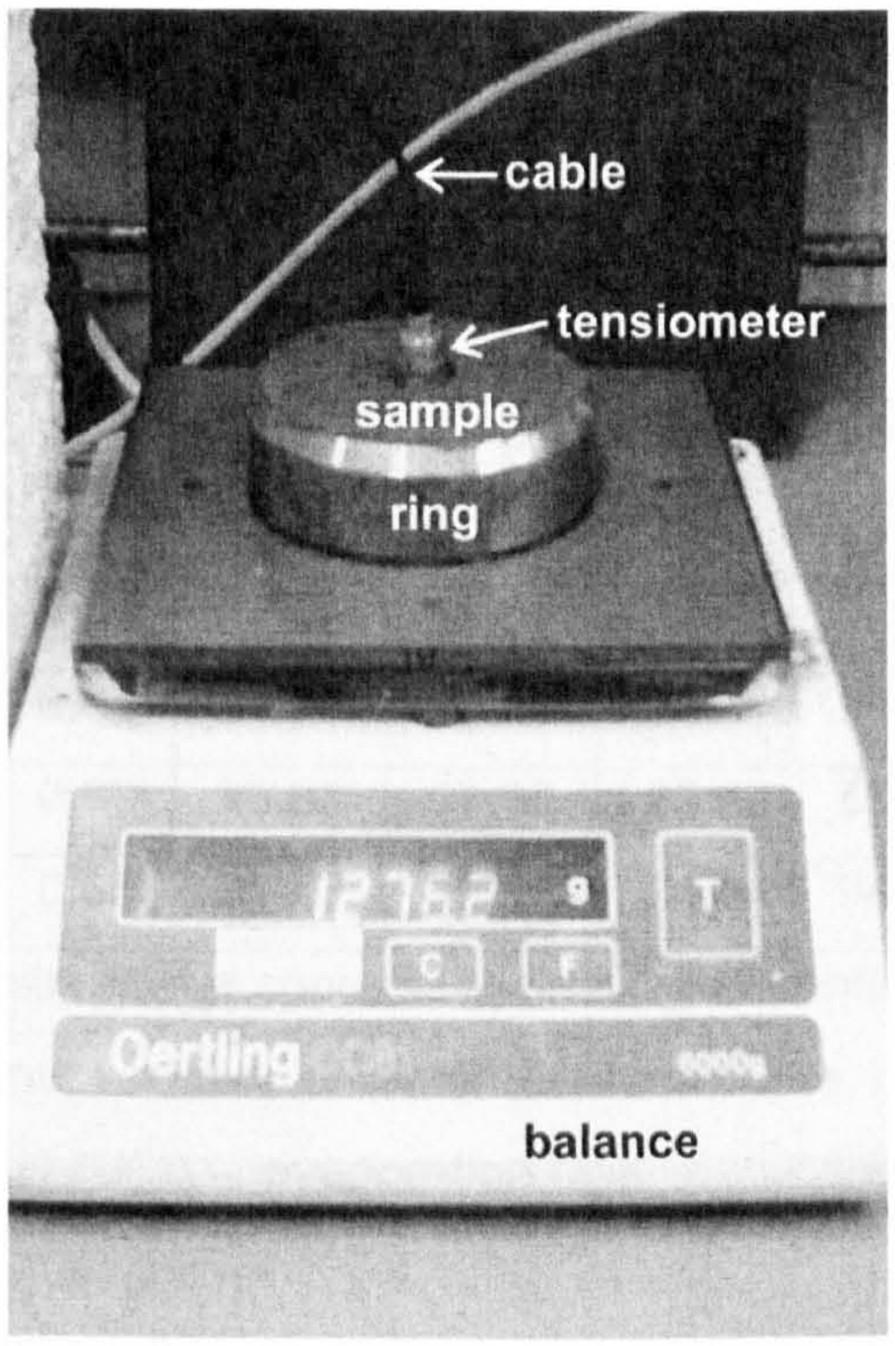

Figure 4.7: Initial set-up for the continuous drying tests

Table 4.1: Testing program for the initial set-up of the continuous drying tests

	compaction	e_i	w_i [%]	w_f [%]	ΔM_w [g]	s_{max} [kPa]	Δt [h]	$\Delta M_w/\Delta t$ [g/h]
Ci1	dynamic	0.52	24.70	18.37	26.0	376.0	25.1	1.06
Ci2	dynamic	0.56	24.76	17.25	30.0	745.2	32.5	0.92
Ci3	dynamic	0.55	24.17	17.23	27.9	584.6	28.4	0.98
Ci4	dynamic	0.49	22.63	16.17	27.0	850.4	25.3	1.07
Ci5	dynamic	0.52	24.57	15.38	37.5	1150.4	34.0	1.1
Ci6	dynamic	0.52	23.53	16.15	30.2	840.8	27.8	1.09
Ci7	dynamic	0.58	26.19	17.06	35.8	1029.3	27.9	-
Ci8	dynamic	0.51	23.73	16.67	29.0	761.1	22.2	1.31
Ci9	dynamic	0.56	24.27	17.03	28.8	851.1	22.3	1.29
Ci10	dynamic	0.59	25.16	16.12	35.3	911.2	26.5	1.33
Ci11	static	0.65	24.77	15.02	38.0	929.8	23.31	1.84
Ci12	static	0.65	24.99	17.25	30.4	949.4	22.97	1.31
Ci13	static	0.65	25.33	17.10	33.6	895.5	23.69	1.42
Ci14	static	0.65	25.43	16.68	34.3	940.9	24.8	1.31

e_i initial void ratio, w_i initial water content, w_f final water content, ΔM_w mass of water evaporated, s_{max} maximum suction of water retention curve, Δt test duration; $\Delta M_w/\Delta t$ evaporation rate

Figure 4.8 shows a typical plot of suction and gravimetric water content against elapsed time. Inspection of Figure 4.8 indicates that the decrease of the gravimetric water content was nearly linear (R^2=0.9993) with respect to time. The entire SWRC was obtained in less than two days. Table 4.1 shows the evaporation rates for all tests were between 0.9g/h and 1.84g/h.

Figure 4.9 shows tests Ci1-Ci10 (dynamically compacted) from Table 4.1. The shapes of the curves are similar but the variation in the water content is greater than 2%. As the curves were quite differently positioned, the tests from Table 4.1 were grouped according to their initial water content (Figure 4.10a w≈24.7-25.2%) and initial void ratio (Figure 4.10b e≈0.51-0.52). The curves tend to fit more closely in both figures, but this may be due to the lower number of tests rather than just the similarity of water content/initial void ratio.

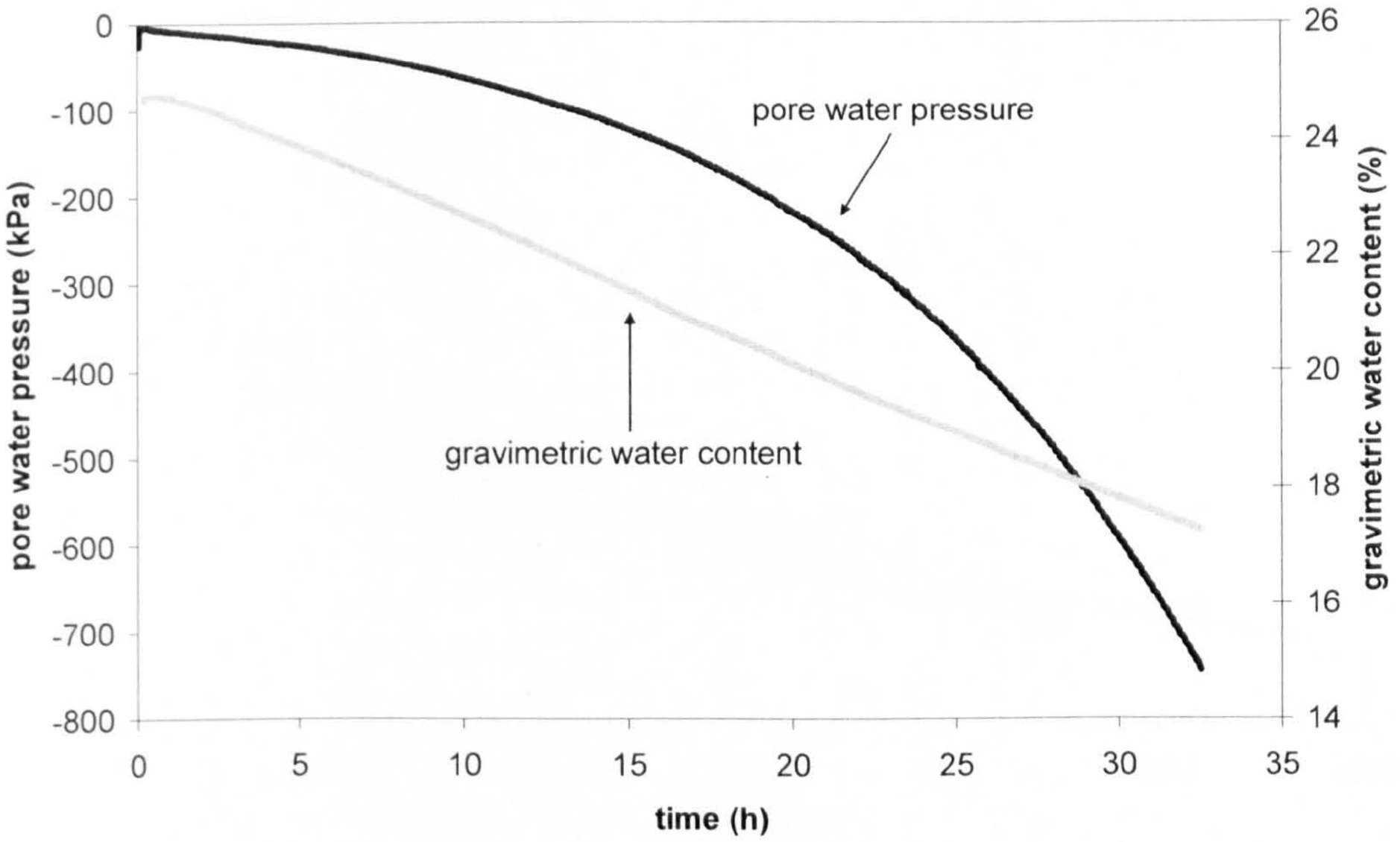

Figure 4.8: Time sequence for test Ci2 (tensiometer II2, BIONICS)

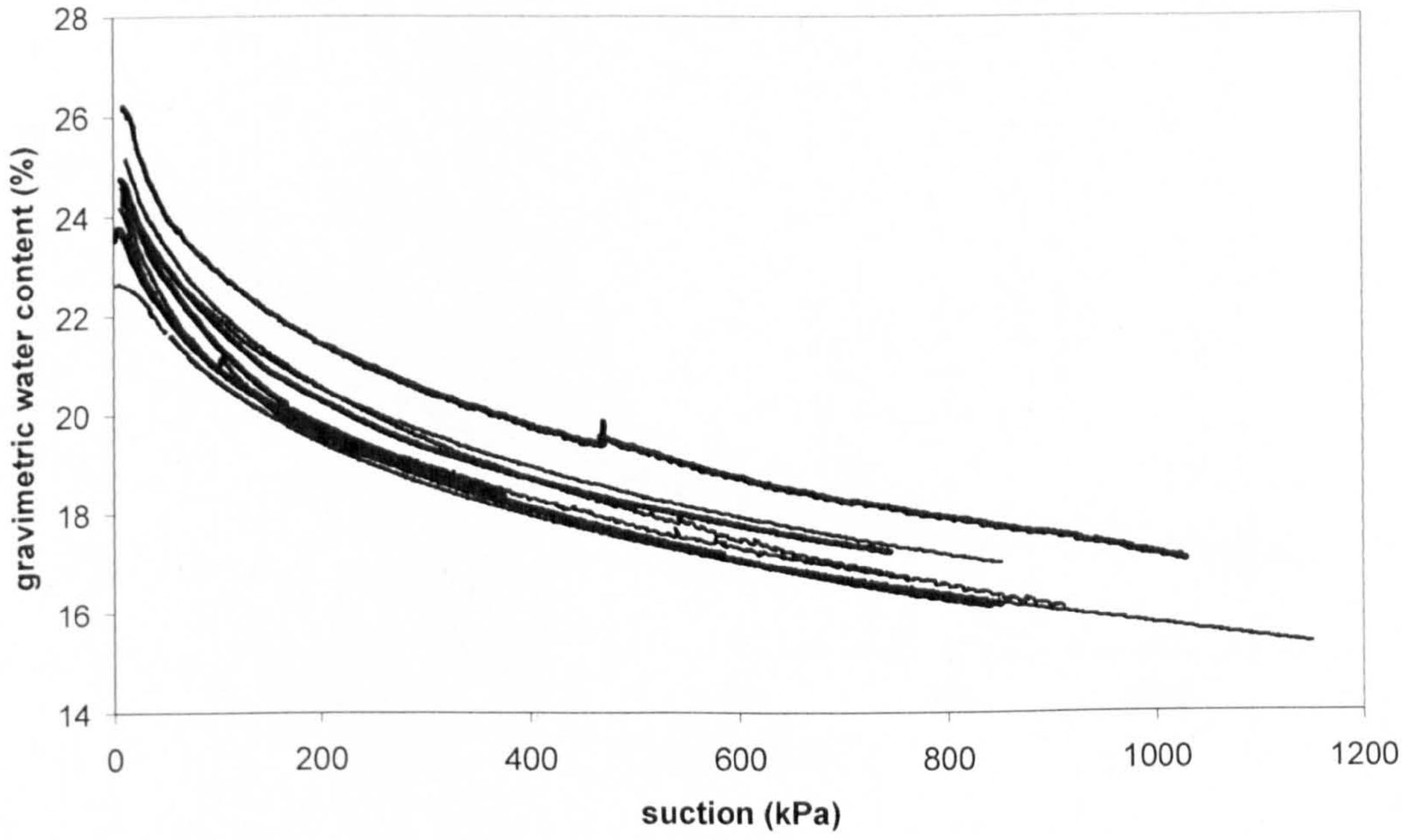

Figure 4.9: SWRCs for tests Ci1 to Ci10 (tensiometers II2, III1, III4, BIONICS)

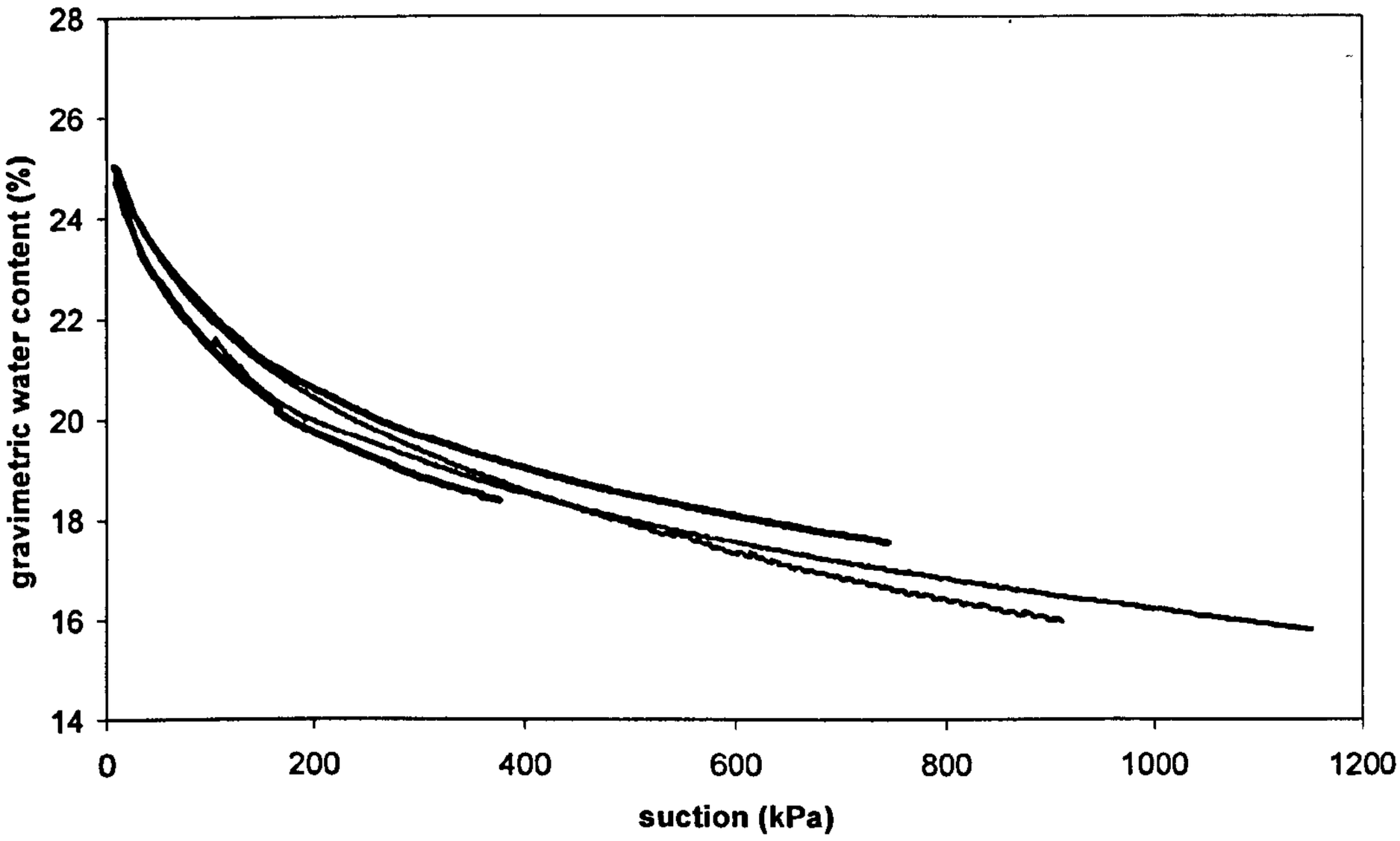

(a)

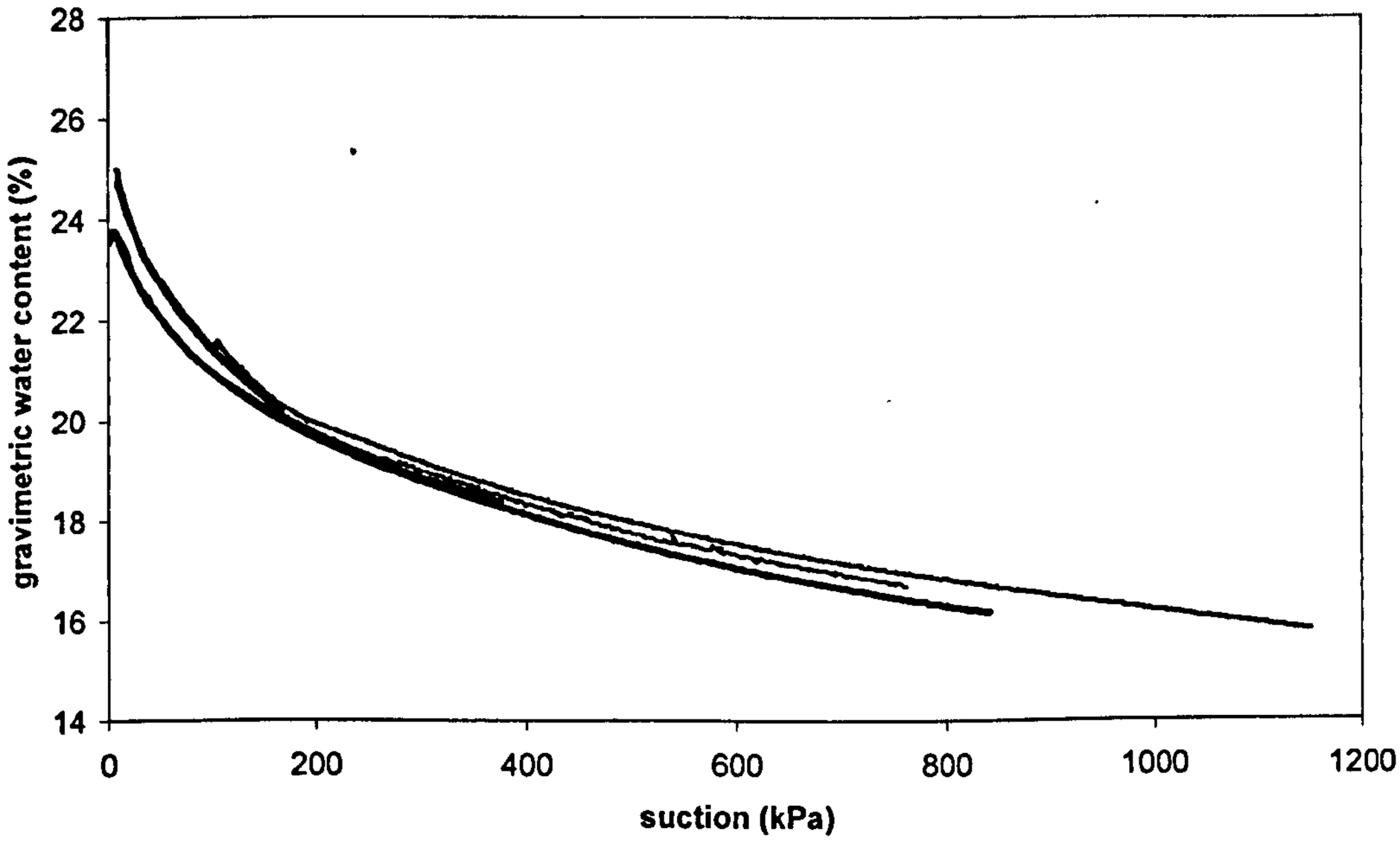

(b)

Figure 4.10: SWRCs for Ci1 to Ci10 (tensiometers II2, III1, III4, BIONICS) for (a) tests with similar initial water content (24.7%-25.2%) and (b) similar initial void ratio (0.51-0.52)

Factors contributing to the spread of curves in Figure 4.9 include:

1. Different as-compacted void ratios

    a. Varying energy of the hammer (falling from different heights) could result in different densities (due to malfunctioning of the device).

    b. Soil heterogeneity
    The distribution of density within the compacted sample might vary which could lead to variation between specimens (which were cut from different positions in the sample, sometimes from the top, bottom or centre).

2. Movements in the tensiometer's cable. Figure 4.11 shows that cable tended to influence the mass readings at the start of the test (Figure 4.11a, Figure 4.11b) or during the test (Figure 4.11b). It could have lead to wrong mass readings and consequently wrong water contents. In the case of Figure 4.11b the second disturbance resulted in a permanent effect, with the inclination of slope changing.

To attempt to remove uncertainty associated with variations in void ratio, a series of tests were carried out on statically compacted specimens (instead of dynamic compaction) as it was possible to control the void ratio more precisely. Four SWRC tests were determined by continuous drying (Ci11 to Ci14 in Table 4.1). The void ratio was 0.65 for the four tests and the water content 24.77-25.43%, which demonstrates that the void ratios of these samples could be controlled with little variation in the initial water content.

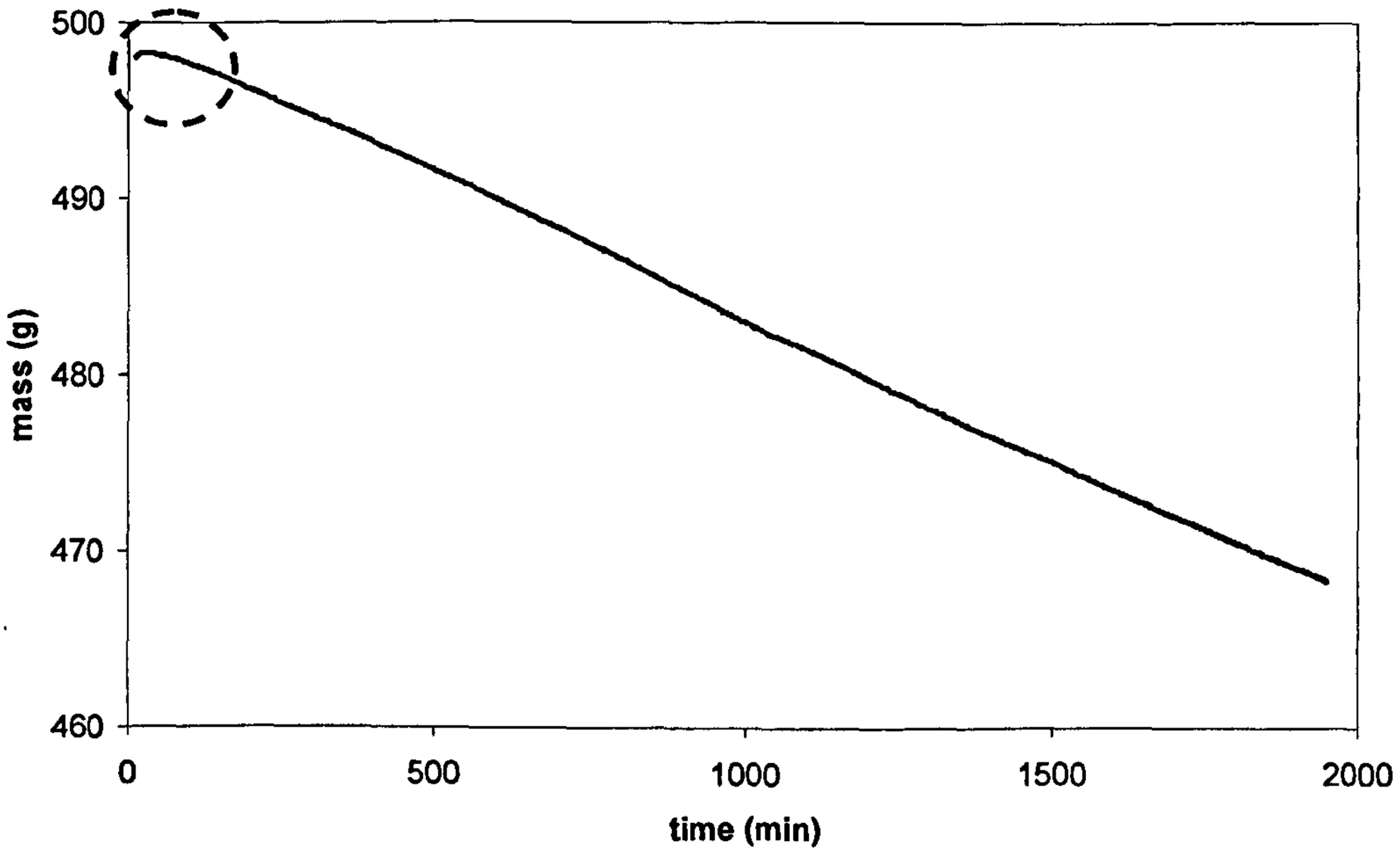

(a)

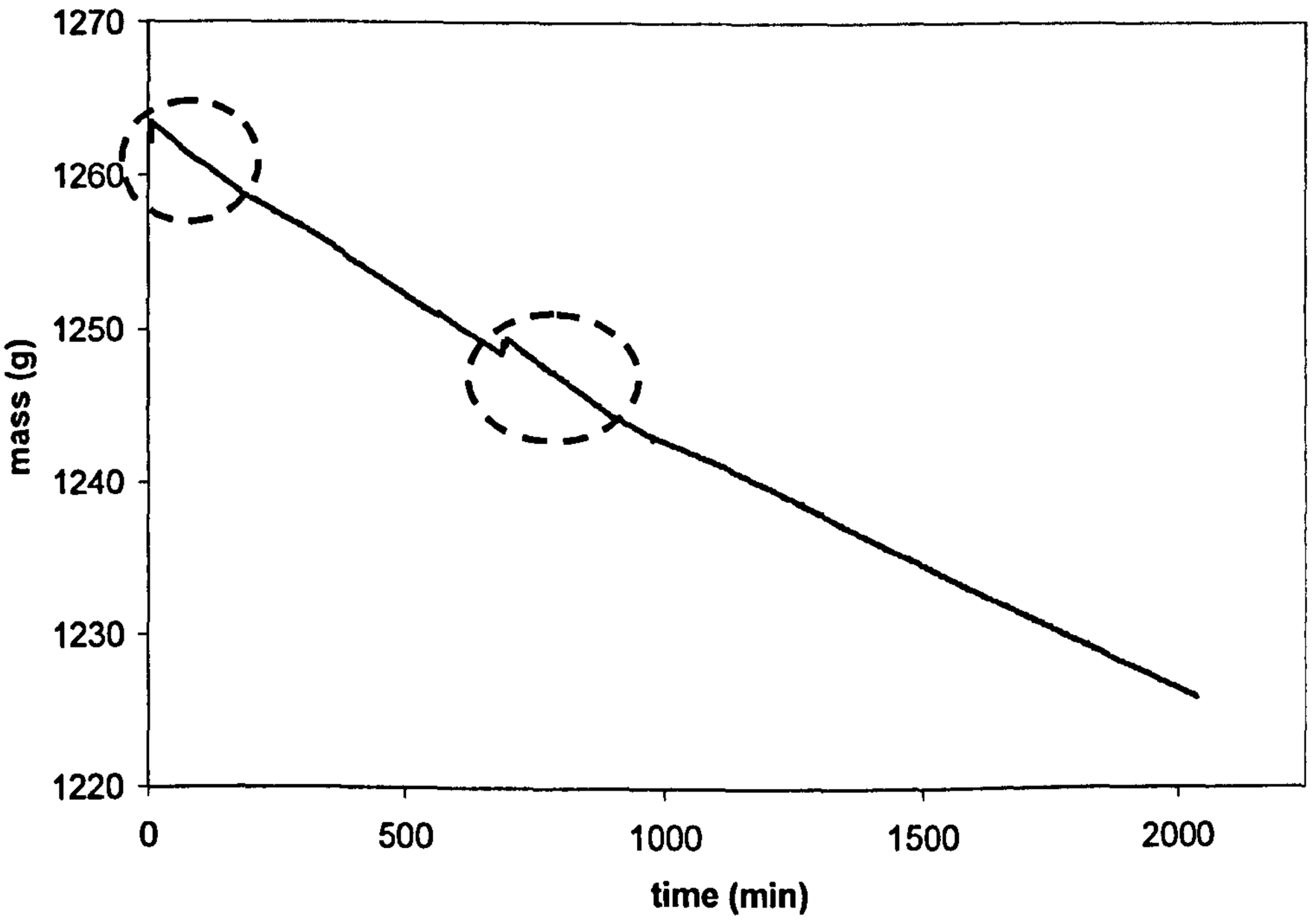

(b)

Figure 4.11: Effect of the tensiometer's cable in the mass measurement, (a) at the start of the test and, (b) during the test

The result for the 4 tests is shown in Figure 4.12. The shape of the curves was again quite different with a variation at the maximum suction of larger than 2%. This meant that differences in void ratio were not causing the variation.

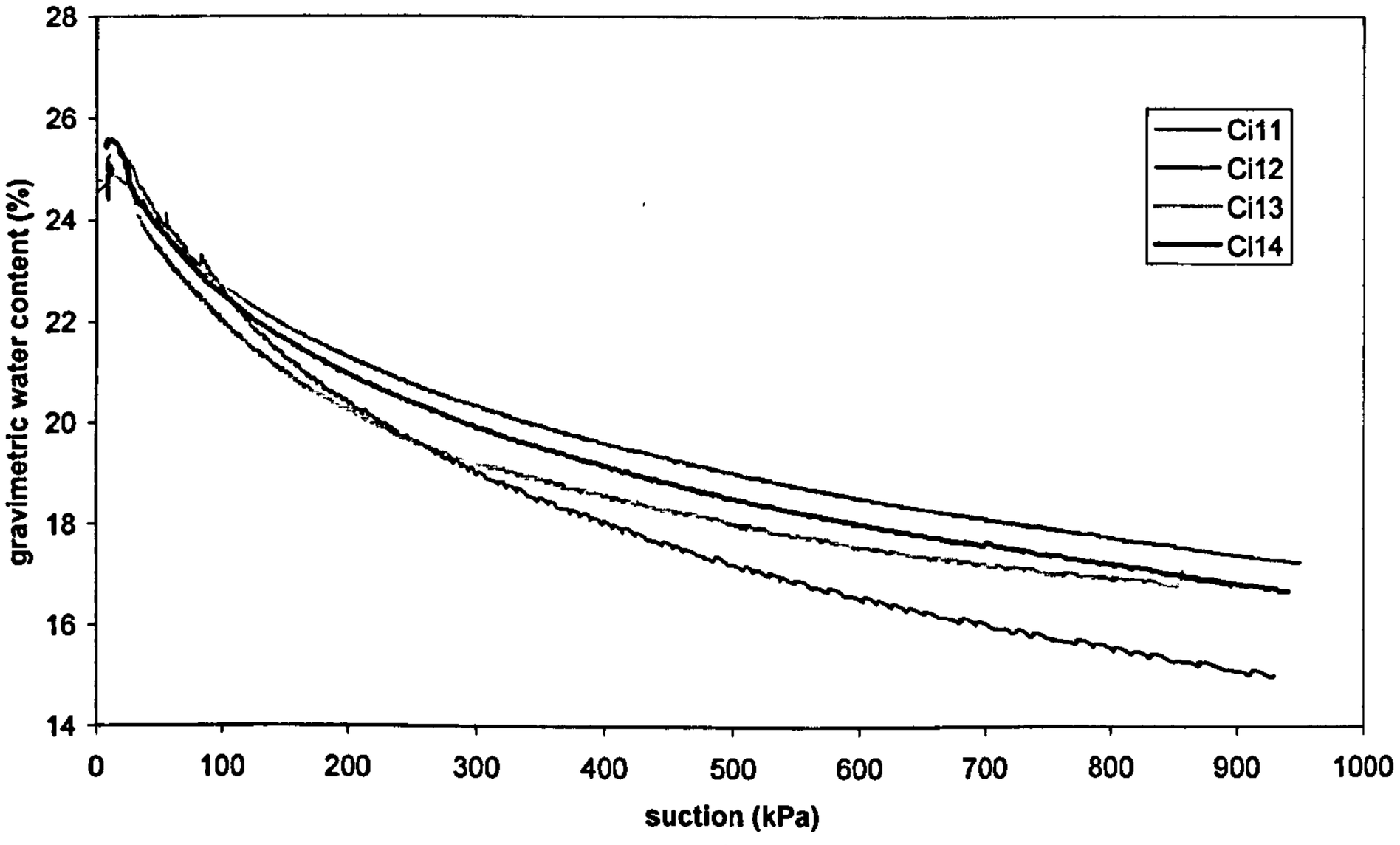

Figure 4.12: SWRCs for tests Ci11 to Ci14 in Table 4.1 (tensiometer III4, BIONICS)

After inspection of all the data the only parameter that did not seem consistent was the evaporation rate. The four evaporation rates show slightly curved lines with different inclinations (Figure 4.13). The rates ranged between 1.84 and 1.31 g/h.

The evaporation curve should have been the same for the 4 tests, provided that the RH of the air in the lab and the surface area of the samples was the same. To confirm this, another group of tests was done. Five samples prepared at the same water content (approximately 25%) and initial void ratio (0.65) were left to dry on the top of the balance (no tensiometer attached).

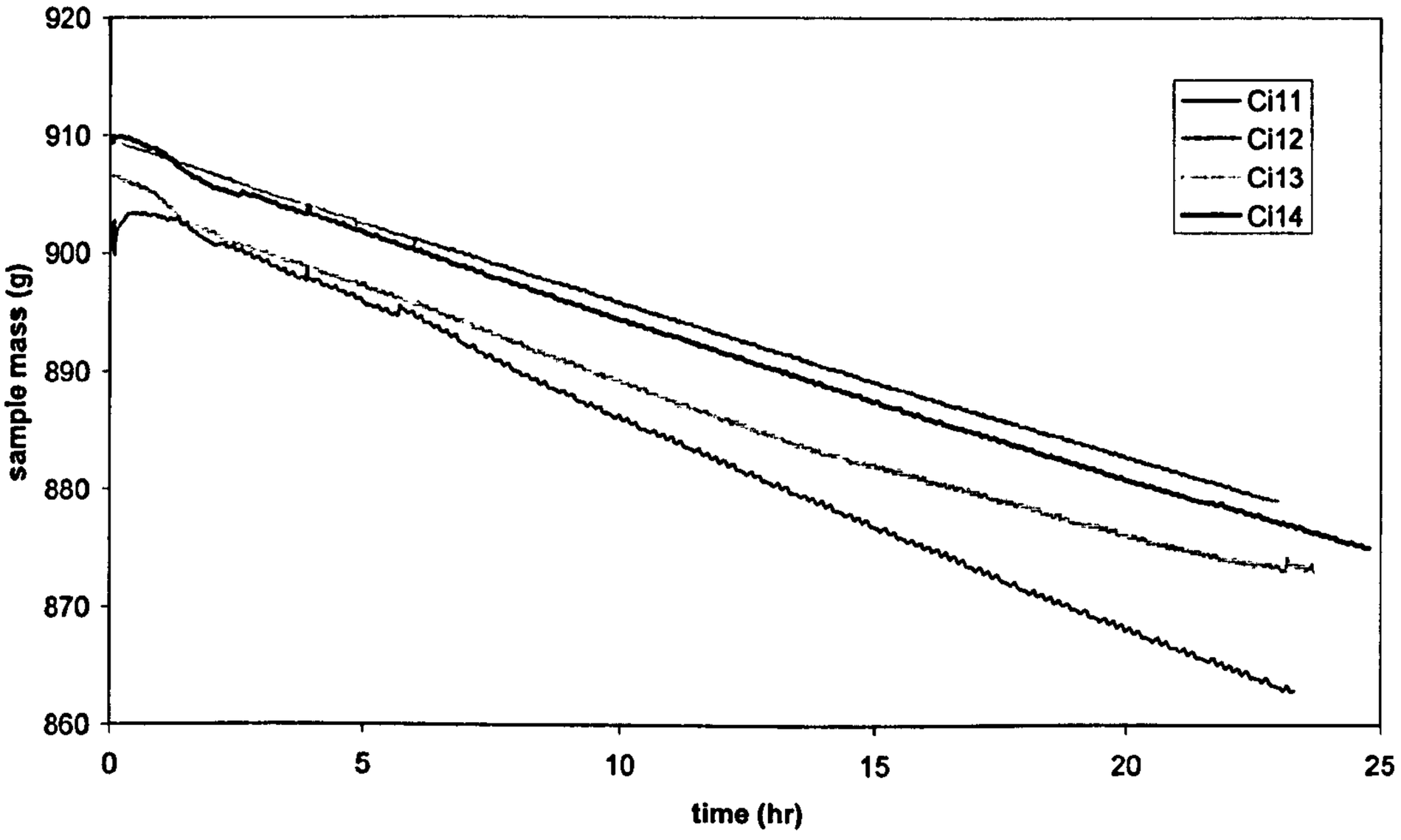

Figure 4.13: Change in sample mass due to water evaporated (with the cable attached) for tests Ci11 to Ci14 in Table 4.1 (tensiometer III4, BIONICS)

Figure 4.14 shows that evaporation is linear but with a small difference in the slope. The minimum rate was 1.21g/h and the maximum 1.34g/h. If we assume that the measured changes in mass for tests Ci11-14 could be in error, we can recalculate the water contents by taking an evaporation rate of 1.34g/h. It can be seen in Figure 4.15 that the error decreases significantly, based on this assumption. For the two curves set most apart the error is below 0.5%. This suggests that the origin of the discrepancies was in the tensiometer's cable affecting the mass measurement and not in the initial void ratio or water content.

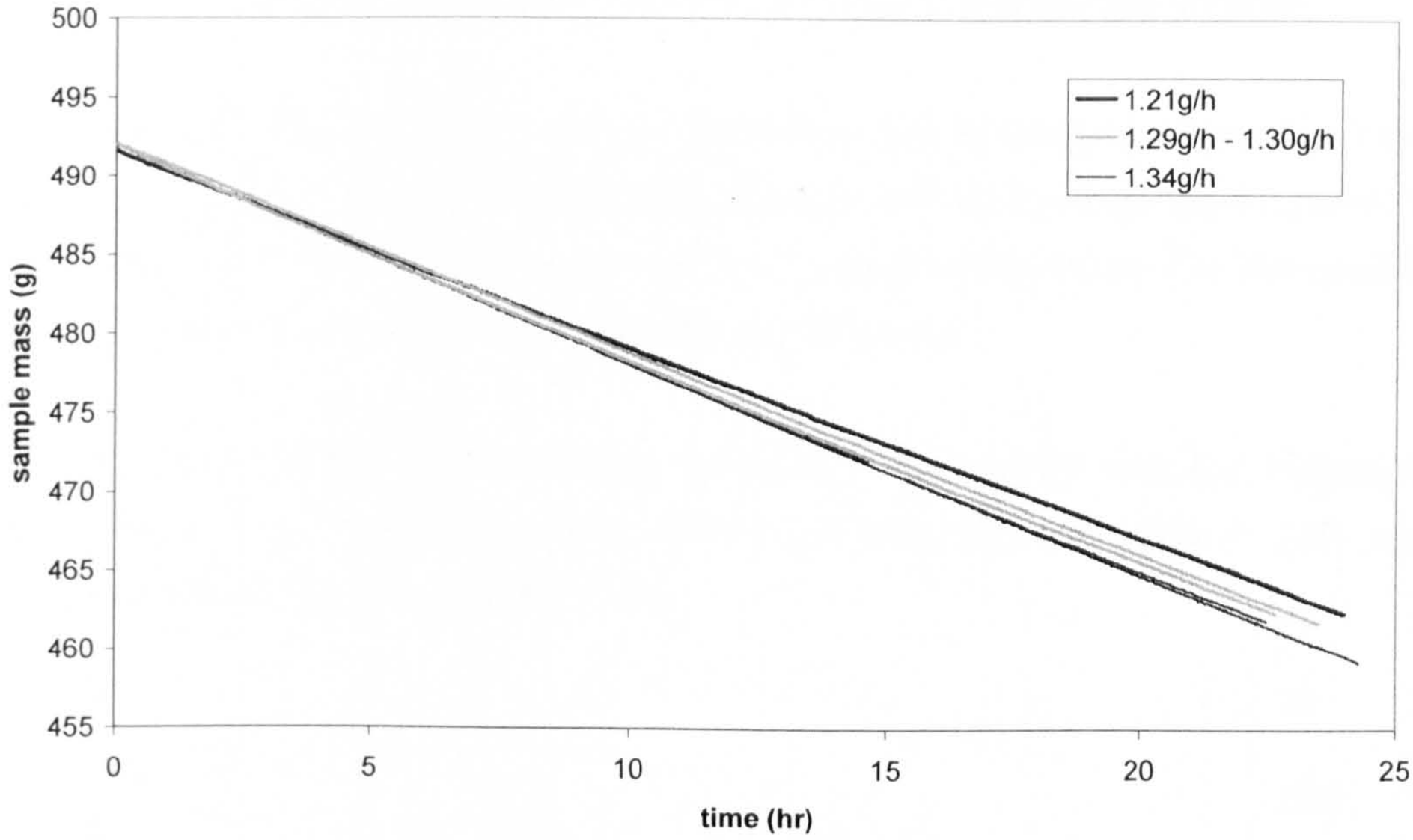

Figure 4.14: Change of sample mass due to water evaporated (no tensiometer on the sample) for a series of samples (tensiometer III4, BIONICS)

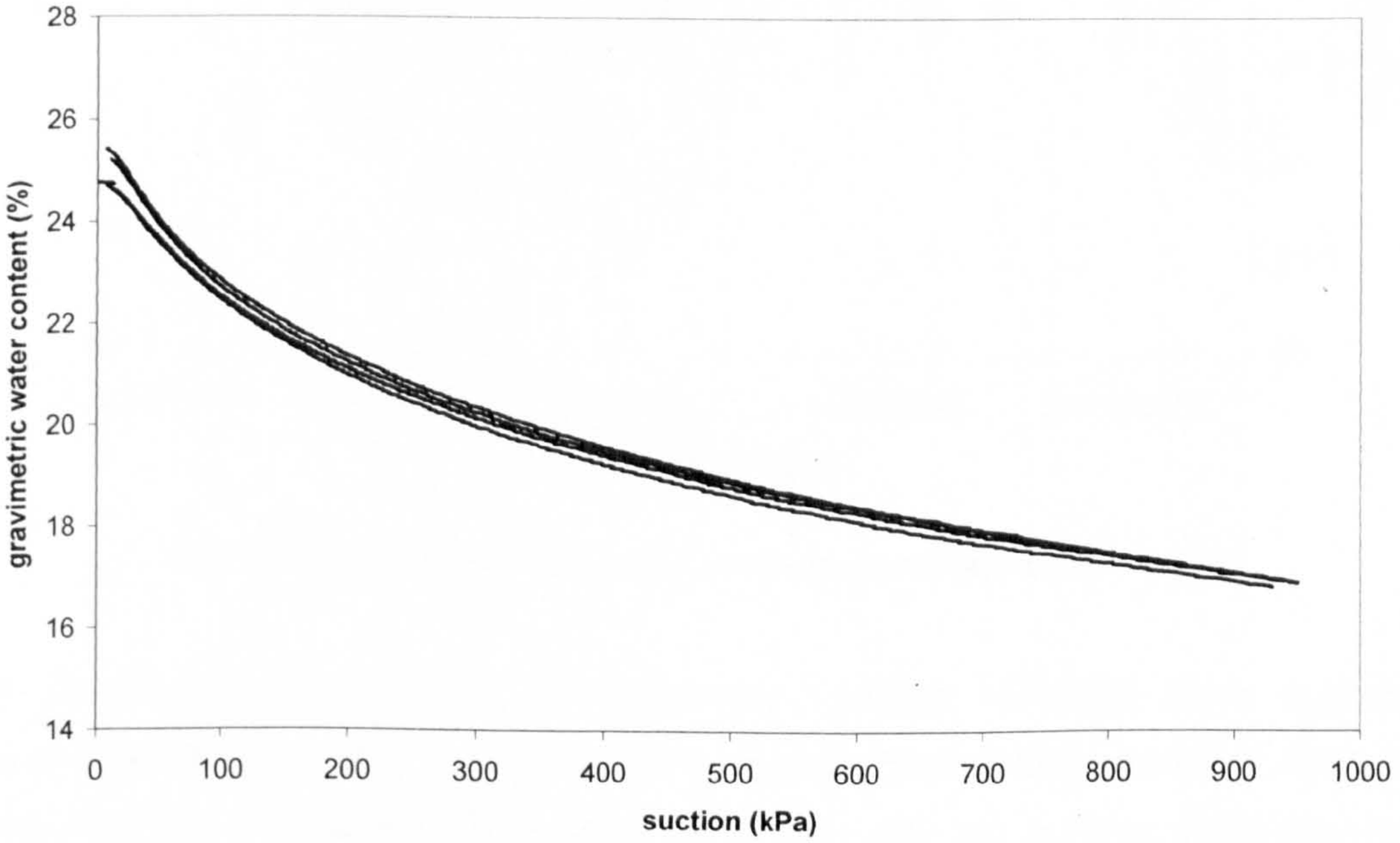

Figure 4.15: SWRCs for tests Ci11 to Ci14 re-drawn for a constant evaporation rate of 1.34g/h

Influence of the sample's exposed surface area to drying and relative humidity

This section presents the effect of the surface area and RH on the evaporation rate. The total surface area exposed to the atmosphere is likely to affect the evaporation rate; larger surface areas should lead to higher evaporation rates. For the relative humidity, lower RH should lead to faster evaporation rates.

The RH was monitored between January'07 and February'07 with the HygroClip probe (Figure 4.16). Some tests were carried out when RH was between 33% and 46% others when the RH was below 33%.

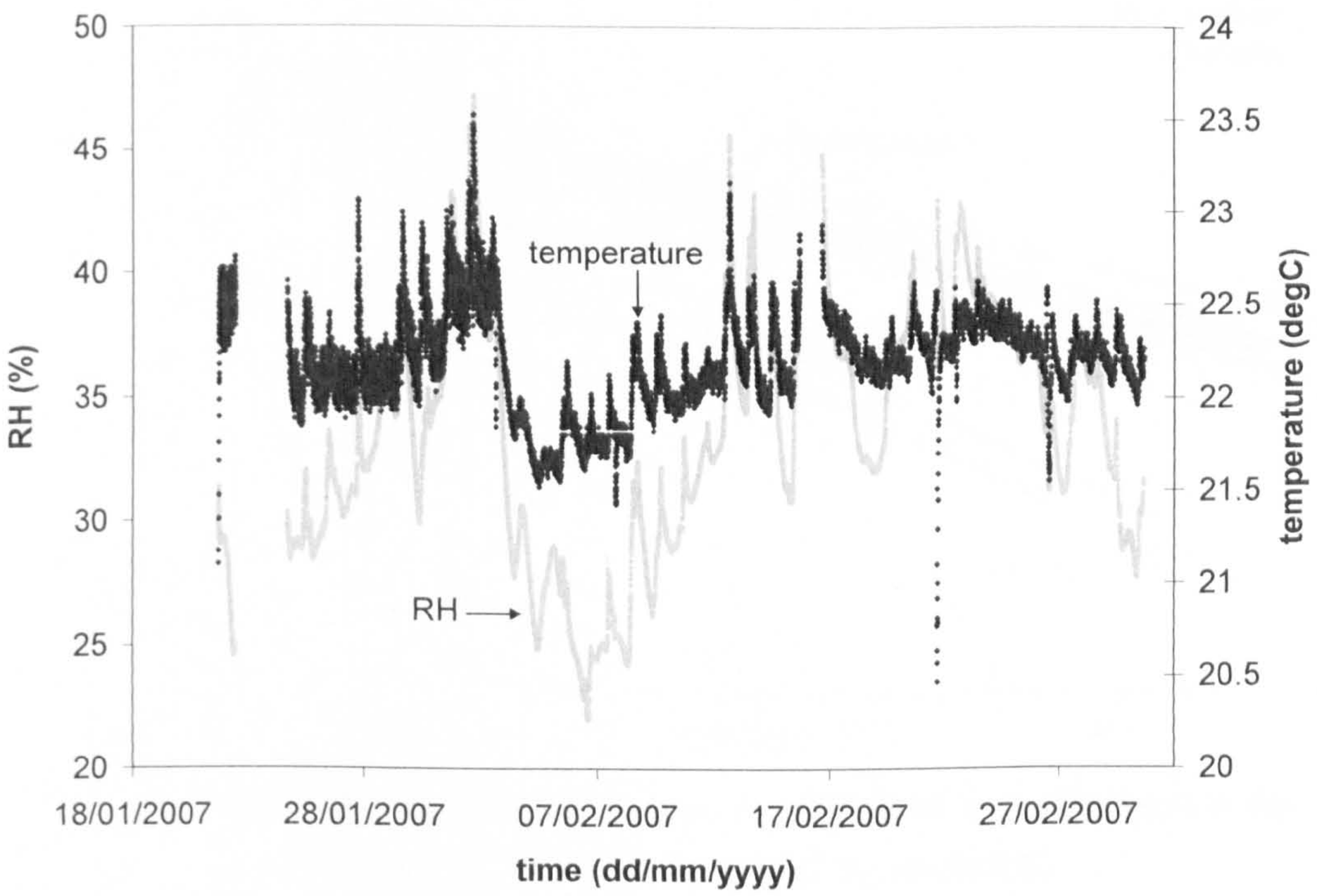

Figure 4.16: Ambient RH and temperature monitored in the lab

To investigate these effects, a further five samples (Ci15-20) were statically compacted at the same void ratio (0.65) and water content (approximately 25%) as tests Ci11-14. Samples Ci15-17 were dried from the top surface only (exposed surface area 78.5cm^2), and samples Ci18-20 were dried from top and sides (exposed surface area 172.7cm^2). Drying from the top was carried out in the same way as all previous tests. To dry from the top and side, the enclosing ring was removed together with the top lid.

Figure 4.17 shows the results for Ci15-20 together with previous tests Ci11-14. The evaporation rate changes with the surface area as would be expected. The evaporation rate was higher for higher surface areas (172.7cm^2). The variation in the evaporation rates can be explained by variations in RH at the time of testing. The upper lines (lower evaporation rates) in each data set are for higher RH's (higher than 33%) and greater evaporation was observed when the RH was less that 33%.

The effect of the exposed surface area on the SWRC will be shown in the following section.

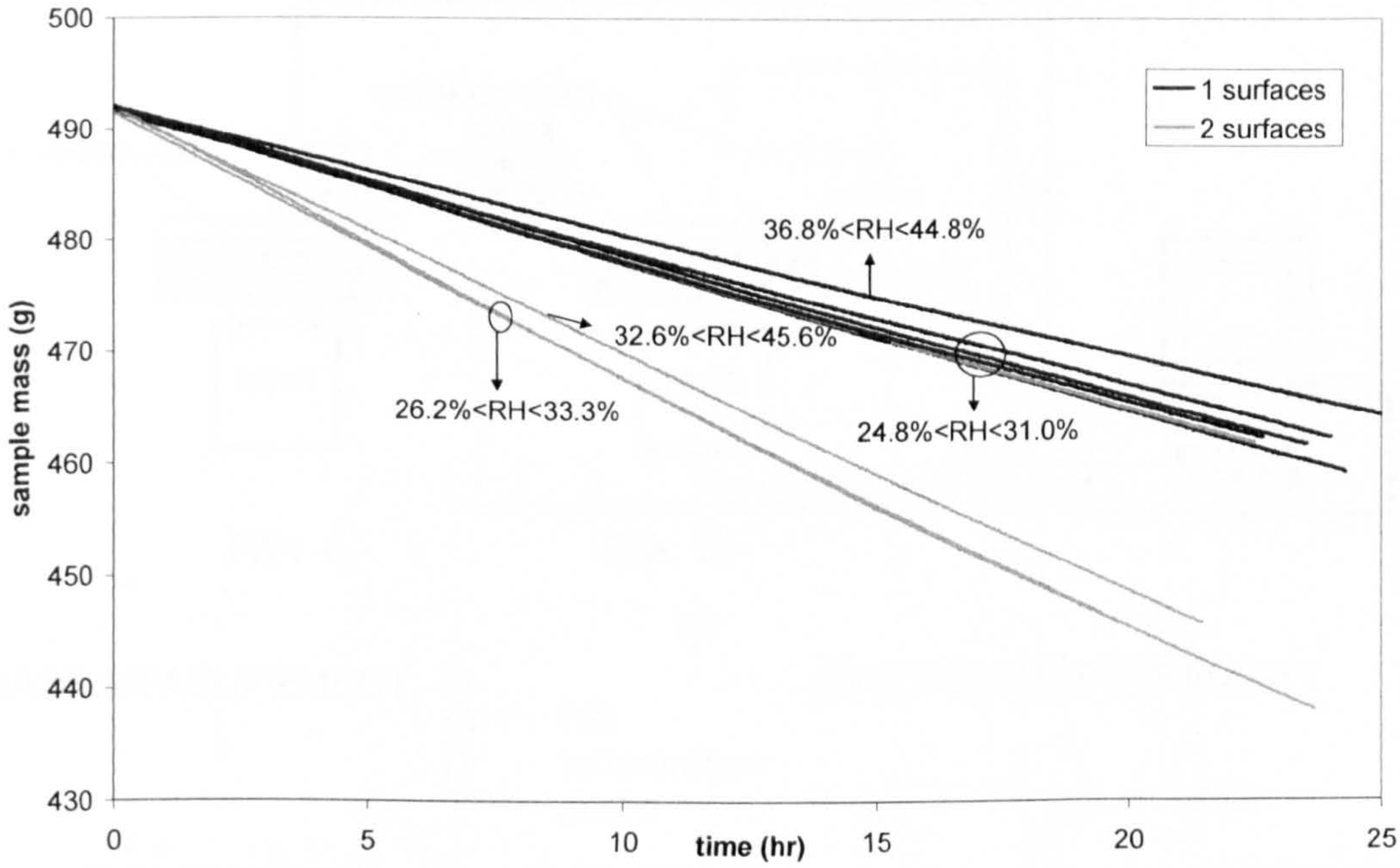

Figure 4.17: Influence of RH and surface area (78.5cm^2 and 172.7cm^2) in the evaporation rate (tests Ci11 to Ci19, BIONICS)

4.4.1.2. Final set-up

The final set-up takes into account the previous results that showed that (1) the cable seems to influence the mass measurements and hence the evaporation curve, (2) greater surface areas lead to a more homogeneous drying of the sample, and (3) using an assumed evaporation rate to draw the SWRC is not accurate enough as variation in RH and temperature will lead to different evaporation rates for each test. In addition, so far the SWRCs have been presented in terms of gravimentric water content. It is clearly of benefit to be able to observe changes in volumetric water content or degree of saturation. For this, volume measurements are needed, so these have been included in the final arrangements.

The procedure was improved by determining the evaporation rate separately from the suction measurement. Wilson et al. (1997) determined evaporation fluxes (the ratio between actual evaporation and potential evaporation) by having two samples next to each other where one (with the sample) determined the actual evaporation and the other (with water) the potential evaporation (Figure 4.18a). A similar approach was followed in this study by having two samples prepared at the same initial conditions, where one was used for suction measurement and the other for the evaporation curve (Figure 4.18b).

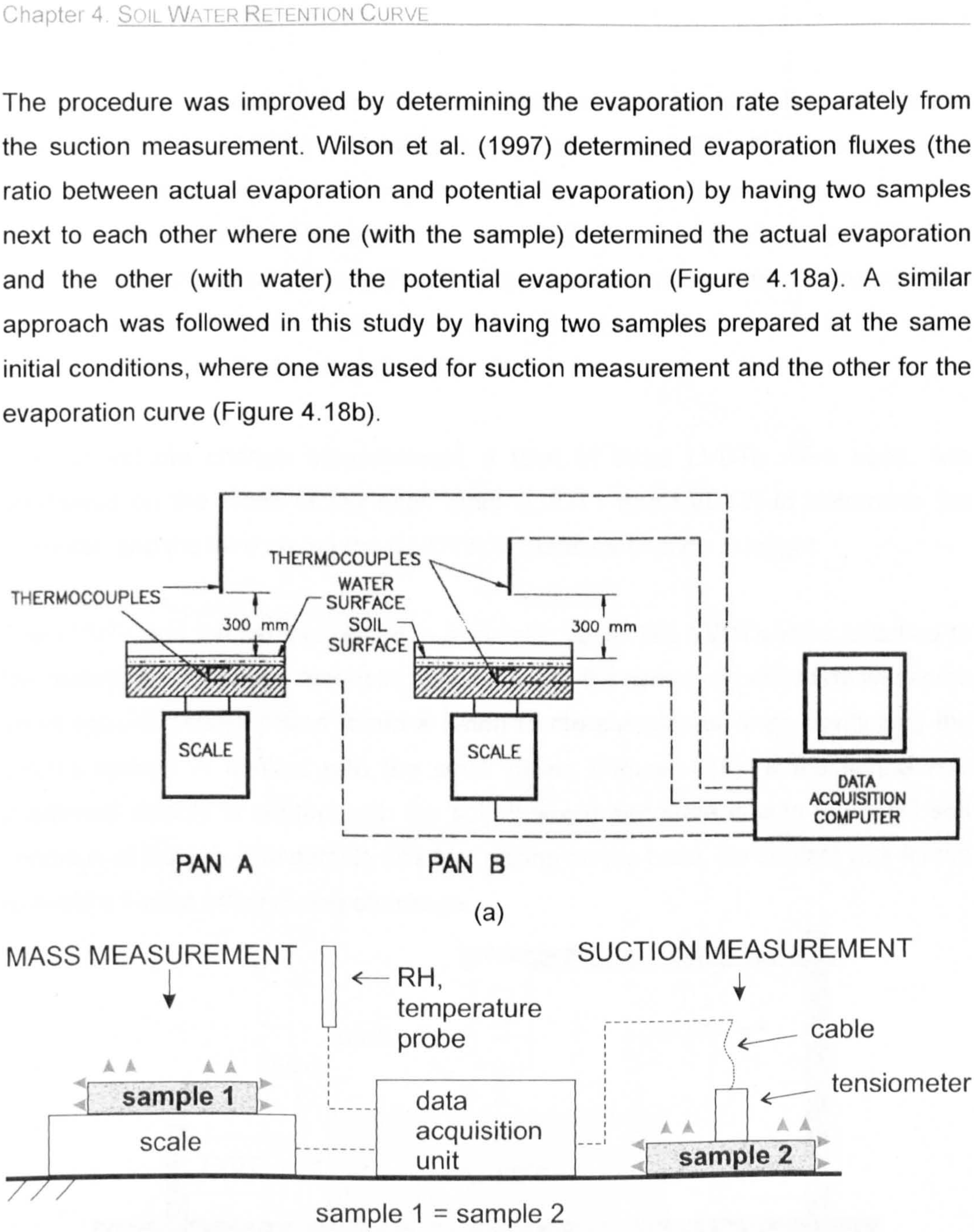

Figure 4.18: Schematic diagram of the new set-up for continuous drying, (a) set-up for the evaporation tests by Wilson et al. (1997), (b) the new set-up for continuous drying (sample is 3cm height by 10cm diameter)

The sample used this time was considerably smaller than all previous tests. It had an initial volume of approximately 30cm^3 (3.0cm height and 3.5cm diameter) and initial wet mass of approximately 60g. The reduction in size was to (1) further restrict water content gradients during drying and (2) to compare the results to discrete drying tests where the sample size had to be decreased to allow measurements in the porometer.

To confirm the new procedure, eight samples were prepared at the same water content (24.23% - 25.70%) and void ratio (approximately 0.73). Four were used for the suction measurement and the remaining four for the mass measurement. The void ratio was considerably larger than the initial set-up (approximately 0.55). The samples were dried continuously from the top and sides with suction measured at the top. In the sample fitted with the tensiometer, suction was measured at the upper surface by inserting the tensiometer by 3mm.

For the volume change measurement a total of three LVDTs were used, two positioned on the sides facing each other (LVDT1 and LVDT2) to determine the diameter, and the third on the top (LVDT3) to measure change in height.

The LVDTs and the sample rested in a metallic base. The LVDTs were attached to the metallic base through magnetic holders and to the sample by attaching first some small square metallic plates (5mm × 5mm) to the sample and then positioning the LVDTs springs in contact with the small plates (Figure 4.19). If the spring was positioned directly in contact with the soil, it would penetrate due to the initial soft condition of the soil. The sample was just resting on the base. No contact was forced to avoid a friction effect during shrinkage.

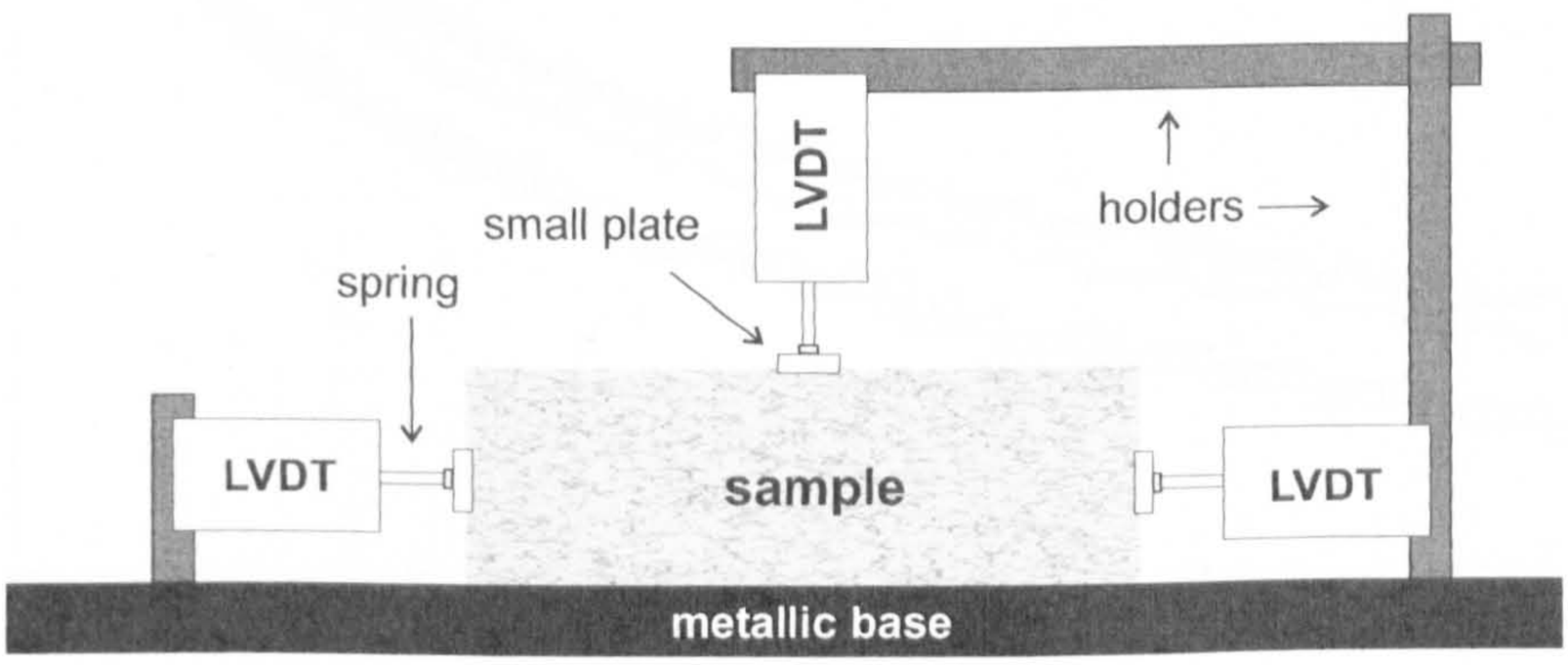

Figure 4.19: Set-up for the shrinkage measurement with LVDTs (sample has a diameter of 10cm and height of 3cm)

Figure 4.20a shows that the evaporation rate is constant for the four samples (Cf1-4) and very similar, between 0.568g/h and 0.582g/h. The SWRCs plotted in Figure 4.20b show a reasonable agreement. The stepping in the curve is due to the resolution of the balance used (0.1g) and small mass variations of the sample (because of the smaller mass of the sample). The variation in water content was less than 2% following the new procedure (for the initial set-up it was higher than 2%).

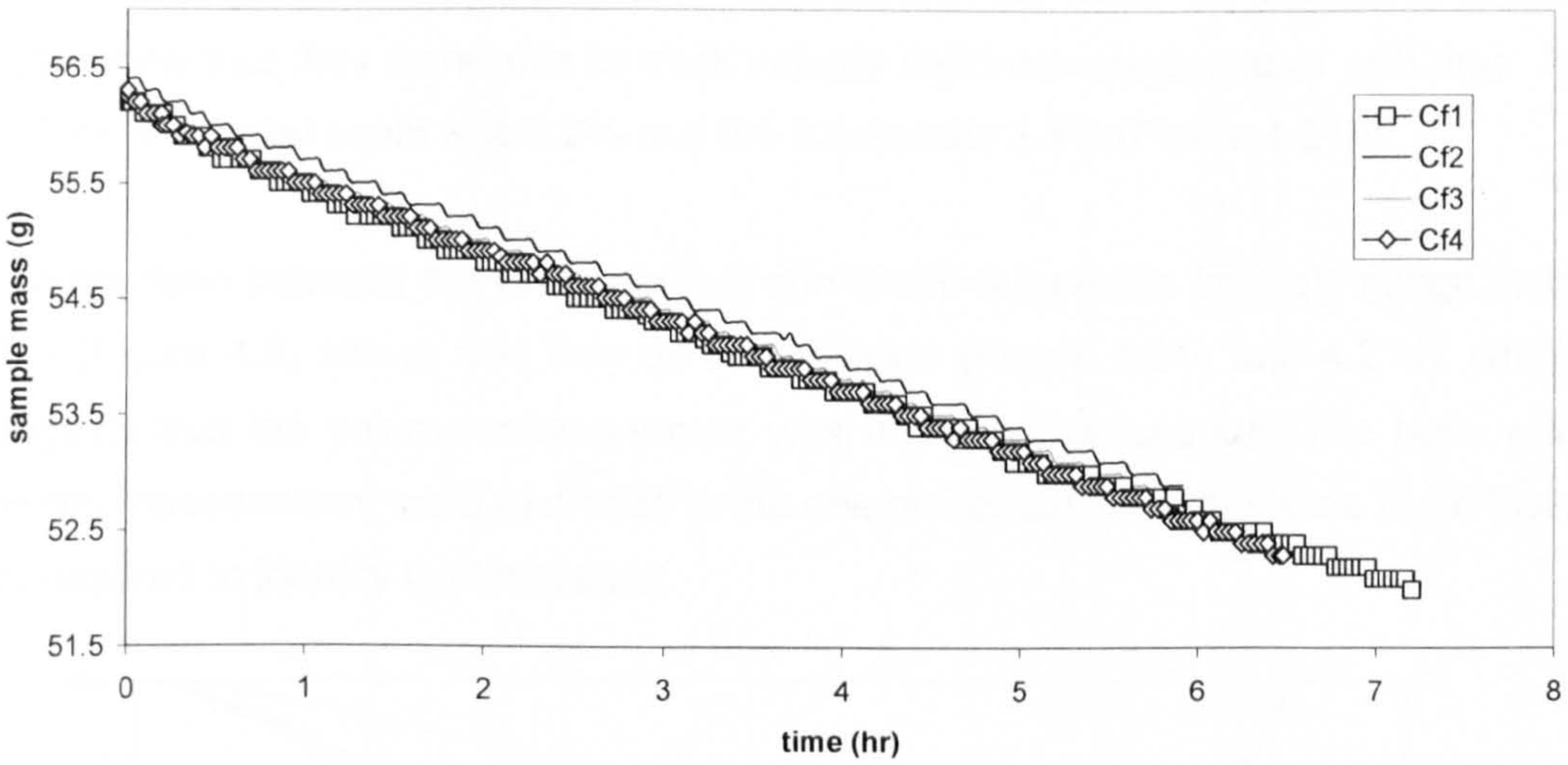

(a)

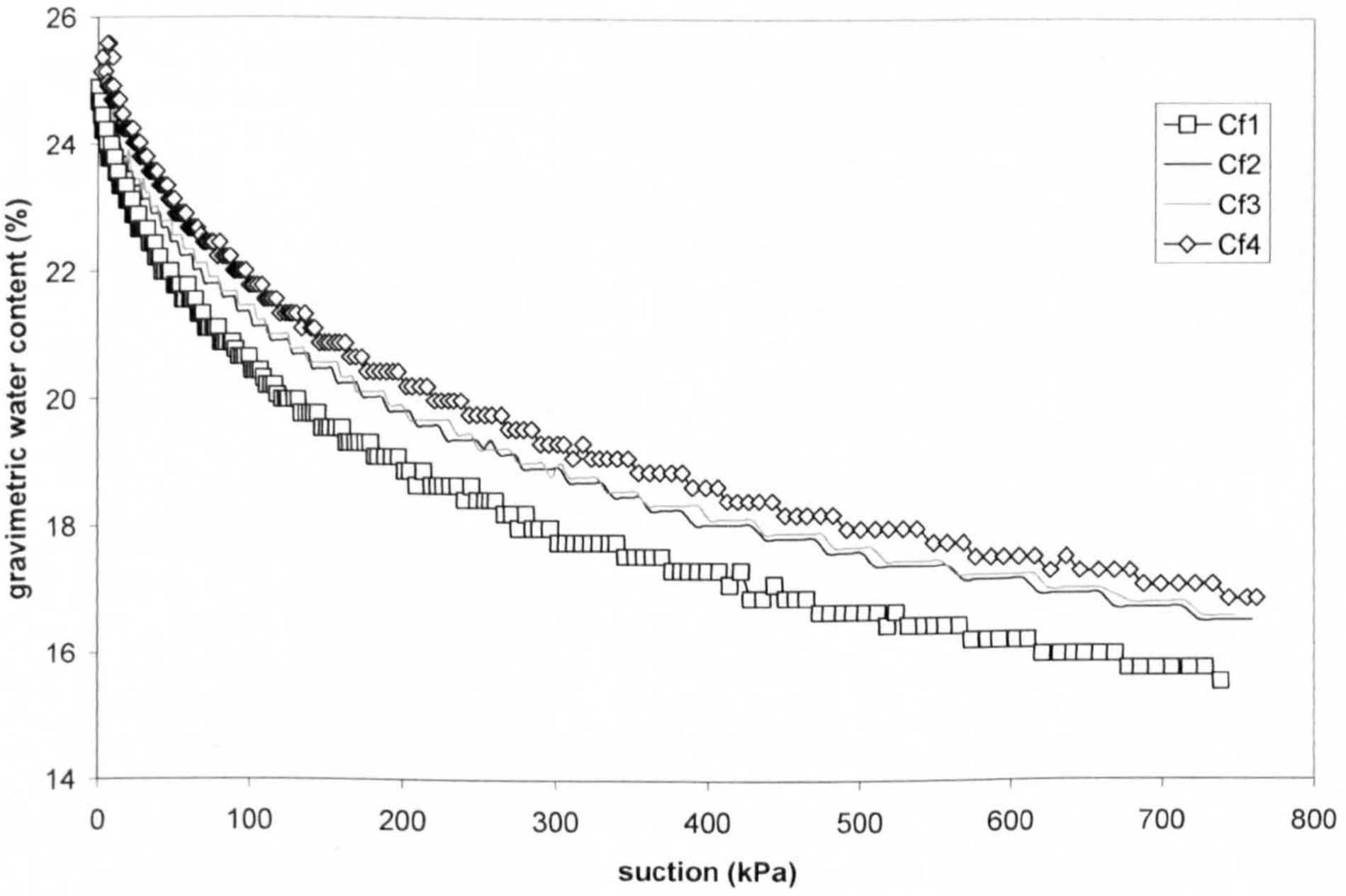

(b)

Figure 4.20: Continuous drying results for the final set-up (tests Cf1 to Cf4, tensiometer III3, BIONICS), (a) evaporation rate, (b) SWRC

Volume change measurements were made on sample Cf5. The results in Figure 4.21a show that they were able to track volume decrease continuously with time. At 800kPa, the radial strain was 3.2% and the axial strain 2.4% (Figure 4.21b).

A comparison between the *Sr-w* and *e-w* curve with the results from shrinkage tests S1-3 (Figure 4.6) shows that they do not coincide (Figure 4.21c and 4.21d), which suggests that the volume measurement was not accurate enough. The tests with volume measurement were restricted to the one presented here, therefore more tests are required to identify the limitations.

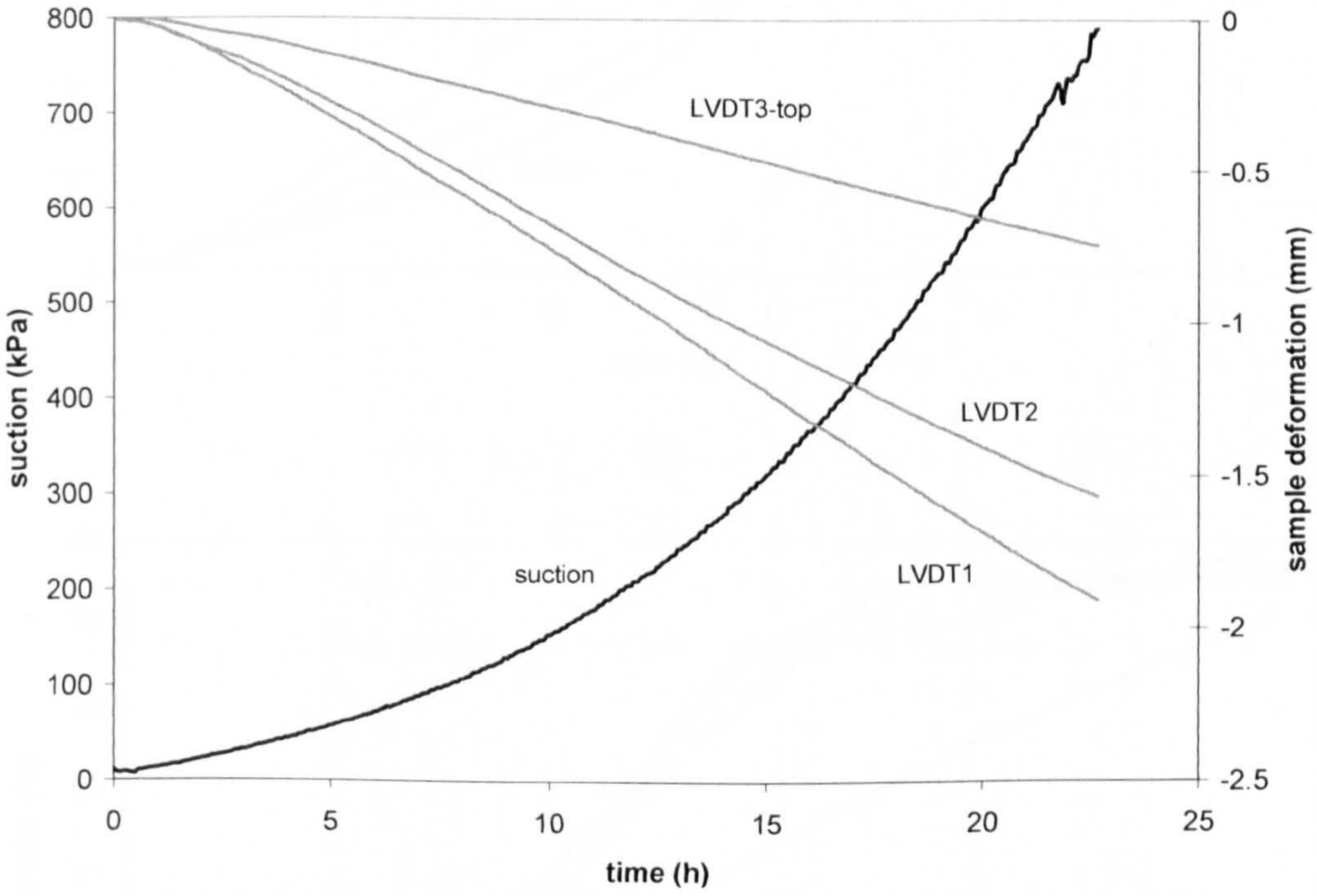

(a)

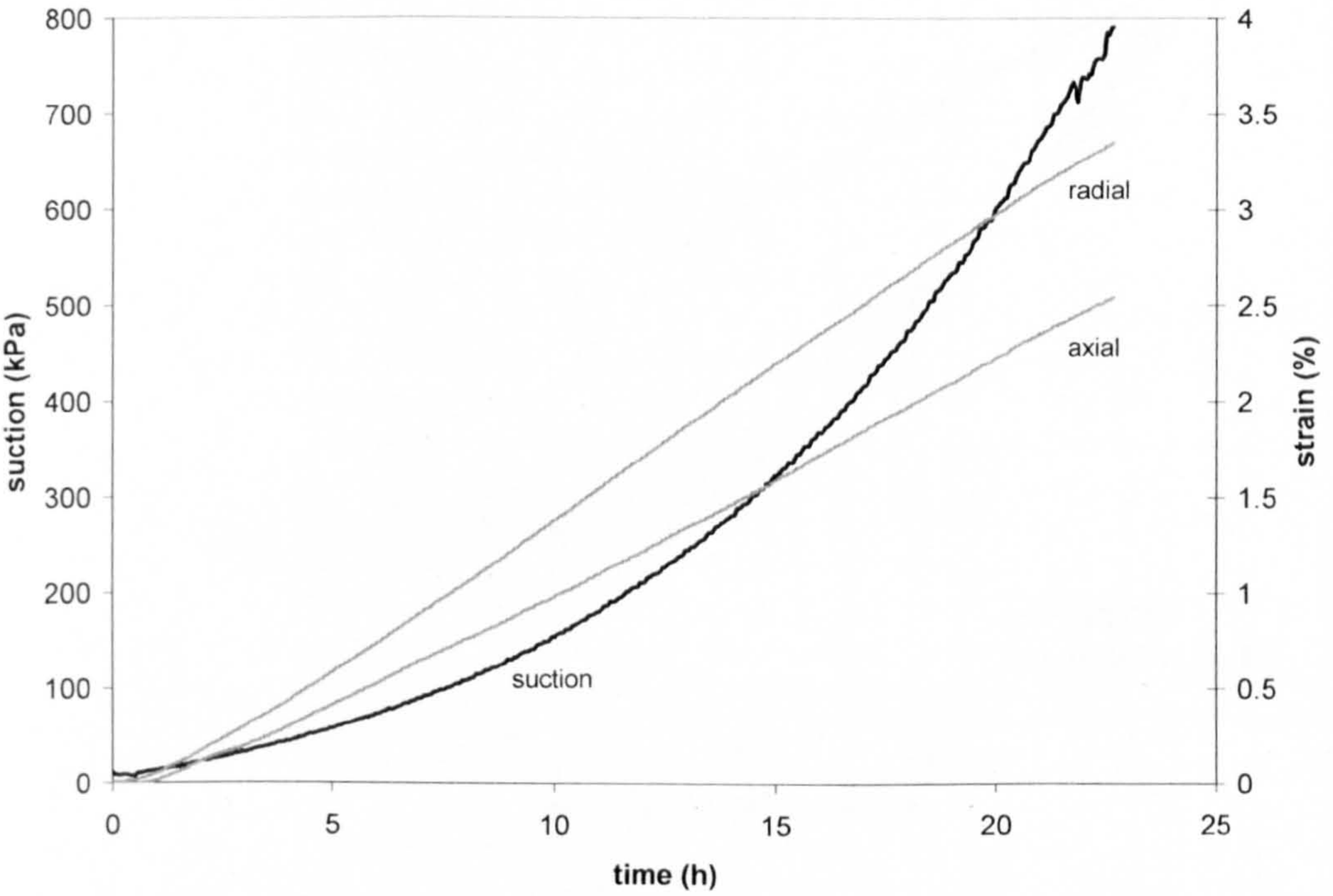
suction (kPa)
strain (%)
time (h)
radial
axial
suction
800
700
600
500
400
300
200
100
0
4
3.5
3
2.5
2
1.5
1
0.5
0
0
5
10
15
20
25

(b)

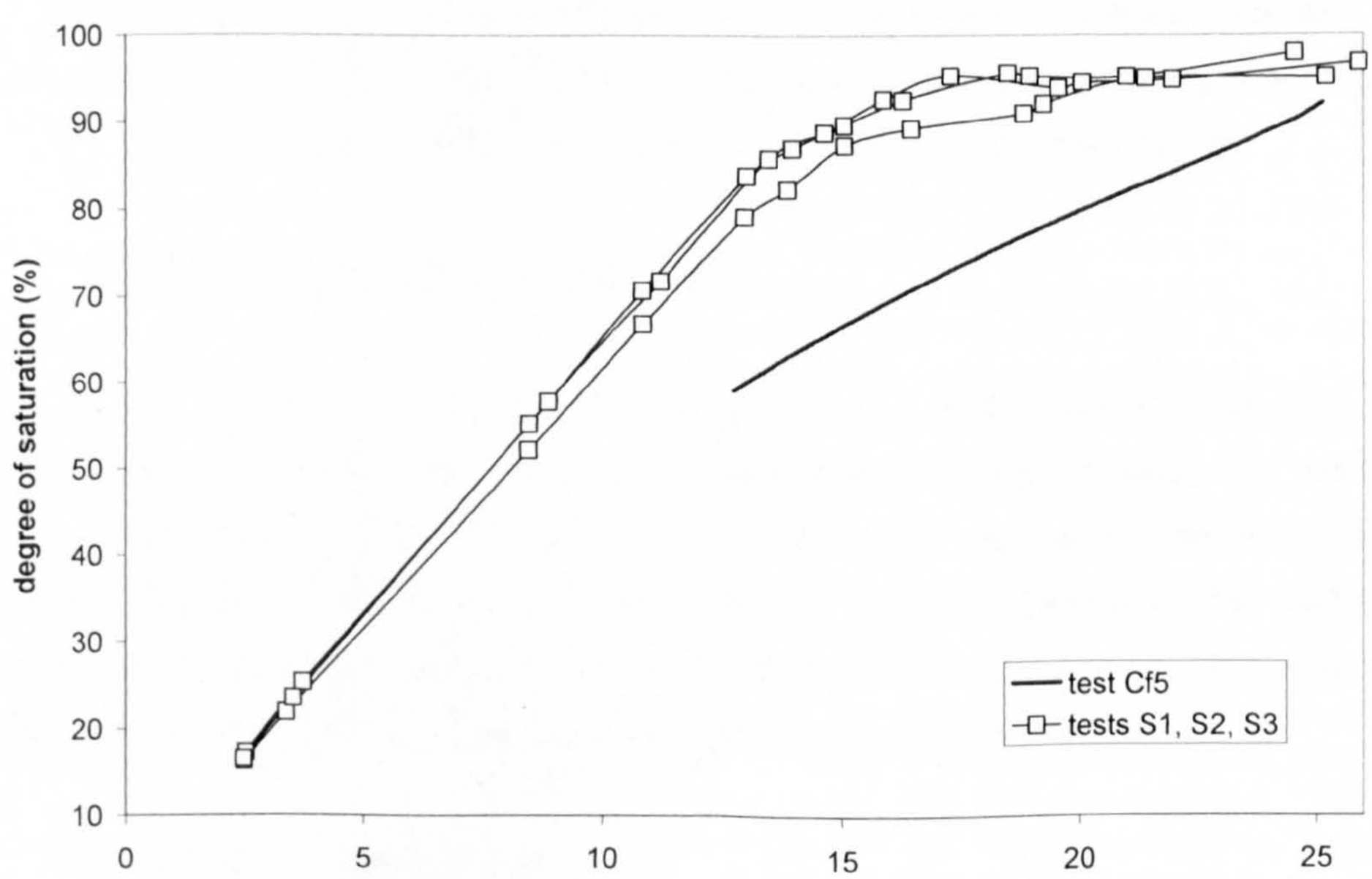
degree of saturation (%)
gravimetric water content (%)
test Cf5
tests S1, S2, S3
100
90
80
70
60
50
40
30
20
10
0
5
10
15
20
25

(c)

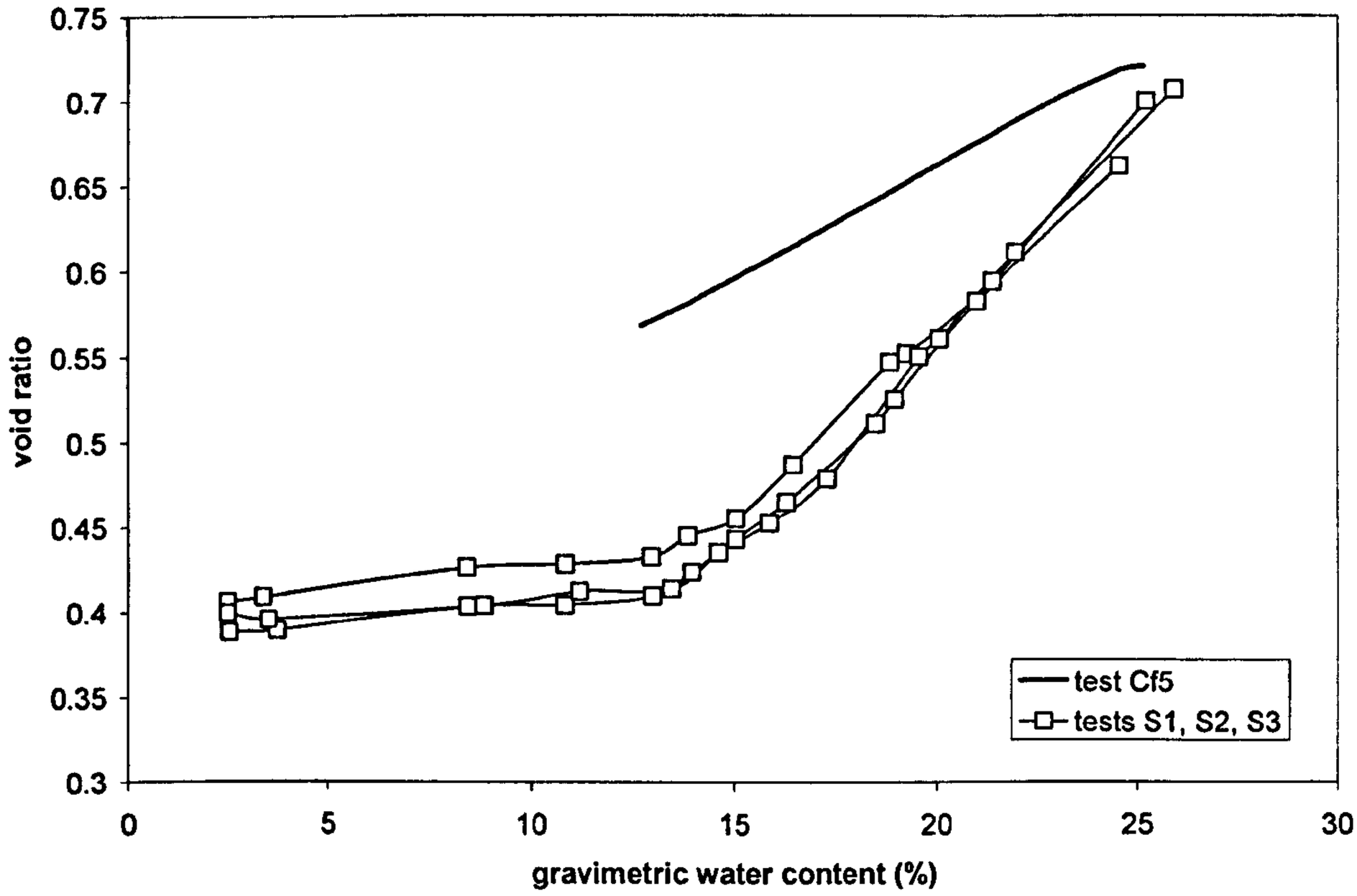

(d)

Figure 4.21: Continuous drying with volume measurement (test Cf5, tensiometer III4, BIONICS), (a) time series, (b) time series with strain data, (c) comparison to the shrinkage limit test of Figure 4.6 in terms of degree of saturation versus gravimetric water content and void ratio versus gravimetric water content in (d)

4.4.2. Discrete drying and wetting

This section presents the technical arrangements to obtain SWRCs following a discrete procedure with high suction tensiometers. Testing followed the same approach as in the continuous procedure: an initial set-up was tested, the limitations identified and a final set-up was proposed and tested again. Details on the wetting procedure and volume measurement are included. With the final set-up, the section ends by presenting drying – wetting cycles conducted on the same sample.

4.4.2.1. Initial set-up

For discrete drying, the SWRC was determined by a sequence of stages of independent drying followed by suction measurement on the same sample. For each drying stage the soil was dried by evaporation. The sample would then be allowed to equilibrate before obtaining suction and sample mass measurements.

The procedure was as follows:

1. Drying: the sample was dried by removing the top plate of the measurement box and allowing the pore water to evaporate to the air for a set period of time. Drying was accelerated by a fan located above the sample;

2. Suction measurement: the top plate was placed back to seal the sample in the cell allowing water redistribution within the soil mass (equalization). The tensiometer was inserted through the bottom plate in contact with the sample and suction was continuously read. A rubber ring with a spring fixed the tensiometer to the box;

3. Mass measurement: after suction became constant indicating equalization, the value of suction was taken and the mass of the sample recorded.

The three stages were repeated until the desired suction or water content level was achieved (or until the tensiometer cavitated). The drying stages were based on the mass measurements, i.e. once the mass had decreased by a certain amount the box was closed to measure suction. At equilibrium conditions (defined in Section 3.5), the value of suction at equilibrium was taken, the mass was measured (the water content was calculated later from the dry mass measured at the end of the test).

Steps 1. to 3. were repeated for a number of data points required to define the entire SWRC. Three tests were carried out following this procedure. The details can be found in Table 4.2 (*D* in the labelling stands for discrete procedure).

Table 4.2: Testing program for the initial set-up of the discrete drying tests

Test no.	e_i	w_i [%]	w_f [%]	ΔM_w [g]	s_{max} [kPa]	Δt [h]
Di1	0.59	24.35	16.88	29.3	568.6	148.8
Di2	0.55	24.80	17.76	33.5	485.5	114.5
Di3	0.54	25.25	14.70	42.5	995.0	171.9

e_i initial void ratio, w_i initial water content, w_f final water content, ΔM_w mass of water evaporated, s_{max} maximum suction measured, Δt test duration

The entire test sequence for the definition of the SWRC by using discrete drying is shown in Figure 4.22a, which includes information of both gravimetric water content and suction for each of the nine drying stages. As expected, the suction equalizes at increasing values (pore water pressure decreases) as the gravimetric water content decreases.

The SWRCs for the three tests are shown in Figure 4.22b. The difference of water content between the two curves furthest apart is less than 2%.

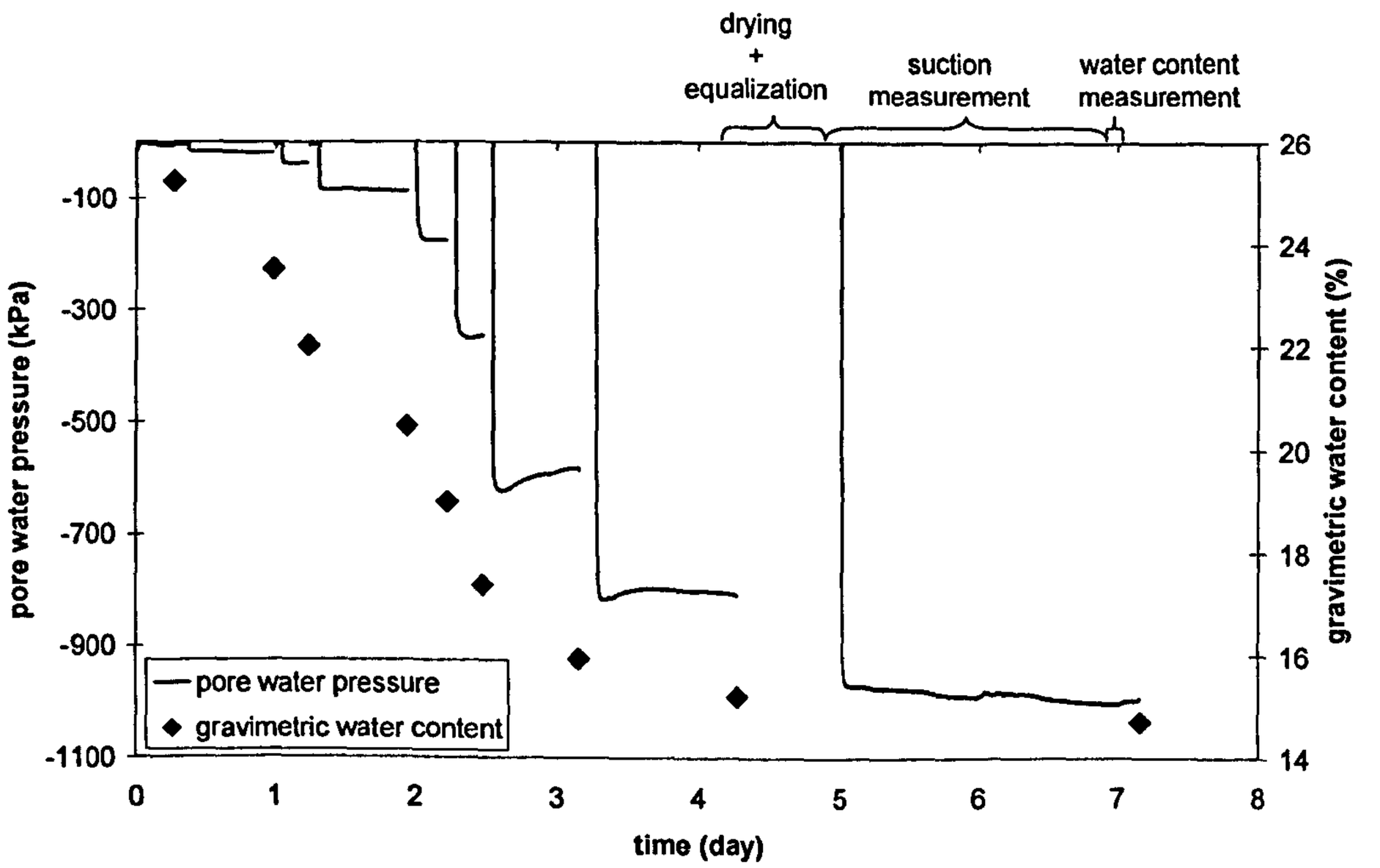

(a)

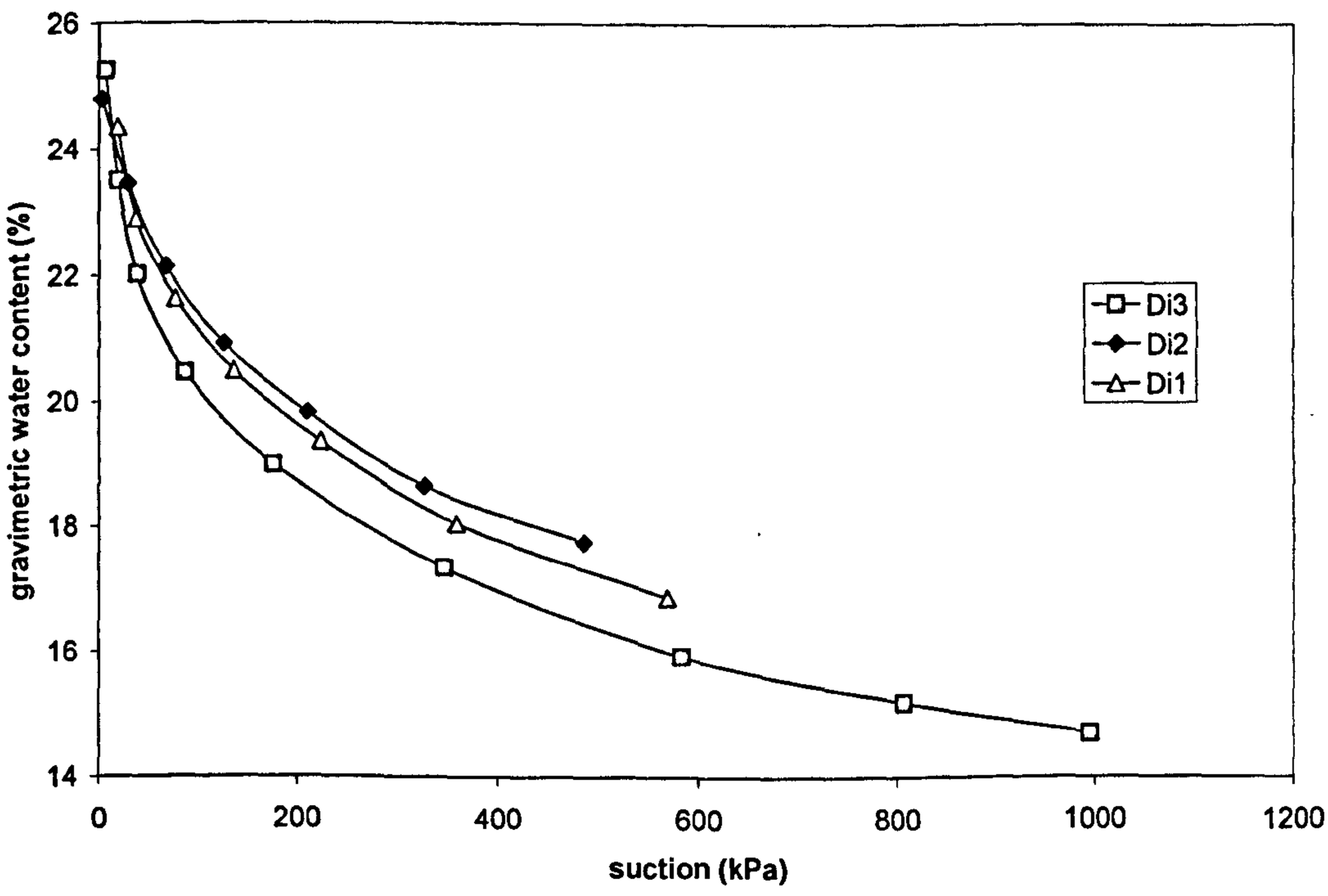

(b)

Figure 4.22: Discrete drying test for the initial set-up, (a) time sequence for test Di3 (tensiometer II2, BIONICS), (b) SWRC for the three tests (Di1 to DI3, tensiometer II1, II2, BIONICS)

4.4.2.2. Final set-up

In order to include volume measurements, the discrete drying procedure was repeated for 4 new samples (Df1-4) with a void ratio of approximately 0.74 and initial water content between 23.2% – 26.3% (Table 4.3). As stated previously, the new samples are smaller to allow volume measurement in the porometer. The procedure consisted in a sequence of four stages (one more stage than before), (1) drying (no fan was used), (2) suction measurement, (3) mass measurement and (4) volume measurement (in this order). Stage (4) was not done for all samples. The four stages were repeated until the desired suction or water content level was reached (or until the tensiometer cavitated). At equilibrium, the value of suction was taken, the water content was calculated from the mass measurements (and final dry mass) and the degree of saturation calculated from the volume measurements.

Table 4.3: Testing program for the final set-up discrete drying tests

Test no.	V_i [cm^3]	e_i	w_i [%]	S_{ri} [%]	w_f [%]	ΔM_w [g]	s_{max} [kPa]
Df1	-	0.75	26.25	92.50	16.55	4.30	660
Df2	29.44	0.74	26.31	94.96	15.14	4.53	865
Df3	-	-	23.23	-	16.84	2.89	703
Df4	-	-	24.53	-	15.85	3.91	867

V_i initial volume, e_i initial void ratio, w_i initial water content, w_f final water content, ΔM_w mass of water evaporated, s_{max} maximum suction measured

The drying paths based on gravimetric water content for the three tests are shown in Figure 4.23. The four curves agree well with an error in the water content of the order of 1.5%.

The same sequence was applied to the wetting tests except that the sample was wetted by placing it in a container fitted with the humidifier (as presented in the equipment section previously).

The volume measurement was done by inserting the sample in the porometer reservoir and filling it with mercury. The volume of the sample was taken once a mercury bubble appeared at an orifice in the top lid. The measurement was repeated three times (the difference was within ±0.01cm ^{3}).

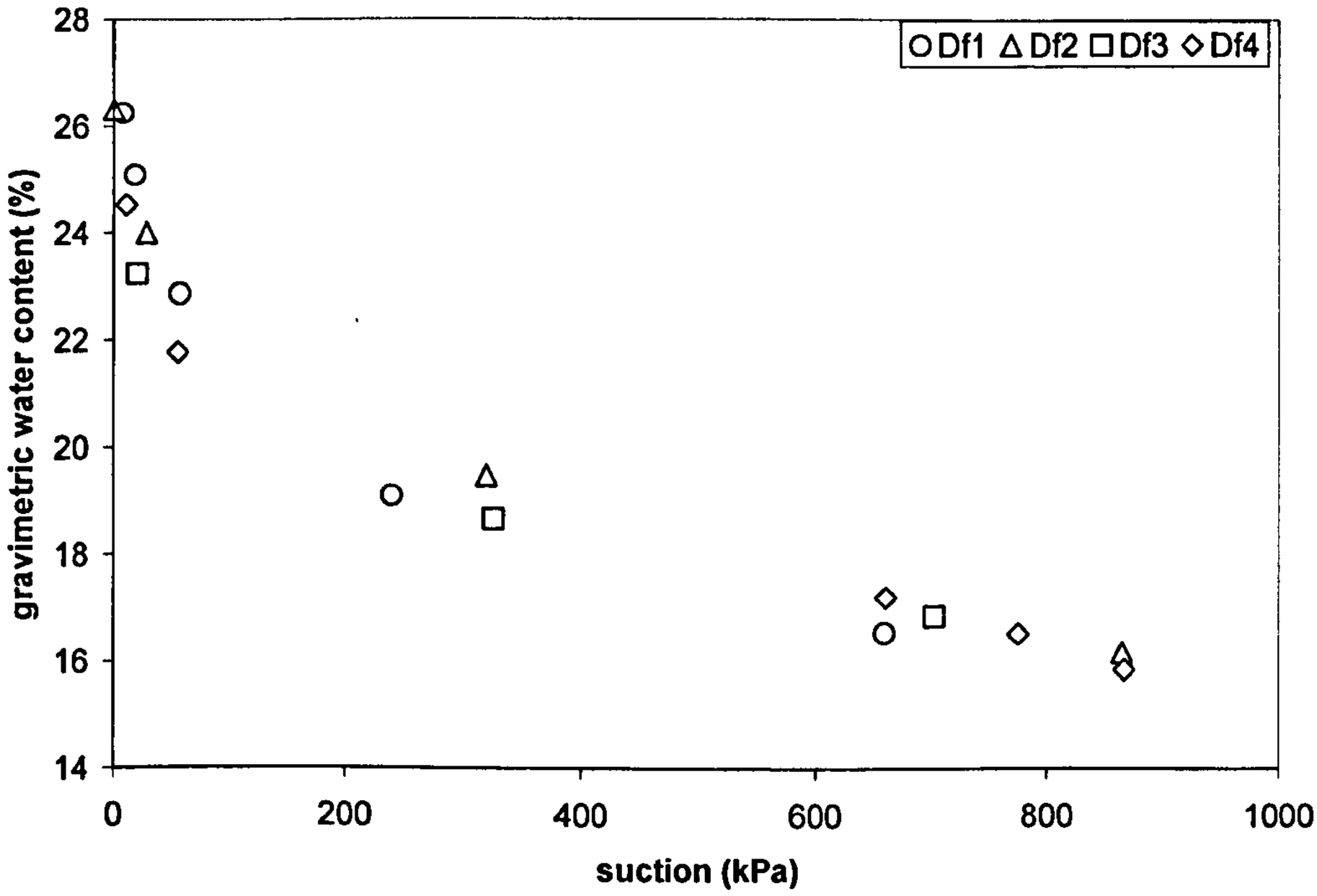

Figure 4.23: SWRC by the discrete drying procedure for the final set-up (tests Df1 to Df4, tensiometer III4, BIONICS)

A wetting path was conducted in sample Df2 and is shown in terms of gravimetric water content versus suction in Figure 4.24a, volumetric water content versus suction in Figure 4.24b and degree of saturation in Figure 4.24c. All figures show hysteresis of the gravimetric and volumetric water content and degree of saturation component with the wetting path positioned below the drying path.

The degree of saturation data should be considered with care since the volume measurements are not accurate enough. It was initially thought that the reason lay in the porometer, but it was later realised that the problem seemed to be linked to the volume changes induced by forcing the tensiometer into the soil. A small depression formed and grew in size with the sequence of measurements.

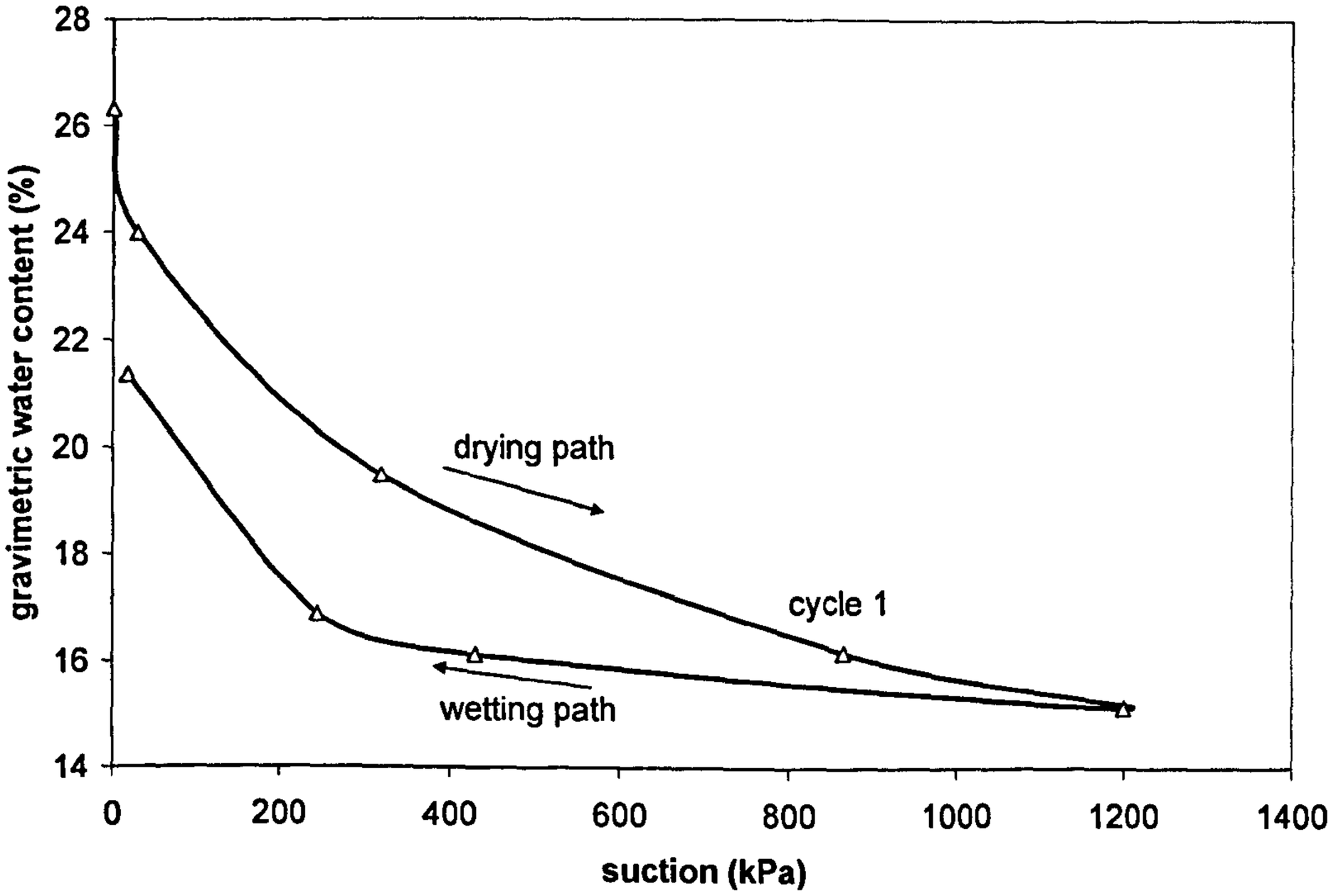
28
26
24
22
20
18
16
14
gravimetric water content (%)
drying path
cycle 1
wetting path
0
200
400
600
800
1000
1200
1400
suction (kPa)

(a)

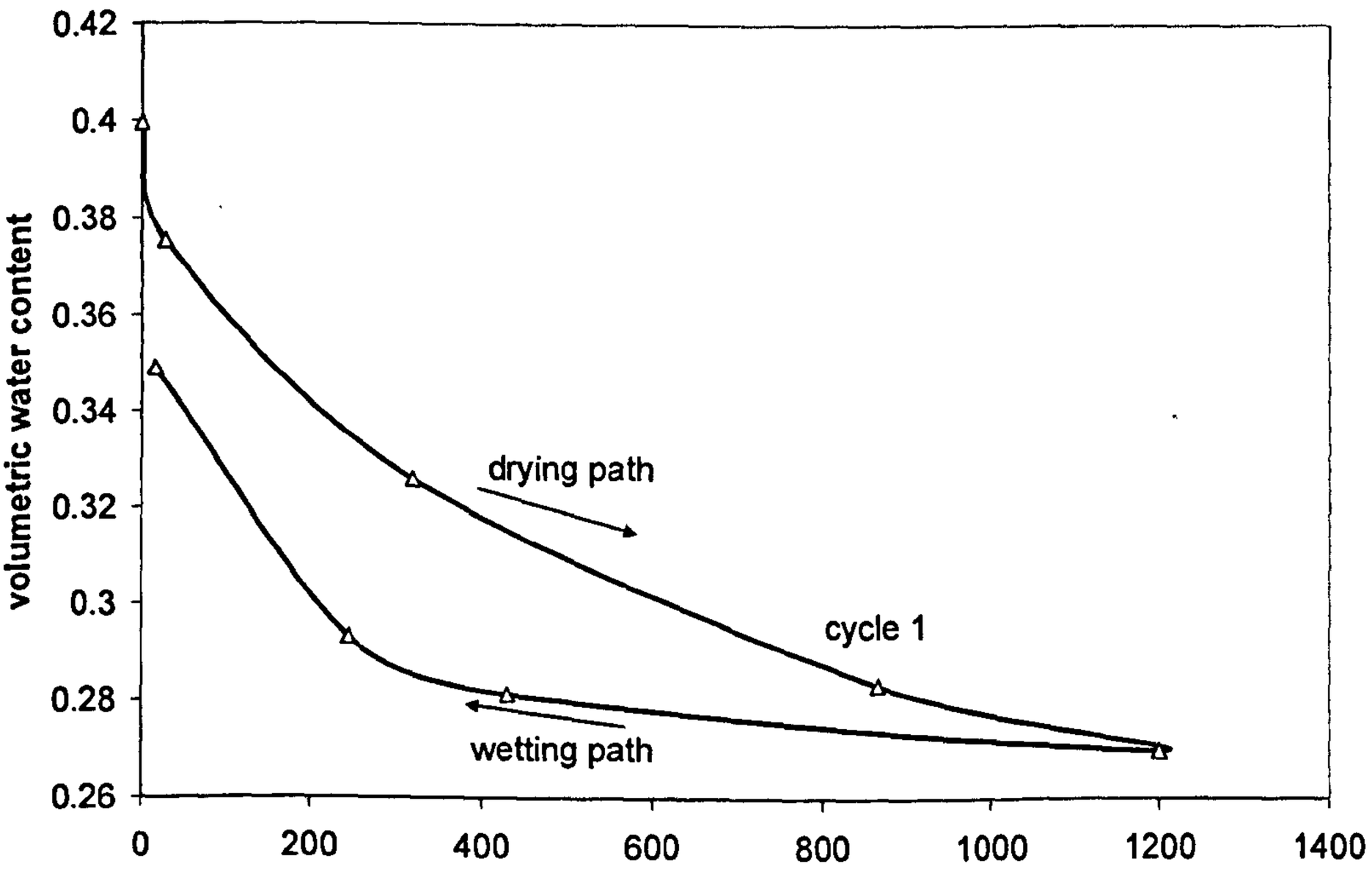
0.42
0.4
0.38
0.36
0.34
0.32
0.3
0.28
0.26
volumetric water content
drying path
cycle 1
wetting path
0
200
400
600
800
1000
1200
1400
suction (kPa)

(b)

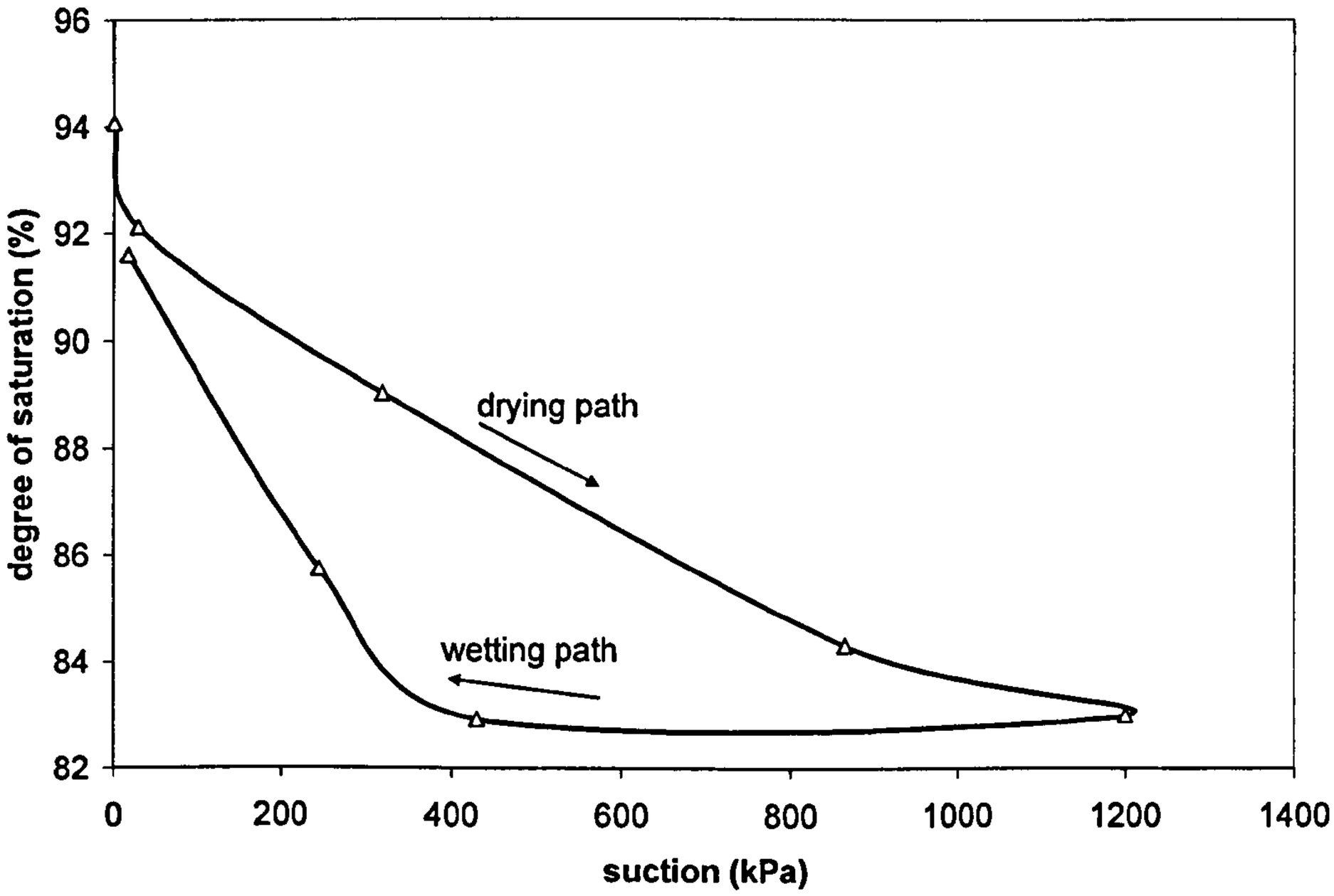

(c)

Figure 4.24: Discrete drying and wetting results for sample Df2 (tensiometer III4, BIONICS), (a) gravimetric water content versus suction, (b) volumetric water content versus suction, (c) degree of saturation versus suction

The drying-wetting cycle of Df2 was further analyzed by comparing to the shrinkage curves of Figure 4.6. Figure 4.25 shows a reasonable agreement between the 2 set of tests in terms of void ratio and degree of saturation versus gravimetric water content.

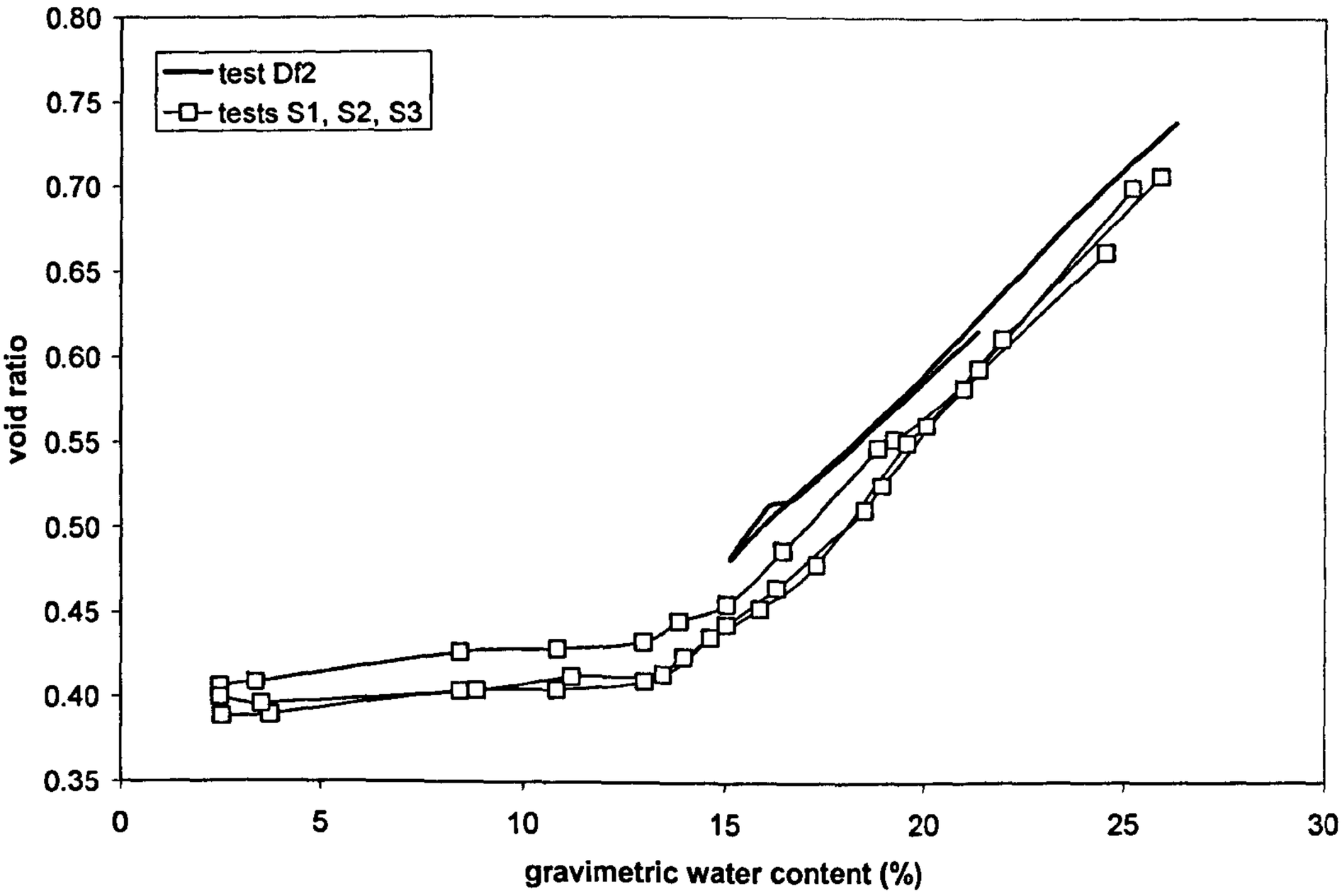

(a)

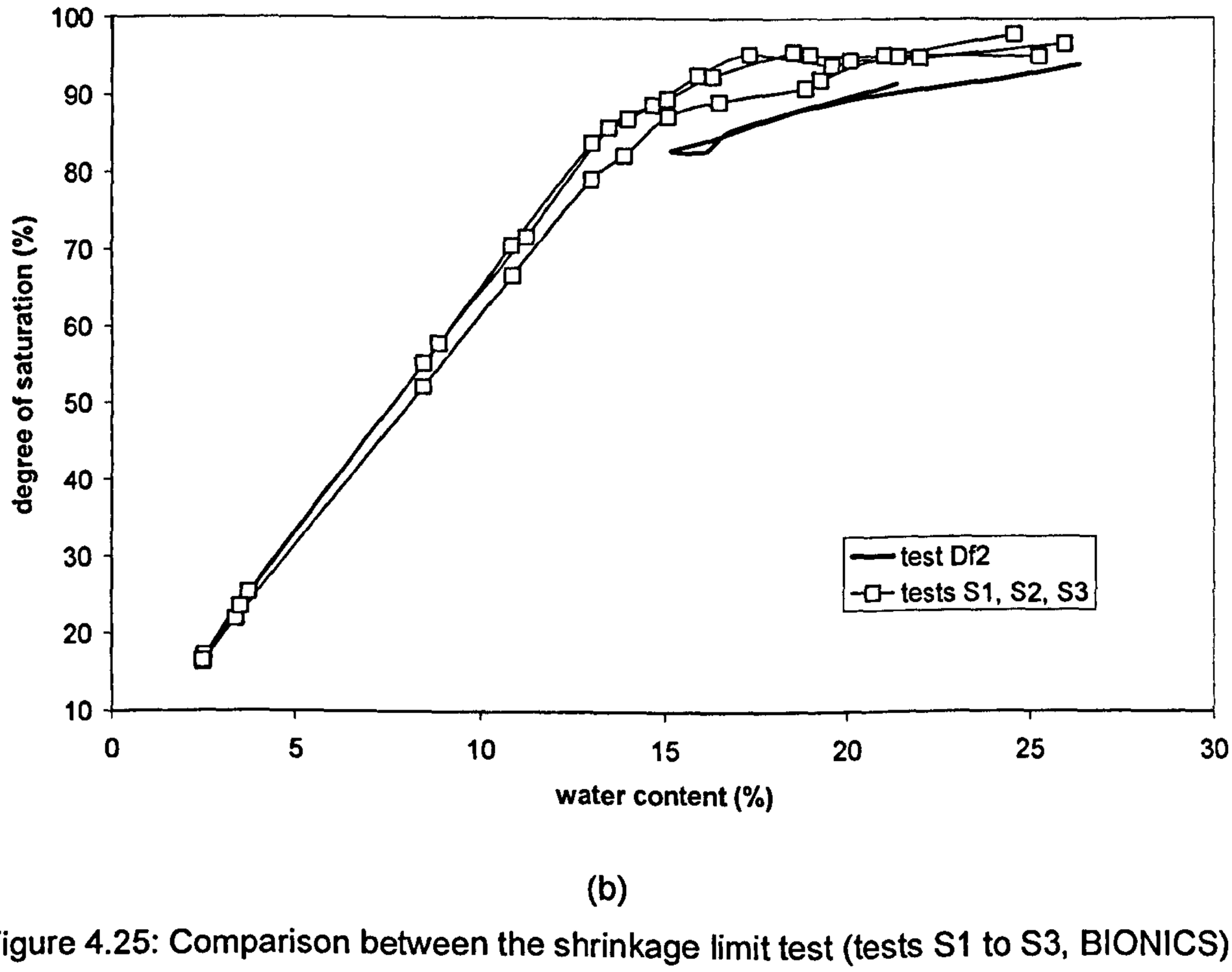

(b)

Figure 4.25: Comparison between the shrinkage limit test (tests S1 to S3, BIONICS) and Df2 (tensiometer III4, BIONICS)

The discrete procedure for the proposed final set-up was employed for several drying-wetting cycles on the same sample. Test Df2 proceeded by performing another two drying-wetting cycles on the same sample (in Figure 4.26), and another three cycles in sample Df3 (in Figure 4.27).

All figures from 4.26 and 4.27 show that it was possible to run a series of cycles of drying and wetting sequences using the discrete procedure. All graphs show a similar trend between the volumetric and gravimetric water content. Volumetric water content variations are within 0.26 and 0.4 (Figure 4.26b) and gravimetric water contents between 26% and 17% for a suction increase up to 900kPa (Figure 4.26a and 4.27). Hysteresis was also clearly visible in all cycles.

Figure 4.26c was the only to show differently shaped curves, the last point of drying curve for cycle 3 is unrealistically high. It shows a difference to cycle 1 and 2 in the order of 4%. The most likely reason is, as discussed previously, an erroneous volume measurement. The reversal of Cycle 2 in Figure 4.27 at approximately 780kPa is due to accidental drying of the sample. The curve should have continued until near 900kPa.

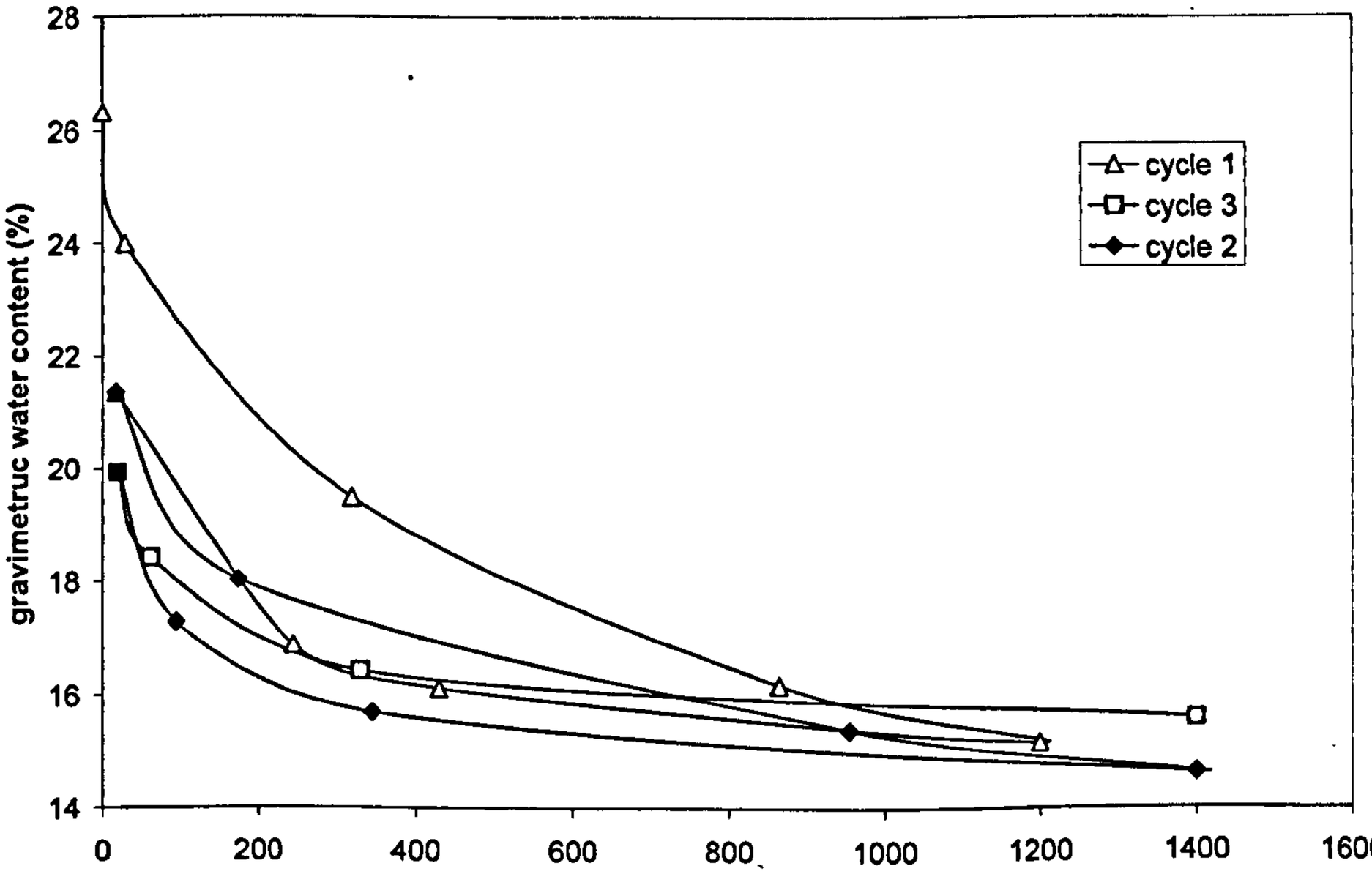

(a)

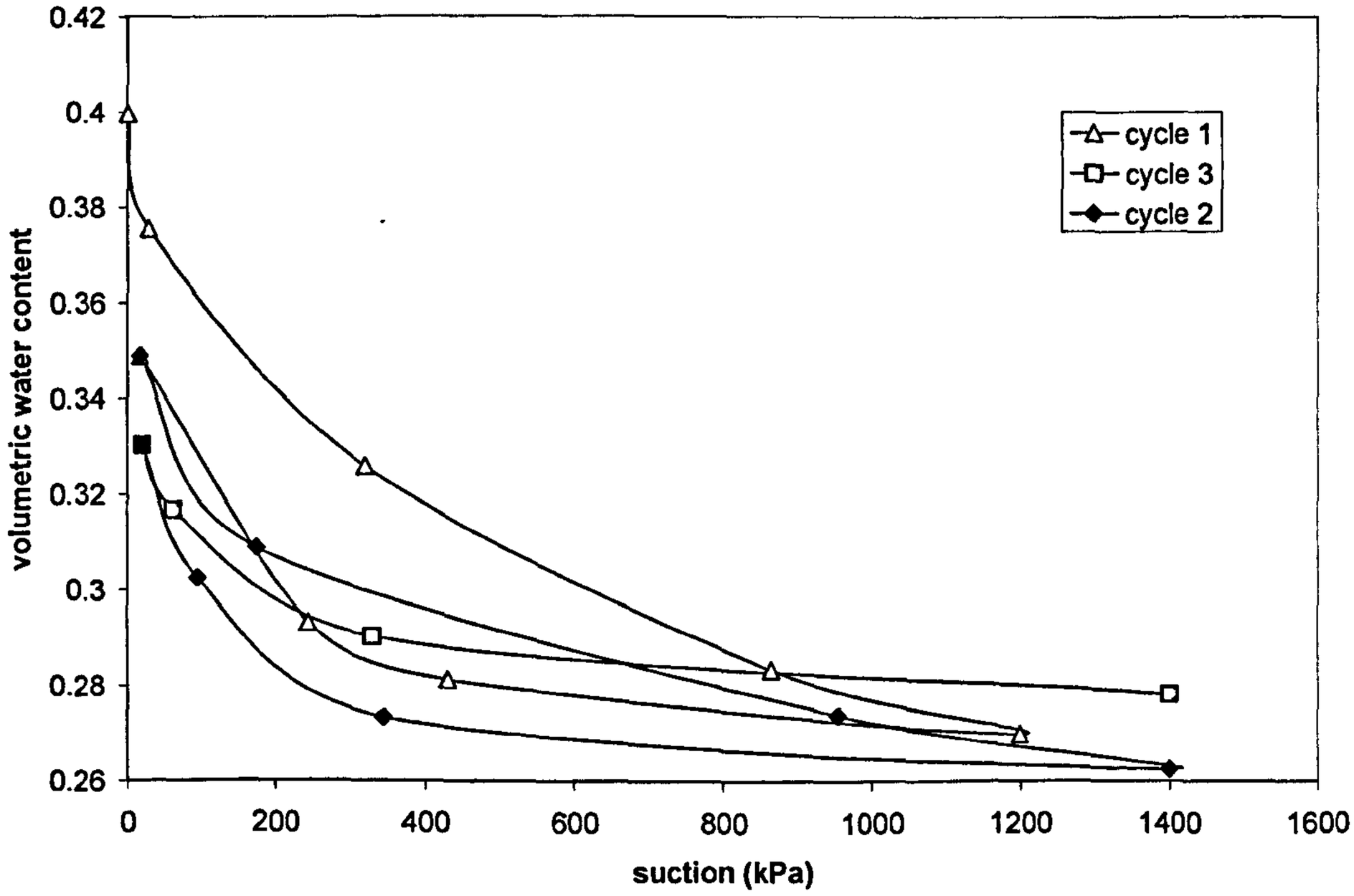
0.42
0.4
0.38
0.36
0.34
0.32
0.3
0.28
0.26
volumetric water content
0
200
400
600
800
1000
1200
1400
1600
suction (kPa)
cycle 1
cycle 3
cycle 2

(b)

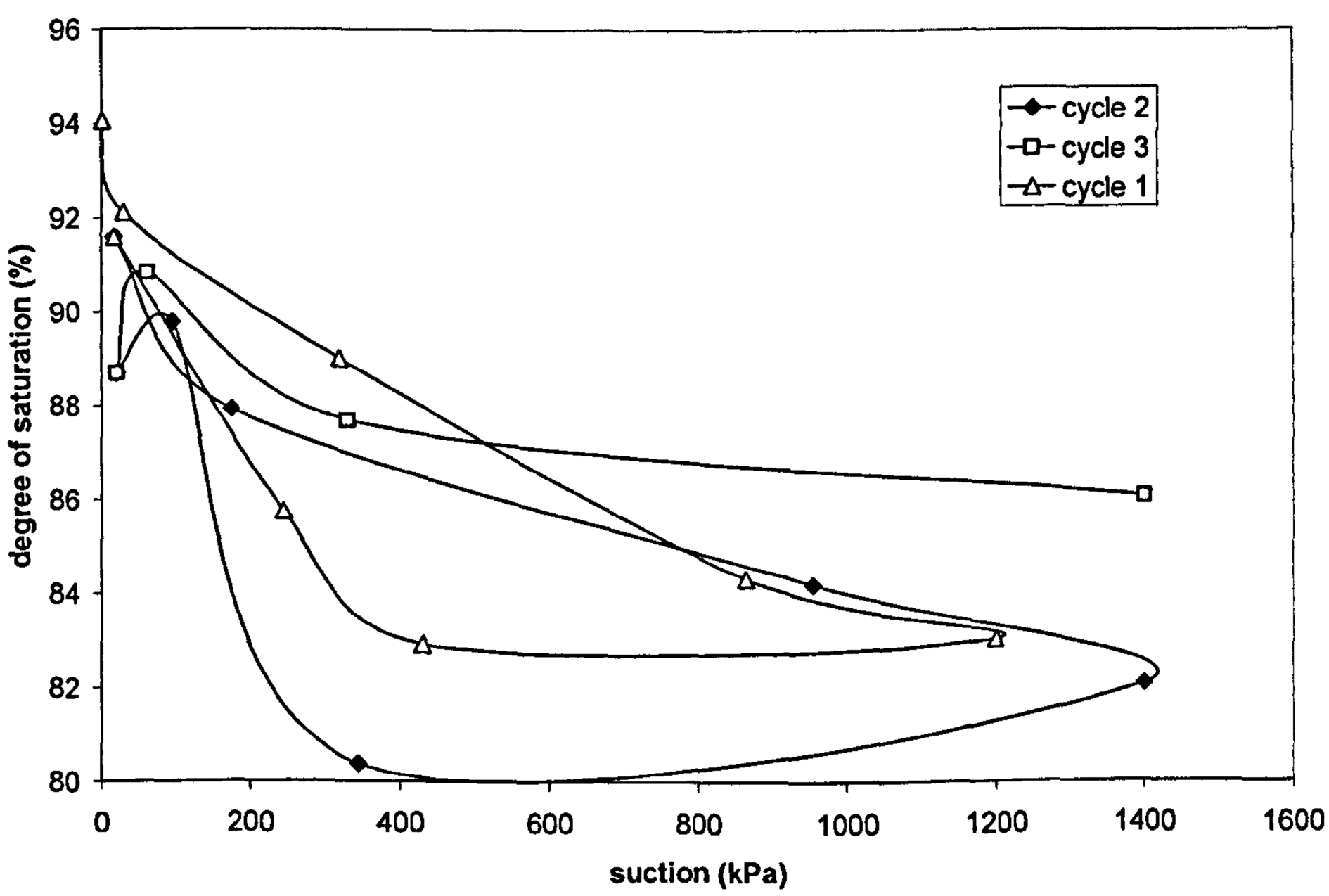
96
94
92
90
88
86
84
82
80
degree of saturation (%)
0
200
400
600
800
1000
1200
1400
1600
suction (kPa)
cycle 2
cycle 3
cycle 1

(c)

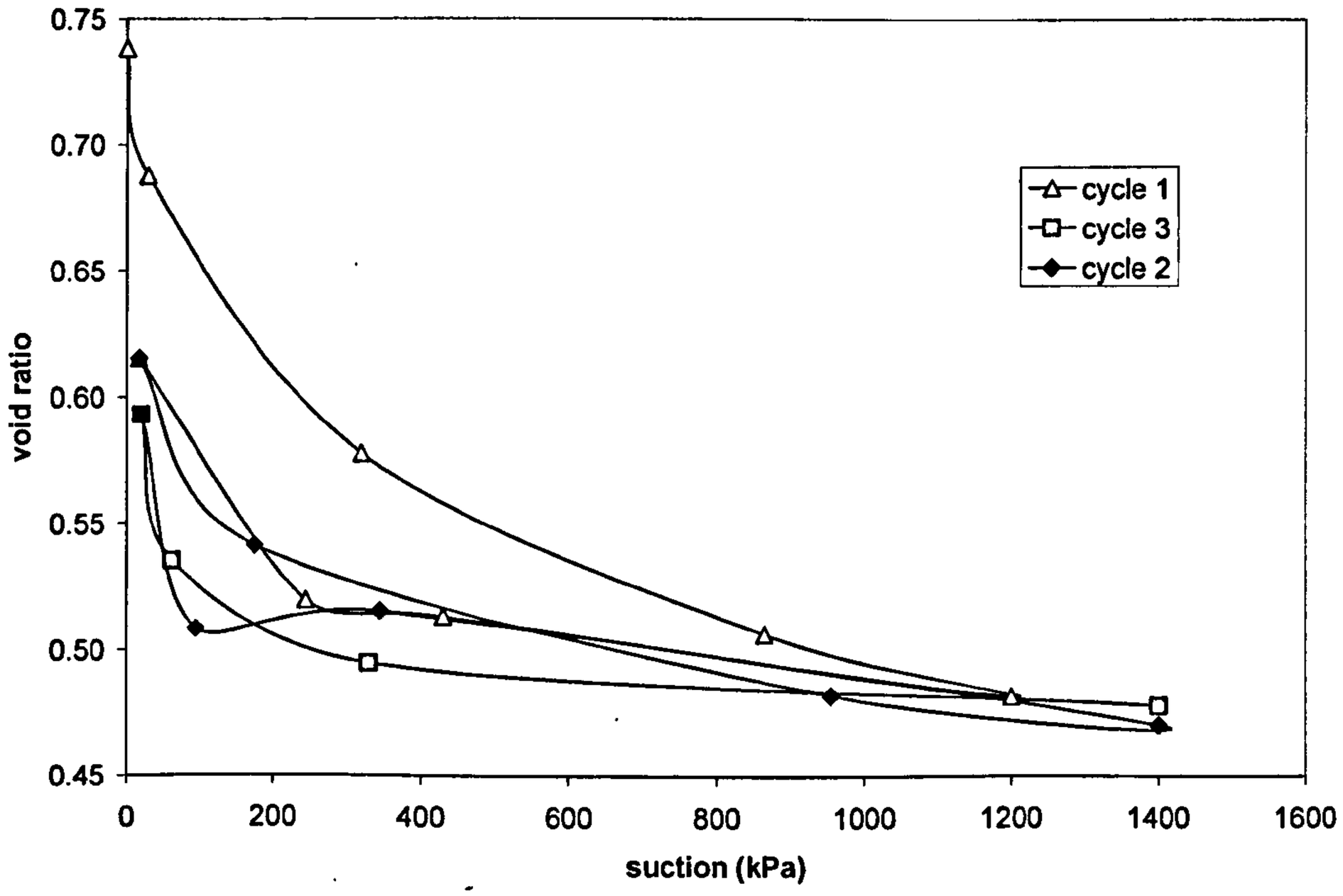

(d)

Figure 4.26: Suction cycles for sample Df2 (tensiometer III4, BIONICS), (a) water content versus suction, (b) volumetric water content versus suction, (c) degree of saturation versus suction, (d) void ratio versus suction

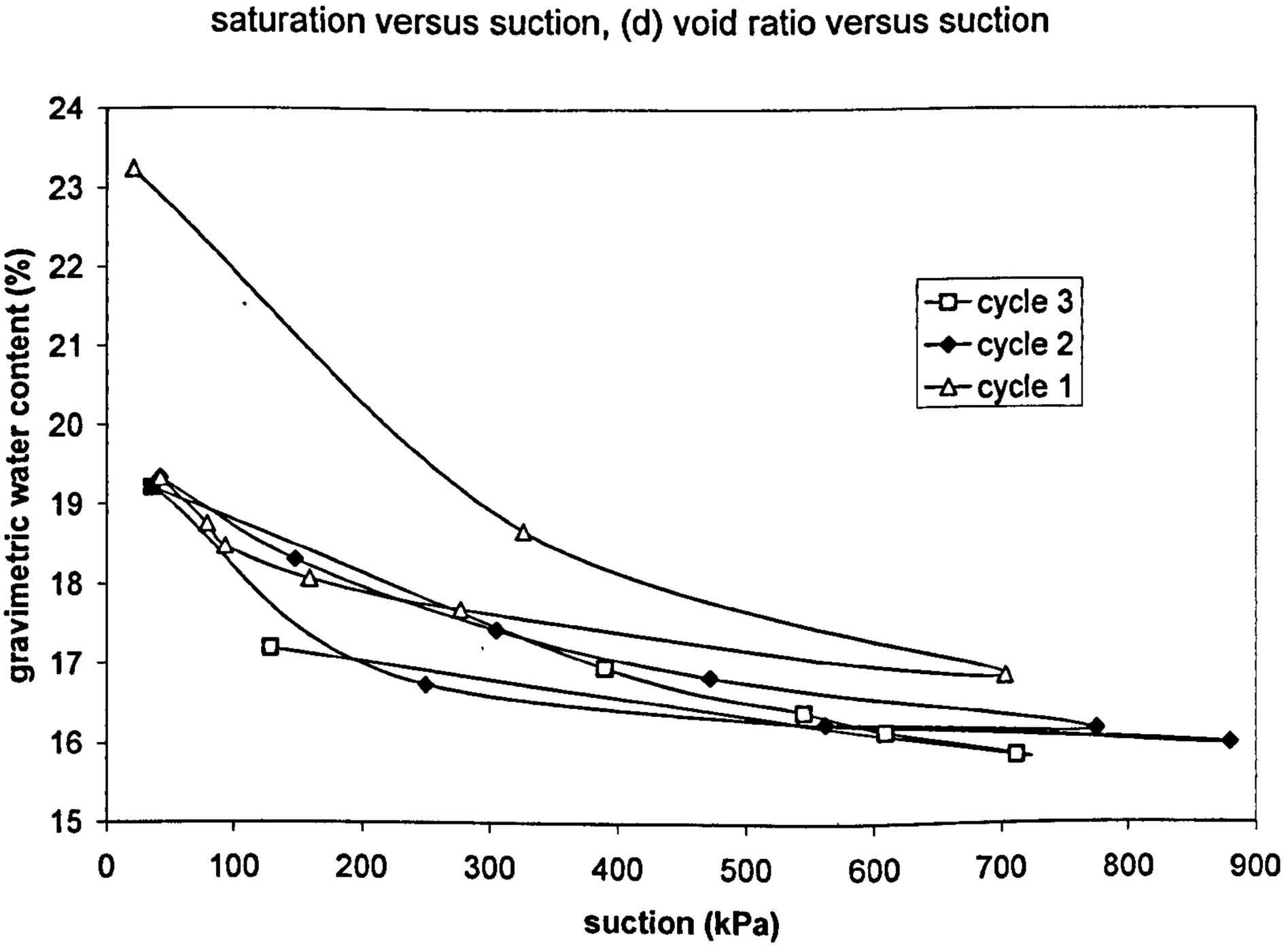

Figure 4.27: Suction cycles for sample Df3 (tensiometer III4, BIONICS)

4.4.3. Pressure plate test

A pressure plate test (test PP) was conducted on a compacted sample with a void ratio of 0.73 and water content of 25.68% (comparable to tests Cf1-4 and Df2-3). Maximum suction was limited to 500kPa due to the air entry value (AEV) of the stone (5bar). Equalization was assumed based on mass readings by regular weighing of the sample. The test was carried out over a period of 7 weeks.

4.5. DISCUSSION

In this section the continuous and discrete procedures are compared and validated against the pressure plate. Section 4.6.3 also presents a characterization of the suction-hydraulic-volumetric behaviour of BIONICS soil that has been used for testing throughout the chapter.

4.5.1. Validation and procedure selection

The analysis of Tables 4.1, 4.2, 4.3, in terms of test completion time indicate that the tests using continuous drying (average duration of 25h for the 235cm^3 samples and 6h for the 30cm^3 samples) were about five times faster than the tests using discrete drying (test duration between 114 and 171h depending on maximum suction), which makes the continuous technique very attractive in terms of time economy.

Figure 4.28 compares both procedures for the initial set-ups. It can be observed that the continuous drying curves appear slightly displaced upwards, which means that suction was higher for the same water content. This could be explained by the fast drying rate to which the soil was exposed, generating an unequal distribution of water content through the sample, and the cable effect on the mass measurements.

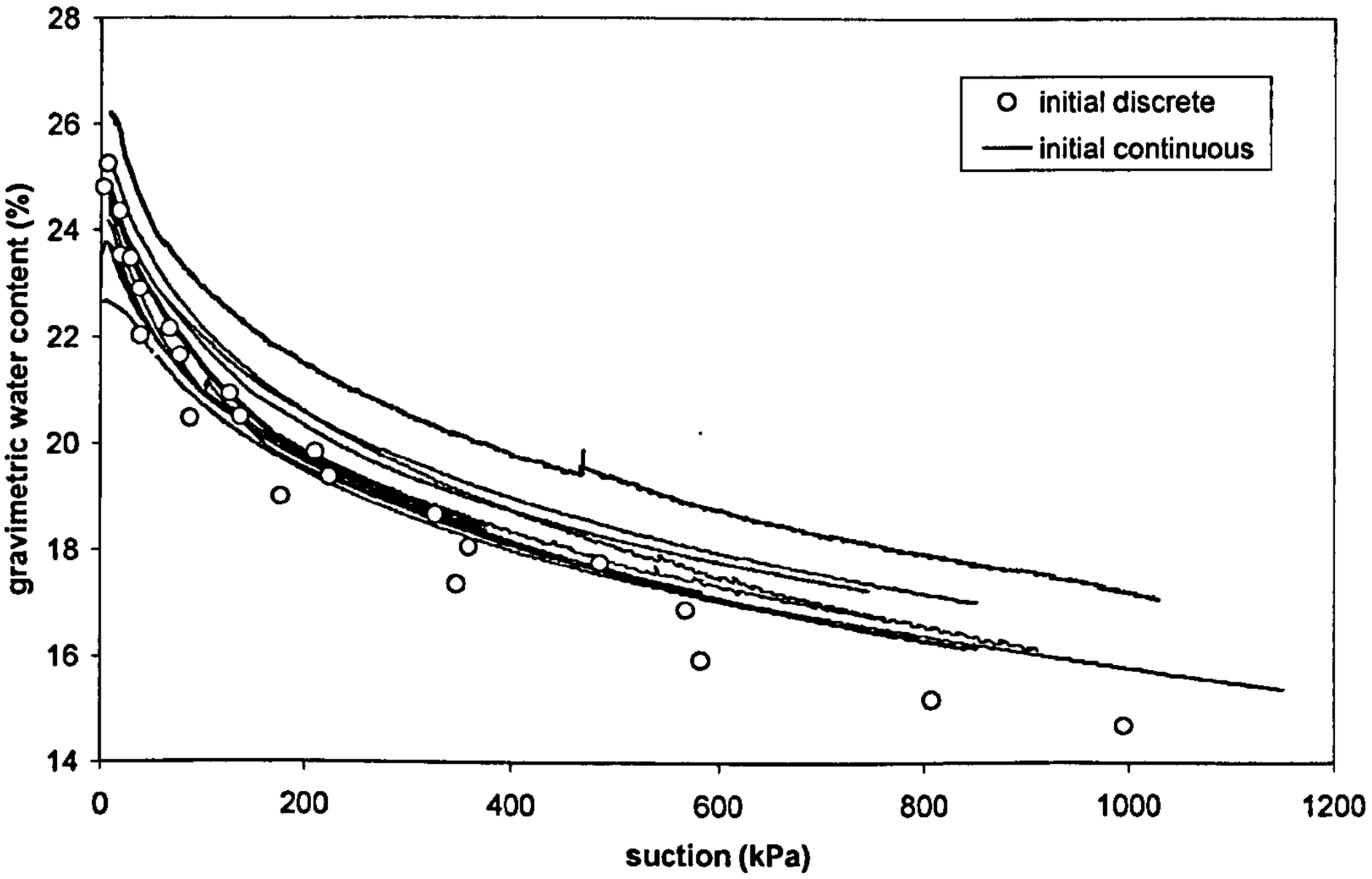

Figure 4.28: Comparison between all drying tests for the initial set-up (tests Ci1 to Ci19 and Di1 to Di 3, tensiometers II2, III1, III4, BIONICS)

The discrete and continuous drying curves for the final set-up curves are compared in Figure 4.29. The two sets of curves show a similar pattern as in Figure 4.28 and are also in better agreement with each other. The error decreased from 3% (Figure 4.28) to 2% in Figure 4.29. Another difference is that the two groups of curves appear differently positioned. For the initial set-up the continuous drying curves are above the discrete drying curves while the opposite happens for the final set-up. This variation could be related to the adoption of the new procedures (no cable used and larger exposed surface area to drying).

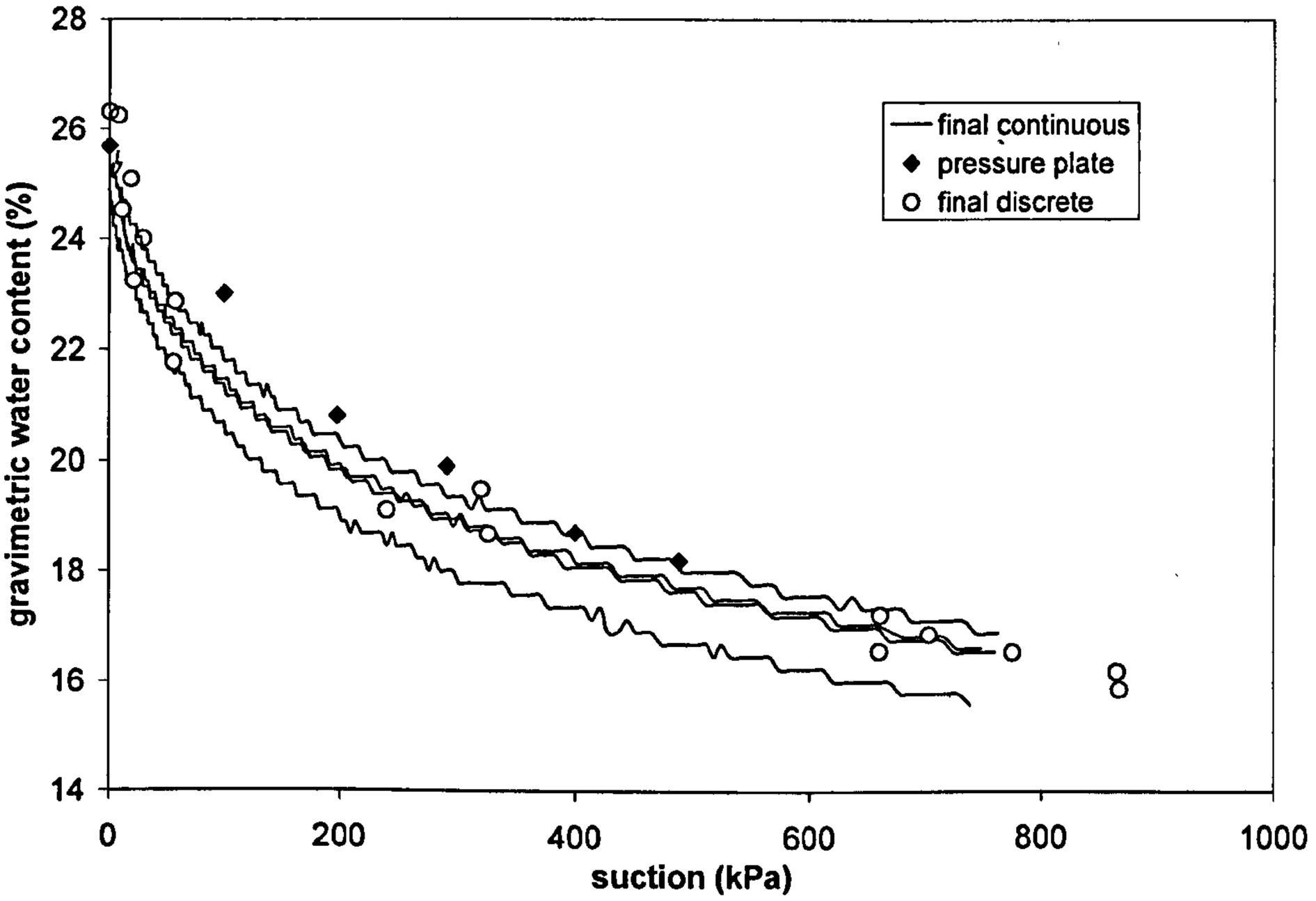

Figure 4.29: Comparison between all drying tests for the final set-up data (tests Cf1 to Cf4 and Df1 to Df4, tensiometer III3, III4, BIONICS)

The tensiometer technique, following both discrete and continuous drying procedures, was validated against the pressure plate technique. The three sets of curves (discrete, continuous and pressure plate) in Figure 4.29, are in general agreement with each other except the pressure plate appears positioned above the discrete and continuous procedure, especially for suctions between 100kPa and 300kPa, although at higher suctions all points tend to converge. No comparison is possible between the pressure plate and initial set-up curves due to difference of void ratio (initial set-up tests have a void ratio within 0.55 and the pressure plate is 0.73).

Teixeira and Marinho (2006) also made a comparison between the discrete drying procedure and pressure plate for a sandy silt of low plasticity (Figure 4.30). Two samples (Am 1 and Am 4) were tested with a high suction tensiometer up to a suction of 500kPa. The pressure plate was used for samples Am 2 and Am 3 until 300kPa. For higher suctions the filter paper method was used (including samples Am 1 and Am 4). The water content error in Figure 4.30c tends to be higher than 5% which the authors considered a good agreement between all techniques.

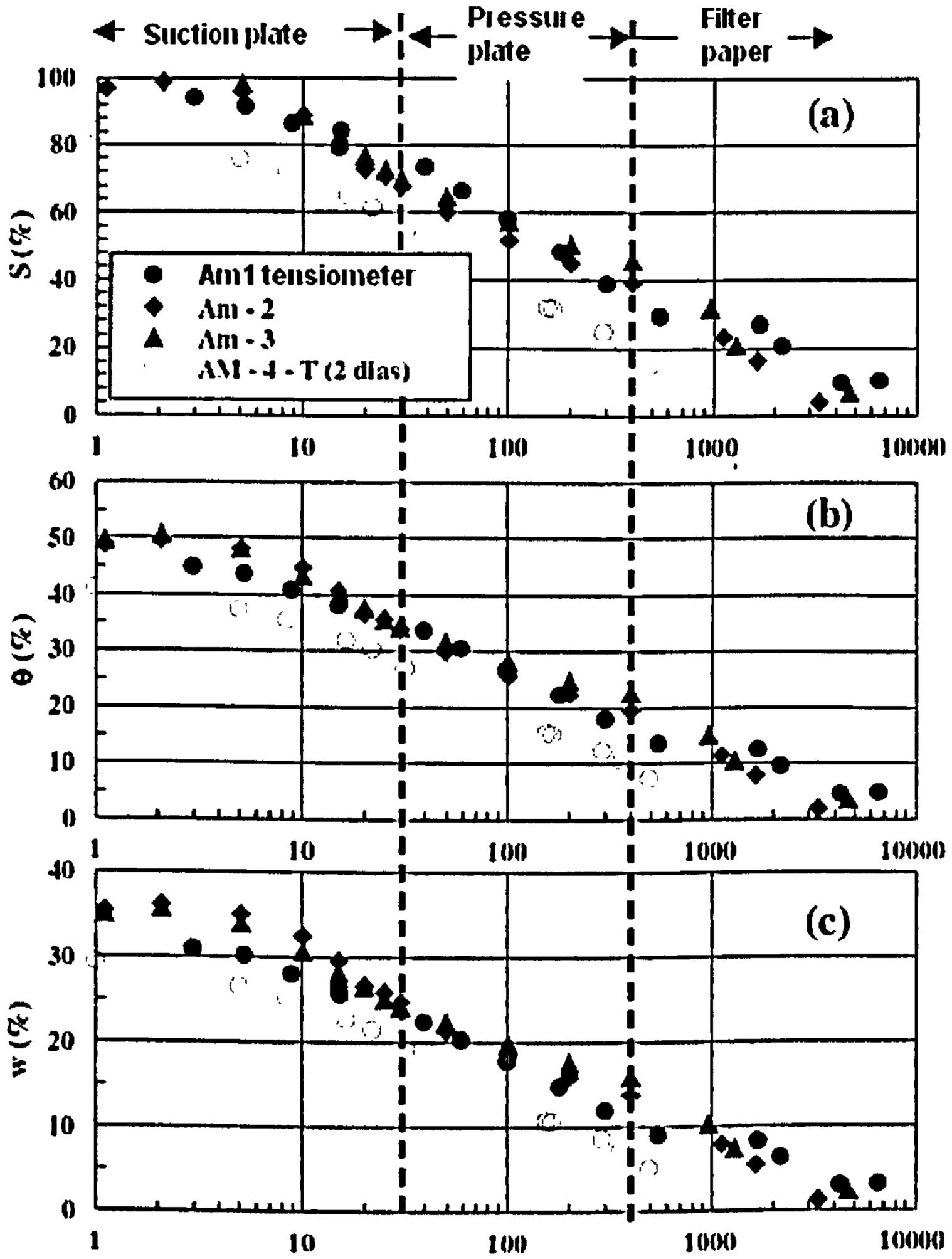

Figure 4.30: The SWRC of a low plasticity sandy silt obtained with the tensiometer, pressure plate and suction plate, (a) degree of saturation versus suction, (b) volumetric water content versus suction, (c) gravimetric water content versus suction (after Teixeira and Marinho, 2006)

The comparison between the filter paper and the tensiometer following the continuous drying procedure by Cunningham (2000) in Figure 2.26b, shows a larger error (between 5% and 10%), as would be expected (since the filter paper technique is an indirect method and subject to further error concerning the calibration relationship).

From Figure 4.29 both procedures (discrete or continuous) seem to be in reasonable agreement with each other. This is encouraging because it means that the SWRC can be done in two days using continuous drying, rather than seven days using discrete drying (Figure 4.22a) for the discrete procedure. It also represents a huge difference with the pressure plate where the test was carried out in 7 weeks. As the material tested has a lower clay content (22% clay-sized particles) it also suggests that it would be suitable for higher permeability materials. However, the error from the curves set furthest apart was small but not negligible: 2%. More work is needed to try to decrease the scatter in the curves.

As the results improved from the initial set-ups where the continuous procedure overestimated suction, any future testing should be done in conditions similar to the final set-up proposed here: the exposed surface area should be as high as possible and the tensiometer cable avoided. However, as the continuous procedure is sensitive to a series of factors, the most conservative solution would be to use the discrete procedure as the suction can be measured at a constant water content. Eventually by doing tests in parallel with the two procedures, and if no difference is observed, then testing could be carried out just with the continuous procedure.

Continuous drying with the new procedure could also be of interest to studies that require a continuous measurement of suction and water content from a soil (e.g. evaporative fluxes from soils).

Figure 4.29 showed that there was not perfect agreement between the continuous or the discrete procedure and the pressure plate. The tensiometer tended to underestimate suction, especially for the middle suction values. Between 100kPa and 300kPa, the error in water content is larger than the 2% but still smaller than the 5% observed by Teixeira and Marinho (2006) and >5% for Cunningham (2000) when compared to filter paper measurements.

This lack of exact agreement could be also due to the techniques used to compare. Cunnigham's results in Figure 2.45 is an example where the error could be mostly related to the filter paper technique rather than the tensiometer. The tendency for the pressure plate to overestimate suction was discussed in the Chapter 3, where it was demonstrated that if no water is present below the stone, a higher suction would be read by the tensiometer. This does not seem to be the case for the test performed here because water was always present below the stone, but still it shows that the

techniques used to impose or measure suction could also be inaccurate. Therefore, even if the agreement between both techniques is not perfect, these early results suggest that the tensiometer can be an alternative for the pressure plate to determine the SWRC.

4.5.2. Limitations

The biggest limitation for the continuous procedure is that it is difficult to wet the sample. It would require imposing a RH of 100%, which is experimentally challenging. Besides the evaporation rates and surface area exposed to drying, the macroscale structure of the soil could influence the sample drying. Figure 4.4a shows preferential pathways through which air could circulate and accelerate the sample drying. This means that the sample would dry in a heterogeneous way, with both preferential inner parts and the external surface drying simultaneously, and could still be further enhanced by drying induced cracking. A third limitation of the continuous drying procedure is the measurement of the volume change. The arrangement to measure deformation based on three LVDTs has not proven accurate enough. This is a limitation in common between both procedures that requires further research.

The discrete procedure has the following limitations: (1) the gravimetric water content determination was affected by the low dry mass of the samples. For instance, an error of 2g for a sample of 400g in the measurement of the mass of the dry sample would be enough to introduce an error in the water content of about 0.5 %. (2) The period of time required for water content equalization in discrete drying must be long enough or excessive evaporation prevented. A rebound is displayed in the suction values once the tensiometer is put in contact with the soil, before equalisation. These suction reversals should be as small as possible to avoid local irreversible changes of volumetric and hydraulic properties of the soil (as discussed in the Measurement Section of Chapter 3). Other factors are the importance of a good contact and the need to have the sample in an air tight environment (also discussed in Chapter 3). (3) The volume measurements with the porometer are not sufficiently accurate (discussed above).

4.5.3. Suction, water retention and volumetric behaviour of BIONICS soil

With the available tests, an attempt was made to characterize the suction-hydraulic-volumetric behaviour of BIONICS soil. The main findings from all SWRC tests are summarized as follows:

(1) Water content versus suction
   a. All tests exhibit a sharp decrease of gravimetric water content (from 25% to ~17%) for a suction increase until 900kPa; from ~18% suction increases considerably for very small decreases of water content.
   b. The soil shows a pronounced hysteresis between the drying and wetting paths.

(2) Degree of saturation versus suction
   a. From Figure 4.26c the soil shows hysteresis in terms of degree of saturation. It is also well visible in terms of void ratio-suction (Figure 4.26d).
   b. Comparing the shrinkage limit test curve in Figure 4.6, the sample seems to remain near full saturation at high degrees of saturation for the tested suction range.

(3) Saturation state: Figure 4.25, which compared Df2 with the shrinkage curves of Figure 4.6, shows that the soil remained at a near saturation state with a degree of saturation higher than 80% for the suction measurement range (up to 1200kPa) with the water content remaining always above the shrinkage limit.

(4) Pores: Figure 4.4a shows a wide range of pore size from 0.5mm to the micron-scale.

(5) Stiffness changes: there is no quantitative information on this, but the soil clearly became stiffer with the cycles of suction for any of the tests presented, particularly after the first drying-wetting cycle.

These findings are interpreted as follows. The soil shows hysteresis in terms of water content and degree of saturation, which suggests that volume variations (shrinkage/swelling) and ink-bottle pores play an important role. However the water content - degree of saturation - suction covered is too small to conclude how each of them influences soil behaviour. This can be further analyzed by comparing the shrinkage limit tests of Figure 4.6. Figure 4.31 shows that the two curves can be divided in three parts. For water contents higher than ~17% (the range covered by the tensiometer) the water content change is essentially controlled by volume change because the degree of saturation remains constant (and above 90%). For water contents lower than the shrinkage limit (~14%) the hydraulic behaviour should be controlled the pores filling/emptying because the void ratio stops decreasing at ~14% while the water content still decreases. Between ~14% and ~17% the soil is in a transition zone.

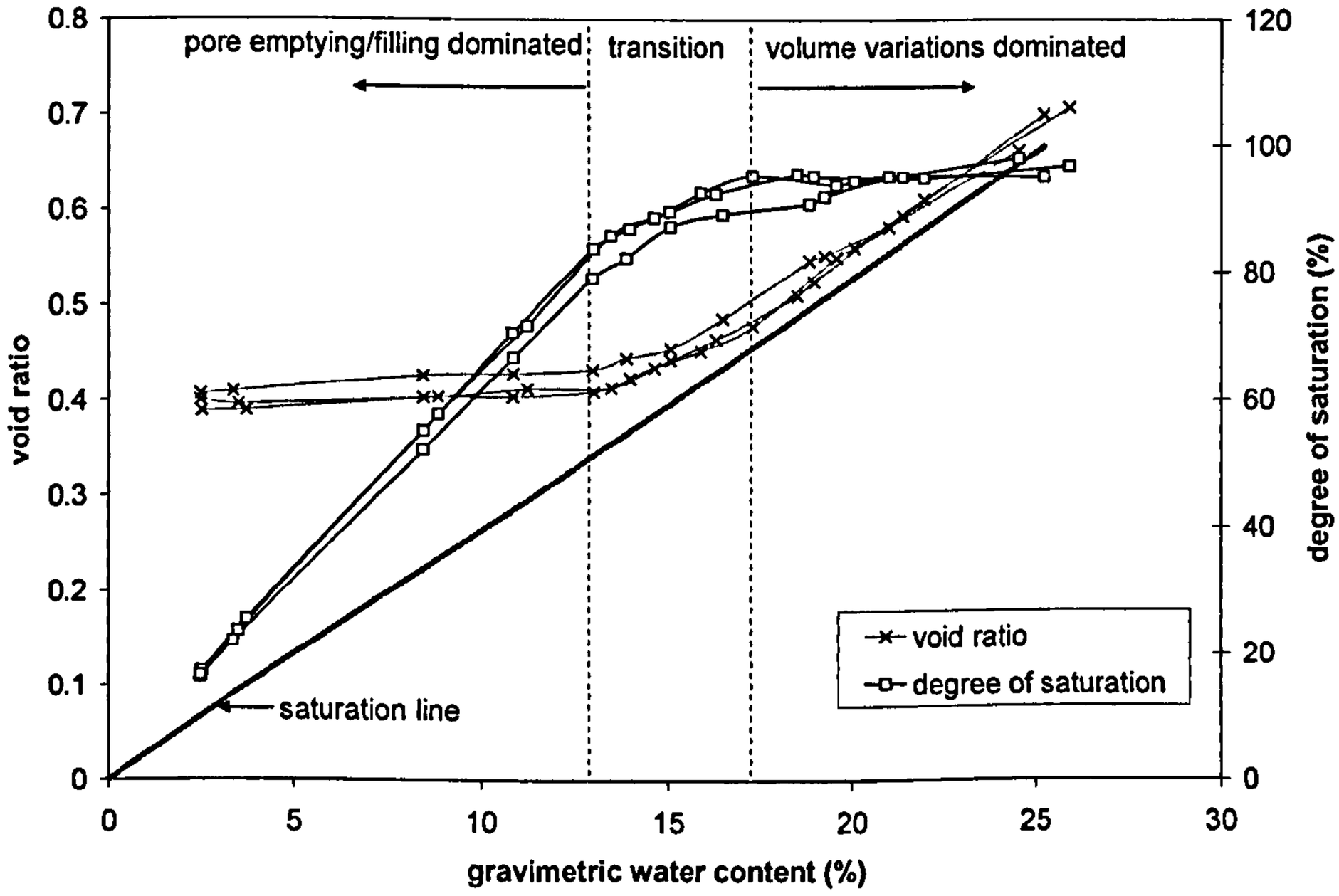

Figure 4.31: Mechanisms controlling drying for the BIONICS soil based on the water content – void ratio – degree of saturation relation (tests S1 to S3, BIONICS)

Even if the soil behaviour seems to be mostly controlled by the deformations (for the range of tested suctions), Figure 4.26 and all other SWRCs presented in this dissertation suggest that there are ink-bottle pores that do not empty/fill at the same suction. Steeper SWRCs at low suctions suggests the presence of large pores that retain larger amounts of water, they are the first to empty (during drying) and the last to fill (during wetting). Therefore, the hydraulic behaviour should essentially be controlled by the larger ink-bottle pores; smaller pores should remain saturated at all times.

In summary, the few data obtained suggests that for the range of tested suctions (0-1200kPa), for the initial void ratio, water content, and compaction procedure used here, the suction-hydraulic-volumetric behaviour of BIONICS soil is essentially controlled by volumetric variations (shrinkage/swelling) with most of the pores remaining near a saturation state. Important changes also seem to occur after the first drying-wetting cycle (eventually due to fabric arrangements), with the soil becoming stiffer (based on qualitative information) and smaller permanent changes in volume.

It is not possible to say exactly in which class of Figure 2.16 fits BIONICS soil. The first impression is that it might fit into Class IIb, just because it shows hysteresis at very low suctions, equivalent to the class IIb in Figure 2.16 that shows hysteresis at high *p/p'*. But the most probable is that the curve has combined patterns of Class IIb and Class IVb (also typical of porous materials).

4.6. CHAPTER SUMMARY

Soil Water Retention Curves (SWRCs) have been determined with high suction tensiometers following continuous and discrete procedures. Volume measurements have been added and SWRCs have also been determined following a wetting path. The procedures and limitations for both techniques have been discussed. It has been demonstrated that both the discrete and continuous procedure using the tensiometer give similar SWRCs to pressure plate testing, although not identical. However, continuous drying is easily influenced by a series of factors and so should not be used as a quantitative measure of the water retention properties of soils, unless it has been shown to be appropriate by comparative testing. The discrete procedure should provide the more correct SWRC.

With the available data on the SWRC of the BIONICS soil, an attempt was made to characterize its suction-hydraulic-volumetric behaviour. For the range of tested suctions and initial conditions, the soil behaviour is essentially controlled by volume changes (shrinkage/swelling) remaining at a near saturation state. Hysteresis can also be seen at low suctions suggesting that large ink-bottle pores are present in the soil.

Chapter 5. SUCTION CONTROL SYSTEM

5.1. INTRODUCTION

A tensiometer based suction control system was developed for triaxial testing including a system for continuous water content measurement and for wetting of samples. This represents an improvement of similar systems reported by Cunningham (2000) and Jotisankasa (2005). The initial system was intended to be vapour based (Figure 5.1) but it was later found that to achieve wetting required the injection of water in the liquid phase.

The initial goal was to circulate air through a soil sample (any soil at different porosities), with the suction and water content varying by vapour transfer from the air to the soil (in the case of wetting) or from the soil to the air (in the case of drying). So, the procedure would be similar to the vapour equilibrium technique (e.g. Blatz and Graham, 2000), but without using chemical solutions to control the suctions (which is suitable for a higher suction range). Suction would be measured by the tensiometer and water content by a balance (assuming that all water lost or gained by the sample would condense or evaporate in the two boxes of Figure 5.1). The system was planned to work in a closed loop, leakage free, to ensure that all losses or gains of moisture originated from the sample.

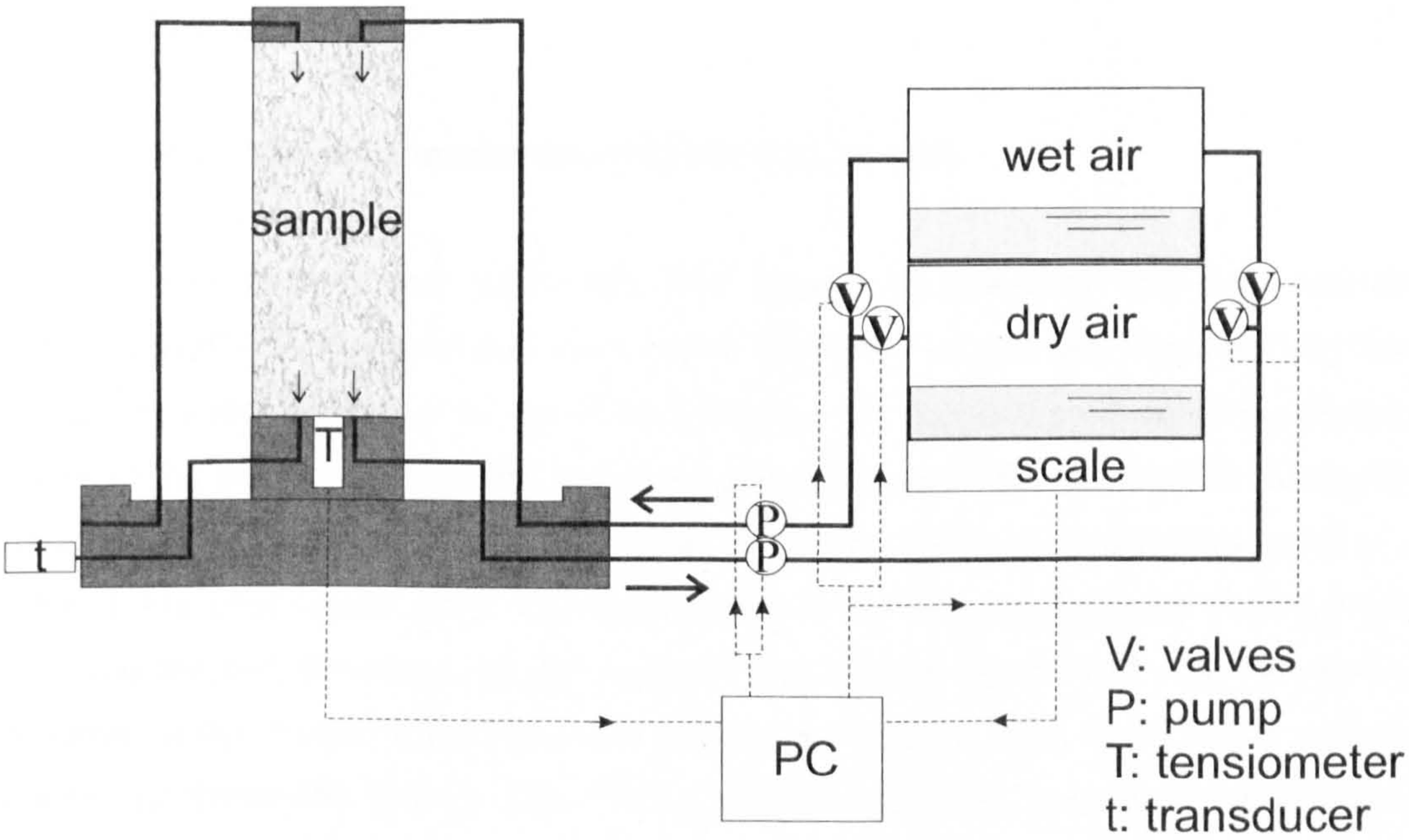

Figure 5.1: Tensiometer based suction control system (ver.1)

The final goal was to develop a tensiometer based suction control system that could dry and wet a confined sample under suction controlled conditions with water content measurement. The intention was to have a system that could control the confining pressure, vertical load, suction and water content, and monitor the air pressure, and the volumetric and axial strain. It was intended to develop a system for triaxial cells.

This chapter reports the development of the tensiometer based suction control system. The development rationale was usually done following the sequence:

(1) Identification of the equipment needed to control or measure parameters (e.g. triaxial cell, balance, tensiometer, pump) and the means of drying or wetting the soil (e.g. liquid water to wet or dry air to dry).

(2) Definition of set-ups, i.e. the physical arrangement of the equipment and how drying and wetting was carried out in relation to the sample.

(3) Establishment of procedures for testing, i.e. for a given set-up, how the equipment was used so that the soil dried or wetted.

5.2. EQUIPMENT

5.2.1. Volume measurement in the triaxial cell

The determination of the void ratio and degree of saturation requires volume measurements. In a triaxial cell, the volume has been traditionally measured by the volume of water flowing in or out of the sample (only for saturated samples) (Head, 1976) or the cell (for unsaturated samples) (e.g. Wheeler, 1986) by means of volume gauges (e.g. Maswoswe, 1985) or differential pressure transducers (Lourenço et al., 2006b). For unsaturated soils, the ideal solution is to measure the water flowing from and into the cell. However, as the material that makes up the cell walls (Perspex) deforms under pressure and absorbs water, calibrations have to be performed to correct for these effects (e.g. Toll, 1988, Zulfahmi, 2008). In order to avoid all these corrections, an adopted solution has been to use double cell structures (Figure 5.2). In the following a distinction will be made between double-walled systems (that have a joint top lid) and double-celled systems (where the inner cell has a separate top lid).

Wheeler (1986) and Yin (2003) used a double-cell structure to restrict creep of the inner wall, where the same pressure is applied to the inner and outer side of the inner cell. Since the inner cell is not subject to any pressure difference it will not deform. In this way, the volume of water flowing out of or into the inner cell corresponds to the change in volume of the sample.

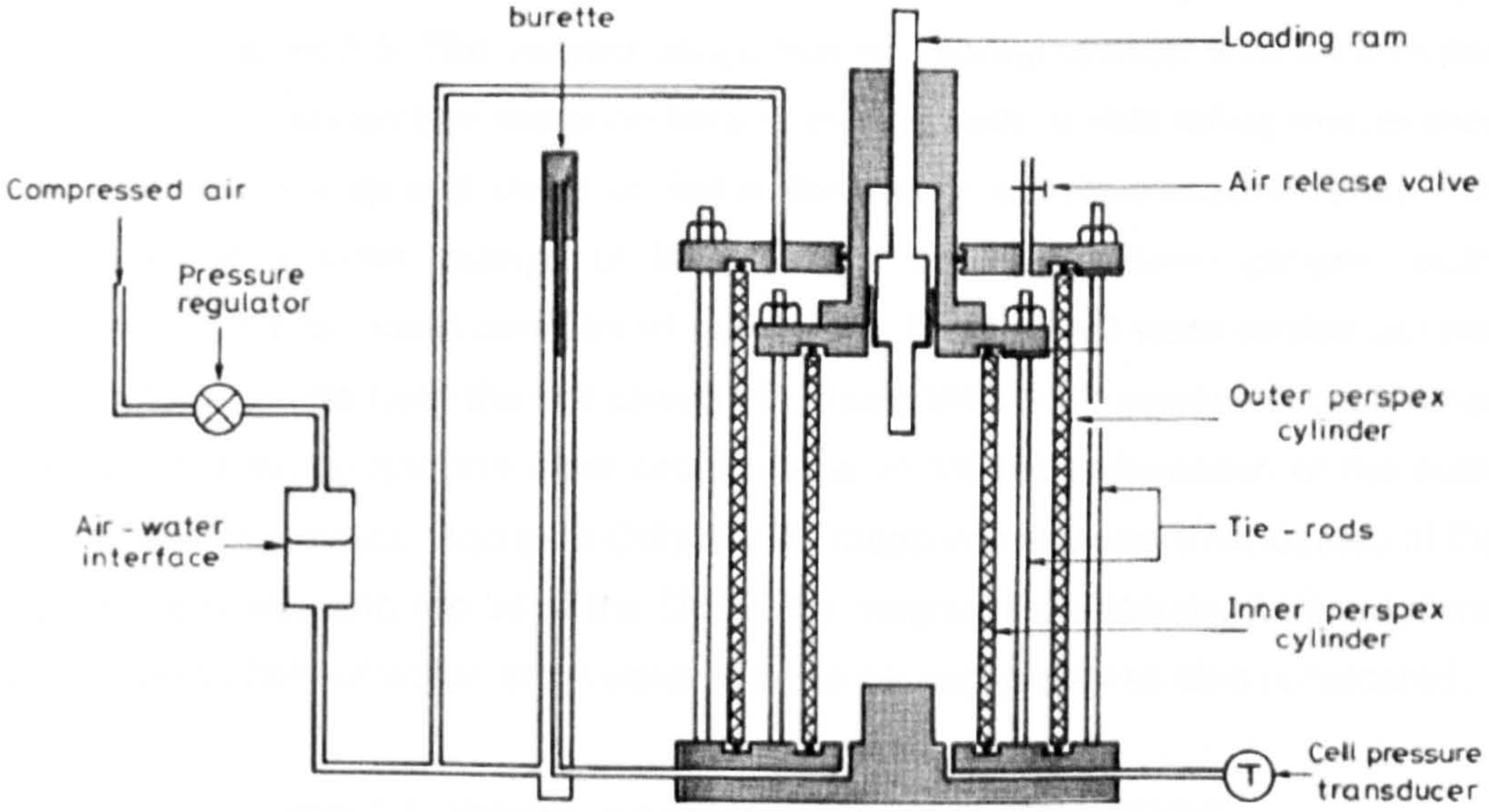

Figure 5.2: The DCTC used by Wheeler (1986)

Initially for this research a double wall triaxial cell was investigated. It was designed as two walls ending in a joint top lid. However, the design was modified to a double cell triaxial cell similar to Wheeler (1986) and Yin (2003) in Figure 5.2. Testing involved measuring the volume of water flowing in and out of the cell (with no sample) for different pressure levels.

5.2.1.1. Double Wall Triaxial Cell

The double wall triaxial cells (DWTC), manufactured by Wykeham Farrance Ltd, were made of an inner glass wall, outer Perspex wall, ending in a joint plate at the top. An inner glass wall was used to prevent water absorption (as can occur with Perspex (Wheeler, 1986)). Glass could be used because the inner wall is not subject to a pressure difference and hence does not have to carry any stress.

While the DWTC was intended to restrict (or even eliminate) any volume change of the cell, it was found that volume change did still occur. The volume change behaviour of the DWTC was investigated for increasing or constant cell pressures (creep). Tests were conducted for different cell pressures (from 800kPa to 2000kPa) with no sample (Table 5.1). Pressure was applied by means of a piston controller. This device has an internal piston inside a reservoir attached to a screw; pressure is applied by a stepper motor that rotates the screw in or out of reservoir under

computer control. Volume change was measured in the inner cell by a volume gauge, as shown in Figure 5.3. The volume gauge has an internal cylinder with a moveable piston that is separated into two chambers at its ends with flexible rolling membranes to allow movement up and down as water flows in or out (Maswoswe, 1985). The contribution to volume change of the different sources (volume gauges, outer Perspex wall, top lid) were considered separately. Tests V1-V3 were carried out just on the volume gauge (with the cell closed off). Tests V4.1-V4.2 measured the change of the volume gauge and the inner cell. In tests V5-V8 the deformation of the outer cell was also measured. Accurate deformation measurements were conducted at the outer Perspex wall and top lid of the DWTC by means of displacement transducers. The compressibility of water, often considered to be negligible was also considered.

Table 5.1: Volume change measurement of the DWTC

Test number	**Parts tested**	**Maximum pressure (kPa)**	**Maximum volume increase of the inner cell (cm^3)**
V1	Volume gauge	~875	0.7
V2	Volume gauge	13 cycles from 0 to 800	From 0.75 to 1.0
V3	Volume gauge	9 cycles from 0 to 800	0.5
V4-1	Volume gauge + inner cell	2000	62.9
V4-2	Volume gauge + inner cell	1000	23.0
V5, V6, V7 , V8	Outer cell deformation	2000	-

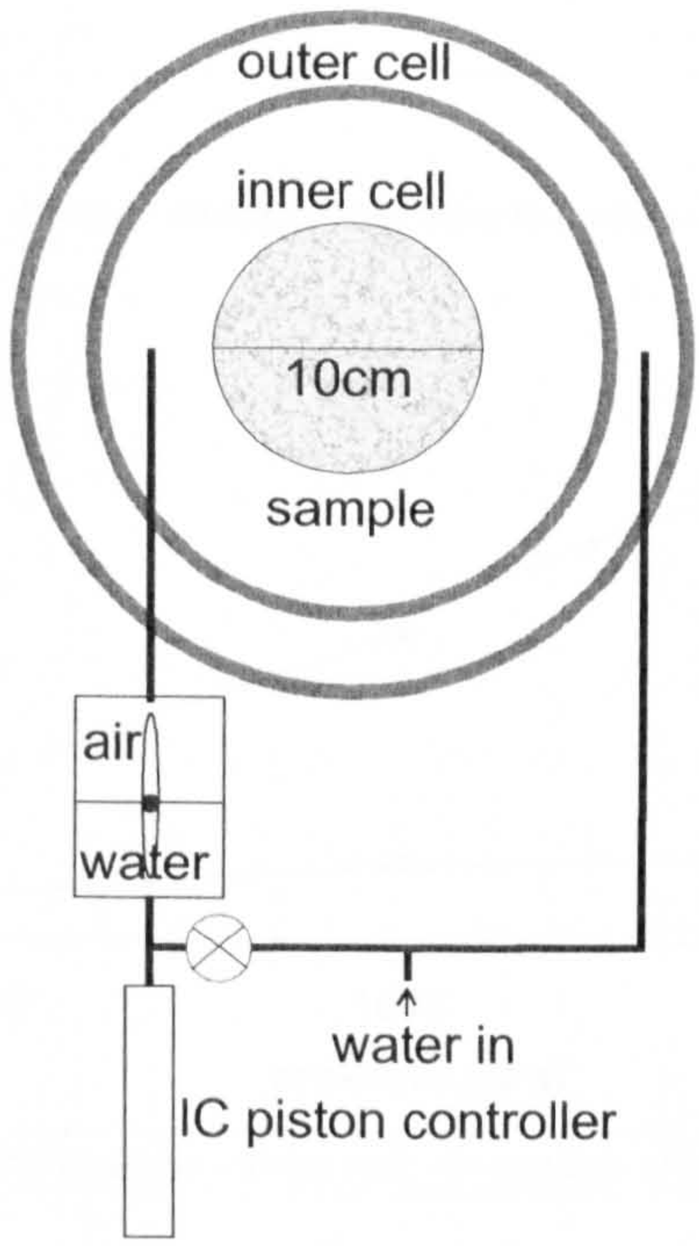

Figure 5.3: Arrangement for the volume change measurement of the inner cell (view from above)

The volume change measurements in Table 5.1 show that from the tests V1, V2, V3, conducted under similar conditions, the apparent volume increase of the volume gauge when subjected to pressure was in the order of 1.0 cm^3 at approximately 800kPa. This indicates the accuracy of volume measurement of this device.

The measured volume change for V4-1 included both inner and outer cell and the results are shown in Figure 5.4; the inner cell showed a volume increase of 62.9cm^3 at 2MPa, while in the outer cell the maximum volume increase was in the order of 389 cm^3. The cell was also observed to creep by 17cm^3 at 2000kPa for a period of 7h. The results of test V4-2 are shown in Figure 5.5. The cell pressure was increased in steps (625kPa, 1250kPa, 1800kPa) to allow refilling of the volume gauges (maximum volume of the volume gauge is 100cm^3). Test V4-2 revealed that water flowed between the inner and outer cells. At 1000kPa, the volume increase rate of the inner cell suddenly increased while that in the outer cell decreased (as indicated by the arrows). This was attributed to a leak of water from the inner to the outer cell.

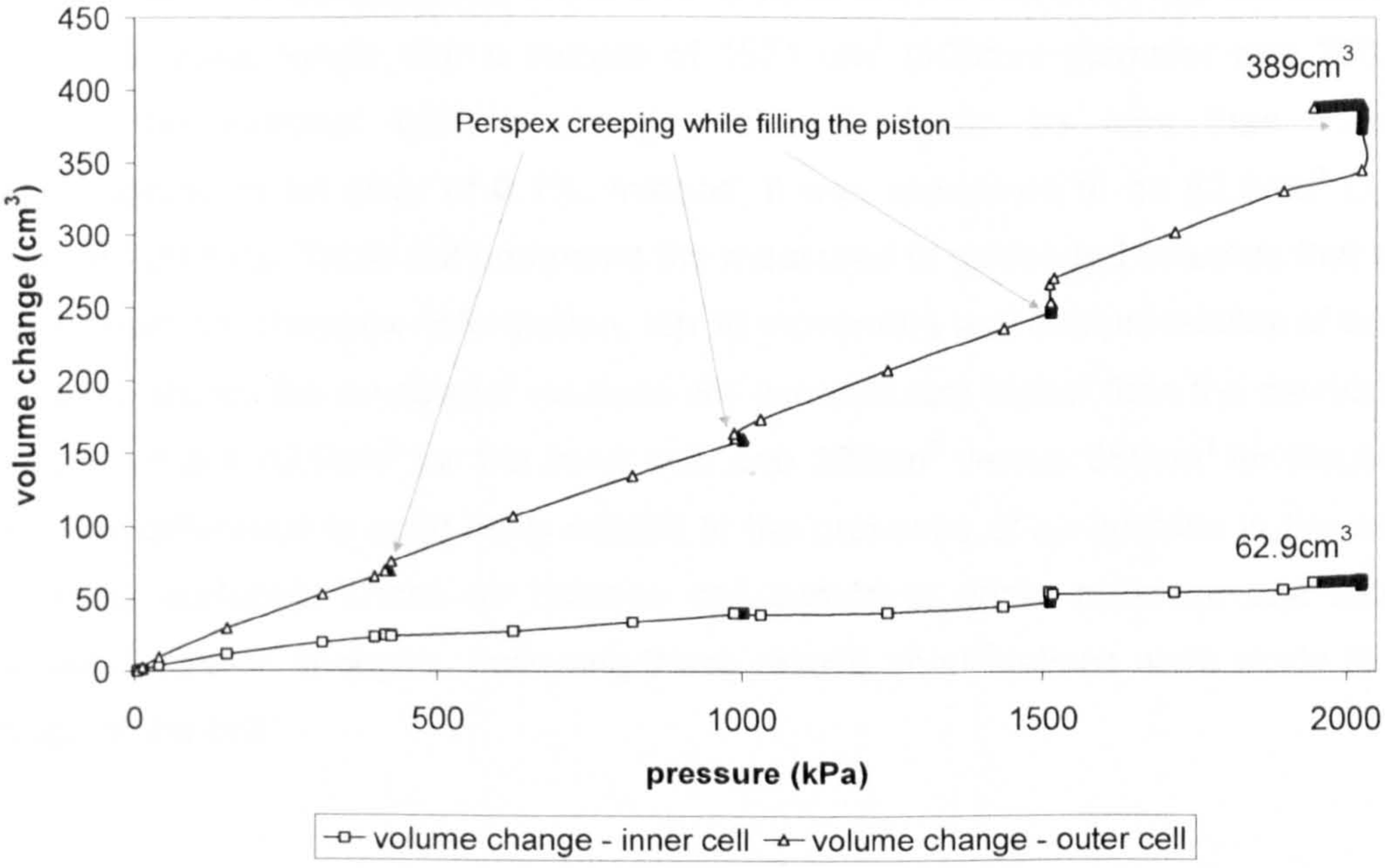

Figure 5.4: Volume change measurement for the inner and outer cell (test V4-1)

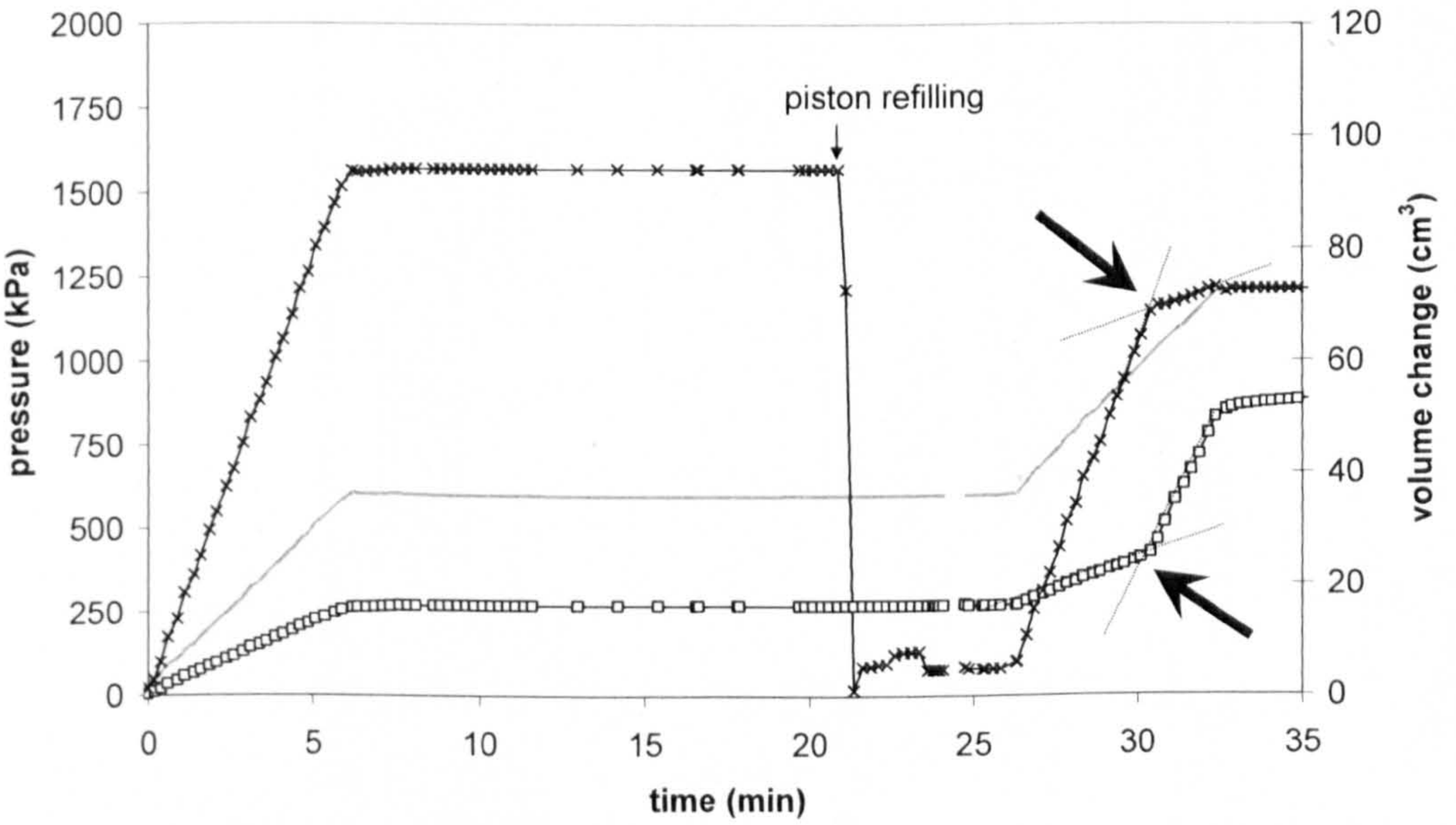

Figure 5.5: Leak from the inner to the outer cell in the DWTC (test V4-2)

The deformations measured in tests V5, V6, V7 and V8 revealed that for a single cell pressure increase from 0-2000kPa the top lid moved upward by an average of 0.68mm, while the outer Perspex wall expanded by 0.93mm (Figure 5.6a). Figure 5.6b also shows the Perspex creep was approximately 0.05mm after 12h.

Volume change measurements in the DWTC have shown that there is a considerable amount of water inflow. For a sample of 1571 cm^3 (100mm diameter and 200mm height), the external volume changes should ideally be less than 1.5cm^3, corresponding to an error of 0.1%. Instead, it was measured to be 62.9cm^3 (3.8% error) at 2000kPa. Table 5.2 compares the measured to calculated volumes that take into account the Perspex deformation, top lid movement and compressibility of water. The table shows the measured volumes are considerably higher than the calculated: 31.1cm^3 versus 62.9cm^3 for the inner cell, and 282cm^3 versus 389cm^3 for the outer cell. This difference is most likely related to the presence of air bubbles in the water and inner surfaces. These air bubbles can compress under pressure and induce additional volume changes. Following these results, modifications were made to the design of the cell.

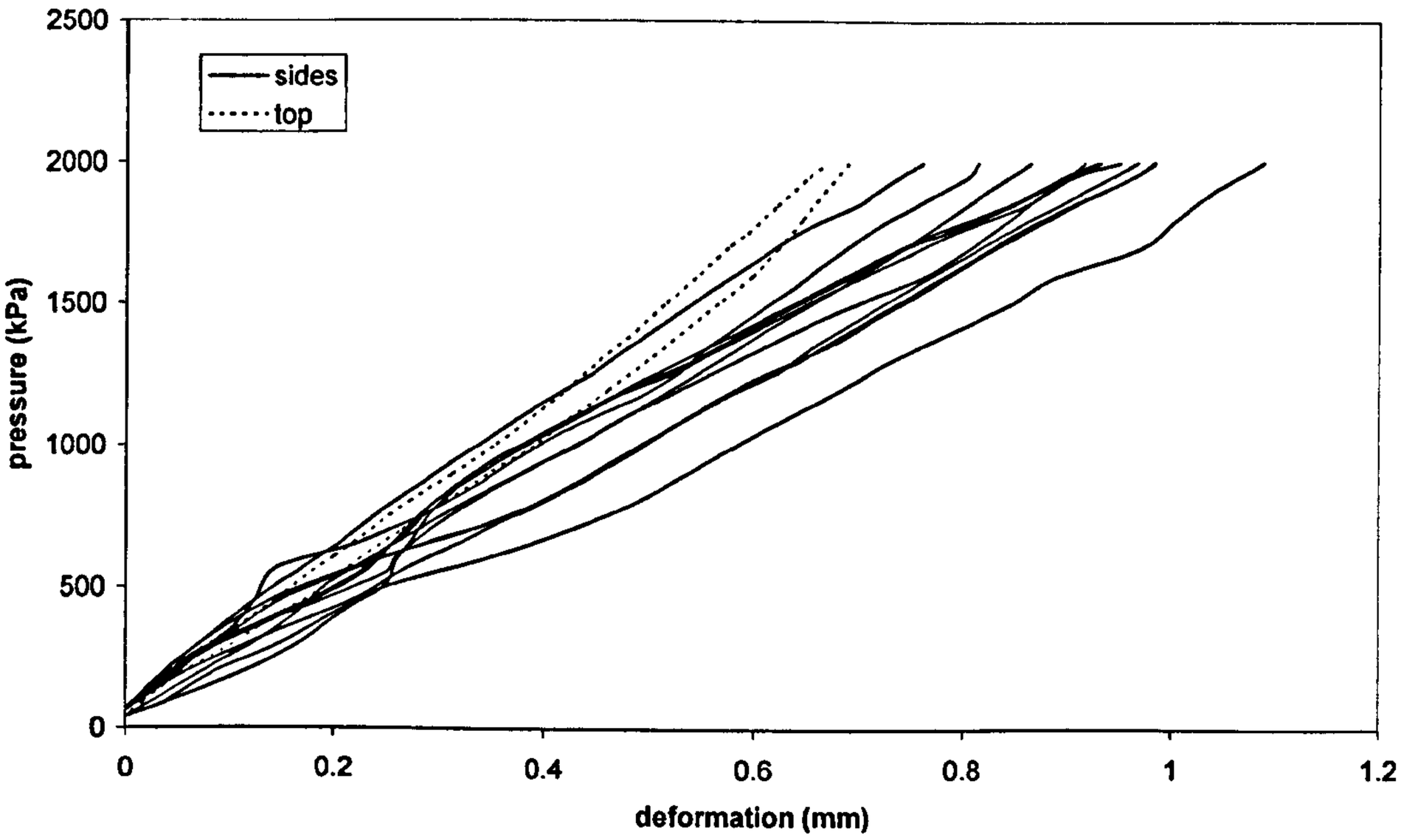

(a)

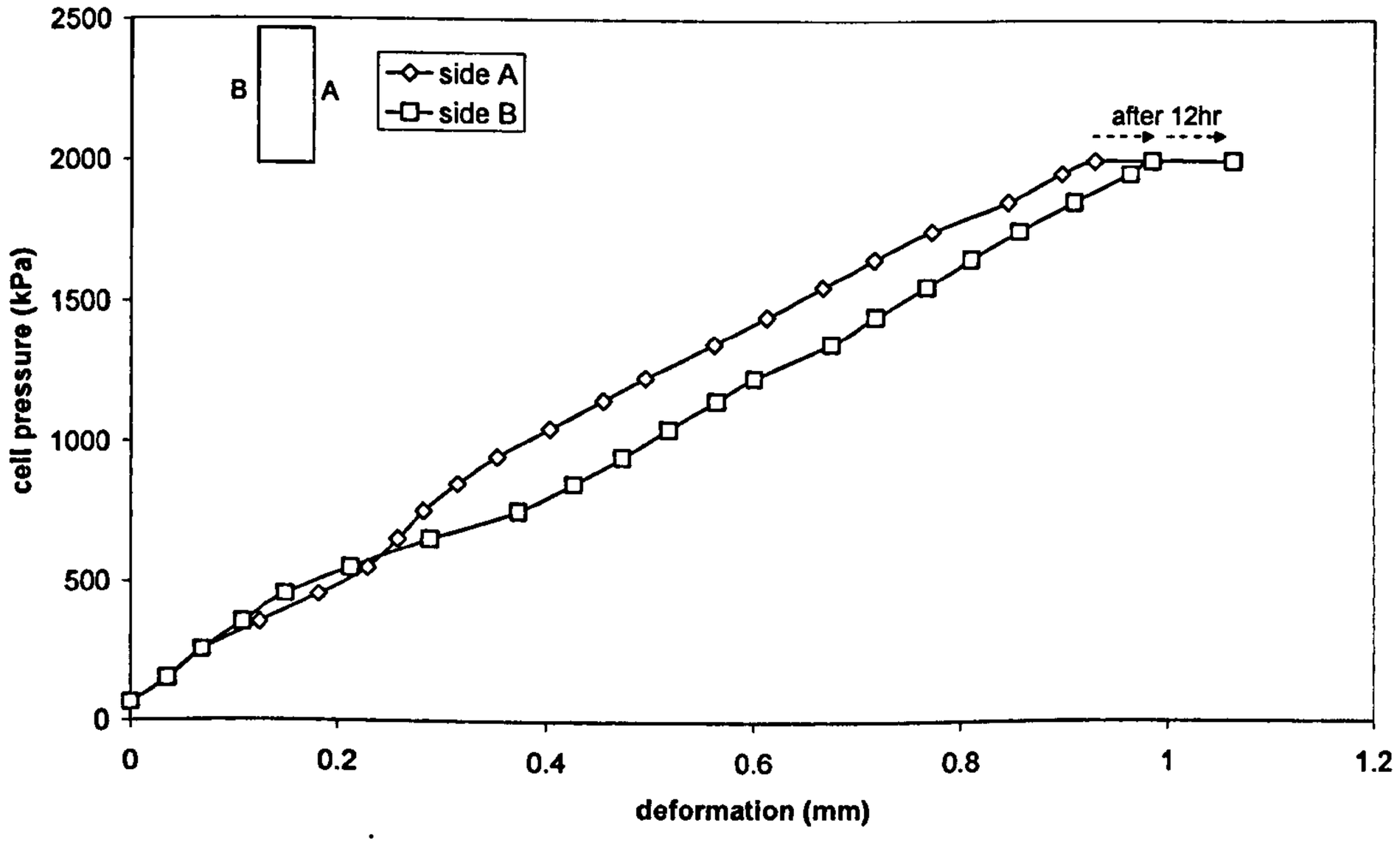

(b)

Figure 5.6: (a) Deformations measured at the top, middle and bottom of the outer Perspex wall and on the top lid of the DWTC (tests V5, V6, V7, V8); (b) creep of the outer wall after 12h at 2000kPa (test V5)

Table 5.2: Volume change details of the DWTC for a pressure increase 0-2MPa

dimensions and other fixed values		**unit**
height	41.6	cm
inner cell inner diameter	19	cm
inner cell outside diameter	20	cm
outer cell inner diameter	22.35	cm
volume of water in the inner cell	11794.8	cm^3
volume of water in the outer cell	3251.66	cm^3
compressibility of water (Tabor, 1969)	0.001	cm^3/cm^3
deformations measured		
cell top deformation (average)	0.068	cm
outer wall deformation (average)	0.093	cm
inner cell volume change		
water flowing in due to cell top deformation	19.28	cm^3
water flowing in due to water compressibility	11.8	cm^3
total INNER CELL	31.07	cm^3
total measured INNER CELL	62.9	cm^3
outer cell volume change		
water flowing in due to Perspex deformation	271.30	cm^3
water flowing in due to water compressibility	3.25	cm^3
water flowing in due to cell top deformation	7.40	cm^3
total OUTER CELL	281.95	cm^3
total measured OUTER CELL	389	cm^3

Yin (2003) did similar measurements in a double cell triaxial system, and obtained a maximum volume increase in the inner cell of 0.4cm^3, at 400kPa. The cell had an inner top cap and the volume of the inner cell was 1500cm^3 (8 times smaller than the DWTC). The inside top cap should have restrained upward deformations, consequently the source of the 0.4 cm^3 could be due to the compressibility of water.

Regarding the DWTC, the cell top movement could be avoided by assembling an inner top cap, i.e. by changing from a double wall system to a double cell system, as used by Yin (2003) and Wheeler (1986). The leaks between the cells required better

sealing by the o-rings (placed at the joint top plate). The water compressibility effect could be restrained by decreasing the volume of water inside, i.e. reducing the cell dimensions. However, this might not be entirely feasible because space is needed to instrument the sample. Regarding the Perspex cell deformation of the outer cell, the only inconvenience of having such high volume of water, is that the piston controller has to be filled several times (capacity of piston is 100cm^3).

It was also observed that the original push-fit fittings supplied by the manufacturer leaked water from the cell to the sample. The working principle of push-fit fittings is based on a differential pressure across the tubing wall that is higher in the interior of the tubing forcing it against an o-ring to seal. In the triaxial cell the situation is the opposite, with the cell pressure higher that the pressure inside the tubing (which could be near atmospheric pressure). The push-fit fittings were substituted by compression fittings.

5.2.1.2. Double Cell Triaxial Cell

The original DWTC was modified into a double cell triaxial cell (DCTC) (Figure 5.7). The new DCTC was checked for volume change at a cell pressure of 300kPa. Figure 5.8a shows, unexpectedly, that water flowed out of the inner cell. This could have been due to temperature effects, because during this time (December 2006) the outdoor temperature decreased. However the cyclic variations show no correspondence with daily fluctuations. The temperature effect is particularly evident in Figure 5.8b. It was noted that the cell expelled more water when there were more people in the lab (increased temperature and humidity).

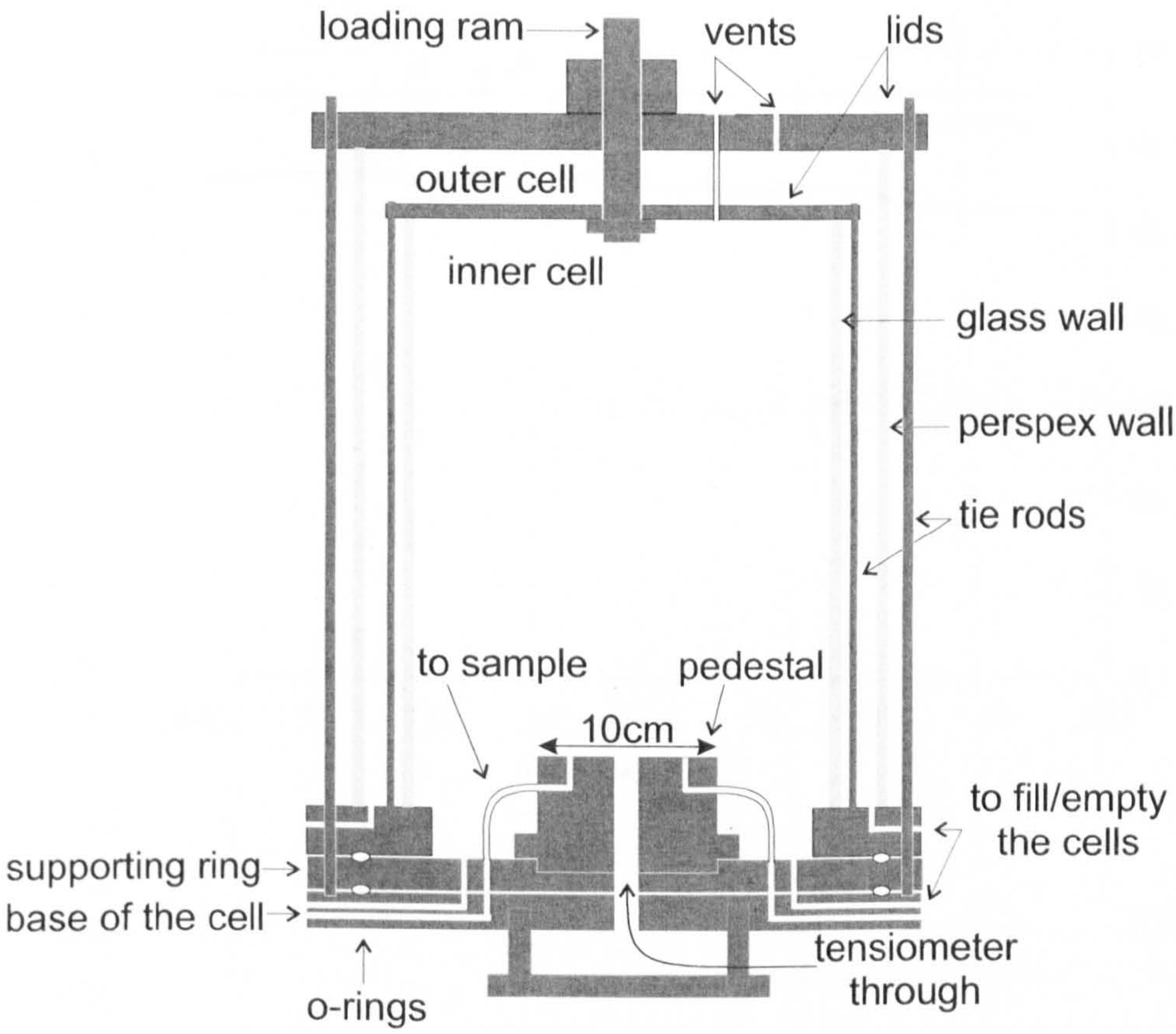

Figure 5.7: The double cell triaxial cell (DCTC)

A new test was conducted to confirm the previous results. The volume change of the inner cell was measured with a volume gauge at a constant cell pressure of 300kPa. After 10 days, the volume gauge was recording no variations at all (Figure 5.9). It was then found that water was able to flow freely between both cells due to a problem with the loading ram that goes through both outer and inner cells. As the inner and outer cell and volume gauge were all connected, the volume increase was not detected by the volume gauges but by the piston controller instead that continued filling the cell as the Perspex wall expanded.

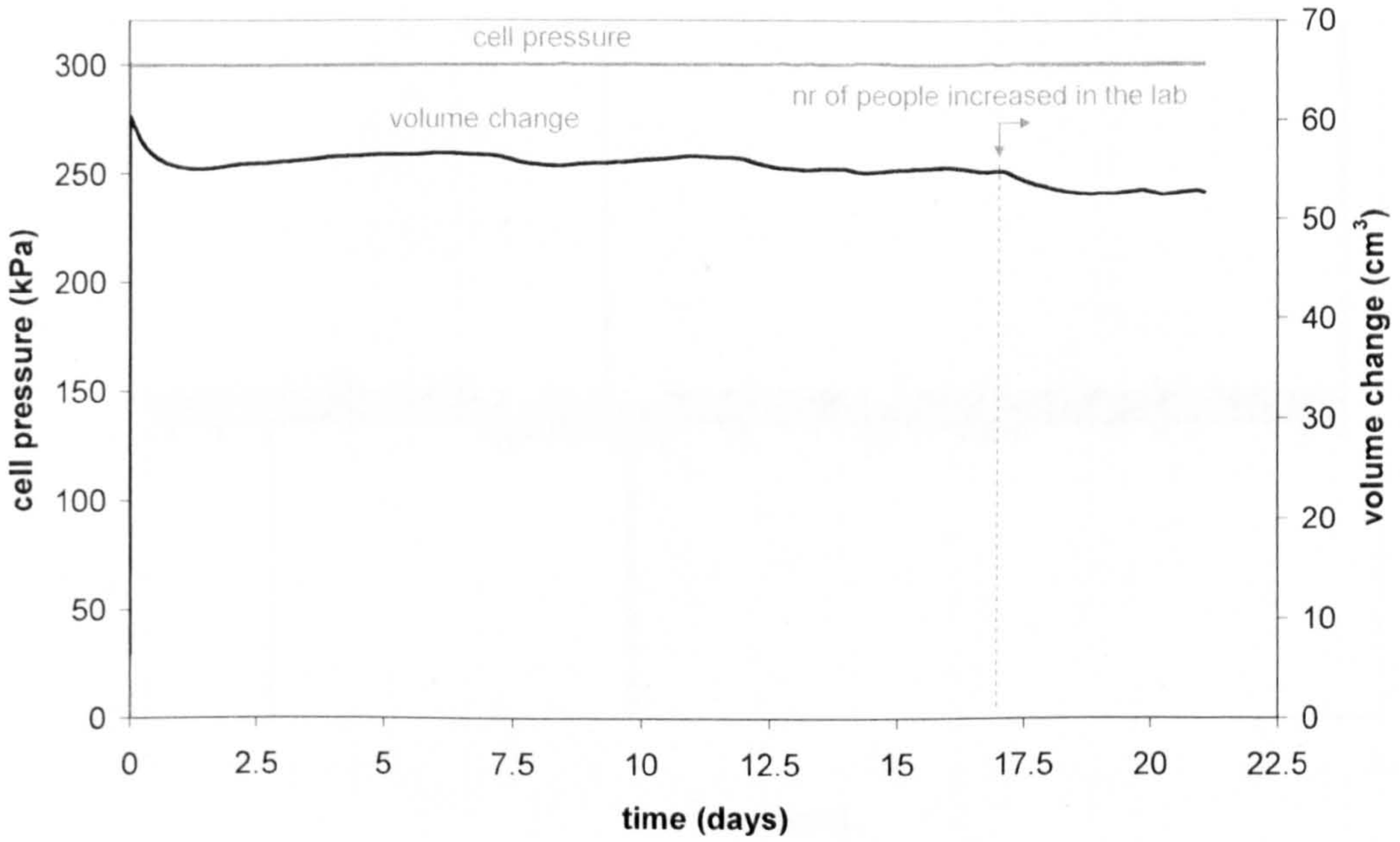

(a)

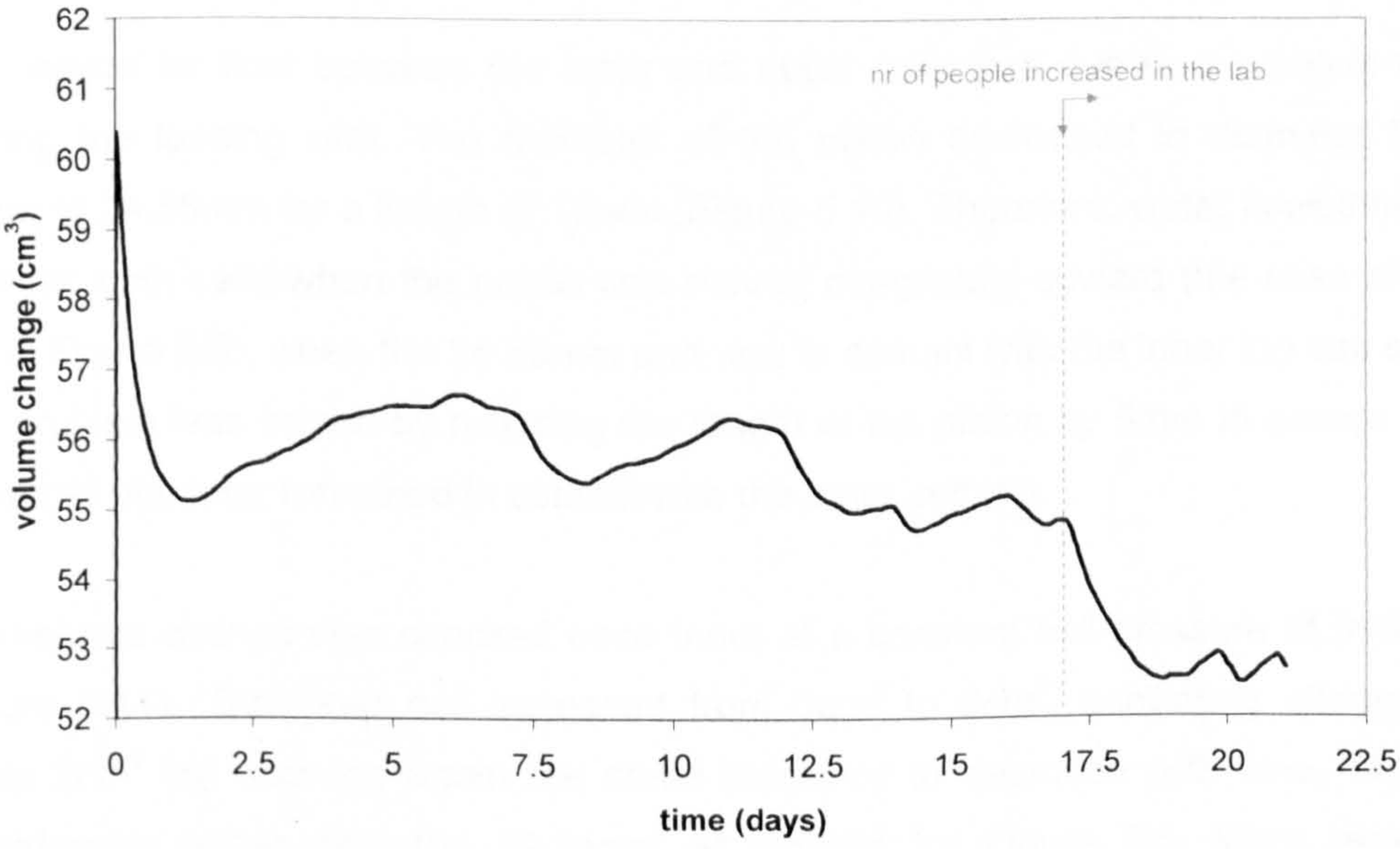

(b)

Figure 5.8: Volume change of the inner cell of the DCTC (test V9), (a) pressure and volume change (b) volume change only shown at expanded scale

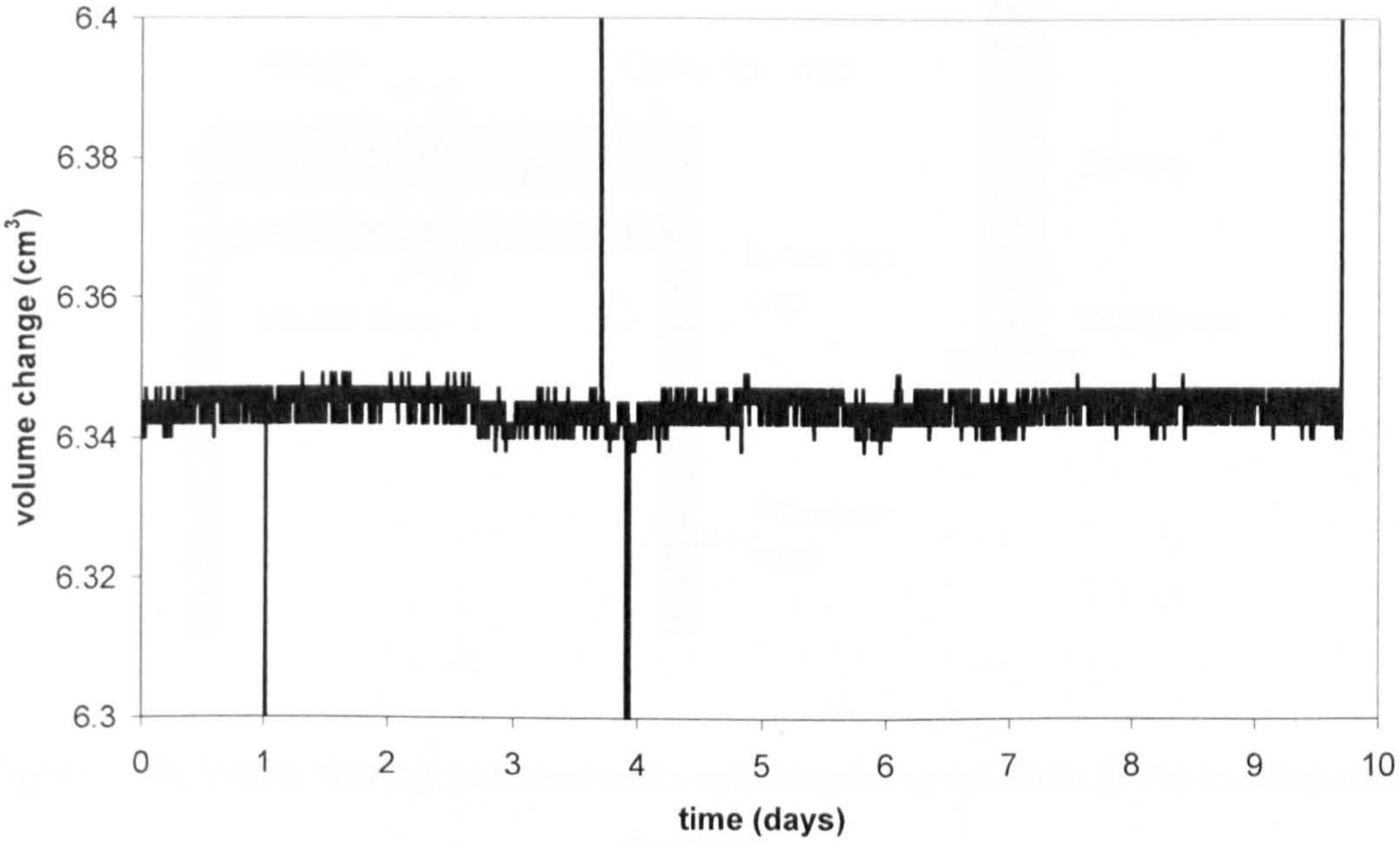

Figure 5.9: Volume change of the DCTC at constant pressure (test V10)

The reason for flow between the inner and outer cells was due to a problem with sealing the loading ram. The diameter of the piston decreased in diameter from 25mm to 24.55mm for a length of 12mm (Figure 5.10). Therefore, water flowed freely between both cells when the piston was moved completely upward (the case of the test in Figure 5.9), when the 24.55mm part was in contact with the inner top cap seal. The problem was solved by reducing the length of the piston by 5mm to ensure that the larger diameter remained in contact with the inner cell top.

The volume change was checked once more at a constant cell pressure of 300kPa (Figure 5.11). The inner cell increased from $0cm^3$ to $6cm^3$, oscillating afterwards within $2cm^3$ but showing again the same tendency to decrease with time. This is considerably better than the $19.34cm^3$ at 300kPa for Figure 5.5. More recently Mendes (2007a) found that water still passed from one cell to the other past the seals of the loading ram. He replaced the o-rings on the ram and the problem was solved.

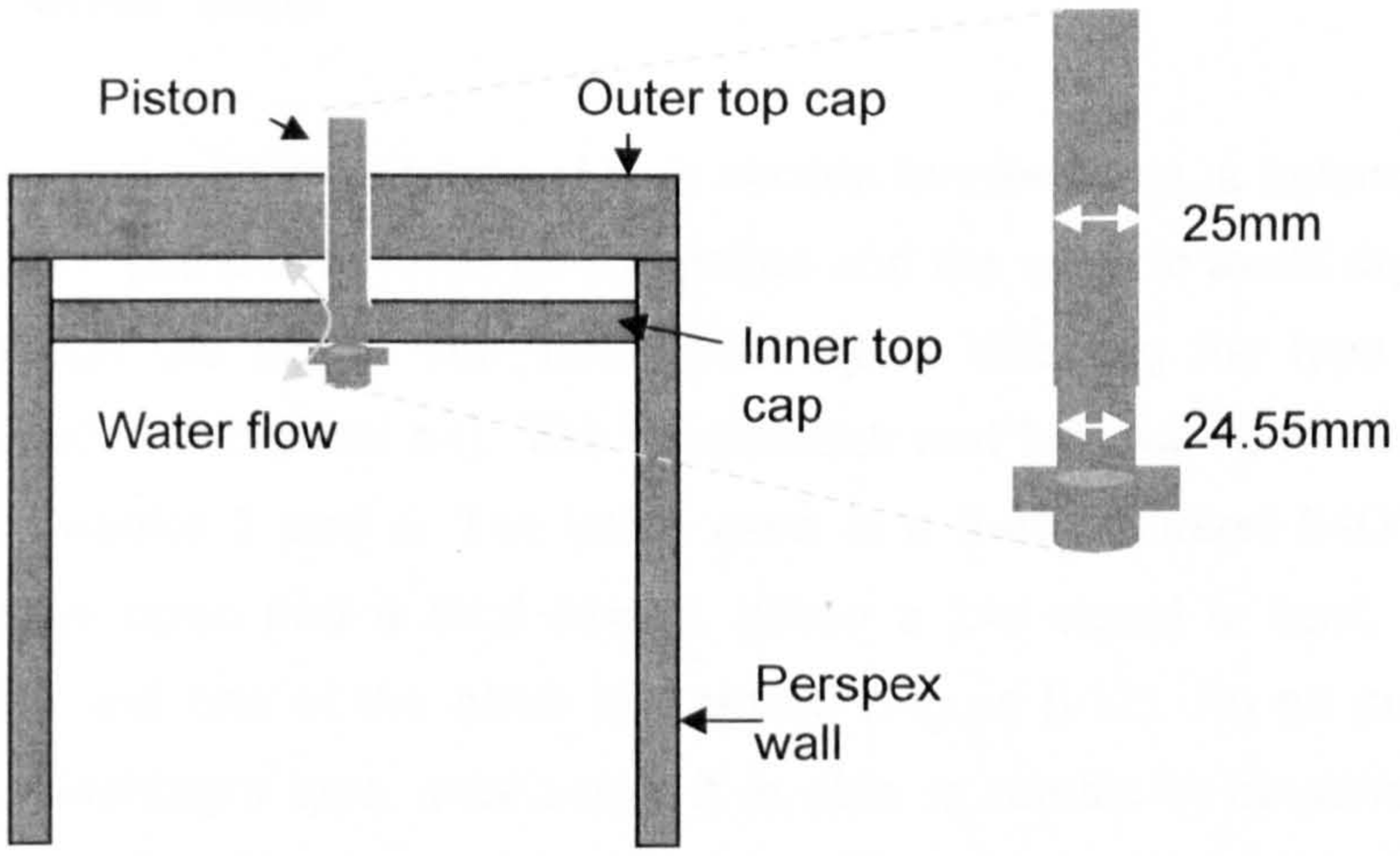

Figure 5.10: Water flowing between both cells due to a reduction in the loading ram diameter

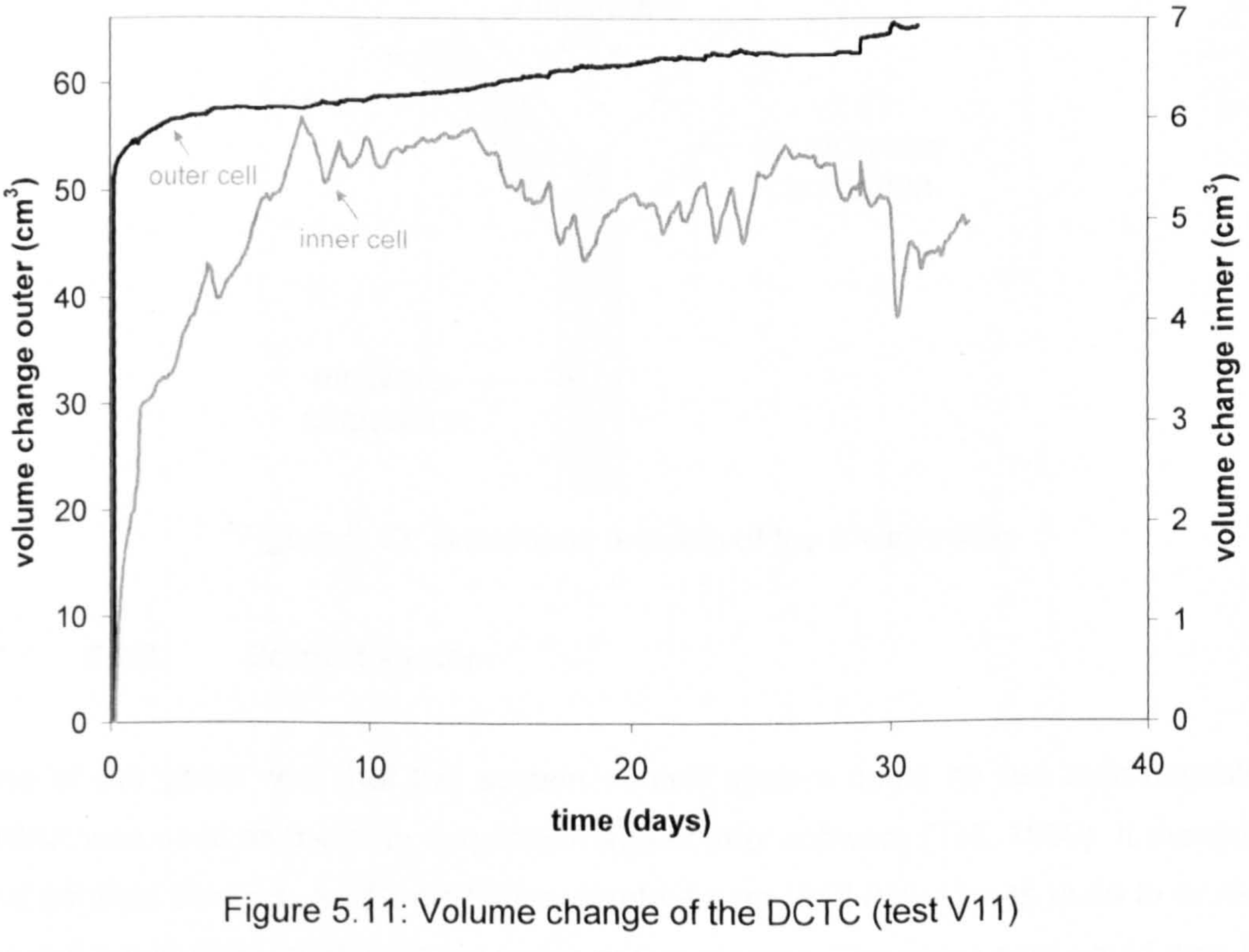

Figure 5.11: Volume change of the DCTC (test V11)

Concluding, the factors controlling the volume measurement in the triaxial were identified and minimized by modifying the design of the cell. However, even though the final values (in Figure 5.11) are better than the initial setup (in Figure 5.5) further work is required to calibrate the cell for temperature variations. Ongoing work by Mendes (2008a) takes this into consideration.

5.2.2. Other parts

The suction control system is made of high suction tensiometers, a balance, a valve, and a pump. The pump is to force air circulation and the valve to avoid dry or wet air migrating through the pipes. The valve also allows selecting the type of fluid to circulate (air/water or dry/wet air). The tensiometer and balance have already been described in Chapter 3 and 4. The valve used is a 3-way Burkert 24DC with two channels always open and a third closed. When a 24v signal is sent, the closed channel opens and one of the other two closes (Figure 5.12). An air pump model Boxer 3114, diaphragm type, was used. It is able to remain in operation for long periods of time (days). The flow rate depends on the voltage (between 6v and 12v). A single value was chosen so that the pump could be switched on and off by a simple control system. For this research the air pump was used at 12v (flow rate ≈12.5l/min according to data supplied by the manufacturer).

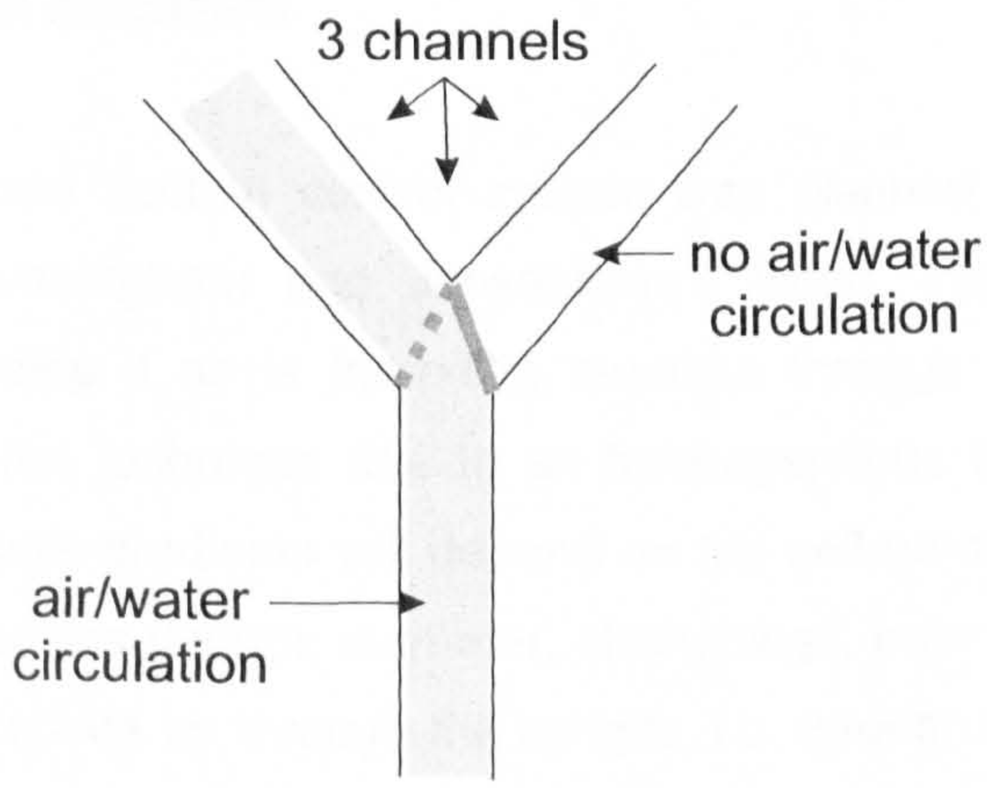

Figure 5.12: Schematic drawing of the 3-way valve

5.2.3. Control system

One of the goals was that the suction control system could be run automatically. TRIAX was used as the data acquisition and control software (Toll, 1999). It monitors and controls devices. A PCI digital input/output card (PCI 836-A) was used to control the cell pressure through stepper motor driven pistons. The same card could also be used to control the pump and valves. It works by sending 5V signals to a voltage converter which converts the signal to 12V to switch the pump on/off and 24V to switch the valve on/off (Figure 5.13). Modifications to the software were carried out by Dr David Toll.

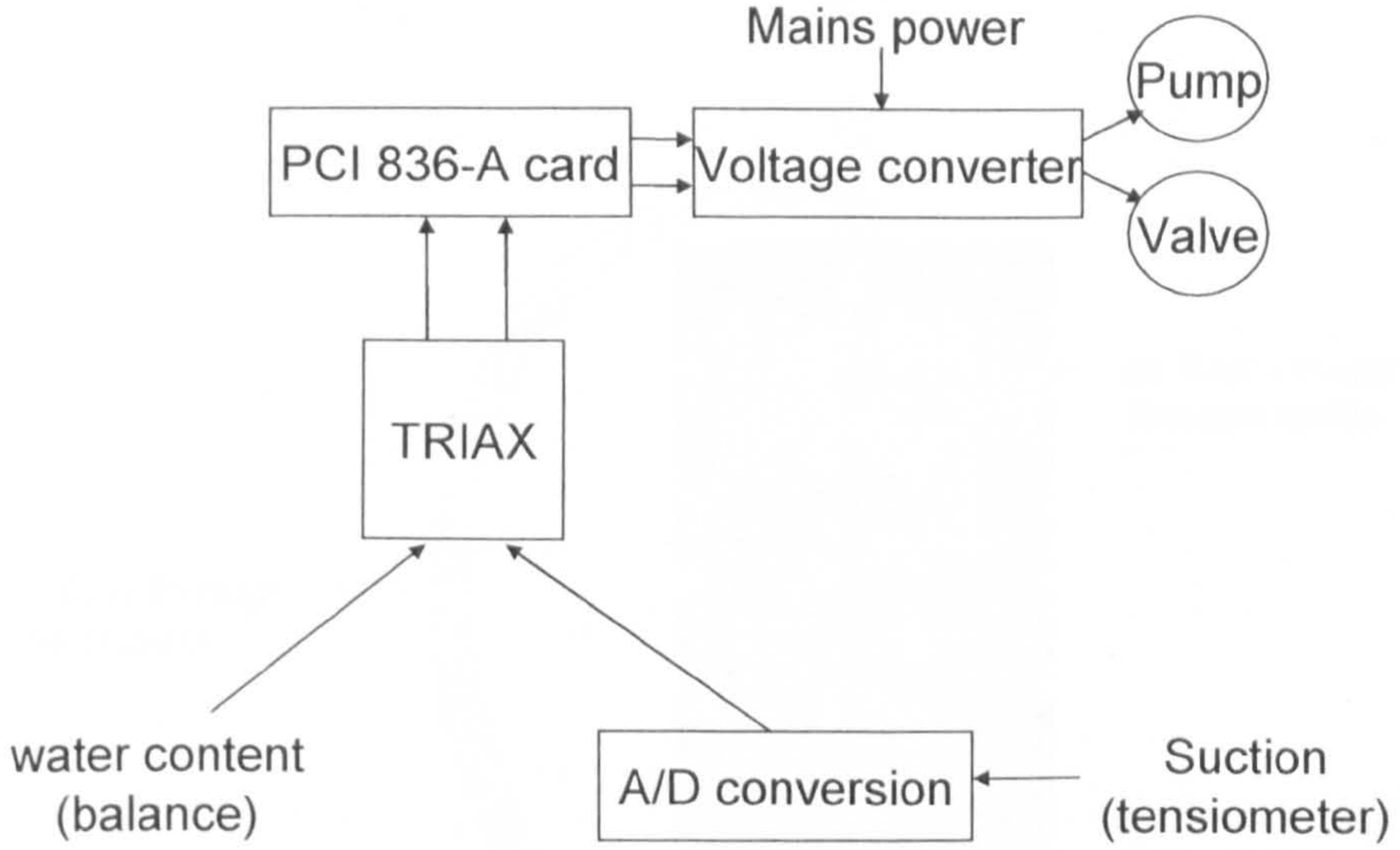

Figure 5.13: Control system

5.3. AIR PRESSURE GRADIENTS

The tensiometer based suction control system was planned to be air circulation based (following Cunningham and Jotisankasa's work). However, air pressure gradients might develop if air is forced to circulate through a soil sample. Such gradients invalidate the technique due to an heterogeneous distribution of the net stress. The air pressure gradients will depend on the soil permeability to air, tubing and fittings characteristics (length, diameter, shortenings, enlargements) and on the technique used to circulate air through the sample, i.e. through the soil itself as done by Cunningham et al. (2003) or around the sides of the sample by using lateral drains (Blatz and Graham, 2000). Air pressure gradients will be higher when air is forced through the sample without side drains or without a bypass between the top cap and bottom pedestal of the sample (Figure 5.14).

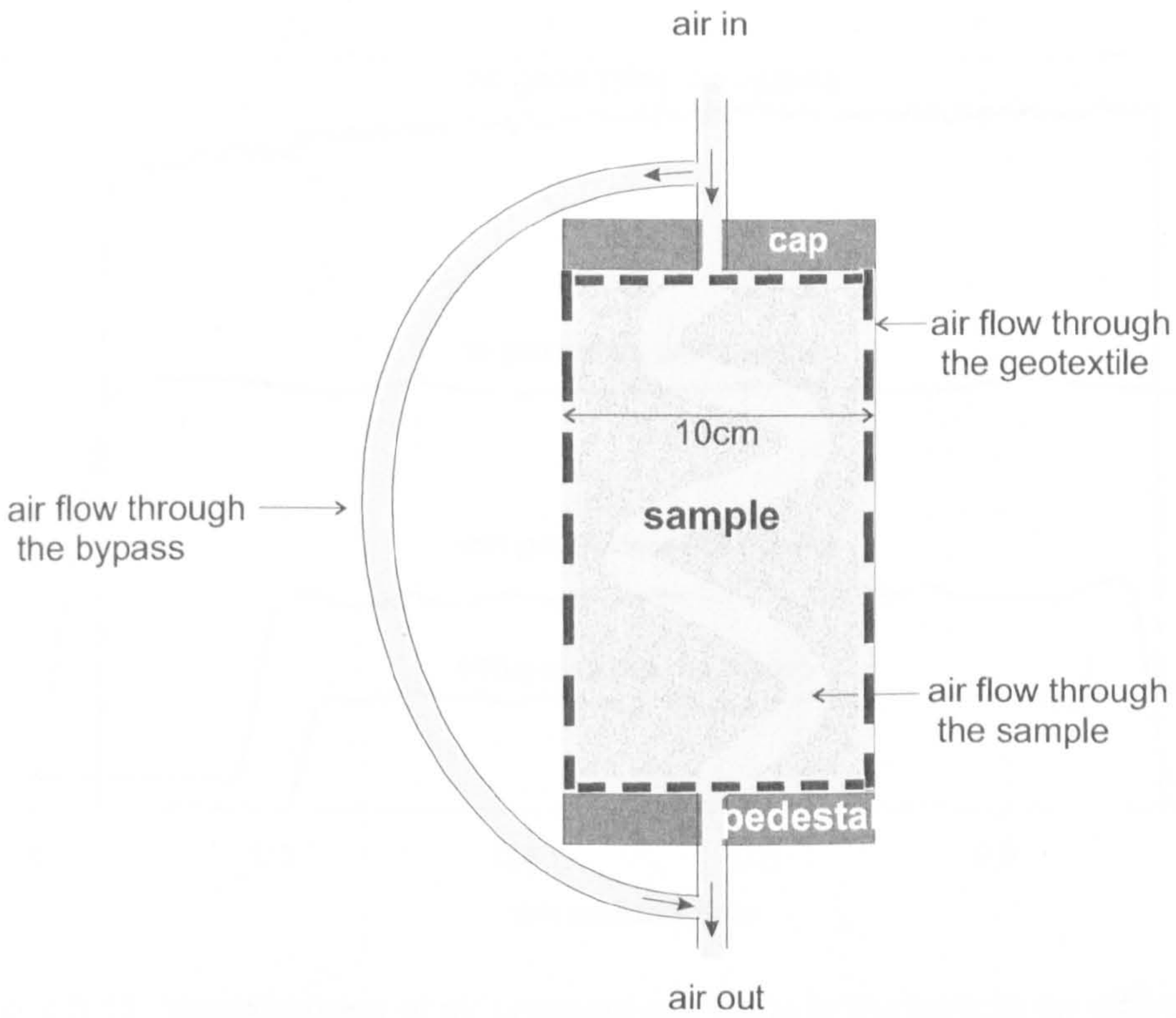

Figure 5.14: Air flow through the soil, bypass or geotextile

A testing program was carried out in order to define the best way to minimise the air pressure gradients in the sample. Tests were conducted with a dummy sample made of 4 porous (sandstone) discs with a water permeability of 10^{-7}m/s. An initial confining pressure of 130kPa was applied to the sample. Air was circulated through the sample for 4 different conditions: (1) sample only, (2) sample with bypass, (3) sample with geotextile, and (4) sample with geotextile and bypass. For the geotextile the porous discs were simply wrapped on the sides between the sample and the loading platens, and for the bypass one pipe was connected between the top cap and pedestal.

The results in Figure 5.15 revealed a pressure difference of approximately 30kPa for the sample only (1), and 5kPa for the geotextile arrangement (3). Pressures for the bypass (2) and combined bypass and geotextile (4) were intermediary. Therefore, according to the data the most important factor decreasing the air pressure gradient was the geotextile, the bypass did not change much.

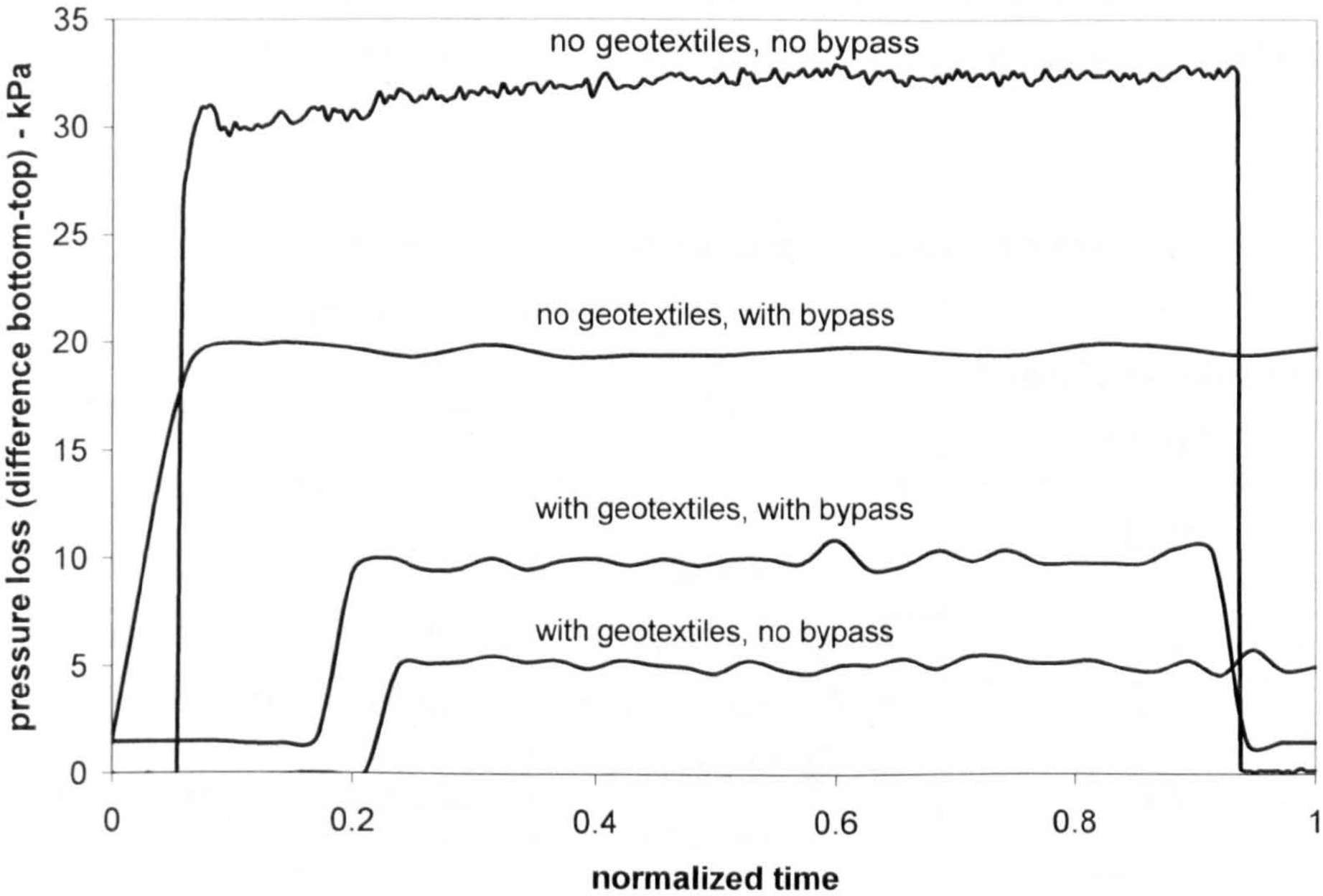

Figure 5.15: Measurement of air pressure gradients in the sample for different conditions (Y-axis denotes the air pressure difference between the bottom and top of the sample) (tests PG1 to PG4, sandstone disks)

5.4. DRYING SYSTEM

5.4.1. Drying measurement and control

Drying was controlled by circulating air through the soil and then through a desiccant. Any moisture released by the soil would be retained by the desiccant and measured based on the mass increase of the desiccant.

5.4.1.1. Dessicant

The desiccant used was silica gel. Silica gel is a synthetic amorphous material with spherical particles of colloidal silica (SiO_2). It is composed of a network of interconnected microscopic pores with different sizes. Average pore sizes range between11Å to 68Å (1Å = 10^{-10}m) (Pesaran and Mills, 1987a) (the distance between the two Hydrogen atoms of the water molecule is 1.515Å). This structure gives a high internal specific surface area (500-900m^2/g), which is responsible for the high

moisture adsorption capacity (kaolin has a specific surface area 40-80 times smaller (10-20m^2/g)). Table 5.3 presents a comparison between different particulate materials.

Table 5.3: Specific surface area for different particulate materials
(from Mitchell, 1993, Sun and Besant, 2005)

Material	Shape	Size	Specific surface area [m^2/g]
Medium sized sand	Rounded	0.50-0.25 mm (grain diameter)	$4.5x10^{-3}$
Kaolin	Platy	0.1-4μm x 0.05-2μm	10-20
Montmorillonite	Platy	>10 Å x up to 10 μm	<840
Silica gel	Spherical	5Å to 3000Å (pore diameter)	<900

Adsorption is controlled by water vapour pressure differences between the silica gel pores and the adjacent air. If water vapour pressure is lower in the pores, water molecules diffuse through the air and adhere to the internal surfaces of the pores (following the introduction in Chapter 2). The amount of adsorbed water is related to the level of water vapour pressure (directly proportional to the relative humidity) of the surrounding air. The higher the humidity, the greater the mass of water adsorbed (Sun and Besant, 2005). If the water vapour pressure is higher in the pores than the adjacent air, moisture transfer occurs and the silica gel loses water (desorption) (Pesaran and Mills, 1987a, Sun and Besant, 2005).

Pesaran and Mills (1987b) identified a hysteric response of silica gel when subjected to drying-wetting cycles, i.e. the adsorption and desorption lines differ. The silica gel used lost >0.8 (kg water/kg humid air) during desorption (drying) and gained >0.6 (kg water/kg humid air) during adsorption (wetting). This behaviour resembles the hydraulic hysteresis of unsaturated soils where the wetting curve of the SWRC lies below the drying curve.

The internal structure of the silica gel was observed by SEM. The image in Figure 5.16 was taken at the maximum possible resolution and amplification (50nm). A lumpy structure with closely packed rounded grains can be distinguished. The darker areas most probably correspond to depressions in the surface rather than pores. The

specifications provided by the manufacturer (MERCK) indicate pores with an average size of 6 nm, approximately 10X times smaller than what is shown. Even if not clearly visible, silica gel's nano-scale structure and homogeneity should justify its high adsorbing capacity of water.

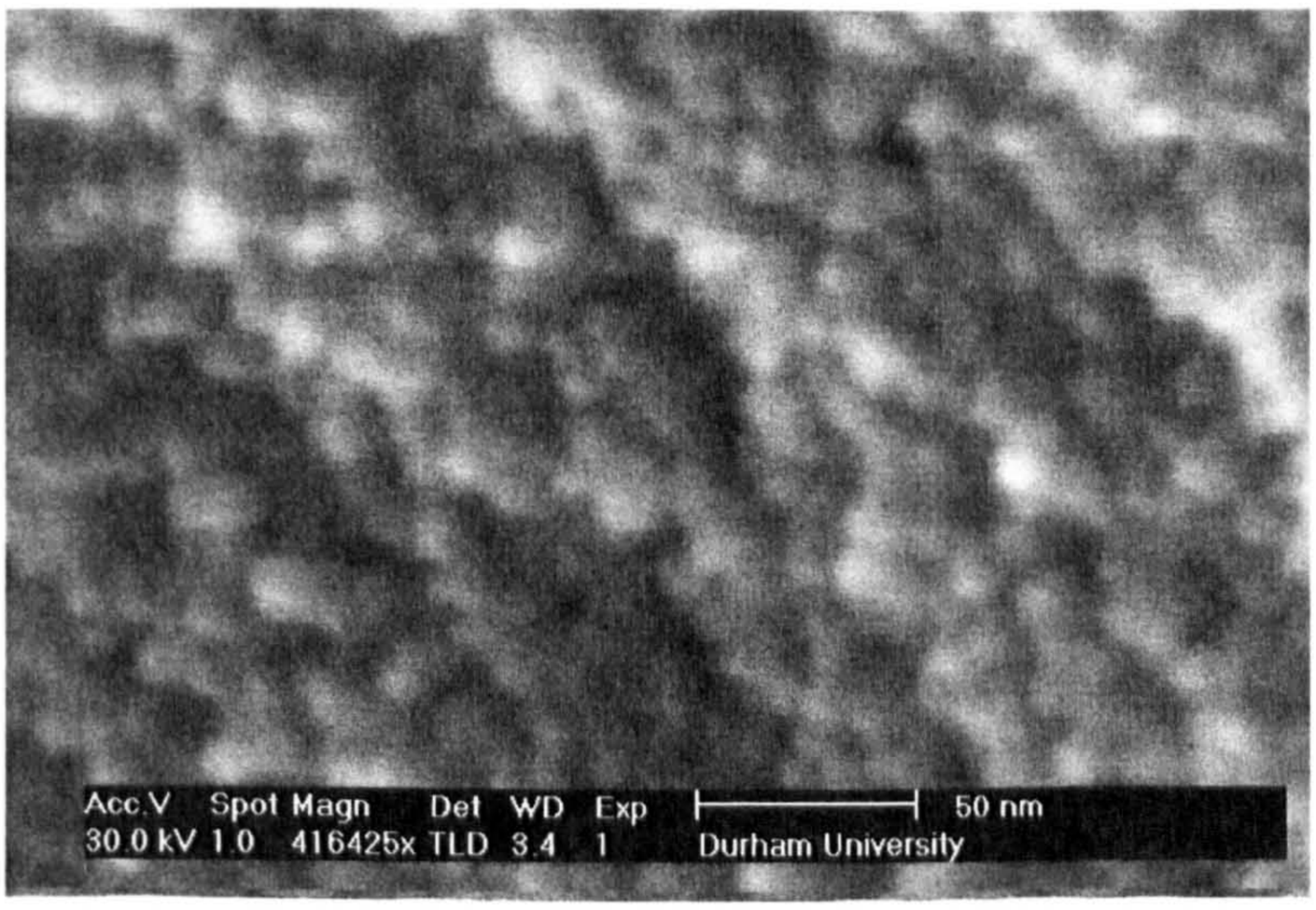

Figure 5.16: SEM microphotograph of silica gel (Photo: Mark Rosamond)

Two silica gels were used: blue and orange. The blue silica gel has an adsorption capacity of approximately 8% of its initial dry weight for a relative humidity (RH) of 55% (Figure 5.17a). Its adsorption capacity was measured by placing the silica gel dry (just removed from the oven) in a balance. The adsorption capacity cannot be directly extrapolated to the suction control tests because the RH in the tubing could be different. Figure 5.17a also shows that the adsorption rate is high once it starts wetting, decreasing afterwards.

The hysteretic behaviour of silica gel due to its porous structure suggests that it should only be used for drying. Water mass fluctuations in the silica gel should be avoided. Otherwise corrections to the hysteresis would have to be included.

The blue silica gel (initially used) was substituted by a new orange silica gel (due to health concerns). Its adsorption capacity was measured and compared to the blue silica gel. Figure 5.17b below shows that orange silica gel absorbs twice the mass of the blue silica gel, an indication that it would not require frequent replacements during testing for the case where large adsorptions of water are expected. The higher adsorption of the orange silica gel could be related to a smaller pore size than the blue silica gel (no information available for the blue silica gel).

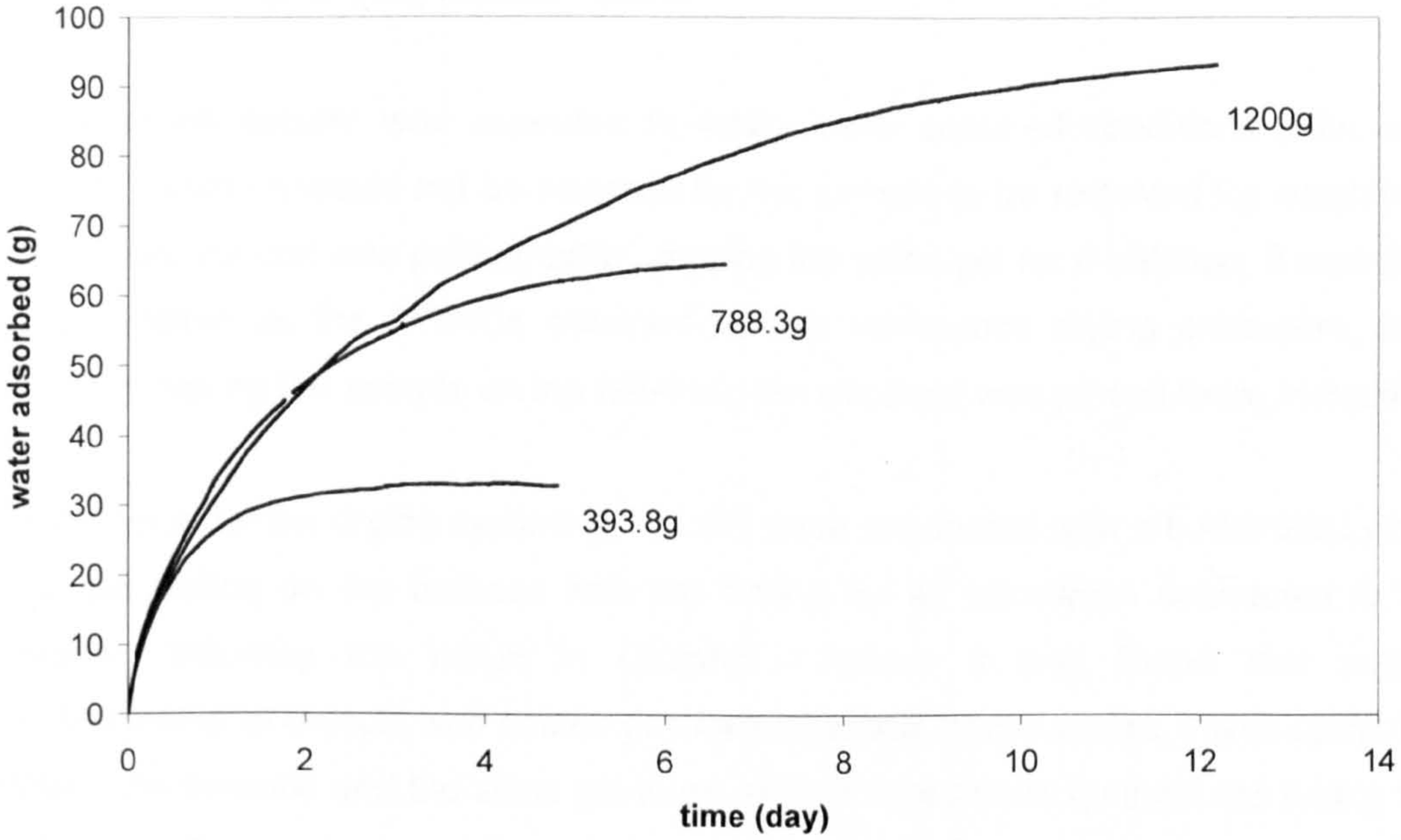

(a)

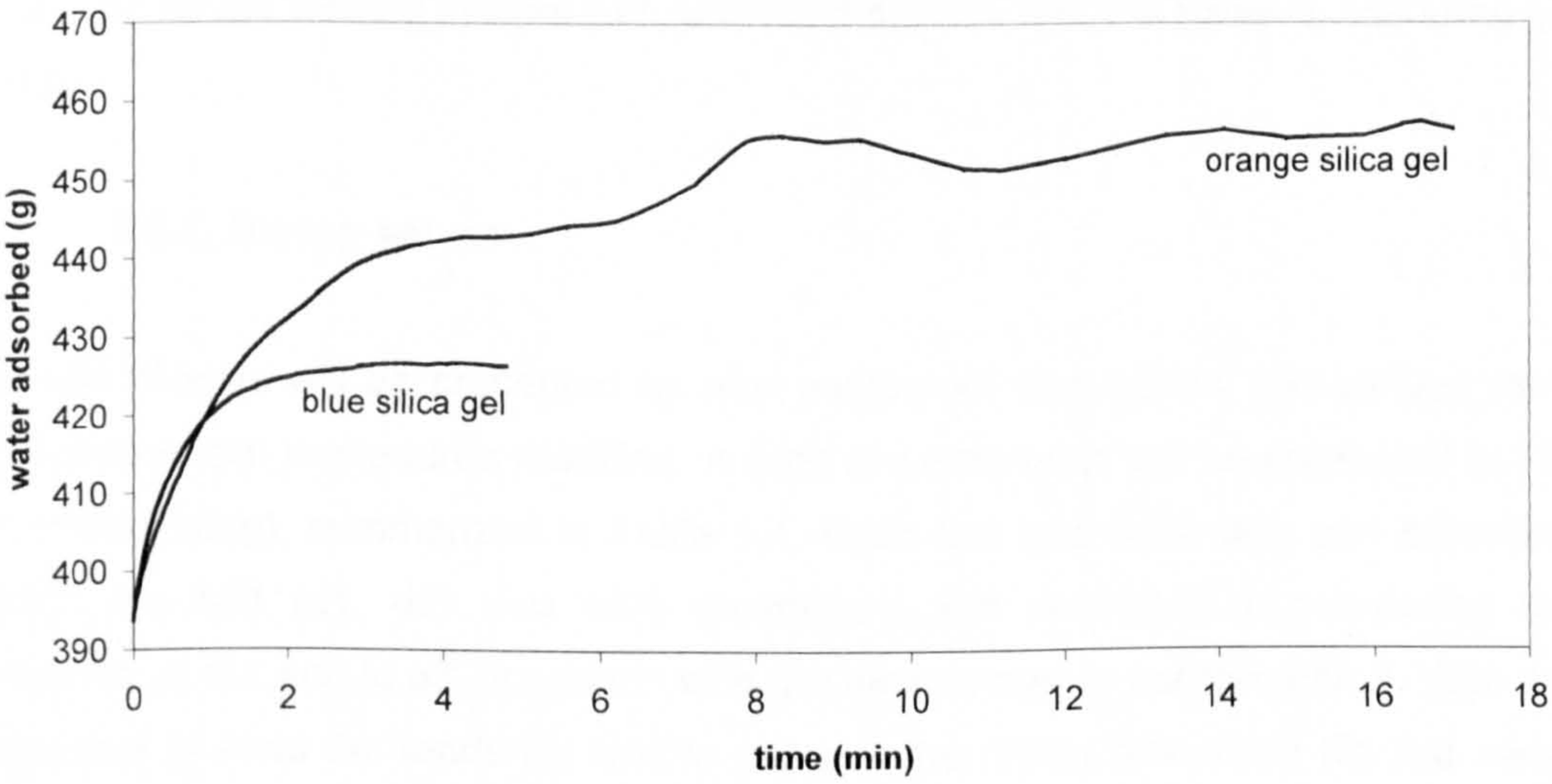

(b)

Figure 5.17: Mass of water adsorbed by the silica gel (tests SG1 to SG4, silica gel), (a) blue silica gel for 3 different initial weights (RH~55%), (b) comparison to the new orange silica gel

5.4.1.2. Drying measurement

As the drying system was expected to work under confined conditions (with cell pressure) where it would not be possible for the sample to be removed for weighing, mass measurement was performed by placing the silica gel on a balance. It was the same principle as the SWRCs obtained by the continuous drying procedure, but instead of having the sample on the balance, the silica gel was placed there instead.

Initially, tests for the drying system (d1 to d7) were conducted with a bottle filled with silica gel resting on the balance with the tubing for air circulation connected to it. However, following the result in Chapter 4 where it was found that mass measurements of objects with cables or tubes attached induce errors, it was opted to enclose the balance and the silica gel in an air tight box and to connect the tubing to the box. All the open spaces were intentionally reduced to the minimum possible in order to accelerate the adsorption of water in the air and reduce equilibration times. The tests for the wetting system (w1, w2) used the box with the balance and silica gel inside.

5.4.2. Drying set-up

Results of tests will be presented as new equipment was added, the set-ups were improved or the procedures modified. A total of seven tests will be presented (d1 to d7, *d* for drying), summarized in Table 5.4. Each test was done with one objective, where the first (d1, d2) was very preliminary and consisted in monitoring the response of the soil to air circulation with the tensiometer in contact with it. With the sequence of tests the tendency was to improve the drying procedure (for the same initial set-up) in d3; automatize the control in d4, d5 and include water content measurement in d6, d7.

Table 5.4: Testing program for the drying tests

test nr.	water content w (%)	void ratio e	material	objective
d1	-	0.94	sand (80%) + kaolin (20%)	to circulate dry air with suction measured by the tensiometer
d2	17	0.51-0.56	BIONICS	same as above
d3	17.3-18.6	0.51-0.56	BIONICS	change of the drying procedure by setting suction targets
d4	17	0.51-0.56	BIONICS	same as above with automatic drying
d5	17	0.51-0.56	BIONICS	same as above with automatic drying to high suctions
d6	17	0.51-0.56	BIONICS	same as above with water content measurement
d7	17	0.51-0.56	BIONICS	same as above

Testing of the drying system started with the set-up shown in Figure 5.18. It uses the drying arrangement for version 1 of the suction control system in Figure 5.1. The drying air source was a tube filled with silica gel, where the moistened air flowing out of the sample would be retained. The goal was to monitor the tensiometer response to dry air circulation.

The system in Figure 5.18 represents a change to the original one shown in Figure 5.1. This original system (with water in a salt solution) was never tested because initial testing with silica gel gave promising results.

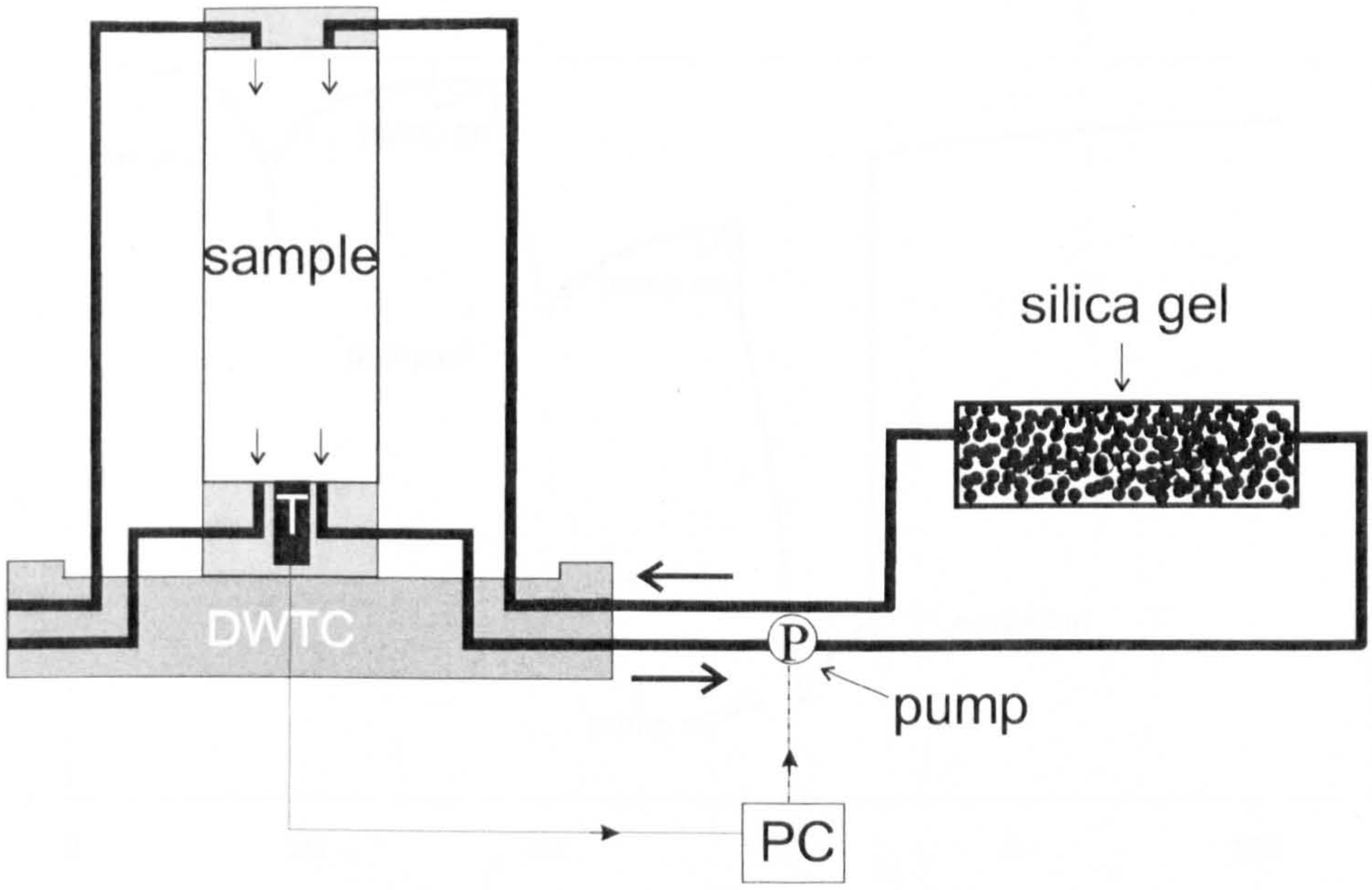

Figure 5.18: Set-up for drying by circulation of dry air through the sample

5.4.2.1. Tests d1, d2

Test d1 (Table 5.4) was conducted on a sand (80%) – kaolin (20%) mixture with a high void ratio (e_0=0.94). The test was conducted with a tensiometer inserted in the pedestal of the DWTC directly in contact with the sample at a cell pressure of 200kPa (no geotextile added). The insertion of the tensiometer in the pedestal is a new design feature and represents an evolution to the initial work by Cunningham (2000) where the tensiometer was placed on the side of the sample through the membrane.

The test (in Figure 5.19) revealed that when the pump was on and air was circulating, suction would increase but when switched off it would decrease and tended to equalize. This was interpreted as the sample drying faster at the surface than at the inner parts. The test ended with early cavitation of the tensiometer.

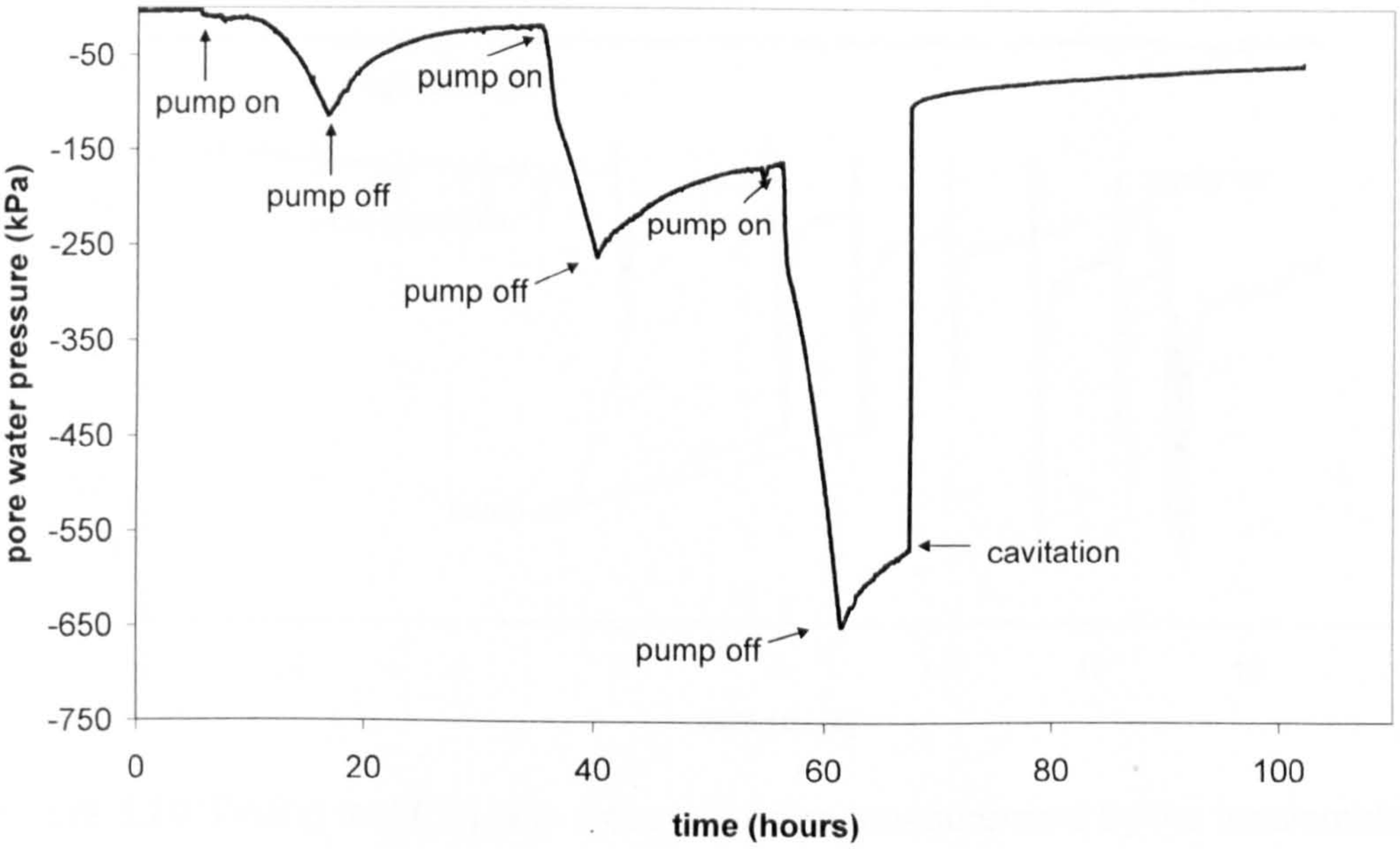

Figure 5.19: Drying test (d1) with suction measurement by the tensiometer (tensiometer II1, sand/kaolin mixture)

The results for test d2 in Figure 5.20 revealed that when the pump was on, suction would increase and when switched off would decrease but would equalise to a value of suction higher than in the previous drying stage. The period of time the pump was on was limited by the suction measured; usually it was switched off when a value of 800kPa was achieved (to reduce the risk of cavitation), although in some cases it was allowed to increase to 1200kPa. Drying progressed slowly, it took almost 2 weeks to increase suction from 50kPa to 400kPa.

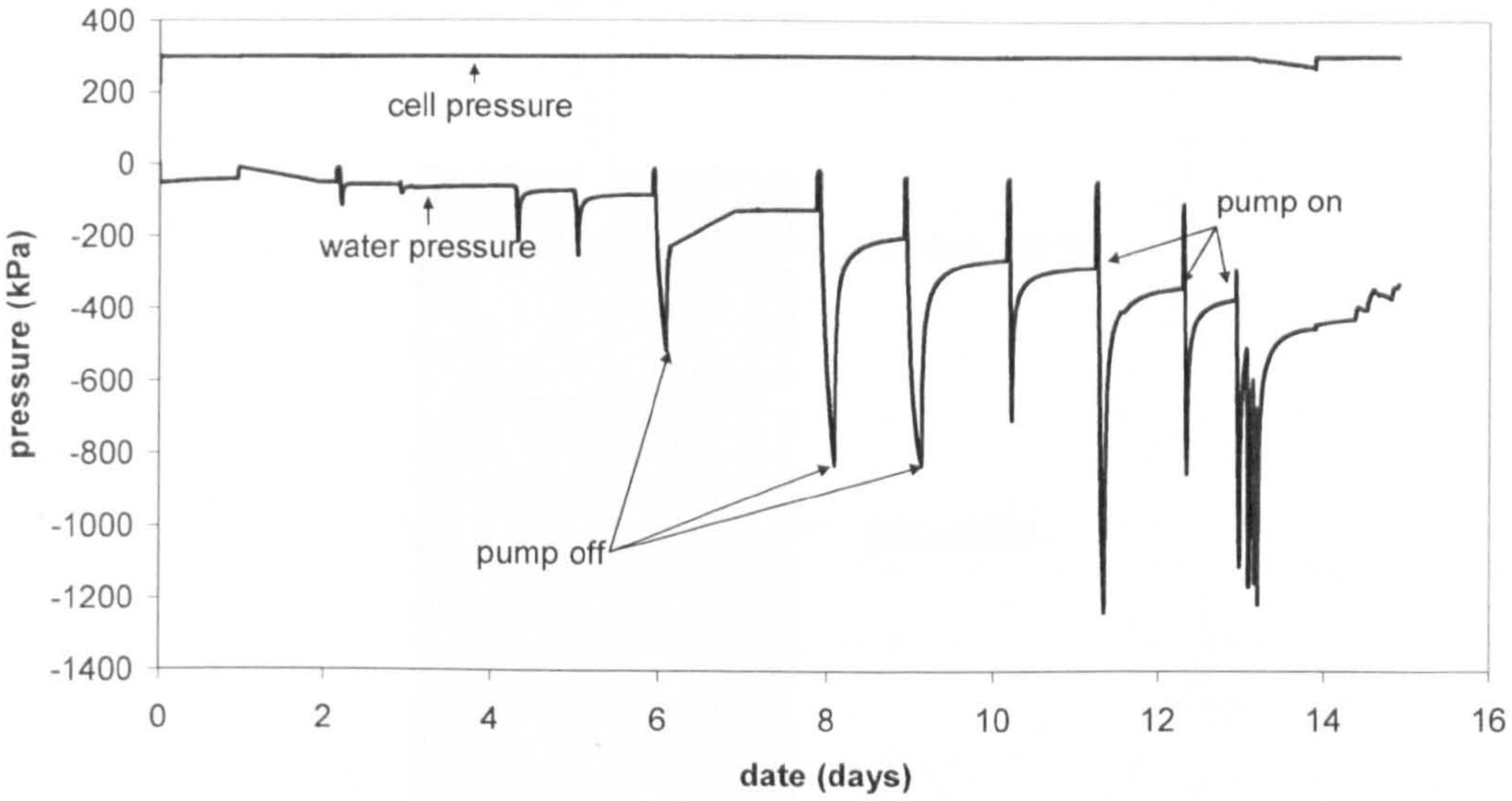

Figure 5.20: Drying test (d2) with water pressure measurement by the tensiometer (tensiometer II1, BIONICS)

5.4.2.2. Test d3

Following the discussion in Chapters 3 and 4 on the importance of avoiding reversals in wetting and drying, as occurred in tests d1 and d2, the drying procedure was reviewed. The new procedure consisted in setting maximum and minimum limits for suction to fluctuate within until equalization.

A compacted sample of BIONICS soil was prepared at w_i=17.3% - 18.6% and placed in the DWTC. The sample height was cut to approximately 30mm (from the 100mm high compacted sample). The sample was enclosed radially by a geotextile and top and bottom by porous stones. Air circulation was done by forcing air to flow in and out through 1 pipe (Figure 5.21). The sample properties at the beginning and end of the test d3 are shown in Table 5.5.

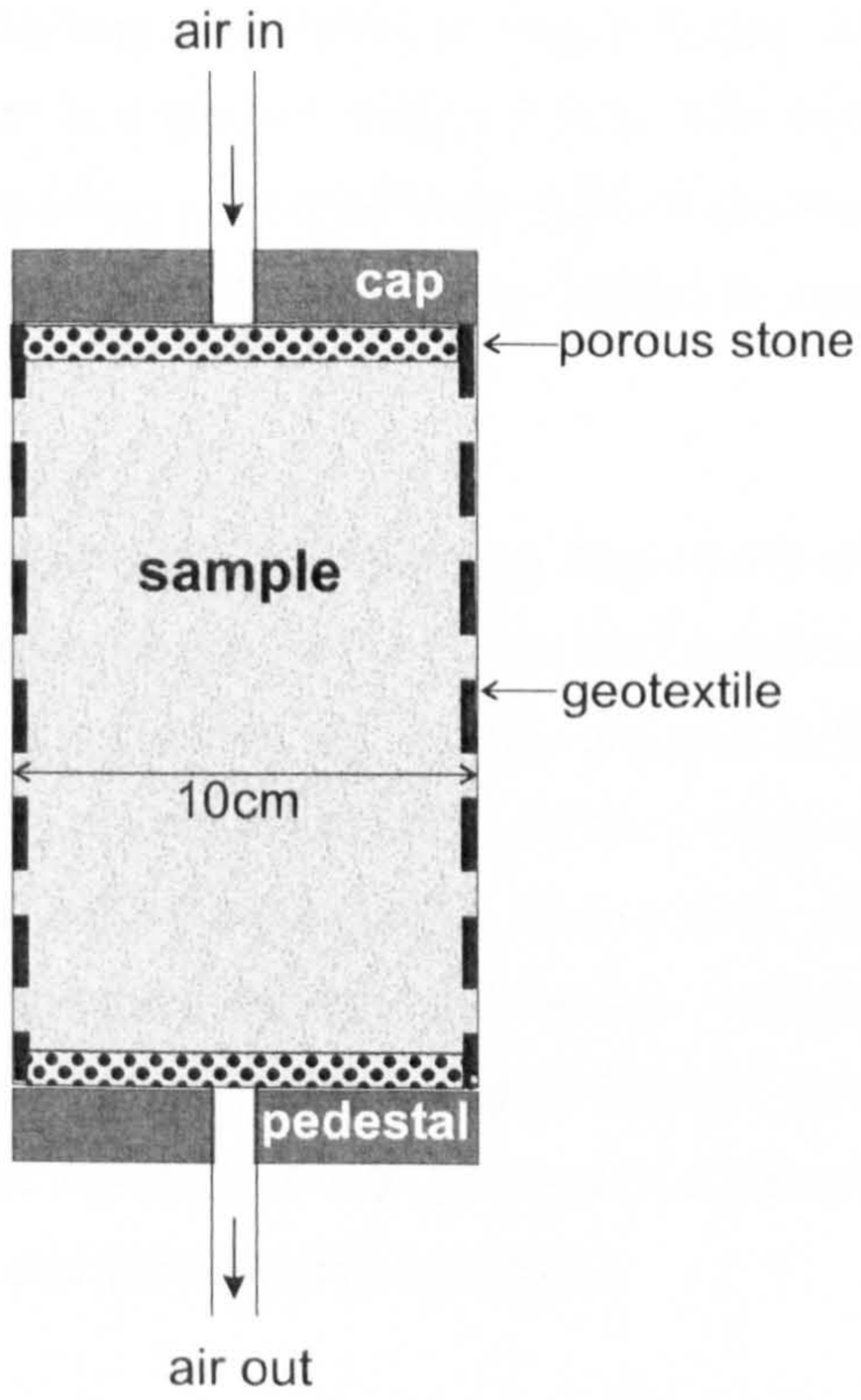

Figure 5.21: Arrangement for the air circulation in the sample

Table 5.5: Soil properties of the tested sample at the start and end of the test d3

dry density ρ (Mg/m³)		**void ratio e**		**water content w (%)**		**degree of saturation S_r (%)**	
initial	final	initial	final	initial	final	initial	final
2.06	2.13	0.51-0.52	0.41	17.3-18.6	13.8	90.4-94.0	88.9

Drying proceeded by setting a target suction (200kPa, 300kPa, 500kPa, 800kPa, 1200kPa, 1400kPa) and controlling suction manually within an interval of ±10kPa, e.g. 490kPa - 510kPa. If suction reached (or exceeded) the upper limit the pump was turned off. If it then dropped below the lower limit the pump was turned back on. Once the value had stabilized the pump was switched on to the next target. For this test, control was carried out by manually switching the pump on/off. The maximum target suction was limited to 1400kPa to prevent air entry or cavitation of the tensiometer. Silica gel was placed in the air circulation system to collect the water droplets in the air. Air pressure in the sample was also monitored to check any obstructions to air flow.

The results for the entire test are shown in Figure 5.22a. An example of a specific suction interval (500kPa) is shown in Figure 5.22b. The suction target intervals are shown by the shadowed area. The maximum suction reached was 1200kPa instead of 1400kPa, because shortly after reaching 1400kPa cavitation occurred in the tensiometer.

As soon as the test started the water pressure decreased until the lower limit of the interval and then increased rapidly to the upper limit when the pump was turned off. As the water pressure equilibrated through the sample with the successive drying cycles, the period of the cycles increased with time (Figure 5.22b) until the water pressure line flattened out. Figure 5.22b also shows that the water pressure decrease (once the pump was switched on) was fast. The water pressure frequently overshoot the lower limit of the interval (Figure 5.22b), even when the pump was switched off at -10kPa of the target water pressure, i.e. the soil would keep drying for some more time before the line inflected upwards.

By the end of the test the sample had dried by 4.15% (20.2g) (w_i-w_f in Table 5.5). The silica gel was also weighted at the start and end of the test and a difference of 5.7% (28g) were recorded. This discrepancy suggests that the system was not entirely closed or that there was an extra source of water humidifying the circulating air. The maximum air pressure recorded was 5kPa which shows that air was flowing easily.

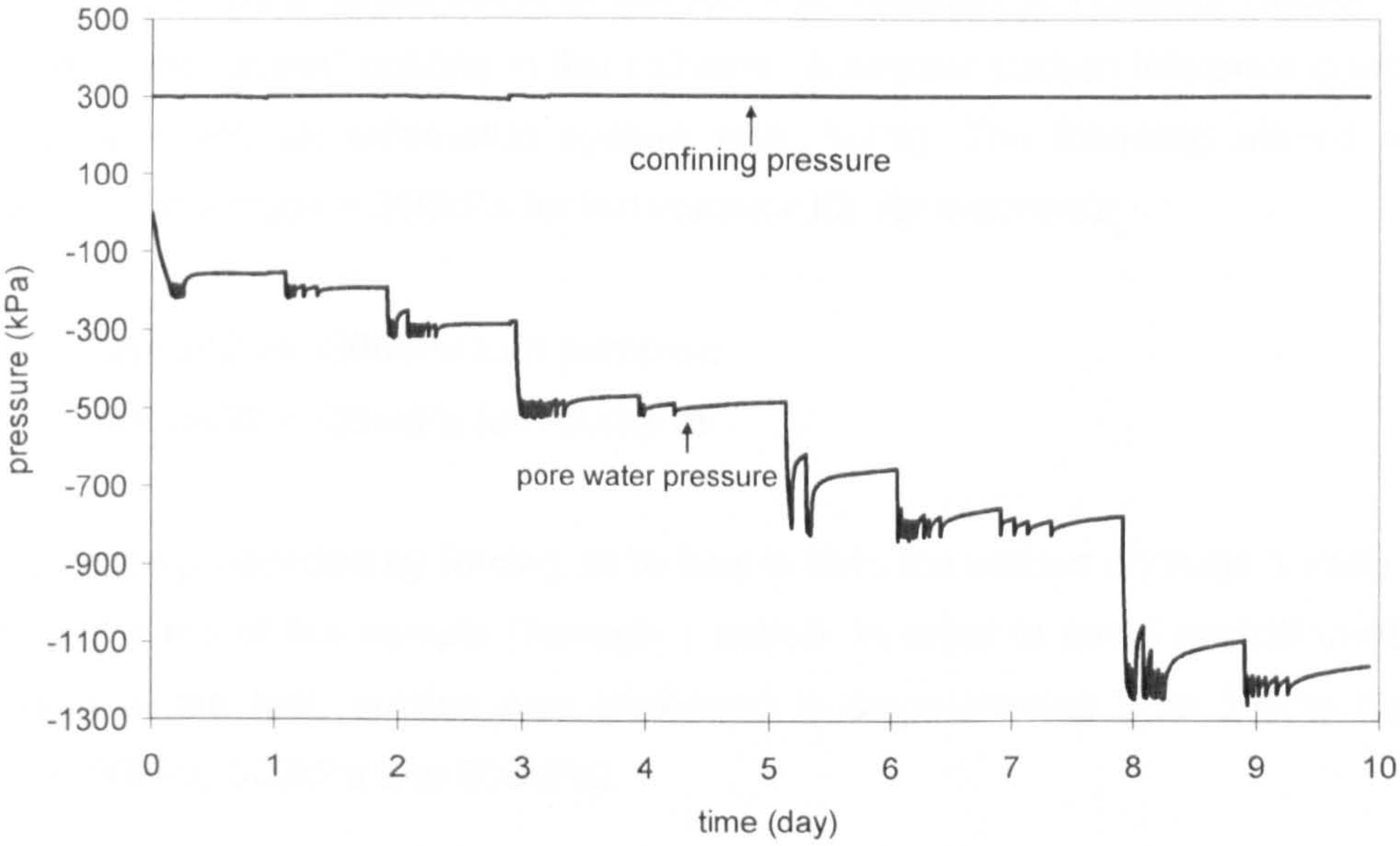

(a)

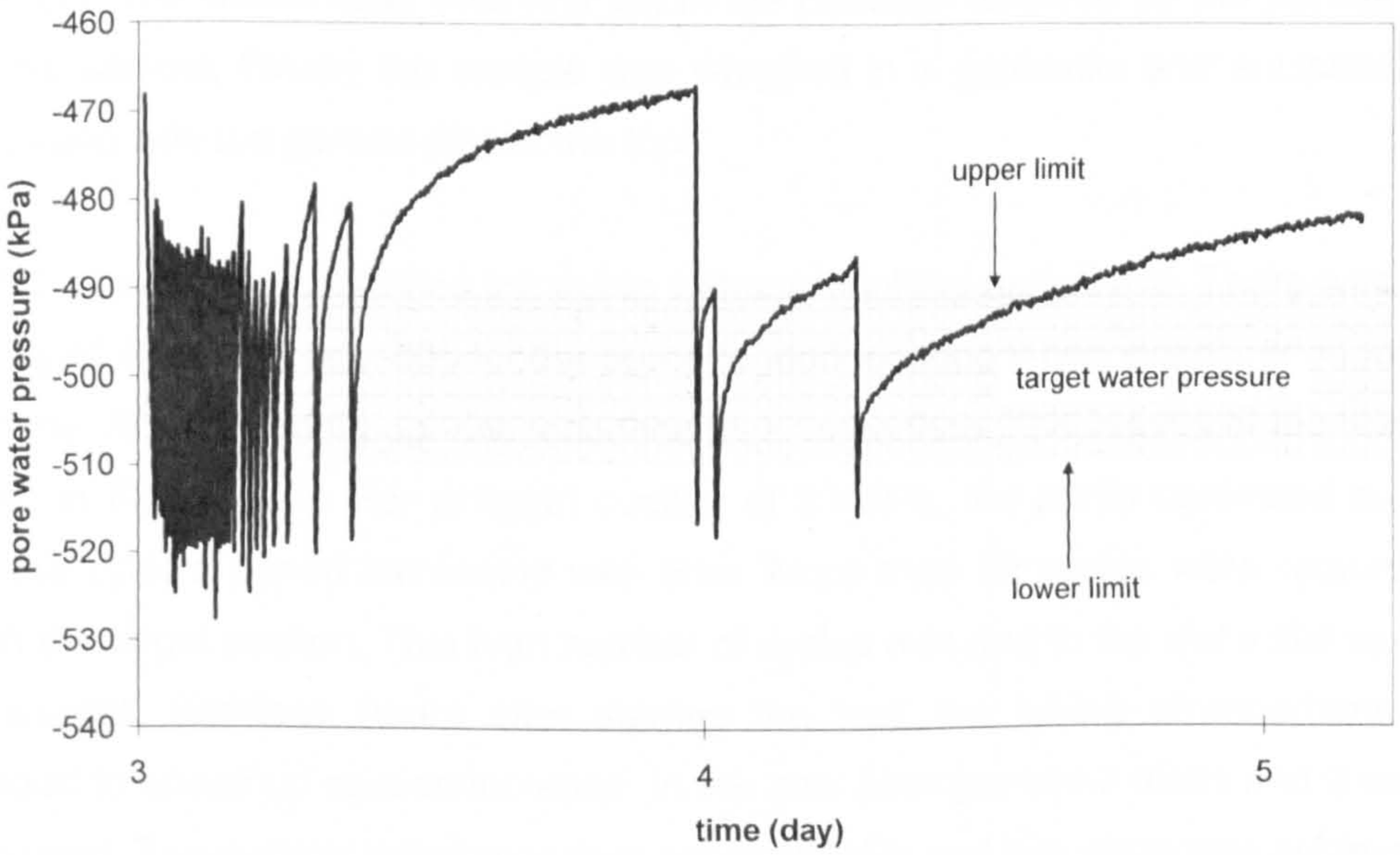

(b)

Figure 5.22: Manual drying of an unsaturated soil sample (test d3, tensiometer II2, BIONICS), a) all test, b) details of 500kPa suction stage

5.4.2.3. Tests d4, d5

The manual drying within a suction range (from low to high suctions) was successful enough to change the drying to a fully automated procedure where the pump is switched on/off once suction exceeds the upper/lower boundary of the interval, respectively. TRIAX version 5.1.4 was used to switch the pump on and off

automatically once a target value of suction was reached or crossed. Suction was selected by the "alarm" options in the software. A smaller suction tolerance could be implemented with an automated system (e.g. 1kPa). The following alarms were chosen (target suction = 300kPa for tensiometer II2, for example):

Alarm 1: tensioII2 >= -300kPa turn pump on
Alarm 2: tensionII2 < -301kPa turn pump off

Air circulation proceeded by forcing air to flow in from the bottom (through 1 inlet) and out from the top of the sample (through 1 outlet). In order to avoid cavitation at the beginning of the test, suction was increased in steps starting from low to higher values (300kPa, 600kPa and 800kPa).

A sample of BIONICS soil was compacted at a water content of 17% and cut to 1/3 of its length. The tensiometer was first set in the pedestal followed by the porous disc and the sample. Finally the sample was wrapped in a geotextile and enclosed in a membrane with the porous disc at the top.

TRIAX successfully controlled the pump without requiring assistance. There was only a delay of approximately 30s for the pump to start working when switching on for the first time. After 'warming up' the response was immediate. The results of the test are shown in Figure 5.23. For a target suction of 300kPa, the pump controlled suction with the cycle's period increasing with time. More than 50 cycles were required to reach the target suction. This high number of cycles was due to the wet initial state of the sample. Eighteen hours after starting the test, the tubing arrangement was changed to speed up suction increase. In the new arrangement 2 inlets and 2 outlets were used. The suction target was then set at 600kPa and this value was achieved in 3 cycles. The target was increased to 800kPa, but shortly after reaching 800kPa cavitation occurred in the tensiometer and the test ended.

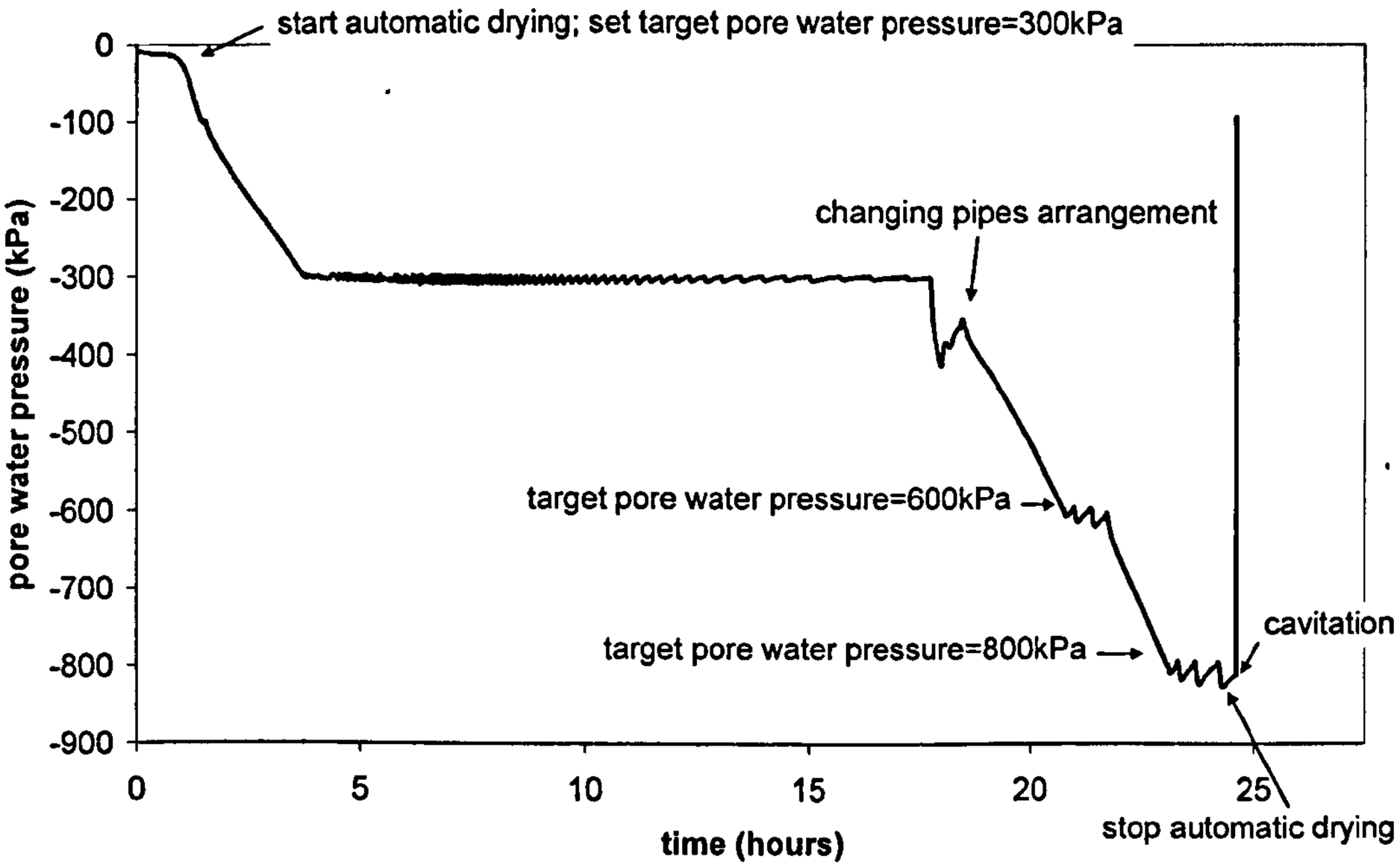

Figure 5.23: Automatic drying of an unsaturated soil (test d4, tensiometer II2, BIONICS)

The previous test by automatic drying was conducted by increasing the target suction in stages, starting from lower to high suctions. One more test (d5) was performed by taking suction directly to a high value (800kPa).

Figure 5.24 shows that suction increased until 800kPa and then was kept within an interval. Due to early cavitation, the test ended without suction fully stabilizing.

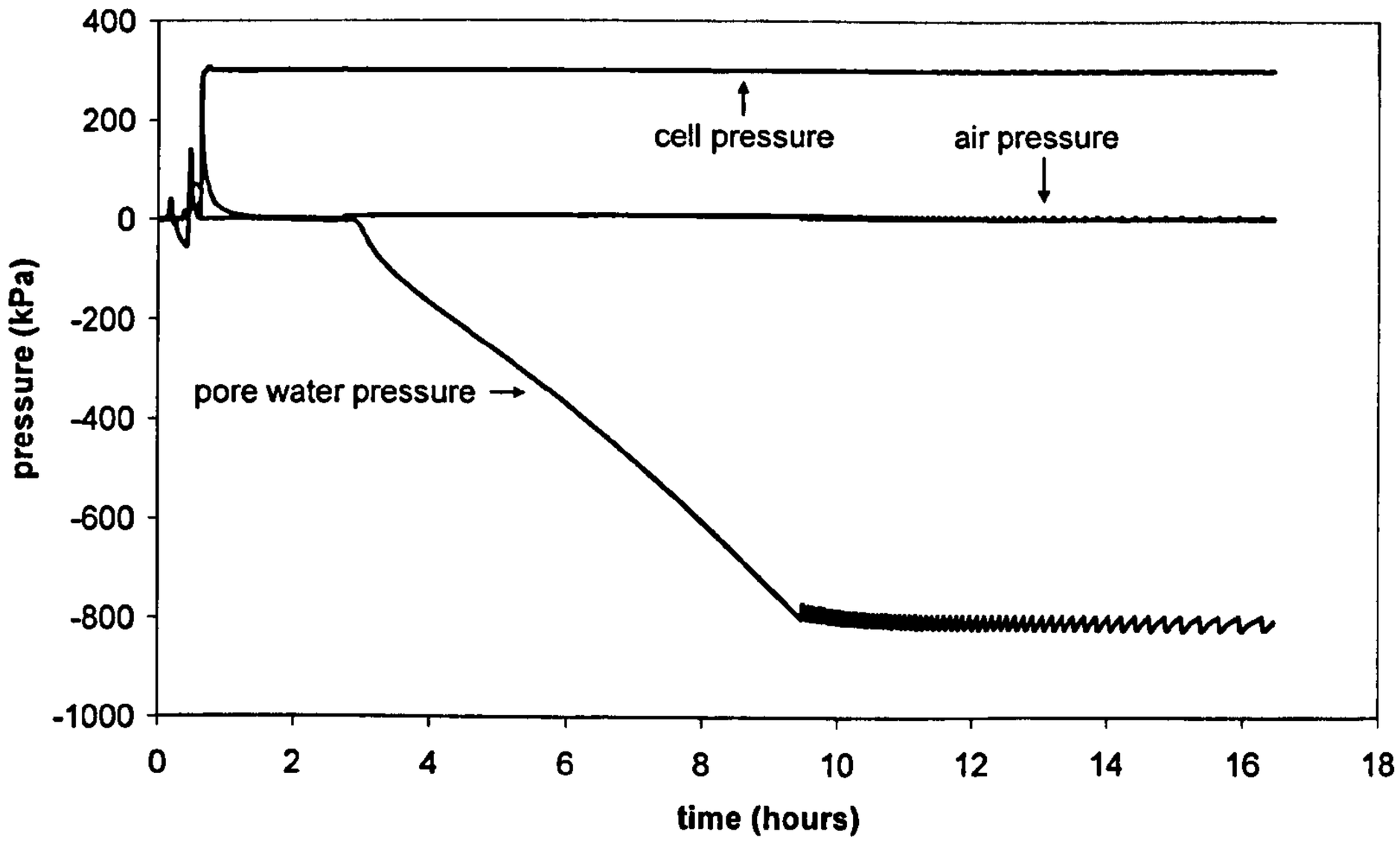

Figure 5.24: Automatic drying of a soil sample within a higher suction value (test d5, tensiometer II2, BIONICS)

As the automatic drying proved sufficiently good to control suction within a suction interval, the development of the suction control technique moved into the next stage: automatic drying with water content measurement. The water content measurement requires measurement of the water lost by the sample. The amount of water lost was measured by using a balance to weight a tube filled with silica gel.

5.4.2.4. Tests d6, d7

The first automatic drying with water mass measurement (test d6) was conducted on a BIONICS soil sample compacted at 17%, with a diameter of 100mm and 30mm height (the same initial conditions as all previous tests). After setting the sample in the DCTC and arranging the water mass measurement system (balance and bottle filled with silica gel), all the area surrounding the equipment was physically protected (to avoid someone knocking it) to keep the mass readings stable.

The results (Figure 5.25) show suction and the mass readings increasing when the sample was drying. Due to an error in setting the correct alarms in TRIAX's control window, the pump worked continuously leading to an early cavitation of the tensiometer. The test still proceeded by switching on the pump for defined periods of time. The results show a good agreement between the periods of time the pump was

on (grey shading) and the mass increase. When the pump was off the mass recordings remained constant. After finalizing the test, the silica gel was weighed, oven dried and weighed again to check if the mass difference was the same as measured by TRIAX (24g). The silica gel measurements were 25.48g indicated a difference of 1.48g. This additional mass adsorbed by the silica gel could be related to some moisture adsorption prior to the start of the test.

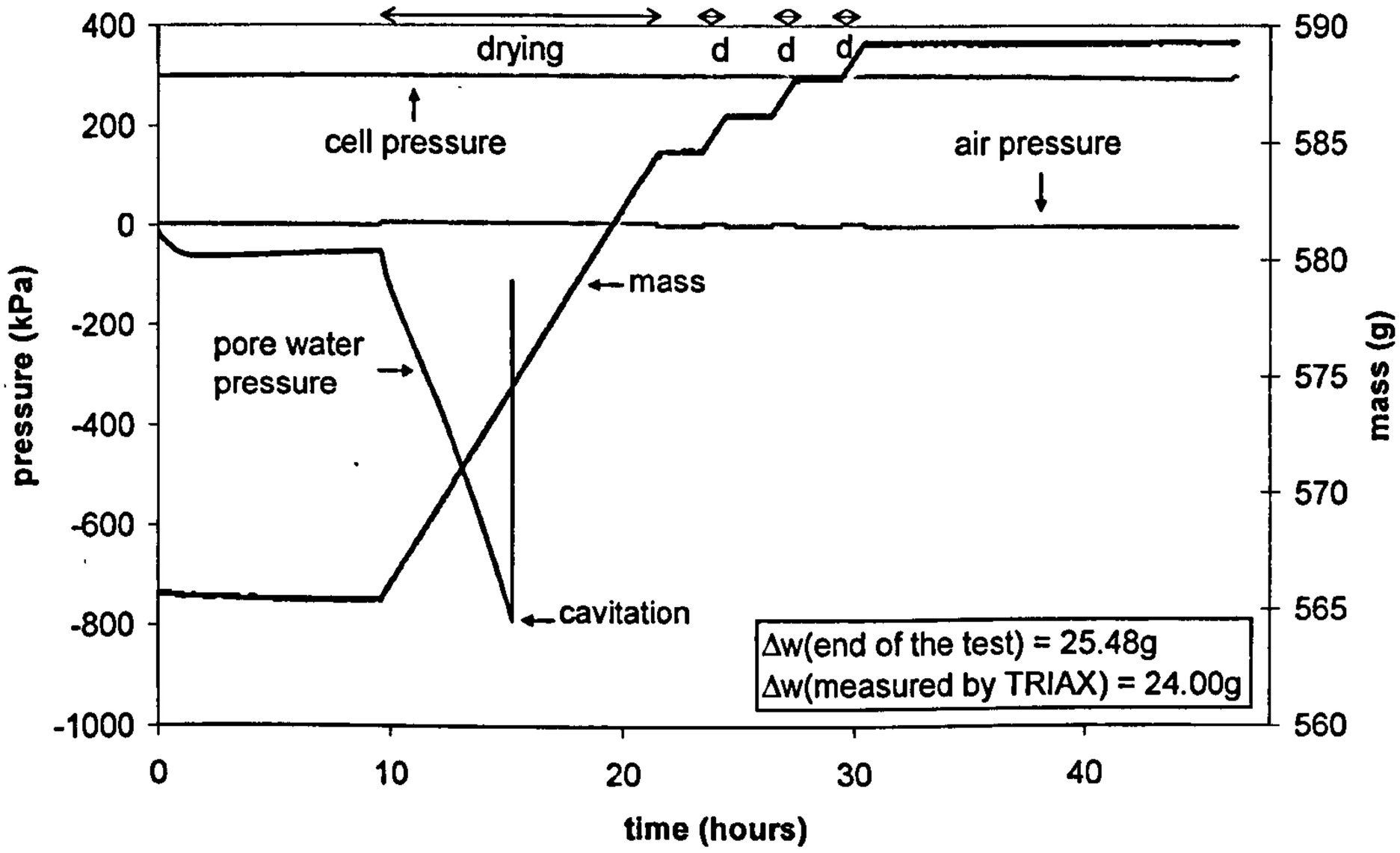

Figure 5.25: Controlled drying test with water mass measurement (test d6, tensiometer III4, BIONICS) (grey shadows in the graph correspond to the drying of the sample)

A second test (d7) was conducted to verify the suction and mass increase behaviour of a drying sample. The sample preparation and testing procedure was the same as d6. The results in Figure 5.26 show suction and mass increasing while the pump was on for longer periods of time, e.g. from the water pressure target of -350kPa to -450kPa. After reaching the suction target the mass still increased slightly becoming reasonably flat afterwards.

The gap in the recorded values at the beginning of the test was produced by an error message saying that TRIAX was unable to communicate with the balance. This happened when the mass values were changing rapidly (e.g. 500.0g to 500.1g). The error message interrupted TRIAX operations and stopped all the devices controlled by TRIAX's control unit (piston controller, pump). Changes to the TRIAX software were made later to correct the problem.

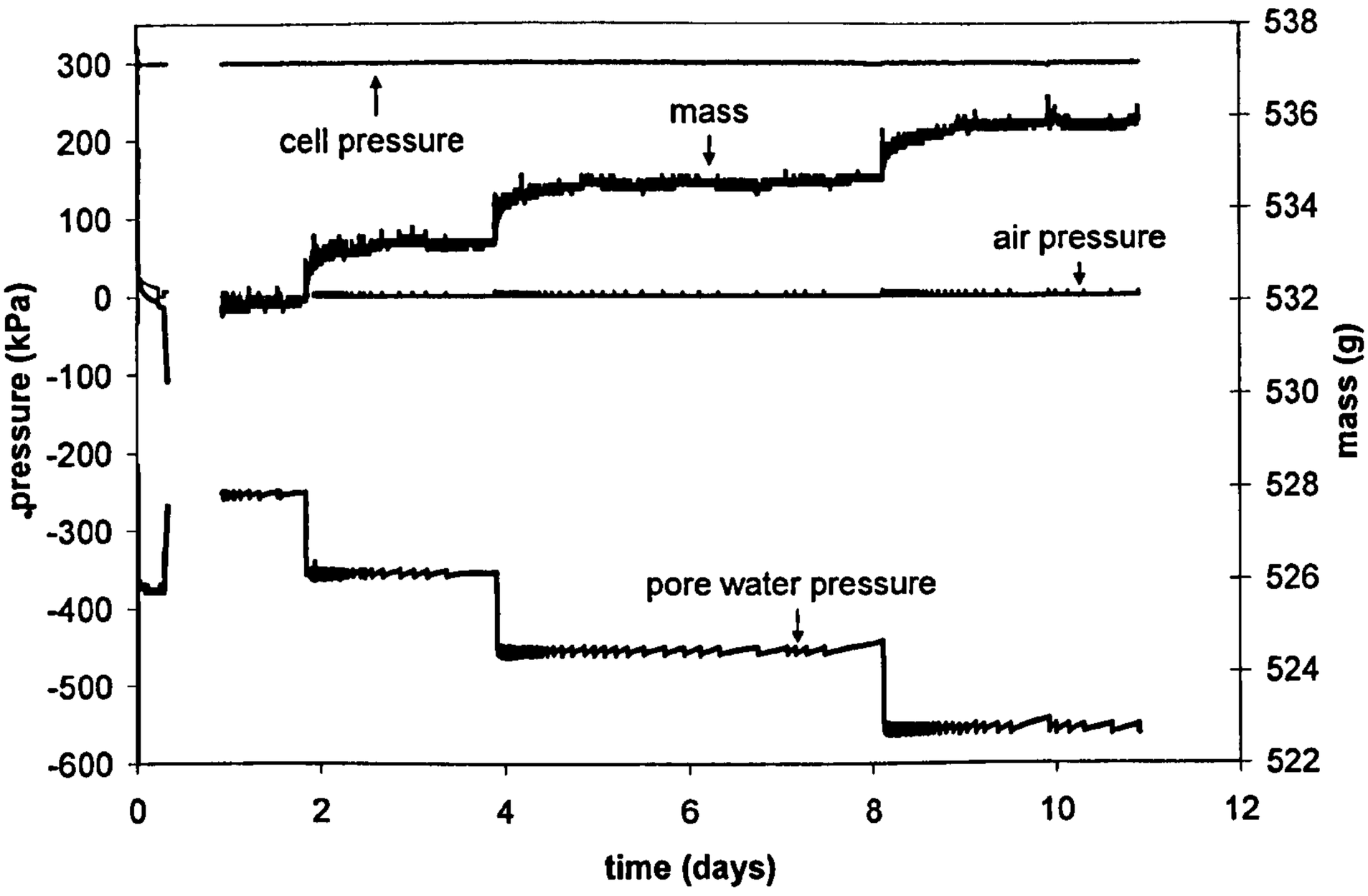

Figure 5.26: Controlled drying test with water mass measurement (test d7, tensiometer III3, BIONICS)

5.5. WETTING SYSTEM

5.5.1. Soil wettability

An early step in the development of the suction control system was to study the wettability of the soil in order to select the appropriate wetting procedure. There were only two choices: soils can be wetted either from vapour or liquid water.

5.5.1.1. From water vapour

The wettability was studied by circulating water vapour and weighing the sample with time. Wetting would be successful if the sample's mass increased. A source of wet air generated by a fogging system in distilled water was used (described in Chapter 4) (Figure 5.27). The fogger was placed between the pump and cell. In some tests the sample was wrapped in a geotextile to facilitate air circulation through the sides. The tests conducted are described in Table 5.6. Most of the samples were made of

statically compacted kaolin but tests A5, A6, A7 and A8 were conducted on a fine material made of industrial gypsum.

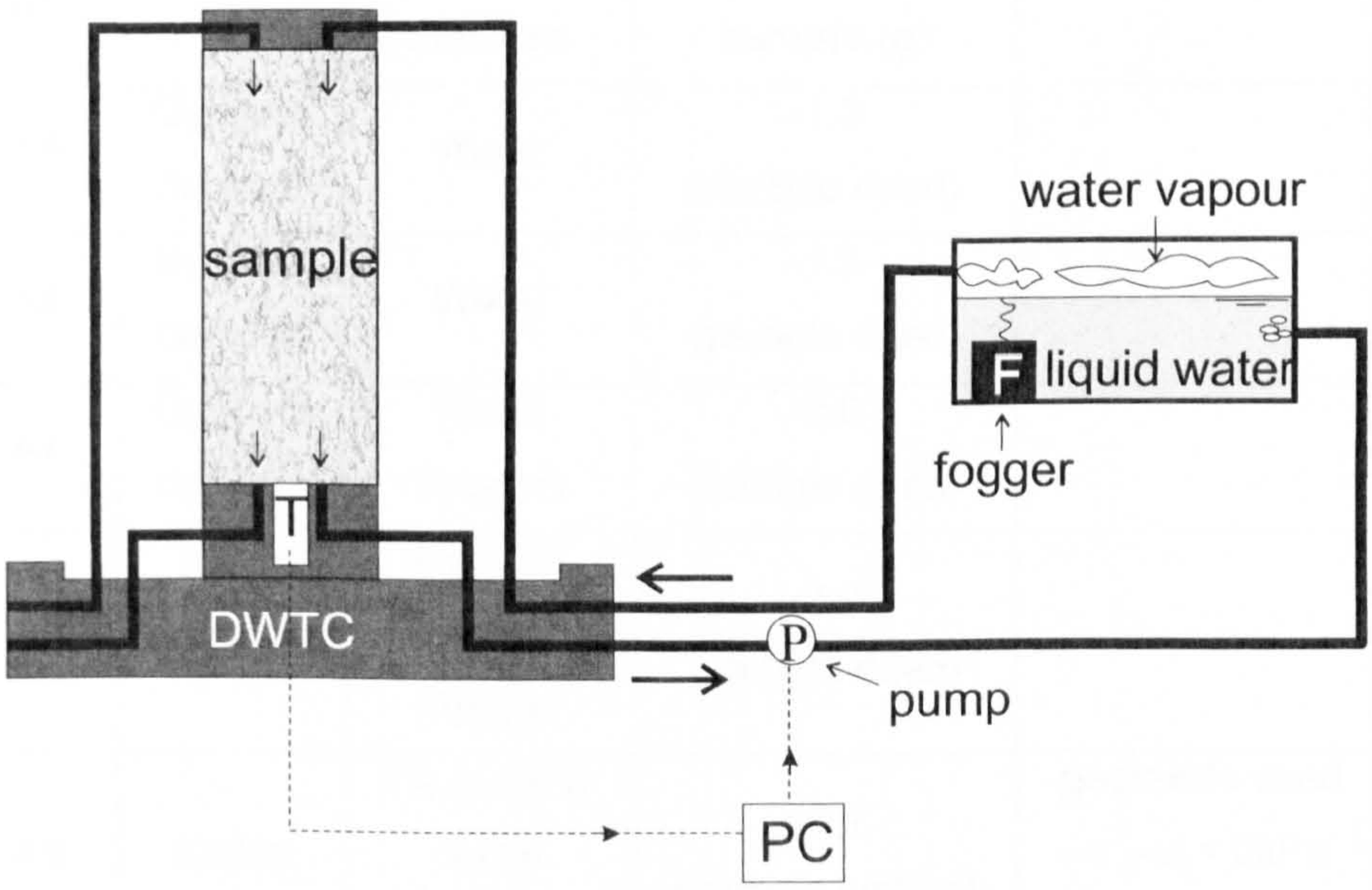

Figure 5.27: Set-up for wetting by circulation of water vapour through the sample

The tendency was for the samples to dry more easily than to wet. Tests A5, A6, A7 and A8 conducted on gypsum all showed drying. The fogger was not used in tests A5 and A6. However, drying was still observed when using the fogger (tests A7 and A8). The difference between the moisture lost and gained (as shown in Table 5.6) is probably due to the RH of the air already in the piping system.

By using de-ionized water with the fogging system the capacity for the sample to wet improved, as shown by tests A9, A10, A11, A12 and A13. It was, however, unclear which of the factors were decisive for the sample to wet: the material used (kaolin), the fogging system, the distilled/de-ionized water or the geotextile. Changing the net stress or the confining pressure had no distinct effect on the sample aptitude to wet; while tests A9, A10 and A11 showed that the moisture gain decreased as the cell pressure increased, tests A12 and A13 showed the opposite.

Table 5.6: Wettability of the soil

Test nr.	Material	Drying/ wetting medium	Moisture gain/loss by the sample (g)	Comments
A5	Gypsum derivate	Water	-1.3 (sample dried)	-
A6	Gypsum derivate	Water	-1.5 (sample dried)	-
A7	Gypsum derivate	Water (fogger)	-2.0 (sample dried)	-
A8	Kaolin	Distilled water (fogger)	-2.0 (sample dried)	-
A9	Kaolin	De-ionized water (fogger)	+8.7 (sample wetted)	-geotextile used - σ_3-u_a= 0kPa -time: 5h
A 10	Kaolin	De-ionized water (fogger)	+3.4 (sample wetted)	-geotextile used - σ_3-u_a =100kPa -time: 5h
A 11	Kaolin	De-ionized water (fogger)	+1.6 (sample wetted)	-geotextile used - σ_3-u_a =200kPa -time: 2½h
A 12	Kaolin	De-ionized water (fogger)	+3.8 (sample wetted)	-geotextile used - σ_3-u_a =100kPa -time: 5h
A 13	Kaolin	De-ionized water ()	+6.4 (sample wetted)	-geotextile used -σ_3-u_a =240kPa -time: 5h
A16	BIONICS	De-ionized water (fogger)	- (sample dried)	-σ_3-u_a =200kPa -time: 2h:50m (x3h)

A further test (A16) was carried out using a tensiometer to monitor suction. The tensiometer was inserted in the pedestal of the DWTC directly in contact with the sample. A sample made of BIONICS soil with an initial water content of approximately 13% was placed in the DWTC with the tensiometer at the bottom. Porous stones were fitted at the top and bottom of the sample. A confining pressure of 200kPa was applied and suction left to equalize. After suction stabilized at a constant value, wet air (from the box with the fogger) was forced to circulate through the sample three times for an equal period of time (2h50m). In the first and second time, air was forced to flow through from the top, while in the third time from the bottom. The air pressure was monitored by a transducer in the tubing connected to the top of the sample.

Figure 5.28 shows that suction actually increased while the pump was on and the wet air was circulating. As soon as the pump was on, the tendency was for the water pressure to decrease. However, following the first period of air circulation, the suction did decrease after the pump was switched off and the soil water pressure was left to equilibrate. For the second and third time, the overall effect was an increase in suction, as the recovery in suction after air circulation was less than the suction increase induced during circulation.

The wettability will depend whether water is transferred from the circulating air to the soil particles or not. For water to be transferred, the suction of the circulating air should be lower than the soil suction. The air suction can be related to the relative humidity (RH) of the circulating air through Kelvin's law (eq. 2.1 in Chapter 2).

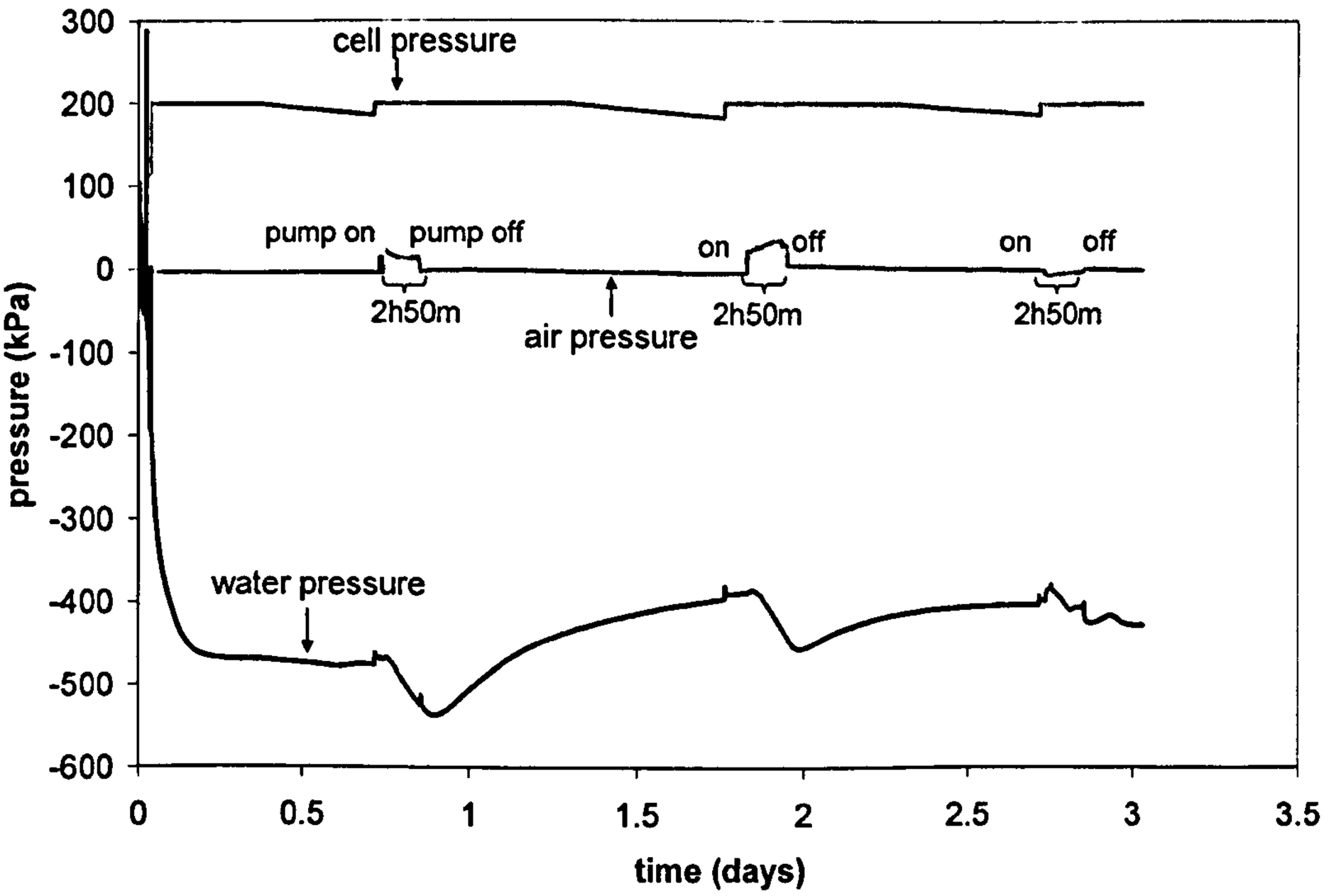

Figure 5.28: BIONICS soil wettability by circulating water vapour; the shaded areas correspond to the period of time the pump was on (the slight decrease of cell pressure was due to interferences of TRIAX with the balance) (test A16, tensiometer II1, BIONICS)

Since the measurement range of the tensiometer is less than 1600kPa, for water to be transferred to the soil skeleton, the air RH should correspond to a suction less than 1600kPa. Applying eq. 2.1, it can be shown that the air RH should be higher than 98.8% for the soil to wet (Figure 5.29a). Figure 5.29b clearly shows that in order to reach more realistic RHs the soil suction has to be in the MPa scale (i.e. beyond the tensiometer measurement range 0-1600kPa). Therefore, although RH was not measured at this stage, this suggests that the RH of the circulating air was lower than the desired (98.8%) for the soil to wet.

A second factor contributing to the difficulty in wetting the samples was water condensation in the pipes. Droplets of water adhering to the internal walls and flowing down were clearly visible, an indication that the system was not in isothermal conditions.

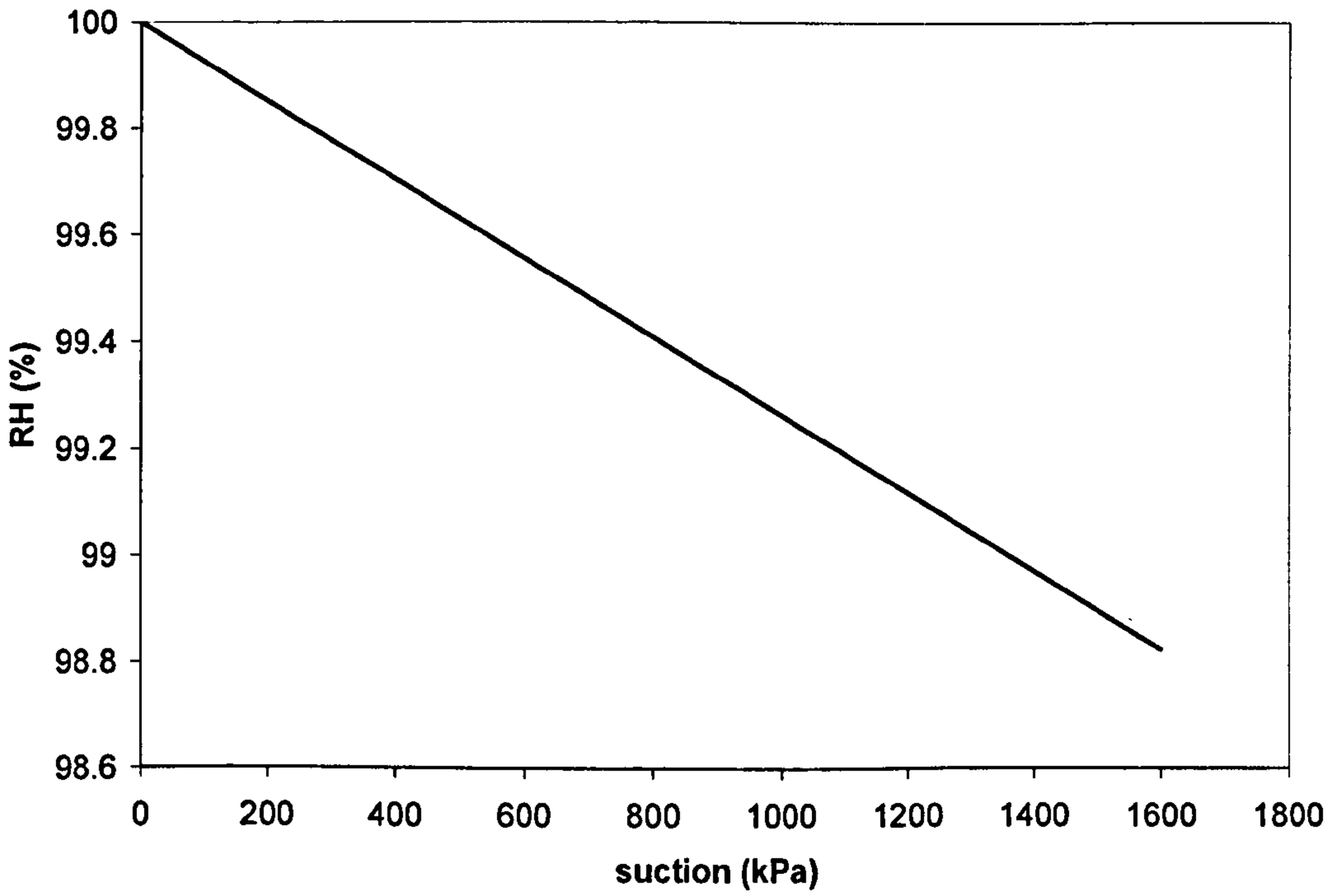

(a)

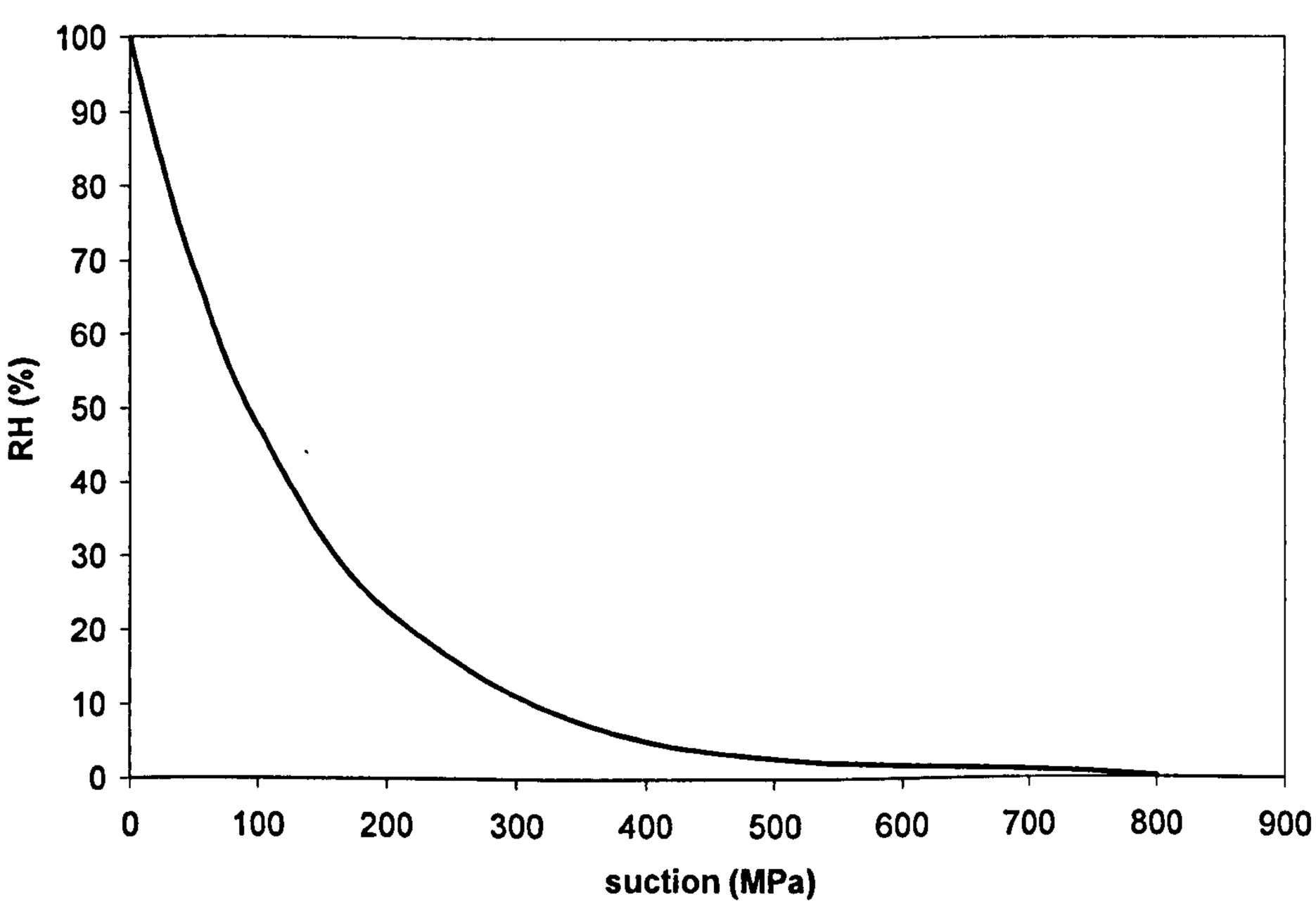

(b)

Figure 5.29: RH versus suction at 20°C, a) RH required to wet the soil within the tensiometer working range, b) full relation RH – suction

5.5.1.2. From liquid water

Previous wetting tests with a system based on water vapour circulation have proven inefficient to wet soil samples, due to water condensation in the tubing and the difficulty of achieving sufficiently high RHs. The system was changed to direct injection of water (as done by Jotisankasa, 2005). If all the water injected is retained by the soil, the water content increase of the sample corresponds to the mass of water injected. Water was injected through a valve set at the top of the DCTC (ver.2 of the suction control system in Figure 5.30).

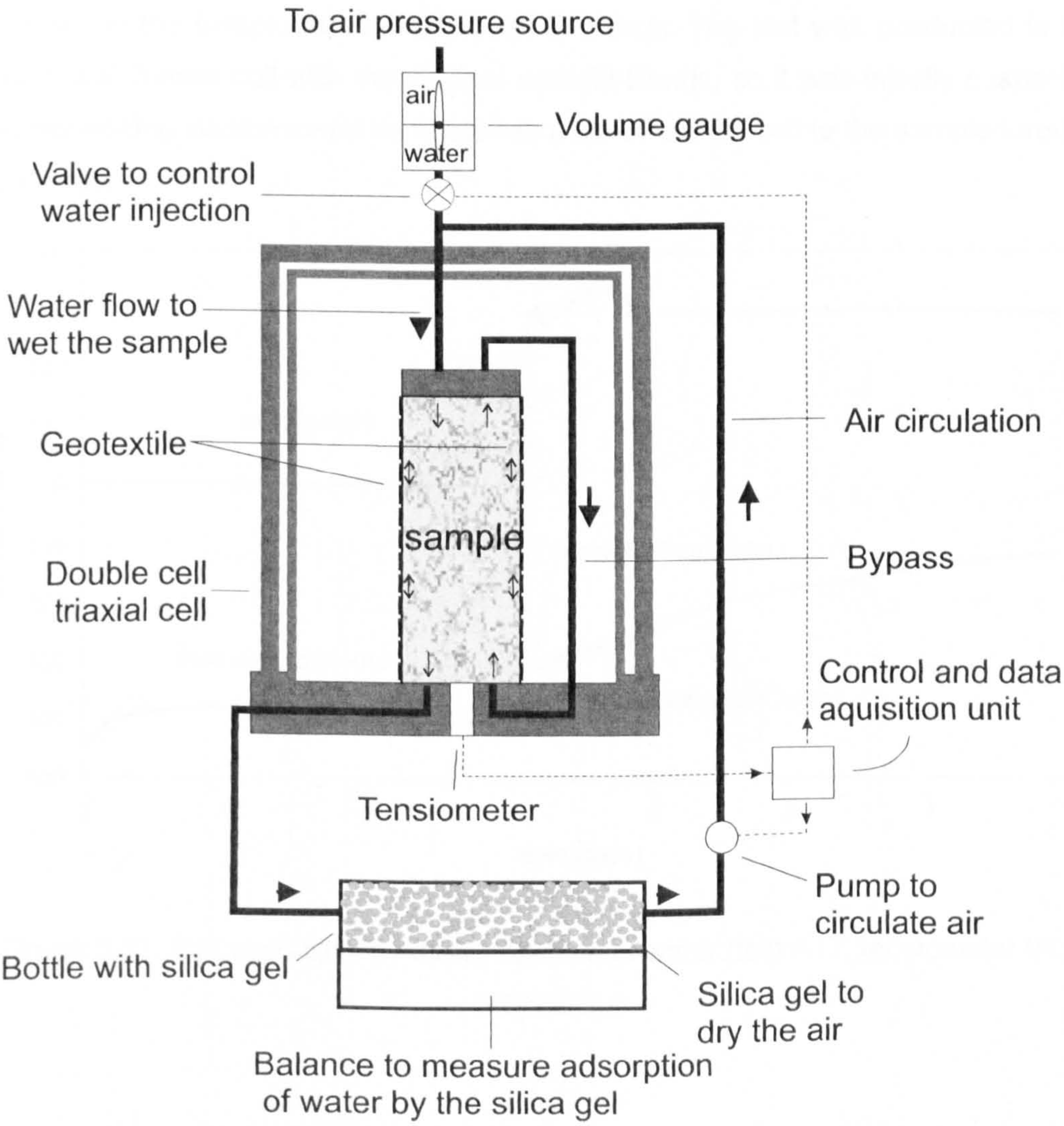

Figure 5.30: Tensiometer based suction control system (ver. 2)

For the test in Figure 5.31 (a continuation of A16 in Figure 5.28) the confining pressure was decreased from the original 200kPa to zero and increased again to 300kPa; 1h later 10cm^3 of water were injected followed by another 5cm^3 after 24h. The sharp step in the suction line is due to the application of the cell pressure, not the water injection. There is a time difference of 1h between the cell pressure increase and water injection.

For both injections suction decreased continuously. It was not clear if this decrease of suction was due to the 15cm^3 of water injected or if water could be leaking from the cell into the sample through the push-fit fittings. The test was conducted in the double wall triaxial cell with the original push-fit fittings, so it was initially suspected that decreasing suction could be related to a leak from the cell to the sample through the fittings.

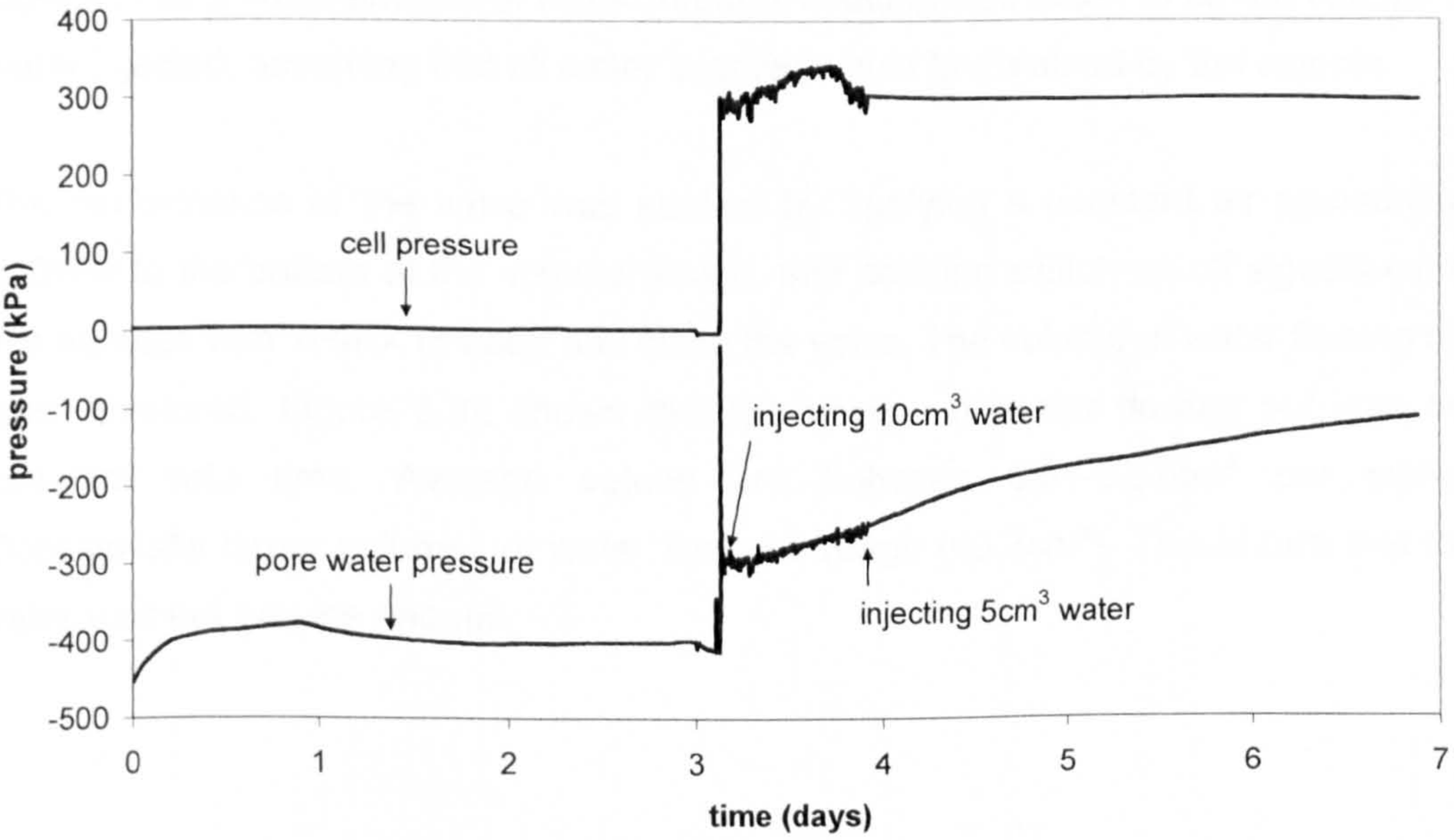

Figure 5.31: Soil wettability by direct injection of water (test A17, tensiometer II1, BIONICS)

Even if the previous test was not conclusive regarding the wettability of soil from liquid water, it seemed obvious that if water were injected directly to the sample, the soil should wet. Therefore, direct injection of liquid water was preferred over circulation of water vapour. As discussed previously, the soil wettability from water vapour can only be enhanced by increasing the RH of the circulating air or, increasing the working suction range of the soil. However, as both options are difficult to achieve the wetting procedure was shifted to injection of liquid water.

5.5.2. Wetting measurement and control

Following the above results, wetting was controlled by directly injecting liquid water into the sample by means of a 3-way valve connected to a water source (a volume gauge). The volume gauge was pressurised at 200kPa and the valve opened and closed to let a small amount of water through. Wetting was taken to be the volume of water injected, assuming that all water injected would be retained by the sample.

The performance of the valve was studied by applying a constant air pressure of 200kPa to the bottom of the volume gauge, and sending switch on-off signals every five minutes with TRIAX to open and close the valve. The volume of water flowing out was monitored. Figure 5.32 shows that the volume of water flowing out was not constant with time. Average values are between 0.01-0.07cm^3 per signal. Occasionally larger volumes of water flowed through (≈0.3cm^3). This shows that the valve was not precise enough.

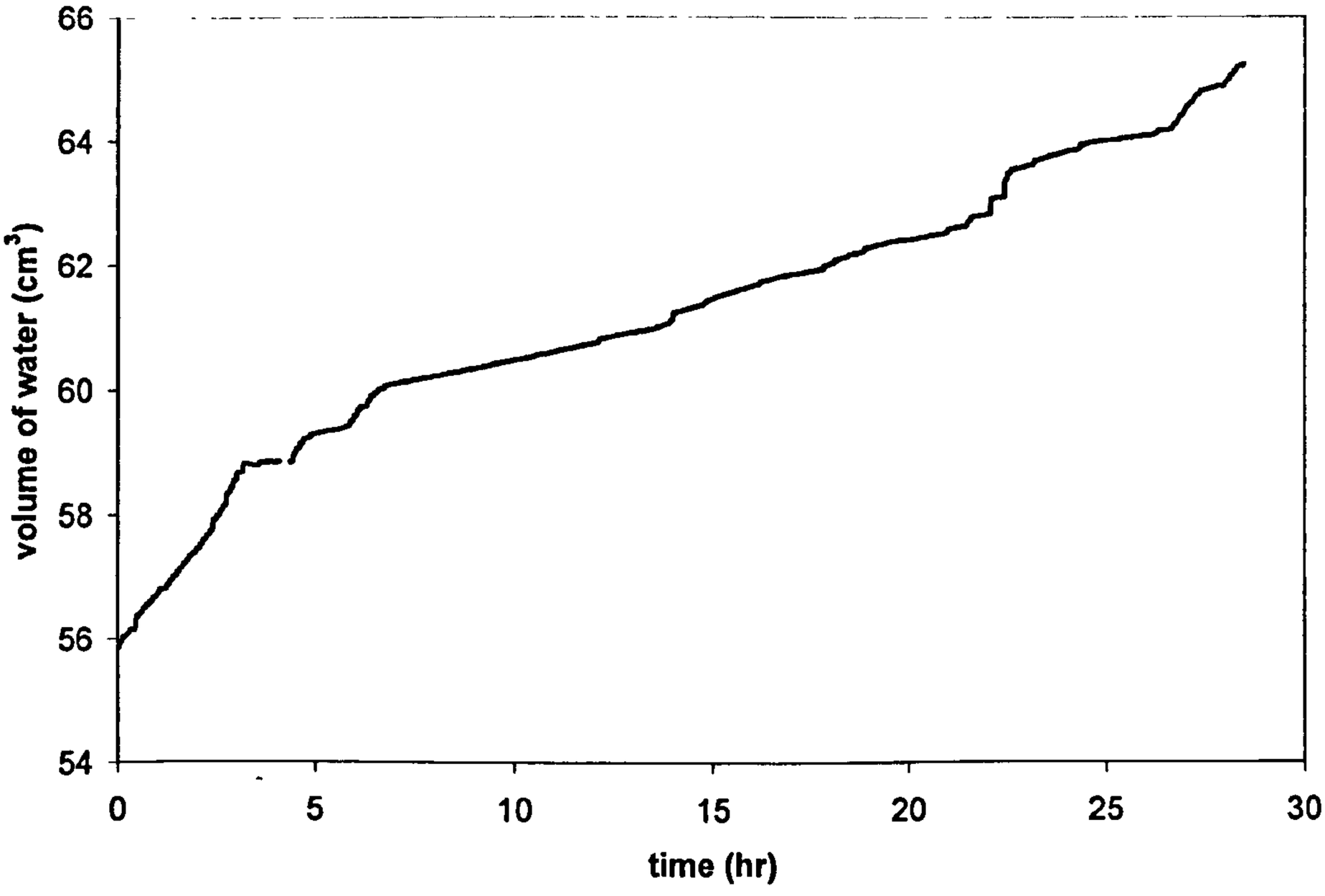

(a)

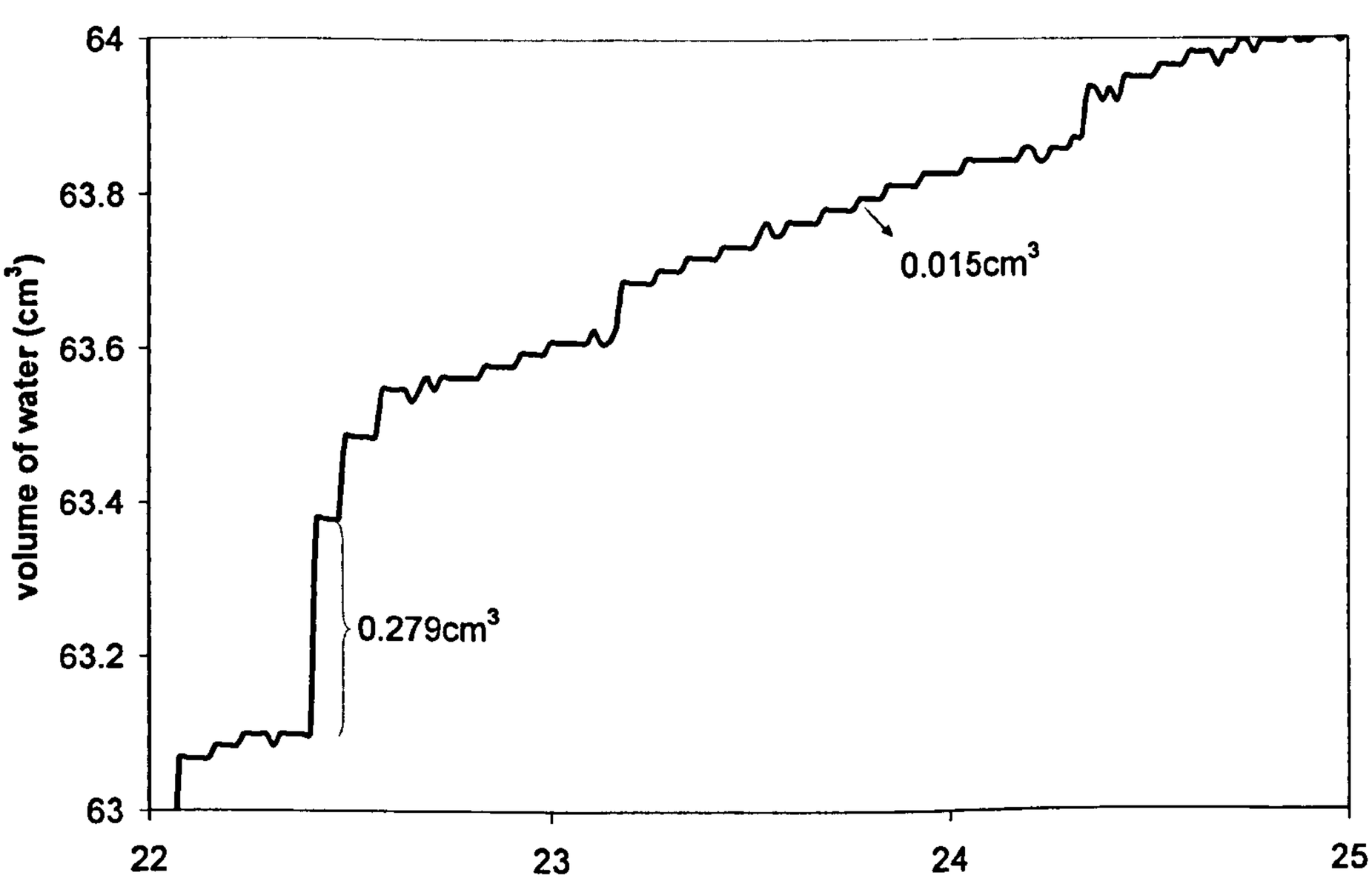

(b)

Figure 5.32: Wetting valve performance (test w0), (a) all test, (b) details

5.5.3. Wetting set-up

Results of tests will be presented as new equipment was added, the set-ups improved or the procedures modified. Two selected tests will be presented (w1 and w2, *w* for wetting), on compacted BIONICS soil at w=17% (for w1) and 17.4% (for w2) and e_0=0.51-0.56.

The objective of the tests was essentially to study the performance of the wetting control system and wetting measurement. However, as the drying control and measurement was reasonably well understood from tests d1 to d7, the tests shown in this section include both drying and wetting with water content measurement. In this way all parts of the tensiometer based suction control system could be tested at once.

5.5.3.1. Test w1

Test w1 was conducted with the suction control system ver. 2 in Figure 5.30, which consisted on injecting water at the top of the sample with the pump working to speed up water infiltration. After reaching the desired level of suction the sample was dried by forcing air to flow through the sample and silica gel. This procedure was repeated in the same sample in a sequence of wetting-drying cycles. This initial wetting test was carried out by injecting a known volume of water from a volume gauge under a continuous pressure of 200kPa. A geotextile was wrapped around the sample together with a bypass connecting the top cap and pedestal to avoid air pressure gradients. Silica gel was used for drying. The volume of water injected by the volume gauge and volume of water adsorbed by the silica gel were monitored. Any moisture expelled by the sample would be retained by the silica gel. Suction was monitored by a tensiometer at the bottom of the sample.

The sample was set in the DCTC and a cell pressure of 335kPa applied. Due to a tubing failure connecting the piston controller to the DCTC, the cell pressure was controlled by the pressure in the water line of the laboratory. Later in the test it was shifted to the piston controller. The sample was then dried to a suction of 400kPa and after stabilizing, wetting started by manually injecting 6cm^3 of water with the pump on. This same procedure was repeated for the following cycles. Eight drying-wetting cycles between 200kPa and 400kPa were applied to the sample (Figure 5.33). The sample had previously been subjected to seven cycles (not shown) although a

preliminary cycle is shown (before cycle 1) when different injection rates were experimented with. Initially a rate of 1 injection/6min was used but did not induce wetting (suction decreased). This was increased to 1 injection/3min which did achieve wetting. This rate was used until cycle 5, when it was found that drying occurred. It should be noted that although the rate was set to 1 injection/3min in this cycle, the 'water in' curve shows a lower inclination comparing to the previous cycles; this seemed to be related to the valve performance discussed previously. Therefore, the injection rate was increased to 1 injection/min for the remainder of the test.

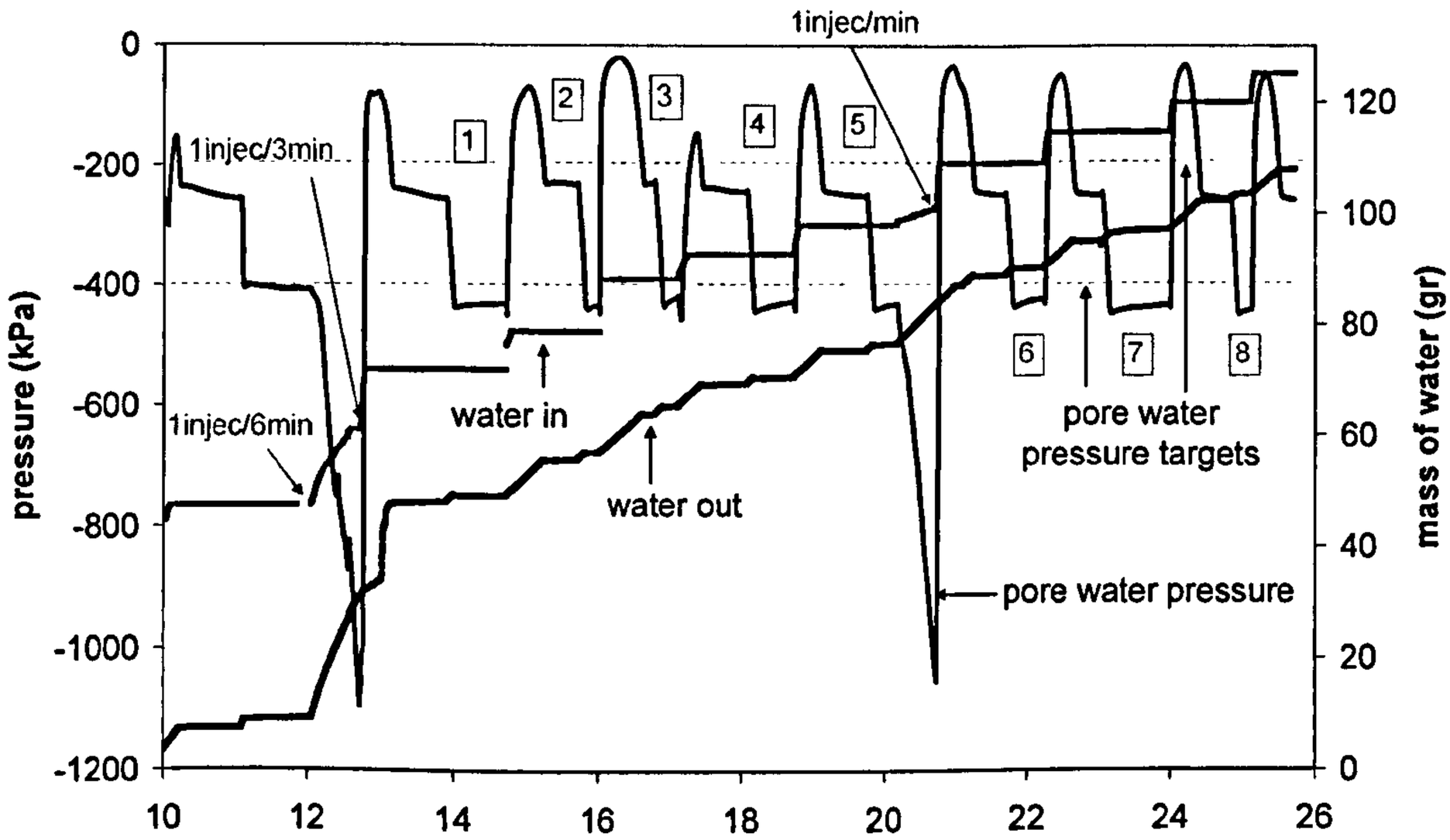

Figure 5.33: Suction cycles for test w1 (tensiometer III3, BIONICS). Numbers 1, 2, 3... denote the number of cycles; the preliminary cycle 0 was not included in the detailed analysis of the data

The following features can be seen in Figure 5.33:

(1) Suction always equalized at a value higher than the target, either after drying (where the target was 400kPa) or wetting (where the target was 200kPa).

(2) During wetting, suction always overshot the target value by as much as 200kPa before drying back to the target value.

(3) Whenever the pump was on the sample also lost water (as shown by the continued upward trend of the Water out curve).

(4) If the rate of water injection was too low (<1injection/min) the sample would dry instead of wet (this is shown in the preliminary cycle 0 and cycle 5).

(5) In the equalization stages, suction would slowly increase (at 200kPa) or slowly decrease (at 400kPa).

If no water is added or lost by the suction control system (e.g. infiltrations from the cell to the sample, condensation in the pipes), the water content of the sample will correspond to the water adsorbed by the sample, which should be the difference between the mass of water injected to the mass of water adsorbed by the silica gel. The total mass of water should also remain unchanged with time, i.e. the difference should be 0 after each cycle. The only exception should be if the sample shrinks, in that case the mass of water required to wet to a certain suction would be less because the void ratio decreased. In this case, the line would displace downwards in a net mass of water versus time graph.

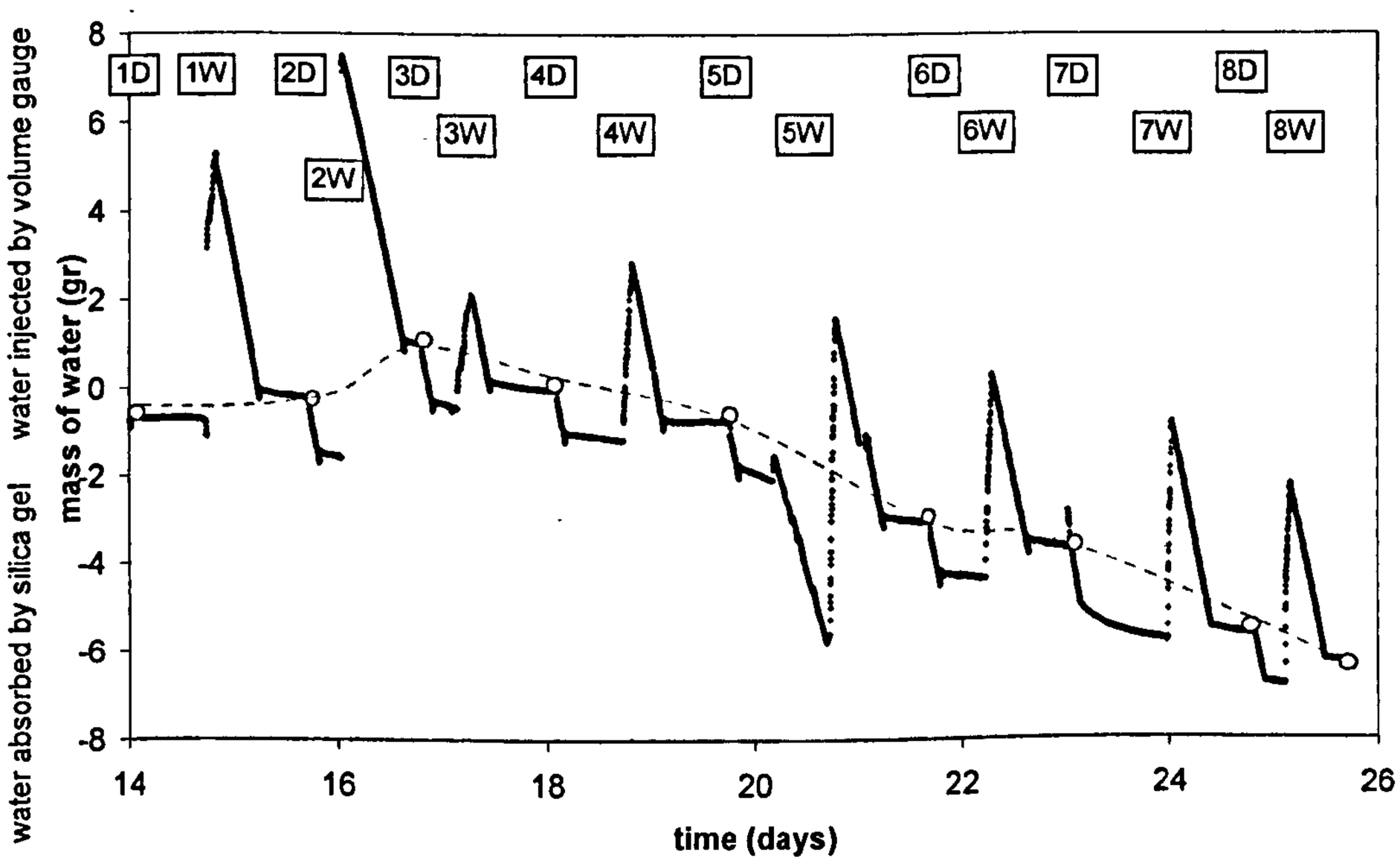

Figure 5.34: Difference between the water injected (by the volume gauge) and the water retained (by the silica gel) against time for test w1 in Figure 5.33; the open circles, connected by the dashed line, indicate the start of drying for each cycle; shaded areas correspond to the wetting and drying stages

Figure 5.34 shows the system was able to monitor the water content throughout the wetting/drying cycles. The net water mass (difference between water injected and adsorbed) became increasingly negative, suggesting the sample was losing water with the suction cycles (an indication of shrinkage) or that extra water could be infiltrating into the system (a total of 6cm^3 in this case). Unfortunately, the wet mass of the sample was not taken at the end of the test; therefore it is not possible to confirm whether the sample dried out. Nevertheless, further testing was done to confirm if water was getting in or out of the system. Three possible effects were studied: (1) water diffusing from the cell to the sample through the membrane, (2) variable temperatures in the system that could lead to condensation or evaporation in various parts of the system, (3) water vapour flowing into the water content measurement box. These three factors will be explored next.

5.5.3.2. Factors affecting the water content measurement

Water diffusion through the membrane

Early studies on the diffusion of water through rubber membranes have shown that the rate of diffusion depends on its thickness, hardness and the rubber saturation with water (Schumacher and Ferguson, 1929). In experiments aiming to determine the rate of diffusion through rubber membranes, Schumacher and Ferguson reached a rate of diffusion of 0.0033mg/h/cm^2. This value was obtained in a vulcanized H_2SO_4 treated rubber with a thickness of 0.048cm (a prevulcanized polyisoprene membrane with a thickness of 0.035cm is used for this research) and it only considers the passage of water by gravity (in our tests there is a confining pressure applied to the membrane). Even if 0.0033mg/h/cm^2 is taken as indicative and adapt it to the current experiments, for the lateral surface area of the sample (94.25cm^2), the mass of water diffusing from the cell to the sample at the end of 12 days (the period of time the test lasted) is 0.09g. This is a much smaller value compared to the 6g difference measured, so clearly other factors must be responsible for the observed difference.

Temperature

A different temperature in the different parts of the system (tubing, sample, pump, valve) might have two effects: (1) migration of water molecules due to variable RHs (the RH depends on temperature), (2) condensation in the cooler surfaces as liquid water or (3) evaporation in warmer surfaces as vapour water. In order to check for temperature effects, one test was conducted with the same arrangement as for the test w1 but with a dummy sample instead. The dummy sample was made of 4 dry sandstone porous disks. Temperature was also measured near the pump (that heats with continuous working) and silica gel. The results in Figure 5.35 show the mass increasing linearly and then, after briefly stopping the pump and restarting, the mass started decreasing. The test was stopped again and air was set to circulate in a loop just between the pump and the bottle with silica gel. As shown in Figure 5.35 the mass kept decreasing, suggesting that the dummy sample was losing water.

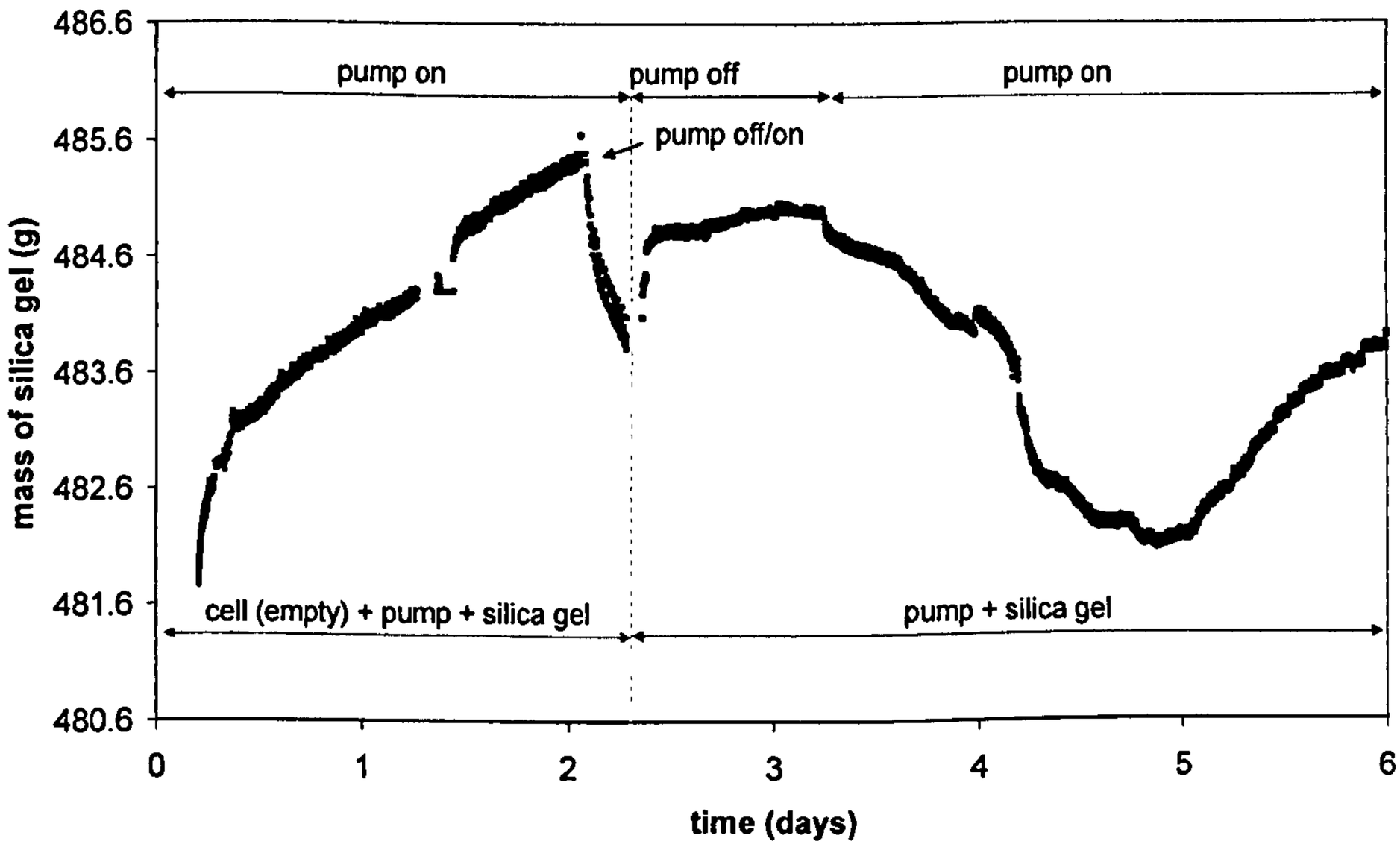

Figure 5.35: Testing the system for temperature effects (test A1, silica gel)

An hypothesis for this response is as follows: silica gel adsorbs water until the water vapour pressure in its pores equals to the water vapour pressure within the tubing and pump (this means the mass recorded by the balance would increase and stabilize), after that if all the system is in isothermal conditions, the mass remains constant with time. However, if some parts of the system have different

temperatures, the saturation vapour pressure would change accordingly and the RH too (according to eq. 5.1 from NPL, 1996). The result is water molecules migrating to the parts with lower RH.

$$RH(\%) = \frac{u_v}{u_{v0}} \times 100 \quad = \frac{\rho}{\rho_s} \times 100 \qquad (5.1)$$

Where *RH* is the relative humidity, u_v is the water vapour pressure or water vapour density, and u_{vs} the saturation vapour pressure or saturation vapour density. Table 5.7 shows the effect of changing the temperature by 1°C at different initial levels of RH and temperature.

Table 5.7: Effect of temperature change of 1°C at various temperatures and RHs (from NPL, 1996)

Relative humidity	**Temperature**				
	10°C	20°C	30°C	50°C	70°C
10%RH	±0.7%RH	±0.6%RH	±0.6%RH	±0.5%RH	±0.5%RH
50%RH	±3.5%RH	±3.2%RH	±3.0%RH	±2.6%RH	±2.3%RH
90%RH	±6.3%RH	±5.7%RH	±5.4%RH	±4.6%RH	±4.1%RH

In the case of this system, the pump heats leading to an increase in temperature in the air flowing through it. The temperature of the air outside the system near the pump was measured to be 29°C and in the silica gel was 23°C. As the temperature increases, the saturation vapour pressure increases and the RH of the air near the pump decreases. The result could be water molecules.transferring from the silica gel to the pump, and the mass monitored by the balance decreasing. This was the opposite of what was observed (mass of the silica gel increasing). Therefore the heating of the pump does not explain the increasing mass of water being adsorbed by the silica gel.

Air leaks into the water content measurement box

The third reason was that the box where the silica gel was kept was not sufficiently air tight. The sealing of the box was then evaluated by enclosing the balance and silica gel in the box. The mass measured by the balance should increase and stabilize at a constant value once all moisture present in the air is adsorbed.

The linear increase in mass in Figure 5.36 shows that possibly there was an air passage from outside to inside the box. The silica gel adsorbed nearly 4g of water. The expected mass of water adsorbed can be calculated from eq. 5.1:

- *saturated vapour density at 22°C (lab's temperature) = 19.42g/m^3*
- *RH in the lab = 55%*
- *actual vapour density = 19.42 g/m^3 x 0.55 = 10.67 g/m^3*
- *For the volume of the box (0.38m x 0.29m x 0.25m), the amount of water is 10.67 g/m^3 x 0.02755m^3 = 0.294g*

If the silica gel adsorbed all the water in the box, for an initial RH of 55% the mass increase should have been 0.294g. It was instead nearly 20 times greater.

Following the above result, a commercial water proof box with a closing system was tested. In order to reduce the amount of adsorbed moisture, one more test was conducted by sealing the o-rings and cable connections with liquid latex rubber. At the end of nearly 2 months the silica gel adsorbed 4.5g (Figure 5.36) giving a rate of approximately 0.07g/day. This is a smaller value but enough to induce errors after a long period of time. It suggests that water vapour is diffusing through the walls of the box.

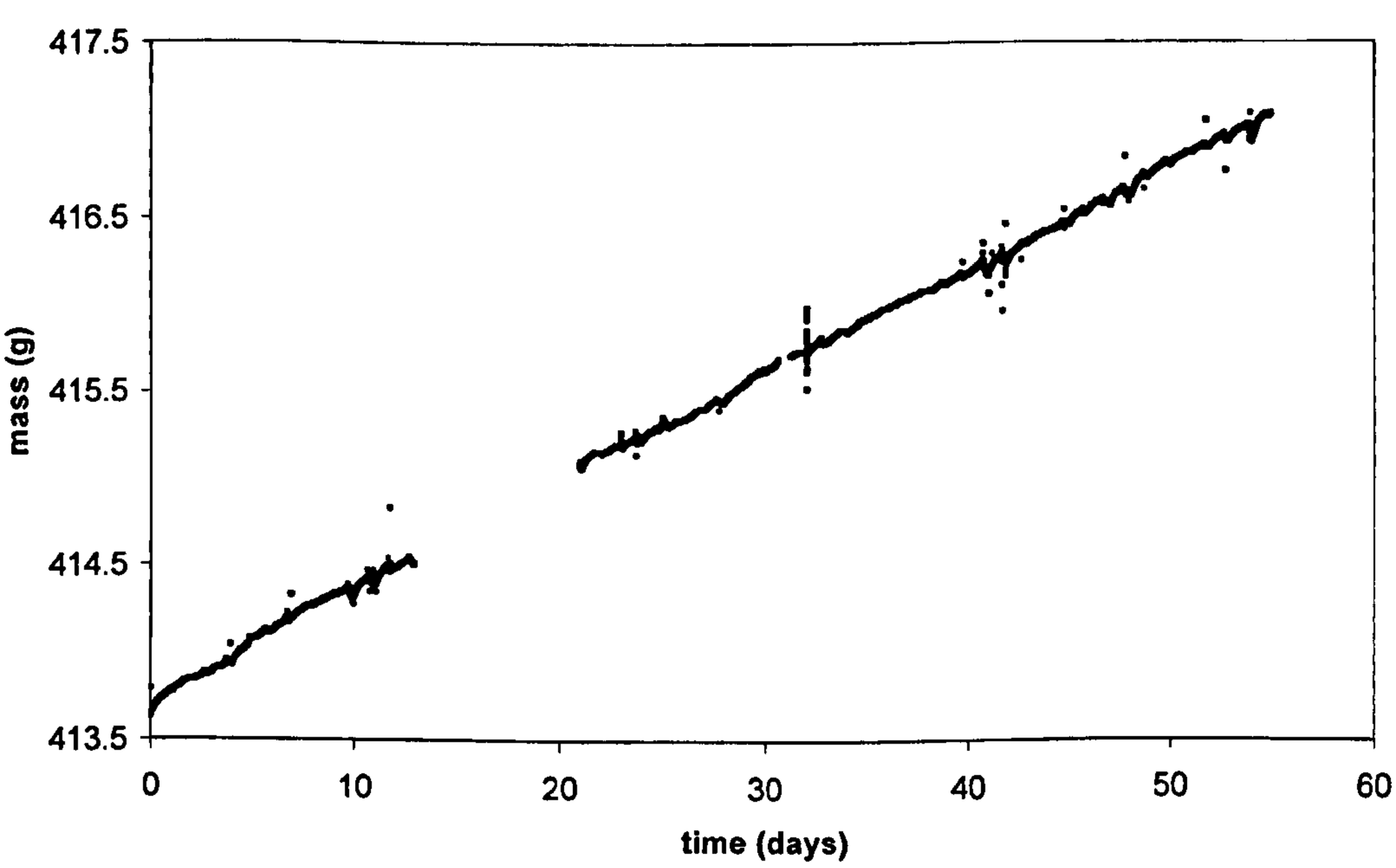

Figure 5.36: Calibration of the water content measurement box (test AI2, silica gel)

Concluding, air leaking or diffusing into the water content measurement box is the only factor capable or contributing to a mass increase by the silica gel. However, if the mass increase by the silica gel was only due to air leaking into the box, the mass increase for the period of the test (12 days) should have been 0.84g (0.07g/day x 12days) and it was instead 6g. Therefore, the obtained results in Figure 5.34 could indicate shrinkage.

Summarizing test w1, version 2 of the suction control system revealed that it was sufficient to dry and wet soil in controlled suction conditions with continuous water content measurement. However, detailed analysis of the data revealed some shortcomings that needed to be addressed. In particular, it was suspected that water vapour infiltrated into the water content measurement box contributing to an increase in the mass readings.

In order to solve the above limitations, modifications were introduced to the version 2 of the suction control system and a new version tested ('version 3') in test w2.

5.5.3.3. Test w2

The fact that suction always stabilized at suctions higher than the target value (either for drying or wetting) was thought to be due to the sharp pressure gradient crossing the sample from the top to the bottom. As the control system was based on a tensiometer located at the bottom of the specimen, further drying or wetting occurred in the sample as suction equalized. This issue was solved by inserting a second tensiometer in the top cap. As the upper surface was the first to be dried/wetted, the tensiometer should be able to stop the pump or valve as soon as suction reached the target value. Regarding the injection rate, the sample was wetted at different rates in order to find an optimum at which suction would not exceed the target value. The improved set-up is shown in Figure 5.37 as version 3.

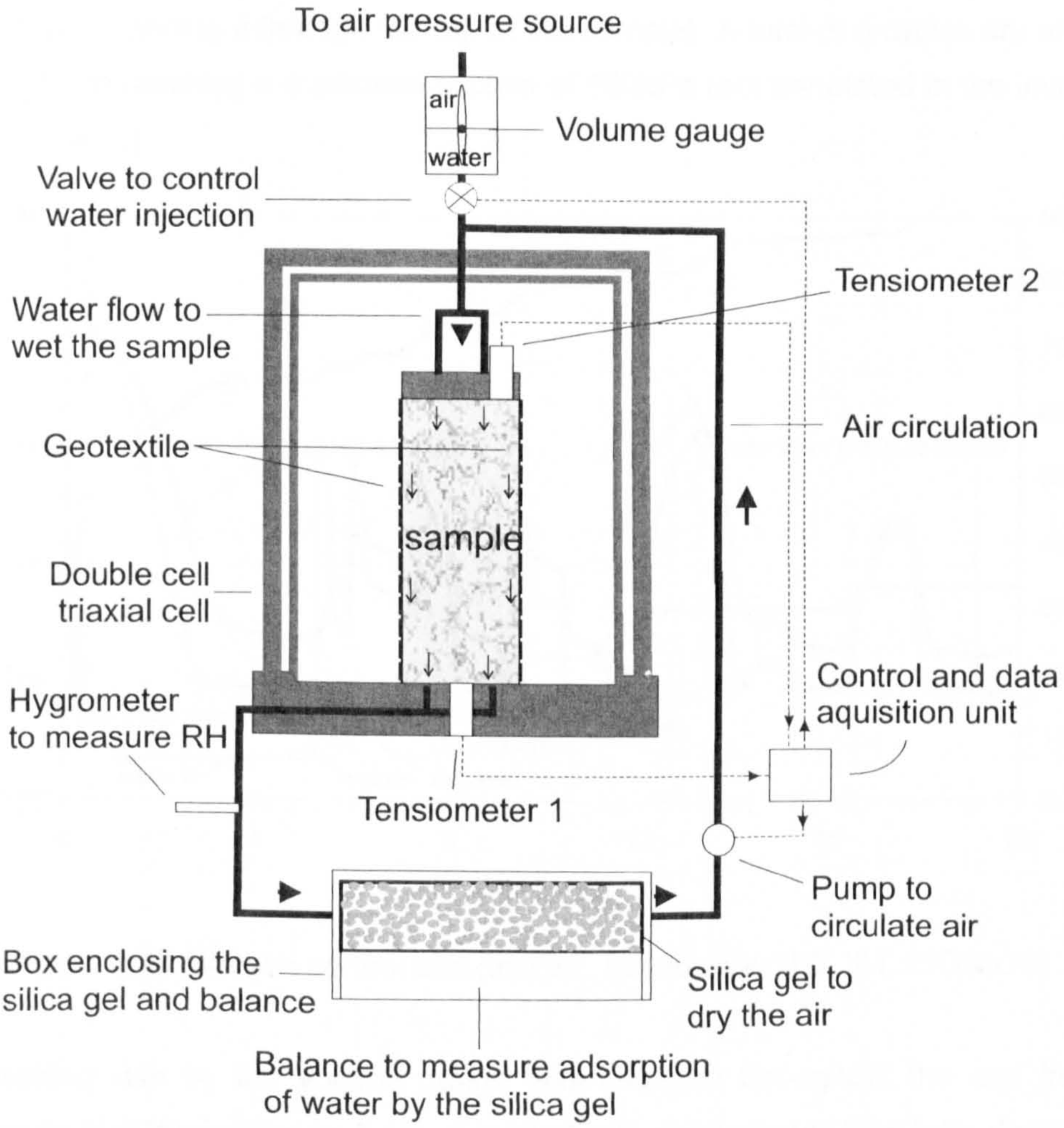

Figure 5.37: Tensiometer based suction control system (ver.3)

A new sample of compacted BIONICS soil was set in the triaxial cell (w=17.4%). It was intended to cycle suction between two high values of suction. However, as suction changed very slowly, it was cycled between 100kPa and 150kPa.

Figure 5.38 shows the suction control test with two tensiometers. When the two tensiometers were set in the sample, suction increased to approximately 130kPa (the initial suction in the sample). Cell pressure was then increased to 305kPa with the tensiometers increasing up to a positive pressure of 200kPa before stabilising at a value of -5kPa. The control system started, and suction increased until 150kPa. The bottom tensiometer followed, increasing up to 130kPa. Later the sample was wetted at different rates and dried. The bottom tensiometer followed but always kept a difference of 20kPa. It is worth noticing that it took 4 days to dry the sample to 150kPa (from nearly 0kPa to 150kPa). The negative air pressure is due to the pump sucking air from the bottom of the sample (where the air pressure transducer is

located) and sending it through the top of the sample). A total of 5 cycles are shown, each of them reaching a maximum suction of 150kPa (not annotated in the image to improve clarity).

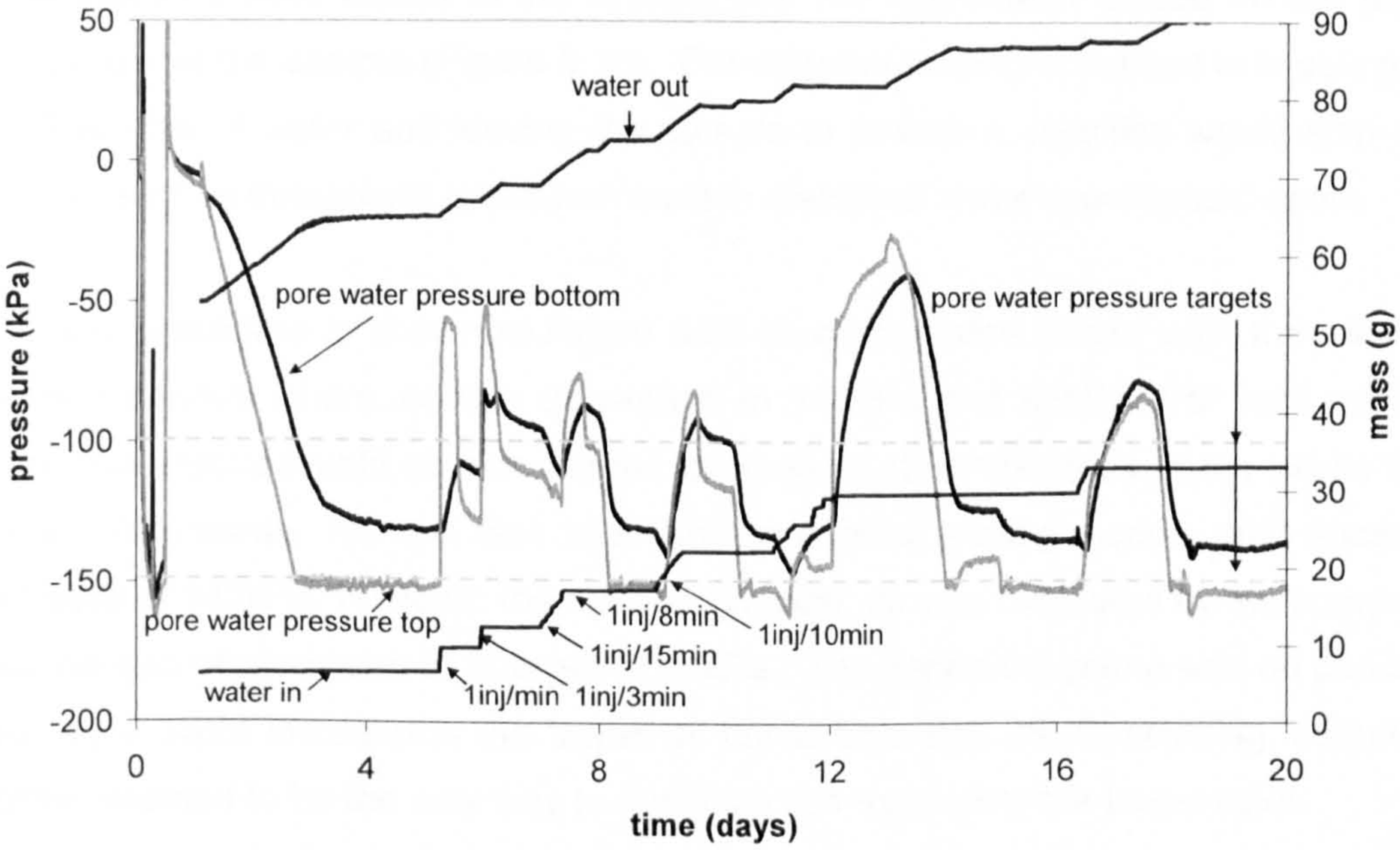

Figure 5.38: Suction control test (test w2, tensiometer III3, III4, BIONICS)

The wetting rate by the volume gauge was changed throughout the test from 1 inj/1min to 1inj/15min (Figure 5.38). It started with 1inj/1min but was later decreased to 1 inj/3min. In both cases suction dropped well below 100kPa. So the injection rate was decreased to 1inj/15min and, as the sample dried instead of wetting, it was increased to 1inj/8min. Suction still dropped below 100kPa, but this time by a smaller amount. The sample was then dried to 150kPa and then wetted at a rate of 1inj/10min. It still overshoot but by an even smaller amount. Finally the sample was dried and then wetted at the same rate as before.

The adopted wetting procedure based on a single target suction did not work. Eventually the sample should have to be wetted in steps, i.e. 150 kPa – 140kPa – 130kPa – 120kPa –110kPa – 100kPa. This would increase the test duration but could avoid dropping below the target suction by a large value.

Further modifications were introduced to the procedures for using ver. 3 by wetting the sample in steps, instead of to a single target suction. The set-up itself (arrangement of the different devices) remained the same except that RH measurements were added to the system with the hygrometer placed on the pipe coming out of the sample (Figure 5.38). The stepped wetting consisted in injecting a small volume of water and leaving the sample to absorb it. Injection would stop as soon as suction decreased, and when suction stabilized water was injected again.

The new procedure is shown in Figure 5.39 (a continuation of test w2). It shows 2 injection periods where suction decreased to 143kPa and 81kPa. For both cases water was injected until suction started decreasing (2 small steps in the 'water in' curve). Afterwards, for the first injection there is a waiting period until suction stabilized at 143kPa. While for the second injection, air was circulated by the pump to limit the suction decrease to a target of 81kPa. The period the pump was on can be seen by a slight increase in the 'water in' curve from day 28. Concluding, stepped wetting seemed to be the only way to avoid suction exceeding the target value.

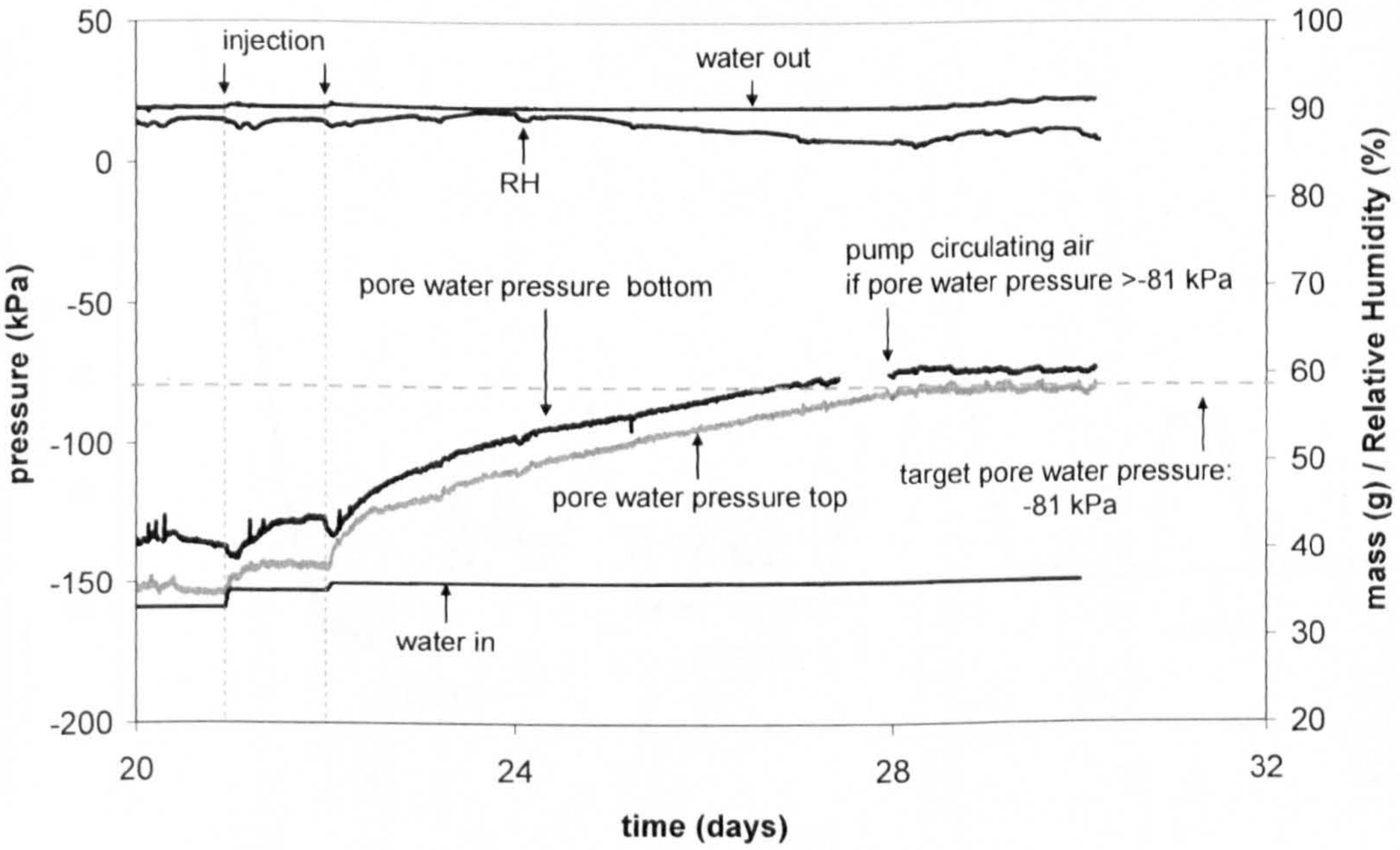

Figure 5.39: Suction control test (test w2, tensiometers III3, III4, BIONICS) showing the successful wetting by injecting water in steps

TRIAX was unable to display data in rates. Therefore, the stepped wetting was done manually by starting the pump/valve once suction had stabilized. RH was fairly constant (approximately 90%) through the test during wetting or drying.

In test w1 (Figure 5.34) the net water mass decreased with the cycles, i.e. the water adsorption by the silica gel was higher that the water injected. For test w2, the results do not show this (Figure 5.40), the net mass variation increased, which would be the case if the sample swells. Again, the wet mass of the sample was not measured after the test, so it's not possible to confirm if the mass of the sample increased. However the results could still be correct, because the first 4 cycles of test w1 in Figure 5.34 also showed a similar tendency for the net water mass to increase. In addition, the mass of the sample in test w2 increased by 1g for the 5 cycles which is comparable the first 4 cycles of test w1. These results also confirm that the increasing negative net water mass measured in test w1 could be due to shrinkage, and not an error induced by water infiltration in the sample or silica gel or a temperature effect as initially assumed.

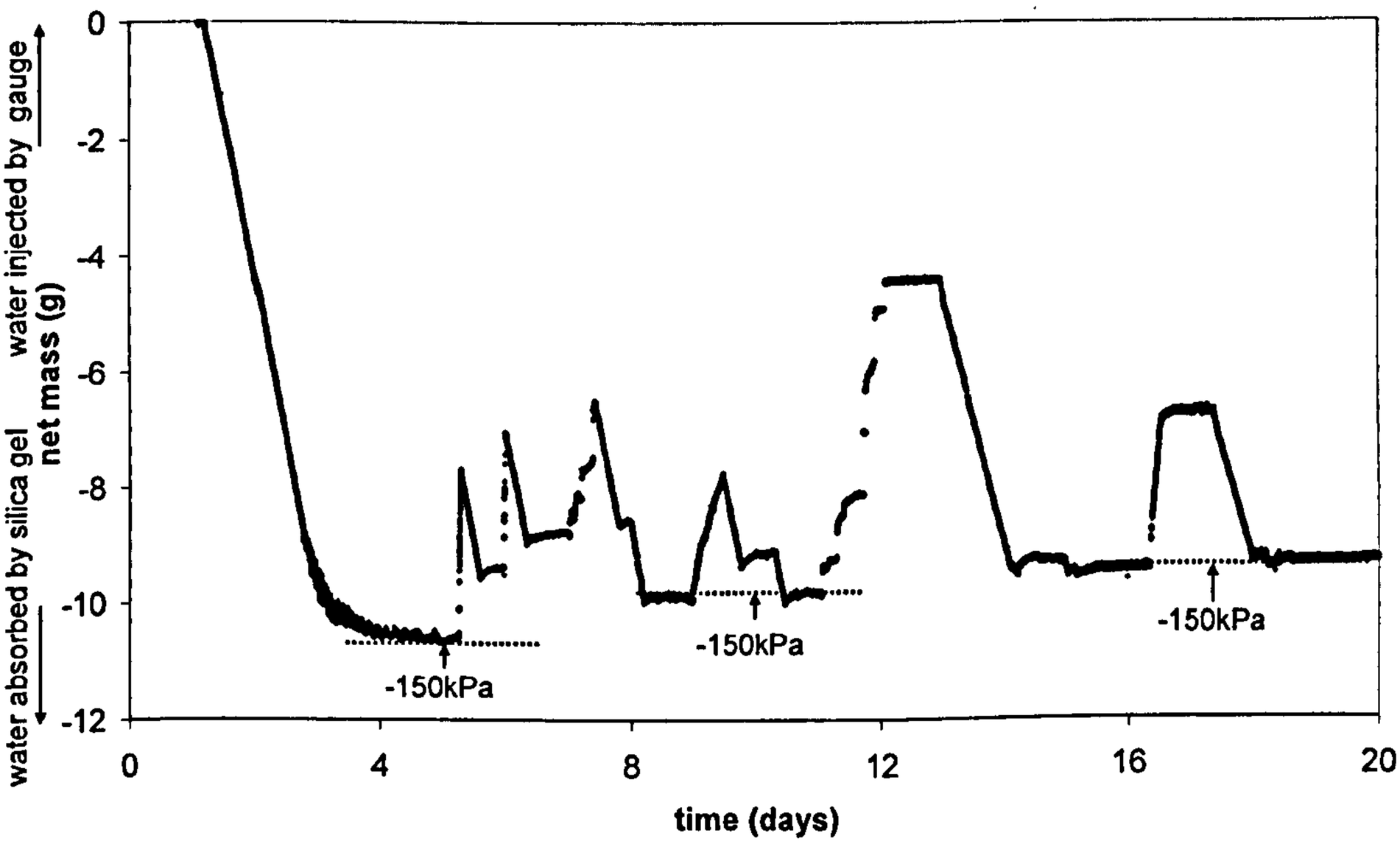

Figure 5.40: Net water mass (test w2, BIONICS)

5.6. FINAL REMARKS

Some of the limitations of final version (ver. 3) of the tensiometer based suction control system are:

- Silica gel has an excellent adsorption effect but, like any other porous material it has hysteretic behaviour with respect to the water content, and has an adsorption capacity (means that it has to be replaced when it reaches the limit).

- The wetting system is complex because:
    - It measures the water content by the difference between the water injected and water adsorption by the silica gel. This is not really a limitation, it just complicates the control.
    - It relies on a number of devices that have their own limitations (e.g. a valve system that does not always inject the same volume of water)
    - There is the possibility that some water droplets get retained in the tubing leading to the top of the sample.

Further work is needed on the wetting system. The stepped wetting was performed manually, so it still has to be automated.

5.7. CHAPTER SUMMARY

This chapter presented the development of a tensiometer based suction control system. The system is able to dry and wet soil, while measuring suction and water content. The system represents an advance on the previous work by Cunningham (2000) and Jotisankasa (2005) because it relies on direct measurements of suction and water content and runs in a closed loop. A desiccant (silica gel) was used as the drying media, and wetting was based on direct injection of water. Suction was measured by high suction tensiometers. Water content was based on the difference between the amount of water injected and retained by the desiccant. The system is able to run automatically, without assistance, controlled by software.

Chapter 6. ENVIRONMENTAL SCANNING ELECTRON MICROSCOPY

6.1. INTRODUCTION

According to the review of Chapter 2, particle level studies relevant to geotechnical engineering have focused on the soil fabric, i.e. on the way clay particles are arranged. Initial studies were conducted using SEMs but have more recently moved to the ESEM, because the latter allows observations of the fabric in situ while the water content of the sample changes. However, the ESEM also has the unique capability of observing air-water interfaces. The curvature and interaction of the air-water interfaces with the particles in an unsaturated soil is significant for its mechanical and hydraulic behaviour, being directly responsible for the meniscus force that pulls particles together and provides the 'extra strength' unsaturated soils are known to have.

While evidence in the form of direct observations of water menisci in soils does not exist (with the exception of Montes-H. et al., 2005), there are published works where water menisci at a small scale have been viewed. Schenk et al. (1998) and Weeks et al. (2005) observed the formation of meniscus water at the contact of a cantilever tip of an atomic force microscope (AFM) and a flat substrate (in Figure 6.1a and Figure 6.1b, respectively). The air-water interfaces are clearly visible with a size in the nm/μm scale. Figure 6.1b shows it to be possible to relate the imposed RH to the meniscus curvature. Lampenscherf et al. (2000) was able to observe growing menisci as RH increased in monosized spheres with different diameters (1.5, 40, 80, 120μm) arranged in 1 layer (Figure 6.1c). The authors were also able to measure indirectly the meniscus force by fixing the spheres into a deformable substrate and measuring its deflection.

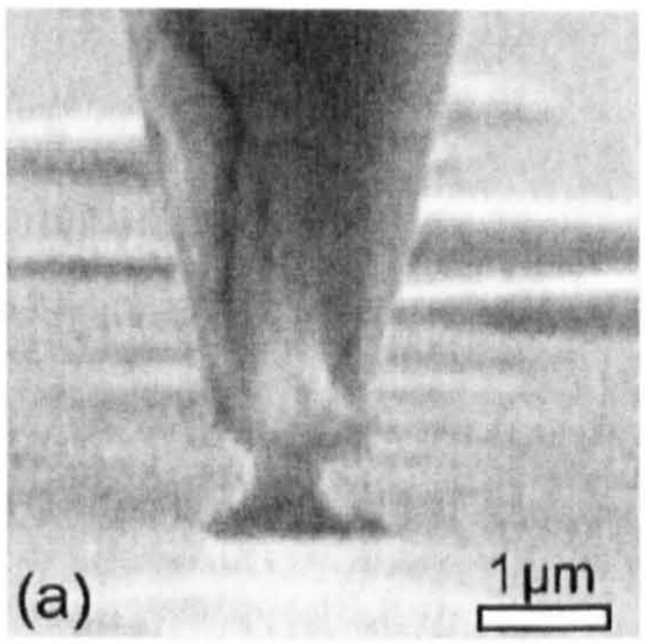

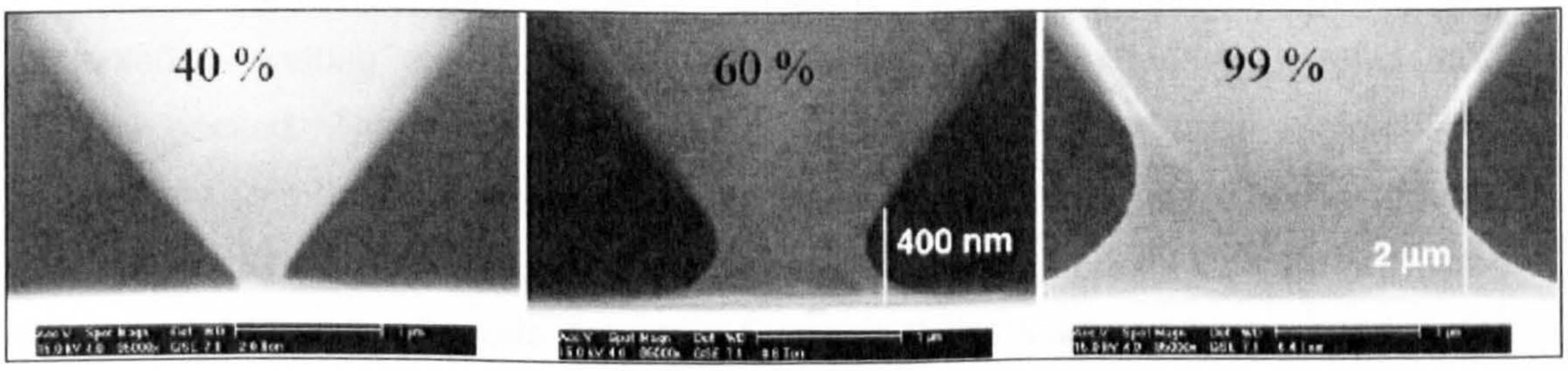

(b)

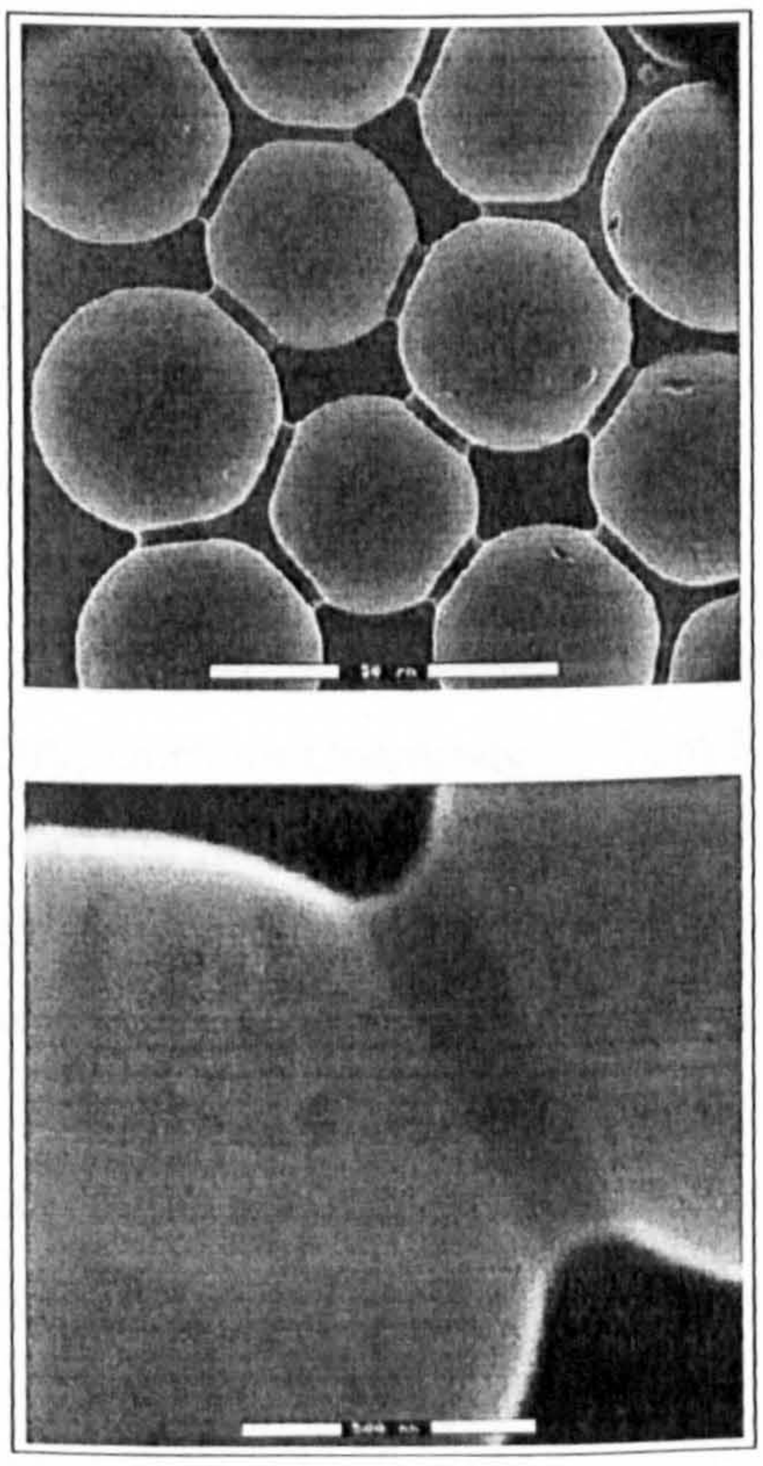

(c)

Figure 6.1: ESEM microphotographs of water menisci, (a) between an tungsten tip and a surface (from Schenk et al., 1998), (b) between a AFM cantilever tip and a surface at different RHs (from Weeks et al., 2005), (c) between glass beads in top image (diameter=40μm) and silica spheres in the bottom image (diameter=1.5μm) (from Lampenscherf et al., 2000)

The aim of this chapter is to use the ESEM to investigate meniscus water behaviour in particulate media under different conditions to demonstrate the possible use of the technique for the study of unsaturated soil behaviour. Instead of using natural soil which would have a variable particle size, shape and a complex fabric, ideal spherical particles were used to simplify matters and to allow direct measurements of dimensions. The particles used are equivalent to clays in terms of size (2μm and 6μm). To resemble the usual testing procedures of unsaturated soils, all tests started from a wet condition with the spheres free to move. The particles were then subjected to wetting and drying cycles in 2 configurations, loosely packed and densely packed. The loose arrangement would enable observation of interface phenomena (e.g. contact angles) and the densely packed its fabric and hydraulic aspects (e.g. the ink-bottle effect during drying) (introduced in Chapter 2). The chapter reports and interprets the main findings of the scanned images and their implications to unsaturated soil mechanics are discussed. Some of the results are reported in Lourenço et al. (2008c).

6.2. EXPERIMENTAL SECTION

6.2.1. Material and equipment

The spheres observed in the ESEM in this study are organosilicates synthesized in the Department of Chemistry, Durham University by Tom Smart and Aileen Congreve according to a modification of the method developed by Miller et al. (2005). They are coated with an amine layer. The spheres have diameters of 2μm and 6μm, there are also smaller random spheres with a diameter <1μm. The spheres were stored and kept in de-ionized water until use in the ESEM. The spheres were developed for research in chemistry. Their characteristics (diameter, coating) were defined by the above authors according to their needs.

The instrument used was a FEI XL-30 field emission ESEM with a gaseous secondary electron detector (GSED) and was equipped with a Peltier stage. The tests were conducted in the same ESEM model and same conditions in two different locations: Department of Chemistry, Durham University (DU) and Institute of Petroleum Engineering, Heriot-Watt University (HWU).

6.2.2. Procedures and programme

A droplet of the aqueous solution with the spheres was placed directly in the stainless steel sample holder, and positioned in the Peltier cooling stage. The loose packing was achieved by adding more de-ionized water while for the dense packing more solution was added. The temperature was set at 5°C and the RH taken to 100%. RH was then cycled between nearly 100% and a minimum of 35%. A working distance (between the stage and the detector) of 7.5 to 10.5mm was used, with an operating voltage of 20kV, and spot size of 4 – 6.3. Under these conditions, it was possible to obtain images up to 10000x magnification. De-ionized water was used as the source of vapour.

The data presented concerns sequences of cycles of water vapour pressure (maximum 3) performed on the same sample. Imaging was done in selected areas. The vapour pressure was changed in steps by visual inspection of the meniscus growth (during wetting) or reduction (during drying). Once it had stabilized, vapour pressure was further increased or decreased. Slight temperature variations occurred when the spheres suddenly wetted or dried, but the test did not proceed to the next stage until the temperature was stable at 5°C. During the waiting periods or whenever changes of water vapour pressure occurred too fast still images were collected. Imaging conducted at HWU started with the samples in a wet condition while at DU the initial wet stage was not recorded.

6.3. IMAGE ANALYSIS

Image analysis was essentially based on observation. Analysis included: observation of the meniscus (shape of the air-water interface, contact angle against the spheres), fabric of the spheres (arrangement in relation to each other and dimensions), meniscus evolution and fabric changes as RH changed. Direct measurements of contact angles and radius were also made.

Tests in Figures 6.2a, 6.2b, 6.3 and 6.10 were affected by a leak in the water line in Durham's ESEM. This lead to condensation at unusually low RH values (91.5%) when it should have occurred at values near 100%. Therefore RH values for these images should only be taken as approximate (they are shown in the figures with the ± sign). RH measurements at HWU are correct.

The main observations will be at first reported below and then interpreted with discussion in Section 6.4.

6.3.1. Interface phenomena

For the 6μm spheres images, it was possible to distinguish clearly the menisci from the spheres and, where the spheres did not pile up it was also possible to distinguish the menisci between the spheres and the substrate. For the 2μm spheres, the menisci were only visible at RH larger than 75%.

The following physical features of the air-water interface and water-solid interface were found:

- At low RHs, water condenses at the interparticle contacts, while at high RHs water condenses at the interparticle contacts and at the sphere surfaces with dome (or mushroom-like) shapes (Figure 6.2a and 6.2b).

- The arrows in Figure 6.2a show that the majority of the menisci have a convex shape. The sequence Figure 6.2a, Figure 6.2b shows that the convex shape develops progressively as RH increases.

- Menisci between the spheres grow upward or to the sides (arrows in Figure 6.2a and Figure 6.2b). The meniscus volume is variable.

- Some menisci break up as they increase in size while others are able to withstand the positive curvature (Figure 6.2b).

- The menisci are linked in Figure 6.2c. They coalesce forming a continuous liquid phase.

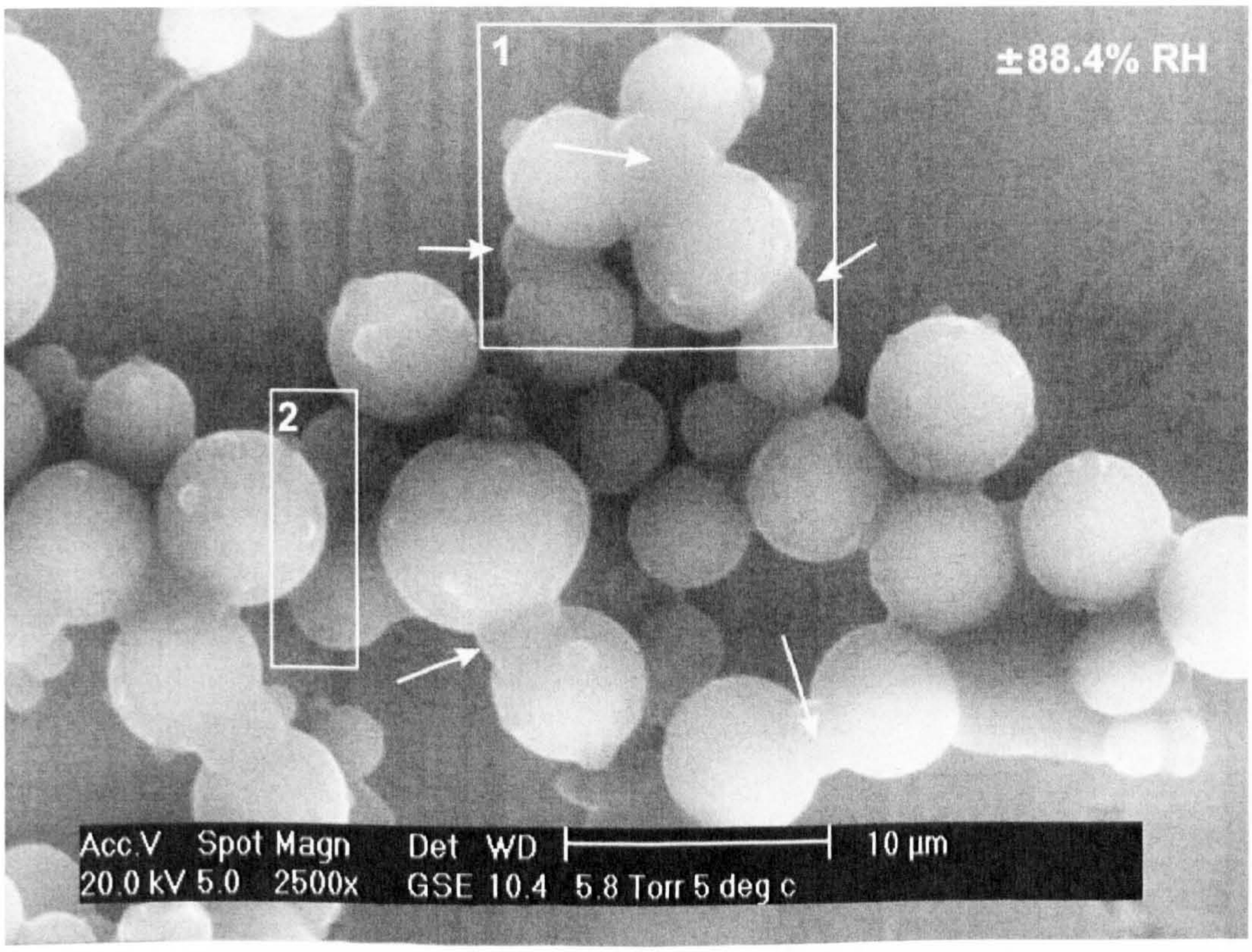
1
±88.4% RH
2
Acc.V Spot Magn Det WD 10 µm
20.0 kV 5.0 2500x GSE 10.4 5.8 Torr 5 deg c

(a)

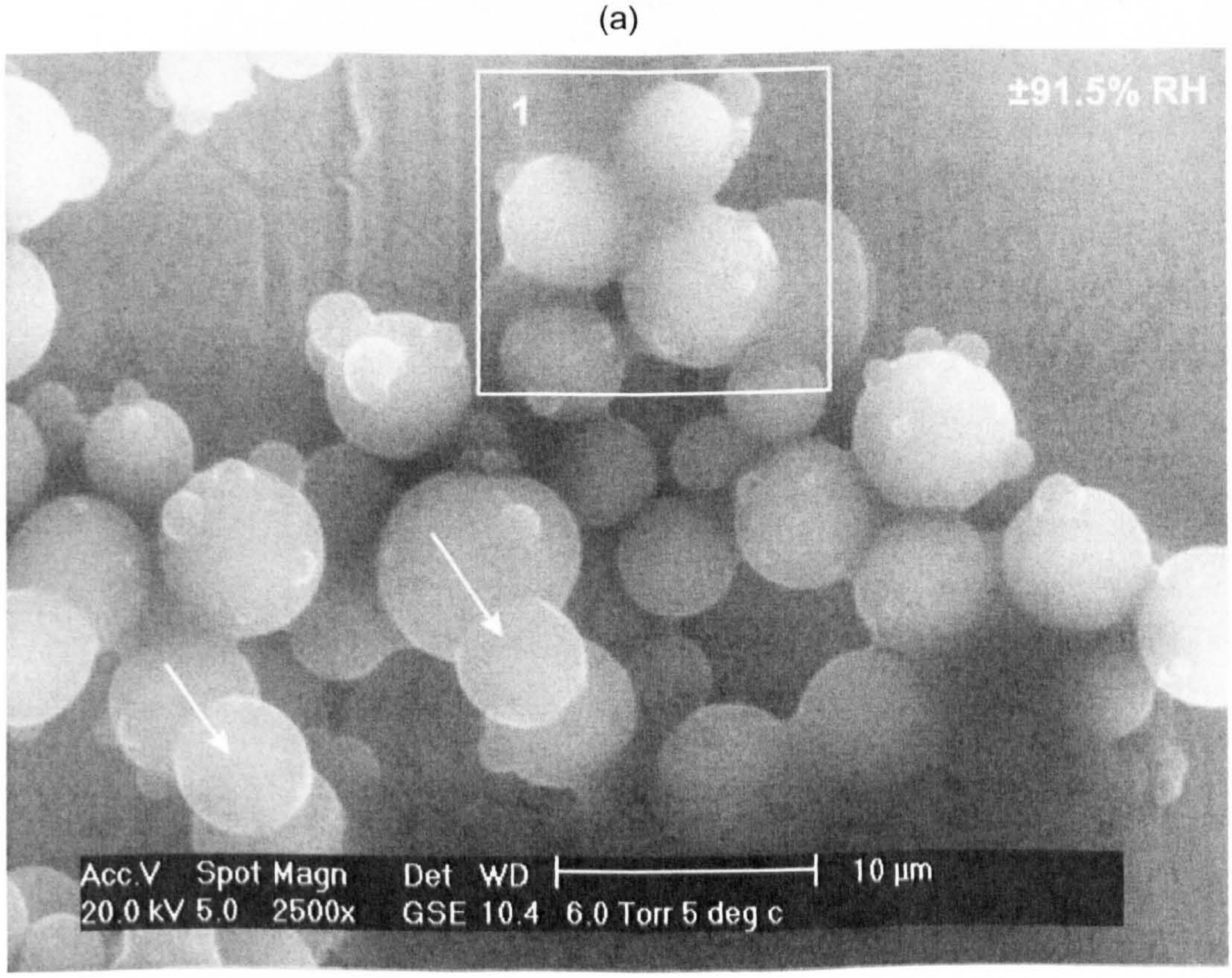
1
±91.5% RH
Acc.V Spot Magn Det WD 10 µm
20.0 kV 5.0 2500x GSE 10.4 6.0 Torr 5 deg c

(b)

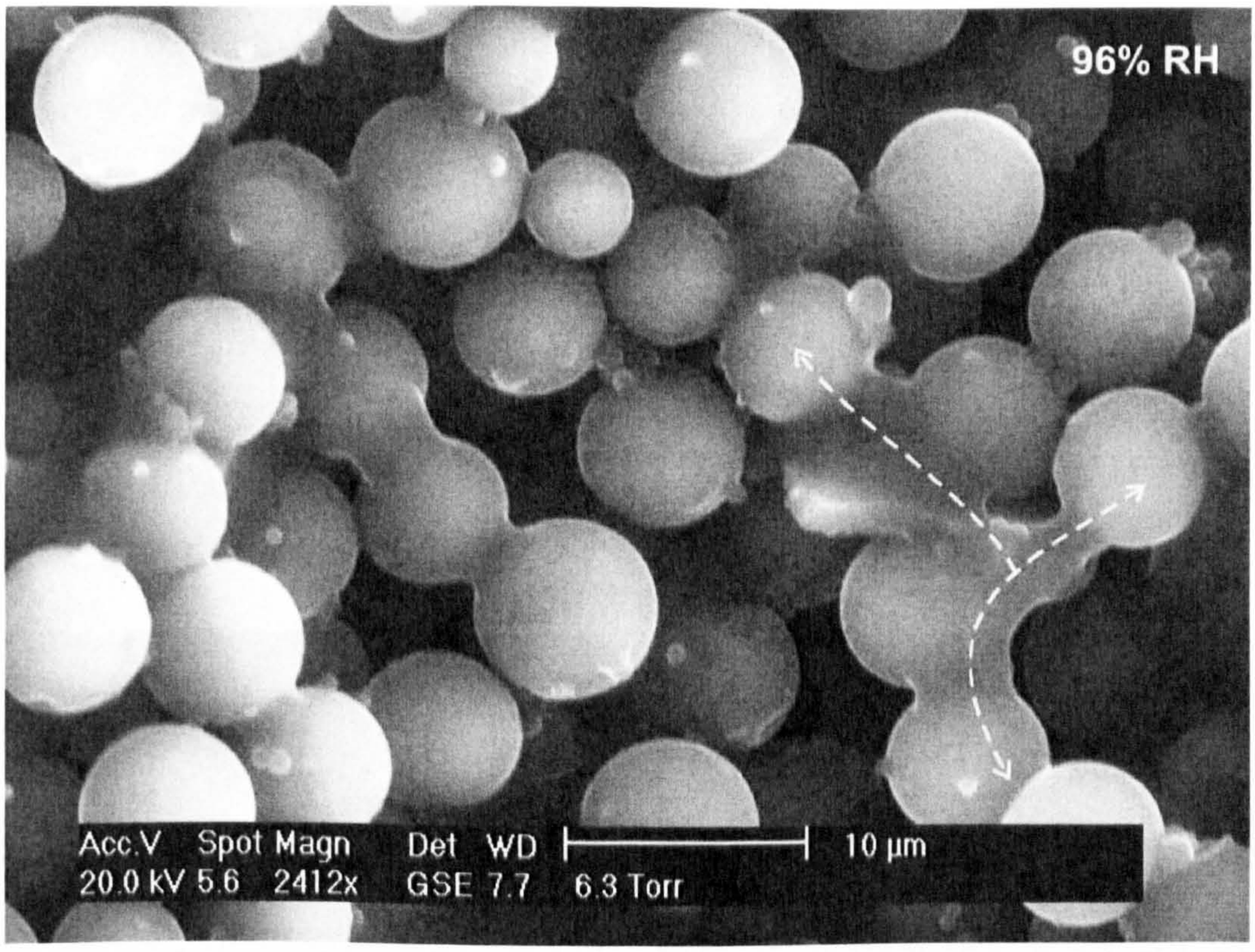

(c)

Figure 6.2: Physical features of the observed menisci; menisci growth with convex shape from a) to b) (test E1, silica spheres); linked menisci in c) leading to a continuous liquid phase (1Torr = 0.133kPa) (test E2, silica spheres)

- Opposite to the convex shapes of Figure 6.3b, Figure 6.3e shows a concave shape for the meniscus, when the same spheres were wetted for a second time. They also did not develop the dome shaped features at the surface.

- The contact angle between the sphere's surface and the menisci was measured manually in Figure 6.3b and Figure 6.3e. Contact angles for the convex menisci on the sides in Figure 6.3b are in the range 75°-85°, while for the concave menisci in Figure 6.3e angles are between 20°-30°.

- The different water regimes can be identified in Figure 6.3: pendular (Figure 6.3a, Figure 6.3c), funicular (closing meniscus in Figure 6.3d) and capillary (Figure 6.3e). Following Orr et al. (1975) classification.

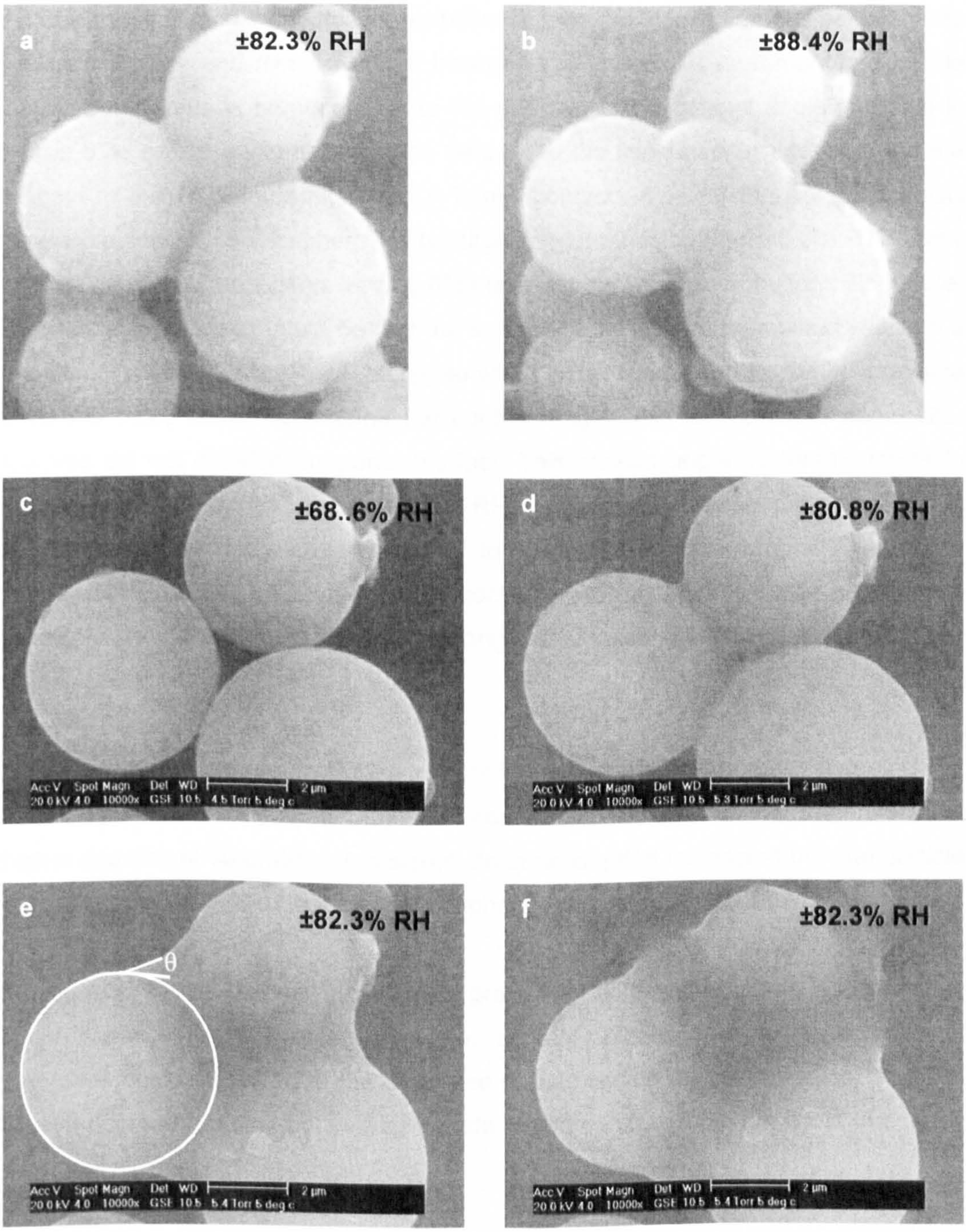

Figure 6.3: Sequence of images scanned during the increase of water vapour pressure (test E1, silica spheres); images *a* and *b* were enlarged from the rectangle in Figure 6.1; the 1st wetting sequence is from *a* to *b*; the 1st drying is in *c*, and the 2nd wetting from *d* to *f*; the measurement of the contact angle θ is shown in *e* (1Torr = 0.133kPa)

An important finding from this description is that the contact angle between the sphere's surface and menisci varied between the cycles. Measurement is possible because the angle is perpendicular to the substrate. The contact angle is drawn in Figure 6.3e as the angle between the tangent to the liquid-vapour interface and the tangent to the solid-liquid interface. A larger contact angle for the convex menisci shows the surface of the spheres to be slightly hydrophobic (Figure 6.3b). The lower contact angle for the second wetting (Figure 6.3e) shows a more hydrophilic nature. A possible explanation could be that the surface of the spheres remained wet with a thin film of water after the first wetting, so when water condensed for the second time it spread more easily decreasing the contact angle. The fact that the dome like-features did not develop supports this fact. This contact angle hysteresis refers to changes between cycles, and not during RH increase or decrease. Lampenscherf et al. (2000) documented a change from 5° to 60° as RH increased from 75% to 95%. Hennig et al. (2004) measured the contact angle of water droplets in a polyimide substract and observed that the contact angle decreased with time at constant water vapour pressure.

Condensation from vapour not only occurs in small spaces and cracks (Israelachvili, 1991). The data clearly show that water condenses in the surface of the spheres at higher degrees of saturation. It is also quite intriguing that menisci at the interparticle contacts grow upward or to the sides of spheres instead of all around.

Figure 6.3c shows that as the menisci grew they coalesced forming a continuous liquid phase. This suggests that water content variations at lower degrees of saturation could be linked to the air phase (condensation and evaporation) and that at high degrees of saturation, water transfer could occur by both the liquid phase (by flow) and air phase (vapour transfer).

6.3.2. Hydraulic hysteresis

Figure 6.4 shows hysteresis of the liquid phase for a drying-wetting cycle. The spheres remained partially flooded while drying until 88.4% RH (Figure 6.4b) but when they were wetted only isolated menisci were visible at 88.4% RH (Figure 6.4d), total condensation did not occur not even at 94.5% RH (Figure 6.4e). Further analysis of images with correct RH measurement revealed that the 2μm and 6μm spheres had full condensation at 94.5-97.5% RH and evaporation at 78-85 % RH. It was initially thought that it was due to a problem with the HWU's ESEM or that water pressure was changed too fast without giving time for the menisci to stabilize. However the sequence of selected images in Figure 6.4 was obtained in 23 min, which was considered to be enough time to menisci to stabilize. In other ESEM studies, Montes-H. (2005) waited 20min, Sorgi and De Gennaro (2007) waited 1h, while Weeks and DeYoreo (2006) reported 10min as waiting time for condensation to occur between the cantilever tip and the substrate.

The ink-bottle effect was not visible for the densely packed spheres. The emptying and filling of pores occurred too fast to allow any observation at intermediate regimes. It was not possible to have a finer control of RH. Water vapour pressure could only be controlled at 0.1torr steps (corresponding to 1.5% RH for >90% RH).

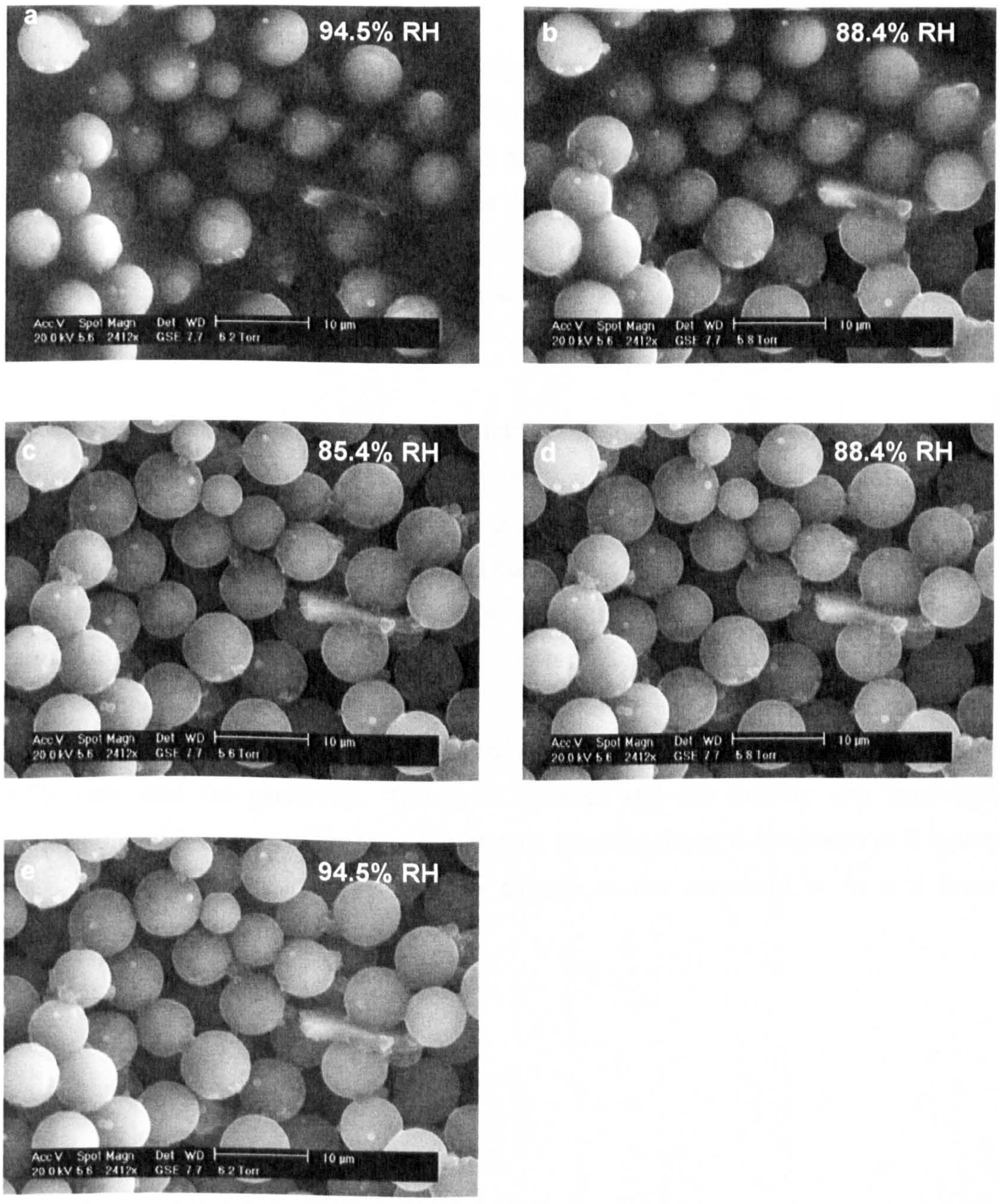

Figure 6.4: Selected images collected from a drying-wetting sequence (*a* to *e*) (test E2, silica spheres); drying is from *a* to *c* and wetting from *c* to *e*; a marked hydraulic hysteresis is shown; at 94.5% the spheres are saturated in *a* and partially saturated in *e* (1Torr = 0.133kPa)

6.3.3. Fabric formation and changes

The spheres with a loose packing are orderly arranged. They are packed in chains, where each sphere has 2 to 3 contacts (Figure 6.5a). Figure 6.5a shows the number of contacts for each sphere. The data was obtained by counting manually the number of contacts for each of the spheres with a diameter higher than 2μm in Figures 6.2a, 6.2b, 6.10. Figure 6.5b and Table 6.1 shows that the number of contacts increased with the diameter. Such an arrangement was not so evident for the densely packed spheres.

An interesting observation is that the fabric for the 2μm spheres was suddenly formed at 82.3% RH. The spheres were underwater at the start of the test (Figure 6.6a) and as evaporation proceeded at the same RH they suddenly piled up creating an edifice of spheres (Figure 6.6b). This was only observed once. The exact sequence could not be tracked because it occurred too fast to be noted and the quality of the image deteriorated as the spheres piled up. Both images were saved with 1 minute difference. Figure 6.6b shows the spheres enclosed by meniscus water. Correspondence between the shape of the spheres in Figure 6.6a and Figure 6.6b. can also be observed. The 6μm spheres did not display any particular behaviour when water evaporated completely. In some areas a maximum of 5 layers were visible, the remaining were lying directly in the substrate or in a 2 layer configuration.

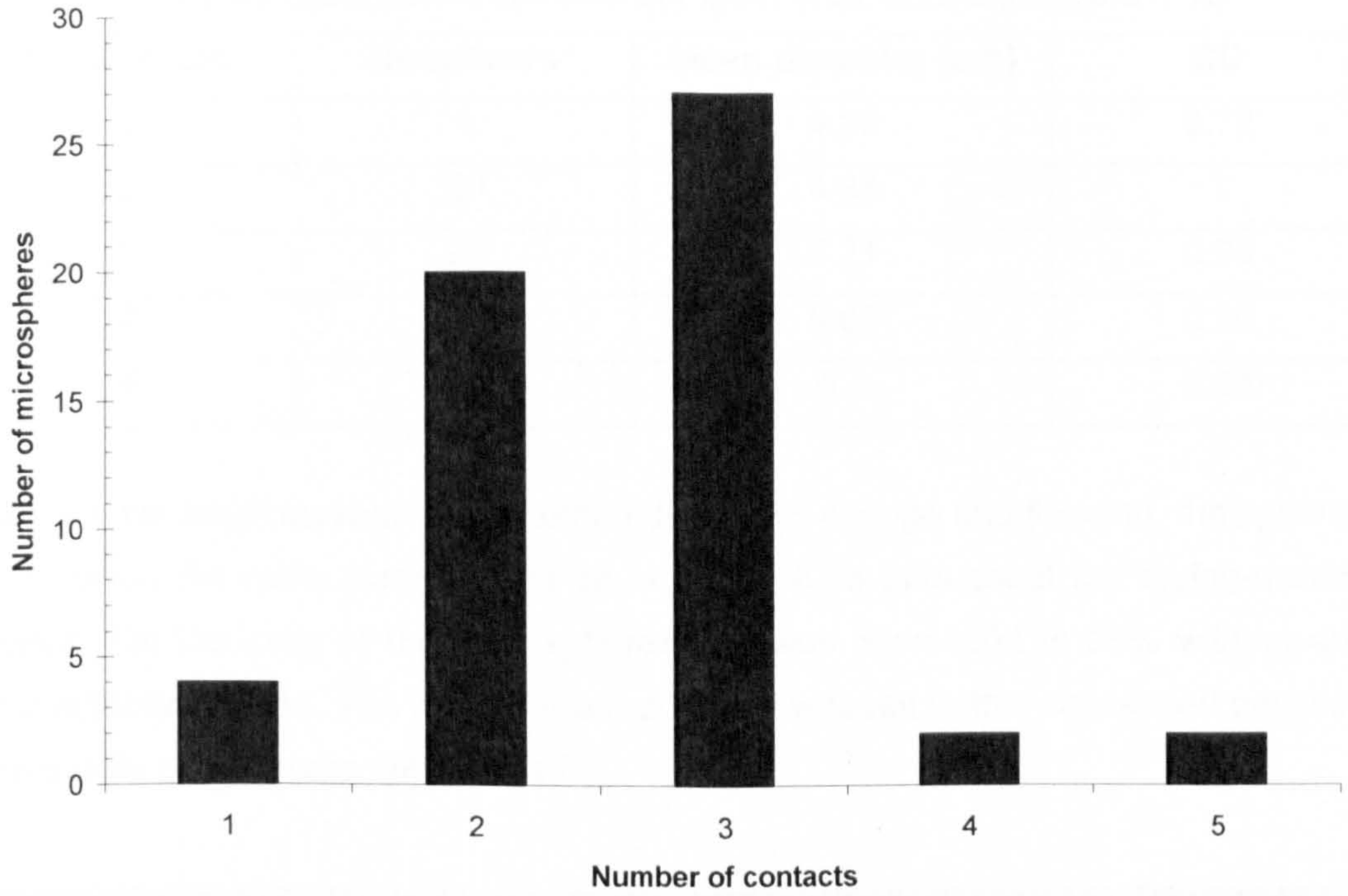

(a)

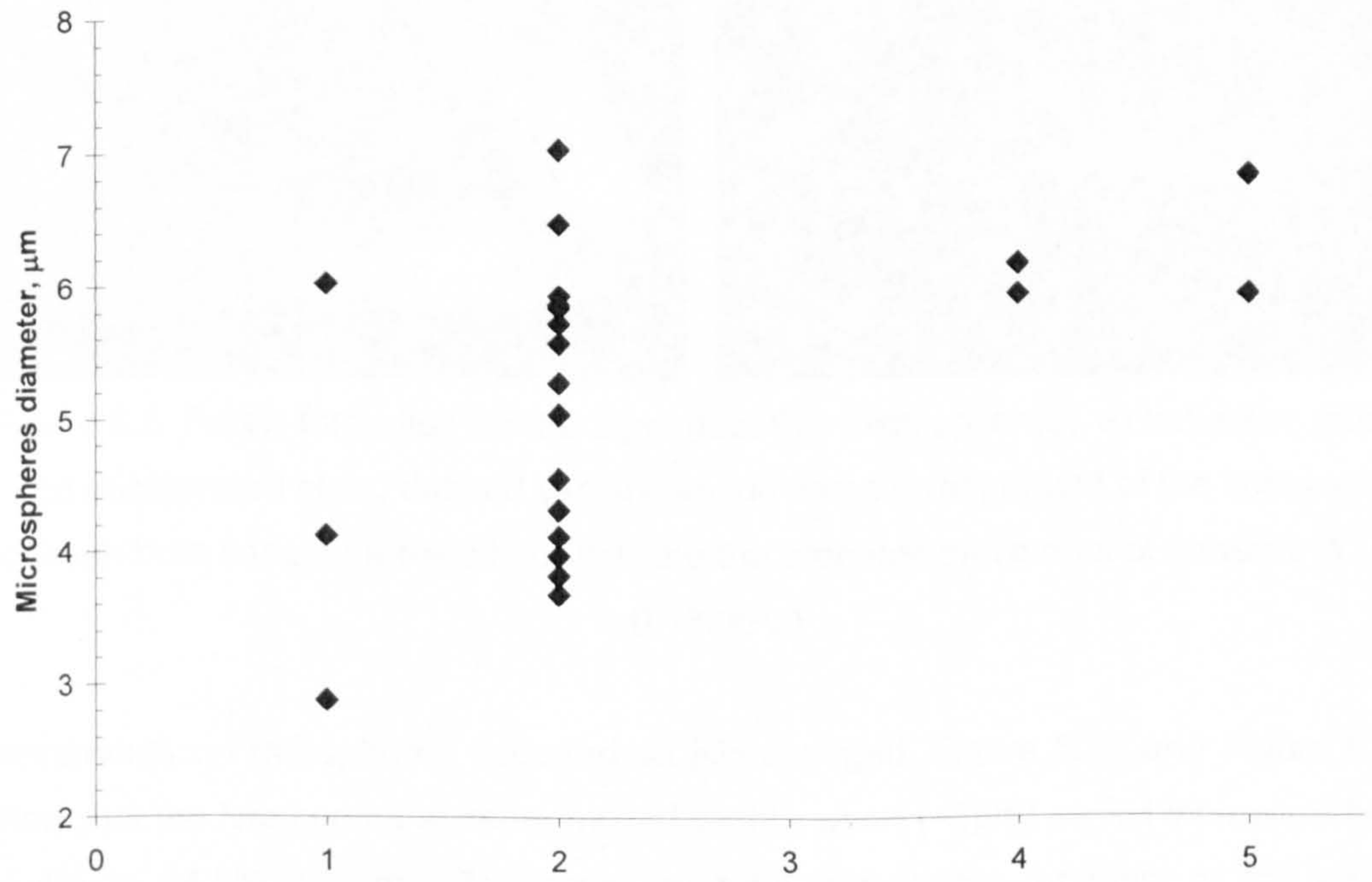

(b)

Figure 6.5: Number of contacts for each sphere of Figure 6.2a, 6.2b and Figure 6.10, (a) number of spheres – number of contacts, (b) spheres diameter – number of contacts

Table 6.1: Average data for the spheres of Figure 6.2a, 6.2b and Figure 6.10

Nr contacts	Nr spheres	Mean diameter (μm)	SD
1	4	4.29	0.72
2	20	4.88	1
3	27	5.21	0.93
4	2	6.06	0.16
5	2	6.4	0.64

Besides the small movements occurring during RH change and flooding, the spheres maintained the same arrangement as in Figure 6.6b throughout the drying-wetting cycles. For the case of the 2μm spheres, RH was decreased to 35% without any visible fabric change. The water vapour pressure was not further decreased because the quality of the image deteriorated.

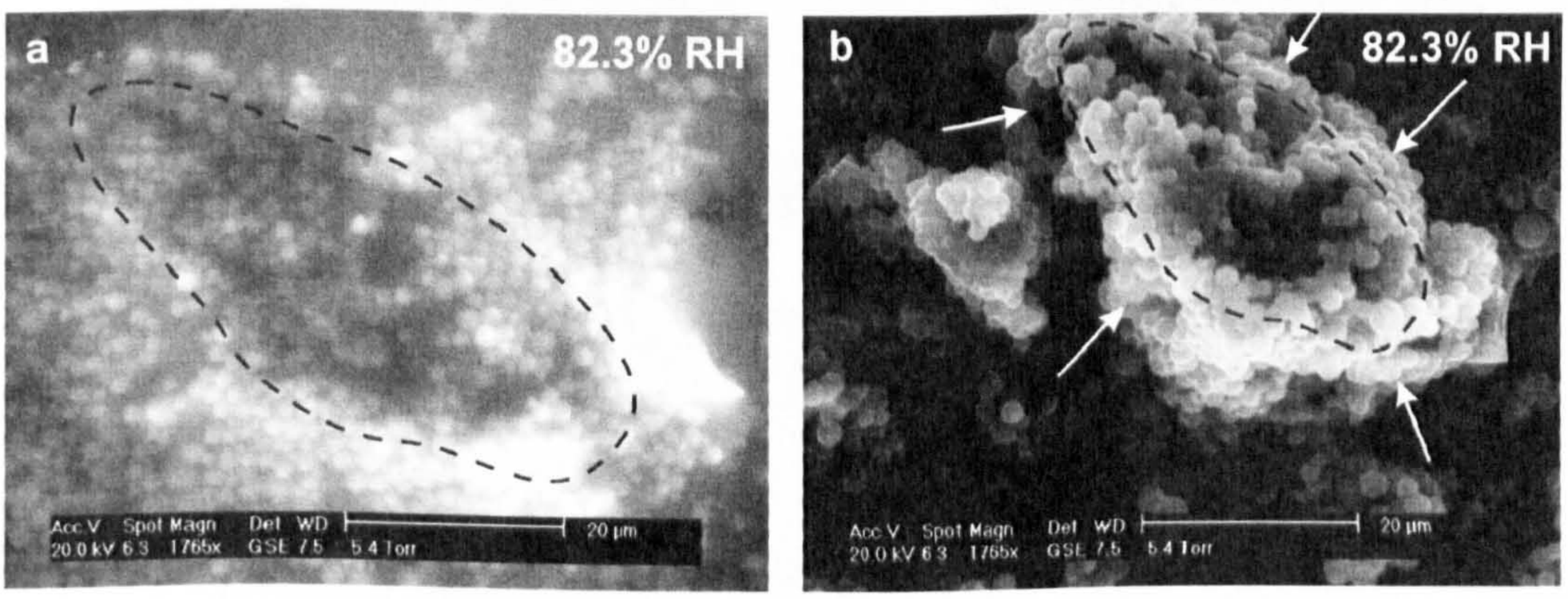

Figure 6.6: Fabric formation for the 2 μm (test E3, silica spheres), a) saturated state, b) unsaturated state; dashed line shows the same arrangement of the spheres between both images; arrows in b) indicate the probable movement of spheres (1Torr = 0.133kPa)

Movements on the spheres occurred as RH changed. Figure 6.7a and Figure 6.7b show that the two central spheres moved slightly apart (<1μm) as RH increased from 85.4% to 94.5%. Figure 6.7c shows the total movements for most of the visible spheres (including the two spheres from Figure 6.7a and Figure 6.7b) for a wetting-drying-wetting cycle. Figure 6.7c was obtained by superimposing two images before and after wetting and drawing each sphere manually. Spheres usually moved upward parallel to the substrate, with the spheres on the right hand side having the largest movement. Left-hand side spheres remained nearly stable. The nature of these movements could be related to the action of the meniscus force pulling the spheres

together or due to gravity with the spheres rolling down because the substrate was inclined or uneven.

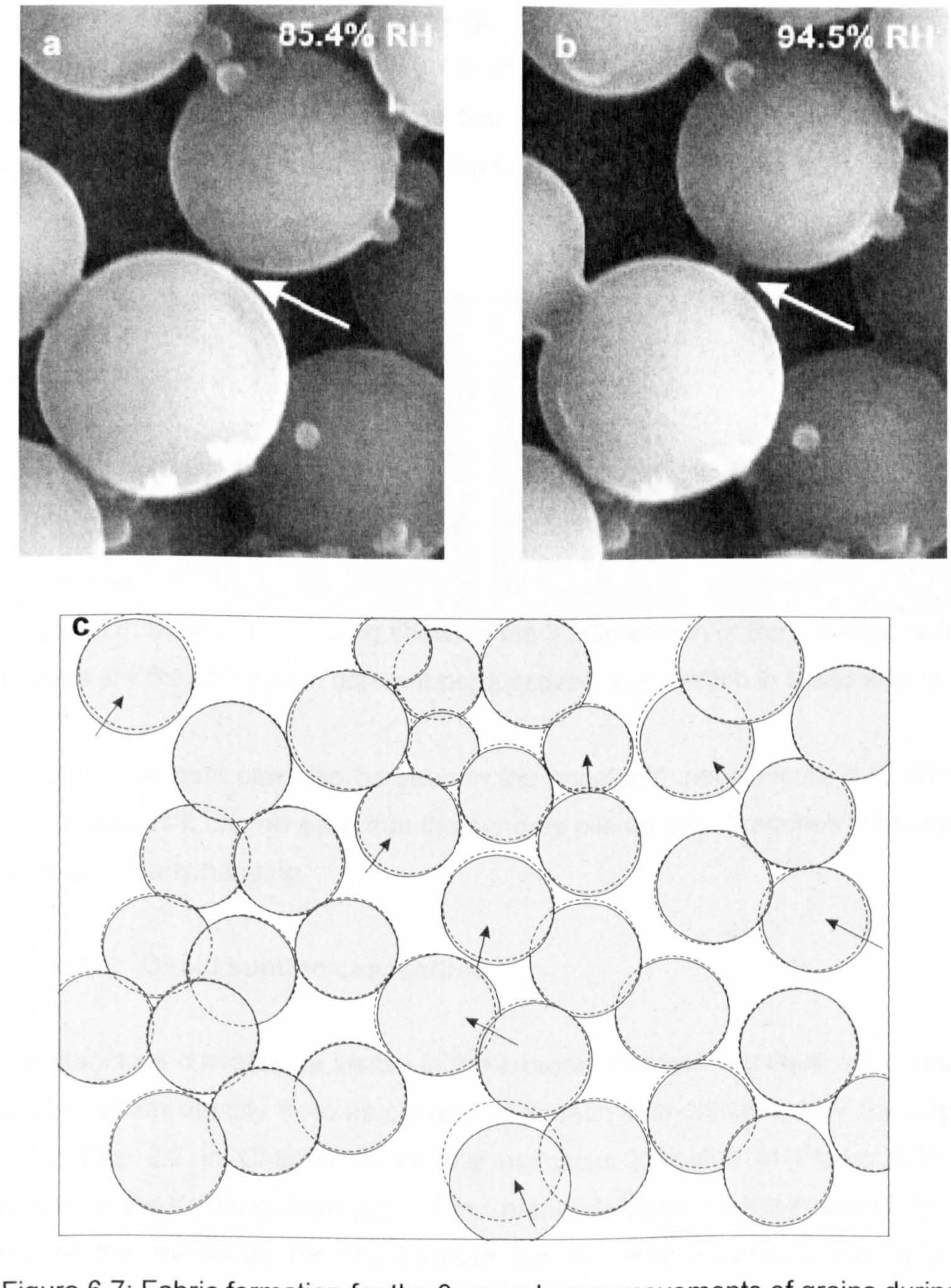

Figure 6.7: Fabric formation for the 6 μm spheres; movements of grains during wetting shown in *a* and *b* (test E2, silica spheres); movements by selected spheres are shown by the arrows in *c*

Further evidence of the meniscus force is given by the position of the spheres in relation to each other. As all images were scanned from above, some spheres hide others (e.g. rectangle 2 in Figure 6.2a) while spheres with different diameters are in contact without hiding each other (rectangle 1 in Figure 6.2a). This suggests that the hidden spheres might not be resting flat on the plate, implying that the meniscus force or some other interparticle force could be holding them. Figure 6.8 shows a schematic example of this, from two views: in elevation in Figure 6.8a and side in Figure 6.8b.

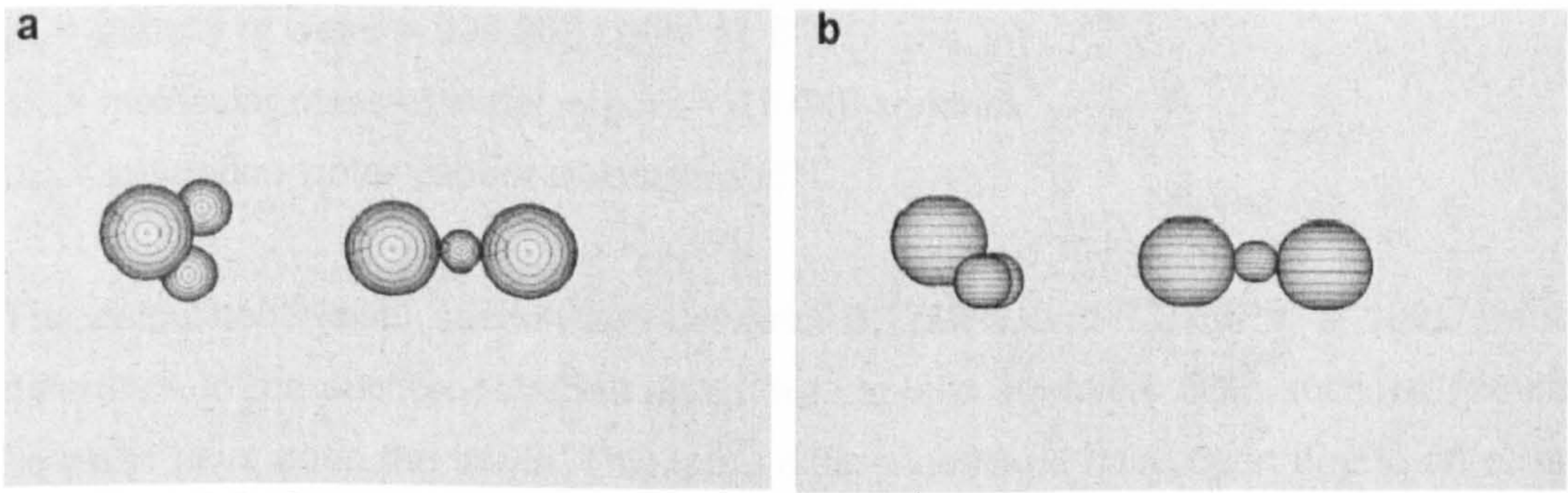

Figure 6.8: Schematic drawing showing the 3rd dimension of the spheres; both images are the same from different perspectives, in elevation in *a* and side in *b*

This 3D arrangement can also be seen in the anaglyph image Figure 6.9. With the aid of 3D glasses it can be seen that the spheres pile up with 'branches' where some spheres are clearly hanging.

6.3.4. Direct suction calculation

As the meniscus curvature is visible in the images, this was a unique opportunity to calculate suction directly from its curvature. Suction was calculated by the Laplace equation (eq. 2.2 in Chapter 2) for the meniscus indicated in Figure 6.10 and compared to the Kelvin suction (eq. 2.1 in Chapter 2) based on the imposed RH. The radius of the meniscus for the Laplace suction was measured manually and converted to the image's scale, while the RH was converted from 5.6torr (for a temperature of 5°C) to suction based in Kelvin's equation.

Laplace suction gives 29.3kPa for:

T, the surface tension of air-water at 5 °C = 0.0749 N/m,

r_1 = 1.01µm

r_2 = -1.67µm.

Kelvin suction was calculated for a RH of 94.5-97.5 % (because of the uncertainty of the RH values given by Durham's ESEM),

R = universal gas constant = 8.31432 $m^3PaK^{-1}mol^{-1}$,

T = absolute temperature = 273.16 + t_o (K), t_o = temperature = 5°C,

ρ_w = density of water = 999.965 kg/m^3 at 5°C,

ω_v = molecular mass of water vapour = 18.016 kg/kmol,

u_{v0} = saturation water vapour pressure at 5°C.

The calculated Kelvin suction lies between 3.17MPa and 7.25MPa, a 100x order difference to the suction obtained using the Laplace equation. Both suctions should however have been the same. This large difference could have been due to an error in the RH measurement in Durham's ESEM linked to a fault in its tubing (discussed previously) or not enough waiting time for the menisci to get in equilibrium with the RH. Nevertheless, the results demonstrate a huge potential for studies related to the validity of Kelvin's or Laplace's laws in granular media.

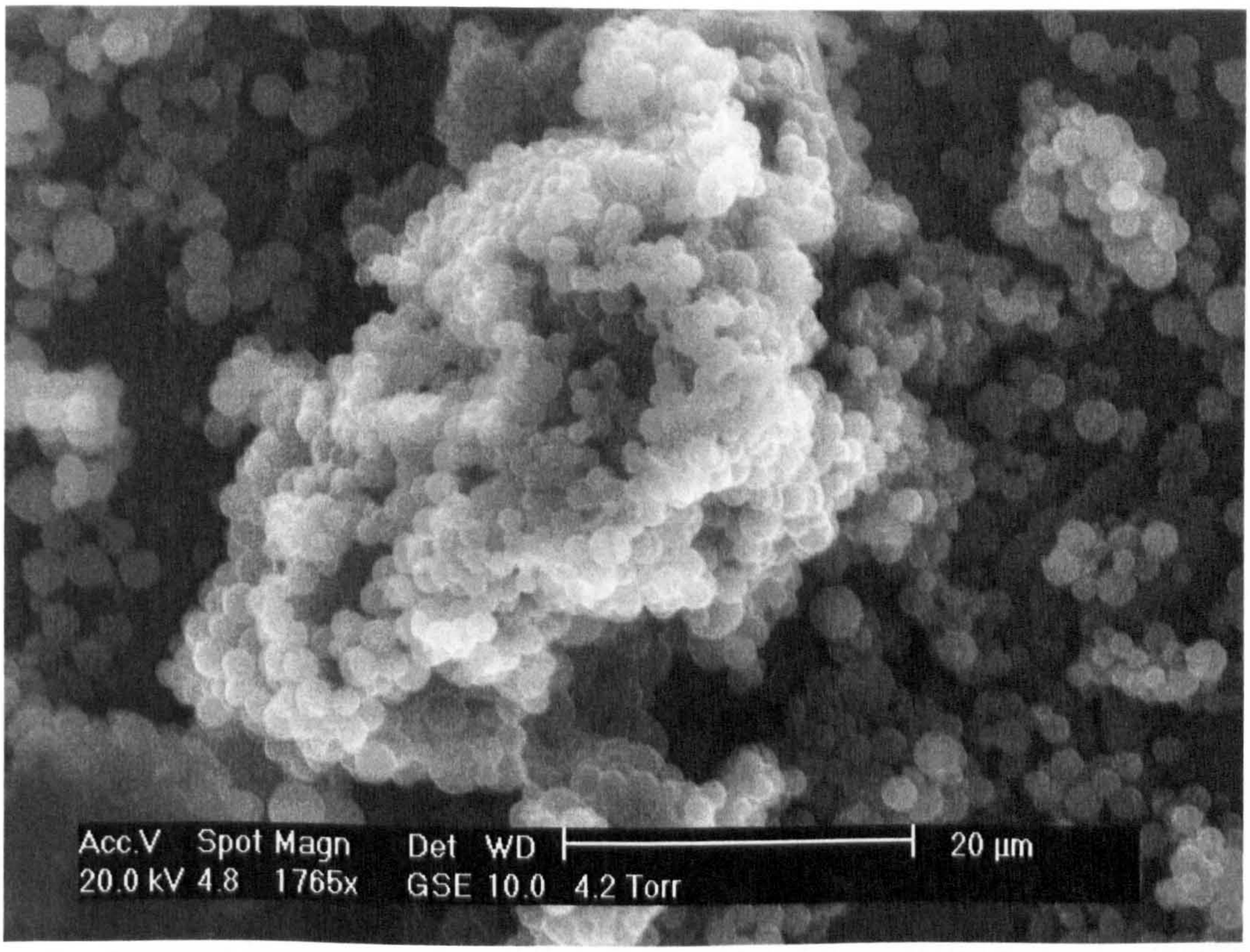

Figure 6.9: ESEM microphotograph of the 2µm spheres in 3D (3D view is possible with anaglyph glasses) (test E3, silica spheres)

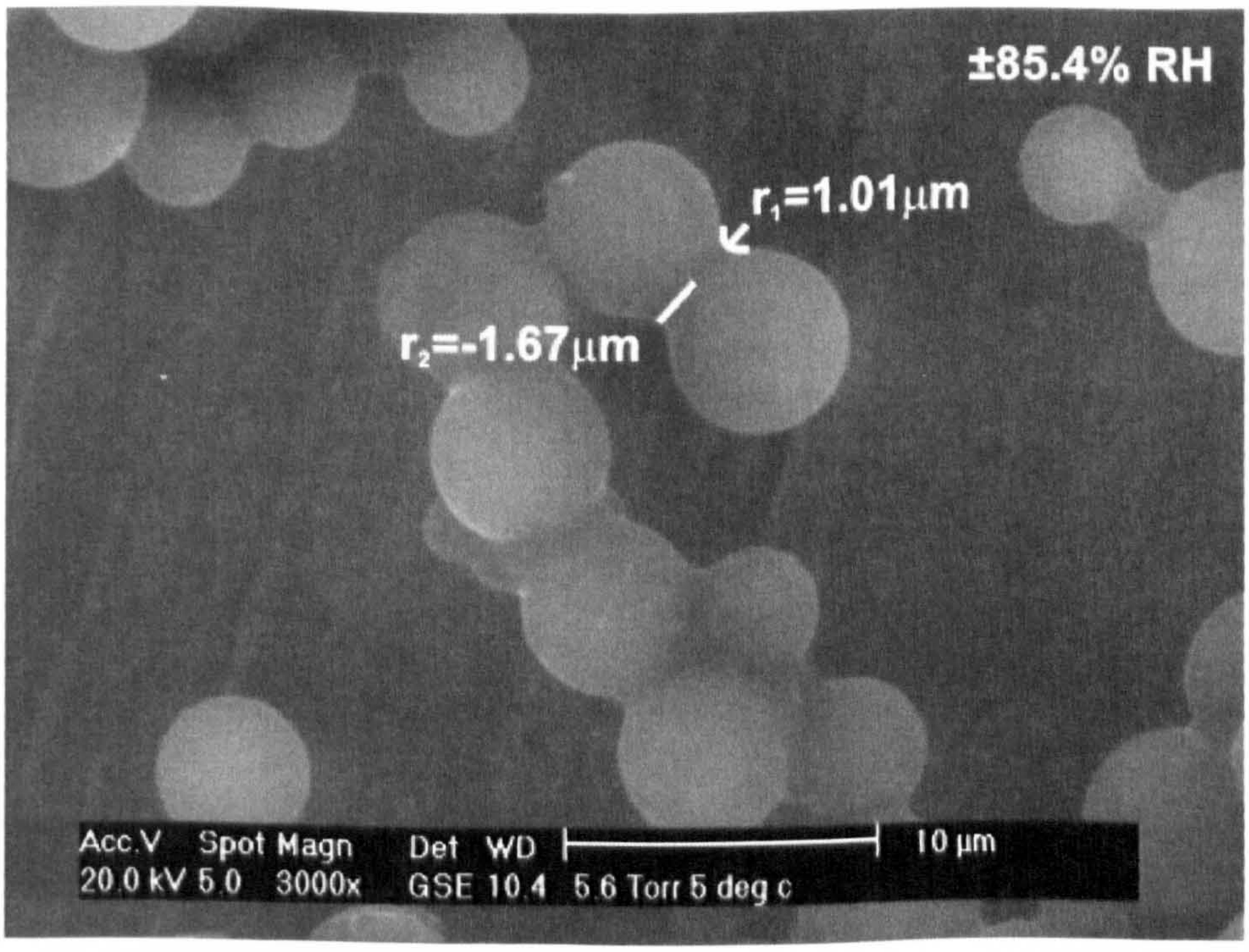

Figure 6.10: r_1 and r_2 measurement to calculate Laplace suction (test E1, silica spheres) (1Torr = 0.133kPa)

6.4. IMPLICATIONS FOR UNSATURATED SOIL MECHANICS

6.4.1. Contact angles

One of the most striking observations from the ESEM images is that the contact angle of the air-water interface against the surface of the spheres is quite variable. In unsaturated soil mechanics, contact angles are usually not taken into account or are assumed to be zero (Fisher, 1926). Based on the published literature from different fields, the goal of this section is to demonstrate that the contact angle of water held in unsaturated soils is likely to be variable, dependent on a variety of factors and that, this variability is likely to affect the mechanical and hydraulic behaviour of unsaturated soils.

6.4.1.1. Factors affecting the contact angle

The factors affecting the contact angle include:

- Direction of movement of the air-water interface. Advancing contact angles are larger than receding contact angles in Figure 6.11 (e.g., de Gennes, 1985).

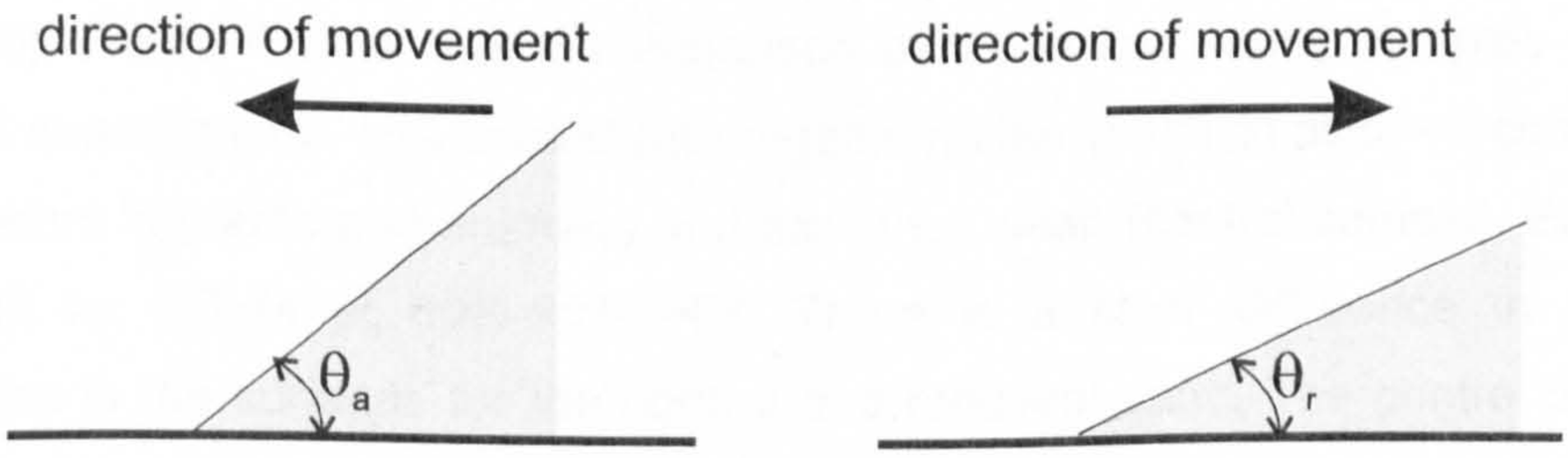

Figure 6.11: The contact angle of a water droplet changes as it moves back and forth; θ_a is the advancing contact angle and θ_r the receding contact angle (after De Gennes, 1985)

- Microasperities in the surface (e.g. Taniguchi and Belfort, 2002).
- Impurities and deposition of solutes (e.g. Fisher and Israelachvili, 1981).
- Velocity of meniscus movement (Hoffman, 1975).
- Sequence of wetting/drying cycles (e.g. Hennig et al., 2004).
- Addition of surfactants to water decreases the water surface tension. Karagunduz et al. (2001) measured a decrease of contact angle from 40° to 10° in sand.
- In water repellency studies of natural soils, also called hydrophobic soils (contact angle greater than 90°), Doerr et al. (2000) showed that water repellency varies with time and is mostly depend on the soil moisture. Drier soils are more hydrophobic than moistened soils.

Contact angle dependence on organic matter

Organic matter increases the contact angle making soils hydrophobic (e.g. Chenu et al., 2000). Figure 6.12 shows a comparison between two sandy samples made of rounded quartz grains, one coated with organic matter (palmitic acid – a common fat acid present in plants and animals) and the other clean (control sample). Both were observed by ESEM at 80%-90% RH. There is a clear difference in moisture adsorption in the surfaces for the control and repellent sand. The control sand has grains with a uniform coating of adsorbed water, while the moisture adsorbed onto the 0.1% treated sand is irregular and with smaller water droplets.

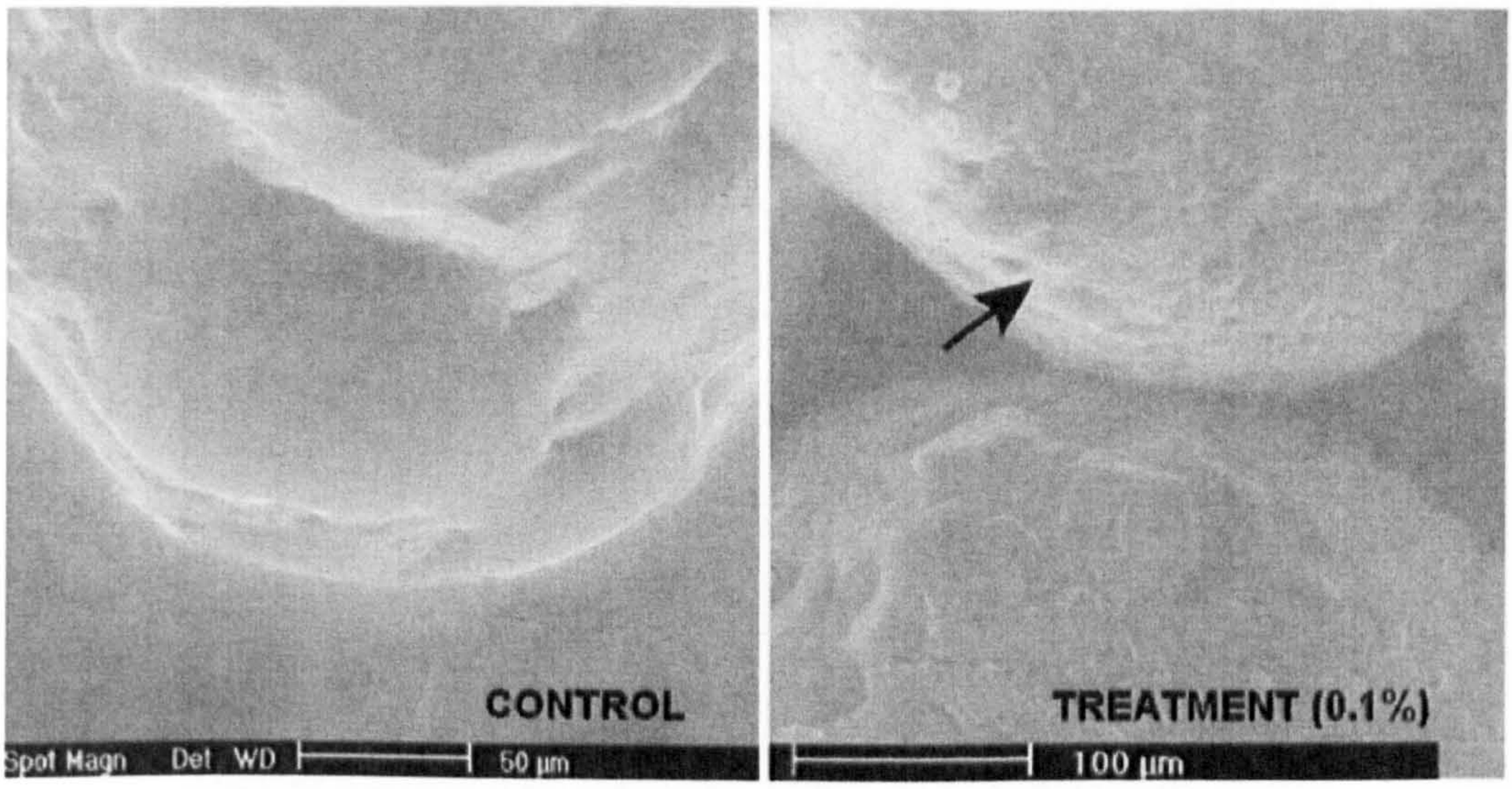

Figure 6.12: ESEM microphotographs of Ottawa sand with no coating (control) and coated with 0.1% palmitic acid in the right-hand side image (from Ravi et al., 2006)

The mechanical behaviour of saturated soils is often considerably affected by the presence of organic compounds in the soil. Cheng et al. (2007) showed that Oostvaardersplasen soils made of silt, clays and organic matter have higher friction angles than non-organic soils. A similar trend was found with Bothkennar clay (Hight et al., 1992) and Athlone clays (Long and O'Riordan, 2001). For these studies the high organic content is due to the existence of animal and plant fossils in the soil, and not usually due to a coating on the grains (as in Ravi et al., 2006) however the effect of the presence of these hydrophobic compounds on the soil in unsaturated conditions could change their mechanical behaviour considerably.

Contact angle dependence on the material

Besides all the previous factors detailed above, the contact angle strongly depends on the material. Letley et al. (1962) found contact angles by wetting experiments in clean soils, of 68.9° for a sandy loam and 65.2° for a clayey soil. Minerals also have different contact angles, 30° for quartz (Fisher and Lark, 1980), dolomite 5.6°-7.6° (Gence, 2006), mica 10° (Byrant et al., 2006). Ceramics are hydrophilic materials according to the Porous Ceramics Catalogue of SMC.

Figure 6.13 and Figure 6.14 shows images of different minerals obtained by ESEM from different sources. Figure 6.13a shows muscovite, a very common mineral in igneous rocks, with very low contact angles. Figure 6.13b and 6.13c show calcite and quartz, respectively. Quartz is the most common mineral in sands. They seem to have high contact angles but not higher than 90°.

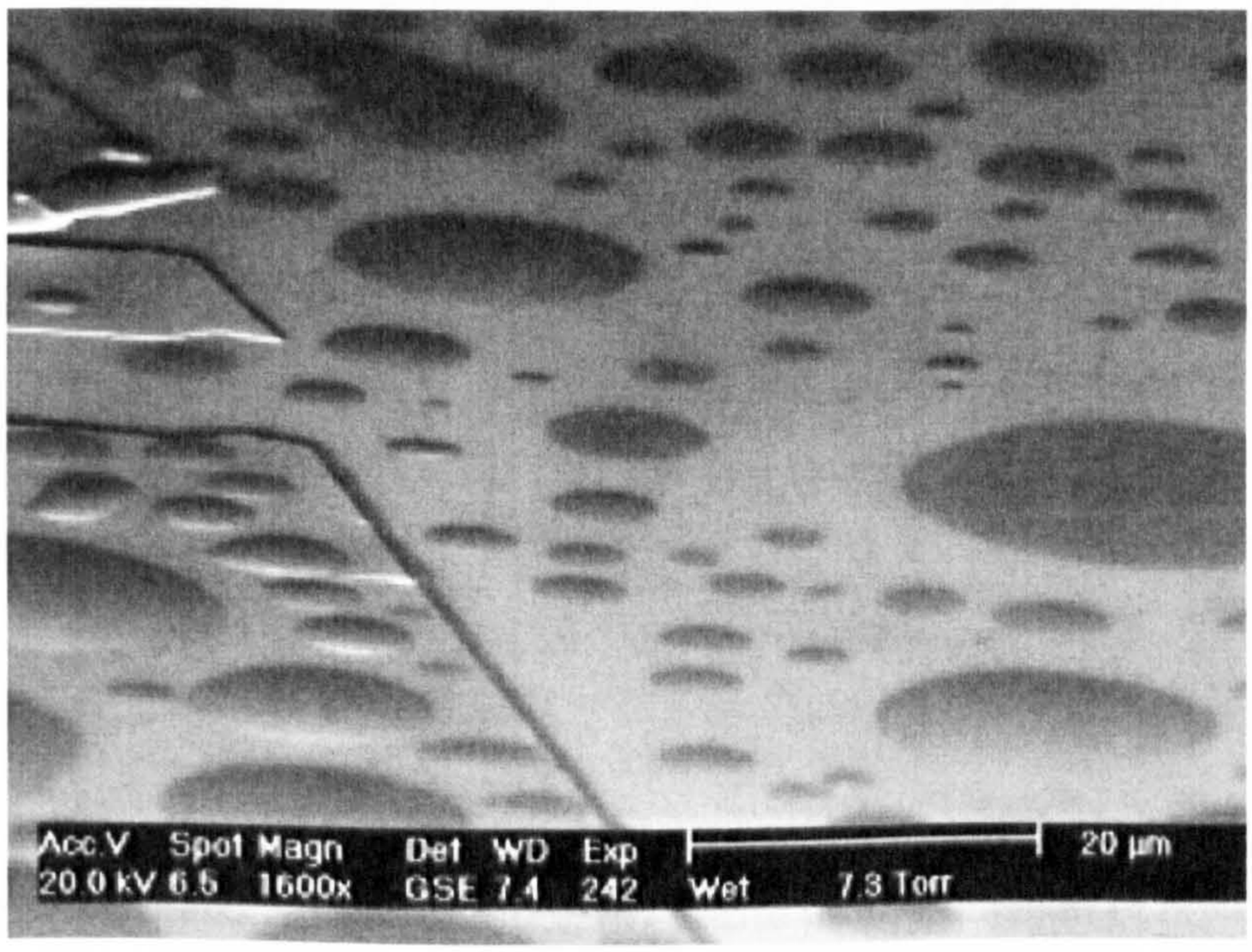

(a)

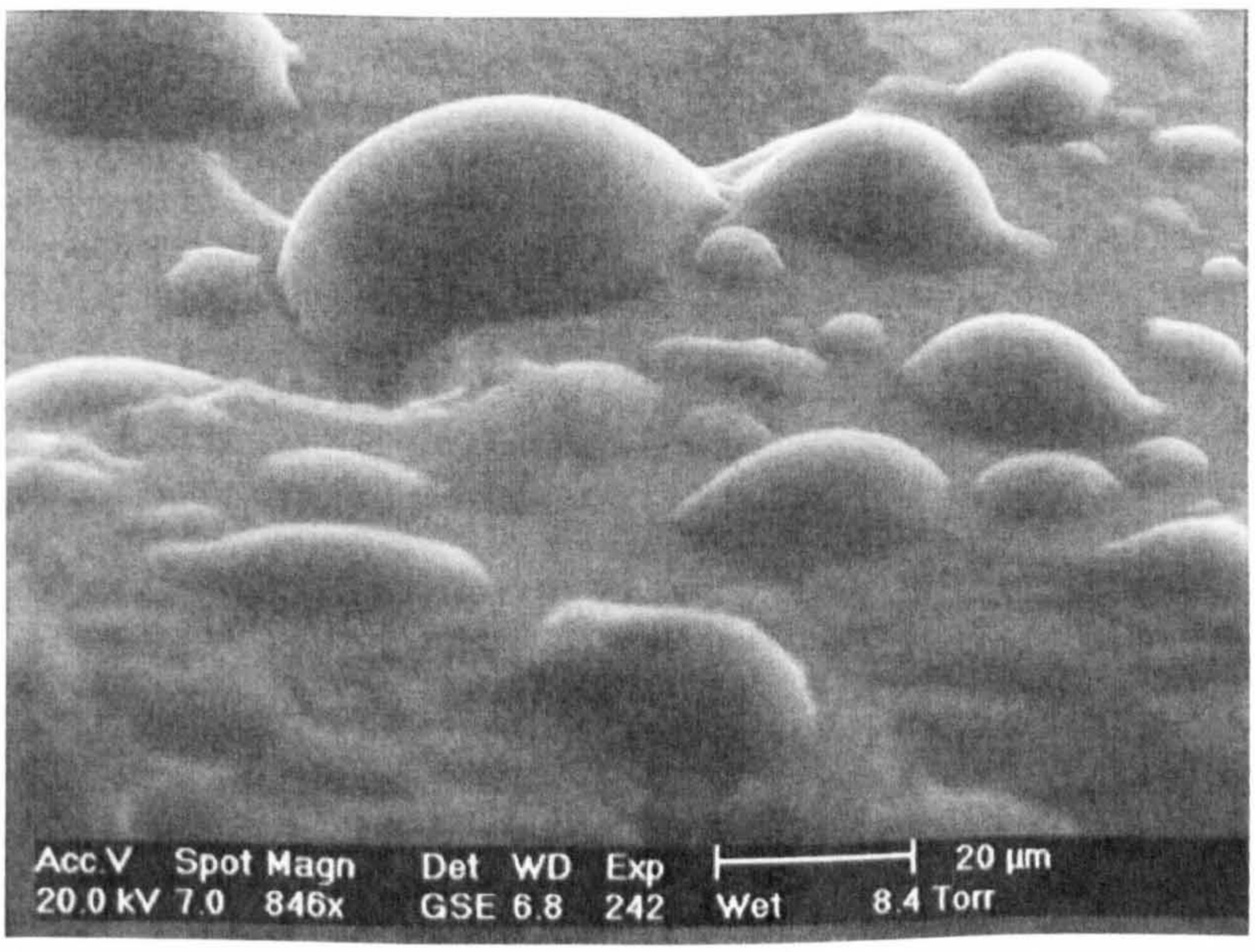

(b)

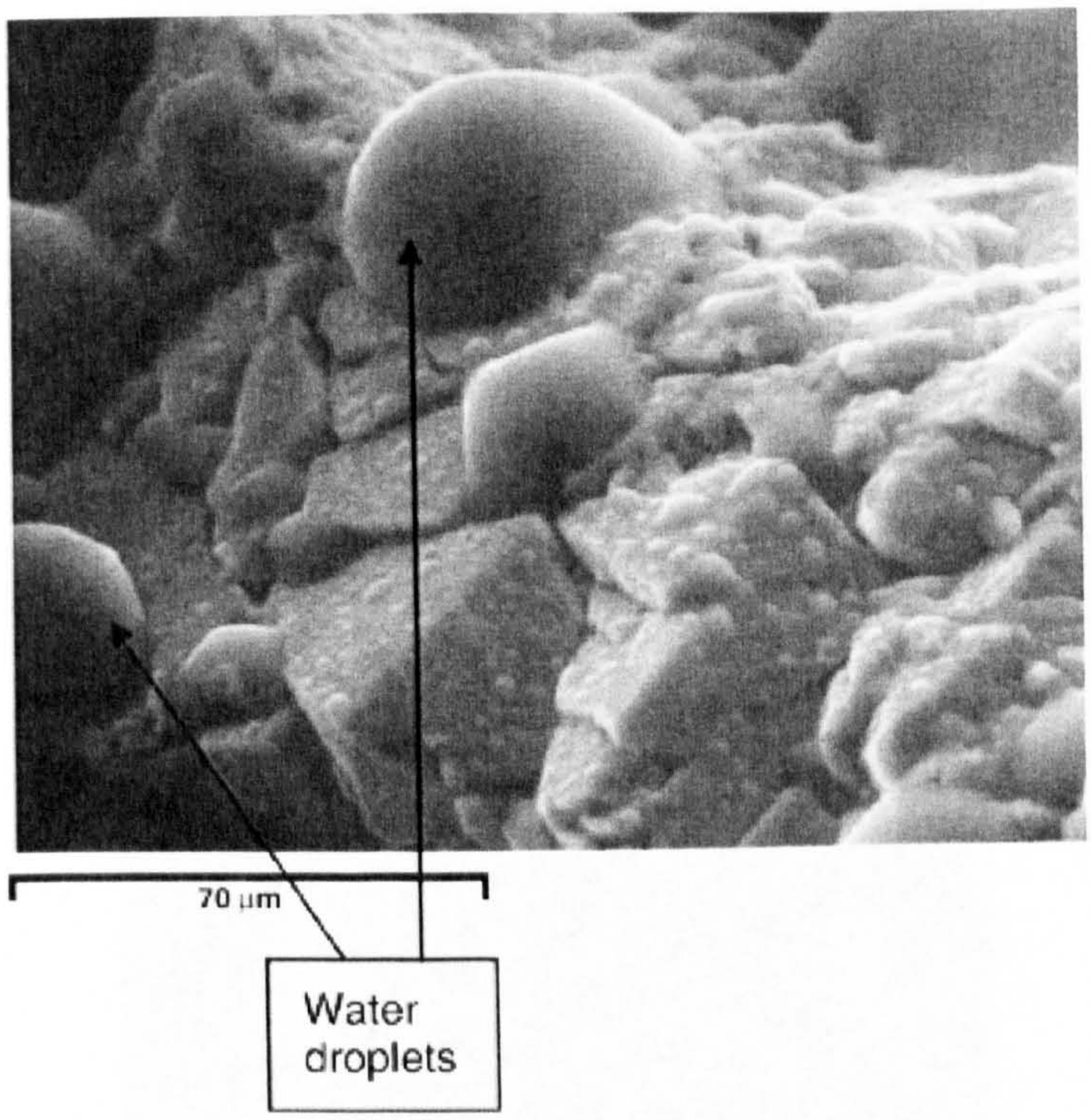

(c)

Figure 6.13: ESEM microphotographs in minerals, (a) muscovite (shows high affinity of water) (from Buckman et al., 2000), (b) calcite (from Buckman et al., 2000), (c) quartz (from Skauge et al., 2006)

As soils are composed of different minerals, variable contact angles can co-exist at a very small scale. Figure 6.14 shows the wetting of a sandstone with quartz and clay minerals in close proximity. Contact angles tend to be higher for the clay minerals than for quartz (Figure 6.14b). 'Mushroom' shaped menisci similar to those obtained in this research (Figure 6.2a and 6.2b) are visible in Figure 6.14a and 6.14c.

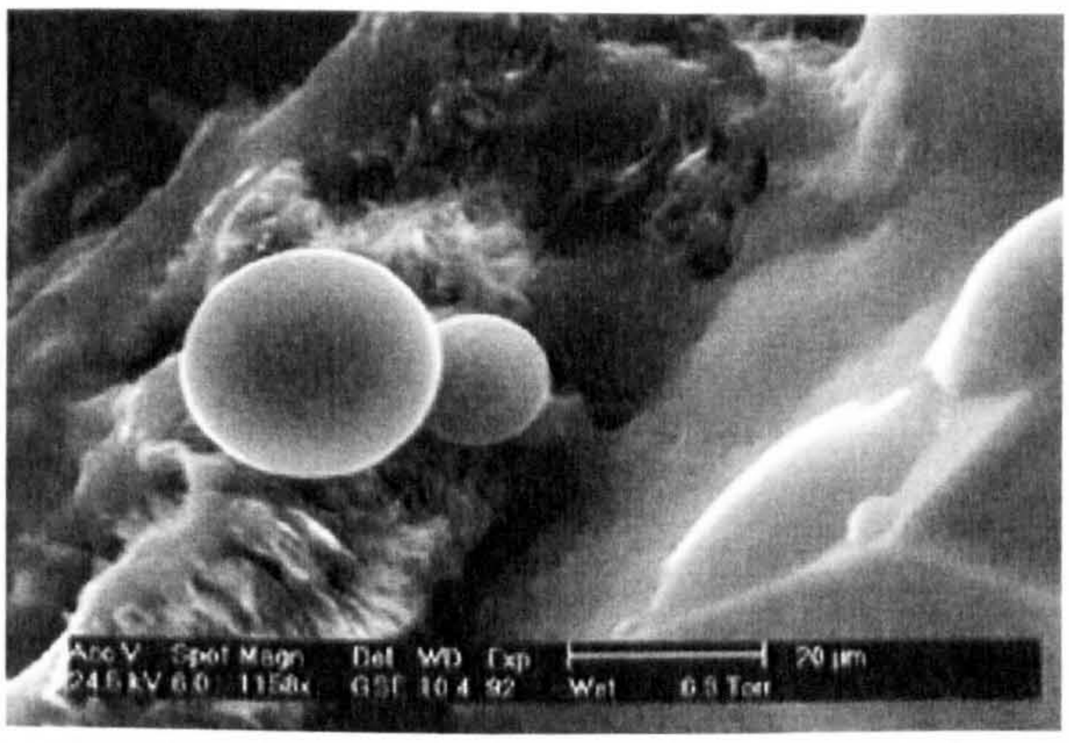

(a)

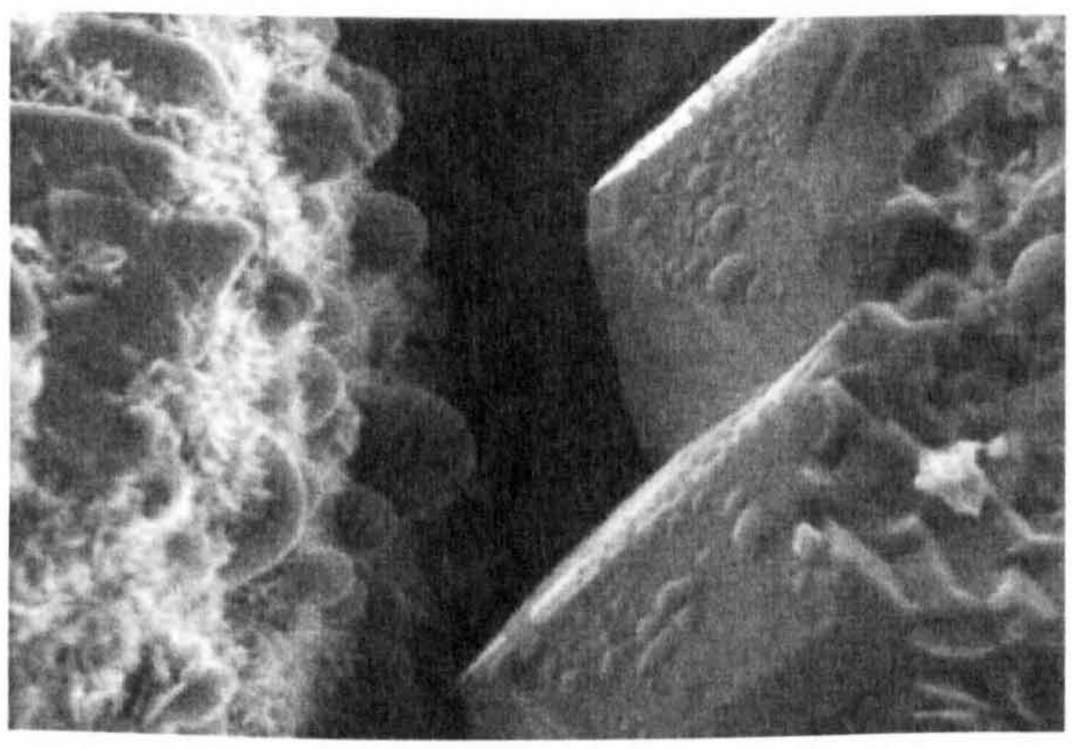

(b)

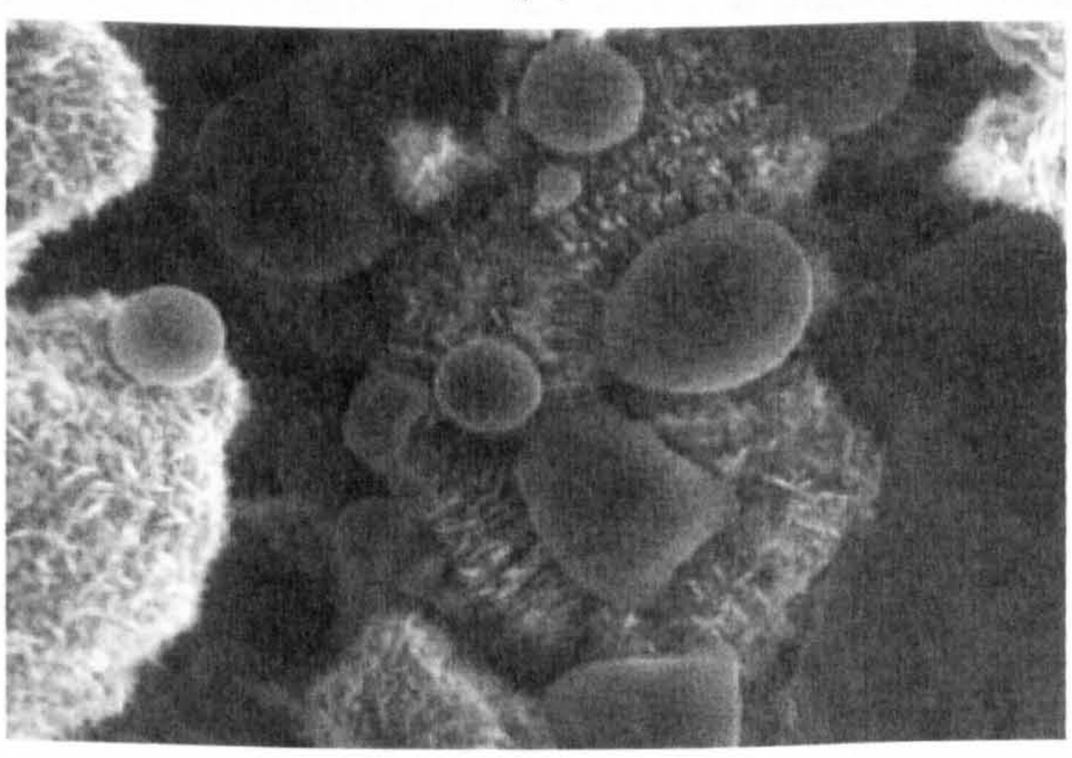

(c)

Figure 6.14: ESEM microphotographs in a sandstone, (a) contact angles in quartz (right) much lower than in kaolin (left), (b) curvature of the menisci different between the quartz (right) and illite (left), (c) water droplets in illite indicating an hydrophobic nature (source of images a, b, c: http://www.pet.hw.ac.uk/cesem/gall_mspet.htm, with permission of Dr Jim Buckman, Heriot-Watt University)

6.4.1.2. Contact angle influence in the mechanical behaviour

Variable contact angles are likely to affect the mechanical behaviour of unsaturated soils. Based on Fisher's (1926) formulation, Ravi et al. (2006) showed that the meniscus force decreases for increasing contact angles. Blanco-Canqui et al. (2005) measured a decreasing tensile strength of macroscopic soil aggregates with increasing organic carbon content. However, the data showed that the density of the aggregates changed as well, so it's difficult to conclude whether the decrease in tensile strength was due to change in the contact angle of soil or decrease in the aggregate density. Even so, the importance of the contact angle on the mechanical behaviour is particularly evident in the case of a soil partially saturated by a non-wettable fluid. In this case the extra cohesion provided by the meniscus force does not exist because the fluid does not adhere to the interparticle contacts or anywhere on the particles' surfaces.

Variable contact angles could affect the accuracy of Kelvin's law in soils. The validity of Kelvin's law, which relates the menisci curvature to an imposed RH in isothermal conditions, has already been discussed in the literature. Fisher and Israelachvili (1981) in condensation experiments of cyclohexane between mica surfaces conclude that it is valid in the range 4-20 nm. The authors also observed that impurities and deposition of solutes affected the accuracy. For the only study with water, Kohonen and Christenson (2000) also studied condensation between mica surfaces and concluded that the equilibrium meniscus curvatures agree with the Kelvin curvatures. The authors attribute this accuracy to the rising of the mica surfaces with dilute acid. In a discussion on the validity of Kelvin's law, Melrose (1989) argues that its validity is universal and that any deviation is related to lack of equilibrium conditions. However Israelachvili (1991) states that there is no evidence than the meniscus will not return to its original position even if waiting for long periods of time. In the case of water in soils, as particles are not clean (and because of all the factors discussed above), application of Kelvin's law to soils might not be straightforward. For instance, the use of saline solutions to impose suction might result in differently shaped menisci and therefore different menisci forces.

In unsaturated soil mechanics the contact angle has been included in theoretical studies by Likos and Lu (2004) and Molenkamp and Nazemi (2003). Molenkamp and Nazemi (2003) related the water volume and the interparticle contact force to suction, contact angle, and size and roughness of the spheres. The authors demonstrate that for a saddle-shaped air water interface (R_1 and R_2 from Laplace equation different at each point of the meniscus) suction depends on the contact angle. The roughness of their surfaces separates the spheres at the contact point creating a non-circular meniscus. Likus and Lu (2004), considered the effect of different contact angles on suction, calculated from the Laplace equation (for a meniscus surface with 1 single r_1 and r_2).

6.4.1.3. Contact angle influence on the hydraulic behaviour

Variable contact angles are likely to affect the hydraulic behaviour of unsaturated soils. Experimental work conducted by soil scientists shows this. In particular, the air-entry pressure is likely to be affected. Wang et al. (2000) demonstrated that the water-entry pressure (defined as the suction level at which water floods the pores) depends on the organic matter content. The authors measured an increase in the water-entry pressure with organic matter content. In similar studies Shirtcliffe et al. (2006) showed experimentally that a contact angle smaller than 50° is necessary for water to infiltrate in many soils.

In a recent paper, Shahidzadeh-Bonn et al. (2007) showed experimentally that the evaporation behaviour from saturated glass beads depends on the affinity of the beads to water. Figure 6.15a shows that the drying rate is much slower for the case of the hydrophobic coating, while for the hydrophilic beads it is linear with an inflection for lower rates when most of the water has evaporated. The saturation profiles of the beads with time are constant for the hydrophilic case (Figure 6.15b) and with a marked drying front moving downwards for the hydrophobic case (Figure 6.15c). The authors justify these results based on the drying pattern. For the case of the hydrophilic beads drying is homogeneous, i.e. once the air entry value is exceeded air penetrates in all the largest pores at once forming a network of linked pores from where water evaporates. For the case of the hydrophobic beads, Figure 6.15c shows that there is a clear drying front progressing downwards. The front separates saturated from dry pores.

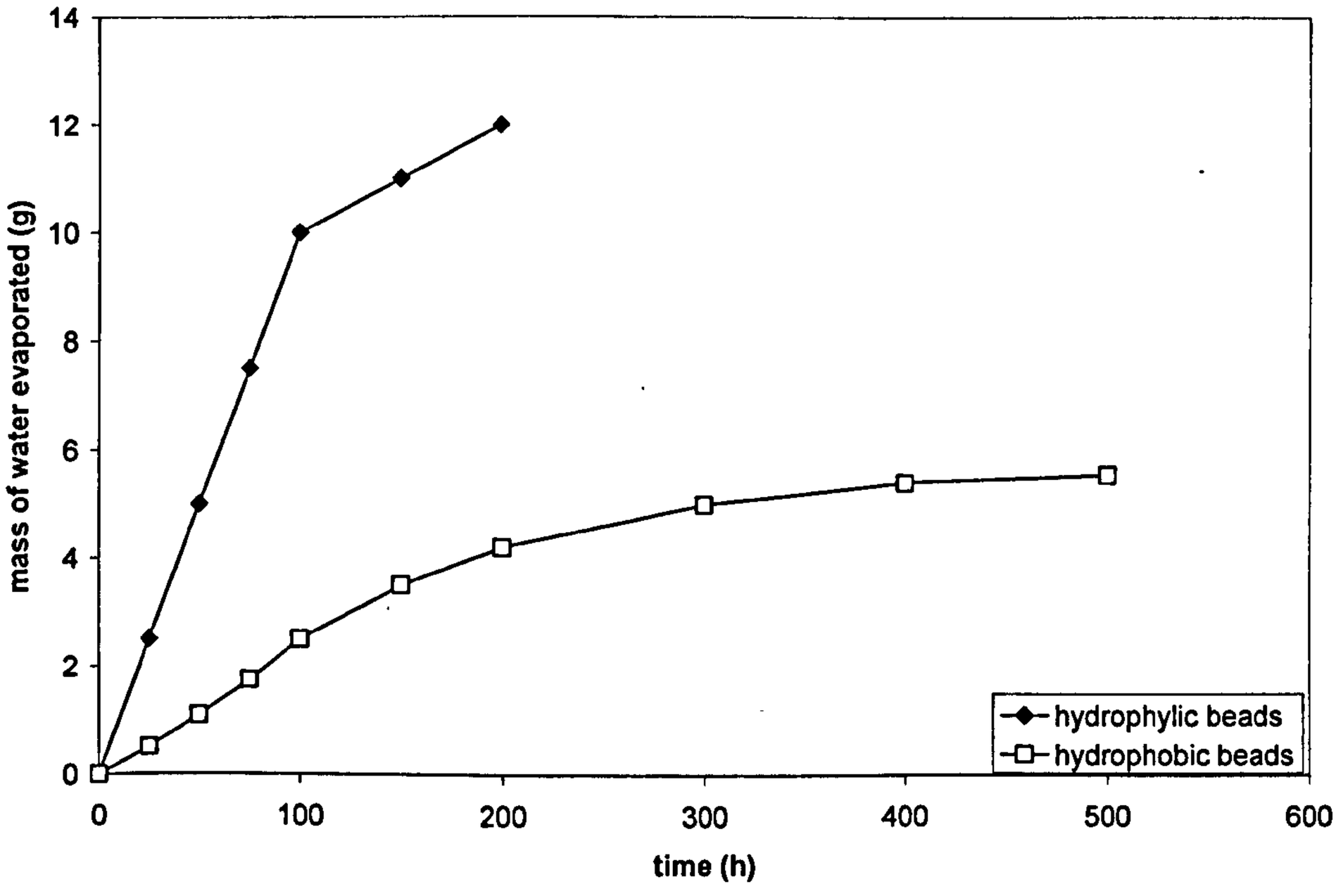

Figure 6.15: Influence of the contact angle of glass beads in evaporation (after Shahidzadeh-Bonn et al. 2007)

6.4.2. Hydraulic hysteresis

Besides the ink-bottle effect, the ESEM images have shown that other mechanisms might also contribute to hydraulic hysteresis. Variable contact angles should be taken into account due to their effects on suction (discussed above), but should be negligible in terms of volume water affected, i.e. the differential volume of water corresponding to a meniscus with either a concave or a convex shape should be much smaller than the volume water related to the emptying or flooding of pores.

This research adds a third type of hysteresis that agrees well with the standard shape of a wetting and drying curve, i.e. according to Figure 6.4 the wetting curve would be positioned below the drying curve in terms of RH versus water content. Weeks et al. (2005) reported a similar hysteretic response of menisci height growth and reduction between the tip of an AFM cantilever and a flat substrate (Figure 6.16), with the sample remaining wet for lower humidities (corresponds to Figure 6.1b). The first explanation for these and the author's results is that there is a time effect, i.e. there is a delay in the condensation and evaporation of water from the sample. However, Weeks et al. (2005) do not question the correctness of their measurements

because RH was changed in steps with sufficient time for meniscus growth or shrinkage; nevertheless no mechanism is presented to justify the results. It is therefore unclear whether the observed hysteresis in this research was equipment induced, or represents a new mechanism (this also applies to Weeks et al., 2005 results).

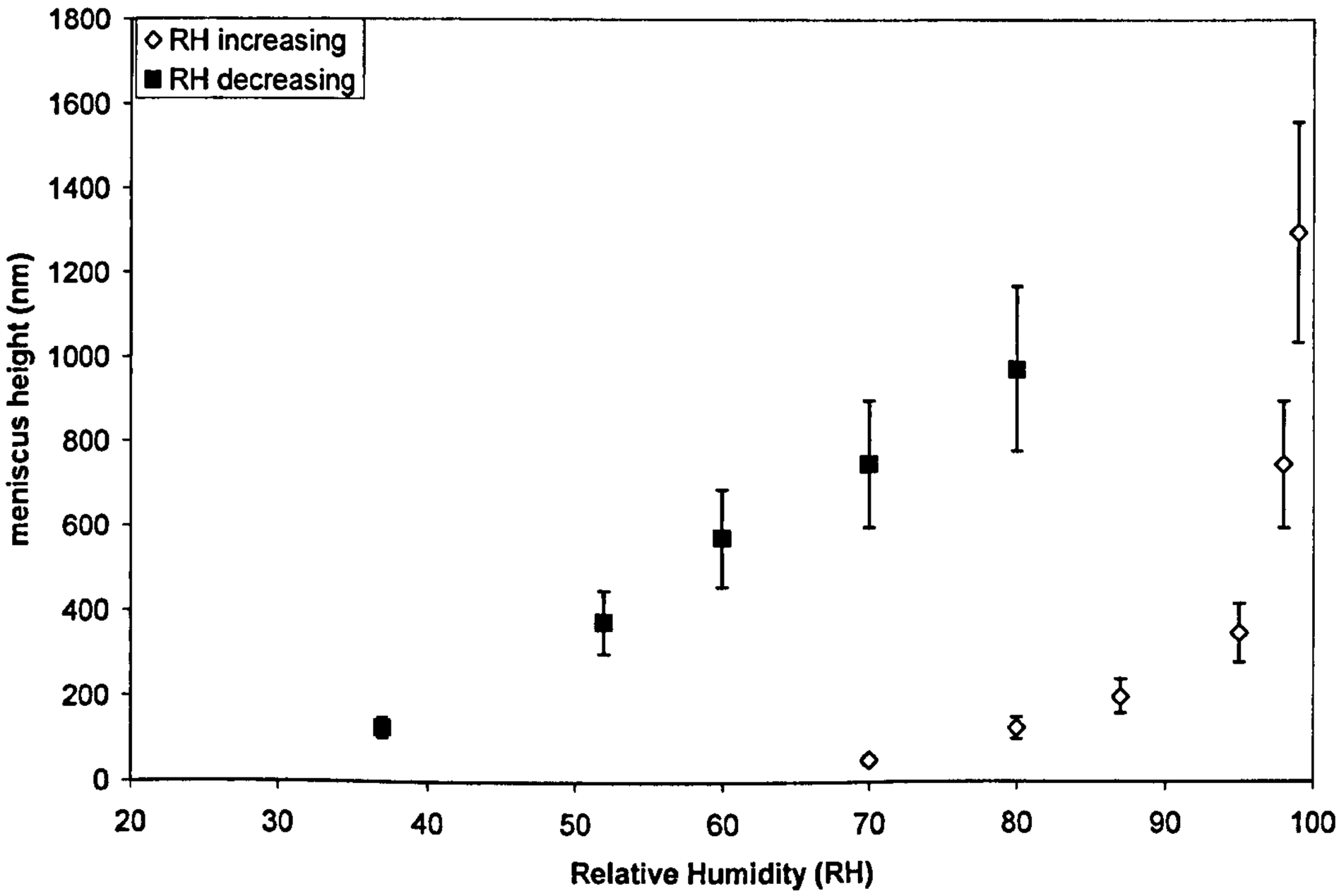

Figure 6.16: Meniscus height measurements during wetting and drying of the AFM cantilever tip of Figure 6.1b (after Weeks et al., 2005)

6.4.3. Fabric

Unsaturated soil behaviour is highly dependent on the fabric (e.g. Gasparre et al., 2007). Clays acquire their initial fabric during the genesis of the soil by sedimentation in a calm aqueous environment (Mitchell, 1993). The piling-up shown in Figure 6.6a to Figure 6.6b took place in a completely different condition, i.e. as water evaporated. To the author's knowledge this observation is new. Piling-up implies particles moving upward, therefore interparticle forces could have acted on the spheres attracting them together.

The fact that the spheres had between 2 and 3 contacts (Figure 6.5) suggests that it is unlikely that the meniscus force controlled the number of contacts. Water menisci form by condensation from vapour at the interparticle contacts, so the spheres had to

be in contact before the meniscus was formed. Therefore the initial fabric formation appears related to interparticle forces other than the meniscus force. It is also improbable that the particles cemented while in the water solution; the amine layer added should have avoided primary valence bonds between the particles.

The interparticle movements of Figure 6.7c could be related to the meniscus force. Lampenscherf et al. (2000) attributed the stress exerted by the spheres in the deformable substrate to the meniscus force. It was however unclear if the observed movements in Figure 6.7c contributed to a separation (equivalent to swelling) or gathering of the spheres (equivalent to shrinkage).

6.4.4. Observations in aggregates

As natural soils are rarely spherical and uniform, observations were also carried on clays. Dry Speswhite kaolin was placed in the ESEM chamber in dry conditions and subjected to an increase of Relative Humidity (RH) from 93% to 96% at a constant temperature of 5°C.

The sequence in Figure 6.17 shows an aggregate composed of clay platelets being enclosed in a water film as RH increased from 93% to 96%. In Figure 6.17c the clay platelets can still be seen through the water film. Note that both Figure 6.17b and 6.17c refer to the same imposed RH of 96%. The differences between these two images are therefore attributable to the fact that in Figure 6.17b equilibrium had not yet been achieved under the imposed RH value. The images are similar to the ones shown by Montes-H. et al. (2005) for bentonite aggregates. Concluding, for the case of aggregates all information obtained is essentially qualitative. Measurements of contact angles, for example, are not possible.

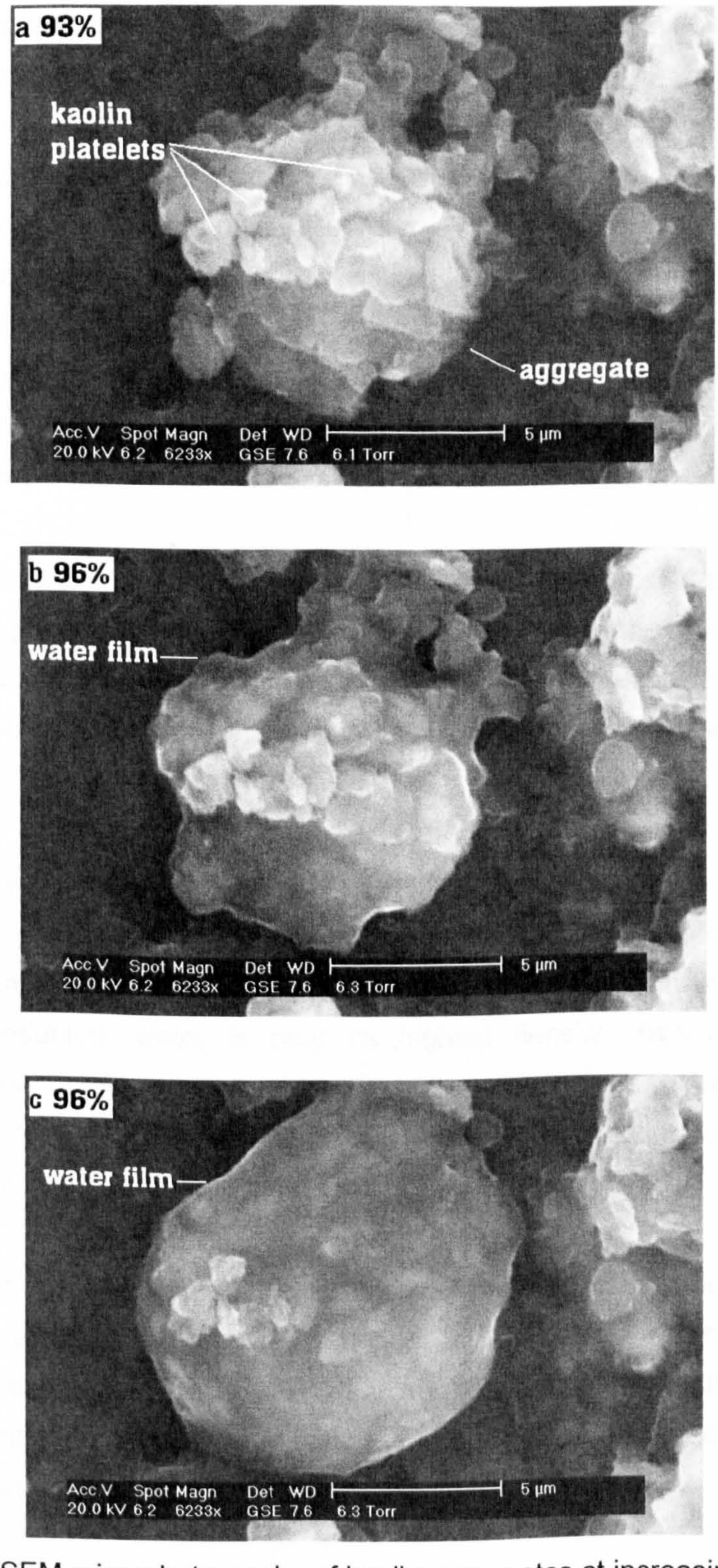

Figure 6.17: ESEM microphotographs of kaolin aggregates at increasing RH (test E4, kaolin) (1Torr = 0.133kPa)

6.5. FINAL CONSIDERATIONS ON THE SUITABILITY OF THE ESEM FOR UNSATURATED SOIL TESTING

- One of the main issues in ESEM imaging is the time required for thermodynamic equilibrium. Published results show varied times. For instance, Montes-H. et al. (2005) waited 10min for equilibrium conditions with bentonite aggregates 95µm large under a RH of 95%; Weeks and DeYoreo (2006) waited the same time for water to condense (under RH = 98%) at the tip of an atomic force microscope cantilever and a flat substrate (with the microscope tip width smaller than 1µm).

- Other factors might also affect the accuracy of the measurements of water vapour pressure and temperature in the ESEM chamber. Temperature, for instance, is imposed by the Peltier stage, which means that temperature gradients could develop in the material if the sample dimensions are relatively large.

- The need to test at low temperatures (to obtain a higher image definition) might be a disadvantage in some situations because water properties change with temperature. At 4°C, near the temperature at which most ESEM studies are conducted, water is near its highest density. This could influence cavitation or air entry. Some soils are also sensitive to temperature and testing at low temperatures could therefore change the response of the material.

- Another limitation is that the ESEM controls the water vapour pressure in 0.1torr steps (at least in the FEI XL-30 models), which for RH>90% corresponds about to 1.5% RH changes. These steps are rather coarse and evaporation or condensation can therefore occur too fast leading to a loss of important information during the wetting/drying process.

- As presented in Chapter 2, mechanical testing is also possible with the ESEM. But with only one study conducted by Stokes and Donald (2000) more testing in different conditions and with different materials are necessary to validate the technique.

6.6. MEASUREMENT OF THE MENISCUS FORCE BY ATOMIC FORCE MICROSCOPY

Meniscus forces at the micron or nano scale have been measured by Atomic Force Microscopy (AFM) (Eastman and Zhu, 1996, Xiao and Qian, 2000, Ouyang et al., 2001, Zitler et al., 2002, Butt et al., 2006, Grobelny et al., 2006). The AFM is an imaging device that is based on the interaction of a nano-sized tip attached to a cantilever and a sample. The cantilever tip (which is attached to a spring) moves along the substrate producing an image. The interaction of the tip with the substrate is also affected by the type of substrate and environment. These side effects are due to attractive forces that develop between the tip and the substrate: van der Walls, electrostatic forces, or meniscus forces when imaging is done in the presence of air.

The force measurement can be done by moving the sample up and down while measuring the cantilever deflection. Due to the attractive forces, the cantilever sticks to the sample while deflecting and then as the spring force overcomes the attractive force the tip releases from the surface and returns to the initial position (Figure 6.18). The cantilever deflection multiplied by the spring constant gives the attractive force, or if it is the case, the meniscus force (Butt et al., 2006, Ouyang et al., 2001).

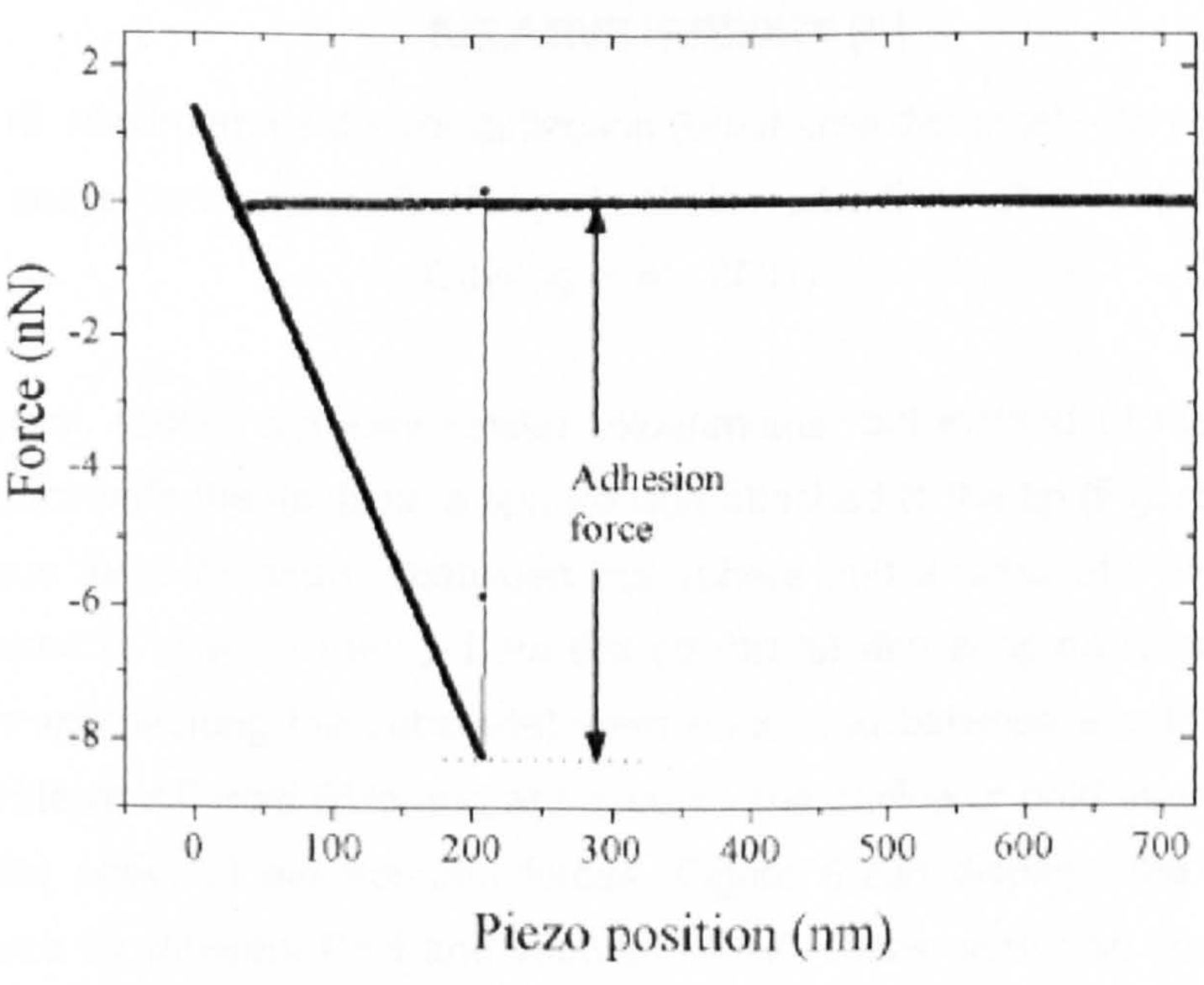

Figure 6.18: Force-piezo position curve measured on mica with an AFM tip at RH 40% (from Butt et al., 2006)

Following the above procedure, the meniscus force can be measured directly between the tip and a substrate at different RHs. Such measurements were made by Ouyang et al. (2001) between three different tips (gold-coated tips, bare Si_3N_4 tips, paraffin-coated tips) and a substrate. Figure 6.19 displays the maximum cantilever deflection (break-free distance) for different RHs. It can clearly be seen that the gold coated tips have the highest deflection and consequently the highest meniscus force.

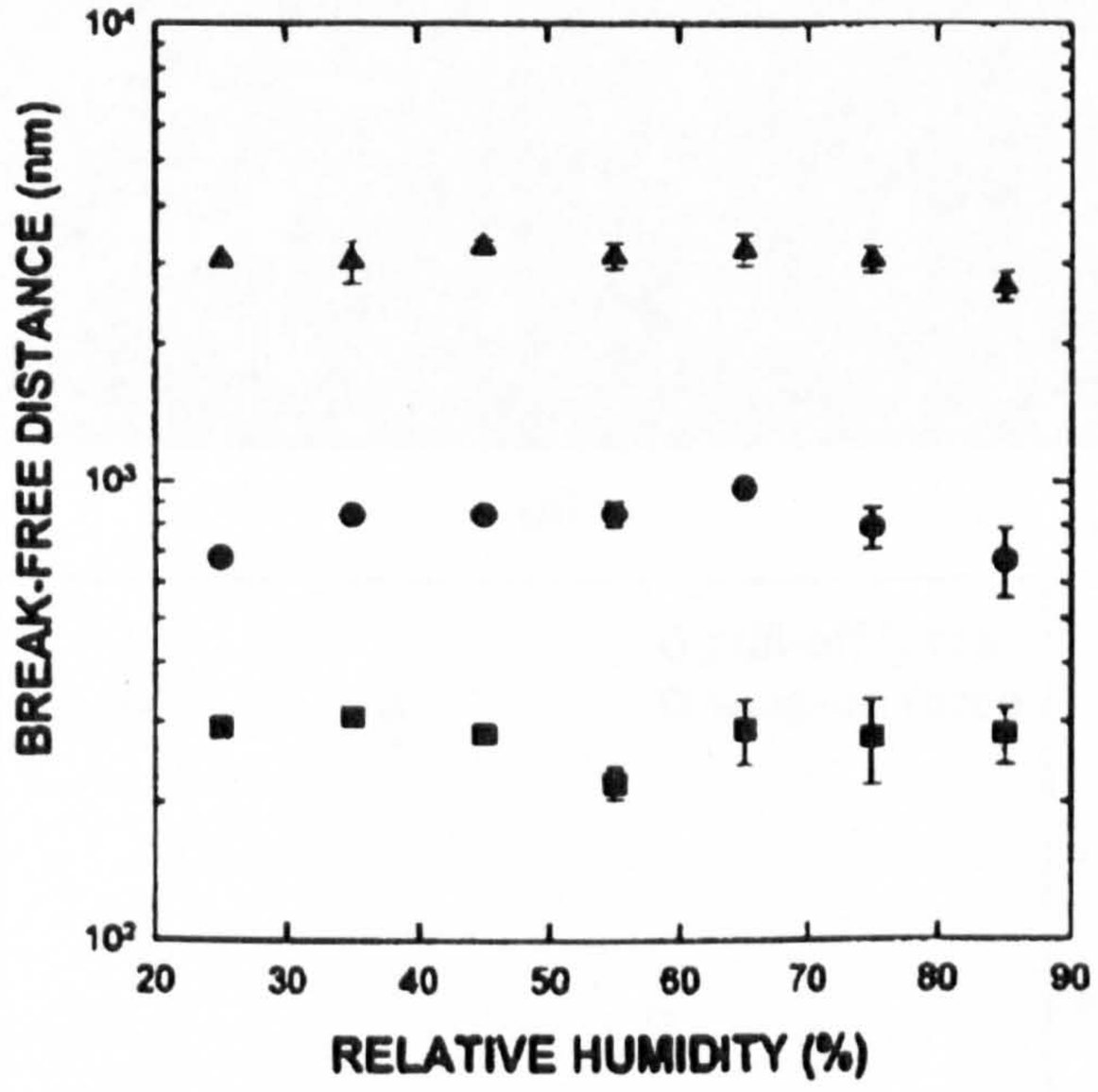

Figure 6.19: Maximum cantilever deflection (break-free distance) – RH for different tips (gold coated in triangles, Si_3N_4 tips in circles, paraffin-coated in squares) (from Ouyang et al., 2001)

Grobelny et al. (2006) did very similar experiments, but instead of measuring the meniscus force with the tip itself, a sphere was attached to the tip (Figure 6.20a) and the meniscus force measured between the sphere and a substrate. Pull-up forces (force required to release the tip from the substrate) and snap-on forces (touching force when approaching the substrate) were measured between a gold sphere and gold substrate at different RHs and at vacuum. The choice of gold materials was to minimize the effect of electrostatic forces. Figure 6.20b displays the pull-up and snap-on force for different RHs and vacuum (UHV). Tests were also conducted in a separate device developed by the authors (adhesion tester). The results show the snap-on force constant and, unexpectedly, the pull–up force decreasing for decreasing RHs. At vacuum (UHV) the pull-up force is equal to the snap-on force, which is expected because no meniscus should be formed.

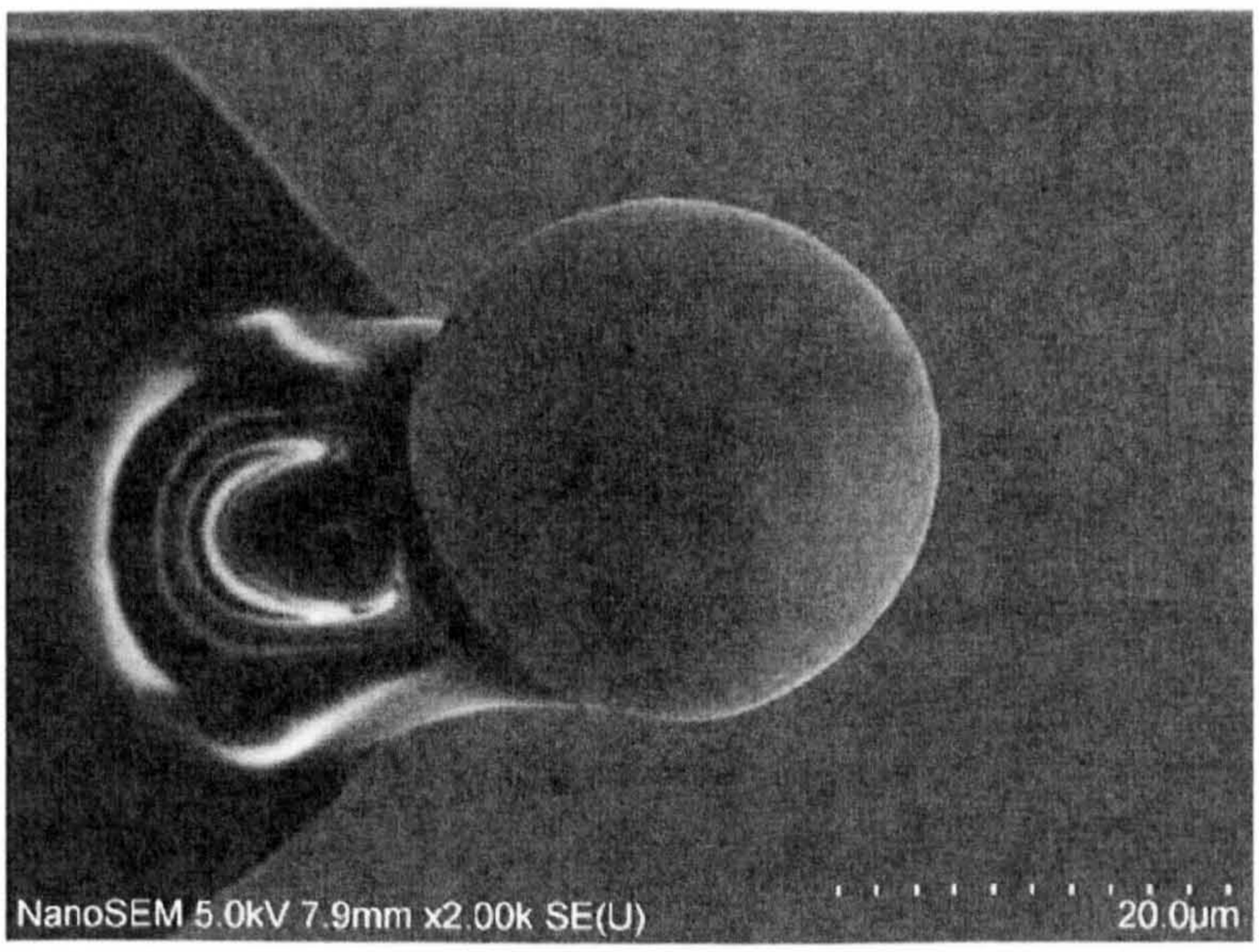

(a)

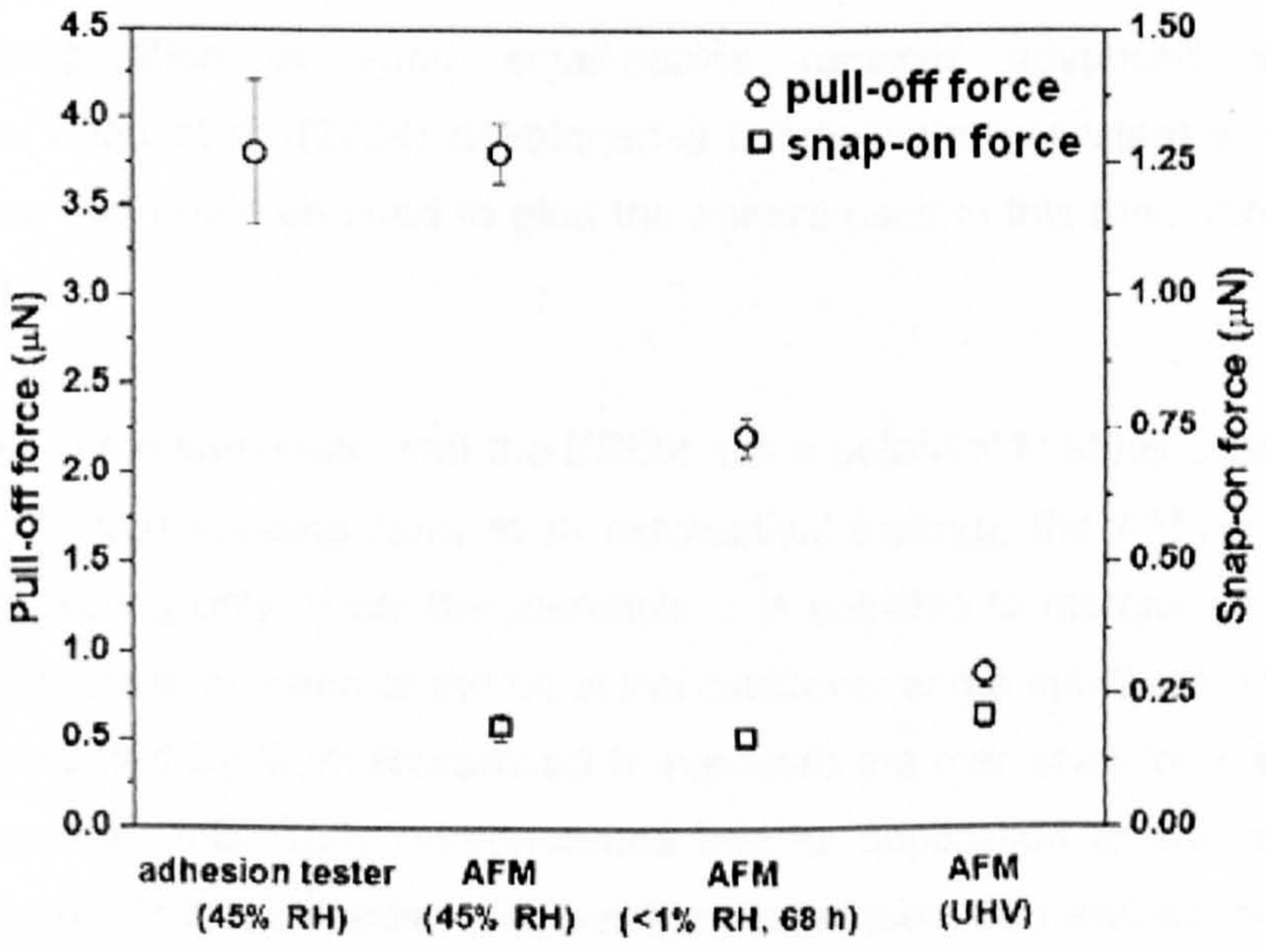

(b)

Figure 6.20: (a) ESEM microphotograph of a gold sphere attached to the end of an AFM cantilever with glue, (b) forces measured at different humidities (snap-on forces are in squares and pull-off forces in circles) (from Grobelny et al., 2006)

Following the work of Grobelny et al. (2006) and using the AFM to measure the meniscus force, it was the author's intention to measure the meniscus force between the silica spheres used for this research. The plan was to glue one sphere to the cantilever tip and measure the meniscus force against another sphere (Figure 6.21a). By using the AFM facilities of the School of Engineering (Durham University), Mark Rosamond (Electronics Group) made several attempts to glue one sphere to the cantilever tip. The many trials conducted by Mark were however unsuccessful because the spheres were mixing and sinking in the glue. Due to this difficulty the testing program was interrupted. Figure 6.21b shows one example where one silica sphere seems to be attached to the cantilever (without glue). The image was taken with an SEM so there should be no water condensing and therefore no meniscus force.

Sample preparation at such small-scales requires advanced manipulation techniques. Zhou et al. (2004) developed a microassembly system with controlled environment that could be used to glue the sphere used in this research against the cantilever tip.

Concluding, in the same way that the ESEM has a potential to study unsaturated soil behaviour through imaging (and even mechanical testing), the AFM is oriented to mechanical testing only. From the literature, it is possible to measure the meniscus force through the interaction of the tip of the cantilever and a substrate. However, the attempt conducted by Mark Rosamond to measure the meniscus force between the spheres used for this study demonstrates that its application to soil might not be straightforward. At least, special manipulation techniques are required for the sample preparation.

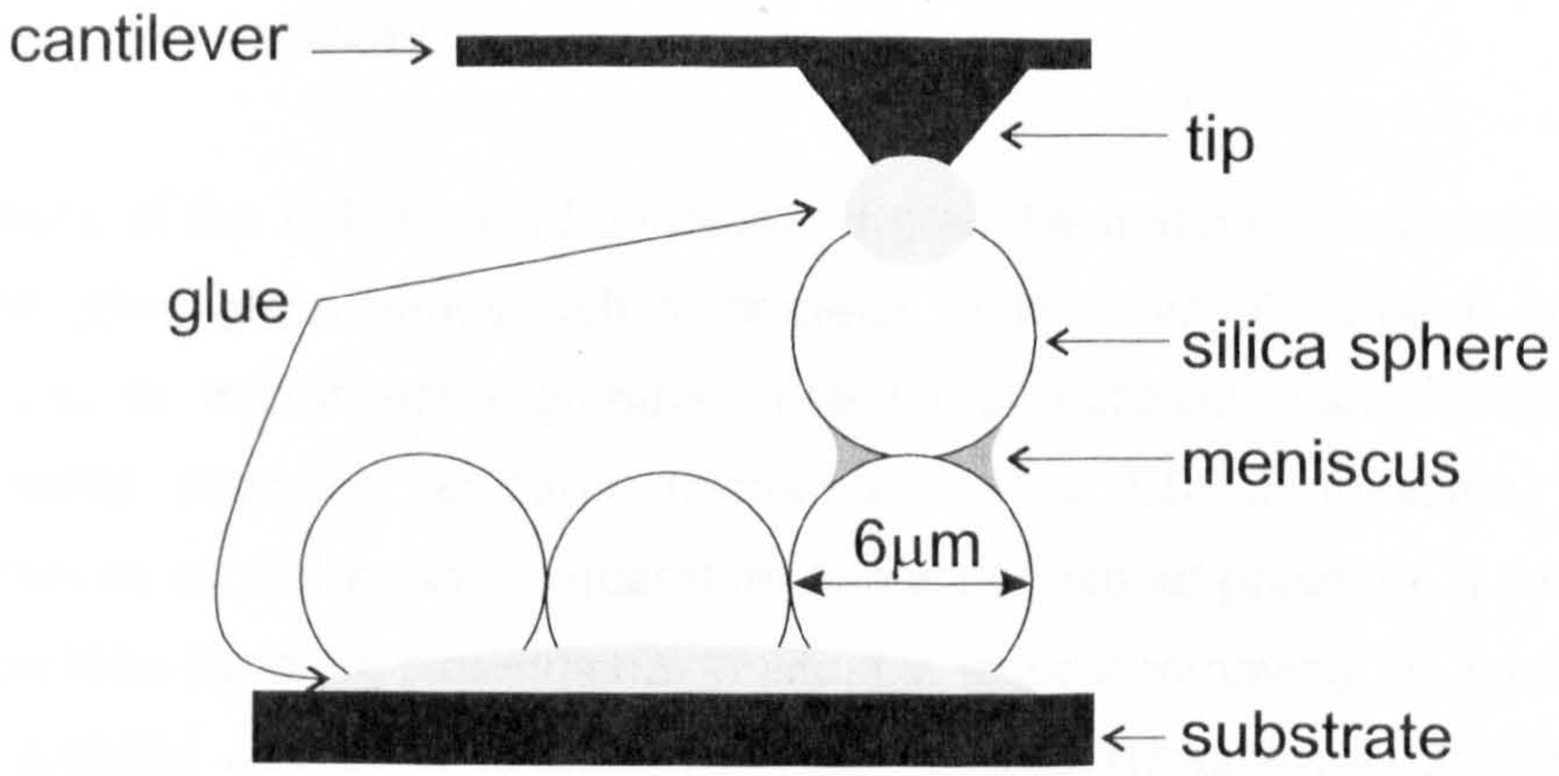

(a)

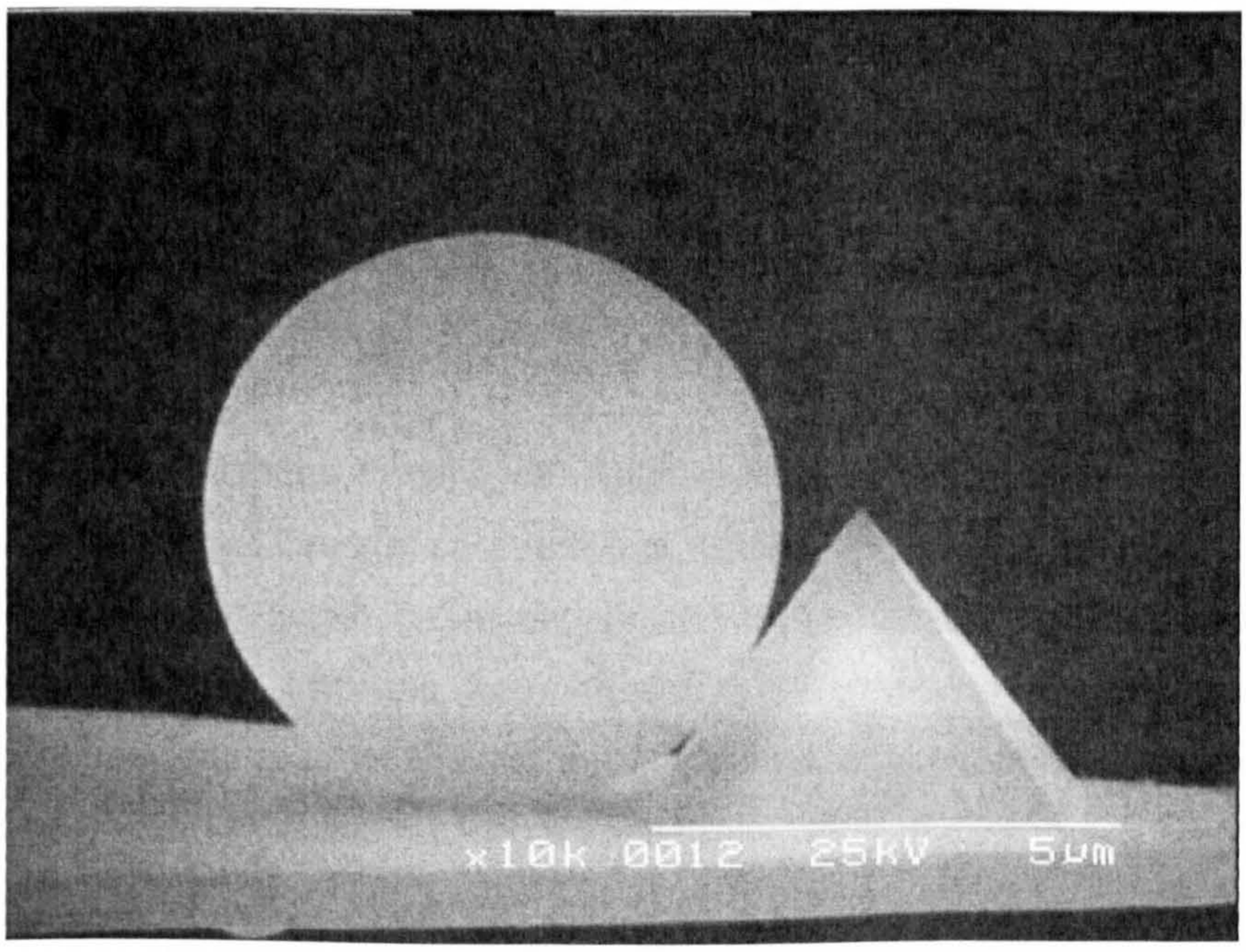

(b)

Figure 6.21: (a) Planned arrangement to measure the meniscus force between the silica spheres, (b) SEM microphotograph with a silica sphere in contact with the AFM cantilever (base of the tip is 5μm long) (test AFM1, silica spheres) (photo: Mark Rosamond)

6.7. CHAPTER SUMMARY

Observations of the behaviour of unsaturated granular materials have usually been conducted using glass beads with a diameter of few mm. Chapter 6 concerned observations in micron-sized granular material at different water conditions by Environmental scanning electron microscopy. The ESEM imposes the wet environment by controlling the temperature and water vapour pressure. It can also be used to perform dynamic experiments in situ, i.e. without removing the sample. This unique capability was used to observe water menisci dynamics in 2μm and 6μm spheres in situ. Testing was conducted by cycling the RH with the spheres loosely and densely packed. The size of the spheres was relevant to unsaturated soils (average clay particle size) but not the shape (spherical instead of platy). Even so, the use of an ideal material simplified observations and allowed the study of water menisci at the interparticle contacts. At the end, observations were also conducted in kaolin.

Contact angles were found to vary with Relative Humidity (RH) cycles. One example shows convex menisci developing in the first wetting followed by concave menisci in the second wetting. A literature review showed that several factors could affect the contact angles in soils, from the material itself to the presence of organic matter. At high RH, menisci increased in size forming dome shapes until collapse or until coalescing with other menisci forming a continuous water phase.

At the end of the testing period, an attempt was conducted to measure the meniscus forces between the spheres by Atomic Force Microscopy. The trials were unsuccessful due to the difficulty in the sample preparation at the micron-scale.

The ESEM has proven a very useful tool to study microscale phenomena in wet granular material with some quantification being possible. It allowed new observations relevant to unsaturated soil mechanics. The abundance of ESEM papers in other fields could be an important source of knowledge to unsaturated soils and could also help to validate observations carried with the ESEM in unsaturated soils.

Chapter 7. CONCLUSIONS AND SUGGESTIONS FOR FURTHER WORK

7.1. DIRECT TESTING OF UNSATURATED SOILS

This thesis describes a testing approach for unsaturated soils where all measurements and techniques read values and control devices directly, with the soil in the same conditions as in nature (i.e. not subject to an elevated air pressure). This is different to commonly available techniques which use intermediary values or devices, or that create unnatural conditions. For instance, relative humidity (RH) equilibrium techniques read an intermediary value that is then related to suction or water content (e.g. a hygrometer reads RH that is then converted to total suction), while the axis translation measures or controls suction by raising the air pressures. The approach, called here 'direct testing of unsaturated soils', relies on the measurement of suction with high suction tensiometers and water content through mass measurements with a balance. With these two devices, techniques were developed to control suction and water content in confined and unconfined conditions. The original contributions of this thesis are detailed next.

7.1.1. Performance of high suction tensiometers

High suction tensiometers are small probes that measure directly the tensile stress in the water present in the soil. The performance of a new high suction tensiometer in terms of saturation, calibration and measurement was evaluated.

1. The Durham University – Wykeham Farrance tensiometer was shown to be capable of sustaining -2 MPa before cavitating.

2. It is demonstrated that the maximum suction that a tensiometer can sustain increases with time and is temperature dependent. It is argued that the time

effect is related to clogging of the stone. The longer time required to saturate tensiometers from dry when they have been used for a long period of time suggested that the porosity of the stone decreases. In this case the pore size would decrease and the air entry pressure increase. Cavitation tests at low temperature also suggest that suction at cavitation can be increased by decreasing to temperatures near 5°C (the temperature at which water is denser). It is also shown that extremely high pressure is not required to saturate the tensiometers, pressurizations up to 1.5MPa were sufficient to reach similar values of suction. Finally, it was observed that the tensiometer records increasing pressures when plunged dry in free water. This provides some clues to the saturation process of the stone, in this case it reveals the porous nature of the stone where water is sucked by capillarity squeezing the trapped air and delaying saturation.

3. From a literature review, it is highlighted that the key element controlling cavitation or the formation of a large bubble is the availability of space for a bubble to grow. Bubbles can grow from anywhere, either within the porous stone or reservoir, but the reservoir is the only place where they can coalesce with others until forming an air discontinuity in the water. Also, a conceptual model for cavitation in high suction tensiometers is presented. It is based on Take (2003) and Jones et al. (1999) and starts with the air being trapped in a crevice until its release.

4. Since high levels of saturation are required for such testing, it is proposed that dissolved oxygen meters could be used as a device to measure the amount of air in water. They are widely used for environmental applications. Several laboratory applications require de-aired water (tensiometer saturation or saturation of soil samples).

5. It is shown that the tensiometer body is sensitive to the way the tensiometer is fixed, i.e. to the external forces holding the device in place. The immediate implication is that the calibration should be conducted under the same external force regime as will be applied to the body of the tensiometer when it is to be used.

6. Techniques to validate the extrapolation of the calibration of high suction tensiometers from the positive to the negative pressure range have shown

that isotropic unloading is the most accurate technique. Axis translation was also used but was seen to be affected by factors related to the technique itself, i.e. tensiometer readings were highly dependent on the water conditions in the stone or below the stone. However, it is dependent on the success in isolating the sample from the water system. It is also shown that the long term use of tensiometers changes the calibration. Therefore, frequent checks of the extrapolation from the positive to the negative are required. Finally, it is suggested that differences between tensiometer types could lead to different results to those observed for the particular tensiometer used in this study, so it is suggested at least one check on the validity of the extrapolated calibration equation should always be done.

7. It is shown that the correctness of the measurements depends not only on the quality of the contact soil-stone, but also on the response time of the tensiometer. The tensiometer was seen to have a variable response time (between 8 and 160 minutes) that did not seem to depend on the water pressure level. The suction measurements conducted in this research also showed that the response time does not necessarily coincide with the time for the sample to reach equalization. This should be taken into consideration when testing samples that are under changing suction (e.g. triaxial tests).

7.1.2. Applications of high suction tensiometers

Techniques to control suction and water content, for unconfined and confined conditions, were developed. The control system required a means of changing suction or water content. The technique for unconfined conditions was specifically developed for the determination of the Soil Water Retention Curve (SWRC). The technique for confined conditions was developed for situations where the soil is enclosed (triaxial cell, oedometer).

1. It is demonstrated that the SWRC can be obtained with high suction tensiometers either by drying continuously to the atmosphere or by drying/wetting in discrete stages. SWRCs by continuous drying were initially obtained by placing the sample in a balance and left to dry. However, the cable was seen to have a considerable influence in the mass measurements. Therefore, a new procedure was proposed where suction and water content where measured separately from 2 identical samples placed next to each

other. For discrete drying/wetting the sample was left to dry or wet and then enclosed for the suction measurement to ensure suction equalisation throughout the sample. The discrete and continuous SWRCs gave similar curves to pressure plate testing, although not identical. However, as the continuous SWRCs were seen to be dependent on a series of factors (e.g., surface area), the discrete procedure should be the better for obtaining the SWRC.

2. Care is needed when measurements are made within an enclosing box. In the presence of large air gaps between the sample and the walls of the box, water evaporating from the sample condenses on the walls and drips back into the sample, which can affect readings.

3. New developments to a tensiometer based suction control system are presented, extending work by Cunningham (2000) and Jotisankasa (2005). The biggest advance was in developing a water content measurement and control system. The sample is wetted by directly injecting water and dried by circulating air through a desiccant (silica gel) within a closed-loop system. Water content measurement is based on the difference between the water injected and adsorbed by the silica gel. The system is able to dry and wet to a required suction, however wetting was not as easily controlled as drying, it tended to overshoot the set values. Further testing is required concerning the accuracy of the water content measurement. The system was used with a double cell triaxial set-up, but could also be adapted for use with oedometers or other devices to test soil. It can be used to perform tests following drying and/or wetting paths. It should also be possible to run suction or water content controlled tests. The developments have identified new problems in unsaturated soil testing, such as the difficulty in imposing appropriate air-tight conditions.

7.1.3. Particle level observations

A distinguishing feature of this research has been the observation of water menisci at the micron-scale by Environmental Scanning Electron Microscopy. It is demonstrated that Environment Scanning Electron Microscopy has applications to unsaturated soils that go beyond fabric studies. Careful analysis of the images revealed a series of phenomena only known from the literature in other fields or apparently unreported at

all. These observations provided evidence at the micron-scale of phenomena previously observed at a scale 1000x bigger.

1. The sphere-water-air interfaces were clearly visible enabling the measurement of contact angles and radiuses and relating them to the imposed RH. The menisci evolution was easily tracked with the pendular, funicular and capillary regimes easily identified.

2. Sphere movements suggested the presence of a meniscus force acting between the particles. It was also possible to identify and measure particle movements while RH changed.

3. The findings indicate that concave and convex menisci can co-exist at the same RH, and the contact angles were seen to change with the wetting-drying cycles.

4. The images demystify a common belief that suction in very fine materials (clays) is mostly controlled by chemical related aspects. It is shown that water condenses in micro sized material with clearly defined menisci and so, meniscus force should still play an important role in the behaviour of very fine materials.

7.2. FURTHER WORK

7.2.1. Advanced laboratory testing

High suction tensiometers

The review in Chapter 2 has shown that tensiometers have been used in different applications, from laboratories studies (e.g. oedometer, triaxial, SWRC) to field measurements. No other technique in unsaturated soil testing matches this versatility. However, even if they measure suctions that could reach 2.5MPa, testing in the geotechnical literature has been limited to lower suctions (up to 1MPa). Further work to improve the tensiometer behaviour at high suctions (or increase suction at cavitation) could include:

- Use of different materials and better control of the porous stone characteristics. Sjoblom (2000) demonstrated that changing the porous stone from the Soil Moisture Corporation to a different material made in Kochi University led to a jump in the measured suction values. Also a better control of the pore size is required. The pore sizes in Table 3.1 are in the order of 0.15μm while in Figure 3.5 they appear to be variable and bigger than that (1-2μm).

- Placing a flexible membrane in the reservoir. Guan (1996) showed that placing a flexible membrane in the reservoir decrease the space for bubbles to grow and led to an increase in the suction at cavitation.

- Improving the affinity of all the internal faces with water could also avoid trapping air and avoid premature cavitation.

- The nature of the hysteresis in the negative range should be understood and quantified in order to obtain accurate measurements, as would understanding the time effect on suction.

Water retention curves

The literature review in Chapter 2 showed that most published wetting SWRCs are, at least in part, scanning curves. In order to obtain primary wetting curves the soil must be dried completely. Obtaining complete SWRCs could show the different regimes of wetting and drying of soils. However, it could be challenging because it requires accurate measurements of suction at very low water contents.

The techniques and knowledge of SWRC in unsaturated soil mechanics could be of interest to environmental science. The retention of contaminants in soils could be done and studied with techniques or principles familiar to unsaturated soil testing. For instance, Cui et al. (2003) studied the retention of oil in a silt by using a multiphase cell to control the oil, water and air pressure (a similar principle as the axis translation technique).

Water content measurement and control

Previously, laboratory testing of unsaturated soils has been focused on suction measurement, with not much attention given to water content. One reason for this is that tests are often run in constant water content conditions (e.g. triaxial tests), or in such a way that the sample can be removed for weighing (e.g. pressure plate). However, continuous measurement with the water content changing is restrained to the work presented in this thesis and the TDR technique. Therefore, the problems found in Chapter 4 and 5 suggest that further work is needed to develop a water content measurement and control system to be employed in confined and unconfined conditions.

Hybrid suction control systems

Depending on the climate and geographical location, soils switch between an unsaturated and saturated state. The system presented in Chapter 5 can only be used in an unsaturated condition. It could be of interest to develop a hybrid system that once reaching a zero suction condition, it could switch to allow positive water pressures to be applied. The tensiometer would fit very well into such system because of its ability to measure positive and negative pressures.

True undrained tests

In the same way that the axis translation imposes unreal conditions by raising the air pressure in unsaturated soils, backpressure is also applied to a saturated soil to avoid cavitation. The undrained unloading tests in Chapter 3 have shown that it is possible to impose and measure negative water pressures well bellow -100kPa in saturated soils. Therefore, triaxial undrained tests could also be run to study the behaviour of dilative soils under true undrained conditions to study the effects of cavitation on the soil behaviour.

Constant shear stress drained tests in unsaturated soil samples

The system developed in Chapter 5 allows wetting/drying under controlled suction with continuous measurements of water content. Applications include the effects of cycles of wetting/drying on the shrinkage/swell of soils (as was the intention early in the research) but also to study shear strength aspects.

One interesting topic is to study the initiation of rainfall-induced landlsides by constant shear stress drained tests (CSD) in unsaturated samples. These tests have been considered the closest to mimic rainfall-induced landslides. The tests have been done but only for saturated samples (e.g. Anderson and Sitar, 1995). Samples are anisotropically consolidated and sheared by wetting. As the material is wetted the stress path moves left towards the failure envelope leading to instability (Figure 7.1).

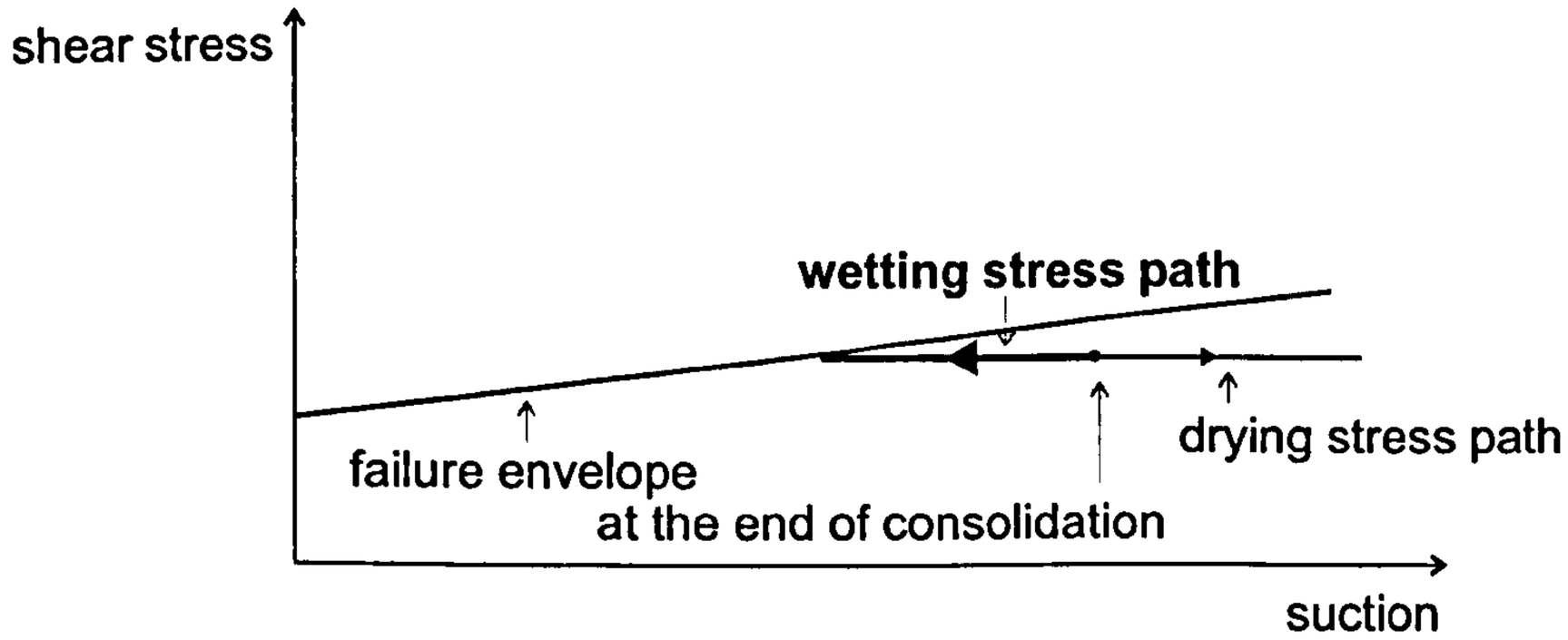

Figure 7.1: Stress paths for constant shear stress drained tests in unsaturated soil samples

7.2.2. Unsaturated soil micromechanics

Chapter 6 provided an insight into aspects of unsaturated soil mechanics at a scale ranging between 1-10μm. For the case of very fine soils, this is the scale at which the phenomena controlling soil behaviour occurs. Meniscus forces at the interparticle or interaggregate contacts, pore emptying/filling, contact angles variations in the clay particles or in the aggregates are likely to take place at a scale not exceeding the micron-level. Unsaturated soil behaviour is therefore controlled at a scale much smaller than, for instance, the standard size samples for triaxial or oedometer tests. The NAS (2006) in a recent policy publication, identifies nanotechnology as a having a potential for the future of geological and geotechnical engineering from medium to low and for microelectromechanical systems (MEMS) and microsensors from medium to high (Figure 7.2a). Unsaturated soil micromechanics would strongly benefit from developments in these two fields. Figure 7.2b shows the different scales between the phenomena happening in the soil and the required technology (current techniques appear completely out of scale).

Nanotechnology

There is available nanotechnology that could be adapted to unsaturated soil testing. ESEM and Atomic Force Microscopy (AFM) are the most obvious devices, but there are others that could be used to study specific aspects. For the case of force measurements, Claesson et al. (1996) reviewed a series of techniques. Among them there is Surface Force Apparatus (SFA) and Total Internal Reflection Microscopy (TIRM). SFA could be particularly useful, it was used by Fisher and Israelachvili (1981) and Kohonen and Christenson (2000) for the validation studies of Kelvin's law (discussed in Chapter 6). However, testing at these scales could also require developing specific technology and appropriate manipulation techniques (Zhou et al., 2004) (also discussed in Chapter 6).

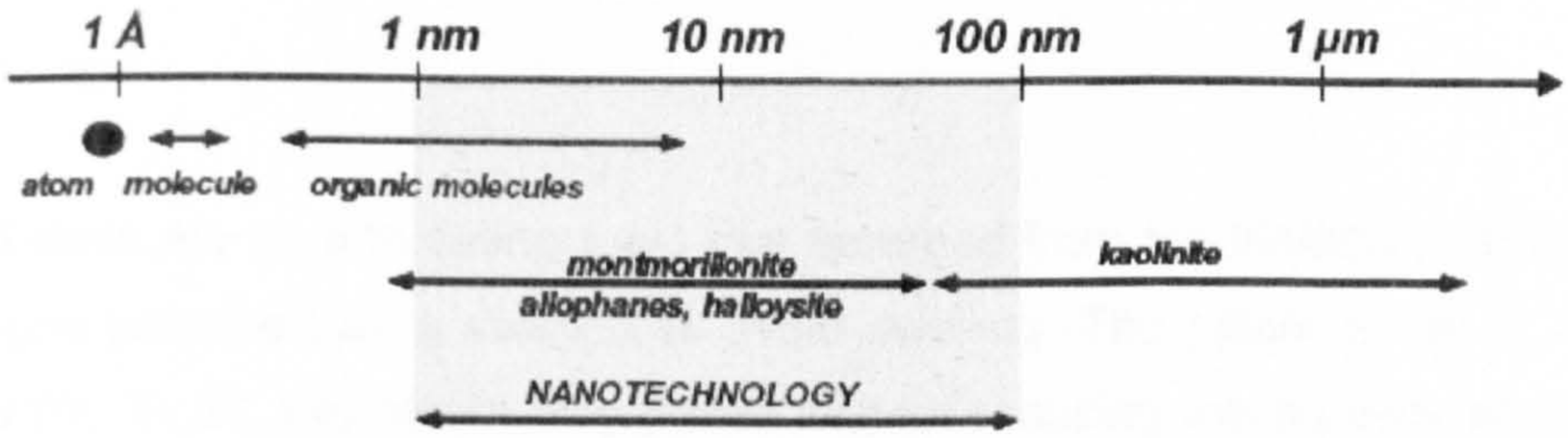

(a)

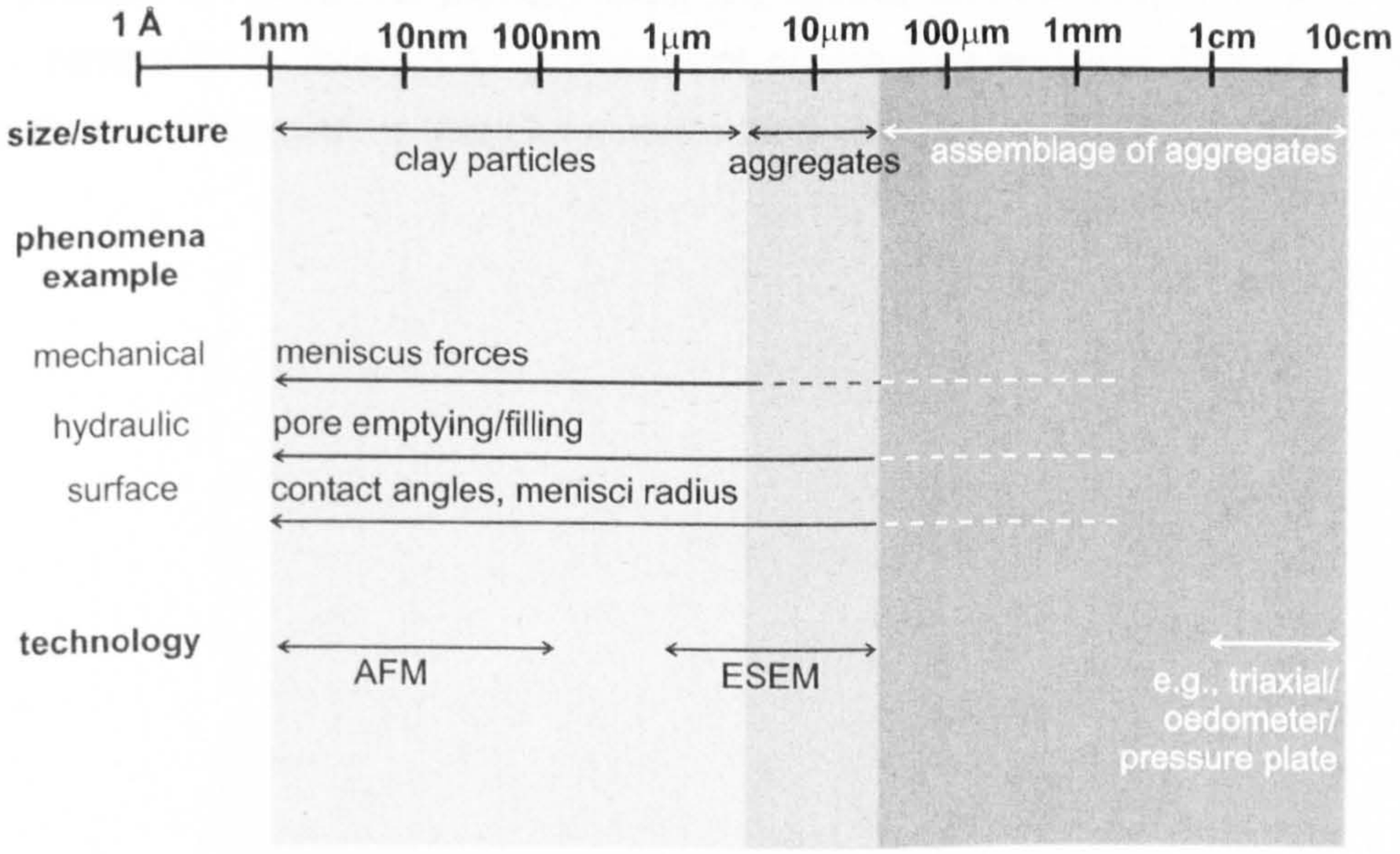

(b)

Figure 7.2: Testing scales, (a) nanotechnology for clay size particles (from NAS, 2006), (b) appropriate technology for different phenomena and clay size/structure (after NAS, 2006)

Contact angles

Following the finding from the ESEM images that contact angles are not zero and are variable, a long discussion was made (based on a literature review) to demonstrate that contact angles can affect both mechanical and hydraulic soil behaviour. However, there are no dedicated experimental studies from a geotechnical point of view. Contact angles can be measured directly with goniometers or by using indirect techniques used in soil science, e.g. water drop penetration time (Letley et al., 2000). It is also a field where it is possible to conduct analytical studies (e.g. influence of contact angle on the meniscus force for different packings/particle shapes). Contact angles could have very practical implications for organic soils, contaminated soils, and mine waste.

Pillared clays

Pillared clays are an interesting topic that emerged from the literature review. They have been proposed as a solution to avoid swelling. The pillars made of different species (Al, Ti, Zr, Fe) attach clay plates without reducing the porosity and surface area, making the clay thermally and volumetrically stable (e.g. Maes et al., 1997). It is also possible to change the porosity according to Aceman et al. (1997). Pillared clays could have a lot of interest to geotechnical engineering because they are able to keep their usual properties that characterize them (low permeability) without swelling.

REFERENCES

Aceman, S., Lahav, N., Yariv, S. (1997). XRD study of the hydration and rehydration behaviour of Al-pillared smectites differing in source of charge, *J. Thermal Anal.* **50**, 241-256

Adamson, A.W., Gast, A.P. (1997). Physical chemistry of surfaces, John Wiley & Sons, 6th Ed., pp.784

Al-Homoud, A.S. Basma, A.A., Husein Malkawi, A.I., Al Bashabsheh, M.A. (1995). Cyclic swelling behaviour of clays, *J. Geotech. Eng. Div.* **121**, 7, 562-565

Ali Rahman, Z. (2008). The Engineering behaviour of a weakly bonded soil including the unsaturated state, PhD Thesis, Durham University

Allam, M.M., Sridharan, A. (1981). Effect of wetting and drying on shear strength, *J. Geotech. Eng. Div.* **107** GT4, 421-438

Alonso, E.E., Romero, E., Hoffmann, C., Garcia-Escudero, E. (2005). Expansive bentonite-sand mixtures in cyclic controlled-suction drying and wetting, *Eng. Geol.* **81**, 213-226

Anderson, S.A., Sitar, N. (1995). Analysis of rainfall-induced debris flows, *J. Geotech. Geoenv. Eng. (ASCE)* **121**, 7, 544-552

Arifin, Y.F., Schanz, T. (2007). Modified isochoric cell for temperature controlled swelling pressure tests, *Experimental unsaturated soil mechanics, T. Schanz (Ed.), Springer,* 229-241

Atchley, A.A., Prosperetti, A. (1989). The crevice model of bubble nucleation, *J. Acoust. Soc. Am.* **86** (3), 1065-1084

Baker, J.C., Grabowska-Olszewska, B., Uwins, P.J.R. (1995). ESEM study of osmotic swelling of bentonite from Radzionkow (Poland), *App. Clay Sc.* **9**, 465-469

Ball, R. (2005). A design for the use of miniature tensiometers in the field, MSc. Dissertation, Durham University

Barrer, R.M. (1989). Clay minerals as selective and shape-selective sorbents, *Pure & Appl. Chem.* **61**, 11, 1903-1912

Baver, L.D., Gardner, W.H., Gardner, W.R. (1972). Soil physics, John Wiley & Sons, 4th Ed., pp.498

Bishop, A.W., Kumapley, N.K., El-Ruwayih, A. (1975). The influence of pore-tension on the strength of clay, *Phil. Trans. Royal Society, London,* **278**, 1286, 511-554

Black, D.K., Lee, K.L. (1973). Saturating laboratory samples by back pressure, *J. Soil Mech. and Found. Div.* **99**, SM1, 75-93

Blanco-Canqui, H., Lal, R., Owens, L.B., Post, W.M., Izaurralde, R.C. (2005). Mechanical properties and organic carbon of soil aggregates in the northern Appalachians, *Soil Sci. Soc. Am. J.* **69**, 1472–1481

Blatz, J., Graham, J. (2000). A system for controlled suction in triaxial tests, *Géotechnique* **50**, 4, 465-469.

Blight, G.E. (2007). Hysteresis during drying and wetting of soils, *3rd Asian Conference in Unsaturated Soils*, 179-184

Boso, M., Romero, E., Tarantino, A. (2003). The use of different suction measurement techniques to determine water retention curves, *Unsaturated soils: Experimental studies, Springer-Verlag Berlin, Schanz T (ed.)*, 171-181

Bremond, N., Arora, M., Ohl, C.-D., Lohse, D. (2005). Cavitation on surfaces, *J. Phys.: Condens. Matter* **17**, S3603–S3608

Brennen, C. E. (1995). Cavitation and bubble dynamics, Oxford University Press, pp. 282

Brunauer, S., Emmett, P.H., Teller, E. (1938). Adsorption of gases in multimolecular layers, *J.Amer.Chem.Soc.* **60**, 309

Buckingham, E. (1907). Studies of the movement of soil moisture, U.S. Department of Agriculture, Bureau of Soils, Bull. 10

Buckman, J.O., Todd, A.C., Hill, P.I. (2000). Observations on a reservoir rock wetability using an environmental scanning electron microscope, *Microscopy and Analysis* **14**, 2, 35-37

Bulut, R., Leong, E.C. (2008). Indirect measurement of suction, *Geotech. Geol. Eng.* (in print)

Butt, H.-J., Farshchi-Tabrizi, M., Kappl, M. (2006). Using capillary forces to determine the geometry of nanocontacts, *J. of Appl. Phys.* **100**, 024312

Byrant, E.M., Bowman, R.S., Bucley, J.S. (2006). Wetting alteration of mica surfaces with polyethoxylated amine surfactants, *J. of Petroleum Sc. and Eng.* **52**, 244–252

Campbell Scientific (2008). TDR100 Reflectometer-based System (Brochure)

Cases, J.M., Berend, I., Besson, G., Francois, M., Uriot, J.P., Thomas, F., Poirier, J.E. (1992). Mechanism of adsorption and desorption of water vapour by homoionic montmorillonite, 1. The sodium-exchanged form, *Langmuir* **22**, 8, 2730-2739

Casini, F., Munoz, J.-J., Lourenco, S., Vaunat, J., Pereira, J.M. (2006). Results of the first centrifuge campaign at LCPC facilities, Nantes, France, MUSE Internal Report, 54pp.

Chen, F.H., Ma, G.S. (1987). Swelling and shrinking behaviour of expansive clays, *Proc. 6th Int. Conf. Expansive Soils, New Delhi,* 127-129

Cheng, X.H., Ngan-Tillard, D.J.M., Den Haan, E.J. (2007). The causes of the high friction angle of Dutch organic soils, *Eng. Geol.* **93**, 31–44

Chenu, C., Bissonnais, Y. L., Arrouays, D. (2000). Organic matter influence on clay wettability and soil aggregate stability, *Soil Sci. Soc. Am. J.* **64**, 1479–1486

Chiu, C.F., Cui, Y.F., Delage, P., De Laure, E., Haza, E. (2005). Lessons learnt from suction monitoring during centrifuge modelling, *Advanced experimental unsaturated soil mechanics, Tarantino, Romero, Cui (eds),* 3-8

Cho, G.C., Santamarina, J.C. (2001). Unsaturated particulate materials – particle level studies, *J. Geotech. Geoenv. Eng. (ASCE)* **127**, 1, 84-96

Claesson, P.M., Ederth, T., Bergeron, V., Rutland, M.W. (1996). Techniques for measuring surface forces, *Adv. Colloid Interface Sci.* **68**, 119-183

Cnudde, V., Masschaele, B., Dierick, M., Vlassenbroeck, J., Van Hoorebeke, L., Jacobs P. (2006). Recent progress in X-ray CT as a geosciences tool, *Applied Geochemistry* **21**, 5, 826-832

Combes, R., Robin, M., Blavier, G., Aidan, M., Degreve, F. (1998). Visualization of imbibition in porous media by environmental scanning electron microscopy: application to reservoir rocks, *J. Petroleum Sc. & Eng.* **20**, 133-139

Croney, D., Coleman, J.D. (1960). Pore pressure and suction in soil, *Proceedings Conference on Pore Pressure and Suction in Soils. London, Butterworths,* 31-37

Cui, Y. J., Delage, P. (1996). Yielding and plastic behaviour of an unsaturated compacted silt, *Géotechnique* **46**, 2, 291-311

Cui, Y. J., Delage, P., Alzoghbi, P. (2003). Retention and transport of a hydrocarbon in a silt, *Géotechnique* **53**, 1, 83-92

Cunningham, M.R. (2000). The mechanical behaviour of a reconstituted unsaturated soil, Ph.D. Thesis, Imperial College of Science, Technology and Medicine, London

Cunningham, M.R., Ridley, A.M., Dineen, K., Burland, J.J. (2003). The mechanical behaviour of a reconstituted unsaturated silty clay, *Géotechnique* **53**, 2, 183-194

Day, R.W. (1994). Swell-shrink behaviour of compacted clay, *J. Geotech. Eng. Div.* **120**, 3, 618-623

De Gennes, P.G. (1985). Wetting: statics and dynamics, *Rev. Modem Physics* **57**, 3, I, 827-863

Delage, P., Romero, E.E., Tarantino, A. (2008). Recent developments in the techniques of controlling and measuring suction in unsaturated soils, *Unsaturated Soils: Advances in Geo-Engineering – Toll, D.G., Augarde, C.E., Gallipoli, D., Wheeler, S.J. (eds.)*, 33-52

Dif, A.E., Bluemel, W.F. (1991). Expansive soils under cyclic drying and wetting, *Geotech. Test. J.* **14**, 1, 96-102

Doerr, S.H., Shakesby, R.A., Walsh, R.P.D. (2000). Soil water repellency: its causes, characteristics and hydrogeomorphological significance, *Earth-Sci. Rev.* **51**, 33-65

Donald, A.M., He, C., Royall, C.P., Sferrazza, M., Stelmashenko, N.A., Thiel, B.A. (2000). Applications of environmental scanning electron microscopy to colloidal aggregation and film formation, *Colloids and Surfaces A: Physicochemical and Eng. Asp.* **174**, 37–53

Donald, A.M. (2003). The use of environmental scanning electron microscopy for imaging wet and insulating materials, *Nature Materials* **2**, 511-516

Donoghue, M. (2006). The performance effects of suction probe saturation in laboratory testing applications, MEng. Report, Durham University

Eastman, T., Zhu, D.-M. (1996). Adhesion forces between surface-modified AFM tips and a mica surface, *Langmuir* **12**, 2859-2862

Eckersley, J. D. (1986). The initiation and development of slope failures with particular reference to flowslides, PhD dissertation, James Cook University of North Queensland

Eckersley, J.D. (1990). Instrumented laboratory flowslides, *Géotechnique* **40**, 489-502

Ekblad, J., Isacsson, U. (2007). Time-domain reflectometry measurements and soil-water characteristic curves of coarse granular materials used in road pavements, *Can. Geotech. J.* **44**, 7, 858-872

Fisher, L.R., Lark, P.D. (1980). The effect of adsorbed water vapour on liquid water flow in pyrex glass capillary tubes, *J. Colloid and Interface Sc.* **76**, 1, 251-253

Fisher, L.R., Israelachvili, J. (1981). Experimental studies on the applicability of the Kelvin equation to highly curved concave menisci, *J. Colloid and Interface Sc.* **80**, 2, 528-541

Fisher, R. A. (1926). On the capillary forces in an ideal soil; correction of formulas by W.B. Haines, *J. Agric. Sci.* **16**, 492–505.

Fleureau, J.-M., Verbrugge, J.-C., Huergo, P.J., Correia, A.G., Kheirbek-Saoud, S. (2002). Aspects of the behaviour of compacted clayey soils on drying and wetting paths, *Can. Geotech. J.* **39**, 1341-1357

Fredlund, D.G., Rahardjo, H. (1993). Soil mechanics for unsaturated soils, John Wiley & Sons, pp.517

Fredlund, D.G., Xing, A. (1994). Equations for the soil-water characteristic curve, *Can. Geotech. J.* **31** (3), 521-532

Fredlund, D.G. (2006). Unsaturated soil mechanics in engineering practice, *J. Geotech. Geoenv. Eng. (ASCE)* **132** (3), 286-321

Gallipoli, D. (2000). Constitutive and numerical modelling of unsaturated soils, PhD dissertation, University of Glasgow

Gallipoli, D., Gens, A., Sharma, R., Vaunat, J., (2003). An elasto-plastic model for unsaturated soil incorporating the effects of suction and degree of saturation on mechanical behaviour, *Géotechnique* **53**, 1, 123–135

Gasparre, A., Nishimura, S., Coop, M. R., Jardine, R. J. (2007). The influence of structure on the behaviour of London Clay, *Géotechnique* **57**, 1, 19–31

Gence, N. (2006). Wetting behavior of magnesite and dolomite surfaces. *App. Surf. Sc.* **252**, 3744–3750

Glendinning, S, Rouainia, M, Hughes, P, Davies, O. (2006). Biological and engineering impacts of climate on slopes (BIONICS): The first 18 months, *10th IAEG international congress 2006, Nottingham, UK,* Paper No. 348

Gregg, S.J. (1968). Surface chemistry study of comminuted and compacted solids, *J. Chem. Ind.* **11**, 611-617

Gregg, S.J., Sing, K.S.W. (1967). Adsorption, surface area and porosity, Academic Press, pp. 371

Grobelny, J., Pradeep, N., Kim, D.-I., Ying, Z.C. (2006). Quantification of the meniscus effect in adhesion force measurements, *Appl. Phys. Lett.* **88**, 091906

Guan, Y. (1996). The measurement of soil suction, PhD Thesis, University of Saskatchewan

Guan, Y., Fredlund, D. G. (1997). Use of the tensile strength of water for the direct measurement of high soil suction, *Can. Geotech. J.* **34**, 604-614

Harvey, E.W., Barnes, D.K., McElroy, W.D., Whiteley A.H., Pease D.C., Cooper K.W. (1944). Bubble formation in animals, *J. Cellular and Comparative Physiology* **24**, 1, 1-22

Hayashi, M., v.d.Kamp, G., Rudolph, D.L. (1997). Use of tensiometer response time to determine the hydraulic conductivity of unsaturated soil, *Soil Sci.* **162**, 8, 566-575

Head, K.H. (1976). Manual of soil laboratory testing, Vol. 3, Pentech Press, London

Hennig, A., Eichhorn, K.-J., Staudinger, U., Sahre, K., Rogalli, M., Stamm, M., A. W. Neumann, A.W., Grundke, K. (2004). Contact angle hysteresis: study by dynamic

cycling contact angle measurements and variable angle spectroscopic ellipsometry on polyimide, *Langmuir* **20**, 6685-6691

Hidayat, S.D. (2006). Comparison of different experimental techniques for suction measurement within the MUSE network, MSc. Dissertation, Durham University

Hight, D. W. (1982). A simple piezometer probe for the routine measurement of pore pressure in triaxial tests on saturated soils, *Géotechnique* **32**, 4, 396-401

Hight, D.W., Bond, A.J., Legge, J.D. (1992). Characterization of the Bothkennar clay: an overview, *Géotechnique* **42**, 2, 303–347

Hilf, J.W. (1956). An investigation of pore water pressure in compacted cohesive soils, US Bureau of Reclamation, Tech. Mem. 654, Denver: US Bureau of Reclamation

Ho, K.M.Y., Tse, J.M.K., Ng, C.W.W. (2007). Influence of drying and wetting history and particle size on state-dependent soil-water characteristic curves (SDSWCCS), *3rd Asian Conference in Unsaturated Soils,* 213-218

Hoffman, R.L. (1975). A study of the advancing interface. I. Interface shape in liquid—gas systems, *J. Colloid Interface Sc.* **50**, 2, 228-241

Hornberger, G.M., Raffensperger, J.P., Wiberg, P.L., Eshleman, K.N. (1998). Elements of physical hydrology, The Johns Hopkins University Press, pp. 301

Ioannou, I., Hall, C., Wilson, M.A., Hoff, W.D., Carter, M.A. (2003). Direct measurement of the wetting front capillary pressure in a clay brick ceramic, *J. Phys. D: Appl. Phys.* **36**, 3176–3182

Ishida, N., Inoue, T., Miyahara, M., Higashitani, K. (2000). Nano bubbles on a hydrophobic surface in water observed by tapping-mode atomic force microscopy, *Langmuir* **16**, 6377-6380

Israelachvili, J.N. (1991). Intermolecular and surface forces, Academic Press, 2nd Edition, pp. 450

Jones, S.B., Wraith, J.M., Orr, D. (2002). Time domain reflectometry measurement principles and applications, *Hydrol. Process.* **16**, 141–153

Jones, S.F., Evans, G.M., Galvin, K.P. (1999). Bubble nucleation from gas cavities - a review, *Adv. in Coll. and Int. Sc.* **80**, 27-50

Jotisankasa, A. (2005). Collapse behaviour of a compacted silty clay, PhD Thesis, Imperial College

Jotisankasa, A., Coop, M., Ridley, A. (2007a). The development of a suction control system for a triaxial apparatus, *Geotech. Test. J.* **30**, 1, 69-75.

Jotisankasa, A., Porlila, W., Soralump, S., Mairiang, W. (2007b). Development of a low-cost miniature tensiometer and its applications, *3rd Asian Conference in Unsaturated Soils,* 475-480

Jotisankasa, A. (2007c). Personal communication

Karagunduz, A., Pennell, K.D., Young, M.H. (2001). Influence of a nonionic surfactant on the water retention properties of unsaturated soils, *Soil Sci. Soc. Am. J.* **65**, 1392–1399

Klute, A., Gardner, W.R. (1962). Tensiometer response time, *Soil Sci.* **93**, 204-207

Kodikara, J., Barbour, S.L., Fredlund, D.G. (1999). Changes in clay structure and behaviour due to wetting and drying, *Proc. 8th Aust.-N. Zeal.Conf. Geomechanics*, 179-186

Kohonen, M.M., Christenson, H.K. (2000). Cappilary condensation of water between rinsed mica surfaces, *Langmuir* **16**, 7285-7288

Lambe, T.W., Whitman, R.V. (1969). Soil Mechanics, John Wiley & Sons, pp. 553

Lampenscherf, S., Pompe, W., Wilkinson, D.S. (2000). Stress development due to capillary condensation in powder compacts: a two-dimensional model study, *J. Am. Ceram. Soc.* **83**, 6, 1333–1340

Langmuir, I. (1916). The constitution and fundamental properties of solids and liquids, Part I – solids, *J.Amer.Chem.Soc.* **38**, 2221

Lee, H.V., Wray, W.K. (1995). Techniques to evaluate soil suction – a vital unsaturated soil water variable, *Unsaturated Soils, Alonso & Delage (eds)* **2**, 615-622

Lehmann, P., Stauffer. F., Hinz, C., Dury, O., Flühler, H. (1998). Effect of hysteresis on water flow in a sand column with a fluctuating capillary fringe, *J. of Contam. Hydrology* **33**, 1-2, 81-100

Leong, E.-C., Tripathy, S., Rahardjo, H. (2003). Total suction measurement of unsaturated soils with a device using the chilled-mirror dew-point technique, *Géotechnique* **53**, 2, 173–182

Leong, E.C., Tripathy, S., Rahardjo, H. (2004). A modified pressure plate apparatus, *Geotech. Test. J.* **27**, 3, 322-331

Letley, J., Osborn, J., Pelishek, R.E. (1962). Measurement of liquid-solid contact angles in soil and sand, *Soil Sc.* **93**, 149-153

Letley, J., Carrillo, M.L.K., Pang, XP (2000). Approaches to characterize the degree of water repellency, *J. Hydrology* **231**, 61-65

Likos, W.J., Lu, N. (2004). Hysteresis of capillary stress in unsaturated granular soil, *J. Eng. Mech.* **130**, 6, 646-656

Litzow, U., Gahr, K.-H.Z., Schneider, J. (2006). Cavitation erosion of advanced ceramics in water, *Int. J. Mat. Res.* **97**, 10, 1372-1377

Long, M.M. O'Riordan, N.J. (2001). Field behaviour of very soft clays at the Athlone embankments, *Géotechnique* **51**, 4, 293-309

Lourenço, S.D.N., Sassa K., Fukuoka H., (2006a). Failure process and hydrologic response of a two layer physical model: implications for rainfall-induced landslides, *Geomorphology* **73**, 1-2, 115-130

Lourenço, S.D.N., Wang G., Sassa K., Fukuoka H. (2006b). Volumetric behaviour of saturated sands under poor drainage conditions, *J. Geophys. Res.* **111**, No. F3, F03004, 10.1029/2005JF000324

Lourenço, S.D.N., Gallipoli, D., Toll, D., Evans, F. (2006c). Development of a commercial tensiometer for triaxial testing of unsaturated soils, *Geotechnical Special Publication (ASCE)* **147**, Vol. 2, 1875-1886

Lourenço, S.D.N., Gallipoli, D., Toll, D., Evans, F., Medero, G. (2007a). Determination of the Soil Water Retention Curve with tensiometers, *Experimental unsaturated soil mechanics, Springer, T. Schanz (Ed.)*, 95-102

Lourenço, S.D.N., Gallipoli, D., Toll, D., Evans, F., Medero, G., (2007b). Discussion "The development of a suction control system for a triaxial apparatus" by Jotisankasa, A., Coop, M., and Ridley, A., *Geotech. Test. J.* **30**, 1, pp. 69-75

Lourenço, S.D.N., Gallipoli, D., Toll, D., Augarde, C., Evans, F., Medero, G. (2008a). Calibrations of a high suction tensiometer *Géotechnique* **58**, 8, 659–668

Lourenço, S.D.N., Gallipoli, D., Augarde, C. Toll, D., Evans, F., Medero, G. (2008b), Evaluation of suction measurement by the tensiometer and the axis translation technique, *Unsaturated Soils: Advances in Geo-Engineering – Toll, D.G., Augarde, C.E., Gallipoli, D., Wheeler, S.J. (eds.)*, 213-218

Lourenço, S.D.N., Gallipoli, D., Augarde, C. Toll, D., Evans, F., Medero, G. (2008c), Studies of unsaturated soils by environmental scanning electron microscope using dynamic mode, *Unsaturated Soils: Advances in Geo-Engineering – Toll, D.G., Augarde, C.E., Gallipoli, D., Wheeler, S.J. (eds.)*, 145-150

Maeda, N., Israelachvili, J.N. (2002). Nanoscale mechanisms of evaporation, condensation and nucleation in confined geometries, *J. Phys. Chem. B* **106**, 3534-3537

Maeda, N., Israelachvili, J. N., Kohonen, M.M. (2003). Evaporation and instabilities of microscopic capillary bridges, *Proc. Natl. Acad. Sci.* **100**, 3, 803-808

Maes, N., Heylen, I., Cool, P., Vansant, E.F. (1997). The relation between the synthesis of pillared clays and their resulting porosity, *App. Clay Sc.* **12**, 43-60

Mahler, C.F., Diene, A.A. (2007). Tensiometer development for high suction analysis in laboratory lysimeters, *Experimental unsaturated soil mechanics, T. Schanz (Ed.), Springer*, 103-115

Mair, R. (1979). Centrifugal modelling of tunnel construction in soft clay, PhD Thesis, Cambridge University

Mantho, A.T. (2005). Soil-atmosphere transfers - application to drought. PhD Dissertation, École National des Ponts et Chaussées, Paris (in French)

Maswoswe, J. (1985). Stress paths for a compacted soil during collapse due to wetting, PhD thesis, University of London

Meilani, I., Rahardjo, H., Leong, E.-C., Fredlund, D.G. (2002). Mini suction probe for matric suction measurements, *Can. Geotech. J.* **39**, 1427-1432

Meisina, C. (2004). Swelling-shrinking properties of weathered clayey soils associated with shallow landslides, *Quart. J. of Eng. Geol. and Hydrogeol.* **37**, 2, 77-94

Melrose, J.C. (1989). Applicability of the Kelvin equation to vapour/liquid systems in porous media, *Langmuir* **5**, 290-293

Mendes, J. (2007a), personal communication

Mendes, J., Gallipoli, D., Augarde, C.E., Toll, D., Medero, G.M. (2007b). Suction measurements of a sandy-clay soil with the filter paper technique, *IV Simposio Brasileiro de Solos Nao Saturados NSAT2007, Recife, Brazil*

Mendes, J. (2008a), Hydro-mechanical characterization of the fill material of the BIONICS embankment, PhD Dissertation, Durham University (in preparation)

Mendes, J., Gallipoli, D., Toll, D., Augarde, C.E., Evans, F.D. (2008b). A System for field measurement of suctions using removable suction probes, *Unsaturated Soils: Advances in Geo-Engineering – Toll, D.G., Augarde, C.E., Gallipoli, D., Wheeler, S.J. (eds.)*, 219-225

Miller, C.R., Vogel, R., Surawski, P.P.T., Jack, K.S., Corrie, S.R., Trau, M. (2005). Functionalized organosilica microspheres via a novel emulsion-based route, *Langmuir* **21**, 9733

Mitchell, J.K. (1993). Fundamentals of Soil Behaviour, John Wiley & Sons, 2nd Ed. pp.437

Montes-H., G. (2005). Swelling–shrinkage measurements of bentonite using coupled environmental scanning electron microscopy and digital image analysis, *J. Colloid and Interface Sc.* **284**, 271-277

Montes-H., G., Geraud, Y., Duplay, J., Reuschle, T. (2005). ESEM observations of compacted bentonite submitted to hydration/dehydration conditions, *Colloids and Surfaces A: Physicochem. Eng. Aspects* **262**, 14–22

Molenkamp, F., Nazemi, A. H. (2003). Interactions between two rough spheres, water bridge and water vapour, *Géotechnique* **53**, 2, 255-264

Musso, G., Morales, E.R., Gens, A., Castellanos, E. (2003). The role of structure in the chemically induced deformations of FEBEX bentonite, *Applied Clay Sc.* **23**, 229-237

National Academy of Sciences – NAS (2006). Geological and geotechnical engineering in the new millennium: opportunities for research and technological innovation, ISBN: 0-309-65331-2, http://www.nap.edu/catalog/11558.html, pp. 222

National Physical Laboratory - NPL (1996). A guide to the measurement of humidity, Institute of Measurement and Control, pp.68

Ng, C.W.W., Pang, Y.W. (2000a). Experimental investigation of soil-water characteristics of a volcanic soil, *Can Geotech. J.* **37**, 6, 1252-1264

Ng, C.W.W., Pang, Y.W. (2000b). Influence of stress state on soil-water characteristics and slope stability, *J. of Geotech. and Geo-Env. Eng. (ASCE)* **126,** 2,157-166

Ng, C.W.W, Zhan, L.T., Cui, Y.J. (2002). A new simple system for measuring volume changes in unsaturated soils, *Can. Geotech. J.* **39,** 3, 757–764

Noborio, K. (2001). Measurement of soil water content and electrical conductivity by time domain reflectometry: a review, *Comp. and Electr. in Agric.* **31**, 213-237

Okada, K., Tomita, T., Yasumori, A. (1998). Gas adsorption of mesoporous γ-alumina prepared by a selective leaching method, *J. Mater. Chem.* **8**, 2863-2867

Oliveira, O.M., Marinho, F.A.M. (2006). Study of the equilibration time in the pressure plate, *Geotechnical Special Publication (ASCE)* **147**, 2, 1865-1874

Oliveira, O.M., Marinho, F.A.M. (2008). Suction equilibration time for a high capacity tensiometer, *Geotech. Test. J.* **31**, 1, 1-5

Orr, F.M., Scriven, L.E., Rivas, A.P. (1975). Pendular rings between solids, meniscus properties and capillary force, *J. Fluid Mech.* **67**, 4, 723-742

Ouyang, Q., Ishida, K., Okada, K. (2001). Investigation of micro-adhesion by atomic force microscopy, *App. Surf. Sc.* **169-170**, 644-648

Peron, H., Hueckel, T., Laloui, L. (2007). An improved volume measurement for determining soil water retention curves, *Geotech. Test. J.* **30**, **1**, 1-8

Pesaran, A.A., Mills. A.F. (1987a), Moisture transport in silica gel packed beds – I. Theoretical study, *Int. J. Heat and Mass Transfer* **30** (6), 1037-1049

Pesaran, A.A., Mills. A.F. (1987b), Moisture transport in silica gel packed beds – II. Experimental study, *Int. J. Heat and Mass Transfer* **30** (6), 1051-1060

Pham, Q.T., Vales, F., Malinsky, L., Nguyen Minh, D., Gharbi, H. (2006). Effects of desaturation–resaturation on mudstone, *J. Phys. Chem. Earth*, in press, doi:10.1016/j.pce.2006.03.012

Poirier, S.E., DeGroot, D.J., Sheahan, T.C. (2005). Measurement of suction in a marine clay as an indicator of sample disturbance, *Proc. Geo-Frontiers 2005 Congress Earth and Space 2005*, **164**, 19

Rahardjo, H., Leong, E.C. (2006). Suction measurements, *Geotechnical Special Publication (ASCE)* **147**, 81-104

Rao, K.S., Satyadas, G.C. (1987). Swelling potential with cycles of swelling and partial shrinkage, *Proceedings 6th Int. Conf. Expansive Soils, New Delhi,* 137-142

Rao, K.S., Rao, S.M., Gangadhara, S. (2000). Swelling behaviour of a dessicated clay, *Geotech. Test. J.* **23**, 2, 193-198

Rao, S.M., Revanasiddappa, K. (2006). Influence of cyclic wetting drying on collapse behaviour of compacted residual soil, *Geotech. and Geol. Eng.* **24**, 725-744

Ravi, S., D'Odorico, P., Herbert, B., Zobeck, T., Over, T.M. (2006). Enhancement of wind erosion by fire-induced water repellency, *Water Resour. Res.* **42**, W11422

Ravikovitch, P.I., Neimark, A.V. (2002). Experimental confirmation of different mechanisms of evaporation from ink-bottle type pores: equilibrium, pore blocking, and cavitation, *Langmuir* **18**, 9830-9837

Redwood, P.S., Lead, J.R., Harrison, R.M., Jones, I.P., Stoll, S. (2005). Characterization of humic substances by environmental scanning electron microscopy, *Env. Sc. and Tech.* **39**, 7, 1962-1966

Reinson, J.R., Fredlund, D.G., Wilson, G.W. (2005). Unsaturated flow in coarse porous media, *Can. Geotech. J.* **42**, 252-262

Renault, P., Mohrath D., Gaudu J.C., Fumanal, J.C. (1998). Air pressure fluctuations in a prairie soil, *Soil Sc. Soc. of Am. J.* **62**, 3, 553-563

Richards, B.E., Trevena, D.H. (1976). The measurement of positive and negative pressures in a liquid contained in a Berthelot tube, *J. Phys. D: Appl. Phys.* **9**, L123-L126

Ridley, A.M. (1993). The measurement of soil moisture suction, PhD thesis, Imperial College, London

Ridley, A.M., Burland, J.B. (1993). A new instrument for the measurement of soil moisture suction, *Géotechnique* **43**, 2, 321-324

Ridley, A.M., Wray, J. B. (1996). Suction measurement: A review of current theory and practices, *Unsaturated Soils, Alonso & Delage (eds)* **3**, 1293-1322

Ridley, A.M., Dineen, K., Burland, J. B., Vaughan P.R. (2003). Soil matrix suction: some examples of its measurement and application in geotechnical engineering, *Géotechnique* **53**, 2, 241-253

Ridley, A.M. (2007). Soil suction – some examples of its measurement and application in geotechnical engineering, 3rd MUSE Workshop, Naples, Italy, http://muse.dur.ac.uk/3rdMuseSchool/Ridley.pdf

Rojas, J.C., Pagano, L., Zingariello, M.C., Giordano, G., Passeggio, G., Mancuso, C. (2008). A new high capacity tensiometer: first results, *Unsaturated Soils: Advances*

in Geo-Engineering – Toll, D.G., Augarde, C.E., Gallipoli, D., Wheeler, S.J. (eds.), 205-211

Rouquerol, J., Avnir, D., Fairbridge, C.W., Everett, D.H., Haines, J.H., Pernicone, N., Ramsay, J.D.F., Sing, K.S.W., Unger, K.K. (1994). IUPAC Recommendations for the characterization of porous solids, *Pure & Appl. Chem.* **66**, 8, 1739-1758

Rouquerol, F., Rouquerol, J., Sing, K. (1999). Adsorption by powders & porous solids, Academic Press, pp. 467

Sánchez, M., Villar, M.V., Gómez-Espina, R., Lloret, A., Gens A. (2008). Swelling pressure in compacted bentonite: Laboratory tests and modelling, *Unsaturated Soils: Advances in Geo-Engineering – Toll, D.G., Augarde, C.E., Gallipoli, D., Wheeler, S.J. (eds.)*, 667-673

Schenk, M., Futing, Reichelt, R. (1998). Direct visualization of the dynamic behavior of a water meniscus by scanning electron microscopy, *J. App. Phys.* **84**, 9, 4880-4884

Sedgewick, S.A., Trevena, D.H. (1976). Limiting negative pressure of water under dynamic stressing, *J. Physics D: Appl. Phys.* **9**, 1983-1990

Shahidzadeh-Bonn, N., Azouni, A., Coussot, P. (2007). Effect of wetting properties on the kinetics of drying of porous media, *J. Phys.: Condens. Matter* **19**, 112101

Sharma, R. S., Wheeler, S. J. (2000). Behaviour of an unsaturated highly expansive clay during cycles of wetting and drying, *Proceedings Asian Conference on Unsaturated Soils, Singapore,* 721–726

Shirtcliffe, N.J., McHale, G., Newton, M.I., Pyatt, F.B., Doerr, S.H. (2006). Critical conditions for the wetting of soils, *App. Phys. Lett.* **89**, 094101

Schumacher, E.E., Ferguson, L. (1929). Diffusion of water through rubber, *Ind. Eng. Chem.* **21**, 2, 158-162

Skauge, A., Spildo, K., Hoiland, L., Vik, B. (2006). Theoretical and experimental evidence of different wettability classes, *J. Petroleum Sc. & Eng.* (in press)

Sjoblom, K. (1996). The mechanisms involved during the desaturation process of a porous matrix, PhD. Thesis, Massachusetts Institute of Technology

Sorgi, C., De Gennaro, V. (2006). Observations at the Environmental SEM of the water influence in the behaviour of marls, *Proceedings J. Nat. Geotech. Geol. de l'Ing.*, Lyon, France, pp. 9 (in French)

Sorgi, C., De Gennaro, V. (2007). ESEM analysis of chalk microstructure submitted to hydromechanical loading, (accepted by Comptes Rendus de l'Academie des Sciences – serie Geoscience) (in French)

Souders, J. E., Jeffrey B. D., Nayak L. P., Michael P. H. (1999). Spatial distribution of venous gas emboli in the lungs, *J. Appl. Physiol.* **87**, 5, 1937–1947

Stokes, D.J., Donald, A.M. (2000). In situ mechanical testing of dry and hydrated breadcrumb in the environmental scanning electron microscope (ESEM), *J. Mat. Sc.* **35**, 599– 607

Stokes, D.J. (2003). Recent advances in electron imaging, image interpretation and applications: environmental scanning electron microscopy, *Phil. Trans. R. Soc. Lond. A* **361**, 2771–2787

Sun, J., Besant, R.W. (2005). Heat and mass transfer during silica gel – moisture interactions, *Int. J. Heat and Mass Transfer* **48**, 4953-4962

Tabor, D. (1969). Gases, liquids and solids, Penguin Books, pp. 290

Take, W.A. (2003). The influence of seasonal moisture cycles on clay slopes, PhD Dissertation, Cambridge University

Take, W.A., Bolton, M.D. (2003). Tensiometer saturation and the reliable measurement of soil suction, *Géotechnique* **53**, 2, 159-172

Tang, A.-M., Cui, Y.-J., (2005). Controlling suction by the vapour equilibrium technique at different temperatures and its application in determining the water retention properties of MX80 clay, *Can. Geotech. J.* **42**, 287-296

Taniguchi, M., Belfort, G. (2002). Correcting for surface roughness: advancing and receding contact angles, *Langmuir* **18**, 6465-6467

Tarantino, A., Mongiovi, L. (2001). Experimental procedures and cavitation mechanisms in tensiometer measurements, *Geotech. and Geol. Eng.* **19**, 189-210

Tarantino, A., Mongiovi, L. (2003). Calibration of tensiometer for direct measurement of matric suction, *Géotechnique* **53**, 1, 137-141

Tarantino, A., Tombolato, S. (2005). Coupling of hydraulic and mechanical behaviour in unsaturated compacted clay, *Géotechnique* **55**, 4, 307–317

Tarantino, A., Ridley, A., Toll, D. (2008). Field measurement of suction, water content, and water permeability, *Geotech. Geol. Eng.* (in print)

Teixeira, P.F., Marinho, F.A.M. (2006). Determination of the soil water retention curve by means of high capacity tensiometers, *XIII Congresso Brasileiro de Mecânica dos Solos e Engenharia Geotécnica, 2006, Curitiba. COBRASEG-2006, 2006.* **1**, 423-427 (in Portuguese).

Tinjun, J.M., Benson, C.H., Blotz, L.R. (1997). Soil-water characteristic curves for compacted clays, *ASCE J. Geotech. Geoenv. Eng. (ASCE)* **123**, 11, 1060-1069

Toker N., Germaine J., Sjoblom K., Culligan P. (2004). A new technique for rapid measurement of continuous soil moisture characteristic curves, *Géotechnique* **54**, 3, 179-186

Toll, D.G. (1988). The behaviour of unsaturated compacted naturally occurring gravel, PhD Thesis, Imperial College of Science, Medicine and Technology, University of London

Toll, D.G. (1999). A Data acquisition and control system for geotechnical testing, *Computing developments in civil and structural engineering (eds. B. Kumar and B.H.V. Topping), Edinburgh: Civil-Comp Press*, 237-242

Toll, D.G., Hight, D.W., On the desaturation and drying of soil, *unpublished*, 27 pp.

Toll, D.G., Ong, B. H., (2003). Critical-state parameters for an unsaturated residual sandy clay, *Géotechnique* **53**, 1, 93–103

Tomlinson, W.J., Matthews, S.J. (1994). Cavitation erosion of structural ceramics, *Ceramics Int.* **20**, 201-209

Tompsett, G.A., Krogh, L., Griffin, D.W., Conner, W.C. (2005). Hysteresis and scanning behavior of mesoporous molecular sieves, *Langmuir* **21**, 8214-8225

Topp, G.C., Davis, J.L., Annan, A.P. (1980). Electromagnetic determination of soil water content: measurements in coaxial transmission lines, *Water Resour. Res.* **16**, 574–582

Towner, G.D. (1980). Theory of time response of tensiometers, *J. Soil Sc.* **31**, 607-621

Trevena, D.H. (1982). Time effects in cavitation experiments, *J. Phys. D: Appl. Phys.* **15**, LIII-114

Tse, E.Y.M., Ng, C.W.W. (2008). Effects of drying and wetting cycles on unsaturated shear strength, *Unsaturated Soils: Advances in Geo-Engineering – Toll, D.G., Augarde, C.E., Gallipoli, D., Wheeler, S.J. (eds.)*, 481-486

University of California, Davis - UCD (2005). Principles of centrifuge modelling, University of California, Davis, Center for Geotechnical Modelling, http://nees.ucdavis.edu/principles.php

Van Liew, H.D., Burkard, M.E. (1993). Density of decompression bubbles and competition for gas among bubbles, tissue, and blood, *J. Appl. Physiol.* **75**, 5, 2293-2301

Van Liew, H. D., Raychaudhuri, S. (1997). Stabilized bubbles in the body: pressure-radius relationships and the limits to stabilization, *J. Appl. Physiol.* **82**, 6, 2045–2053

Vanapalli, S.K., Fredlund, D.G., Pufahl, D.E. (1999). The influence of soil structure and stress history on the soil-water characteristics of a compacted till, *Géotechnique* **49**, 2, 143-159

Vaunat, J. (2006). Physical modelling of the response of a foundation on unsaturated silty layer, Powerpoint Presentation, 2nd MUSE Workshop, ENPC, Paris

Venaruzzo, J.L., Volzone, C., Rueda, M.L., Ortiga, J. (2002). Modified bentonitic clay minerals as adsorbents of CO, CO_2 and SO_2 gases, *Microporous and Mesoporous Mat.* **56**, 73–80

Vercraeije, V. (2007). Performance of tensiometers in different types of soils, MEng. Project, Durham University

Wang, Z., Feyen, J., Van Genuchten, M.T., Nielson, D.R. (1998). Air entrapment effects on infiltration rate and flow instability, *Water Res. Research* **34**, 2, 213–222

Wang, Z., Wu, L., Wu, Q.J. (2000). Water-entry value as an alternative indicator of soil water-repellency and wettability, *J. Hydrology* **231–232**, 76–83

Wang, X., Benson, C.H. (2004). Leak-free pressure plate extractor for measuring the soil water characteristic curve, *Geotech. Test. J.* **27**, 2, 163-172

Weeks, B.L., DeYoreo, J.J. (2006). Dynamic meniscus growth at a scanning probe tip in contact with a gold substrate, *J. Phys. Chem. B* **110**, 10231-10233

Weeks, B.L., Vaughn, M.W., DeYoreo, J.J. (2005). Direct Imaging of Meniscus Formation in Atomic Force Microscopy Using Environmental Scanning Electron Microscopy, *Langmuir* **21**, 8096-8098

Weeks, E.P. (2002). The Lisse effect revisited, *Ground Water* **40**, 6, 652-656

Wenzel, W.W., Wieshammer, G. (1995). Suction cup materials and their potential to bias trace metal analyses of soil solutions: a review, *Int. J. Environ. Anal. Chem.* **59**, 277-290

Wheeler, S.J. (1986). The stress-strain behaviour of soils containing gas bubbles, PhD Dissertation, University of Oxford

Wheeler, S.J., Sivakumar, V. (1995). An elasto-plastic critical state framework for unsaturated soil, *Géotechnique* **45**, 1, 35-53

Wheeler, S.J., Sharma, R.S., Buisson, M.S.R., (2003). Coupling of hydraulic hysteresis and stress-strain behaviour in unsaturated soils, *Géotechnique* **53**, 1, 41-54

White, N.F., Sunada, D.K., Duke, H.R., Corey, A.T. (1972). Boundary effects in desaturation of porous media, *Soil Sc.* **113**, 1, 7-12

Wildenschild D., Hopmans, J.W., Vaz, C.M.P., Rivers, M.L., Rikard, D., Christensen, B.S.B. (2002). Using X-ray computed tomography in hydrology: systems, resolutions and limitations, *J. Hydrology* **267**, 285-297

Williams, J., Prebble, R.E., Williams, W.T., Hignett, C.T. (1983). The influence of texture, structure and clay mineralogy on the soil moisture characteristic, *Australian J. Soil Res.* **21**, 1, 15 - 32

Wilson, G.W., Fredlund, D.G., Barbour, S.L. (1997). The effect of soil suction on evaporative fluxes from soil surfaces, *Can. Geotech. J.* **34**, 145-155

Wong, C.K., Wibowo, R. (2000). Tomographic evaluation of air and water flow patterns in soil column, *Geotech. Test. J.* **23**, 4, 413-422

Wong, J.C., Rahardjo, H., Toll, D.G., Leong, E.C. (2001). Modified triaxial apparatus for shearing-infiltration tests, *Geotech. Test. J.* **24**, 4, 370-380

Yesiller, N., Miller, C.J., Inci, G., Yaldo, K. (2000). Dessication and cracking behaviour of three compacted landfill liner soils, *Eng. Geol.* **57**, 105-121

Yin, J.-H. (2003). A double cell triaxial system for continuous measurement of volume changes of an unsaturated or saturated soil specimen in triaxial testing, *Geotech. Test. J.* **26**, 3, 353-358.

Yount, D.E., Strauss, R.H. (1976). Bubble formation in gelatine: a model for decompression sickness, *J. App. Phys.* **47**, 11, 5081-5089

Xiao, X., Qian, L. (2000). Investigation of humidity-dependent capillary force, *Langmuir* **16**, 8153-8158

Zhang, Y.S., Sun, W., Li, J.Z. (2005). Hydration process of interfacial transition in potassium polysialate (K-PSDS) geopolymer concrete, *Mag. Concrete Res.* **57**, 1, 33-38

Zhou, Q., Aurelian, A., Chang, B., del Corral, C., Koivo, H.N. (2004). Microassembly system with controlled environment, *J. of Micromechatronics* **2**, 3, 227-248

Zitzler, L., Herminghaus, S., Mugele, F. (2002). Capillary forces in tapping mode atomic force microscopy, *Phys. Rev. B* **66**, 155436

Appendix TESTING PROGRAM

test	tensiometer	equipment	material	purpose	figure
Td1	III6	-	-	tensiometer design	3.4a
T11	II1	saturation vessel	kaolin	tensiometer saturation	-
T12	II1	saturation vessel	kaolin	tensiometer saturation	-
T13	II1	saturation vessel	kaolin	tensiometer saturation	-
T15	II2	saturation vessel	kaolin	tensiometer saturation	-
T16	II2	saturation vessel	kaolin	tensiometer saturation	-
T18	II3	saturation vessel	kaolin	tensiometer saturation	-
T20	II4	saturation vessel	-	tensiometer saturation	-
T24	II5	saturation vessel	-	tensiometer saturation	3.8
T25	II2	saturation vessel	kaolin	tensiometer saturation	-
T27	II3	saturation vessel	kaolin	tensiometer saturation	3.9a
T28	II4	saturation vessel	-	tensiometer saturation	3.11
T29	II3	saturation vessel	-	tensiometer saturation	-

test	tensiometer	equipment	material	purpose	figure
T30	II4	saturation vessel	-	tensiometer saturation	-
T31	III4	saturation vessel	-	tensiometer saturation	3.10
T34	II1	saturation vessel	-	tensiometer saturation	-
T35	II1	-	-	tensiometer post-cavitation	3.15
T36	II2	saturation vessel	-	tensiometer saturation	3.19
Tt1	III3	-	-	tensiometer temp. effect	3.14
Tt2	III4	-	-	tensiometer temp. effect	3.14
Tt3	III4	-	-	tensiometer temp. effect	3.14
Tt4	II2	-	-	tensiometer temp. effect	3.14
Tt5	III4	-	-	tensiometer temp. effect	3.14
Tt6	II2	-	-	tensiometer temp. effect	3.14
Tt7	III4	-	-	tensiometer temp. effect	3.14
Tt8	III3	-	-	tensiometer temp. effect	3.14
Tt9	III4	-	-	tensiometer temp. effect	3.9b, 3.14
Tt10	II2	-	-	tensiometer temp. effect	3.13, 3.14
Tt11	III3	-	-	tensiometer temp. effect	3.14
Tt12	III3	-	-	tensiometer temp. effect	3.14
Tt13	II2	-	-	tensiometer temp. effect	3.14
Tt14	III4	-	-	tensiometer temp. effect	3.14

test	tensiometer	equipment	material	purpose	figure
Tpc1	III5	-	-	tensiometer post-cavitation	3.16a
Tpc2	III5	-	-	tensiometer post-cavitation	3.16b
Tpc3	III5	-	-	tensiometer post-cavitation	3.17a, 3.17b
Tpc4	III5	-	-	tensiometer post-cavitation	-
Tpc5	III5	-	-	tensiometer post-cavitation	-
Tc1	III3	saturation vessel	-	tensiometer calibration positive	3.39
Tc2	III3	saturation vessel	-	tensiometer calibration positive	3.39
Tc3	III3	triaxial	-	tensiometer calibration positive	3.39, 3.40
Tc4	III3	triaxial	kaolin	tensiometer calibration positive	3.39
Tc5	III4	triaxial	-	tensiometer calibration vacuum	3.42
Tc6	II1	triaxial	kaolin	tensiometer calibration unloading	-
Tc7	II2	triaxial	kaolin	tensiometer calibration unloading	-
Tc8	II1	triaxial	kaolin	tensiometer calibration unloading	-
Tc9	III4	triaxial	kaolin	tensiometer calibration unloading	-

test	tensiometer	equipment	material	purpose	figure
Tc10	III3	triaxial	kaolin	tensiometer calibration unloading	-
Tc11	III6	triaxial	kaolin	tensiometer calibration unloading	-
Tc12	III6	triaxial	kaolin	tensiometer calibration unloading	-
Tc13	III4	triaxial	kaolin	tensiometer calibration unloading	3.44
Tc14	III6	triaxial	kaolin	tensiometer calibration unloading	-
Tc15	III4	triaxial	kaolin	tensiometer calibration unloading	3.45b, 3.46
Tc16	II1	pressure plate	kaolin	tensiometer calibration axis translation	3.48a, 3.49a
Tc17	II1	pressure plate	kaolin	tensiometer calibration axis translation	-
Tc18	II2	triaxial	kaolin	tensiometer calibration axis translation	-
Tc19	II3	triaxial	kaolin	tensiometer calibration axis translation	3.49b
Tc20	II2	triaxial	kaolin	tensiometer calibration axis translation	-
Tc21	II2	triaxial	buckley	tensiometer calibration axis translation	-
Tc22	II1	triaxial	kaolin	tensiometer calibration axis translation	-

test	tensiometer	equipment	material	purpose	figure
Tc23	II2	triaxial	kaolin	tensiometer calibration axis translation	3.48b
Tc24	III4	triaxial	kaolin	tensiometer calibration axis translation	3.50
Tc25	III4	triaxial	kaolin	tensiometer calibration axis translation	3.51
Tc26	III5	-	-	tensiometer calibration	3.54
Tc27	II1	-	BIONICS	tensiometer calibration	3.55, 3.59a
Tm1	III3	suction meas. box	BIONICS	tensiometer measurement	3.60
Tm2	III1	-	-	tensiometer measurement	-
Tm3	III5	-	-	tensiometer measurement	3.61
Tm4	II3	triaxial	lime	tensiometer measurement	3.63
Tcen1	II1, II2	centrifuge	Jossigny silt	tensiometer centrifuge	3.67b
Tcen2	III2, III4, III5	centrifuge	Jossigny silt	tensiometer centrifuge	-
Tcen3	III3, III4, III6	centrifuge	Jossigny silt	tensiometer centrifuge	3.67a
S1	-	Hg Porometer	BIONICS	sample volume measurement	4.6, 4.21c, 4.21d, 4.25, 4.31
S2	-	Hg Porometer	BIONICS	sample volume measurement	4.6, 4.21c, 4.21d, 4.25, 4.31
S3	-	Hg Porometer	BIONICS	sample volume measurement	4.6, 4.21c, 4.21d, 4.25, 4.31
Ci1	III1	balance	BIONICS	SWRC	4.9, 4.10a, 4.28

test	tensiometer	equipment	material	purpose	figure
Ci2	II2	balance	BIONICS	SWRC	4.8, 4.9, 4.10a, 4.10b, 4.28
Ci3	II2	balance	BIONICS	SWRC	4.9, 4.28
Ci4	III4	balance	BIONICS	SWRC	4.9, 4.28
Ci5	III4	balance	BIONICS	SWRC	4.9, 4.10b, 4.28
Ci6	III4	balance	BIONICS	SWRC	4.9, 4.10b, 4.28
Ci7	III4	balance	BIONICS	SWRC	4.9, 4.28
Ci8	III4	balance	BIONICS	SWRC	4.9, 4.10b, 4.28
Ci9	III4	balance	BIONICS	SWRC	4.9, 4.28
Ci10	III4	balance	BIONICS	SWRC	4.9, 4.10a, 4.28
Ci11	III4	balance	BIONICS	SWRC	4.12, 4.17, 4.28
Ci12	III4	balance	BIONICS	SWRC	4.12, 4.13, 4.17, 4.28
Ci13	III4	balance	BIONICS	SWRC	4.12, 4.13, 4.17, 4.28
Ci14	III4	balance	BIONICS	SWRC	4.12, 4.13, 4.17, 4.28
Ci15	-	balance	BIONICS	SWRC	4.17
Ci16	-	balance	BIONICS	SWRC	4.17
Ci17	-	balance	BIONICS	SWRC	4.17
Ci18	-	balance	BIONICS	SWRC	4.17
Ci19	-	balance	BIONICS	SWRC	4.17
Cf1	III3	balance	BIONICS	SWRC	4.20, 4.29
Cf2	III3	balance	BIONICS	SWRC	4.20, 4.29
Cf3	III3	balance	BIONICS	SWRC	4.20, 4.29
Cf4	III3	balance	BIONICS	SWRC	4.20, 4.29
Cf5	III4	balance	BIONICS	SWRC	4.21, 4.29
Di1	II1	balance, suction meas. box	BIONICS	SWRC	4.22b, 4.28

test	tensiometer	equipment	material	purpose	figure
Di2	II1	balance, suction meas. box	BIONICS	SWRC	3.59c, 4.22b, 4.28
Di3	II2	balance, suction meas. box	BIONICS	SWRC	4.22a, 4.22b, 4.28
PP	-	pressure plate	BIONICS	SWRC	4.29
Df1	III4	balance, suction meas. box	BIONICS	SWRC	3.59b, 4.23, 4.29
Df2	III4	balance, suction meas. box	BIONICS	SWRC	4.23, 4.24, 4.25, 4.26, 4.29
Df3	III4	balance, suction meas. box	BIONICS	SWRC	4.23, 4.27, 4.29
Df4	III4	balance, suction meas. box	BIONICS	SWRC	4.23, 4.29
Df5	III3	balance, suction meas. box	BIONICS	SWRC	3.59d
V1	-	triaxial, volume gauges	-	triaxial volume change	-
V2	-	triaxial, volume gauges	-	triaxial volume change	-
V3	-	triaxial, volume gauges	-	triaxial volume change	-
V4-1	-	triaxial, volume gauges	-	triaxial volume change	5.4
V4-2	-	triaxial, volume gauges	-	triaxial volume change	5.5

test	tensiometer	equipment	material	purpose	figure
V5	-	triaxial, LVDT	-	triaxial volume change	5.6a, 5.6b
V6	-	triaxial, LVDT	-	triaxial volume change	5.6a
V7	-	triaxial, LVDT	-	triaxial volume change	5.6a
V8	-	triaxial, LVDT	-	triaxial volume change	5.6a
V9	-	triaxial, volume gauge	-	triaxial volume change	5.8
V10	-	triaxial, volume gauge	-	triaxial volume change	5.9
V11	-	triaxial	-	triaxial volume change	5.11
PG1	-	triaxial	sandstone disks (4)	air pressure gradients	5.15
PG2	-	triaxial	sandstone disks (4)	air pressure gradients	5.15
PG3	-	triaxial	sandstone disks (4)	air pressure gradients	5.15
PG4	-	triaxial	sandstone disks (4)	air pressure gradients	5.15
SG1	-	balance	silica gel	adsorption capacity	5.17a, 5.17b
SG2	-	balance	silica gel	adsorption capacity	5.17a
SG3	-	balance	silica gel	adsorption capacity	5.17a
SG4	-	balance	silica gel	adsorption capacity	5.17b
d1	II1	triaxial	sand, kaolin	drying control	5.19
d2	II1	triaxial	BIONICS	drying control	5.20
d3	II2	triaxial	BIONICS	drying control	5.22
d4	II2	triaxial, suction control sys.	BIONICS	drying control	5.23

test	tensiometer	equipment	material	purpose	figure
d5	II2	triaxial, suction control sys.	BIONICS	drying control	5.24
d6	III4	triaxial, suction control sys.	BIONICS	drying control	5.25
d7	III3	triaxial, suction control sys.	BIONICS	drying control	5.26
A5	-	triaxial	gypsum	soil wettability	-
A6	-	triaxial	gypsum	soil wettability	-
A7	-	triaxial	gypsum	soil wettability	-
A8	-	triaxial	kaolin	soil wettability	-
A9	-	triaxial	kaolin	soil wettability	-
A10	-	triaxial	kaolin	soil wettability	-
A11	-	triaxial	kaolin	soil wettability	-
A12	-	triaxial	kaolin	soil wettability	-
A13	-	triaxial	kaolin	soil wettability	-
A16	II1	triaxial	BIONICS	soil wettability	5.28
A17	II1	triaxial	BIONICS	soil wettability	5.31
W0	-	wetting valve	-	valve performance	5.32
W1	III3	triaxial, suction control sys.	BIONICS	wetting control	5.33, 5.34
W2	III3 (top) II2 (bottom)	triaxial, suction control sys.	BIONICS	wetting control	5.38, 5.39, 5.40
AI1	-	balance, silica gel box	silica gel	air leakage monitoring	5.35
AI2	-	balance, silica gel box	silica gel	air leakage monitoring	5.36
E1	-	ESEM	6μm silica spheres	water menisci observations	6.2a, 6.2b, 6.3, 6.10
E2	-	ESEM	6μm silica spheres	water menisci observations	6.2c, 6.4, 6.7a, 6.7b
E3	-	ESEM	2μm silica spheres	water menisci observations	6.6, 6.9

test	tensiometer	equipment	material	purpose	figure
E4		ESEM	kaolin	water menisci observations	**6.17**
AFM1	-	AFM	6µm silica spheres	meniscus force measurement	**6.21b**